DEEP-SEATED MAGMATISM,

ITS SOURCES AND THEIR RELATION TO PLUME PROCESSES

Глубинный магматизм, его источники и их связь с плюмовыми процессами

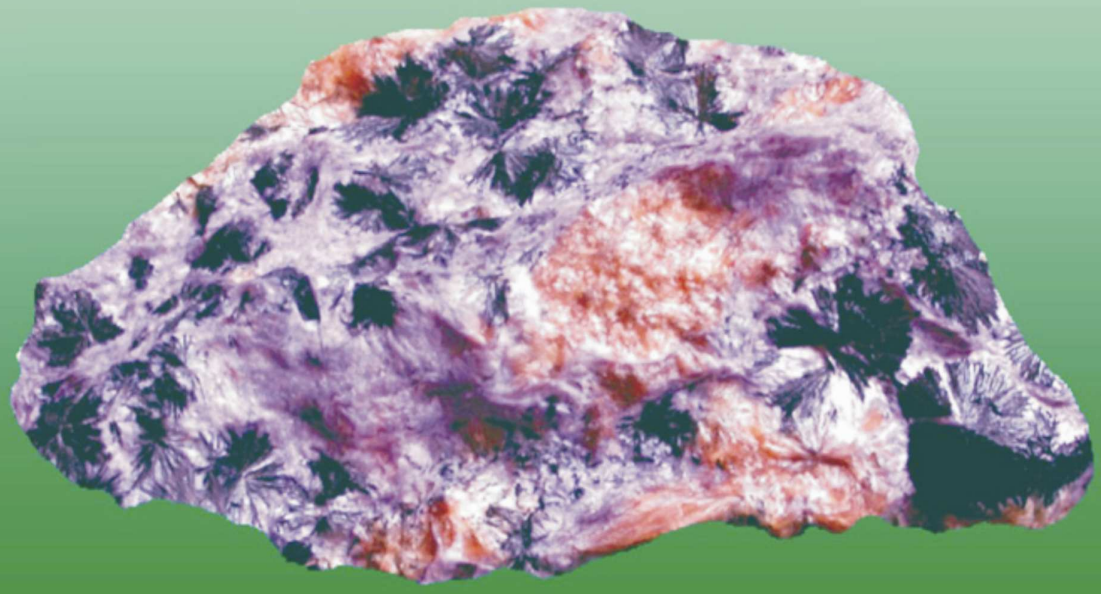

IRKUTSK - ULAN-UDE
2004

Russian Academy of Sciences
Vinogradov Institute of Geochemistry
Siberian Branch of RAS
Geological Institute
Siberian Branch of RAS
Russian Foundation of Basic Research

Deep-seated magmatism, its sources and their relation to plume processes

(Глубинный магматизм, его источники и их связь с плюмовыми процессами)

PROCEEDING
of International Workshop
« Deep-seated magmatism,
its sources and their relation
to plume processes »

Edited by Dr. N.V. Vladykin

IRKUTSK
ULAN-UDE

2004

UDK 552.33+ 552.32

Deep-seated magmatism, its sources and their relation to plume processes. Proceedings of the 4 Interntional Conference. Ulan-Ude. Publishing House of the Institute of Geography SB RAS, 2004, 315 p., ISBN 5-94797-046-5.

The given book presents invited reports of the 4th International Similar «Deep-seated magmatism, its sources and the association with plume processes», 2004, Ulan-Ude.

The invited reports discuss the features of alkaline, carbonatite and kimberlite magmatism. Volatile component flows in the upper shells of the Earth caused by deep-seated geodynamic processes are considered in the reports. The review of stages in alkaline magmatism in the Earth's history is given. New data concerning carbonatites of Namibia and new carbonatite occurrence «Veseloe» in Northern Transbaikalia are presented. The phenomenon of the carbonatite metasomatism when forming Fernando de Noronha Island carbonatites, Brazil is considered. Silicate-carbon-sodium-saline separation in inclusions of the alkaline melt in minerals of early rocks of carbonatite complex is of particular interest. The diagram to determine the mantle sources of carbonatites is compiled based on studies of C and O isotopes of carbonatites occurrences in Siberia and Mongolia. Sr and Nd isotope geochemistry in carbonatites and kimberlites of Siberia is discussed.

The book is of great importance for petrologists, geochemists, and specialists studying deep alkaline and kimberlite magmatism, students and teaching staff of universities.

Published following the decision of the Scientific Council of Vinogradov Institute of Geochemistry SB RAS

Editor: Prof. N.V. Vladykin

Reviewers: Prof. O.M. Glazunov and Prof. V.S. Antipin

Original-model: A.B. Perepelov

ID№ 05215 от 28.06. 2001г.

Institute of Geography SB RAS
664033, Irkutsk, Ulanbatorskaja str. 1

ISBN 5-94797-046-5

TABLE OF CONTENTS

FOREWORD

Alkaline rocks are unique formation on the Earth. They have been of particular interest for researchers. Large Nb, Ta, Zr, Y, TR, Cu, P deposits, gemstones of charoite, Cr-diopside, dianite are associated with alkaline rocks. The Australian lamproites are connected with diamonds. The complicated processes of their formation provoked multi-year scientific disputes, which are still the case. The new methods of investigations provided much information on the composition of alkaline rocks. The data on geochemistry of isotopes confirm the mantle sources of the substance of alkaline rocks. The new stage of the plume tectonics deepened the interest of scientists to the alkaline rocks from the viewpoint of plate tectonics. The deep-seated Earth's geodynamics can be interpreted using these data.

These problems were discussed during International Seminars held in 2001 at the Institute of Geochemistry, SB RAS, Irkutsk, in 2002 at the Far-East Geological Institute, Vladivostok, and in 2003 at Institute of Tectonics and Geophysics, Khabarovsk. The given book presents invited reports of the 4th International Seminar «Deep-seated magmatism, its sources and the association with plume processes», 2004, Ulan-Ude.

The invited reports discuss the features of alkaline, carbonatite and kimberlite magmatism. Volatile component flows in the upper shells of the Earth caused by deep-seated geodynamic processes are considered in the reports. The proceedings contain review of stages in alkaline magmatism stages in the Earth's history. The reports give new data concerning carbonatites of Namibia and new carbonatite occurrence «Veseloe» in Northern Transbaikalia. The phenomenon of the carbonatite metasomatism when forming Fernando de Noronha Island carbonatites, Brazil is considered.

Silicate-carbon-sodium-saline separation in inclusions of the alkaline melt in minerals of early rocks of carbonatite complex is of particular interest. The diagram to determine the mantle sources of carbonatites is compiled based on studies of C and O isotopes of carbonatites occurrences in Siberia and Mongolia. Sr and Nd isotope geochemistry in carbonatites and kimberlites of Siberia is discussed. The reports are translated into English by the authors.

The book is of great importance for petrologists, geochemists, and specialists studying deep alkaline and kimberlite magmatism.

Chief Editor **Dr. N.V. Vladykin**

UDK 548.4

Volatile component flows in the upper shells of the Earth caused by deep-seated geodynamic processes

Yarmolyuk V.V.[1], Kovalenko V.I.[1], Naumov V.B.[2]

[1] *Institute of Geology, Mineralogy and Ore Deposits, RAS, Moscow, Russia*
[2] *Vernadsky Institute of Geochemistry and Analytical Chemistry, Moscow, Russia*

The study reports on the distribution of volatile flows between mantle and external shells of the Earth: crust, hydrosphere and atmosphere. This analysis is based on the knowledge on the balance between masses of volatiles carried by magmatic melts onto the Earth surface, the masses of these volatiles consumed in the Earth interior by the subducted lithosphere, as well as masses contained in the external shells. The geodynamic concepts applied for the model of balance consist in the essential contribution of lithosphere plates tectonics and geodynamics of mantle plumes to the Earth formation. Besides, it was assumed that the velocities of geological processes varied insignificantly through geological time.

The average contents of volatile components in magmatic melts of important geodynamic settings were defined from the data on contents of water, chlorine, fluorine and sulfur in melt inclusions and quenched glass. These settings are: mid-oceanic ridges (MOR), oceanic islands and lava plateau (OI), island arcs and active continental margins (ACM), and intracontinental magmatic areas (CR). Using these data, the masses of volatile components, transported with onto the Earth surface since it had been formed, were evaluated. The amount of descending flows of volatile components were recognized through applicatioin the data on abundances of these volatiles and assessment of the amount of oceanic and continental crust buried in the subduction zones through geological history. The schemes of the balance indicate presence in the Earth of a thick primary exosphere, its composition largely defined by water and chlorine, while proportions of sulfur and fluorine were not essential. The mass of water in the primary exosphere exceeded its mass contained in the recent hydrosphere and crust more than 1.5 times. The processes of subduction were very important for existence of the primary ocean. Through geological history these zones consumed enormous volumes of water comparable with its abundance in all recent external shells. The calculations of the balance show that entire amount of chlorine of the primary exosphere of the Earth and predominant mass of sulfur and about 60 % of fluorine, which were released with melts through geological history, were recycled through these zones. Recycled lithosphere is also responsible for emergence of enriched mantle sources feeding magmatism of intraplate settings. The direct evidence is yielded by the data on enrichment of magmas with OI and CR against melts MOR H_2O > 1,5 times, Cl >over 2,5 times, F > 4 times. The paper also considers the issues on the relationships between thick primary aqueous exosphere of the Earth and the features of its geodynamic development.

INTRODUCTION

Formation of external shells of the Earth (continental and oceanic crust of hydrosphere and atmosphere) basically result from global geodynamic changes of our planet, which led it from the state of cosmic material blend to the recent outlook. Volatile components (H_2O, CO_2, Cl, F, S) contributed considerably to these processes, for they represented principal or essential components of hydrosphere, atmosphere and lithosphere. In all recent external shells of the Earth volatile components are derived from the mantle. It appears that magmatic differentiation in the mantle caused formation of external shells. Modern geodynamic concepts consider descending substance flows, along with ascending ones, as being crucial. They are associated with consumption of lithosphere material in zones of subduction and collision, and thus compensating growth of oceanic crust in mid-oceanic ridges. These motions bring silicate matter and part of volatile components back into the mantle, that is recycling of the latter takes place. Considering this idea, the balance should occur between the masses of volatile components in exosphere and deep shells of the Earth or between the masses of these components, on the one hand, which were transported into the upper shells of the planet jointly with magmatic melts from the mantle, and on the other hand, involved into reverse processes of recycling. In the present article we look at the dynamics of volatile components between shells of the Earth based on the balance controlled by lithosphere plates tectonics and deep geodynamics of plumes [28]. Their combination assumes non-linear character of geological processes responsible for formation of important geospheres of the Earth. This aspect of the Earth sciences is being developed by Puscharovsky in [14, 15]. Evaluation of substance balance in geodynamic processes is of particular significance for volatile components, which dominate in the exosphere, hydrosphere and atmosphere included, and are easily redistributed between it and the mantle. So far, the two extreme models of formation of the Earth's exosphere are being discussed: (i) magmatic degassing and (ii) cosmic accretion [23]. With the balances of volatile components applied, it is feasible to regard these models to be in agreement. Also note that recycling of volatile components in the deep mantle is believed to be responsible for mantle heterogeneities [35], which produce non-linear effects in the mantle geodynamics. In particular, it was shown that the temperature of the descending plate in the subduction zone drops non-linearly with increase of subduction velocity. It was fairly high in the Cretaceous, Early Paleozoic and possibly Early Archean epochs of the Earth. Thus, cold subducting material in the epochs of the fast (to 20 cm/yr) subduction descend to larger depths as compared to the ordinary velocities (3-12 cm/yr), and it makes up the mantle heterogeneities mentioned above. Characteristically, rheology of subduction processes, as well as mantle circulation have changed. The article is based on the materials reported at the conference "Deep-seated fluids and geodynamics" at Geological Institute, Moscow (2003). The geochemical aspects of global balance of chlorine and water and geochemical specifics of these elements in different geodynamic settings were previously discussed in [6].

APPROACHES TO EVALUATE THE BALANCE OF VOLATILE COMPONENTS IN GEOLOGICAL PROCESSES

The general scheme of the balance of volatile components, provided in Figure 1, is based on the following principles:

1. The main masses of volatiles involved in geological processes in the upper shells of the Earth, are formed due to their primary content in the exosphere of the embryo Earth and due to juvenile additives associated with their supplies from the mantle during magmatic activity (flows ***a, b, c*** and ***c**** in Figure 1). The balance of the recent distribution of volatile components from these two sources is defined from the ratio of contents of these components in the external shells (oceanic and continental crust and hydrosphere), and their content in the composition of recycled lithosphere (flow ***d*** in Fig.1)

2. The main volume of mantle magmas is erupted in mid-oceanic ridges (MOR), on oceanic islands and plateau (OI), in continental rifts and in intracontinental areas (CR), related to hot spots, and in island arcs and active continental margins (IA+ACM). During magmatic eruptions the volatile components contained in magmas are partly degassing from melts, are accumulated in the atmosphere and hydrosphere, are conserved in the magmatic rocks of the crust.

3. In the settings IA+ACM volatiles are transported into magmatic melts due to melting of subducted lithosphere (flow ***b**** Fig. 1 – recycled component of ascending flow of volatiles) and due to partial melting of the mantle wedge (flow ***a**** Fig. 1 – juvenile component).

4. After partial melting of rocks of subducted crust the preserved portion of volatiles subsides together with lithosphere down the mantle depth (flow ***d*** Fig.1), thus ensuring its return (deep-seated recycling) to the deep mantle, where their juvenile flows came from.

Thus, the idea of the balance is resolved to comparison of the two totally different and oppositely directed flows of volatiles acting between the mantle and exosphere of the Earth. One of them, directed upwards from the mantle, is distinguished as a juvenile component in the balance scheme. The other flow is directed down the mantle and is realized in the settings of convergent boundaries of lithospheric plates, serving as the zones of the lithosphere substance discharge into the Earth's mantle. Besides, the scheme of the balance contains the hypothetical element characteristic of the primary exosphere of the planet, most likely arising in its accretion. It was distinguished because we cannot ignore the existence of the latter at the early stages of the Earth development. Later on it will be shown, that involvement of this exosphere in the balance of volatiles is decisive, at least for water and chlorine.

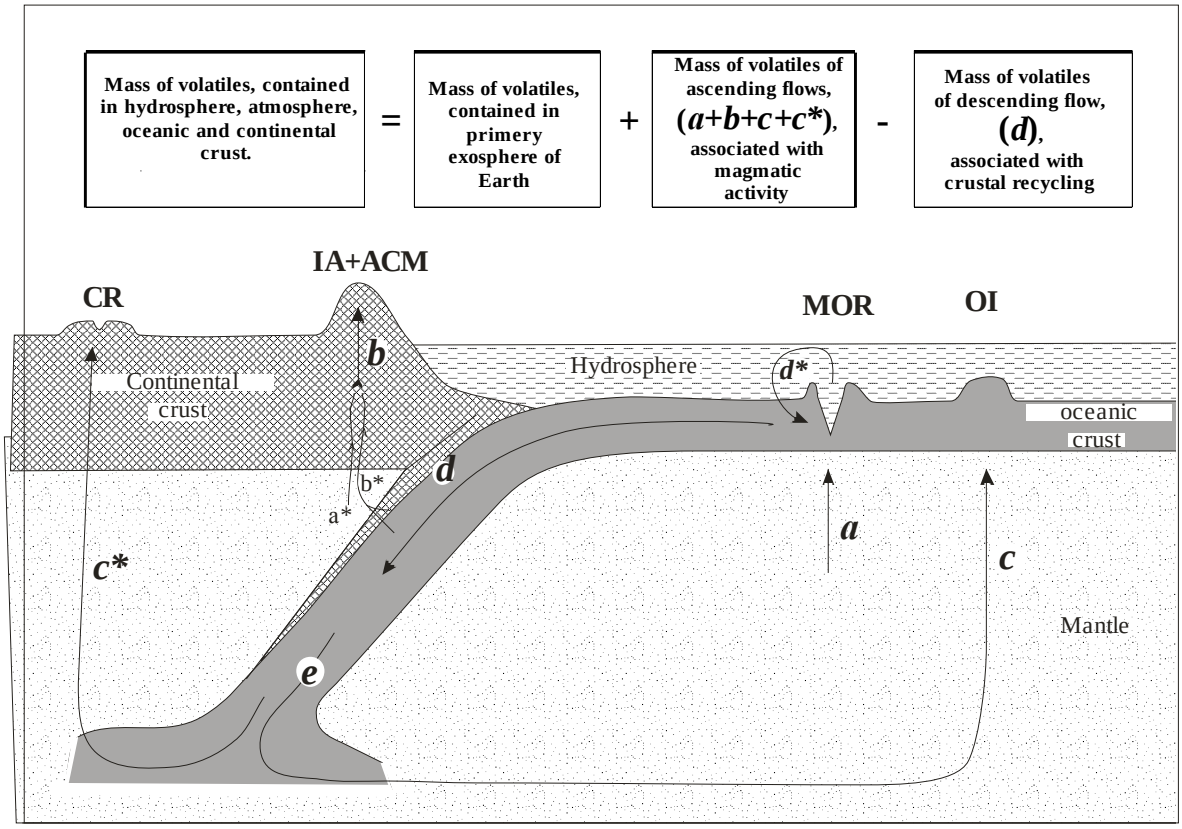

Fig.1. **Model of balance of volatile component masses and distribution of their flows in the structures of different geodynamic settings.**

Geodynamic settings: MOR – mid-oceanic ridges, OI – oceanic islands and lava plateau, IA+ACM – island arcs and continental margins, CR – continental rifts. Volatiles flows: 1 - ascending, related to magmatism: ***а*** - MOR, ***б*** – IA+ACO (its branches included - a*, formed by melting of mantle wedge, and б*, formed by melting of subducted plated), ***в*** - OI, ***в**** - CR; 2 – descending, representing masses of volatiles in rocks: г – subducted plate, д – subducted plate, after thermal processing in subduction zone.

It is important that in constructing the models of balance we postulated on the considerable contribution of tectonics of lithosphere plates and mantle plumes or deep-seated geodynamics [1, 28] to the processes of formation and transformation of the continental and oceanic crust throughout geological history, with its duration accepted to last 4,5 billion years. The following assumptions have been made:

- it was magmatism that mostly supplied crustal material onto the Earth surface,
- velocity of geological processes varied insignificantly during the Earth' history,
- contribution of magmatism of different geodynamic settings to formation of continental and oceanic crusts, and velocity of growth of the crust and its destruction on the convergent boundaries of lithospheric plates remained constant during the geological history,
- the abundance of volatiles in the rocks of both continental and oceanic crust, as well as in magmas of different geodynamic settings primarily through Mesozoic and Cenozoic also did not change in time.

All these assumptions enabled us to propose the model of distribution of main geodynamic flows of water, chlorine, fluorine and sulfur between upper shells of the Earth (Fig. 1). This model is aimed to cover entire geological history. Volatile components are transported by magmas MOR (flow «***a***»), are partly remained in the oceanic crust, and may partly leave for hydrosphere. Oceanic crust is becomes hydrated due to convective hydrothermal systems with marine water involved, and somewhat enriched, at least with water and chlorine (flow «***d****» in Fig. 1). Lithosphere with hydrated oceanic crust and fragments of tectonically eroded continental crust travels to suduction zones (flow «***d***»). For simplicity, we consider that fluid composition of magmas IA+ACM (flow ***b*** in Fig.1) resulted from interaction of products of mantle wedge melting (flow «***a****») and subducted oceanic and continental crust (flow «***b****»). Volatile components preserved in the descending plate (flow «***e***» in Fig. 1) are transported deep into the mantle, participating in formation of OI and CR sources through recycling of lithosphere. It is apparent that for a balance assessment of all these flows it is necessary to know average contents and masses of these components in hydrosphere, continental and oceanic crust, in magmas MOR, OI, IA+ACM and CR, as well as masses of water and chlorine, recycled during geological history of the Earth.

ASSESSMENT OF VOLATILE COMPONENTS ABUNDANCE IN GEOLOGICAL SETTINGS

The relationship of volatile components with geodynamics can be revealed using reliable values of volatile components abundance in natural mantle magmas of different geodynamic settings, in the Earth's crust, hydrosphere and atmosphere, as well as reconstruction of volatile flows between geospheres. It is most difficult to define contents of volatiles in magmatic melts, which have been tentative so far, and they have been defined by direct methods fairly recently. These definitions were made by attracting the data of local analysis of volatile components in melt inclusions in the minerals of magmatic rocks [3-5, 10-13]. These inclusions represent the fragments of natural magmas captured by growing crystals and conserved up to the point of their exposition for the study. Besides, the data on the contents of volatiles in magmas were supplemented by the results on quenched glasses formed by deep-seated eruptions onto the bottom of oceans and seas, when the pressure of water column is higher than the internal pressure of volatiles in melts, and thus it hinders formation of the gaseous phases and release of volatiles from melt (glass).

The analyses of volatile components in melt inclusions and quenched glass were performed by ion (H_2O, F) and electronic (Cl, S) microprobes [29], FTIR (H_2O, [28]), as well as high-T mass spectrometry [21]. The analytical parameters of these methods were provided in some publications, and the overview of

Table 1.

Contents and masses of volatile components in the melts, which made up the lithosphere shell, in crustal rocks and hydrosphere

Shells of the Earth (1) and their mass (2) after [18]		Content* (a) and mass** (b)							
		H_2O		Cl		S		F	
1	2	a	b	a	b	a	b	a	b
		In the melts***, which formed the crust							
Continental and subcontinental crust, including subducted crust for time span 4,5 billion years, including the crust formed in the settings of:	3348		44,11		3,94		2,71		2,29
Island arcs and active continental margins (IA+ACM)	2243	1,69	37,91	0,14	3,14	0,078	1,75	0,051	1,14
Continental rifts and hot spots (CR)	184	1,17	2,15	0,248	0,46	0,099	0,18	0,2	0,37
Oceanic uplifts, plateau and islands (OI)	921	0,44	4,05	0,037	0,34	0,085	0,78	0,085	0,78
Oceanic crust formed in MOR for geological history:	22000	0,33	72,6	0,014	3,08	0,111	24,42	0,023	5,06
Total volume, which formed in formation of oceanic and continental crust:	25348		116,71		7,02		27,13		7,35
		In the rocks, making up the crust, and in hydrosphere							
Recent continental crust	2232	0,77	17,19	0,071	1,58	0,11	2,46	0,064[3]	1,43
Recent oceanic crust	614	0,85	5,22	0,019	0,12	0,101	0,62	0,019	0,12
Total of the recent crust	2846		22,41		1,70		3,08		1,55
Hydrosphere	135,8		135,8	1,9	2,7	0,09	0,13		<0,01
Total in hydrosphere, oceanic and continental crust	2981,8		158,21		4,40		3,21		1,55
Recycled crust: continental -	1116	0,77	8,59	0,071	0,79	0,11	1,23	0,064	0,71
oceanic -	21386	0,85	181,8	0,019	4,06	0,101	21,6	0,019	4,06
Total -	22502		190,39		4,85		22,83		4,77

Note. * content in mass %; ** mass in 10^{22} g; *** on approaches to assess the average content of volatiles in melts of different geodynamic settings, see text

analytical approached to the study of volatile components content variations in magmatic processes is given in the monograph [4]. This paper contains both original data of the authors and the results of numerous analyses, which have been included into the databank on melt inclusions [3, 15-18]. Table 1 yields the values of volatile component contents in melts of different geodynamic settings.

To characterize the representative sampling of volatile in magmas of different geodynamic settings we point out about 20000 definitions of their contents have been employed. Sampling sites were schematically shown on the map of Figure 2. Sampling was made in the rocks of the main recent geodynamic settings of magmatism process, and from the rocks of their paleo-analogs (ophiolite and island arc complexes, assemblages of rocks of ancient ACM, continental collision, and the areas of the ancient intraplate activity.

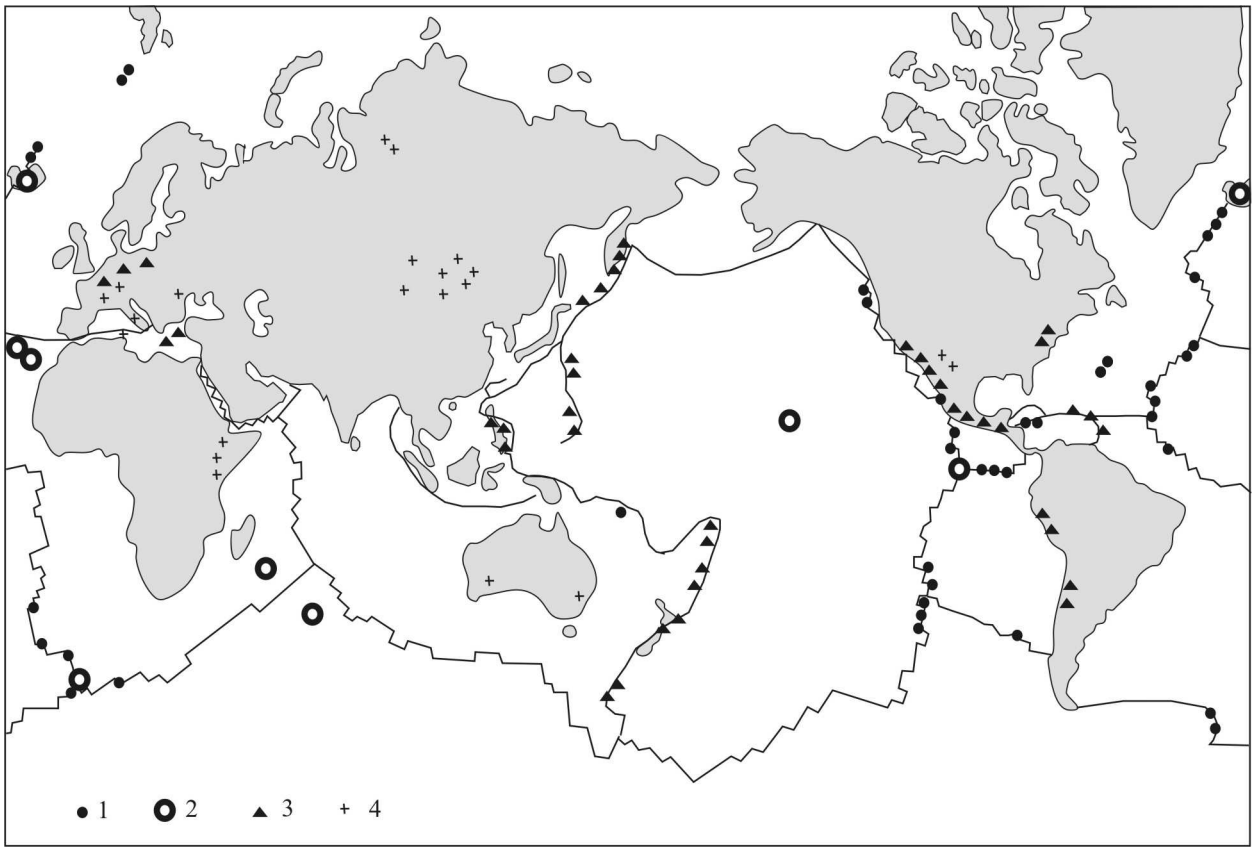

Fig. 2. **Location of sampling sites. Results are yielded in the database on the volatiles contents in magmatic melts of different geodynamic settings.**

1 – mid-oceanic ridges, 2 – oceanic islands, 3 – island arcs and active continental margins, 4 – continental rifts.

The average contents of H_2O, Cl, S, F in the rocks of oceanic and continental crust and in hydrosphere are estimated by Ronov et al. [17-33], specified later [8-18] and presented in Table 1. The content and mass of these volatiles in the Earth's shells were calculated based on the model of its structure and composition

proposed by Ronov et al. [19, 33]. The model is empirical and is based on the materials on the distribution and chemical composition of rocks making up sedimentary and granite-metamorphic shells of the Earth [17]. In this paper the data on the comparison with previous publications are supplemented with new materials describing the results of detailed geochemical conducted investigations in «model regions» (ancient East-European and Siberian and young Skiff platforms, Uralian, Caucasian, Carpathian and Central-European fold zones). The results of similar investigations within crystalline shields and basements of platforms, within the sedimentary layer of the Pacific, Atlantic and Indian oceans have also been considered. Ronov with co-authors [19] analyzed few thousands of samples to characterize different types of rocks and sediments in certain tectonic zones. Currently these data, at least for stratosphere, are believed to be mostly reliable in the geological literature.

EVALUATION OF THE CONTRIBUTION OF ROCKS OF DIFFERENT GEODYNAMIC SETTINGS TO CRUST FORMATION

To substantiate the scheme of balance it is also necessary to assess the masses of oceanic and continental crust, including their recycling through the geological history (see estimates in Table 2). They represent the reconstructions of the volume, mass and composition of the crust, accomplished by Ronov et al. [19, 33], and approaches to define the scales of crust-forming processes reported in [22, 32]. Like other authors, we consider that formation of the continental block of the Earth proceeded in the geodynamic setting IA+ACM, and due to collisional and subductional processes of subcontinental terminology by [22, 32] crust, arising in the OI and CR settings. In accordance with the data by Ronov et al [19, 33] the continental crust mass makes up $2232x10^{22}$г ($8,10x10^{9}$ km^3) and consequently, its annual increase is 1,8 km^3/yr. This is close to figure 1,72 km^3/yr, obtained by Reimer and Schubert [32], which indicates that the recent growth of the crust is ensured by the input of magmatic products of magmatic arcs (67 mass %), oceanic islands and plateau (27,5 mass %), and intracontinental (intra-plate) magmatic areas (5,5 mass %) (Table 2). These estimates of the crust growth disclose about 2/3 of its total growth, while one third of newly formed crust is consumed in subduction zones due to tectonic erosion. Extending these estimates onto the geological history we get the volume of the existing and subducted continental crust and input of products of geodynamic origin (Table 2). We note that magmas of different composition were involved in formation of IA+ACM. Following the data from [19], we accepted that the composition of the continental crust, like that of magmatic complexes ACM, is equivalent to the composition of magmatic rocks of different composition, taken in proportion (volume %): basic – 56.5, average – 33.9, acid – 9.6, without consideration, as mentioned above, that these ratios varied in time. This allowed us to evaluate the average content of volatiles in rocks IA+ACM [6]. In the processes of intra-plate magmatism (OI and CR) the magmas of mean and acid composition played minor role. Thus, the evaluation related to

this magmatism of volatile flows was performed using the data on their contents in basic melts.

The rocks of oceanic sector of the Earth fix only that volume which was formed for about the last 150 million years of the geological history of the Earth.

Table 2.

Input of rocks of different geodynamic settings into composition of oceanic and continental crust of the Earth and masses of these rocks involved in recycling for geological history (based on data by [32, 33])

Type of crust	Recent growth of crust per km^3/year	Mass of recent crust in 10^{22} g	Mass of recycled crust for geological history in 10^{22} g	Total mass of crust formed for geological history in 10^{22} g
Oceanic crust (OC)	17	614	21386	22000
Continental and subcontinental crust (CC)	1,8	2232	1116	3348
Including that formed in settings (in brackets portion in composition CC in %):				
Island arcs, active margins and back-arc basins	1,2 (67)	1495	748	2243
Oceanic plateau and islands	0,5 (27,5)	614	307	921
Intracontinental magmatic regions	0,1 (5,5)	123	61	184

More ancient magmatic rocks of the oceanic block are considered to be subducted (recycled) in the Pre- Late Mesozoic geological history and were not preserved up to now. However, such magmas evidently erupted earlier [7, 22, 36], therefore we spread the recent velocity of the oceanic crust growth (~17 km^3/year) over entire history of the Earth, and obtained the total mass weighing $22000x10^{22}$g. The recent mass of the oceanic crust weighs $614x10^{22}$g, thus showing that through geological history of the Earth no less than $21386x10^{22}$g of this crust, driving into the Earth interior significant masses of water, chlorine, fluorine, sulfur, which were considered in the calculations of the balance

Below the parameters of balance constructions are given separately for each volatile component.

BALANCE OF WATER (Fig. 3**)**

The data on water distribution in melts and rocks of different geodynamic settings are given in Table 1. It follows that through geological history magmas transported the volume of water equal to (в 10^{22} г):

- in formation of oceanic crust in the environment MOR - 72,6,
- in formation of continental and subcontinental crust in the environments of island arcs and active margins (37,91), continental rifts and hot spots of mantle (2, 15), oceanic islands, plateau and uplifts (4,05) – 44,11.

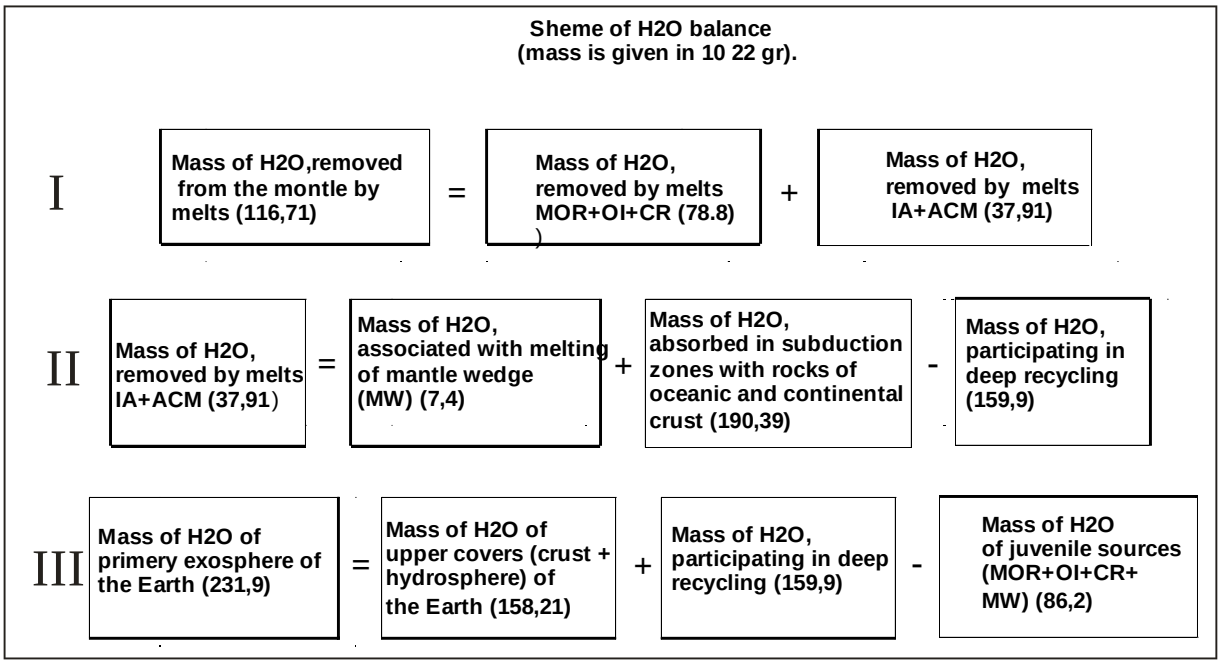

Fig.3. **Scheme of balance and distribution of water masses in flows of volatiles in the upper geospheres of the Earth.**

I –H_2O mass, transported by melts MOR+OI+CR (on divergent boundaries of lithosphere plates and in intraplate regions) and melts IA+ACM (on the convergent boundaries of lithopshere plates);
II – masses and sources of H_2O, involved in differently directed flows in the settings of convergent boundaries of lithosphere plates; III – balance of water mass, involved in the flows of volatiles between the mantle and upper shells of the Earth, and contained in crustal rocks and in hydrosphere.

Thus, magmatic melts recovered from the Earth interior 116,71 x 10^{22} g of water (Table 1, Fig. 3). In the external shells, including their recycled masses, about 212,8 x 10^{22}g in the crust and 135,8 x 10^{22} g of water were recorded in the crust and hydrosphere, accordingly (Table 1). That is, each shell contains more water than it was transported from the mantle. It follows that the balance of water between its parts, evacuated with magmas from the mantle and contained in the external shells, is not observed.

We now consider the particularities of balance scheme, used when studying the balance of the other volatiles, based on the analysis of water flows occurring

between different shells. The calculations of the balance considered the following key points:

Setting MOR. Among water flows ascending from the mantle the largest flow was associated with the melts, forming oceanic crust in mid-oceanic ridges (Fig. 4, flow **a**). The content of water in MOR melts makes up ~0,33 mass %, which enables to assess its volume, carried out by melts for geological history as amount $72{,}6 \times 10^{22}$g. This water is partly redistributed into hydrosphere and atmosphere (Fig. 4, flow **a'**), and conserved in magmatic rocks. Strong convective hydrothermal systems, driving oceanic water into the rocks of the ocean bottom, operate under conditions of mid-oceanic ridges (Fig. 4, flow **b**). The average content of water in the rocks of the oceanic crust, including magmatism-related

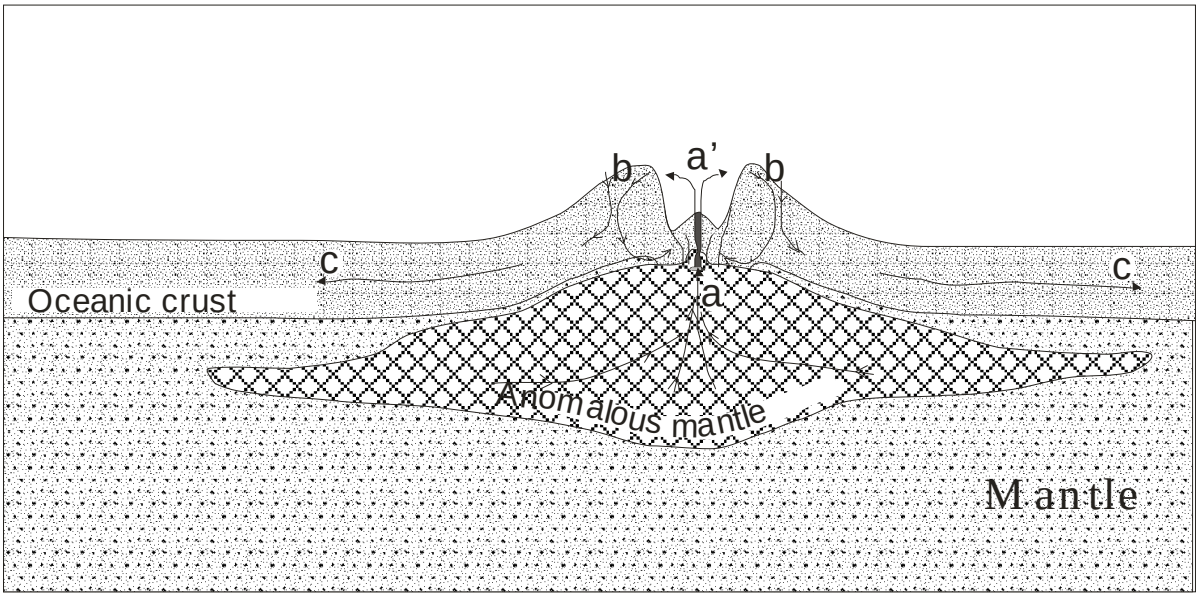

c	=	**a**	-	**a'**	+	**b**
Mass of the component, in rocks of the oceanic plate.		**Mass of the component, removed from magmatic melts.**		**Mass of the component, transformer from the melt into hydrosphere and atmosphere.**		**Mass of the component brought info the rocks with marine water**

Fig. 4. **Distribution of masses and flows of volatiles in the setting of mid-oceanic ridges.**

sedimentary rocks, is estimated to be 1 mass% and thus, following other researchers, it may be stated that rocks of the oceanic crust, after its formation are essentially enriched with marine water. The hydrated oceanic crust (including its recycled part) incorporates $181{,}8 \times 10^{22}$g of water, which (Fig. 4, flow ***c***) is supplied with rocks into subduction zone.

Setting IA+ACM. Distribution of water flows at convergent boundaries of lithosphere plates is illustrated in Figure 5. The zone of subduction contains the rocks of oceanic crust and tectonically altered rocks of continental crust [31]. The

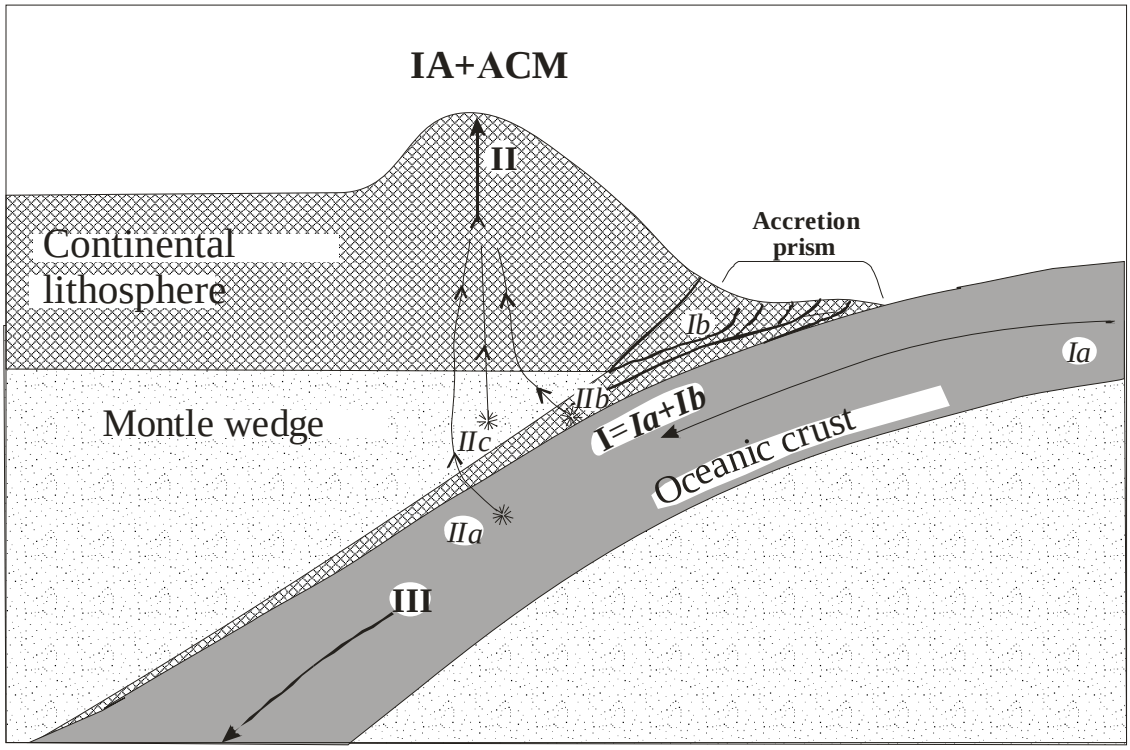

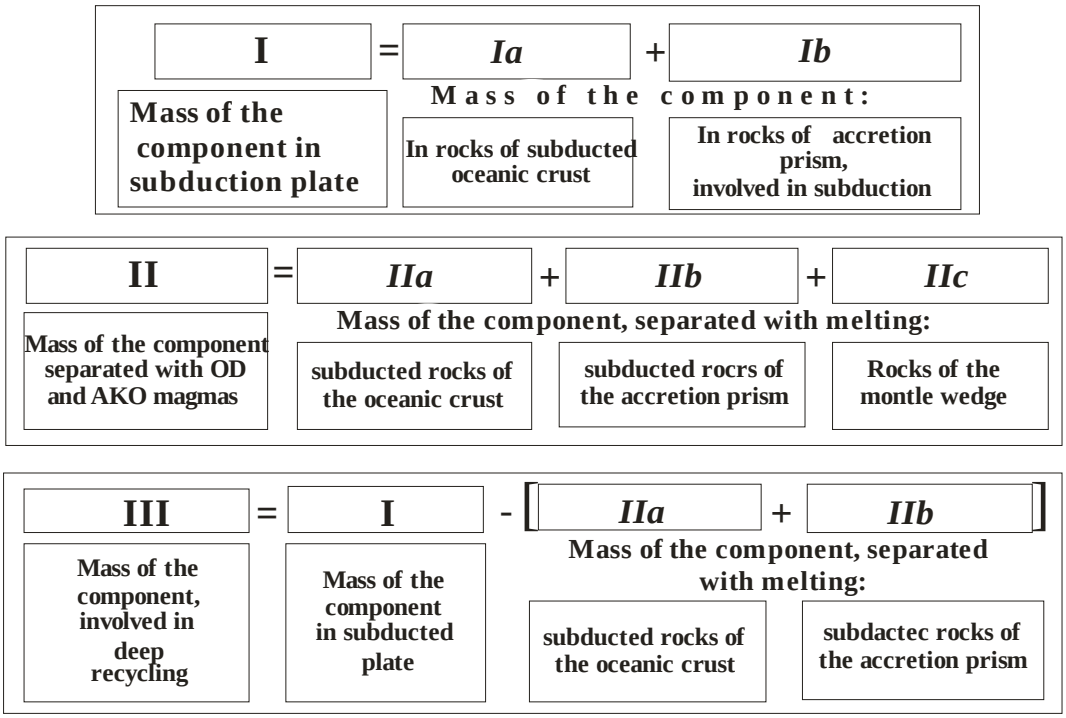

Fig. 5. **Distribution of masses and flows of volatiles in the settings of convergent boundaries of lithosphere plates.**

amount of water transported (recycled) into the Earth interior jointly with rocks of oceanic crust is estimated to be 181,8 x 10^{22} g (Table 1, flow ***Ia*** in Fig. 5). The average content of water in the continental crust makes up 0,77 mass % (Table 1) and, consequently, the amount 8,59 x 10^{22} g H_2O with subducted continental crust

(flow ***Ib*** in Fig. 5) was returned into the mantle. Всего же на конвергентных границах в мантию было рециклировано не менее The total of 190,39 x 10^{22} g of water was recycled on the convergent boundaries into the mantle (Fig. 5). The opposite (ascending) direction on these boundaries is common for the volatile flow associated with magmatism IA+ACM. It value reaches 37,91 x 10^{22} g. Some part of this flow has juvenile mantle source related to melting of rocks of mantle wedge (flow ***IIc*** in Fig. 5). But the contribution of juvenile component should not exceed that amount of water, which would have been released in formation of oceanic crust, equal to the mass of continental crust, from mantle MOR. This amount is estimated from the calculation: oceanic crust mass, equal to mass of crust IA+ACM, multiplied the average content of water in magmas MOR, and thus it is not higher than 7,4 x 10^{22} g of H_2O. However, the released amount was much higher (37,91 x 10^{22} g, Fig.3). The excess as the volume 30,51 x 10^{22} g of H_2O, was most likely involved as a result of dehydration of the material of subducted lithosphere in its melting (flows ***IIa*** and ***IIb*** in Fig. 5). But this amount of water makes up only 16% of water, recycled together with subducted crust.

Distribution of water under deep recycling conditions. The mass of water preserved in the subducted lithosphere amounts to 159,88 x 10^{22} g (190,39 - 30,51) (Fig. 3). This water is involved into deeper levels of mantle and takes part in the deep mantle recycling (flows «***∂***» in Fig. 1 and **III** in Fig. 5). It is believed that it was partly involved into sources of intraplate magmatism (OI and CR), due to which melts of these settings were enriched in H_2O against melts MOR. However, it is evident that the greater part of this water did not take part in magma formation, as in the mantle component OI and CR the ratio of water to chlorine is lower (<12) compared to their ratio in flows «***∂***» in Fig. 1 equal to 33 (159,9/4,85). If we consider that all chlorine in flow «***∂***» (Fig. 1) is present in sources of intraplate magmas and accept the water ratio to be 12, only 58,2 x 10^{22} g of water must be involved in intraplate magma formation, which makes up only 36% of water flow «***∂***» (Fig. 1). Its larger part is remained in the mantle, or in the water-rich magmas unable to move, or as an agent of mantle hydration [6]. Thus, the Earth mantle acquired 159,9 x 10^{22} g of water as a result of subduction for entire geological history (Fig. 3). The velocity of water consumption in the mantle is on average 3,6x 10^{14} g/yr or about 0,36 km^3/yr.

Primary exosphere of the Earth. The excess of water, equal to the difference between masses of water which is contained in hydrosphere and in the crustal rocks on the one hand, and was transported from the mantle by melts, on the other hand, is estimated to be 231,9 x 10^{22} g. Our view (Fig. 3), is that this excess is as much as the water volume existing in the primary external exopshere of the Earth. If we consider the amount of juvenile water (86,2 x 10^{22} g), released for the geological history, the total water volume involved in the geological processes in the upper shells of the Earth makes up not less than 318 x 10^{22} g. Part of this water was in the crust and hydrosphere of the Earth (158,21 x 10^{22} г), and nearly the same part (over 160 x 10^{22} g) was involved оказалась in the intra-mantle recycling.

So the conclusion is that at the initial stages of development the Earth possessed voluminous water atmosphere, with the water mass exceeding that in the recent ocean 1,5-fold. The condensation of this atmosphere should lead to origination of the ocean with the average depth about 4 km.

BALANCE OF CHLORINE (Fig. 6)

The main parameters of the balance model of chlorine behaviour in geodynamic processes are given in Table 1. Based on the available data the magmas removed chlorine as amount of 10^{22} g:

- In formation of oceanic crust in setting MOR - 3,08,

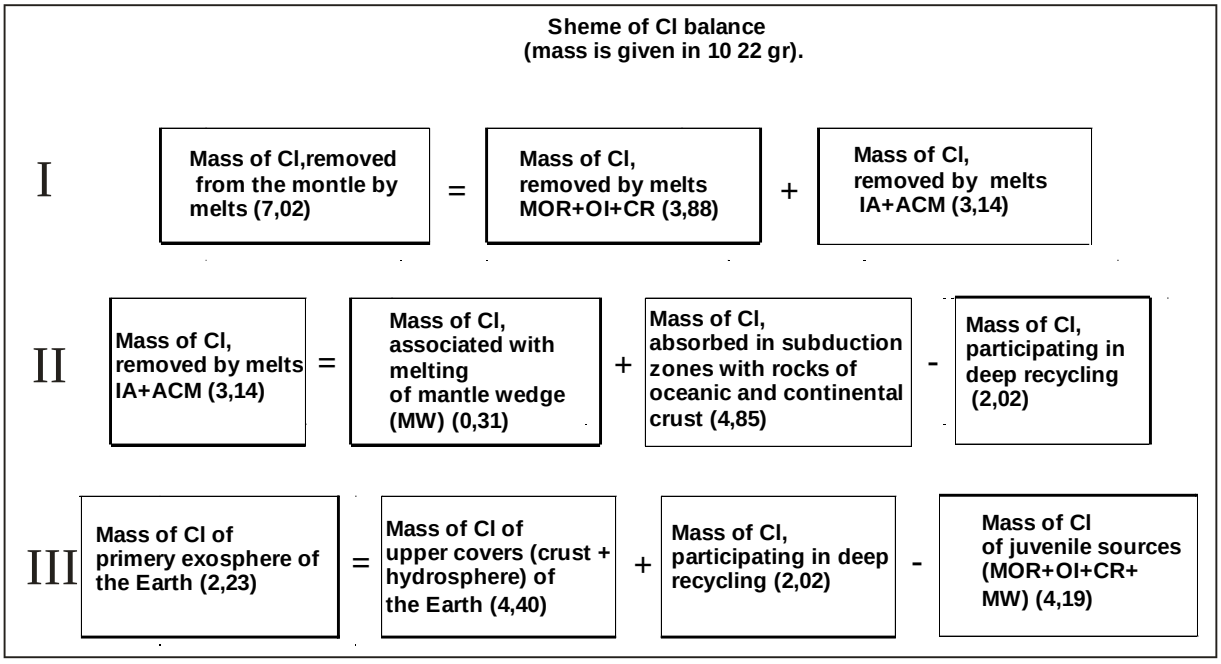

Fig. 6. **Scheme of balance and distribution of chlorine mass in the flows of volatiles and in the upper geospheres of the Earth.**

I – Cl mass, transported by melts MOR+OI+CR (on the divergent boundaries of lithosphere plates and in intra-plate regions) and melts IA+ACM (on convergent boundaries of lithosphere plates); II – masses and sources of Cl, involved in differently directed flows in the settings of convergent boundaries of lithosphere plates; III – balance of Cl masses, involved in the volatile component flows between mantle and upper shells of the Earth, and contained in crustal rocks and in hydrosphere.

- In formation of continental and subcontinental crust, recycled included, in the settings of island arcs and active margins, continental rifts and hot spots of the mantle, oceanic islands, plateau and uplifts this figure is 3,94. Total of 7,02 x 10^{22} g Cl (Table 1) was recovered from the Earth interior with melts of different geodynamic settings for entire history of the Earth.

- In the external shells, including recycled masses, the crust contains 6,55, x 10^{22} g and hydrosphere contains 2,7 x 10^{22} g of water (Table 1), and thus, we get excessive mass of chlorine ($2,23x10^{22}$г) in the external shells against its amount released from mantle melts.

Thus, the behaviour of Cl in the main flows of volatiles is as follows:

In setting MOR chlorine behaves like water [6]. Its content in melts is lower than in rocks. This indicates hydration of magmatic rocks after their formation under the effect of hydropthermal-convective systems. Therefore, if melts in COX settings removed $3{,}08 \times 10^{22}$ g of Cl, the oceanic crust, recycled part included, the mass of chlorine, is estimated to be $4{,}06 \times 10^{22}$ g and consequently, chlorine makes up 25% , borrowed from marine water.

Setting IA+ACM (Fig. 5)**.** On the convergent boundaries of lithosphere plates the amount of chlorine $4{,}85 \times 10^{22}$ g was consumed, contained in thin these rocks on the convergent boundaries of lithosphere plates due to subduction of rocks of the oceanic and continental crust (flow ***Ia*** and ***Ib*** **in** Fig. 5). While descending to the subduction zone the total flow of subducted chlorine (flow **I,** Fig. 5) is divided into two branches with the balance described as:

Cl(**I**) = Cl(***IIa+IIb***)↑ + Cl(**III**)↓**,** where arrows show the ascending and descending branches**.** The total outcome of chlorine with magmas at convergent boundaries is:

$Cl_{\mathbf{IA+ACM}}$ = Cl(***IIa+IIb***) + Cl(***IId***), where flow Cl(***IId***) is connected with melting of mantle wedge. As stated before, in melting of depleted mantle of the mantle wedge the extraction of volatile into melts should not be over that existing in melting of mantle in the zones of mid-oceanic ridges. Thus, the contribution of chlorine of the mantle wedge to formation of magmas IA+ACM or continental crust cannot be in excess of its amount which would have been released in formation of of equivalent volume of the oceanic crust from mantle MOR. This input should be over value $0{,}31 \times 10^{22}$ g Cl (Fig. 6). In reality, the amount was one order of magnitude greater, i.e. $3{,}14 \times 10^{22}$ g Cl. The excess as amount $2{,}83 \times 10^{22}$ g Cl, was due to dehydration in melting of rocks of subducted plate. With this in mind, the mass of chlorine in the latter is 4.85×10^{22} g. So, the conclusion is that greater part of chlorine is redistributed into ascending fluid flows associated with magmatism of marginal belts.

Distribution of chlorine under deep recycling conditions. The amount of Cl $2{,}02 \times 10^{22}$g in the descending plate, is involved into mantle depth (flow **III,** Fig.5). This chlorine is involved in recycling, covering the upper mantle. Increased (against melts of oceanic ridges) the contents of chlorine in melts OI and regions CR, are likely related to the emergence of this recycled chlorine in the sources of intraplate magmatism. This agrees with the recent geodynamic models [25].

Primary exosphere of Earth. Now we assess the mass of chlorine, which likely existed in the external exosphere of the early Earth. So we assess (following the scheme of balance, (Fig. 1) the mass of chlorine of juvenile origin to be $4{,}19 \times 10^{22}$g, i..e. recovered by magmas from mantle sources. The mass of chlorine of primary exosphere is thus $2{,}23 \times 10^{22}$ g of Cl. This is about the amount of chlorine in the recent hydrosphere ($2{,}7 \times 10^{22}$ g). Чpart of Cl of the primary exopshere probably retained in the upper shells of the Earth (about $0{,}21 \times 10^{22}$ g = $4{,}40_{\text{external}}$

$_{shells}$ – 4,19 $_{juvenile\ sources}$), the remaining part was redistributed into fluid flows of supra-subducted zones and in intra-mantle recycling.

We may estimate what [6] volume of Cl was recycled by different geological processes for the geological history. As was stated, the Cl abundance in the oceanic crust is higher than was removed by MOR melts through entire Earth history. Excess is 1,1 x 10^{22} g Cl. It appears that this is the amount of Cl which additionally arrived into oceanic lithosphere (flow ***b*** in Fig. 4). The amount of 2,83 x 10^{22} g Cl was returned to the upper shells of the Earth from the subducted crust (Fig. 5). Finally, the considerable part of Cl 2,02 x 10^{22} g was involved into deeper recycling covering entire sub-lithosphere mantle. Thus, for entite geological history the amount 5,98 x 10^{22} g Cl was recycled, which is in a greater excces of its amount contained in the Earth's crust and hydrosphere.

FLUORINE FLOWS (Fig. 7)

Following data of Table 1 the amount of 7,35x10 ^{22} g of fluorine could be recovered from the earth [20,2] interior (Table 1, scheme of balance Fig. 7). However, not over 6,32 x10^{22} g F was accumulated in the rocks of lithosphere and hydrosphere shells, recycled parts included, Divergence of estimates of released

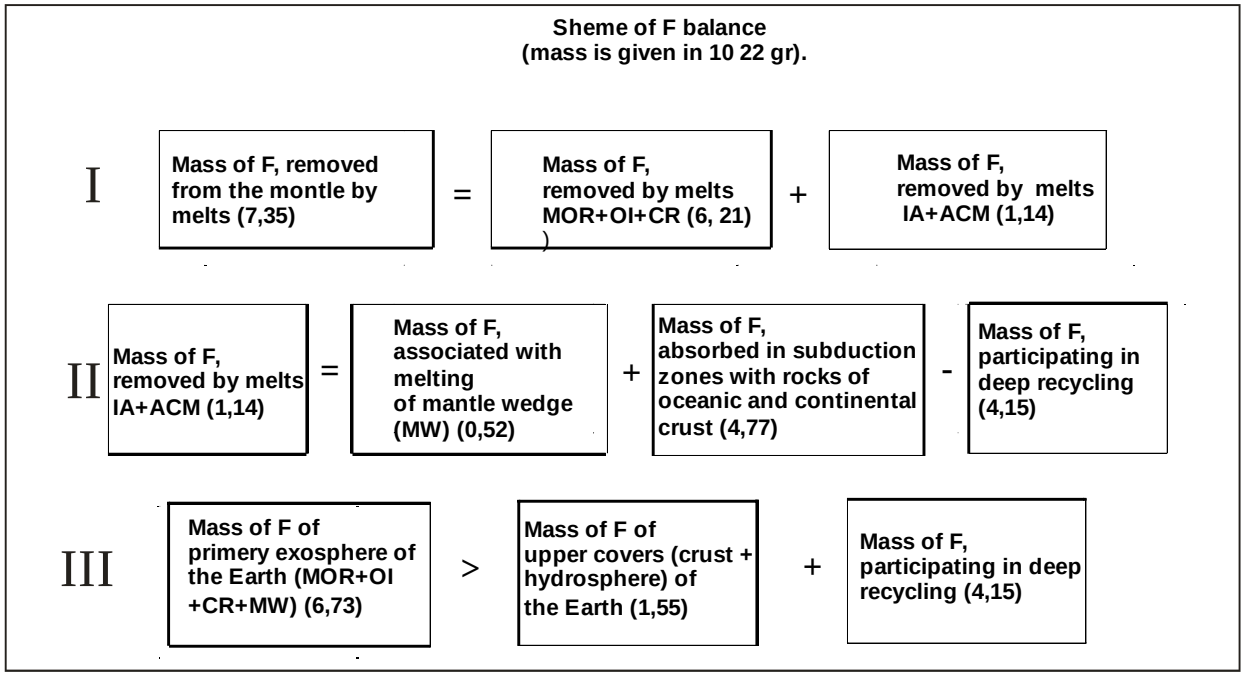

Fig. 7. **Scheme of balance and distribution of fluorine masses in volatiles flows in the upper geospheres of the Earth.**

I – mass F, evacuated by melts MOR+OI+CR (on the divergent boundaries of lithosphere plates and in internal regions) and melts IA+ACM (on convergent boundaries of lithosphere plates); II – masses and sources of F, involved in differently directed flows in the settings of convergent boundaries of lithosphere plates; III – balance of F masses, involved in the flows of volatiles between mantle and upper shells of the Earth, and contained in crustal rocks and in hydrosphere.

and accumulated fluorine makes up over 16%, with evident dominance of F of the primary mantle sources. It is likely that this discrepance lies within the errors in the

definitions of average fluorine contents in the rocks and melts. We remind that our estimates of volatiles contents in magmatic melts are based on the data on the Late Phanerozoic rocks.

As follows from Table 1, the average contents of fluorine in the melts of rocks of oceanic plateau and islands are 4-fold, and in melts of rocks of continental rifts are 10-fold higher than its contents in the melts of basalts of mid-oceanic ridges. In the existing geodynamic models the formation of oceanic islands and continental rifts is linked with the activity of mantle plumes. The The vital source of tjis mantle is recycled lithosphere enriched in many incompatible elements, e.g. fluorine. Its mean content in recycled crust is 0,021 mass.% (Table 1). So, the melts formed in melting of recycled lithosphere, even if mixed with products of melting of non-depleted mantle might be enriched in F. This agrees well with the data on higher F contents in melts related to mantle intra-plate sources (see Table, settings OI and CR).

General scheme in Fig 1 displays behavior of F in geological processes.

Setting MOR. Emergence of juvenile F in the structures of lithosphere shells of the Earth is related to magmatic eruptions within mid-oceanic ridges and formation of oceanic crust. In formation of the oceanic crust the amount of F was 5,06 x 10^{22} g, with the average abundance in melts to be ~0,023 мас.%. The rocks of oceanic crust contain lower fluorine (0,019 mass %), which indicates its redistribution from magmatic centers MOR into hydrosphere and atmosphere as 0,88 x 10^{22} (flow **a'** in Fig. 4). The content of fluorine in hydrosphere is by two orders of magnitude lower, so we assume that fluorine released from melts was chemically bound in the rocks of continental crust.

Setting IA+ACM. The content of fluorine in basalt melts of island arcs and active margins [11] is three times higher than that in similar melts of mid-oceanic ridges (see Table, settings IA+ACM). So this amount is not possible to explain only due to melting of substance of mantle wedge, which cannot provide fluorine greater than mantle of mid-oceanic ridges. It seems that the main input of F into magmas IA+ACM was ensured by recovery from rocks of subducted lithosphere.

The rocks of subducted crust (Table 1), both oceanic and continental, consume 4,77 x 10^{22} g F. (flow **I,** Fig. 5). Within zone of subduction this flow is divided into descending and ascending branches (Fig. 5). The mass of fluorine, recovered from the suibducted lithopshere with meltsis assessed based on the ratio:

F_{IA+ACM} = F (***IIa+IIb***) + F (***IId***), where flow of F (***IId***) is associated with melting of mantle wedge.

Proportion of fluorine of mantle wedge F(***IId***), assessed from its content in the products of melting of depleted mantle is evaluated as 0,52 x 10^{22} g. Therefore, when subducted lithosphere melts, the ascending flow additionally obtains about 0,62x x10^{22} g F (F_{IA+ACM} – F(***IId***)).

Behaviour of chlorine under deep recycling. After subduction alteration of the rocks of the descending plate preserved in these rocks part of F (4,15x x10 ^{22} g F) is involved in the deeper horizons of the mantle (flow **III** in Fig. 5). In our opinion, this recycling of F into mantle ensures its higher contents in magmatic melts related to activity of plumes.

Primary exosphere of the Earth. The disbalance between juvenile fluorine and that contained in the shells indicates it cannot be important in the primary exosphere of the Earth. This could explained by that the abundance of F could vary with time in the melts of some geodynamic settings Most likely they could take place in intra-plate settings, in which the sources remain to be isolated from melting areas through long periods of time (1 – 3 billion years), So, appearance of F-enrished recycled component in the upper geospheres could be essentially delayed compared to the other flows. Thus, it is assumed that intra-plate melts are enriched in F at the last stages of geological history. This could be the reason why the input of rocks of intra-plate settings into total balance of fluorine in the lithosphere shell of the Earth could be lower than the calculated one. Assuming that initial contents of F in melts OI and CR could be compararble with its contents in melts MOR, in this case the input of fluorine of all magmatic sources (6,45x x10 ^{22} g) would in balance with its contents in the crust and hydrosphere.

FLOWS OF SULFUR (Fig. 8)

The data on sulfur redistribution in melts and rocks of different geodynamic settings are given in Table 1. The analysis of the composition of volcanic glasses showed that on average sulfur is present as amount of 0,107 mass %. This estimate is close to the data on the sulfur content in the rocks of oceanic bottom, obtained by Silantiev et al. (Oral comm.) and the data on quenched glass MOR [27]. Besides, it is close to sulfur content in the basic melts of all geodynamic settings, and its content in the rocks of continental crust. It appears that sulfur does not fractionate in crystallization of melts, and consequently in the rocks of oceanic crust its contents are expected to be close to those in melts and common for quenched glasses of MOR basalts.

Magmatic melts removed total of 27,13 x10 ^{22} g of sulfur. The amount of sulfur available in the rocks of continental and oceanic crust, recycled included, is evaluated to be 26,04x10 ^{22} g. Thus, the balance of sulfur between its masses removed with melts and conserved in the rocks of the different crust types is observed in the first approximation. In the recent crust and hydrosphere this amount is around 3,21x10^{22}g of sulfur. The remaining amount (~22,83x10^{22}г) is involved in the processes of deep recycling.

So, the behaviour of sulfur is described in the geological processes as follows:

In setting MOR the volume of 24,42 x 10^{22} g S was removed with magmas for the geological history. It is practically not redistributed into other media and is preserved in the rocks of oceanic crust (22,22 x 10^{22} g).

Setting IA+ACM. The mass of sulfur buried in subduction zones on the convergent boundaries is estimated to be $22{,}83 \times 10^{22}$ g. However, melts removed $1{,}75 \times 10^{22}$ g S. This is lower than probable input of sulfur of the mantle wedge (***II_d*** in Fig.5), which could be calculated with the other technique as $2{,}48 \times 10^{22}$ g. We believe that such a low removal of sulfur is associated with heightened content of water in the melts of convergent boundaries, due to which sulfur behaves as a compatible element, and remains in resthite not only in melting of the mantle wedge but in melting of subducted crust. Therefore, against other volatiles sulfur is to the least extent redistributed in the settings of convergent boundaries.

Behaviour of sulfur under deep recycling. In magmas OI and CR sulfur has lower contents relative to those in melts MOR. This fact indicates on participation of recycled lithosphere in formation of intraplate sources of magmatism. These sources are enriched in water which affects behaviour of sulfur and defines its predominant preservation in resthite in melting in magma.

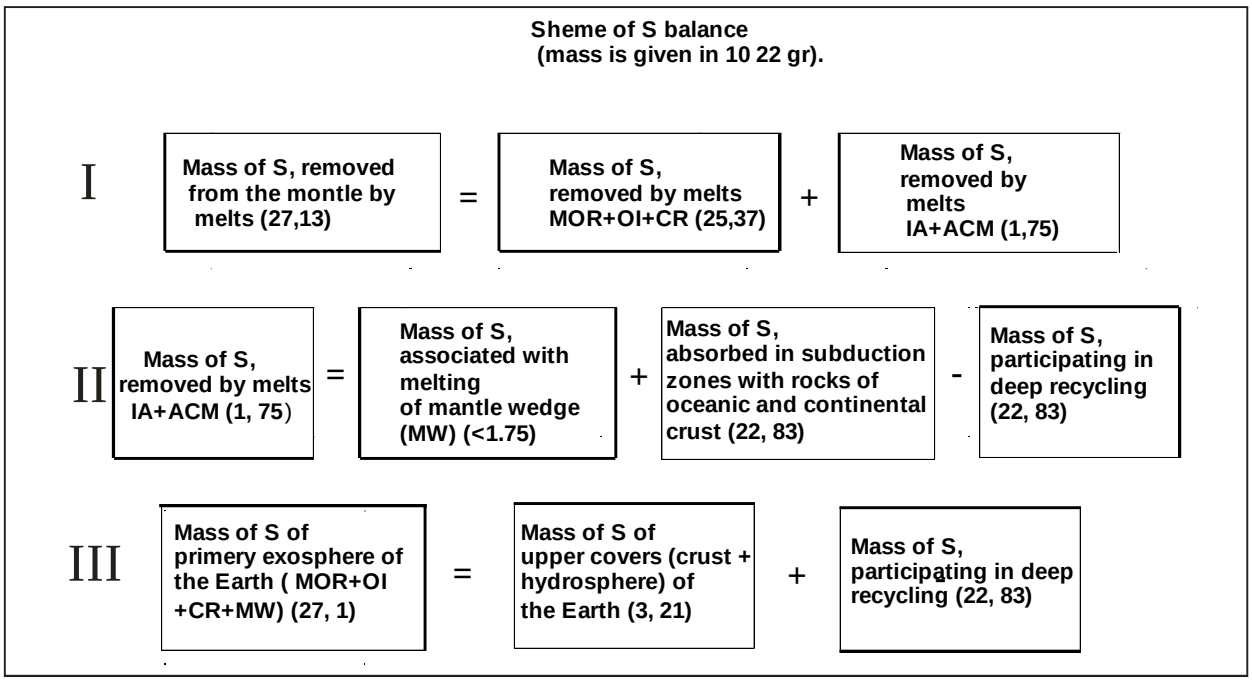

Fig. 8. **Scheme of the balance and distribution of sulfur masses in the flows of volatiles and in the upper geospheres of the Earth.**

I – mass of S, evacuated with melts MOR+OI+CR (on the divergent boundaries of lithosphere plates and in internal regions) and melts IA+ACM (on convergent boundaries of lithosphere plates); II – masses and sources of S, involved in differently directed flows in the settings of convergent boundaries of lithosphere plates; III – balance of S masses, involved in the flows of volatiles between the mantle and upper shells of the Earth and contained in the rocks and in hydrosphere.

DISCUSSION

General remarks The principal idea of the study was representation on differently directed flows of volatiles, operating in the upper shells of the Earth. The ascending (juvenile) flow evacuates volatiles from the mantle together with

magmatic melts, while the descending flow provides transport of (recycling) of lithosphere material into the Earth interior in subduction zones. As was indicated, the behaviour of the volatiles in these flows is different. Thus, water and chlorine made composed the primary Earth's exosphere. The amount of water involved in recycling is in excess of juvenile component supplies, so in the geological history its content in the upper shells gradually decreases. In contrast, the abundance of chlorine and fluorine progressively increased in hydrosphere and crustal rocks because of dominating juvenile component over recycling. Sulfur behaves primarily as the element compatible with basic melts and is basically not redistributed into external shells in eruptions, so its content remains to be constant in the melts of different geodynamic settings and in the rocks of continental and oceanic crust.

The above results indicate involvement of volatiles in the recycling processes. They were mostly effective at convergent boundaries of lithopsheric plates in settings ACM+IA, in which the melts are highly enriched in H_2O, Cl, F against melts of mid-oceanic ridges, which is explained by extraction of the part of these volatiles from the subducted crust. The effect of recycling is due to enrichment with water, fluorine and chlorine of melts, arising in mantle plumes. Compared to these volatiles, sulfur is fairly moderately involved in recycling.

The proposed model of the balance is the first approximation for there is no systematic evidence to quantitatively consider the change of the ratios between the volumes of magmatic products of different composition and different geodynamic settings during geological history of the Earth. Particularly problematic is the issue on the composition of the oceanic crust into the moon, nuclear and cratonal (Archean – Early Proterozoic) stages of the Earth evolution [7]. In the Early Archean the authors assume [36] generation of komatiite crust, basite crust as the analogs of oceanic crust. They originated at much higher length of the global system MOR or with a high velocity of spreading, and different variants of the oceanic crust composition with the other rocks involved. Unfortunately, there is no reliable data on the contents of water, chlorine, fluorine and sulfur in the magmas (e.g. from melt inclusions). In this connection, the balance of volatile components requires specifying further acquired data on the contents of these components in the magmas of the early stages of the geological history of the Earth.

It is assumed that the approach proposed is more or less acceptable. The criterion for such a conclusion is observance of the balance between ascending and descending flows, which was established for chlorine, water and sulfur, although the issues of the model (average contents of volatiles in magmas and rocks, and the ideas on the insignificant change in time of the velocity of the crust-forming processes with the dominant role of tectonics of lithosphere plates) were independent between each other.

Now consider some consequences, which are derived from the models of the balance of volatiles in the geodynamic processes.

Volatiles and recycling processes. The previous studies [3-5] showed that during magmatic differentiation and crust formation water, chlorine and fluorine behave as incompatible components accumulated in the atmosphere, hydrosphere and the products of a deeper differentiation of magmatic melts. At the same time, the important result on the balances reported was the conclusion on participation of volatiles in different processes of recycling, that is in the processes of their transition from atmosphere and hydrosphere into crustal rocks and return to the mantle together with latter. The processes of recycling start operating in setting MOR in hydration of newly formed crustal rocks and their enrichment, as compared to melts, with water and chlorine.

The processes of recycling proceeded mostly effectively at the convergent boundaries of plates. The magmas of these settings, against products of melting of the depleted mantle in MOR, are enriched in water 5-fold, chlorine 10-fold and fluorine 2-fold. As compared to crustal rocks, they are more rich in water and chlorine more than 2 times. Therefore, over half of these volatiles transported on the convergent boundaries of lithospheric plates, was returned to hydrosphere and atmosphere. The excessive content of volatiles in magmas IA+ACM, compared to magmas MOR, may be only related to participation in the processes of melting of the subducted plate enriched in these components. This water makes up over 80% of the total water mass, involved in magmatism IA+ACM. Also note that, melts take out about 65% of the total recycled chlorine and about 25% of fluorine onto the Earth surface on the convergent boundaries of redistribution. The zones of island arc and marginal-continental magmatism are the most widespread structures of the Earth's surface, which suggests the main contribution of subduction to the processes of recycling through geological history.

After reworking of lithosphere in the subduction zones the volatiles preserved are involved into a profound recycling. The geodynamic models relate recycled lithosphere to the emergence of mantle sources, feeding magmatism of intraplate settings: oceanic islands and lava plateau, continental rifts and the regions, which originated above hot spots. We also obtained the data the data on enrichment of magmas of these geodynamic settings with water, fluorine and chlorine, which fits well in these models concepts. As was revealed by the latest seismic computer-aided tomography, the regions of mantle plume origination are distributed over depth irregularly. This was pointed out by Puscharovsky [15] who marked that they were confined to intra-mantle seismic-tectonic domains [16], along which the subducted material is distributed when subsiding into the mantle. It is necessary to remind, that the origin of plumes is interpreted at least in two ways. On the one hand, they are believed to have thermal origin, on the other hand, they are explained by the density inhomogeneity of the mantle. Our data, which indicate on enrichment of melts in settings OI and CR with water, chlorine and fluorine, and that mantle plumes have certain chemical and mineralogical differences from the composition of usual mantle. Thus, ascending of plumes to the surface could be defined both thermal and deep-seated tectonic movements, and density difference

of its material from the surrounding mantle, for instance due to presence of volatile components in its composition, while the distribution of foci of their origination could be defined by the levels of lithosphere burial (or seismographic boundaries). The possibility for volatiles to be recycled at depth is affected by subduction velocity. At high subduction velocities the more low-T parts of subducted plates descend to large depths, preserving volatile components due to low temperatures (with this pressure). If high velocities of spreading and subduction were typical for the early stages of the Earth's history one may assume that emergence of the main mantle heterogeneities being the source of plumes at that particular time.

Composition and extent of primary exosphere of the Earth. The balance compilations point out that it is vital to accept thick gaseous exosphere of the Earth, beginning from the earliest stages of its development. Of particular interest is the scheme of water balance. The most intriguing is that subduction zones consume more water than it is evacuated with melts of all geodynamic settings. Nevertheless, the gigantic water reservoir is available on the Earth. Note that the idea on consumption of marine water in the mantle was reported earlier [9, 24, 25, 31]. However, we were able to reliably substantiate it with factual materials in terms of geological history and to carry out a comprehensive analysis.

The apparent non-balanced distribution of water between geospheres could be discussed in two versions. Thus, it is supposed that at the early stages of development the Earth was devoid of atmosphere. In this case it is assumed that in Pre-Phanerozoic time the intensity of water release from melts was much higher than recently (i.e. melts were more water-saturated), and the water content in the rocks of subducted crust, on the contrary, was very low. These assumptions have no foundation, because basic (mantle) rocks which formed from water-saturated melts (primarily amphibole-bearing basalts) in the Precambrian complexes were spread not more than in the young formations.

The second version suggests presence of the thick exosphere at the early stage of the Earth development. The composition of this exosphere was mostly made of water and chlorine as the ratio 100:1 (in the recent ocean ~ 100:2), while sulfur and fluorine were not too significant. The water mass in the primary exosphere of the early Earth is estimated to be $231{,}9 \times 10^{22}$ g . This 1.5 times greater than the mass of the recent ocean. The condensation of such atmosphere should have resulted in origination of the ocean with the average depth about 4 km. The processes of subduction evidently played subduction processes. During the geological history the volume of water, comparable to its content in all recent external shells, including hydrosphere, has been consumed through the zones of subduction. Even if the considerable amount of juvenile component appeared, the average recent depth of the ocean diminished 1.5-fold and is estimated to be 2,7 km. Simply speaking, the Earth "drinks" its hydrosphere through subduction zones, which resulted in «flooding» of its mantle. Note that assumption of higher velocities of spreading and subduction at the early stages of the Earth development leads to the

conclusion on the more essential water content in the primary astenosphere and consequently, on its more considerable redistribution into the planet mantle.

VOLATILES AND THEIR POSSIBLE ROLE IN GEODYNAMICS OF PLANETS OF THE EARTH GROUP

It is apparent that presence of water medium, as the independent shell in geological processes, defined a number of important differences of the Earth from the other planets of the Earth group. Thus, no evidence of lithospheric plate tectonics was found on any of these planets. Besides, they have long come through the peak of its geological activity. It is assumed that the reason of the different tectonic history of the Earth development was presence of the thick water atmosphere and its activity in recycling, particularly on the convergent boundaries of plates. Magmatism of these settings, which contributed to the formation and transformation of the Earth, is characterized by a high differentiation with predominance of mean and acid rocks (andesites, dacites, rhyolites and their plutonic equivalents) and high degree of saturation of melts with water, increasing with increasing silicate contents. Due to water participation the temperature interval of melt formation is sharply displaced towards lower temperatures. But these melts, like the sites of their melting, serve as lubricants on the boundaries of subducted plates. It may be stated that without water in the convergence zones the processes of subduction would have ceased due to wedging of the descending plate. This is indirectly confirmed by absence of structures equivalent to zones of convergence in the Mars and Venus, being water-devoid. It is believed that water supply into the interior at the convergent boundaries of lithosphere plates could have become the decisive factor which supported subduction throughout the history of the Earth.

It appears that the processes of deep-seated recycling of volatiles could be related to the deep geodynamics of the Earth. A gradual enrichment of the mantle with water could have brought to the drop of melt temperatures and as a result, could cause replacement of high-T komatiite magmatism with tholeiitic one. This could prolong the magmatic evolution on the Earth. Finally, if origination and dynamics of plumes is controlled both thermal processes and chemical heterogeneity of the mantle, the processes of recycling, e.g. recycling of volatiles, could be the key mechanism in supporting the plume activity of the earth activity.

The paper is prepared with the financial support of the Russian Foundation for Basic Research (projects 02-05-64191, 02-05-64196, 02-05-64518), Program of Science School, grant NS-1145.2003.5, project 1.2 «Catastrophic processes» («Global changes of environment and climate»), Programs №5 RAS.

REFERENCES

1. **Dobretsov, N.L., Kirdyashkin, A.G., Kirdyashkin, A.A.** Deep-level geodynamics. // Novosibirsk. Izdatel'stvo SB RAS, branch GEO. 2001. 407 pp.

2. **Ivanov V.V.** Complex geoecological approach to decreasing of resisting of man and nature. M. Publishin House IMGRE, 2003, 61 pp.
3. **Kovalenko V.I., Naumov V.B., Yarmolyuk V.V. et al.** Signficance of magmtism in water concentration in outer covers of the Earth. In: Global changes of the environment. Publishing House SB RAS OIGGM, 1998. p. 117-126.
4. **Kovalenko, V.I., Naumov, V.B., Yarmolyuk, V.V., and Dorofeeva, V.A.** Volatile components (H_2O, CO_2, Cl, F, and S) in basic magmas of various geodynamic settings: data on melt inclusions and quenched glasses. // Petrology (2000), №2, pp. 131-164.
5. **Kovalenko, V.I., Naumov, V.B., Yarmolyuk, V.V., and Dorofeeva, V.A.** Volatile components (H_2O, CO_2, Cl, F, and S) in magmas of intermediate and asid compositions from distinct geodynamic environments: evidence from melt inclusion and chill glasses. // Petrology (2000), №6, pp. 585-617.
6. **Kovalenko, V.I., Naumov, V.B., Dorofeev, V.A., and Migdisov, A.A.** Balance of H_2O and Cl between the earth's mantle and outer shell. // Geochemistry (2002), №10, pp. 1041-1070.
7. **Magmatic rocks.** Evolution of the magmatism in the Earth's history. M. Nauka1987. 439 p.
8. **Migdisov A.A., Bredanova N.V., Yaroschevskyi A.A.** New data of element distribution in sedimentary cover, 2002 (in press)
9. **Monin A.S.** Earth's history, L, Nauka, 1977. 288 p.
10. **Naumov, V.B., Kovalenko, V.I., and Dorofeeva, V.A.** Fluorine concentration in magmatic melts evidence from inclusions in minerals. // Geochemistry (1998), № 2, pp. 147-157.
11. **Naumov, V.B., Kovalenko, V.I., Ivanitskii, O.M.** Volatile components (H_2O, Cl, S, CO_2) concentration in magmas: evidences from melt inclutions in minerals. // Doclady RAS (2004), V. 347, № 3, pp.391-393.
12. **Naumov, V.B., Kovalenko, V.I., Ivanitskii, O.M., Savel'eva, N.I.** Chlorine content in magmatic melts according to mineral inclusion data. // Geochemistry (1995), №6, pp.798-808.
13. **Naumov, V.B., Kovalenko, V.I., Yarmolyuk, V.V., and Dorofeeva, V.A.** Volatile components (H_2O, Cl, F, S, and CO_2) in magmatic melts of various geodynamic environments. // Geochemistry (2000), №5, pp. 555-564.
14. **Puscharovskyi Yu.M.** Some recent problems of Earth's tectonics, 2004 (in press)
15. **Pushcharovsky, Yu.M.** Linearity and nonlinearity in geology. // Geotectonics (1999), №3, pp. 42-49.
16. **Pushcharovsky, Yu.M. and Pushcharovsky, D.Yu.** Geospheres of the earth's mantle. // Geotectonics (1999), №1, pp. 3-14.
17. **Ronov A.B.** Stratoshpere or sedimentary cover of the Earth (quantitativestudies. M. Nauka, 1993.
18. **Ronov A.B., Migdisov A.A.** quantitative regularitiesin the structure and composition of sedimentary sequences of the East-European Platform of Russian plate and their location in series of ancient platforms of the world // Lithology and useful minerals. 1996. № 5. p. 451-475.
19. **Ronov A.B., Yaroschevskyi A,A., Migdisova.A.** Chemical structure of the earth's cover and geochemical balance of main elements. M.:Nauka, 1990. 183 p.
20. **Yarmolyuk, V.V., Ivanov, V.G., Kovalenko, V.I.** Sources of intraplate magmatism of Western Transbaikalia in the Late Mesozoic-Cenozoik: trace-element and isotope data. // Petrology (1998), V. 6, № 2, pp. 115-138.
21. **Aggrey K.E., Muenow D.W., Batiza R.** Volatile abundances in basaltic glasses from seamounts flanking the East Pacific Rise at 21^o N and $12\text{-}14^o$ N // Geochim. et Cosmochim. Acta. 1988. V. 52. № 8. P. 2115-2119.
22. **Condie K.C.** Plate tectonics and crustal evolution. 4^{th} ed. Oxford, UK: Butterworth-Heinemann. 1997, 282p.
23. **Davies J.H., Stevenson D.J.** Physical model of source region of subduction zone volkanics // J. Geophys. Res. 1992. V. 97. № B2. P. 2037-2070.
24. **Dickinson W.R., Luth W.C.** A model for plate tectonic evolution of mantle layers. // Science. 1971. V. 174. P. 400-404.
25. **Fyfe W.S.** The evolution of the earth's crust: modern plate tectonics to ancient hot spot tectonics? // Chem. Geol. 1978. V. 23. P. 89-114.

26. **Hofmann A.W.** Mantle geochemistry: the message from oceanic volkanism. // Nature. 1997. V. 385. P. 219-229.
27. **Jambon A.** Earth degassing and large-scale geochemical cycling of volatile elements // Carroll M.R. and Holloway J.R., eds. Volatiles in magmas. Rev. Mineral. 1994. V. 30. P. 480-517.
28. **Maruyama S.** Plume tectonics. // Journ.Geol.Soc.Japan. 1994. V.100. N1. P.24-49.
29. **Michael P.** Regionally distinctive sources of depleted MORB: Evidence from trace elements and H_2O // Earth Planetary Sci. Lett. 1995. V. 131. P. 301-320.
30. **Michael P.J., Schiling J-G.** Chlorine in mid-ocean ridge magmas: Evidence for assimilation of seawater-influenced components // Geochim. et Cosmochim. Acta. 1989. V. 53. P. 3131-3143.
31. **Peacock S.M.** Fluid processes in subduction zones. // Science. 1990. V. 248. P. 329-337.
32. **Reymer A., Schubert G.** Phanerozoic addition rates to the continental crust and crustal grouth. // Tectonics. 1984. V. 3. P. 63-77.
33. **Ronov A.B., Jaroshevsky A.A., Migdisov A.A.** Chemical structure of the Earth's crust and major element geochemical balance // International Geological Reviews. 1991. № 10. P 941-1031. № 11. P.1032-1085.
34. **Staudigel H., King S.D.** Ultrafast subduction: the key to slab recycling efficiency and mantle differentiation?// EPSL. 1992. V.109. p.517-530.
35. **Volatiles in magmas.** Carroll M.R. and Holloway J.R., eds.// Rev. Mineral. 1994. V. 30. 550 p.
36. **Windley B.F.** The evolving continents. 1995. John Wiley a. Sons. Chichester-New York-Brisbanee-Toronto-Singapore. 526 pp.

UDK 552.33; 550.42

Carbonate Metasomatism of the Oceanic Mantle Beneath Fernando de Noronha Island, Brazil

Kogarko L.N.[1], Kurat G.[2], and Ntaflos T. [3]

[1] *Vernadsky Institute of Geochemistry and Analytical Chemistry, Moscow, Russia*
[2] *Naturhistorisches Museum, Vienna, Austria*
[3] *Institute of Petrology, University of Vienna, Vienna, Austria*

We present evidence for carbonate-immiscibility phenomena in the upper mantle based on data from a set of strongly metasomatized xenoliths in a basanitic lava flow from Fernando de Noronha Island (south-west Atlantic).

Petrological and geochemical study of lherzolitic and harzburgitic xenoliths revealed that the oceanic mantle of this region has been affected by very strong carbonate metasomatism. The metasomatism led to wehrlitization of the primary mineral assemblage (ol, opx, sp). The wehrlitization was the result of interaction between a possibly ephemeral sodic dolomitic melt or fluid with the mantle peridotite according to the reactions:

$$4MgSiO_3 + CaMg(CO_3)_2 = 2Mg_2SiO_4 + CaMgSi_2O_6 + 2CO_2$$
$$3CaMg(CO_3)_2 + CaMgSi_2O_6 = 4CaCO_3 + 2Mg_2SiO_4 + CO_2.$$

The olivine has abundant micro-inclusions consisting of Na-Al - rich glass, Fe, Ni, Cu-mono-sulfide, Ca-rich carbonate and dense CO_2. The interrelationships between the glass, sulfide and carbonate inclusions permit us to speculate that silicate, sulfide and Ca-rich carbonatite melts were in equilibrium with each other and originated from partial melting of metasomatized and wehrlitized peridotite underneath Fernando de Noronha Island.

These results support a two stage model of Ca-rich carbonatite formation:

1st stage - metasomatic wehrlitization and carbonatization of mantle rocks;

2nd stage - partial melting of the carbonate-bearing wehrlitic rock resulting in Ca-кich carbonatitic melt or three immiscible liquids: silicate, carbonate, sulfide and ultimately generation of calciocarbonatites.

INTRODUCTION

Mantle metasomatism is a very powerful process of global geochemical differentiation as well as mixing. The large-scale mass transportation in the upper mantle is closely connected with the origin of alkaline and carbonatitic magmatism. For example, isotopic data for Kola Peninsula alkaline rocks, carbonatites and related gigantic rare metal deposits suggest that they originated from a relatively depleted mantle source: ($\varepsilon Nd = 4.5$; $Sr^{87}/Sr^{86} = 0{,}7035 - 0{,}7038$ [22, 25]. So there is a paradox: on the one hand these rocks are extremely enriched in rare elements and on the other they have an isotopic signature corresponding to mantle rocks depleted in trace elements. The enormous concentration of rare

elements in the alkaline rocks of this region is mostly related to large-scale processes of mantle metasomatism confined to a very narrow time span (371-361 Ma), so the primary isotopic signature of the depleted rocks stayed unchanged.

Metasomatism, cryptic and patent, has been observed in upper mantle rocks world wide [36]. The metasomatizing agent appears to be either highly mobile silicate and/or carbonate liquids or fluids dominated by CO_2, N_2, or H_2O. Fluids appear to be the most effective agent which, because of the lack of surface tension, can enter any space offered down to the atomic scale. Fluids provide also the best vehicle for mass transport and are likely to precipitate one phase at a time, offering a direct way for the formation of monomineralic upper mantle rocks [16, 30, 33].

Various researchers have suggested that primary carbonate melts could be efficient metasomatizing agents, forming second generation clinopyroxene, olivine and spinel and minerals enriched in light rare earth elements (LREEs) such as apatite, kirschsteinite etc [8, 18, 19, 23, 43, 57, 58]. Recently, we demonstrated [23] that the sub-oceanic harzburgitic mantle of Montana Clara Island (Canary Archipelago) had previously been metasomatized by primary dolomitic melt following the reaction:

$$enstatite + dolomite = forsterite + diopside + CO_2$$

At Montana Clara Island the carbonatized and wehrlitized mantle was partially melted during adiabatic decompression, which resulted in the formation of three immiscible liquids (sulfide, carbonate and silicate). This was the first reported occurrence of a primary magma within peridotites which had the composition of calciocarbonatite. We proposed that the investigated Montana Clara assemblage represented a micro-model for the generation of the Ca-rich carbonatitic magmas during partial melting of carbonatized and metasomatized oceanic mantle.

Later Yaxley et al. [58] reported a very similar mineral assemblage in mantle nodules hosted by the Newer Volcanics of south-eastern Australia. In this assemblage, nearly pure primary calcite is mostly found as rounded blebs within the silica-rich glass patches in association with clinopyroxene and second generation olivine. The study provided evidence for the existence of sodic dolomitic melts in the lithosphere beneath south-eastern Australia. These melts are believed to have metasomatized the lithosphere, producing apatite and calcite-bearing wehrlites enriched in Th, Zr, Nb, Sr, Y, and LREE. Yaxley et al. [58] suggested that the carbonate in the Australian assemblage represents cumulus crystals.

Seifert and Thomas [46] found wehrlite xenoliths in the Grosser Winterberg tephrite (Germany) containing grain-boundary melt pockets consisting of silicate glass with immiscible (Ca, Fe, Mg)-carbonate globules. They interpreted the generation of the Ca-rich carbonate melt as a result of mantle metasomatism by CO_2-dominated fluids. Pyle and Haggerty [40] described an assemblage of

globules of Ca-rich carbonate and Na-Al glass in metasomatized eclogite xenoliths from South African kimberlites. They attributed the silicate-carbonate textural relationships to liquid immiscibility in the upper mantle. Other workers have found Mg-rich carbonate in mantle peridotites from Spitsbergen in association with silicate glasses and have interpreted these assemblages as evidence of liquid immiscibility [2, 18].

The presented examples of carbonate-silicate liquid immiscibility in the upper mantle were considered in the light of the experimental data of Koster van Groos [29], Freestone and Hamilton [11], Kjarsgaard and Hamilton [20], Baker and Wyllie [4], and Hamilton and Kjarsgaard [13]. These experimental studies have demonstrated the immiscibility between Na-rich carbonatite and silicate magmas over a wide range of pressures (2-25 kbar).

However, Lee and Wyllie [31, 32] have pointed out a number of limitations on this hypothesis. They presented evidence that crystalline calcite can grow in silicate-carbonate liquids with a remarkably rounded morphology simulating the characteristics of melts. On the basis of the available experimental evidence they concluded that the compositions of carbonate aggregates situated in the aluminosilicate glass in mantle xenoliths makes these aggregates unlikely candidates for Ca-rich carbonate liquids immiscible with silicate liquids. Recently, Ionov [17] presented new information for Ca-rich carbonates in mantle xenoliths from Mongolia and Spitsbergen. The low alkali contents in the carbonate pockets are likely to be consistent with their origin as crystal cumulates rather than as quenched liquids. But Ionov [17] pointed out that "the origin of the textural relationships between the carbonate globules and silicate glass remains enigmatic".

The genesis of Ca-rich carbonatitic melts in the upper mantle still remains unsolved, so new mineralogical observations on the interrelationships between carbonate and silicate material in deep-seated xenoliths remain very important. Although mantle xenoliths provide convincing evidence for the presence of primary Ca-rich carbonates, comparable evidence has not yet been presented for the role of carbonate-silicate immiscibility phenomena in the upper mantle. In this paper we present such evidence based on data from a set of strongly metasomatized xenoliths in a basanitic lava flow from Fernando de Noronha Island (south-west Atlantic).

GEOLOGICAL SETTING

Fernando de Noronha Island is situated in the south-west Atlantic, 345 km off the coast of Brazil. The island consists of three complexes of intrusive and effusive rocks and has an area of 16.9 km^2 [1, 38]. The oldest formation, the Remedius complex, is represented by phonolitic, trachytic, alkalitrachytic plugs, dykes and stocks pyroclastic rocks including agglomerates, breccias, lapilli-tuffs and ash. The composition of pyroclastic material is mostly phonolitic and trachytic. Dykes of the Remedius complex include different types of foidite, basanite, tephrite and phonolite. The second oldest formation, Quixaba, overlaps the Remedius rocks in

two isolated occurrences. In marked contrast the Remedius formation, Quixaba rocks are almost entirely extrusive and of olivine nephelinitic composition. The youngest rocks of Fernando de Noronha Island are those of the Sao Joze formation, which are of basanitic composition. They outcrop on the islets of Chapeo de Nordeste and Sao Joze [1, 38].

The basanite lava flows of the islets contain large amount of upper mantle xenoliths. The xenoliths were first noted by Almeida [1] and later briefly described by Meyer and Svisero [37] who give some information on the mineral composition of these xenoliths.

ANALYTICAL METHODS

Minerals were analyzed at the university of Vienna using a Cameca SX100 electron microprobe operated at 15kV accelerating voltage and 20 nA beam current. Natural and synthetic minerals were used as standards for calibration. Counting times were 20 s for all elements. Ca in olivine was analyzed using pure wollastonite as primary standard and San Carlos olivine as secondary standard at 20 kV accelerating voltage and 40 nA beam current. Counting times were 100 s for both peak and background positions. To prevent loss of alkalis during analysis of glasses and glass inclusions we used defocused electron beam (5 μm in diameter) and decreased the counting time to 10 s, but even in these cases some alkalis might have been lost. PAP correction was applied for all data [39].

Rare earth element abundance have been determined for 15 representative samples by instrumental neutron-activation analysis (INAA) [28] in Vernadsky Institute of Geochemistry and Analytical Chemistry using reactor facilities provided by Moscow Engineering Physical Institute.

SAMPLES, TEXTURAL RELATIONSHIPS AND CHEMICAL COMPOSITIONS

We collected mantle xenoliths from the Sao Jose formation during a 1991 oceanic expedition by the Scientific Vessel Academician Boris Petrov. Most xenoliths are within the size range 0.5 - 25 cm, very rarely up to 35 cm. The xenoliths are all ultramafic and compositionally form two main groups: (1) spinel lherzolites and harzburgites (predominant) and; (2) pyroxene-rich rocks and wehrlites (less common). We found no garnet-bearing ultramafitites.

Most of the spinel lherzolites and harzburgites have granoblastic texture. Xenoliths with porphyroclastic texture are less common. The modal proportions of the four principal minerals are variable: olivine - (65 - 80 vol%), orthopyroxene - (7 - 25 vol%), clinopyroxene and spinel - (0.5 - 10 vol%). Pyroxene-rich ultramafitites and wehrlites are rare. The proportions of clinopyroxene, olivine and spinel in the pyroxene-rich peridotites are highly variable.

Both types of rocks show clear evidence for patent metasomatism characterized by the presence of Ca-rich carbonate, apatite and second generation

Table 1. **Chemical compositions of bulk rocks, minerals and melt inclusions**

Sample	SiO_2	TiO_2	Al_2O_3	FeO	Fe	MnO	Cr_2O_3	NiO	Ni	MgO	CaO	Na_2O	K_2O	Zn	Cu	S	Sum
Xenoliths FN-20	44.3	0.2	2.7	8.6	-	0.1	0.2	-	-	40.0	2.2	0.3	0.1	-	-	-	98.7
Olivine (I)	40.9	-	-	9.9	-	0.1	-	0.3	-	48.5	0.1	-	-	-	-	-	99.8
Olivine (II)	40.6	0.1	-	10.1	-	0.2	0.1	0.2	-	47.5	0.2	-	-	-	-	-	99.0
Orthopyroxene (I)	54.1	0.1	4.7	6.3	-	0.1	0.5	0.1	-	32.1	0.8	0.1	-	-	-	-	98.9
Clinopyroxene (I)	51.1	0.2	5.7	3. 4	-	0.1	0.9	-	-	15.8	18.7	1.2	-	-	-	-	97.1
Clinopyroxene (II)	53.1	1.00	1.2	2.9	-	-	1.2	0.1	-	18.1	22.7	0.6	-	-	-	-	100.9
Spinel (I)	0.1	0.1	45.5	17.8	-	0.1	16.2	0.3	-	17.8	-	-	-	-	-	-	97.9
Spinel(II)	0.1	68.5	1.3	11.7	-	0.1	1.6	-	-	11.3	0.1	-	-	-	-	-	94.7
Carbonate inclusion	2.9	0.7	1.0	1.3	-	-	-	-	-	4.3	45.5	0.5	0.4	-	-	-	56.6
Carbonate	0.3	-	-	0.3	-	-	-	-	-	1.0	52.4	0.1	-	-	-	-	54.1
Glass inclusion	57.5	1.0	25.4	1.6	-	-	-	-	-	-	1.0	9.0	3.9	-	-	-	99.4
Sulfide inclusion	-	-	-	-	32.7	-	-	-	32.5	-	-	0.1	-	-	-	34.0	99.3
Sulfide in carbonate micro-inclusion	-	-	-	-	33.3	-	-	-	31.8	-	-	-	-	2.6	0.8	31.4	99.9
Kirschsteinite	30.9	0.1	0.3	19.7	-	0.4	-	0.1	-	15.8	31.4	-	-	-	-	-	98.78
Cpx (host lava)	47.4	2.5	4.5	6.8	-	0.4	-	0.2	-	12.3	25.2	0.7	-	-	-	-	100.0

assemblages consisting of fine-grained olivine (5 - 40 μm, clinopyroxene (1 - 35 μm, spinel (1 - 15 μm, carbonate (10 up to 200 μm, glass (up to 1 - 2 mm) and sulfides (0.5 - 10 μm. In one xenolith we found kirschsteinite (Table 1). First generation olivine, orthopyroxene, spinel and clinopyroxene are very coarse-grained, sometimes up to 3 - 5 mm across. They are crossed by numerous veinlets of a fine-grained assemblage which also often surrounds orthopyroxene as reaction zones (Figs. 1, 2, 3). In these zones second generation clinopyroxene replaces primary orthopyroxene and occasionally second generation olivine (Fig. 3).

The composition of first generation olivine, orthopyroxene, clinopyroxene and spinel (Table 1) is typical of upper mantle lherzolites. Second generation olivines are richer in calcium (up to 0.27 wt% CaO) than the primary olivines (0.06 - 0.08 wt%). Second generation clinopyroxenes are more Ca- and Mg-rich and less aluminous and sodic compared with the original clinopyroxenes. However, in some second generation clinopyroxenes the sodium concentration reaches up to 2.55 wt% Na_2O, which is higher than that of the primary clinopyroxenes.

Armalcolite is found in the second generation assemblage in close association with glass. Polycrystalline carbonate fills irregularly-shaped, round or vermicular pockets with sharp curvilinear boundaries with the glass and is closely associated with the clinopyroxene and olivine of the second generation situated in reaction zones. In one reaction aureole we found Ba-Sr sulfate (barian strontianite) in association with calcite, second generation clinopyroxene, spinel, olivine, glass and primary orthopyroxene (Fig. 1).

In some rocks networks of veinlets are present (up to 2 μm wide and up to 100 μm long) which are filled only with Ca-rich carbonate. The carbonate composition is Mg-bearing calcite with an atomic Ca/(Mg+Ca+Fe+Na) ratio in the range of 0.85 - 0.96 and which contains minor amounts of Si, Fe, Al and Na (Table 1). In one thin section kirschsteinite is present in close association with olivine and carbonate in second generation assemblages (Table 1).

Interstitial patches of brownish Na-Al glass incorporate second generation olivine, clinopyroxene, spinel and carbonate. Quench crystals of Cl-bearing apatite (Cl content is up to 0.65 wt%) and rutile are also present in the glass. The composition of the glass is variable (Fig. 4) ranging from that of basaltic andesite to those of highly evolved melts: trachytic, phonolitic and dacitic. In some cases the glasses are partly crystallized and contain quench plagioclase and potassium feldspar. Very similar glass compositions have also been reported in upper mantle xenoliths from many other continental and oceanic localities [8, 10, 15, 18, 23, 45, 49, 57, 58].

Glasses often include Fe-Ni sulfide globules with compositions typical for primary mantle sulfides (Table 1). The globules mostly contain nickeliferous pyrrhotites, pentlandite or possibly monosulfide solid solutions with minor amounts of Cu, Co, and in some cases Zn (up to 2.62 wt%).

Fig. 1. **Back-scattered electron image of orthopyroxene being replaced by fine-grained mineral assemblage.**

Opx - orthopyroxene, Ol - olivine, X - clinopyroxene, Gl - glass, C - carbonate, B - barian-strontianite, Pl -plagioclase.

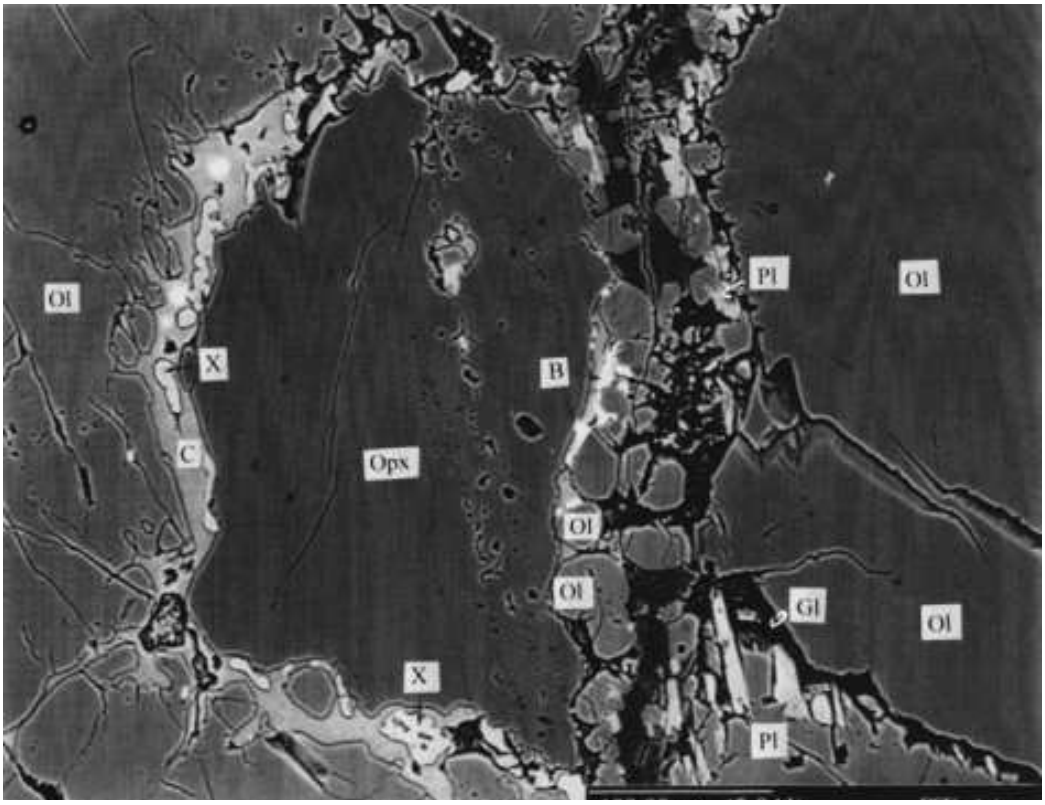

Fig. 2. **Back-scattered electron image of orthopyroxene being replaced by fine-grained mineral assemblage.**

Opx - orthopyroxene, Ol - olivine, X -clinopyroxene, Gl - glass, C - carbonate.

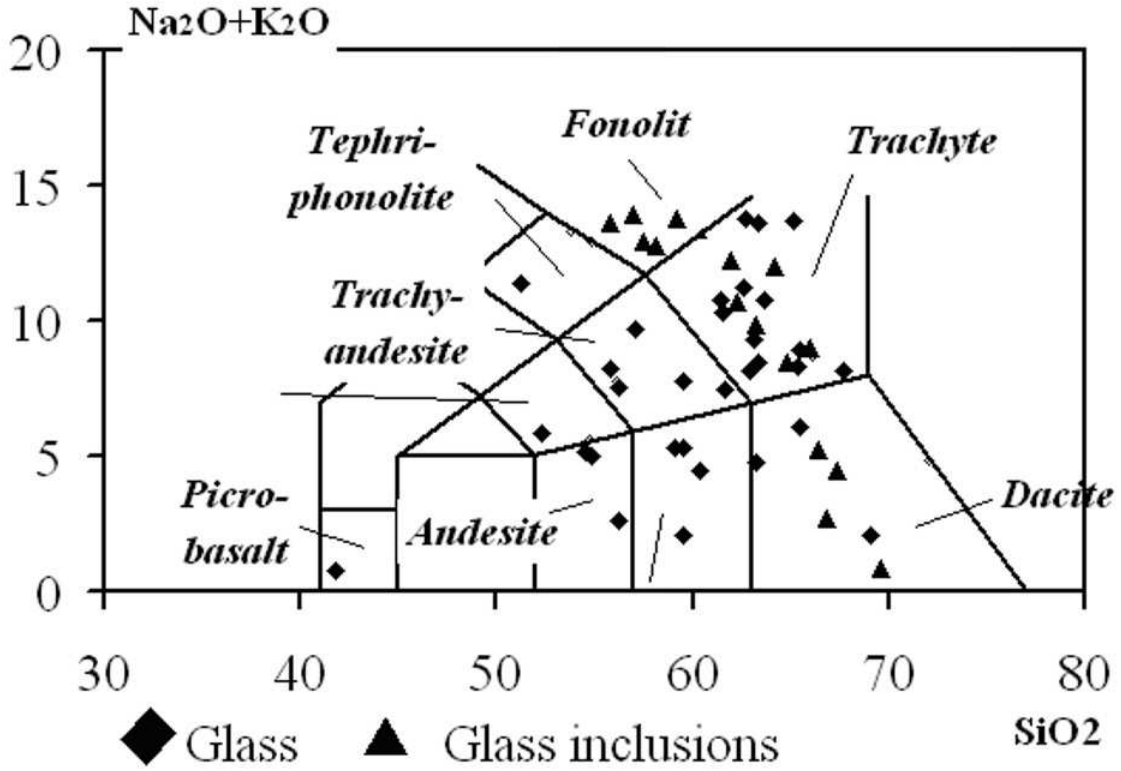

Fig. 3. **The chemical composition of glass inclusions in olivine and glass from reaction zones in Fernando de Noronha xenoliths projected into the alkali-silica diagram.**

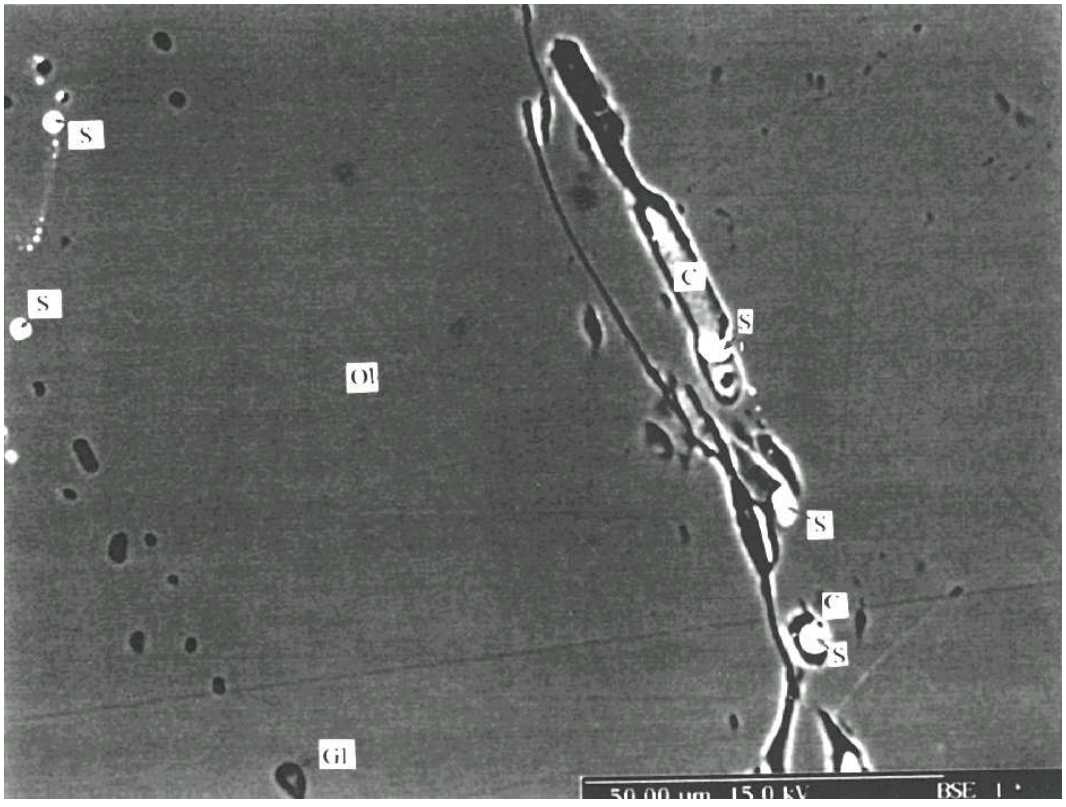

Fig. 4. **Back-scattered electron image of inclusions in the first generation olivine.**

Bright white: sulfide melt inclusions (S); white: cabonate inclusion containing a sulfide globule (C), inclusion is partly leached; gray: inclusions of trachytic phonolitic glass (G).

The olivines contain abundant micro-inclusions filled with Na-Al siliceous glass, monosulfide of Fe, Ni, and Cu, carbonate, and dense CO_2. The glass inclusions form blebs of round, oval or negative crystal shapes (0.5 up to 30 μm). They are isotropic, but in rare cases show very weak birefringence. Occasionally, these micro-inclusions also contain droplets of Fe-Ni sulfides or a bubble (Figs. 5 and 6). The glass of these inclusions usually has a chemical composition similar to that of peralkaline phonolites, trachytes or dacites (Table 1).

Sulfide micro-inclusions with sizes from 0.5 to 5 μm form accumulations sometimes containing linear arrays of inclusions varying from spheres to equant negative crystals (Figs. 5 and 6). The sulfide inclusions are dominantly nickeliferous mono-sulfide with minor amounts of Co and Cu. In one rock we found a pyrrhotite-chalcopyrite association. In some sulfide inclusions we noted up to 2.65 wt% Zn. To the best of our knowledge, Zn has not previously been reported from upper mantle sulfides.

Some micro-inclusions are filled with polyphase assemblages containing silicate glass and mono-sulfide with curved boundaries between phases (Fig. 6).

The carbonate micro-inclusions form elongated rods, tubes or negative crystals. They usually show traces of leaching of carbonate material (Figs. 5 and 7). In one inclusion (Figs. 5 and 7), Ni-Fe-sulfide (Table 1) is enclosed in the carbonate with distinct curved menisci (Fig. 7). Glass, sulfide and carbonate inclusions are closely related and confined to the same planes in the olivine crystals (Fig. 5), testifying for a simultaneous trapping of these micro-inclusions as droplets of melt.

All major silicate phases of the rocks are rich in CO_2 inclusions, especially olivine.

REE analyses of investigated xenoliths are shown in Fig. 11. Chondrite-normalized REE patterns of the investigated peridotites in the majority of cases exhibit complex S-like shapes: the normalized abundances drop from La to Pr, then increase with atomic number to reach a maximum at Tb and subsequently decrease to Lu. Some specimens also exhibit a very weak negative Eu anomaly.

DISCUSSION

The close connection of alkaline and carbonatitic magmatism with mantle metasomatism and fluid migration initiated by rifting is widely accepted. It is generally assumed on the basis of isotope (Menzies and Murthy, 1980; Menzies and Wass, 1983), trace element [22, 52] and experimental studies [7, 55] that mantle metasomatism is an inevitable precursor for the generation of alkaline and carbonatitic magmas. A small degree of partial melting of carbonate-bearing peridotite at pressures above 20 kbar generates dolomitic [53, 54,] or sodium-rich dolomitic melts [51] which could be a very active metasomatizing agent forming carbonate-bearing wehrlitic assemblages: clinopyroxene, olivine, spinel and carbonate [18, 19, 23, 43, 57]. Dalton and Wood [7] showed that at lower pressure

(15 kbar) Ca-rich carbonatite melt (with Ca/(Ca+Mg+Fe+Na) ratios up to 0.96) could be produced in the mantle as the result of wall-rock reaction of less calcic

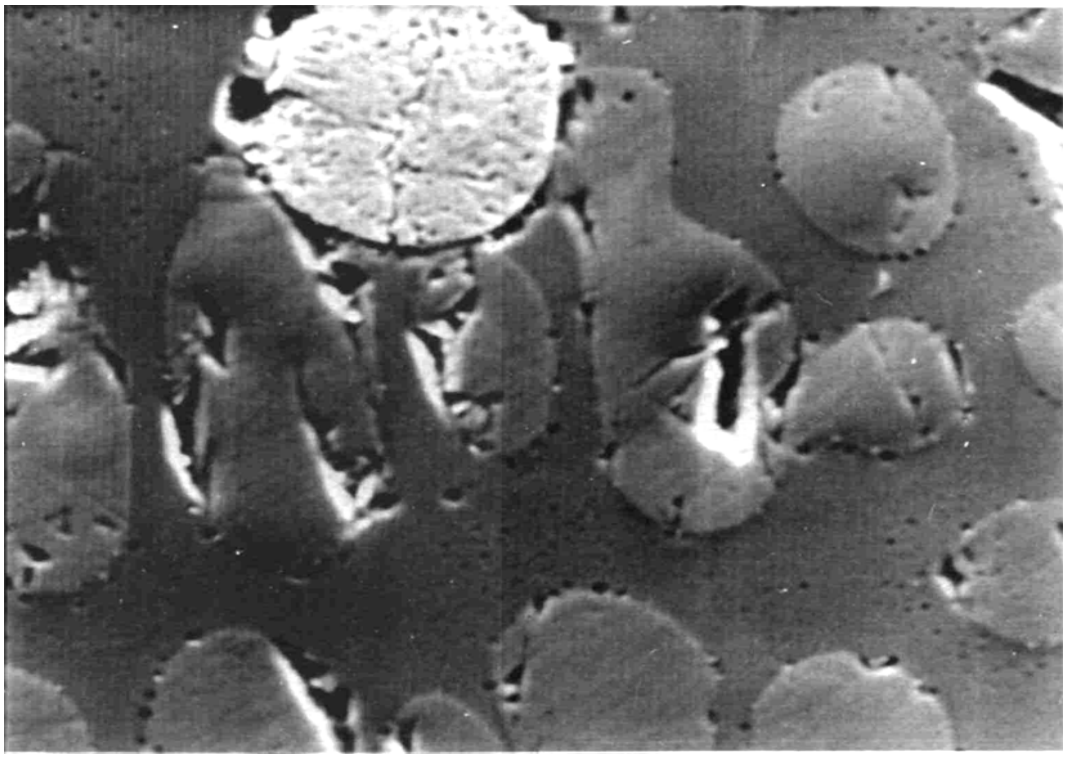

Fig. 5. **Back-scattered electron image of a melting experiment product, T = 1220 °C, p = 8 kbar.**

Sulfide-silicate-carbonate immiscibility, S - sulfide liquid, C - carbonate liquid, Gl - glass, silicate liquid (Kogarko, Slutsky, 2004, in press).

melts with a wehrlitic assemblage. The Mg/Fe ratio in carbonate also increases during this process.

Textural evidence and the mineral compositions of the investigated xenoliths indicate very active metasomatic interaction between primary dolomite melt (or fluid) and oceanic mantle below Fernando de Noronha following the reactions:

$$2Mg_2Si_2O_6 + CaMg(CO_3)_2 = 2Mg_2SiO_4 + CaMgSi_2O_6 + 2CO_2 \quad (1)$$
orthopyroxene melt olivine clinopyroxene fluid

$$3CaMg(CO_3)_2 + CaMgSi_2O_6 = 4CaCO_3 + 2Mg_2SiO_4 + CO_2 \quad (2)$$
melt clinopyroxene melt olivine fluid

A second generation of minerals and numerous CO_2 inclusions occurring in olivine, and less often in other minerals, appears to have formed as the result of these reactions. Mineral chemical features of the second generation assemblage (more Ca and Mg in clinopyroxene and high Ca contents of olivine) also imply that the metasomatic agent was enriched in Ca and Mg and dramatically depleted in silica, being unstable with orthopyroxene and in equilibrium with more Ca- and Mg-rich clinopyroxene and Ca-enriched olivine (Table 1). The replacement of second generation olivine by clinopyroxene in some xenoliths (Fig. 3) suggests

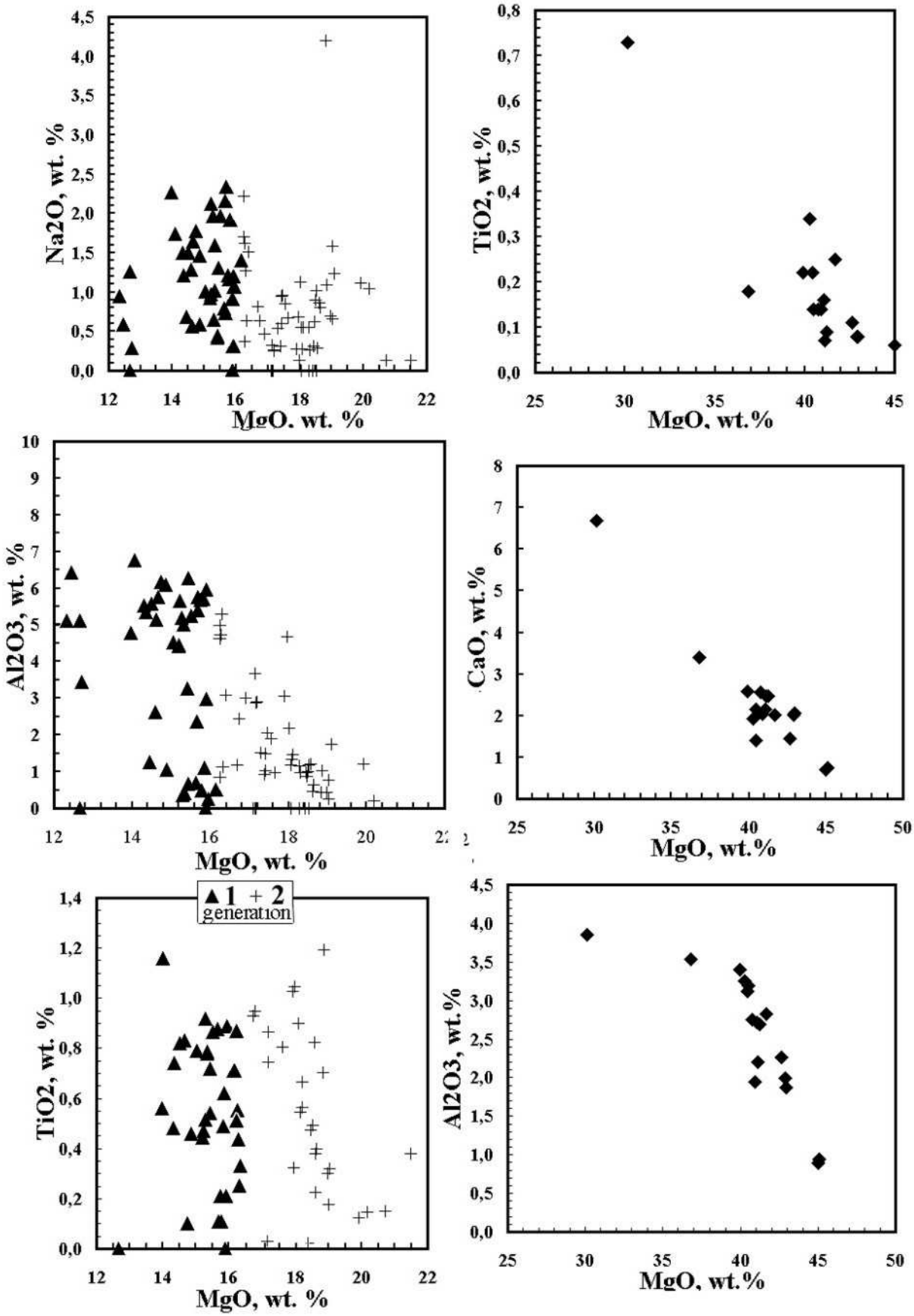

Fig. 6. **Co-variations of MgO - CaO, MgO - Al_2O_3, and MgO - TiO_2 in xenoliths from Fernando de Noronha.**

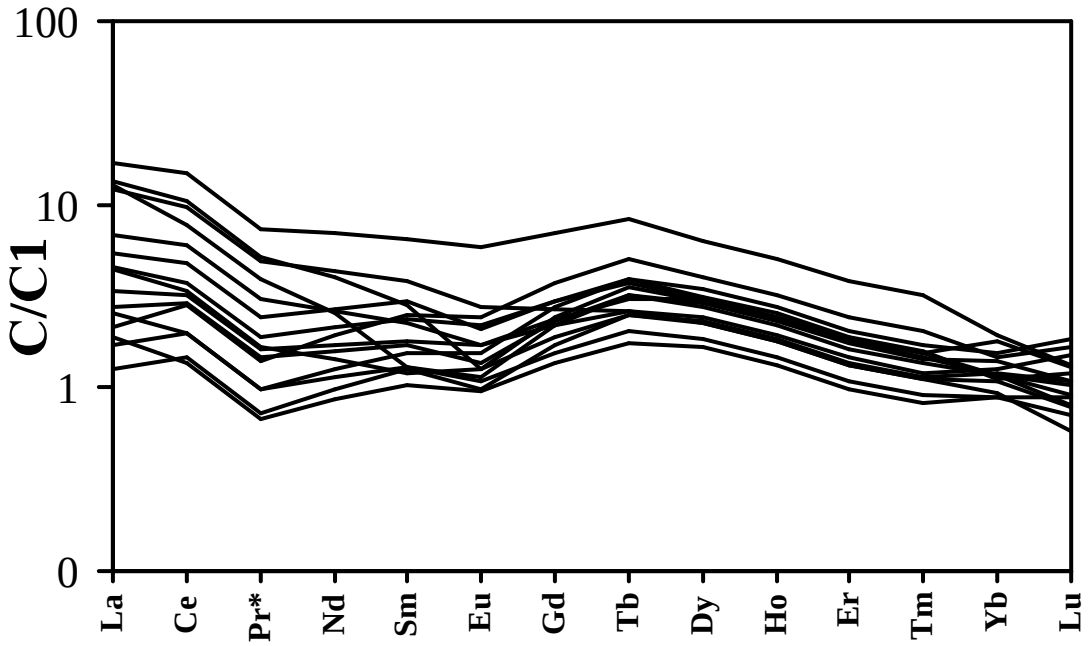

Fig.7. **The abundances of rare earth elements in upper mantle xenoliths from Fernando de Noronha normalized to CI chondrite (data of Taylor and McLennan, 1985).**

that under increasing CO_2 pressure or decreasing temperature reaction (2) moved to the left.

The calcium-rich carbonate confined to the wehrlite veinlets of the Fernando de Noronha xenoliths has very high Ca/(Ca+Mg+Fe+Na) (0.84 - 0.91) and Mg/(Mg+Fe) ratios (0.81 - 0.86) (Table 1). Using two-pyroxene geothermometry and Ca-in-olivine geobarometry [5], the lower equilibration temperature limit for the second generation minerals was 1050 - 1105 ^{o}C and the pressure 11 - 14 kbar. This is close to the pressure at which the Dalton and Wood [7] experiments were done which produced high-calcium carbonate melts. It should be pointed out that the equilibration pressure and temperature ranges for the first generation of minerals are 18 - 23 kbar and 1255 - 970 ^{o}C, which may imply that the uplift of mantle material was simultaneous with carbonatite metasomatism. This conclusion is in agreement with the data on CO_2 micro-inclusions. These inclusions had melting temperatures of -57.1 ^{o}C, which indicates that the trapped fluid is CO_2 with minor amounts of other volatile species. These inclusions homogenized at -25 ^{o}C into a liquid phase with a density of 1.06 g/cm^3, estimated from CO_2 vapor-liquid equilibria [41]. We calculated the lower limit for the trapping pressure (8.4 kbar) using the formation temperature for the second generation assemblage (1105 - 1050 ^{o}C). Low-density CO_2 inclusions appeared to be confined to healed micro-fractures in host olivine (Fig. 8). Their homogenization into a liquid phase at +26 ^{o}C corresponds to a very low trapping pressure of about 1 kbar at 1105 - 1050 ^{o}C. The presence of kirschsteinite in metasomatic zones suggests the invariant reaction:

$$3Ca(Mg,Fe)SiO_4 + CO_2 = Ca(Mg,Fe)Si_2O_6 + (Mg,Fe)_2SiO_4 + 2CaCO_3.$$

Using the temperature range of the second generation assemblage and the thermodynamic database of Shapkin et al. [47], we obtain $p(CO_2)$ of 0.9 - 1.5 kbar. This suggests that the reaction may have occurred at a very shallow level of 3 - 5 km.

In spite of the low sodium concentrations (0.1 - 0.7 wt% Na_2O) in the carbonate from the investigated xenoliths, we assume that the primary carbonate melt was to a large extent enriched in sodium because clinopyroxene in the second generation assemblage contains up to 2.5 wt% Na_2O. According to our calculations, based on the experimental data of Dalton and Wood [7] and Yaxley and Green [58], this Na_2O content of the clinopyroxene corresponds to about 30% Na_2CO_3 in the co-existing melt/fluid. Therefore, it appears likely that the metasomatic assemblage of secondary minerals was in equilibrium with a sodium-rich dolomitic melt.

It is probable that sodium was carried away by the residual low temperature fraction of the melt/fluid. From experimental data [9] one may also conclude that nyererite, which is the main sodium compound in natrocarbonatites, is dissolved incongruently under the conditions of a low temperature hydrothermal process. Sodium carbonate enters the solution during the interaction of sodium-bearing carbonate with a hydrothermal fluid, while the solubility of calcium carbonate is lower by an order of magnitude. Another possibility is that alkalis have been lost as chlorides in an aqueous fluid where sodium solubility is practically unlimited. The presence of Cl-bearing apatite in metasomatic zones points to a substantial role of chlorine in the fluids.

REE patterns of investigated xenoliths possibly reflect the complex history of the mantle under Fernando de Noronha. The rocks were strongly depleted in light rare earth elements (LREEs) in the past probably by extraction of a melt fraction. Subsequently they experienced an enrichment in trace elements from a LREE-enriched fluid which, however, did not fully precipitate the most incompatible elements like La and Ce. Such a behavior can be expected from a sodium dolomitic melt/fluid.

Thus, we concluded that the primary carbonate melt or fluid which metasomatically interacted with the oceanic lithosphere below Fernando de Noronha had a sodium-bearing dolomitic carbonatite composition.

SILICATE-SULFIDE-CARBONATE LIQUID IMMISCIBILITY

It is generally accepted that glass patches in deep-seated xenoliths are mostly a result of partial melting of metasomatized mantle substrate [18, 23, 42, 45, 57]. The strongly evolved glass composition of the Fernando de Noronha xenoliths implies that these melts were not in equilibrium with the minerals of the first generation but rather formed during incongruent melting of jadeitic clinopyroxene from metasomatized veinlets [23].

The presence of quenches apatite and rutile in the glass may be attributed to the rapid evolution of such melts leading to saturation by these minerals. The presence of armalcolite and second generation clinopyroxene containing more Ti than the primary minerals testifies for a Ti enrichment of the metasomatized zones. Metasomatic clinopyroxenes from Mongolia and Spitsbergen xenoliths also show higher Ti values as compared to first generation clinopyroxene [17]. This means that Ti was introduced into the oceanic mantle together with dolomite melt.

The glass containing abundant sulfides globules was also saturated with respect to sulfides. Numerous sulfide micro-inclusions occur in all minerals of the rocks, especially in olivine. In some cases, glass inclusions contain also sulfides (Fig. 6). The morphology and composition of sulfide inclusions indicate that they were trapped as droplets of immiscible melt. Andersen et al. [3] and Amundsen [2] have presented convincing evidence for silicate- sulfide liquid immiscibility in partially melted mantle rocks.

As noted before, the second generation phase assemblage has abundant carbonate patches with sharply curved menisci, immersed in felsic glass. These textural interrelationships between carbonate and silicate glass resemble immiscible melt relations.

We interpret the presence of the three different types of melt micro-inclusions, glass, sulfide and carbonate, all confined to the same plane in olivine crystals (Fig. 5), as clear, unambiguous evidence of a liquid immiscibility relationship between sulfide, silicate and carbonatite melts. The formation of the system of veins in the investigated rocks filled by carbonate is very difficult to be explained by the accumulation of calcite during the crystallization of silicate-carbonate melt. It is much more likely that the low-viscosity Ca-rich carbonate melt or fluid percolated through the mantle material forming the series of carbonate veins. A melt similar in composition to Ca-rich carbonatite was generated during the partial melting of wehrlitized mantle material containing calcite. The shape of the segregations of Ca-rich carbonate and the presence of three types of inclusions controlled by the same planes may also imply that the origin of Ca-rich carbonatites may be due to the processes of liquid immiscibility. Experimental investigations suggest that liquid immiscibility plays a leading role in the genesis of carbonatites [11, 21]. Experiments have demonstrated the presence of extensive fields of two immiscible liquids in the system (SiO_2 + Al_2O_3 + TiO_2) - (MgO + FeO + CaO) - (Na_2O + K_2O) - CO_2. The immiscibility gap expands with increasing pressure and alkali content. According to Lee and Wyllie [32], the immiscibility gap also expands with decreasing magnesium concentration. However, Lee and Wyllie [31, 32] have pointed out a number of limitations to this hypothesis and maintain that there cannot be a single process responsible for the formation of all carbonatites. Their recent experimental results [32] indicate that carbonate-silicate immiscibility is strongly restricted to alkali-rich melts containing at least 5% Na_2CO_3.

Our calculations based on clinopyroxene composition and experimental data of Dalton and Wood [7] and Yaxley and Green [58] show that up to about 30 wt% of Na_2CO_3 in the carbonatite liquid being in equilibrium with the metasomatic mineral association in wehrlites of Fernando de Noronha. Assuming equilibrium between silica-rich and carbonatite melts, one can estimate the alkali component of the latter using the partition coefficient of alkalis as determined Hamilton et al. [14]. The calculated amounts fall in the range of 12 - 45 wt% Na_2CO_3.

Studies of crystallized melt inclusions provide new evidence for quite high alkali concentrations in carbonatite melts of some of the world's largest carbonatitic complexes - Guli, Kovdor and Gardiner [26, 50]. Veksler et al. [50] have concluded that "potential carbonatite melts of Kovdor and Gardiner would be alkaline-bearing". Thus Ca-rich carbonatites may originate from primary Na-rich carbonatite melt by fractional crystallization with subsequent wall-rock reactions and loss of alkalis to the fluid phase.

We attribute the leaching phenomena in carbonate micro-inclusions (Figs. 5 and 7) to the activity of aqueous fluids in mantle peridotites below Fernando de Noronha. From the above consideration it is thus possible to suggest that the immiscibility of carbonate, sulfide and silicate melts took place during the partial melting of upper mantle material below the island. The original carbonate melt initially could have contained significant amounts of alkalis, which possibly continued to move further and thus were lost.

The immiscibility between silicate and sulfide melts has been known for many years. However, the immiscibility in carbonate-silicate-sulfide systems has so far not been revealed. Using a piston-cylinder apparatus, we have investigated the immiscibility in the system Ca-rich carbonate - Fe,Ni sulfide - silicate melt of phonolitic composition containing F. The experiments were made at 1250 ^oC and 4 - 15 kbar. The investigated system showed clear immiscibility: sulfide and carbonate melts were present in the form of small globules in silicate liquids (Fig. 9). Sulfur solubility in silicate melt varies from 0.15 to 0.35 wt% and in carbonate liquid it ranges from 0.02 to 3.7 wt% depending on alkali content [24, 27].

CONCLUSIONS

Our investigations have revealed a very complicated multi-stage geological history for the mantle rocks below Fernando de Noronha Island. The MgO - CaO and MgO - Al_2O_3 co-variations in the bulk composition of the investigated rocks (Fig. 10) reflect varying degrees of partial melting during which the initial substrate lost the so-called basaltic elements: Ca, Al, Ti, Na and incompatible trace elements. Sulfur should have been lost during this process due to the low melting temperatures of mantle sulfides. Later this depleted mantle material was invaded by a carbonate melt/fluid with a prevailing dolomitic component and containing sodium and possibly potassium, sulfur, light rare earth elements (LREEs), titanium, strontium, barium and phosphorous. Geochemical data demonstrate a strong influx of LREE (Fig. 11). During the metasomatic reactions partial

wehrlitization took place along veinlets and fissures. This process was accompanied by the uplift of mantle material from depths of about 60 km to 30 km, as suggested by our calculations, which indicate that the metasomatic mineral assemblage probably formed at relatively low pressures.

Later, during very rapid ascent of mantle material (otherwise primary carbonate would not survive), the wehrlitic mineral assemblage containing carbonate melted as result of decompression and produced Ca-rich carbonatitic melt. In some cases three immiscible liquids - carbonate, sulfide, and silicate were formed. The last equilibration between mineral phases appears to have been reached under very low pressures of about 1 kbar at 3 - 5 km depth.

Generalization of our data and that published earlier [18, 19, 23, 43, 45, 57] indicate that mantle carbonatite metasomatism is a very wide-spread phenomenon. However, to the best of our knowledge only four cases of carbonate metasomatism occurring in oceanic lithosphere have been reported so far: Samoa Island [15], Grande Comore [6], the Canary Archipelago [23], and the Cape Verde Islands [44]. We suggest a close connection between carbonatite metasomatic processes in the oceanic lithosphere and the origin of very Ca-rich, silica-undersaturated and carbonatitic magmas in some of the Canary and Cape Verde islands and Fernando de Noronha.

ACKNOWLEDGEMENTS

We are grateful for fruitful discussions to Drs. A. Woolley and B. Close.

This work was financially supported by the Russian Foundation for Basic Researchers, Project 99-05-64835, INTAS 1010-CT93-OO18, the Austrian FWF and the Austrian Academy of Sciences.

REFERENCES

1. **Almeida, F.F.M.** (1958). Geologia e petrologia do Arquepelago de Fernando de Noronha. - Div. De Geol e Min., Depto. Nac. Prod. Min., Ministr. Da Agric., Monog. 13 Rio de Janeiro.
2. **Amundsen, H.E.F.** (1987). Evidence for liquid immiscibility in the upper mantle // Nature 327: 692-695.
3. **Andersen, T., Griffin, W.L., O'Reilly, S.Y.** (1987). Primary sulfide melt inclusions in mantle-derived megacrysts and pyroxenites // Lithos 20: 279-294.
4. **Baker, M.B., and Wyllie, P.J.** (1990). Liquid immiscibility in a nepheline- carbonate system at 25 kbar and implication for carbonatite origin // Nature 346: 168-170.
5. **Brey, G.P., Koehler, T.** (1990). Geothermobarometry in four-phase lherzolites II New thermobarometers, and practical assessment of existing thermobarometers // J. Petrol. 31: 1353-1358.
6. **Coltorti, M., Bonadiman, C., Hinton, R.W., Siena, F., and Upton, B.G.J.** (1999). Carbonatite matasomatism of the oceanic upper mantle: evidence from clinopyroxenes and glasses in ultramafic xenoliths of Grande Comore, Indian Ocean // J. Petrol. 40: 133-165.
7. **Dalton, J.A., Wood, B.J.** (1993). The composition of primary carbonate melts and their evolution through wallrock reactions in the mantle // Earth Planet. Sci. Lett. 119: 511-525.

8. **Dautria, J.M., Dupuy, C., Takherist, D., Dostal J.** (1992). Carbonate metasomatism in the lithospheric mantle: peridotitic xenoliths from a melilitic distric of the Sahara basin // Contrib. Mineral. Petrol. 111: 31-52.
9. **Dernov-Pegarev, V.F., Malinin, S.D.** (1976). Solubility of calcite in high temperature aqueous solutions of alkali carbonate and the problem of the formation of carbonatites // Geokh. 5, 643-657 (in Russian), translated as: Geochem. Internat. 13: 1-13.
10. **Edgar, A.D., Lioyd, F.E., Forsyth, D.M., Barnett, R.L.** (1989). Origin of glass in upper mantle xenoliths from the Quaternary volcanics of Gees. West Eifel, Germany // Contrib. Mineral. Petrol 103: 277-286.
11. **Freestone, I.C. and Hamilton, D.L.** (1980). The role of liquid immiscibility in the genesis of carbonatites // Contrib. Mineral. Petrol. 73: 105-117.
12. **Green, T.H., Adam, J. and Sie, S.H. (**1992). Trace element partitioning between silicate minerals and carbonatite at 25 kbar and application to mantle metasomatism // Mineral. Petrol. 46: 179-184.
13. **Hamilton, D.L., Kjarsgaard, B.A.** (1993). The immiscibility of silicate and carbonate liquids // South African J. Geol. 96: 139-142.
14. **Hamilton, D.L., Bedson, P. and Esson, J.** (1989). The behaviour of trace elements in the evolution of carbonatites // In: Bell K. (ed) Carbonatites. Genesis and Evolution. London: Unwin Hyman, 405-427.
15. **Hauri E.N., Shimizu N., Dieu J.J., Hart S.R.** (1993). Evidence for hot-spot-related carbonatite metasomatism in the oceanic upper mantle // Nature 365: 221-227.
16. **Hess, H.H.** (1960). Stillwater igneous complex Montana: a quantitative mineralogical study // Geol. Soc. Amer. Mem. 80, 230 pp.
17. **Ionov, D.** (1998). Trace element composition of mantle-derived carbonates and coexisting phases in peridotite xenoliths from alkali basalts // J. Petrol. 39: 1931-1941.
18. **Ionov, D. A., Dupuy, C., O'Reilly, S.Y., Kopylova, M.G., Genshaft, Y.S.** (1993). Carbonated peridotite xenoliths from Spitsbergen: implications for trace element signature of mantle carbonate metasomatism // Earth Planet. Sci. Lett. 119: 283-297.
19. **Ionov, D.A, Hofmann, A.W., Shimizu, N.J.** (1994). Metasomatism induced melting in mantle xenoliths from Mongolia // J. Petrol. 35: 753-785.
20. **Kjarsgaard, B.A., Hamilton. D.L.** (1989). The genesis of carbonatites by immiscibility // In: Bell K. (ed) Carbonatites Genesis and Evolution. Unwin Hyman. London. 388-404.
21. **Kjarsgaard, B.A., Peterson, T.D.** (1991). Nepheline-carbonatite liquid immiscibility at Shombole volcano, East Africa // Mineral. Petrol. 43: 293-314.
22. **Kogarko. L.N.** (1996). Geochemical models of supergiant apatite and rare-metal deposits related to alkaline magmatism // Geochem. Internat. 33 (4): 129-149.
23. **Kogarko, L.N., Henderson, C.M.B., Pacheco, H.** (1995). Primary Ca-rich carbonatite magma and carbonate-silicate-sulfide liquid immiscibility mantle // Contrib. Mineral. Petrol. 121 267-274.
24. **Kogarko, L.N., Henderson, M., Ntaflos, T., Slutsky, A.B., Pacheco, A.** (1998). Carbonate metasomatism of oceanic lithosphere and carbonate-silicate-sulfide liquid immiscibility // Mineral. Mag. 62A (2): 797-798.
25. **Kogarko, L.N., Kramm, U., Grauert, B.** (1983). New data on age and genesis of Lovozero alkaline rocks (Rb-Sr signature) // Dokl. Acad. Sci. USSR, 268 (4): 970-972.
26. **Kogarko, L.N., Plant, D.A., Henderson, C.M.B., Kjarsgaard, B.A.** (1991). Na-rich carbonate inclusion in perovskite and calzirtite from the Guli Intrusive Ca-carbonatite, Polar Siberia // Contrib. Mineral. Petrol. 109: 124-129.
27. **Kogarko, L.N., Slutsky, A.B.** (1999). Carbonate-silicate-sulfide liquid immiscibility // Dokl. Acad. Sci. (in press).

28. **Kolesov, G.M.** (1994). Determination of trace elements: neutron-activation analysis in geochemistry and cosmochemistry // J. Analytical Chem. 49 (1): 50-58
29. **Koster van Groos, A.F.** (1975). The effect of high CO_2 pressure on alkalic rocks and its bearing on the formation of alkalic ultrabasic rocks and the associated carbonatites // Amer. J. Sci. 275: 163-185.
30. **Kurat, G., Palme, H., Embey-Isztin, A., Touret, J., Ntaflos, T., Spettel, B., Brandstätter, F., Palme, C., Dreibus, G., and Prinz, M.** (1993). Petrology and geochemistry of peridotites and associated vein rocks of Zabargad Island, Red Sea, Egypt // Mineral. Petrol. 48: 309-341.
31. **Lee, W-J., Wyllie, P.J.** (1994). Experimental data bearing on liquid immiscibility, crystal fractionation and the origin of calciocarbonatites and natrocarbonatites // Internat. Geol. Rev. 36: 797-819.
32. **Lee, W-J., Wyllie, P.J.** (1996). Liquid immiscibility in the join $NaAlSi_3O_8$ -$CaCO_3$ to 2.5 GPa and the origin of calciocarbonatite magmas // J. Petrol. 37: 1125-1152.
33. **Loomis, T.P., Gottschalk, R.R.** (1981). Hydrothermal origin of mafic layers in alpine-type peridotites: evidence from the Seiad Ultramafic Complex, California, USA // Contrib. Mineral. Petrol. 76: 1-11.
34. **Menzies, M.A., Murthy, V.R.** (1980). Nd and Sr isotope geochemistry of hydrous mantle nodules and their host alkali basalts: implications for local heterogeneities in metasomatically veined mantle // Earth Planet. Sci. Lett. 46: 77-85.
35. **Menzies, M. A., Wass, S. Y.** (1983). CO_2- and LREE-rich mantle below eastern Australia: a REE and isotopic study of alkaline magmas and apatite-rich mantle xenoliths from the Southern Highlands Province, Australia // Earth Planet. Sci. Lett. 65: 287-302.
36. **Menzies. M.A., and Hawkesworth, C.J.** (1987). Mantle Metasomatism. Acad. Press, London, 472 pp.
37. **Meyer, H.O.A., Svisero, D.P.** (1987). Mantle xenoliths in South America // In: Nixon, P.H. (ed.) Mantle Xenoliths. Chichester: J. Wiley & Sons, 85-93.
38. **Mitchel-Thome, R. C.** (1970). Geology of the South Atlantic Islands. Gebrüder Borntraeger, Berlin, Stuttgart. 367p.
39. **Pouchou, J.L., Pichoir, F.** (1991). Quantitative analysis of homogeneous or stratified microvolumes applying the model "PAP". // In: K.F.J. Heinrich and D.E. Newbury (Editors), Electron Probe Quantitation, Plenum Press, pp. 31-75.
40. **Pyle, J. M., Haggerty, S.E.** (1994). Silicate-carbonate liquid immiscibility in upper-mantle eclogites: Implications for natrosilicic and carbonatitic conjugate melts // Geochim. Cosmochim. Acta 58: 2997-3011.
41. **Roedder, E.** (1984). Fluid inclusions in minerals // Rev. Mineral. 12: 109-148.
42. **Rosenbaum, J.M., Zindler, A., Rubenstone, J.L.** (1996). Mantle fluids: evidence from fluid inclusions // Geochim. Cosmochim. Acta 60: 3229-3252.
43. **Rudnick, R.L., McDonough, W.F., Chappell, B.W.** (1993). Carbonatite metasomatism in the northern Tanzanian mantle: petrographic and geochemical characteristics // Earth Planet. Sci. Lett. 114: 463-475.
44. **Ryabchikov, I.D., Brey, G., Kogarko, L.N., Bulatov, V.K.** (1989). Partial melting of carbonated peridotite at 50 kbar // Geokh. 1: 3-9. (in Russian).
45. **Schiano, P., Clocchiatti, R., Joron, J.L.** (1992). Melt and fluid inclusions in basalts and xenoliths from Tahaa Island. Society Archipelago: evidence for a metasomatised upper mantle // Earth Planet. Sci. Lett. 111: 69-82.
46. **Seifert, W., Thomas, R.** (1995). Silicate-carbonate immiscibility: A melt inclusion study of olivine melilitite and wehrlite xenoliths in tephrite from the Elbe Zone, Germany // Chem. Erde 55: 263-279.

47. **Shapkin, A.I., Garanin, A.V. and Khodakovskii, I.L.** (1986). DIANIK GEOKHI.Russian Acad.Sci. Computer complex for chemical thermodynamics Project. In Direct and Inverse Thermodynamic Tasks.Nauka, Novosibirsk, 80-88.
48. **Taylor, S.R., and McLennan, S.M.** (1985). The continental crust: its composition and evolution. Blackwell, Oxford, 312 p.
49. **Varella, M.E., Clocchiatti, R., Kurat, G., Schiano, P.** (1999). Silicic glasses in hydrous and anhydrous mantle xenoliths from Western Victoria, Australia: at least two different sources // Chem. Geol. 153: 151-169.
50. **Veksler, I.V., Nielsen, T.F.D., Sokolov, S.V.** (1998). Mineralogy of crystallized melt inclusions from Gardiner and Kovdor Ultramafic alkaline complexes: implications for carbonatite genesis // J. Petrol. 39: (11&12): 2015-2031.
51. **Wallace, M.E., and Green, D.H.** (1988). An experimental determination of primary carbonatite magma composition // Nature 335: 343-346.
52. **Wass, S.Y., and Rogers, N.W.** (1980). Mantle metasomatism - precursor to continental alkaline volcanism // Geochim. Cosmochim. Acta 44: 1199-1206.
53. **Wyllie, P.J., and Huang, W.-L.** (1976). Carbonation and melting reactions in the system CaO-MgO-SiO_2-CO_2 at mantle pressure with geophysical and petrological applications // Contrib. Mineral. Petrol. 54: 79-107.
54. **Wyllie, P.J.** (1987). Discussion of recent papers on carbonated peridotite, bearing on mantle metasomatism and magmatism // Earth Planet. Sci. Lett. 82: 391-397.
55. **Wyllie, P.J.** (1989). Origin of carbonatites: evidence from phase equilibrium studies. In Carbonatites: Genesis and Evolution (K. Bell, ed.). Univ. Human, London: 500-545.
56. **Wyllie, P.J., Lee, W.-J.** (1998). Kimberlites, carbonatites, peridotites and silicate-carbonate liquid immiscibility explained in parts of the system CaO-(Na_2O+K_2O)-(MgO+FeO)-(SiO_2+Al_2O_3)-CO_2. Extended abstracts 7th Internat. Kimberlite Conf. Cape Town: 974-976.
57. **Yaxley, G.M., Crawford, A. J., Green, D. H.** (1991). Evidence for carbonatite metasomatism in spinel peridotite xenoliths from western Victoria, Australia // Earth Planet. Sci. Lett. 107: 305-317.
58. **Yaxley, G.M., Green, D.H., Kamenetsky, V.** (1998). Carbonatite metasomatism in the southeastern Australian lithosphere // J. Petrol. 39: (11&12), pp. 1917-1930.

UDK 552.33

An illustration of the evolution and alteration of carbonatites using REE, Sr –rich carbonatites at Nkombwa, Zambia

Wall F.

The Natural History Museum, London, f.wall@nhm.ac.uk

The Nkombwa Carbonatite Complex, Zambia consists of ferroan dolomite-ankierite carbonatites, including some with monazite-isokite-quartz mineralization. There are no associated calcite carbonaties or silicate rocks. The carbonatites have been studied by backscattered electron imagery and electron microprobe analysis. The mineral associations and compositions record a history of magmatic evolution and post magmatic mineralization that is common to many carbonatites and raises an important question about the role of external fluids in carbonatite systems. The magmatic evolution can be followed by zoning in apatite and the appearance of inclusions of burbankite-like compositions ($(Na,Ca)_3(Sr,Ba,Ce)_3(CO_3)_5$), strontianite and monazite-Ce). Finally this assemblage changes to monazite, REE fluocarbonates and strontianite, seen as small pools in the magmatic rocks. A pegmatite stage is marked by ferroan dolomite cabonatite containing many blebs of burbankite. Then comes postmagmatic mineralization in the form of monazite-(Ce), isokite ($CaMgPO_4F$), and dolomite veinlets and monazite-(Ce), isokite, quartz metasomatic pseudomorphous replacement of carbonates. These stages, albeit with slightly varying mineral assemblages are common to many carbonatites that contain REE mineralization. Burbankite is an indicator of the late magmatic – transition environment and is unstable in the later hydrothermal environments. The role of silica is problematic in these environments. Several studies of similar mineralization find no substantial groundwater involvement, but it seems highly likely, especially given the mapping of silicification at Nkombwa, and common occurrence of quartz rocks in the out areas of complexes that the silica is being dissolved from the country rock. At Nkombwa, REE-rich dolomite veinlets could be exclusively carbonatite-derived fluids whilst the quartz-bearing assemblage may involve groundwater. More work, perhaps with novel tracers, is required to understand properly the role of groundwater in carbonatite systems.

INTRODUCTION

The REE and Sr are key elements in carbonatites because of their high contents and thus use as tracers of mantle source characteristics [6]. The high concentrations can also produce potential economic deposits of these elements. In this paper the aim is to use the Nkombwa carbonatite as an example of how Sr and REE minerals can be used to trace the evolution and alteration of carbonatite.

GEOLOGICAL BACKGROUND

Nkombwa (N'kumbwa) is a prominent hill, 600 m by 1200 m, rising 300 m above the surrounding countryside at 32°51'E 10°09' N, 25 km east of the town of Isoka, Zambia [15, 17]. It consists of veined ankeritic dolomite carbonatite surrounded by a 100 m- wide breccia zone and a 2 km zone of potassic and sodic fenitization. A zone of silicification is mapped through the centre (Fig. 1). Nkombwa is intruded into upper Proterozoic Irumide basement gneisses [17, 28] and has been dated by K-Ar at 689 +-20 Ma [16, 17], placing it in the north Nyasa igneous province. This study is based on samples donated to The Natural History Museum by T. Deans and by D. Appleton of the British Geological Survey.

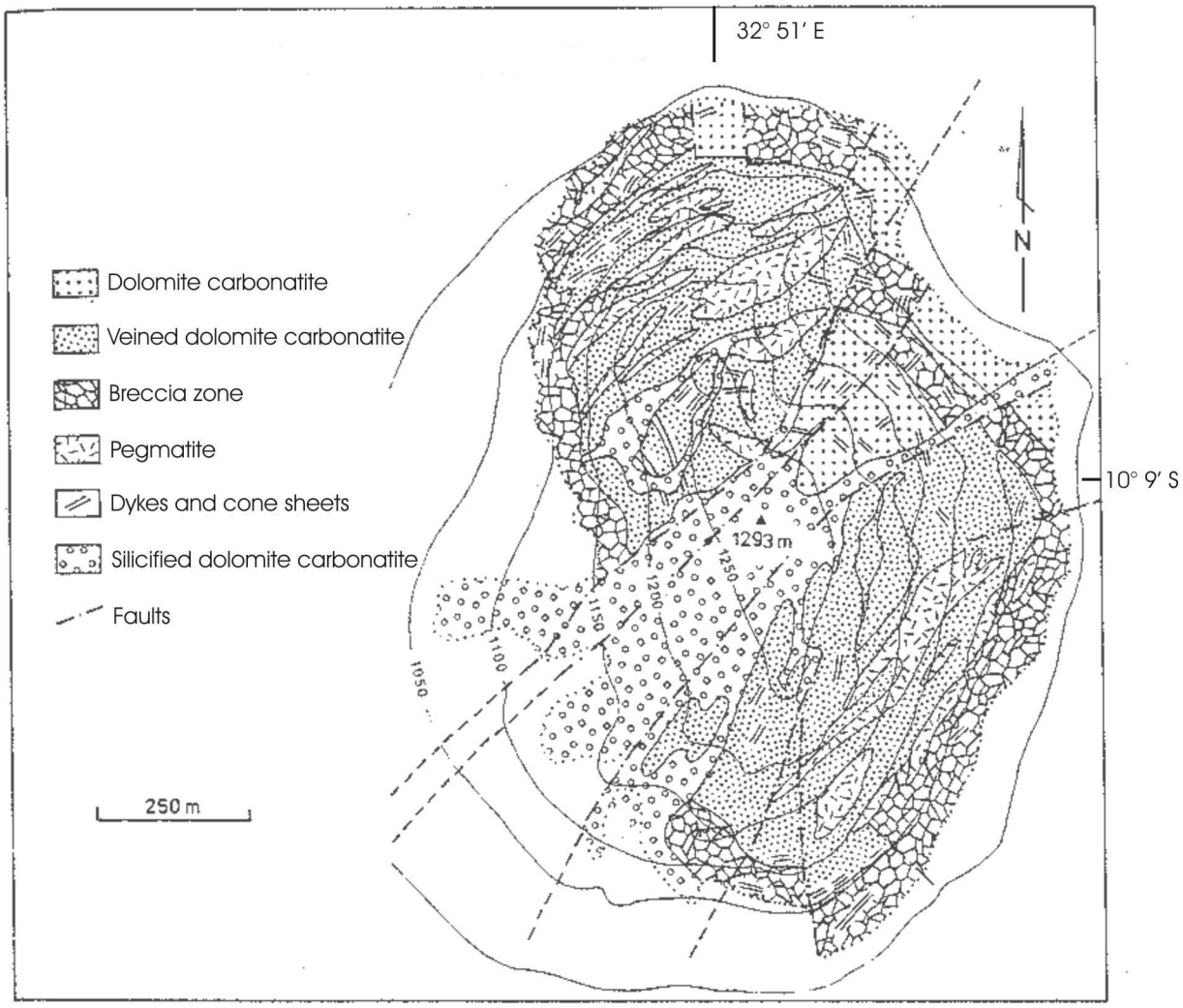

Fig. 1.

ANALYTICAL TECHNIQUES

The samples were studied using SEM/EDS, EPMA and cathodoluminescence petrography at The Natural History Museum, London. EDS analyses were carried out on a Hitachi S2500 SEM equipped with a Link AN10/55S analysis system, operated at 15 kV and 1 nA specimen current measured on a vanadium calibration

standard, with a 100 s livetime and ZAF matrix correction. The WDS analyses were obtained on Cambridge Instruments Microscan 9 operated at 20 kV and 25 nA measured on a Faraday cage and processed using a ZAF matrix correction and on a Cameca SX50 operated at 20 kV and 20 nA with a $\phi\rho z$ matrix correction. Empirical corrections were made for REE elemental overlaps. The primary standards were a mixture of synthetics and natural minerals and quality control standards, selected from amongst the mineral standards, were used during all analytical sessions. Sodium-bearing carbonates such as burbankite present particular problems; they are easily damaged by the electron beam and subject to sodium loss. Analyses were carried out by EDS at 15 kV and 1 nA specimen current, using either a 1 µm spot with short, 10 s, counting times combined to produce the spectrum, or rasters on approximately 5x5 µm areas. The latter technique gave better results where the burbankite was large enough to allow it to be used.

NKOMBWA CARBONATITES

The carbonatites at Nkombwa may be grouped into four categories. (1) light-coloured apatite-bearing ferroan dolomite carbonatite, (2) massive, pegmatitic, crystalline, light coloured dolomite carbonatite, (3) apatite-rich carbonatite, (4) monazite and isokite-rich carbonatite (Table 1). Some of the monazite and isokite-rich rocks contain a high proportion of quartz and less than 50% carbonate and so are not carbonatites. They are called here, monazite-isokite-quartz rocks. There are no calcite carbonatites at Nkombwa and no associated igneous silicate rocks. Some of the carbonatites contain magnesite-siderite series minerals and these were the subjects of a previous study [24].

EVOLUTION OF APATITE TO A SR, REE MINERAL ASSEMBLAGE

The lowest modal concentration of REE and Sr minerals occurs in light-coloured fresh-looking ferroan dolomite carbonatite (BM 1993, P6 (52), Table 1). This rock has the sugary texture typical of many carbonatites and also a very common amount, 5-10 modal %, of lozenge-shaped apatite (Fig. 2a). All of the apatite is concentrically zoned with rims enriched in Sr and REE (Fig. 2b, Table 2). Small, ca. 1 µm, inclusions in the apatite are closest in composition to burbankite-carbocernaite (Fig. 2b, Table 3). Near the edge of the apatite crystals there are cavities containing monazite-(Ce) and strontianite and around the edge there are crystals of strontianite, monazite-(Ce) and barite (Fig. 2b, Table 3).

There are also two types of inclusions in the ferroan dolomite. The first consists of <1 µm – 4 µm diameter blebs of burbankite and strontianite (Fig. 2d); the second consists of pools of strontianite, quartz and REE,Ca fluocarbonates (Figs 2c and d). The two assemblages are never found in direct association but are always separated by ferroan dolomite (Fig. 2d).

Table 1.

Examples of Nkombwa carbonatites

Sample number	Description
BM 1993, P6 (52)	*Light-coloured apatite-bearing ferroan dolomite carbonatite*. Sugary, fresh, medium-coarse grained. Ferroan dolomite is equant, 0.4-1 mm diameter with lobate interlocking margins and enclosing apatite, 5-10 modal % apatite lozenge grains, 300 x 600 – 900 µm, with occasional carbonate inclusions. 1 modal% anhedral, 100-200 µm phlogopite. Pools of Ca,REE fluocarbonate, barite, strontianite, quartz. Blebs of burbankite and strontianite, burbankite and strontianite-monazite in apatite
BM 1993, P6 (92)	*Monazite-isokite-quartz rock*. Rich in green spherulitic and axiolitic monazite-(Ce), spherulitic isokite, quartz and carbonate in radiating pseudomorph structures, 1 mm (up to 4 mm) diameter by 4 mm long. Isokite replaces carbonate. Matrix is light – dark brown carbonate, rich in limonitic Fe oxide, with some isokite and quartz.
BM 1993, P6 (98)	*Massive crystalline, light coloured dolomite carbonatite.* Very coarse-grained, (crystals > 5 mm) grey carbonatite with marked rhombohedral cleavage. Dolomite contains many 2 µm blebs of yellow cathodoluminescent burbankite. Occasional monazite, a few µm diameter associated with strontianite. Veinlets 200-500 µm wide cross-cut each other and contain carbonate, Fe oxides, Ba,Mn oxides, phlogopite(?), 100 µm isokite spherulites, occasional monazite and strontianite.
BM 1993, P6 (102)	*Apatite-rich carbonatite.* Rich in apatite laths which have discontinuous core-rim zoning in Sr. Plus Fe oxide, a little find-grained monazite and carbonate and accessory sellaite.
BM 1993, P6 (131)	Two distinct carbonatites: *Massive rhombic, crystalline, light coloured dolomite carbonatite plus brown, medium grained monazite and bastnäsite-bearing dolomite carbonatite.* Light carbonatite has interlocking (recrystallised) dolomite) Dark carbonatite contains limonitic Fe oxide, monazite and bastnäsite and a little carbonate.
BM 1993, P6 (132)	Mon*azite-quartz rock.* Heterogeneous 1 mm patches of green spherulitic and axiolitic monazite in brown Fe oxide-stained quartz (up to 300 µm diameter) pseudomorphing prismatic, radiating crystals. Minor 200 x 400 µm barite. Other nearby areas consist of pink carbonate (dolomite) with a texture similar to the outline of the pseudomorphs.
BM 1993, P6 (134)	Pale brown mottled *apatite-bearing ferroan dolomite carbonatite.* Ferroan dolomite-ankerite plus apatite crystals 100-150 µm diameter. Minor 100-200 µm pyrochlore. Minor strontianite associated with magnesite-siderite. Blebs of barite in the ferroan dolomite.

Given these relationships it is possible to construct a paragenetic sequence (Fig. 3). The first minerals to crystallise were apatite and ferroan dolomite. There was then a continuous fractionation to higher contents of Sr and REE, accommodated in apatite and in 'burbankite-like' and strontianite inclusions in apatite and ferroan dolomite. In the final stages of crystallization came the assemblages of monazite-(Ce), barite, REE fluocarbonates, strontianite and quartz. It is notable that the burbankite is not associated with the other REE minerals and always occurs separately.

BLEBS OF BURBANKITE-LIKE COMPOSITIONS IN PEGMATITE CARBONATITE

Some of the dolomite carbonatite is pegmatitic with pronounced rhombic cleavage. In thin section the large dolomite grains exhibit strained extinction indicative of recrystallization. They contain many blebs of burbankite-like composition (Fig. 4a). These blebs cathodoluminesce yellow and are sometimes

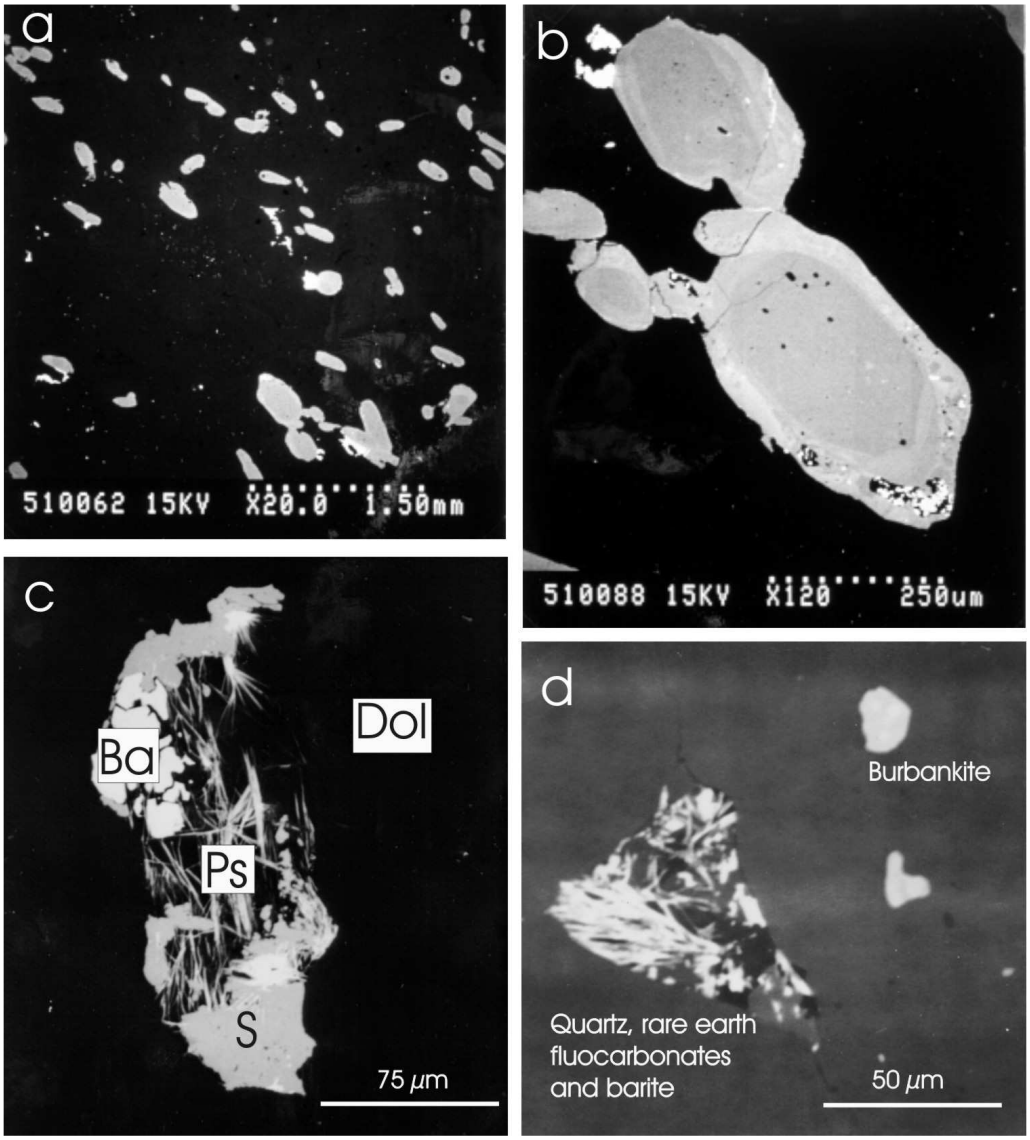

Fig. 2.

	Magmatic	- - - - - - - - - -	Hydrothermal
Ferroan dolomite	———	———	
Phlogopite	———		
Apatite with low Sr, REE	———		
Apatite with high Sr,REE		———	
Burbankite		———	
Strontianite		———	———
Monazite-(Ce)		———	———
Barite			———
Basnäsite and REE,Ca fluocarbonates			———
Quartz			———

Fig. 3.

Table 2.

Electron microprobe analyses of apatite from Nkombwa (wt%)

BM	1993, P6 (52)				1993, P6 (102)		1993, P6 (132)	
Anal. no.	1	2	3	4	5	6	7	8
Na_2O	0.9	-	-	0.4	0.2	-	-	-
MgO	-	-	-	-	-	-	0.7	0.6
SiO_2			-	-	0.2	-	0.2	-
CaO	50.4	53.8	51.6	50.6	51.4	44.7	55.1	53.9
SrO	2.2	0.6	1.9	2.3	5.4	13.0	2.2	2.9
Ce_2O_3	1.5	-	0.7	-	-	-	-	-
Nd_2O_3	0.6	-	-	-	-	-	-	-
P_2O_5	42.9	44.2	43.0	42.3	40.8	40.7	41.8	40.6
Total	98.4	95.5	97.3	95.5	98.0	98.3	100.4	98.0
Formula calculated to 10 cations in the Ca sites								
Na	0.292	-	-	0.138	0.056	-	-	-
Mg	-	-	-	-	-	-	0.172	0.153
Ca	9.356	9.941	9.756	9.629	9.410	8.643	9.624	9.573
Sr	0.216	0.059	0.197	0.233	0.534	1.357	0.204	0.274
Ce	0.096	-	0.047	-	-	-	-	-
Nd	0.039	-	-	-	-	-	-	-
Total	10.000	10.000	10.000	10.000	10.000	10.000	10.000	10.000
P	6.290	6.850	6.411	6.362	5.892	6.216	5.765	5.700
Si	-	-	-	-	0.034	-	0.028	-
Total	6.290	6.850	6.410	6.360	5.926	6.216	5.793	5.700

Note. Analyses 1 to 4 are from zoned, lozenge-shaped crystals, 5 and 6 are from zoned laths, 7 and 8 are associated with isokite. Analyses by EDS. Elements not listed or not given are below detection limit of about 0.1 wt%. F was not analysed.

associated with strontianite but never with monazite or any other REE minerals. Monazite and strontianite are found together though, as 5–50 μm anhedral crystals.

The carbonatite is cut by veinlets of dolomite, Fe oxide, phlogopite, isokite and monazite (Fig. 4a).

Burbankite, $(Na,Ca)_3(Sr,Ba,Ce)_3(CO_3)_5$, and carbocernaite, $(Ca,Na)(Sr,Ce,Ba)(CO_3)_2$, were identified on the basis of their compositions (Table 3). The blebs in ferroan dolomite are always zoned (Fig. 4b) with some areas having compositions consistent with burbankite (Table 3) and other areas being closer to carbocernaite. Other areas of the "burbankite" blebs with low BSE coefficients are distinct in that they have no REE (Table 3). They appear to be a member of the burbankite family because of the high Na content of 8.44 wt% oxide but do not correspond to any known composition. The formula for the Nkombwa mineral is $(Na_{1.79}Ca_{1.16})_{\Sigma 3.0}Sr_3(CO_3)_5$ and so it seems to be a Sr end member, REE-poor new member of the group. Unfortunately the small grain size precluded further work. Despite the considerable variation in the amount of REE in the various burbankite/carbocernaite carbonates, the degree of light rare earth-enrichment remains reasonably constant with ratios of $La/\Sigma REE_{wt\%}$ of about 0.3. The exception

is carbocernaite from BM 1993, P5(1) which is associated with daqingshanite and has a $La/\Sigma REE_{wt\%}$ ratio of about 0.4.

Table 3.

Electron microprobe analyses of burbankite $(Na,Ca)_3(Sr,Ba,Ce)_3(CO_3)_5$, carbocernaite, $(Ca,Na)(Sr,Ce,Ba)(CO_3)_2$, and strontianite from Nkombwa (wt%)

	burbankite?	burbankite	burbankite?	carbocernaite	bleb in apatite	strontianite	strontianite
BM 1993	P6 (98)	P6 (98)	P6 (98)	P5(1)	P6 (52)	P6 (52)	P6 (52)
Comment			avg of 3				
Na_2O	6.28	8.10	8.44	5.24	3.11	0.23	
CaO	3.05	10.08	9.86	3.57	6.76	0.97	1.01
SrO	34.82	49.29	46.31	24.27	31.41	68.69	68.65
BaO	5.59	1.39	-	8.46	5.52	-	-
La_2O_3	7.59	1.07	-	10.08	5.48	-	-
Ce_2O_3	13.40	2.58	-	12.14	10.28	-	-
Pr_2O_3	-	-	-	-	1.25	-	-
Nd_2O_3	3.58	1.26	-	1.90	2.80	-	-
CO_2*	33.11	36.95	33.39	28.96	30.38	30.09	29.94
Total	107.42^+	110.73^+	98.00	94.62	96.99	99.98	99.60
Formula calculated to 5(O) for carbocernaite and burbankite and 2(O) for strontianite							
Na	1.347	1.556	1.794	1.284	0.727	0.022	-
Ca	0.361	1.070	1.159	0.484	0.873	0.051	0.053
Sr	2.233	2.832	2.944	1.779	2.195	1.939	1.947
Ba	0.242	0.054	-	0.419	0.261	-	-
La	0.310	0.039	-	0.470	0.244	-	-
Ce	0.542	0.094	-	0.561	0.453	-	-
Pr	-	-	-	-	0.055	-	-
Nd	0.141	0.045		0.086	0.121	-	-
Total	5.177	5.689	5.897	5.084	4.927	2.011	2.000

Note. - = below detection limits of about 0.5 wt %. Total Fe as FeO. CO_2 calculated by stoichiometry. $^+$ high totals are probably the result of beam damage. Carbocernaite has a 5:5 ratio of cations to carbonate whereas the burbankite group has a ratio of 6:5. Analyses are calculated to 5(O) to facilitate this comparison. The quality of the analyses is good enough to allow comment and discussion but care should be taken before incorporating into any wider database.

There is a contrast between the main rock-forming carbonate in this pegmatitic carbonatite which is ferroan dolomite and the composition of the cross-cutting veinlets which are composed of dolomite with less than 0.5 wt% FeO (Table 4). Up to 1.2 wt % SrO is present in the veinlet dolomite (Table 4). Magnesite-siderite is also present in this rock and may be associated with burbankite (Table 4).

Previous studies of ferroan dolomite and magnesite-siderite series carbonates at Nkombwa [24] and also at Chipman Lake, Ontario, Canada [14] have found an evolution towards the Fe-rich compositions. There is further important observation at Nkombwa in that the late, probably hydrothermal, veinlets are composed of Fe-free, yellow cathodoluminescent, dolomite. So this makes a series of ferroan

dolomite, ankerite and magnesite-siderite with increasing Fe through magmatic fractional crystallization followed by hydrothermal Fe-free dolomite.

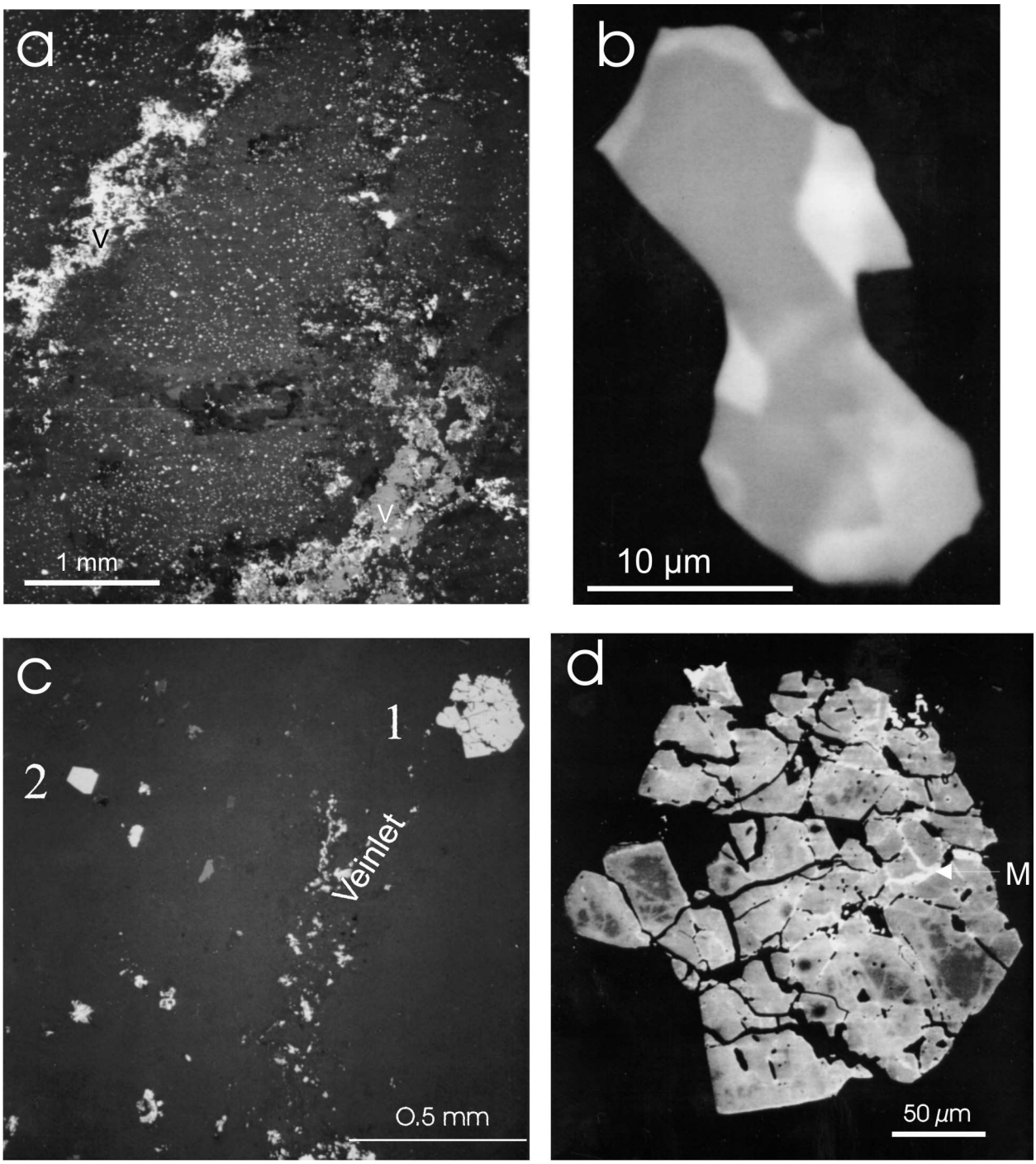

Fig. 4.

ALTERATION OF PYROCHLORE BY SR,REE-RICH FLUIDS

A pyrochlore and apatite-bearing, light-coloured, fresh-looking ferroan dolomite carbonatite (BM 1993 (134)) has a different kind of late-stage feature. The rock is cut by a monazite-bearing vein and where this meets pyrochlore, the pyrochlore is highly fractured and altered from pyrochlore *s.s.*,

$(Ca,Na)_2Nb_2O_6(OH,F)$, to a Sr-bearing pyrochlore (Figs 4c and d). Cracks in the pyrochlore crystal contain monazite (Fig. 4d). Away from the veinlet, the pyrochlore is unaltered (Fig. 4c). Although alteration of pyrochlore *s.s.* to Sr-

Table 4.

Electron microprobe analyses of the Nkombwa rock-forming carbonates: ferroan dolomite, dolomite, and magnesite (wt%)

BM	1993, P6 (98)	1993, P6 (98)	1993, P6 (98)	1993, P6 (98)
Mineral	**ferroan dolomite**	**dolomite**	**dolomite**	**magnesite**
Occurrence	host carbonate	in vein with isokite and monazite	in vein with isokite and monazite	next to burbankite
MgO	19.9	20.7	20.8	21.3
CaO	28.4	28.7	27.8	0.2
MnO	1.0	-	-	4.4
FeO	2.8	0.5	-	27.1
SrO	0.6	0.9	1.2	-
CO_2*	46.6	45.8	45.0	42.8
Total	99.3	96.6	94.7	95.8
Formula calculated to 2(O)				
Mg	0.931	0.987	1.009	1.087
Ca	0.957	0.983	0.968	0.007
Mn	0.027	-	-	0.129
Fe	0.070	0.014	-	0.777
Sr	0.011	0.017	0.023	-
Total	2.000	2.000	2.000	2.000

Note. - = below detection limit of 0.1 wt%. Total Fe as FeO. CO_2* calculated by stoichiometry. See also [24] for analyses of Nkombwa rock-forming carbonates, including ankerite with up to 11 wt% FeO.

bearing pyrochlore is best known from lateritic weathering [8,10,21,22] it has also been observed as a result of hydrothermal alteration at various localities [e.g. 11 and author's unpublished data from Chilwa Island, Malawi]. It is concluded to be the result of hydrothermal alteration at Nkombwa.

EVOLUTION OF APATITE TO SR-RICH COMPOSITIONS

Apatite-bearing carbonatite has been described above but one variety of carbonatite is distinctive in being particularly rich in laths of apatite (Fig. 5b). The laths are typically 100 x 500 µm and closely packed together. They have high Sr contents (up to 13 wt% SrO, Table 2) and have a marked discontinuous core-rim zoning, becoming most enriched in Sr at the rim. The matrix is dolomite, which appears oxidised in hand specimen. The contact with equigranular ferroan dolomite carbonatite is sharp suggesting this is a different phase of carbonatite intrusion.

Monazite-(Ce) – isokite – quartz mineralization, including pseudomorphs.

Monazite $(Ce,La)PO_4$ (Table 5) and isokite $(CaMgPO_4F)$ (Table 6) are common components of the Nkombwa rocks and occur in sub-mm carbonate veins, as well as in ferroan dolomite carbonatite and silicified carbonatite. The rocks in which they occur are typically heterogeneous and have been oxidised to

Table 5.

Electron microprobe analyses of monazite-(Ce) from Nkombwa (wt%)

BM 1993	P5(1)	P6 (52)		P6 (73)				P6 (132)		P6 (133)			P6 (134)
Anal.	1	2	3	4	5	6	7	8	9	10	11	12	13
SiO_2	-	-	-	-	-	0.53	0.59	0.22	0.53	0.4	-	-	-
P_2O_5	29.45	31.57	29.02	28.21	27.31	29.35	29.14	28.97	29.27	30.6	29.9	30.31	29.6
CaO	0.52	0.84	1.39	5.39	4.56	1.41	1.16	1.75	1.64	1.9	0.7	1.09	0.7
FeO		0.43	2.60	-	-	0.20	-	-	-	-	-	-	-
SrO	2.81	2.73	3.84	1.83	2.31	4.04	3.93	4.44	4.30	4.4	2.3	2.03	3.5
BaO	0.08	-	-	0.12	0.09	0.05	0.13	0.30	0.25	-	0.5	0.29	1.1
La_2O_3	23.95	21.76	12.95	23.14	24.75	23.58	24.28	22.94	23.55	21.7	24.9	24.71	12.5
Ce_2O_3	31.63	32.98	29.89	27.64	28.97	30.42	30.04	33.33	33.22	33.6	32.6	31.98	31.4
Pr_2O_3	2.14	2.31	3.81	1.89	1.57	1.95	1.84	1.79	1.72	3.0	2.7	2.10	3.3
Nd_2O_3	5.94	6.84	11.85	4.64	3.73	5.47	5.11	5.27	5.34	6.6	5.7	5.61	12.0
Sm_2O_3	0.08	-	-	0.22	0.03	0.17	0.14	0.11	0.13	-	-	0.22	-
ThO_2	-	0.87	4.01	-	-	-	-	-	-	-	-	-	-
SO_3	-	-	3.40	3.23	3.45	-	3.06	3.06	-	-	-	3.09	-
Total	96.60	100.33	102.76	96.31	96.77	97.17	99.42	102.18	99.95	102.3	99.3	101.43	94.2
Formula to 16(O)													
Mg	0.000	0.000	0.000	0.000	0.000	0.000	0.000	0.000	0.000	0.000	0.000	0.044	0.000
Ca	0.090	0.137	0.236	0.941	0.810	0.239	0.199	0.297	0.274	0.312	0.115	0.183	0.113
Fe	0.000	0.055	0.344	0.000	0.000	0.026	0.000	0.000	0.000	0.000	0.000	0.000	0.000
Sr	0.262	0.241	0.352	0.173	0.222	0.371	0.364	0.407	0.389	0.388	0.212	0.184	0.331
Ba	0.005	0.000	0.000	0.008	0.006	0.003	0.008	0.019	0.015	0.000	0.032	0.018	0.071
La	1.420	1.222	0.756	1.391	1.513	1.377	1.431	1.338	1.356	1.208	1.443	1.424	0.753
Ce	1.860	1.837	1.730	1.648	1.757	1.762	1.756	1.929	1.898	1.858	1.874	1.829	1.872
Pr	0.125	0.128	0.220	0.112	0.095	0.113	0.107	0.103	0.098	0.164	0.155	0.120	0.195
Nd	0.341	0.372	0.670	0.270	0.221	0.309	0.292	0.298	0.298	0.358	0.322	0.313	0.700
Sm	0.004	0.000	0.000	0.012	0.002	0.009	0.008	0.006	0.007	0.000	0.000	0.012	0.000
Th	0.000	0.030	0.144	0.000	0.000	0.000	0.000	0.000	0.000	0.000	0.000	0.000	0.000
Total	4.107	4.021	4.451	4.555	4.625	4.211	4.163	4.396	4.335	4.289	4.153	4.126	4.035
P	4.007	4.068	3.887	3.891	3.832	3.934	3.941	3.879	3.868	3.914	3.980	4.010	4.082
Si	0.000	0.000	0.000	0.000	0.000	0.084	0.094	0.035	0.083	0.066	0.000	0.000	0.000
Total	4.007	4.068	3.887	3.891	3.832	4.018	4.035	3.914	3.951	3.980	3.980	4.010	4.082

Note. Total Fe as FeO. Analyses by WDS except for 10,11,13 which are by EDS. - = below detection limit. Monazite in BM 1993, P6 (52) is associated with apatite, (2) is at the edge with strontianite and barite and (3) is an inclusion in apatite; in (73) the monazite is axiolitic along relict cleavage planes; in BM 1993, P6 (132) and (133) the monazite is spherulitic and axiolitic and associated with isokite; in BM 1993, P6 (134) the monazite is associated with strontianite; in BM 1993, P5(1) monazite is associated with daqingshanite.

release iron oxide from the carbonate. Much of the monazite is green in hand specimen, although its colour varies from almost colourless to yellow-green to bright green. In many specimens it highlights pseudomorphs (Fig. 5a).

Monazite in pseudomorphs and other silicified carbonatite often occurs as distinctive 10 µm-diameter spherulites and axiolites. The axiolites preserve relict crystal margins and rhombohedral cleavage planes of carbonate. They are about

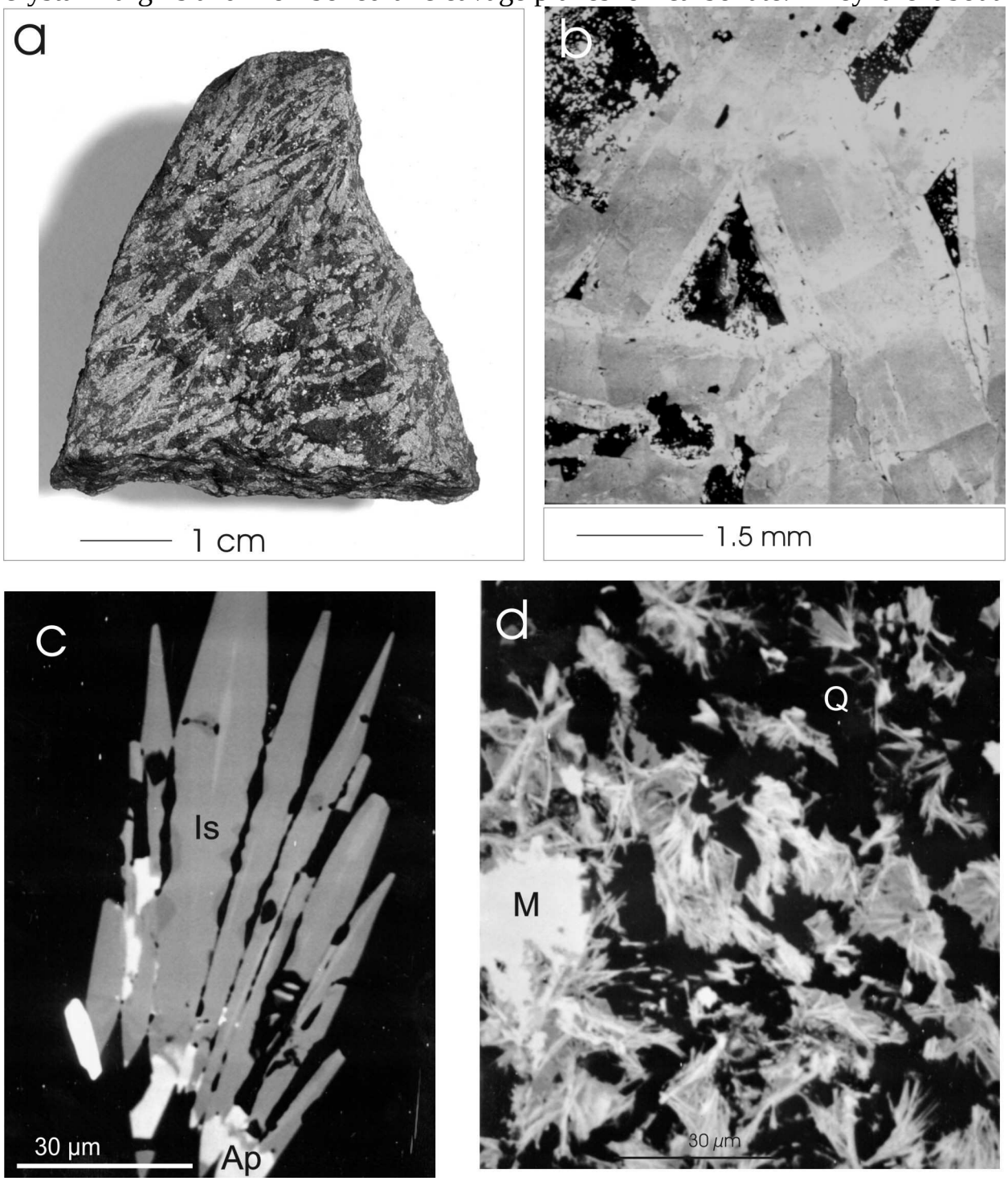

Fig. 5.

10 µm diameter and often have a fine line of limonitic Fe oxide at their centre and often also a concentration of 5µm Fe oxide grains at their outer margin. They define textures of what was probably originally a much coarser grained rock with >0.5 mm crystals. The monazite is usually hosted by quartz or microcrystalline quartz and/or dolomite.

The isokite typically occurs as much larger, 200 to 400 µm, spherulites which often enclose monazite and also often have a peppering of 10 µm sub-euhedral

Table 6.

Electron microprobe analyses of isokite ($CaMgPO_4F$) from Nkombwa (wt%)

BM 1993, P6	**(133)**	**(133)**	**(133)**	**(132)**	**(132)**	**(132)**
Anal. no.	1	2	3	4	5	6
Na_2O	-	0.4	-	-	0.3	0.3
MgO	20.3	20.9	21.3	20.4	21.0	20.7
Al_2O_3	2.5	-	-	-	-	-
SiO_2	-	-	-	0.2	-	0.2
CaO	30.5	29.9	32.2	29.8	29.5	30.0
SrO	1.1	2.1	0.5	1.4	3.9	1.5
BaO	0.5	-	-	-	1.0	0.7
P_2O_5	39.5	39.4	40.8	38.7	41.0	39.5
Total	94.6	92.5	94.8	90.6	96.6	92.9
Formula to 18(O)						
Na	-	0.080	-	-	0.060	0.060
Mg	3.590	3.780	3.740	3.770	3.690	3.740
Ca	3.870	3.890	4.060	3.950	3.720	3.890
Sr	0.080	0.150	0.030	0.100	0.270	0.110
Ba	0.020	-	-	-	0.050	0.030
Total	7.560	7.900	7.830	7.820	7.790	7.830
P	3.960	4.060	4.070	4.050	4.100	4.060
Si	-	-	-	0.030	-	-
Al	0.030	-	-	-	-	
Total	3.930	4.060	4.070	4.080	4.100	4.060

Note. 1 spherulitic, 2 spherulitic, around monazite, 3 not spherulitic, around monazite, 4 zoned, 5 Sr-rich zone, brighter on BSE, 6 not spherulitic, with apatite, zoned. Analyses by EDS. Elements not listed or not given in the table are below detection limits of about 0.1 wt%. F was not analysed.

opaques at their margin. It is difficult to determine the exact nature of the nucleus of the spherulites but occasionally there is apatite intimately intergrown with the isokite at the base of the spherulitic crystals (Fig. 4c). The apatite never occurs in the outer parts of the spherulites and therefore it seems to be associated with the initial growth, perhaps nucleating first, and then being partially replaced by the isokite. Nkombwa isokite contains small amounts of Sr but, unlike apatite, has no detectable substition of REE (Table 6).

The rare mineral daqingshanite ($(Sr,Ca,Ba)_3(Ce,La)PO_4(CO3)_{3-x}(OH,F)$, x about 0.8) also occurs associated with monazite and isokite and was described

previously from Nkombwa [5]. It is highly light REE-enriched with one composition having La predominant over Ce; daqingshanite-(La) rather than daqingshanite-(Ce) (Table 7).

Veins of isokite and monazite (Fig. 4a) contain dolomite with 0.5 wt% FeO which cathodoluminesces yellow-orange and is distinct from the more iron-rich main rock-forming ferroan dolomite, as discussed above.

Table 7.

Electron microprobe analyses of daqingshanite-(Ce) from Nkombwa (wt%)

Rock no.	BM 1993, P5 (1)			
P_2O_5	10.7	12.5	11.3	12.6
CaO	1.2	0.4	1.2	0.3
SrO	40.3	46.2	43.2	47.8
BaO	5.4	0.9	3.6	0.7
La_2O_3	11.5	12.1	11.4	11.6
Ce_2O_3	10.7	12.1	11.4	11.6
Pr_2O_3	-	-	-	-
Nd_2O_3	-	1.4	2.0	1.5
Total	79.7	83.9	81.4	84.1

Note. Analyses by EDS. F not analysed. Elements not listed, or where no figure is quoted, are below detection limit of about 0.5 wt%.

CHANGE IN MONAZITE-(CE) COMPOSITION

Monazite-(Ce) from Nkombwa is mostly highly enriched in the light REE, with La/ΣREE wt% usually 0.38-0.42 (Table 5, Fig. 6). However, the earliest monazite – inclusions in apatite and crystals associated with strontianite in ferroan dolomite carbonatite - is less light REE-enriched than the monazite-(Ce) in the main metasomatic monazite-isokite-quartz mineralization and has La/ΣREE wt% ratios of 0.21-0.41 (Table 5, Fig. 6a). Between 2 and 4.5 wt% SrO is consistently present in the monazite-(Ce). Th is usually below the detection limit of about 0.5 wt% and this is typical of much monazite from carbonatite [18,23]. Some of the analyses of spherulitic monazite have low totals, of about 96 wt%, as in BM 1993, P6 (76) for example. There seem to be two types of monazite-(Ce), one that produces good totals and one with always has lower totals. One possibility is that the mineral with the low analysis total is rhabdophane but this was not detected by XRD or infrared spectroscopy (C. Sweeney at De Beers Industrial Diamonds). It is possible that the monazite-(Ce) is hydrated to balance the substitution of Sr [23] or that the low totals are an artefact of the spherulites. Up to 3.4 wt% sulphate was detected in some crystals; an observation consistent with sulphate-bearing monazite has been described previously from dolomite carbonatites and quartz carbonate veins at Vuoriyarvi and Kandaguba, Kola Peninsula, Russia and interpreted as precipitating from carbohydrothermal solutions [9,7].

BASTNÄSITE AND MONAZITE-BEARING QUARTZ ROCK

Acicular needles of bastnäsite-(Ce) associated with monazite in a rock containing abundant limonitic iron oxides in a matrix of quartz (Fig. 5d). The

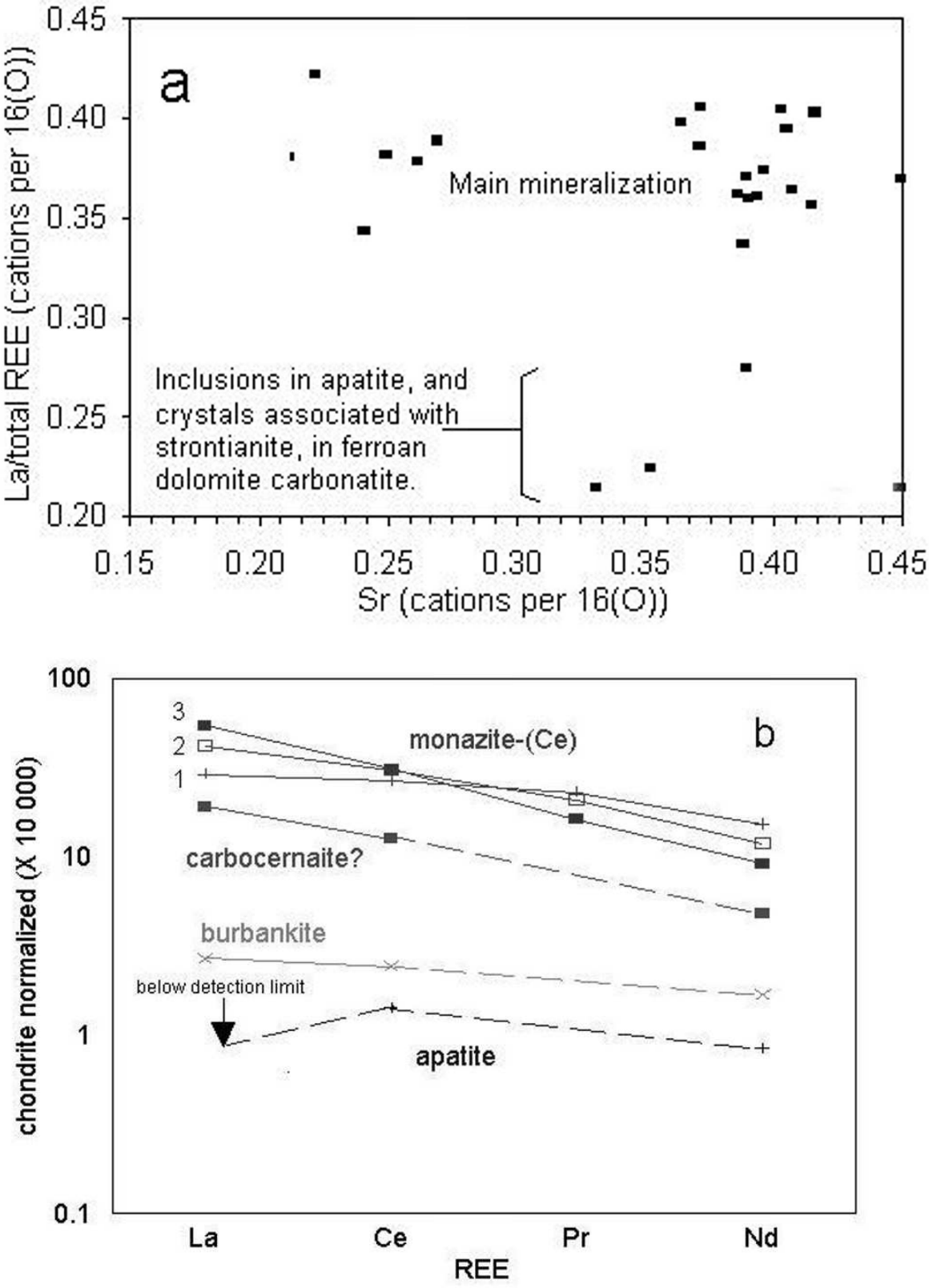

Fig. 6 (a, b).

bastnäsite needles always occur with the Fe oxide. Bastnäsite-(Ce) was previously reported at Nkombwa as needles replacing monazite in xenoliths of bastnäsite, barite, monazite and dolomite in ferrocarbonatite sills and dykes and silicified carbonatite [28]. These textures are similar to that of the bastnäsite in Figure 5d. It was concluded that the bastnäsite had formed by post-magmatic alteration of monazite to form a bastnäsite-rich rock which was then picked up and carried as xenoliths in later ferrocarbonatite dykes although no evidence of any equivalent xenoliths was found in this study. The acicular nature of the bastnäsite is similar to that reported in many other carbonatites [20] and thought to be indicative of hydrothermal formation [13].

NKOMBWA PARAGENETIC SEQUENCE

A general paragenetic sequence for Nkombwa carbonatites (Fig. 7) emphasizes the role of ferroan dolomite, lozenge-shaped apatite, pyrochlore and phlogopite as early, magmatitc, 'liquidus' phases; with burbankite, strontianite and monazite-(Ce) precipitating at the end of the magmatic phase in a transition environment and then the later suite of dolomite (low Fe), isokite, monazite-(Ce), bastnäsite-(Ce), daqingshanite, barite, sulphides, Fe oxides and quartz. This later

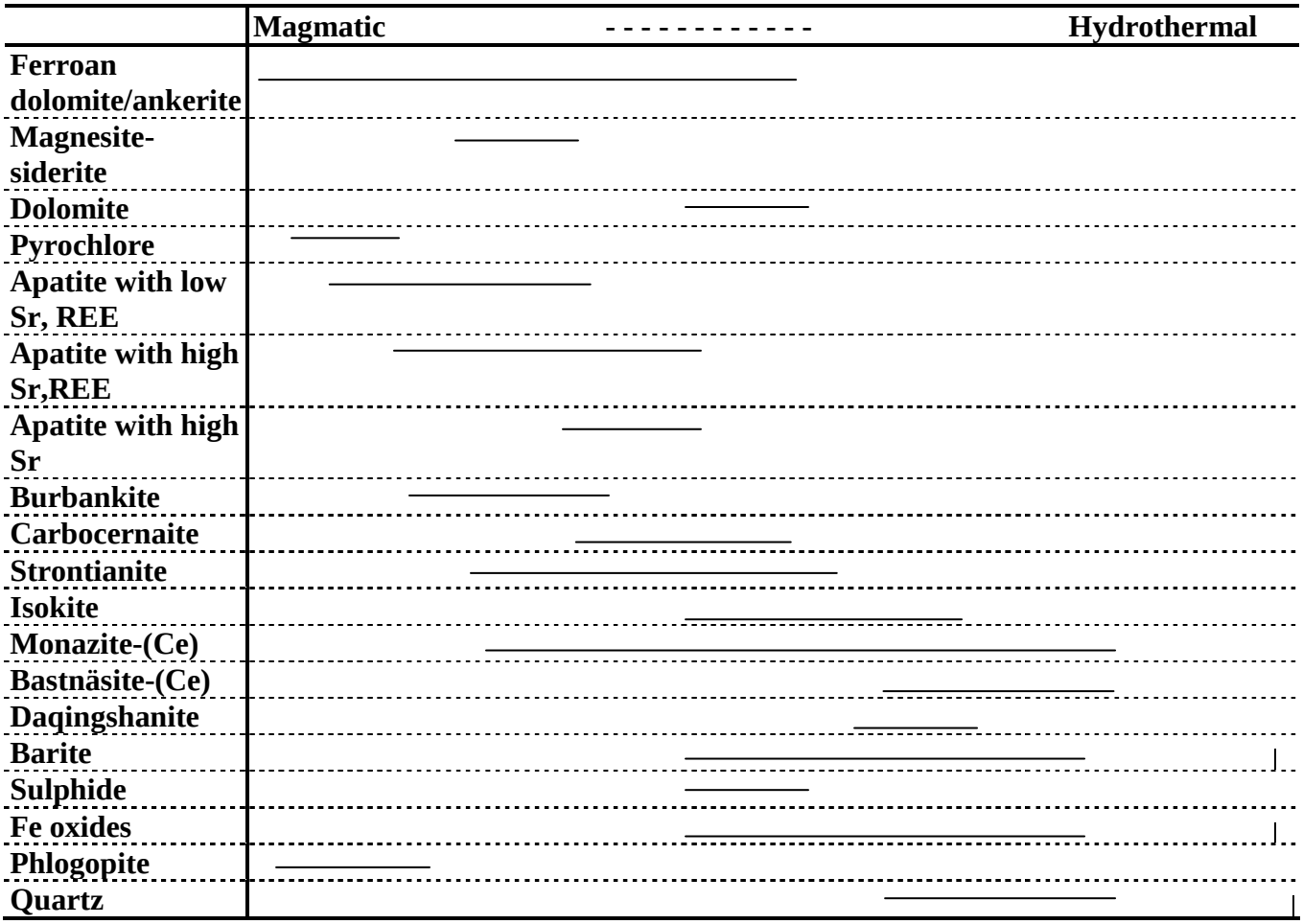

Fig. 7.

suite generally lacks apatite but contains isokite (Mg phosphate) instead. The magnesite-siderite carbonates are difficult to interpret but they are probably later than most of the ferroan dolomite. Quartz is part of the Sr,REE mineralization rather than a later introduction through weathering.

All of the minerals at Nkombwa are light REE-enriched but the degree of enrichment in the lightest REE, La and Ce increases through the paragenetic sequence. This is well illustrated by using the assemblage in apatite ferroan dolomite carbonatite (BM 1993, P6 (52) in which the minerals become progressively more rich in La from the apatite, to burbankite and carbocernaite to monazite-(Ce) (Fig. 6b). The mineralization is more light REE enriched than the magmatic and transition phases, as described for monazite above and the highest degree of light REE –enrichment occurs as a late phase in the mineralization, daqingshanite-(La).

MAGMATIC EVOLUTION

The mineral compositions and inclusions record a magmatic evolution towards more Sr and REE-rich compositions as crystallization of dolomite and apatite proceeded. The evolution differs slightly for different varieties of Nkombwa ferroan dolomite carbonatite, for example one type (sample BM 1993, P6 (102) has outer zones of apatite richer in Sr but not REE; this may be indicative of separate magma batches.

ROLE OF BURBANKITE – PEGMATITIC TRANSITION ENVIRONMENTS

The role of burbankite and miinerals of burbankite-like composition is potentially important because of the distinct occurrence and lack of association with other REE minerals. Burbankite, and carbocernaite are known from a number of carbonatites [23]. For example, blebs of burbankite were found in dolomite in dolomite and ankerite carbonatite at Chipman Lake, Ontario but not in a later ferrocarbonatite nor in the later REE mineral assemblage [18]. At Khibiny, Kola Peninsula, burbankite is the earliest in the sequence of rare earth minerals and forms pegmatitic crystals that are then pseudomorphed by an assemblage of ancylite-(Ce), REE fluocarbonates, strontianite and barite [26]. At Vuoriyarvi, Kola Peninsula, burbankite and calcioburbankite form both pegmatitic crystals that are pseudomorphed by a different REE mineral assemblage and also form blebs in host calcite or dolomite [23]. The conclusion is that burbankite is commonly the earliest in the sequence of REE minerals – and the question is to explain why. Fractional crystallization could produce the increase in the incompatible elements and Na required to form burbankite, leading to its crystallization in the final stages when the incompatible element concentrations are at their highest and pegmatitic crystallization most likely. Taking into account all occurrences, including Nkombwa, the main differences in composition between the later REE mineralising assemblages and earlier burbankite are the absence of sodium, and

presence of hydrated minerals (e.g. ancylite) and occasionally F, P and Si. The loss of burbankite represents a distinct change from a pegmatitc stage into a fluid-dominated, often metasomatic open system stage, of post-magmatic mineralization [23].

POST-MAGMATIC ALTERATION - ROLE OF SILICA AND REACTION WITH GROUND WATER AND COUNTRY ROCK

The post-magmatic mineralization at Nkombwa consists of veinlets of dolomite, monazite-(Ce), isokite and metasomatic replacement of carbonate by monazite-(Ce), isokite and quartz. The zone of silicification is mapped as a large area through the centre of Nkombwa (Fig. 1, [17, 28]) along the direction of faults. Stable and radiogenic isotope studies on similar monazite-(Ce) quartz mineralization in the Kangankunde carbonatite, Malawi [18, 19] show carbonatite-derived fluids with no evidence of significant contamination from surrounding country rock in all mineralization within the main complex. At 1.5 km from the main complex, it is possible to detect a crustal contribution in Sr and Nd isotope ratios [18, 19]. At Vuoriyarvi and Khibiny, isotopic study [25] showed some limited crustal contamination but the mineralising fluids are dominated by magmatic signatures. Of course, Nd and Sr levels in carbonatite, especially in REE-rich carbonatite are high so that they are insensitive to crustal contamination (see discussion of isotope systematics of REE-rich carbonatites in [4, 23, 25]. The burbankite may be destabilized when fluids exsolve from the magma and the most soluble components, notably Na, are dissolved away. These fluids react with previously crystallized material, producing pseudomorphs, and may either carry residual magmatic silica, or collect silica from the country rock (although again there is not yet any direct evidence for this country rock interaction). The Si is intimately linked to the mineralization (e.g. pools of strontianite, quartz and REE,Ca fluocarbonates in fresh carbonatite at Nkombwa (Fig. 2, c and d), and stable isotopic evidence from Kangankunde, Malawi [18]) and not introduced by subsequent weathering. Interaction with groundwater has been proposed as the main mechanism by which REE-rich hematite carbonatite formed from ferrocarbonatite at Fen, Norway [2, 3] but this reaction involved a 70% volume reduction and produced distinct La-depleted chondrite-normalised patterns in the minerals [1]. Neither feature is observed at Nkombwa, nor in most other late mineralization in carbonatites. Evidence of groundwater interaction was also detected in REE mineralised rocks with lower Sr contents at Barra do Itapirapuã, Brazil [4] where a two stage process was proposed: (1) a REE-rich hydrothermal fluid overprint to form the REE minerals and then (2) penetration by crust-derived fluids (groundwater).

RELATIONSHIP TO FENITIZATION

The relationship between fenitization, present at Nkombwa and the other similar localities mentioned above, and the REE mineralization has between

reconciled as two main stages of fluid release by analogy with granitic magmas [18]. First boiling occurs owing to pressure release as the magma rises, releasing a Na, K-rich fenitising fluid and initiating crystallization. A second boiling event occurs after build up of the remaining volatile (fluid) components in the magma during crystallization and this forms the REE mineralising fluid.

A perennial question regarding fenitization is whether silica, depleted in fenite with respect to country rock, could have exchanged back into the carbonatite magma. The first and second boiling hypothesis means that the fenitization and mineralization processes are closely linked and the country rock may be a source of the silica in the mineralization, but there is no direct evidence yet of any such link.

CONCLUSIONS

The Sr and REE contents of minerals and mineral assemblages and compositions record three phases in the evolution of the Nkombwa carbonatite complex. These stages are probably common to many carbonatites including Kangankunde, Malawi; Khibiny and Vuoriyarvi, Russia; Barra do Itapirapuã, Brazil; Chipman Lake, Canada.

1. A simple magmatic evolution occurs in dolomite carbonatite, increasing Sr and REE concentrations. Fe contents also increase in rock-forming carbonates.

2. A pegmatitic stage follows, for which burbankite is an indicator mineral.

3. Post-magmatic REE mineralization consists of veinlets and metasomatic alteration. At Nkombwa this consists of monazite-(Ce), isokite +/- low Fe dolomite and quartz The fluid components are largely carbonate-derived but local crustal and groundwater interaction may occur, especially to form the quartz-rich rocks. Results from different complexes vary and more work is required to clarify how hydrothermal systems function around carbonatites.

4. A further stage of alteration caused by weathering or intense hydrothermal alteration may cause considerable volume reduction and further concentrate REE, as at Fen, Norway, but is not the main factor in most REE-rich carbonatites.

ACKNOWLEDGEMENTS

I would like to express my thanks to the organisers of the conference for their kind invitation to contribute this paper.

REFERENCES

1. **Andersen, T.** (1986) Compositional variation of some rare earth minerals from the Fen complex (Telemark, SE Norway): implications for the mobility of rare earths in a carbonatite system. Mineralogical Magazine, 50, 503-509.
2. **Andersen, T.** (1987) A model for the evolution of hematite carbonatite, based on whole rock major and trace element data from the Fen complex, southeast Norway. Applied Geochemistry, 2, 163-180

3. **Andersen, T.** (1987) Mantle and crustal components in a carbonatite complex, and the evolution of carbonatite magma: REE and isotopic evidence from the Fen complex, southeast Norway. Chemical Geology (Isotope Geoscience Section), 65, 147-166.
4. **Andrade, F.R.D., Möller, P., and Höhndorf, A.** (1999) The effect of hydrothermal alteration on the Sr and Nd Isotopic Signatures of the Barra do Itapirapuã Carbonatite, Southern Brazil. Journal of Geology, 107, 177-191.
5. **Appleton, J.D., Bland, D.J., Nancarrow, P.H., Styles, M.T., Mambwe, S.H. and Zambezi, P.** (1992) The occurrence of daqingshanite-(Ce) in the Nkombwa Hill carbonatite, Zambia. Mineralogical Magazine, 56, 419-422.
6. **Bell, K. and Blenkinsop, J.** (1989) Neodymium and strontium isotope geochemistry of carbonatites. Pp 278-300 in: Carbonatites: genesis and evolution (K. Bell, editor) Unwin Hyman, London.
7. **Bulakh, A.G., Nesterov, A.R., Zaitsev, A.N., Pilipuk, A.N., Wall, F. and Kirillov, A.S.** (2000) Sulfur-containing monazite-(Ce) from late-stage mineral assemblages at the Kandaguba and Vuorijarvi carbonatite complexes, Kola Peninsula, Russia. Neues Jahrbuch für Mineralogie Monatschefte, 2000, 217-233.
8. **Deans, T.** (1966) Economic mineralogy of African carbonatites. In: Carbonatites. (O.F.Tuttle and J. Gittins, eds) John Wiley & Sons, New York, 385-413.
9. **Kukharenko, A.A., Bulakh, A.G. and Baklanova, K.A.** (1961) Sulfate-monazite from carbonatites of the Kola peninsula. Zapiski Vserossiskogo Mineralogicheskogo Obshchestva, 90, 373-381.
10. **Lapin, A.V.** (1989) Typomorphism and genesis of strontiopyrochlore and bariopyrochlore, Doklady Earth Science Section, 296, 151-155.
11. **Lumpkin, G.R. and Ewing, R.C.** (1995) Geochemical alteration of pyrochlore group minerals: pyrochlore subgroup. American Mineralogist, 80, 732-743.
12. **Mariano, A.N.** (1989) Nature of economic mineralization in carbonatites and related rocks. In carbonatites: genesis and evolution (K. Bell, ed.). Unwin Hyman, London, 149-176.
13. **Mariano, A.N.** (1989) Economic geology of rare earth minerals. In Geochemistry and mineralogy of rare earth elements, B.R. Lipin and G.A. McKay (eds), 307-37. Mineralogical Society of America, Reviews in Mineralogy, 21.
14. **Platt, R.G. and Woolley, A.R.** (1990) The carbonatites and fenites of Chipman Lake, Ontario. Canadian Mineralogist, 28, 241-250.
15. **Reeve, W.H. and Deans, T.** (1954) An occurrence of carbonatite in the Isoka District of Northern Rhodesia. A preliminary account. Colonial Geology and Mineral Resources, 4, 271-281.
16. **Snelling, N.J.** (1965) Age determinations on three African carbonatites. Nature, 205, 491.
17. **Turner, D.C., Andersen, L.S., Punukollu, S.N., Silwa, A. and Tembo, F.** (1989) Igneous phosphate resourced in Zambia. In: Phosphate Deposits of the World, Volume 2: phosphate rock resources. Eds A.J.G. Notholt, R.P. Sheldon and D.F. Davidson, Cambridge University Press, Cambridge, 247-257.
18. **Wall, F.** (2000) Mineral chemistry and petrogenesis of rare earth-rich carbonatites with particular reference to the Kangankunde carbonatite, Malawi. PhD thesis, University of London, 340 pp.
19. **Wall, F., Barreiro, B.A. and Spiro, B.** (1994) Isotopic evidence for late-stage processes in carbonatites: rare earth mineralization in carbonatites and quartz rocks at Kangankunde, Malawi. V.M. Goldschmidt Conference Extended Abstracts, Mineralogical Magazine, 58A, 951-952.
20. **Wall, F. and Mariano, A.N.** (1996) Rare earth minerals in carbonatites: a discussion centred on the Kangankunde Carbonatite, Malawi. In: Rare Earth Minerals: chemistry,

origin and ore deposits (A.P. Jones, F.Wall and C.T. Williams, eds) The Mineralogical Society Series, 7, Chapman & Hall, London, UK, 193-225.

21. **Wall, F., Williams, C.T., Woolley, A.R. and Nasraoui, M.** (1996) Pyrochlore from weathered carbonatite at Lueshe, Zaire. Mineralogical Magazine, 60, 731-750.
22. **Wall, F. Williams, C.T. and Woolley, A.R.** (1999) Pyrochlore in niobium ore deposits. Mineral Deposits: Processes to Processing. Stanley et al. (eds) Balkema, Rotterdam, 687-690.
23. **Wall, F. and Zaitsev, A.N.** (2004, in press) Rare earth minerals in Kola Carbonatites. In: Phoscorites and carbonatites from Mantle to Mine: the Key Example of the Kola Alkaline Province. (F. Wall and A.N. Zaitsev, editors) Mineralogical Society Series, 10, Mineralogical Society, London.
24. **Woolley, A.R. and Buckley, H.A.** (1993) Magnesite-siderite series carbonates in the Nkombwa and Newania carbonatite complexes. South African Journal of Geology, 96, 126-130
25. **Zaitsev, A.N., Demény, A., Sindern, S. and Wall, F.** (2002) Burbankite group minerals and their alteration in rare earth carbonatites - source of elements and fluids (evidence from C-O and Sr-Nd isotopic data). Lithos, 62, 15-33.
26. **Zaitsev, A.N., Wall, F. and Le Bas, M.J.** (1998) REE-Sr-Ba minerals from the Khibina carbonatites, Kola Peninsula, Russia: their mineralogy, paragenesis and evolution. Mineralogical Magazine, 62, 225-250.
27. **Zambezi, P.** (1995) Geochemistry of the Nkombwa Hill Carbonatite Complex of Isoka District, Northeast Zambia, with special emphasis on economic minerals. Thesis, Free University of Amsterdam, 121 pp.
28. **Zambezi, P., Voncken, J.H.L., Hale, M. and Touret, J.L.R.** (1997) Bastnäsite-(Ce) at the Nkombwa Hill carbonatite complex, Isoka District, northeast Zambia. Mineralogy and Petrology, 59, 239-250.

UDK 550.311:551.24:553.061.12

Mantle cycles: a modern insight

Balashov Yu.A., Glaznev V.N.

Geological Institute, Kola Science Centre, Russian Academy of Sciences, Apatity, Russia

The statistic analysis of the geochronological database (over 14200 datings) has been performed using the method of stochastic total information description individually for Earth's upper mantle and crust through the whole interval of geological time. The evolutional dynamics of the two upper covers has been established to differ, i.e. mantle processes were intensive in the period of simultaneous endogenous activation within the both covers, while the abrupt reduction in the upper mantle activity occurred in the periods of endogenous attenuation. The difference is an objective criterion for identifying maximum duration of the mantle cycles, which turned out to be different for the Early-Middle Archean, Late Archean-Proterozoic and Phanerozoic. These conclusions have been checked by the examples of geochronological data systematization according to the total data and the samples of various subalkaline and alkaline rock types. It has been shown that the distribution of five groups of subalkaline and alkaline rocks in the interval of the Late Archean-Phanerozoic compilies with the stages of the mantle cycles recognized by the total data for the upper mantle igneous rocks. Since the rocks of increased alkalinity represent one type of plume magmatism, their permanent participation in every revealed mantle cycle emphasizes the importance of this magmatism in the evolution of the crust-mantle system through the geological history of the Earth. The Sr and Nd initial isotope ratios in the alkaline series are divided into two groups, one of them having isotope parameters typical of the mantle, the other being characterized by the crustal values. The mantle isotope ratios are generally traced on the whole geological interval of the rocks dated, and the role of the crustal isotope tracers increases from the Archean towards the Phanerozoic, this reflects on the whole an intensified fluid effect on the magmatic processes both at the initial magma generation, and at the magma consolidation in the crust. Since the source of the alkaline magmas formed during the mantle metasomatism, which enriched magma-generating zones with incoherent elements, repeated acts of such a process in the separate mantle zones should result in the abnormal element accumulation, and that would affect generated alkaline magmas.

INTRODUCTION

More than 40 years ago the irregularity in the evolution of the continental crust-forming processes [1], which is now called «megacyclicity» [2], was first discovered. Over this time the issue of the crustal growth has over and over again been discussed, and if the unique assumption [3] that the whole crust formed at the early stage of the Earth's life, would be left our, the other authors primarily on the basis of geochronological data consider the megacyclicity as a reflection of successive, but irregular crust growth in the course of the geological time. These ideas bore initially on combination of the datings on the rocks and minerals of the

crust and upper mantle into the uniform system. Such an approach to the data systematization either postulated essentially geochronological identity between the endogenous events within the upper mantle and crust, or disregarded forcedly possible distinctions, and thereby estimated only roughly the boundaries of the supposed megacyclicity. The difficulties in interpreting the results were aggravated with the fact that the revealed peaks and boundaries between the megacycles varied depending on the use of the data obtained by K-Ar, U-Th-Pb, Rb-Sr dating techniques [1]. The same difference was corroborated with the advent of fresh statistic generalizations including the Sm-Nd [4] and U-Pb [5] data, their correlation with the earlier publications [1, 2 etc.]. It is reasonable that the issues on the causes of these differences arose, and as a consequence, the resolution of the problem concerning the global cyclicity took again on current importance.

As far back as the 80-ies of the last century it was shown that the continental crust contained excess bulk of some lithophile elements (Rb, K, Th, U, Sr, LREE) as compared with their content in the upper mantle, if its initial composition would be identical with the average mantle composition [6]. The same conclusion is even obvious, if we compare the budget of the continental crust with the real depleted upper mantle sources for the oceanic and island arc basalts [7 etc.].

The last decade was the epoch of the comprehensive investigations in the field of the upper mantle hot spot and lower mantle superplume substance origin and transfer into the external geospheres, which have been regarded as a most probable mechanism of the endogenous activation. Hence, there appeared two interrelated aspects of work: tectonic and petrological-geochemical, which were clarified after the new paradigm of the global tectonics had been formulated. The paradigm unified the ideas of plate tectonics and lower mantle plumes [8], and that served in fact as a basis for the development of modern ideas of the deep geodynamics, and met the actual confirmation:

- in the latest seismic data on the structure and physical properties of the lower mantle (tracing the subduction down to the lower mantle boundary, identifying the boundary layer D”, estimating the levels of the middle mantle and transitional layer) [9, 10 etc.];
- in the detection of the anatomy of the properties and the rotation of the inner core[11];
- in the model estimations of the ultradeep liquid core energy and lower mantle flow properties effect on the conditions of incipient and moving superplumes into the upper mantle and crust [12-14];
- in the development of the petrological and geochemical mantle metasomatism criteria under the subduction and in the zones of the upper mantle under the influence of plumes [15-17];
- in the model estimations of the plume-lithosphere interaction [16-18];
- geological, petrological and geochemical criteria for identifying the effect of the superplume on the upper mantle magmatism, were concurrently worked out [19-28 etc.].

However, almost all listed model arguments and actual observations concern primarily the modern structure of the mantle and core, and do not overstep the limits of the Phanerozoic mantle magmatism. Therefore, the issues of the mantle magmatism evolution within the 4.5 Ga history of the Earth's history remain relevant.

Thus, today we should again appeal to the analysis of the geochronological information in order to reveal and ground the criteria of the endogenous cyclicity in the Earth's mantles, to the generalization of the isotope-geochemical data in order to elucidate the intensity of the interaction of these processes between the crust and mantle, taking into account the effect of the Earth's surface tectonics and deep geodynamics. This paper focuses mainly on some aspects of these global problems.

STOCHASTIC DESCRIPTION OF GEOCHRONOLOGICAL DATA

Recently examples of statistic time data systematization [29-31] through the factorisation on the infinite and infinite bases, including method of correlation degree of stochastic processes, have appeared.

This paper focuses on the methods of stochastic time data analysis considering problems of a significant variation range with the precision of actual geochronological datings and nonequilibrium presentation of data on various rock types. Given approach to the geochronological information deals with the age datings regarded as normal stochastic processes, which are realized within some determined interval [32], and to which one can apply slightly transformed advanced modern analyzing techniques for steady-flow and transient processes [33, 34]. Numerical presentation implementation is possible only at the discrete step, Δt, which should answer the settled tasks of signal analysis. Thus, for example, if the analysis with a 10-20 m.y. step, which answers on average the precision of individual age estimations of endogenous processes, is suitable for revealing the statistic mechanisms for the Precambrian, the processing with a 2-5 m.y. step (or an even less step if the case is the Miocene or Quaternary), which is on average correspond to the existing chronostratigraphic scales, should be employed for the Phanerozoic. It stands to reason that the resulting probability density plot depends on the time log, Δt, but the most essential in this idea is the possibility to apply the whole body of signal analysis to the obtained probability estimations, $P(t)$ (e.g., plotting wavelet spectrograms for probable process density etc.) [33, 34].

TWO TYPES OF MEGACYCLICITY ?

Over the last 10-15 years a huge body of geochronological information has been accumulated. Its further generalization allows addressing to the problem of

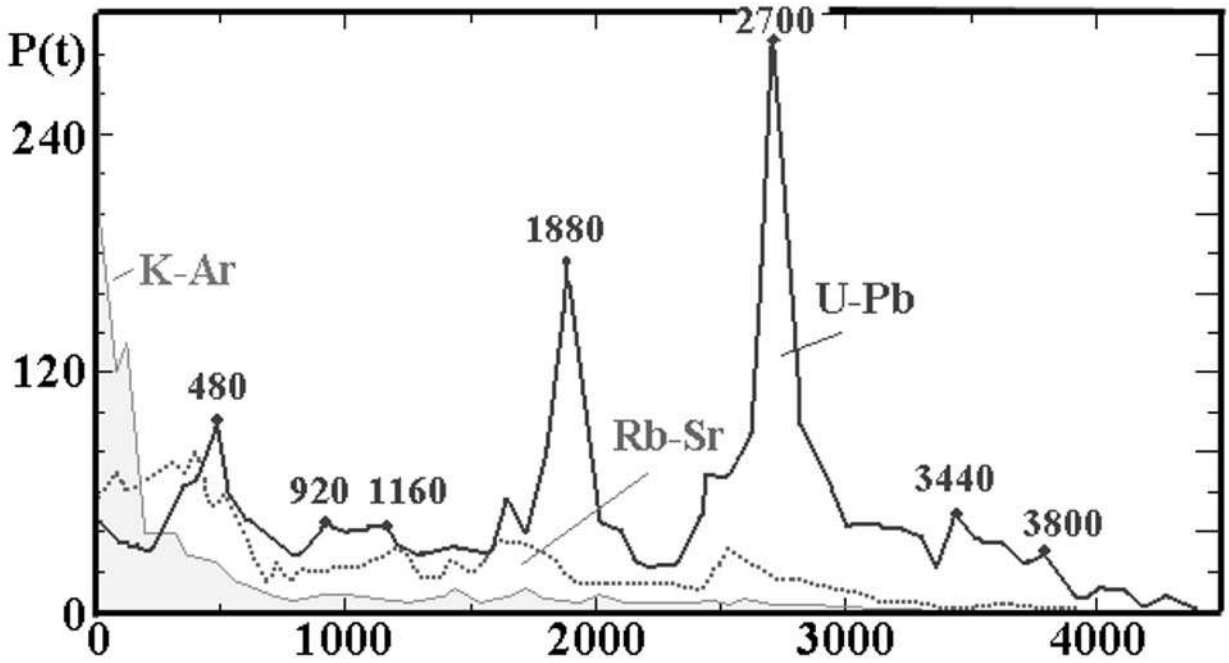

Fig. 1. **Prevalence hystogram of datings obtained by three geochronological methods for total of the upper mantle and crust rocks and minerals.**

Statistic evolvent ($P_t \approx$ number of datings) is carried out with the averaging step in 20 m.y. For plotting the diagrams for each method only maximum values of P_t, which were logged within the interval of 0-4400 m.y. Digits in rectangles indicate U-Pb peaks of megacyclicicty.

megacyclicity. And this is more relevant, since modern achievements in the field of the Earth's structure and deep geodymanics' investigations have provoked into modernizing essentially the geological-tectonic, petrological and geochemical ideas of the mantle and crust evolution. Thus, there arose a need to correlate various aspects of geological attainments with geochronology, which provides quantity measure for judging the dynamics of crust-forming processes reflected in the plate and plume tectonics, and to associate them with the evolution of the Earth's internal mantles and core's energy and with the possible external effect on some mantles.

Before we move to the discussion of the problems settled, let us look into the possibilities and restrictions in applying the geochronological methods to the phenomenon of megacyclicity. The paper deals with the fundamental databank (over 14200 datings), which collects together published data obtained by different methods: U-Th-Pb (or U-Pb) – 8229; Rb-Sr – 3330; K/Ar + $^{40}Ar/^{39}Ar$ +FT (or K-Ar) - 2054; Sm-Nd – 650 datings. It should be noted that each method is represented by a large body of datings, this, on the basis of the stochastic description technique, allows apparently drawing some well-reasoned conclusions. The results of systematization show (Fig. 1) that the information fields for each method differ essentially. As it should have been expected, the U-Pb data are most ambient, except for the Meso-Cainozoic interval. In contrast, K-Ar and Rb-Sr

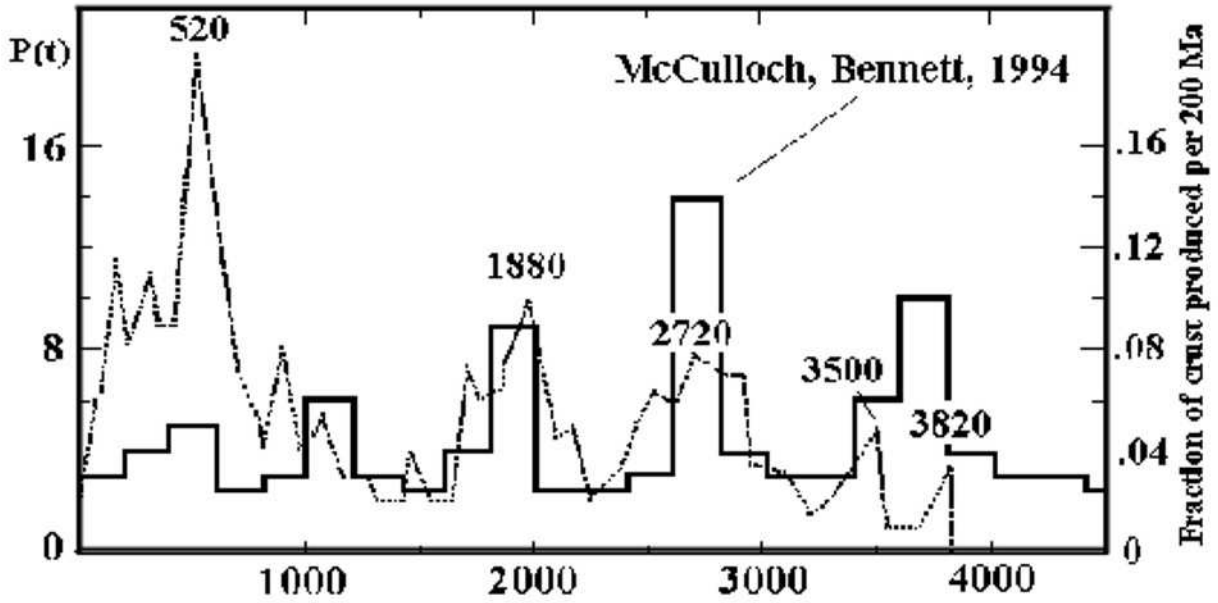

Fig. 2. **Correlation of Sm-Nd data systematization results obtained using the method of nonparametric statistic (P_t) in the range of 0-4.5 Ga by all maximums revealed at the averaging step of 20 m.y., and model method of statistic averaging step of 200 m.y. [4].**

In the latter case, the peak height is given as a part of the total crust mass formed over 4.5 Ga. Rectangles show the age of maximal megacyclicity peaks after the new data.

dating yielded the main data file on the endogenous events in the Phanerozoic. The information with the use of these two methods reduces abruptly at the transition from the Phanerozoic to the Proterozoic and Late Archean, but in the range of more than 3.1 Ga it is hardly representative for revealing peaks of megacyclicity. The only histogram registering stages of the continental crust growth with the use of Sm-Nd dating technique was published by M.T. McCalloh and V.S. Bennett [4] after the data for Australia. The correlation of the sample from our databank (650 datings for different regions) and the data for Australia indicates a satisfactory similarity, in spite of the difference in the averaging step (Fig. 2). The Sm-Nd ages of maximums are possible to clarify.

The result for main peaks (Ma) by the Sm-Nd system (3820, 3500, 2720, 1880, 520) conforms with the maximal U-Pb peaks (3800, 3440, 2700, 1880, 480).

By detecting the Rb-Sr megacyclicity peaks, sampling from our databank included 3330 datings, that exceeds about three times the data (1108 datings) used by Yu.D. Pushkarev [2] for the same purpose. Though, between the two systematizations, in spite of the difference in the methodology, there is a similarity in distribution of maximum megacyclicity peaks for the whole interval of the geological time (Fig. 3; detailed Phanerozoic – Fig. 4). The peak ages – our data / data after [2] correspond (Ma) : 3660-3620 /≈ 3600; 2520/ 2600; 1620-1720/1650; 1220/1100; 405/420; 125/160.

The K-Ar method yielded the ages of maximum peaks of (Ma) 2600, 2020, 1720, 1440, 330, 125, 80, 0-15 (Fig. 1 and 4). In the both cases maximum Rb-Sr and K-Ar peaks no not coincide with the U-Pb and Sm-Nd systematization, being

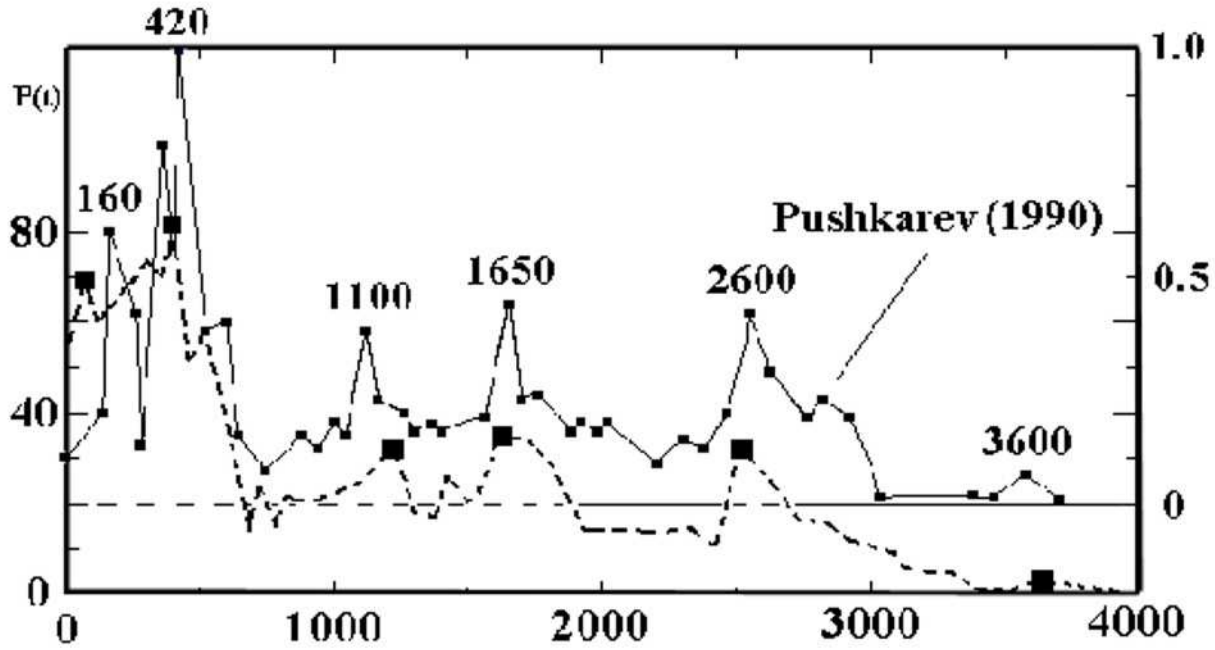

Fig. 3. **Correlation of Rb-Sr dta systematization results obtained using the method of nonparametric statistic (P_t) in the range of 0-4 Ga by all maximums revealed at the averaging step of 20 m.y., and using the moving-average method for an elementary square200 m.y.on side [2] and conditional normalization be maximum peak (taken as1 1).**

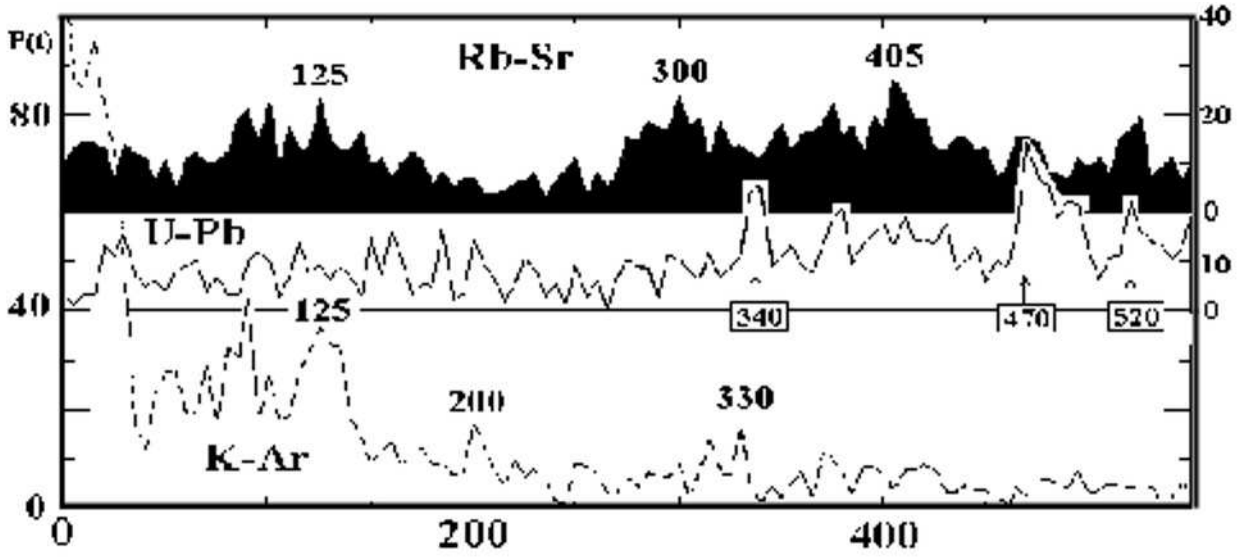

Fig. 4. **Refinement of the age position of main megacyclicity peaks by the data for different geochronological methods using nonparametric statistic (P_t) with a step of 5 m.y.**

essentially shifted towards rejuvenation by 50-100-200 Ma. It should be noted that this conclusion is not a novel, since it can be easily drawn in the first work «on the distribution of mineral data in time and space» [1].

Thus, there is formal evidence of the two types of megacyclicity. The U-Pb and Sm-Nd isotope systems are regarded by the majority of geochronologists as

the most proof against late superimposed processes in comparison with Rb-Sr and K-Ar systems, that is particularly important for the Precambrian. All stated above implies that dating by various methods fixed predominantly different endogenous events and in different proportions. If we compare the observed data on the megacyclicity with the modern insight [8] into the deep geodynamics, such a megacyclic bifurcation does not disclose the essence of the effect of two main processes – plate and plume tectonics. Searching for the acknowledgment of these ideas on geodynamics on the basis of total information on geochronology of the two upper shells is fruitless.

The principle of uniting the information on the crust and the upper mantle itself seems to date old-fashioned and useless for interpreting the set of the processes which controlled the cycling of the crust-forming processes. Such a conclusion arises from the chain of contradictions. The first is related to the huge range of the difference in datings' amount, which are joined into one or another geochronological method, that is reflected in the difference of maximum (megacyclic) peak age estimation, and chiefly in the contrast of the relative endogenous intensity estimation (i.e., in presence or absence of the Phanerozoic megacycles). On the other hand, the published geochronological data on the different types of igneous rocks do not coincide with the considerable variations in the middle and regional prevalence of the main rock types. Second, the significant contrast in the prevalence of the rocks between the Precambrian and Phanerozoic regions has been ignored. These facts cause a false summation of theb geochronological information, since such an approach obviates the importance of concrete geological processes. The same is applied to the attempt [35, 36 etc.] of searching for the global (100 m.y.) periodicity in the relative prevalence of the rocks by the total data on the crust and mantle. In this case it would be turned out that the «abnormal» peaks, which occur within the 100 m.y. cycles and are higher or equal to the adjacent ones, prevail during the last 2 Ga in regard to the deeper Precambrian. As a result, as well as analyzing the grater event of megacyclicity, no unambiguous solution of the process types is possible to arrive at. One may just suggest that such a situation results from the superimposing of the diverse events proceeded in the crust and mantle and/or within each of the geospheres. Thus, there appears a need for more specified original research of the crustal and mantle events.

CRUST - UPPER MANTLE SYSTEM

Since today there is sufficient information separately for the crust and mantle, the first step should concern examining the features of the endogenous events in either of the two upper Earth's shells in order to decide a point of similarity and discrepancy measure in the dynamics of their evolution. Let us note that the summation of the geochronological data by the separate shells does not remove all the contradictions which have been stated above for the «bulk» analysis by the

total data for the crust and mantle, but provides corrections to the difference of processes between the two shells.

The overall distribution histogram of the datings (Fig. 5) obtained by every method separately for the crust (9808 datings) and mantle (4435 datings) allows surely asserting that the megacyclicity is registered in the two upper shells with major, maximum («megacyclic») peaks, which tend on the whole to the U-Pb systematization for the total crustal and upper mantle data. It is possibly a consequence of the prevalent U-Pb datings in the body of the information. Almost all megacyclic and other peaks conform roughly to each other for the two shells (crust/mantle, Ma): peaks for the Early and Middle Archean - 3800/3820, 3620/3640, 3520/3500, 3300/3310, 3220/3220 are almost equal in height for the crust, and it keeps from revealing any major peak among them, for the mantle the highest peaks have the ages of 3440 and 3500 Ma; for the late Archean there is a single megacyclic maximum of 2680/2710 Ma and two less clear peaks of 2920/2920, 2820/2810 Ma; for the Proterozoic there is one megacyclic peak of 1880/1880 Ma and many minor ones of 2520/2500, 2420/2440, 2320/2320, 2220/2200, 2100/2100, 2020/1980, 1720/1720, 1660/1640, 1500/1520, 1420/1440, 1300/1340, 1220/1260, 1140/1140,1020/1000, 920/920, 820/800, 720/740 Ma, where it is not possible to isolate reasonably other megacyclic varieties, since for the crust and mantle such maximums can differ in time of appearance and intensity (i.e., for the interval of 1400-900 Ma); for the Phanerozoic scale with a step of 20 m.y. is rough and discloses only one megacyclic peak with the age of 400/410 Ma, and at a step of 5 m.y. one can observe a similarity only for the peaks of 475/475, 400/410, 375/375 and 90/90 ma; the rest maximum peaks for the crust and mantle are not consistent (i.e., there is a individual peak for the mantle with the age of 120 Ma, Fig.5). This is evident of the signs of the certain autonomy in the evolution of the endogenous processes within the shells for the Phanerozoic. In this connection let us note that the clearest megacyclic peak of the Late Archean splits into two datings: ca. 2710 Ma for the mantle, 2680 Ma for the crust (Fig. 5), that can also be regarded as a sign of difference in the intensity of endogenous activity between the two shells.

In order to contour the duration of megacycles to a first approximation, using the episode of fall in or loss of the endogenous activity in the crust and mantle shows considerable promise. Similar episodes are divided roughly into two groups (Fig. 5). The first group corresponds with the almost simultaneous for the two shells release of the endogenous activity, and is marked by vertical arrows at Figure 5. The second one is predominantly for the crust or mantle. The minimum ages of the first group can be considered as natural boundaries of the megacycles. Such an interpretation of these boundaries was earlier proposed [2]. The data on the first group yield the following datings (Ma) : ≈ 3900, ≈ 3600, 3380, 3140, 2260, 1360, 940-960, 880, 645, 210 and 60. This list can be expanded or reduced at discretion of the researcher. At this approach, the accepted criteria of falling endogenous activity exclude completely or partially the data on the second group,

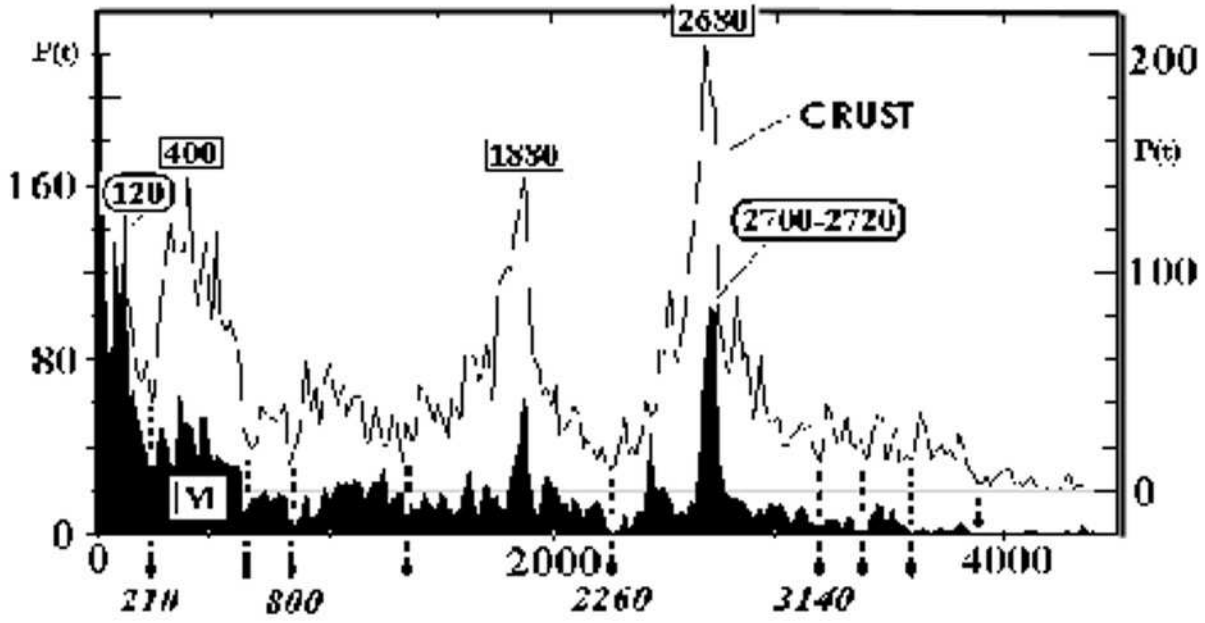

Fig. 5. **General lines of the endogenous evolution in the mantle (M) and crust registering irregularity in the crust evolution – stages of maximum and minimum activation in the two shells.**

Dash-spot lines with arrows indicate clearest episodes of minimums correlated in the mantle-crust system. The diagram is plotted using statistic parameter (P_t) with an averaging step of 20 m.y. Digits in rectangles indicate the age of megacyclicity peaks for the crust, digits in ovals – for the upper mantle.

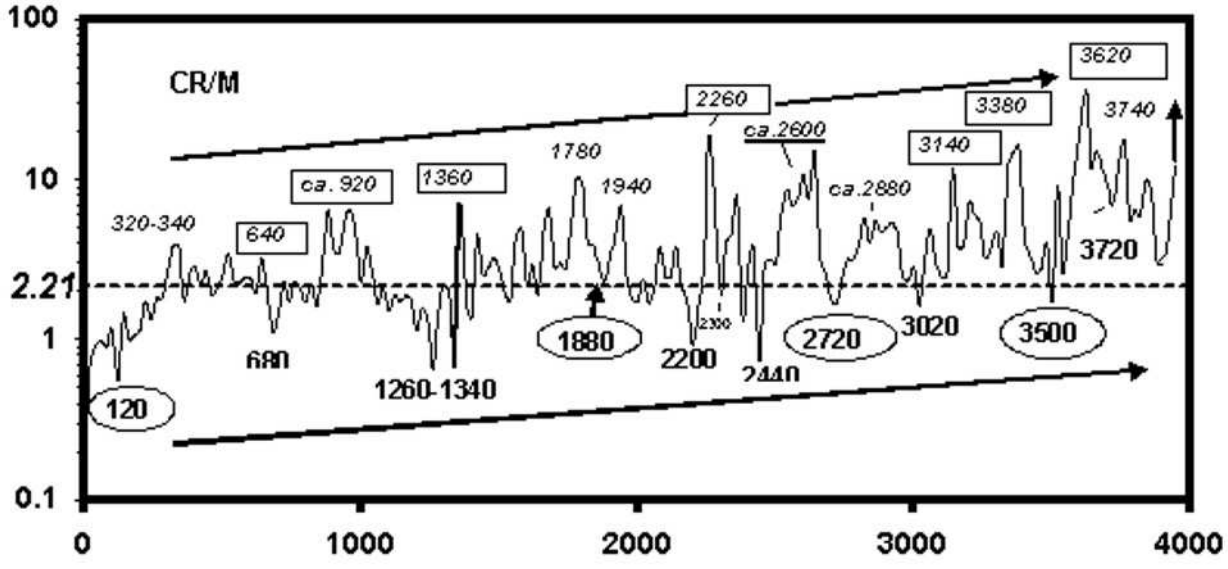

Fig. 6. **Variation in the ratio of datings' amount between the crust and upper mantle (CR/M) in the range of 0-4000 m.y.**

Digits in ovals correspond to the age of megacyclicity peaks, digits in rectangles – to the age of minimal endogenous activity in the two shells (after Fig. 5). Arrows show tendency to enhancing CR/M ratio from the Phanerozoic to the Precambrian. The averaging step is 20 m.y.

this provides subjectivity when outlining the boundaries. In order to get factual picture of the variation in the endogenous intensity within the two shells, let us employ the ratio of crust/mantle peaks (CR/M) in the range of 0-4.0 Ga (Fig. 6). This approach allows excluding «apparent effect» (Fig. 5) of the simultaneous influence of the megacyclic activation of the processes in the mantle on the endogenous intensity in the crust. Since the initial average ratio of the crustal and mantle datings is 9808/4935 = 2.21, it can be regarded as a basis for the comparison of the CR/M values and their variation through the geological time. It should be noted that the maximum CR/M values correspond to the datings of simultaneous minimums revealed at the histogram of the crustal and mantle peaks, and minimum ones – to the megacyclic maximums (Fig. 5). Moreover, Figure 6 fixes a series of other peaks in the two zones of the extreme CR/M values, which were left out of account when analyzing the data (Fig. 5). It is obvious that the so-called megacyclic peaks are not different from the other ones. Furthermore, among the megacyclic peaks there are varieties with less contrast CR/M values. However, the fact that the intervals of simultaneously falling activity in the two shells are evident of the primary reducing mantle endogenous activity is more substantial. In other words, against the background of loss or abrupt attenuation of the mantle processes, the crustal ones go on. In contrast, the areas with the minimum CR/M peaks, including unique megacyclic, correspond to the abrupt predominance of the upper mantle endogenous processes over crustal ones.

The existence of the extreme deviations from the average CR/M ratio (Fig. 6) allows describing rigorously the boundaries and cycle amount, but the cycles themselves acquire some different contents and thus indicate the relative activation of the processes in the crust and mantle. If we use an age series of the maximum CR/M ratios, that is consistent by implication to the optimal fall in the mantle endogenous events, and thus to the registration of the boundaries of the mantle cycles, the obtained series of the intervals (shown in brackets) can be divided into three groups:

1) in the Phanerozoic group, according to the refined data (Fig. 7) for the interval of 0-330 Ma, the mantle magmatic CR/M values of more than 2.21 prevail sharply, that makes it difficult to estimate reliably the cycles, among whose for the youngest (Cainozoic) episodes there is just a relative division into the episodes of 0-10 (10), 15-30 (15) and 35-40 (5) Ma; moreover, by the maximums of the CR/M ratios there are episodes of 40-60 (20), 60-100 (40), 100-145 (45), 145-210 (65), 210-265 (55), 265-330 (65), 330-415 (85), 415-515 (100) and 515-645 (130) Ma, that reflects on the whole the directed growth in the duration of the mantle cycles toward the Precambrian systems;

2) the Proterozoic cycles are restricted by the intervals of 640 – ≈ 920 (≈ 280), ≈ 920 -1360 (≈ 440), 1360-1780 (420), 1780-2260 (480) and 2260-2600 (340), which define on average the cycle duration of ca. 390 Ma; these cycles are close in duration to the «Wilson's cycles», which have been long defined in the geotectonic reconstructions;

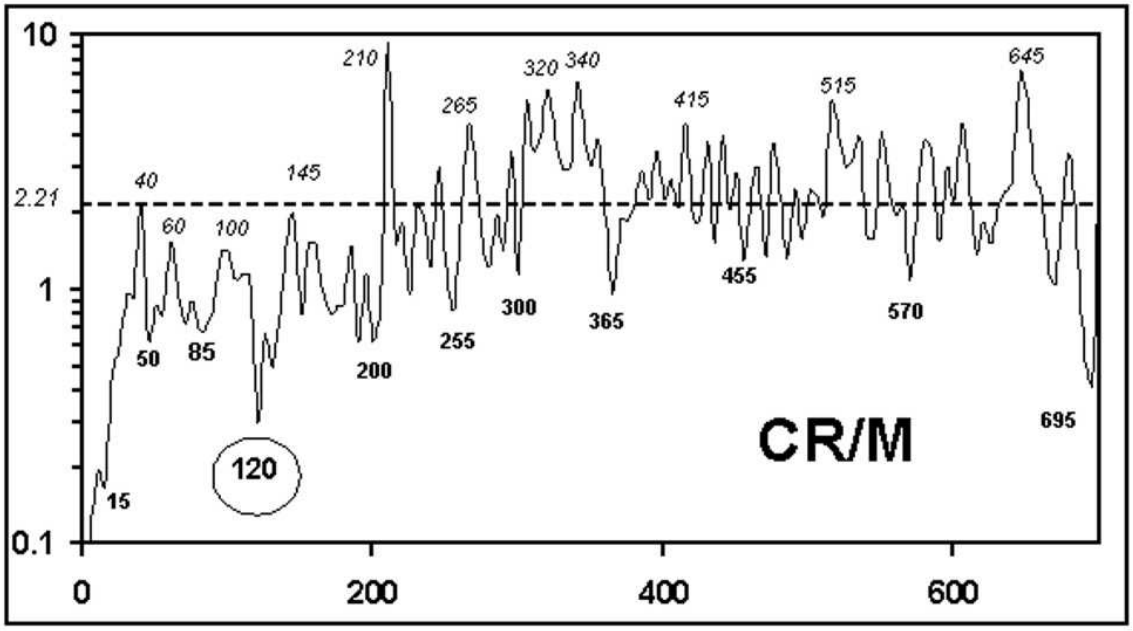

Fig. 7. **Specification of the variation in the CR/M ratio in the Phanerozoic, averaging step is 5 m.y.**

The digit in oval corresponds to the mantle peak showed at Figure 5.

3) for the Archean cycles there is a sequence of 2600-2880 (280), 2880-3140 (260), 3140-3380 (240), 3380-3620 (240) and 3620 – ≈ 3920 (≈ 300), which corresponds to the average value of ca. 265 Ma; limitation of the information for the early Archean determines relative estimation of two larger ancient cycles and extrapolation into the interval of 3900-4100 Ma, for which according to the data on the detrital zircons, the 100- and 200 m.y. cycles are possible.

Thus, there is alternation in the relative activation of the endogenous processes in the crust and upper mantle and difference in the duration and position of the mantle cycles in the geological history, this denotes unambiguously the contrast in the evolutional dynamics of the two upper shells of the Earth. To a first approximation the cyclicity considered can reflect «retarding» and more delayed (time-expanded) reaction of the crust on the processes, which were initiated in the upper mantle, and had themselves different duration in the different geological periods. Let us here emphasize especially that the more fractional division of the large mantle cycles, which arises when analyzing the diagram at Figure 6, is not included in the paper, and will be discussed separately.

The offset of all CR/M ratios from the Phanerozoic to the Precambrian ends to the optimal prevalence of the crustal activation (shown by arrows at Figure 6). It reflects most likely the dependence on the processes of the secondary reworking of the crust and/or on the decrease in the degree of preservation (or denudation) of the primary mantle rocks passing on to the older cratonic areas. The geological investigations revealed in fact that the granitoid rocks and gneisses are optimally spread in contrast to the other Precambrian rocks in the Karelain, Kola, Ukranian, Aldan, Canadian etc. shields.

INTENSITY OF ALKALINE MAGMATISM

It has been already noted that the most promising application of the statistic generalization of the geochronological data is the analysis of the mantle activation as applied to the natural rock series, which can be distinguished by the geochemical and petrological features. These rock series include in particular the rocks of high alkalinity, whose cyclic evolution in the geological time is considered below.

Among various types of the endogenous processes defining the continental crust growth rate, a special place is assigned to the alkaline magmatism, since its evolution reflects most clearly the overall interaction result of virtually all the Earth's shells. According to the modern concepts, the generation of the alkaline magmas is controlled chiefly by the core and upper mantle energy. This interaction should vary because of general cooling of the internal Earth's shells, that must be reflected in the geological time first in the directed evolution of the alkaline magma composition (this has still not been studied in detail) , and second in the changing intensity of their generation. L.N. Kogarko [16] demonstrated that the abrupt expansion of the alkaline rock generation is registered at the transition from the Late Archean to the Phanerozoic. Moreover, it became clear [37] that the evolution of the alkaline magmatism itself related predominantly with the plume activity, had a discrete nature. However, the designated ranking of the mantle events is rather rough and does not disclose factual scales and dynamics of the plume activation.

On the other hand, alkaline magmatism represents a unique example of the mantle magmatism, in which evolution the effect of the external factor connected with the release of free oxygen in the atmosphere and with the inflow of the oxidized material during the subduction into the upper mantle, is most clearly manifested. As a result, changing oxygen fugacity in the mantle promoted an abrupt intensity of the primary metasomatized mantle enrichment in the incoherent elements (origination of the enriched mantle reservoirs) and generated alkaline magmas [16, 37]. It might seem that the unambiguous solution of the problem on the causes of the initial accumulation of the incoherent and volatile elements in the mantle had been found. However, among hundreds of known subalkaline and alkaline massifs there are only a few instances of «heavy» enrichment in these elements to the extent of ore concentrations. Hence, it is necessary to draw in supplementary reasoning.

For the stochastic statistic analysis of the alkaline magmatism evolution with the geological time, all the types of the alkaline rocks can be represented as the natural assemblages of increasing alkalinity according to the petrochemical and petrological classification [38, 39]. These are syenogranite, monzogranite, quartz syenite and monzonite, and their volcanogenic analogues (quartz trachyte and latite) form the most primitive subalkaline group («granosyenite» - 411 datings in the databank), which is often represented in the crust by independent massifs. The stenite, monzonite and their foid-bearing analogues and volcanites, which occur as

differentiates in the gabbrodiorite massifs and as individual intrusions and volcanic rocks (234 datings), are regarded as to the second subalkaline («syenite») group. The foid-syenite, foid-monzonite, foidolite and their volcanogenic analogues, as well as melanocratic intrusive and effusive varieties, lamprophyre and carbonatite are united in the Na-alkaline («foidolitic») group (679 datings). The independent group of alkaline rocks («alkaline granite») is represented by alkaline granite and granosyenite and their volcanogenic analogues (komendite, pantellerite), which occur as independent massifs and are identical petrochemically and geochemically to the A-type granitoids, as differentiates of gabbro-anorthosite magmas, foidolitic intrusions of the central type and ocean island alkaline basalts (94 datings). Kimberlites, lamproite along with leucitic volcanites are united into the group of «high potassium rocks» (182 datings).

In view of geology alkaline magmatism is typical of oceanic hot spots. It takes place in islands and seamounts, and is inland confined to the areas of deep faults in the collision zones, to the contact of the ancient blocks of different age and to the continental rifts or to the huge plate basaltic flows or to the island arc series, where it in most cases closes the evolution of the preceding basaltic magmatism. On the whole, alkaline magmatism is a result of the magma generation at a different mantle depth, from the asthenosphere zones to the lower mantle – core boundary. However, the signs of the generation fom the middle or lower mantle are rather sporadic and are fixed by the combination of isotope-geochemical anomalies (high $^{3}He/^{4}He$, $^{186}Os/^{188}Os$, $^{187}Os/^{188}Os$ ratios; increased $^{87}Sr/^{86}Sr$ ratio and low $^{143}Nd/^{144}Nd$ ratio in comparison with the oceanic basalts), which are presumably typical of the lower mantle and external core [18; 21, 24, 25 etc.], or by the presence of ancient phenocrysts in the kimberlites, which retain relic textural features denoting the rock generation in the middle or lower mantle [26, 27 etc.], and also by the tomographic features of the reduced S-wave velocity zones at depths of ca. 500 km in the mantle under the surface manifestation of hot spots, or by the geological features of the stretched chains or ranges of such a type of magmatism [40].

The total distribution of the subalkaline and alkaline (SALK) rocks (1600 datings) shows several characteristics in the geological time (Fig. 8). First, there is a clear cyclicity, which boundaries are fixed by the episodes of minimum mantle activation. The ages of these episodes coincide with the boundaries of the mantle cycles established through the total databank for the endogenous events in the crust and upper mantle (Fig. 6). This means that the considered SALK magmatism is a constant component of the upper mantle cyclic activation in the range of at least 0 – 3.5 Ma. Since the alkaline magmatism is regarded genetically as the deepest mantle one, it is possible to assert that the dynamics of its evolution reflects pulsating energy and substance inflow from the different mantle levels.

When the total statistics of the rock series under the consideration allows designating some maximum (“megacyclic”) peaks (2660, 1860, 1160, and for the Phanerozoic – 520, 360, 280, 120, 80 and 0-10 Ma), we have probably a chance to

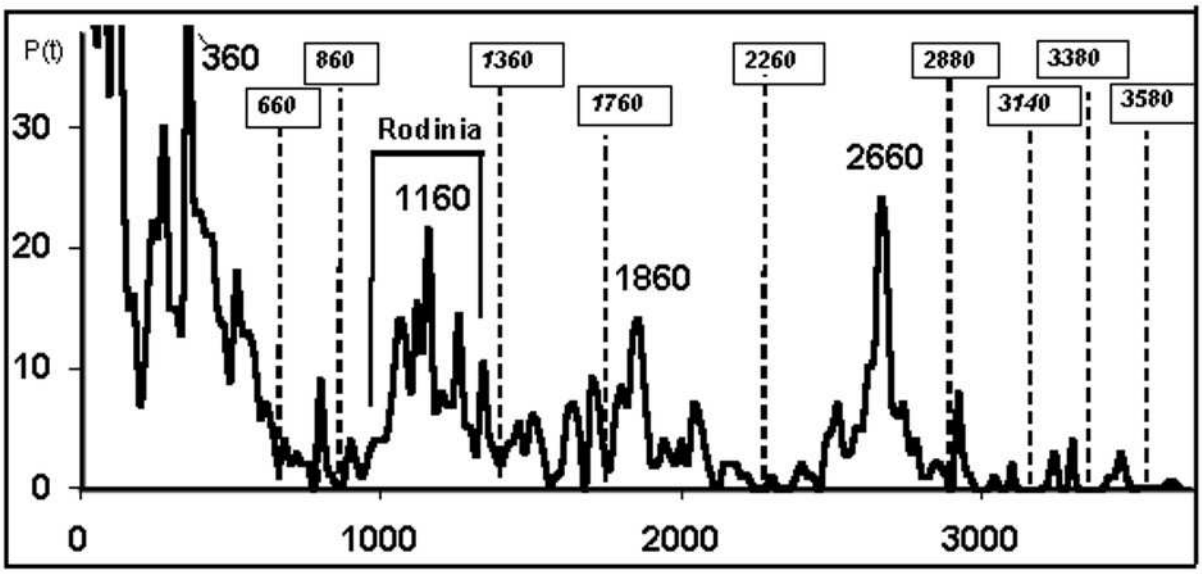

Fig. 8. **Cycles of the total subalkaline and alkaline magmatism activation, which boundaries are revealed by the abrupt fall in the magmatism evolution.**

The data systematization has been carried out using the method of stochastic statistics, where $P_t \approx N$ – amount of datings (averaging step of 20 m.y.). The minimum mantle activation is shown by dotted line, and digits in rectangles indicate age (Fig. 6). Rodinia – the interval of the alkaline cycle identical with the duration of its existence.

estimate the nature of these peaks, using separately the data on the subalkaline and alkaline natural assemblages (Fig. 9).

Primarily, it should noted that except for «granosyenite» subalkaline series, the rest shows a steady raising of the intensity from the Archean to Phanerozoic at the clear cyclicity in the all series which has already been described (Fig. 8). This conclusion agrees with the ideas cited in [16, 37]. It should only be added that the distinguished changing in the intensity of the alkaline magmatism evolution is related most likely to the thickening of the lithosphere during the Earth's cooling, and resulting displacement of the magma melt generation at the great depths in the upper mantle, and rise of the plume hearths in the middle and upper mantle. The same trend is traced for instance in the kimberlite diamond-bearing melts, which have the deepest source and entrap usually different xenoliths of the mantle peridotites and xenocrysts of some minerals. As it was turned out [41] the highest values of the P-T parameters for the peridotite xenoliths from the Premier Pipe (South Africa) with the age of 1202±72 Ma [42] correspond 58 kbar (ca. 185 km), for the Udachnaya Pipe (Yakutia) with the age of 360±10 Ma [43] – 80 kbar (ca. 250 km), and the baddeleyite xenocryst from the 70 Ma Mbuya-Mauya kimberlite (South Africa) [26, 27] shows evidences of the lower mantle genesis. The second factor is a sequential influx of oxidated crust products together with volatiles into the mantle during the numerous episodes of subduction in the late Archean, Proterozoic and Phanerozoic. This defines a substantial expansion of the enriched in incoherent elements mantle zones, and intensification of the geochemical

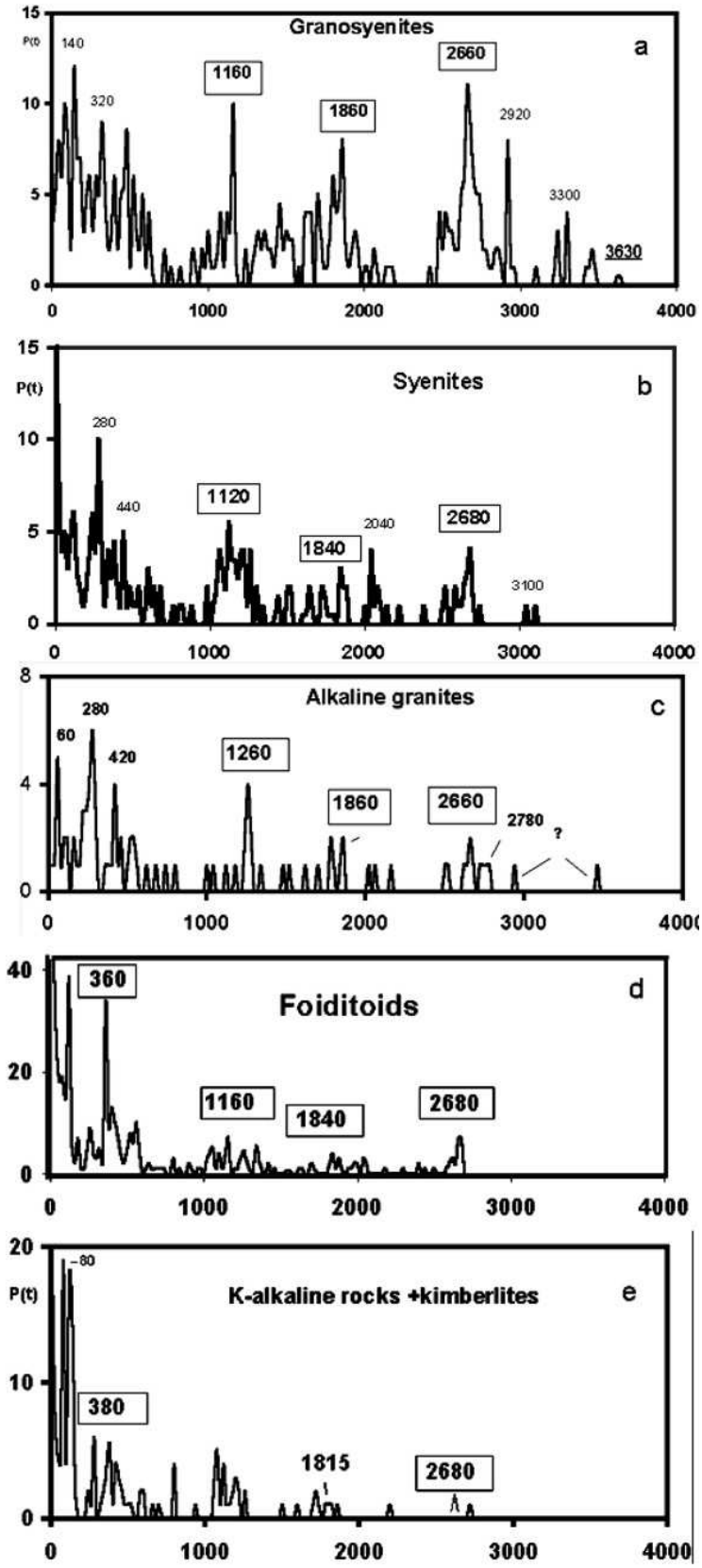

Fig. 9. **Detailed elaboration of the subalkaline and alkaline magmatism evolution by the types of the natural series.**

The rectangles indicate concordant ages of maximum plume peaks in the evolution of the each series. Averaging step is 20 m.y.

heterogeneity of the mantle itself, that is realized in the increasing frequency of the alkaline magma generation towards the Phanerozoic [16].

The time of the initial occurrence of any SALK series rock differs (Fig. 9). The oldest rocks are represented by rare primitive subalkaline varieties (quartz monzonite and monzogranite), which occur in the Western Australia (Pilbara Block, 3200-3630 Ma) [44], where the first occurrence of alkaline granite (3466±2 Ma), which is occasionally dated to be Late Archean (2946±6 and 2762±4 Ma). However, these rocks demonstrate here and there signs of late transformations [44], that complicates the accurate identifications of the ancient «alkaline» granite. The initiation of the rest series is ascribed to the Late Archean. The second alkaline group is represented by the oldest varieties, i.e. by the Barberton syenite (3105±10 Ma) [45] and trachytic tuffs (3048±19) in the Pilbara Block [44]. The Na- and K-alkaline series have the oldest age of 2700 Ma. The ultrapotassium rocks (pyroxenite, syenite and shoshonite) of the Ukduska massif (Aldan Shield) yielded recently the age similar to the same boundary (2719±14 Ma) [46].

The kimberlites and lamproites formed much later, the oldest kimberlite (≈ 2200 Ma) and lamproit (1815±14 Ma) are known in Australia [47, 48].

A mutual data overview for all the series has shown that the interval of 2680-2660 Ma enclosed the first powerful («megacyclic») magmatism peak, that has already been taken note of [49]. The peak is represented by the numerous stocks and intrusions of monzodiorite, monzonite, syenite, nepheline syenite, carbonatite, lamprophyre dikes, trachytic and leucitic volcanites. The overwhelming majority of these rocks occur in the southern Canadian Shield (Ontario-Quebek), in the south-eastern Greenland and West Australia [50-52, 44 etc.]. As for the Baltic Shield, in the central and eastern parts of the Kola Peninsula, similar SALK massifs turned out to be coeval with the Canadian and Greenland rocks: for the quartz monzodiorite of the Pyatn'yavr region – from 2715±8 to 2650±15 Ma [53], for the monzonite-latite series of the Marijok River region - 2657± 8.4 Ma [53], for the monzonite of the Tsaga anorthosite massif - 2662±10 Ma [54], for the alkaline syenite of the Sakharjok massif - 2682±10 [55], for the lamprophyre of the Porosozero massif - 2680±10 [56]. But the most sensational result was obtained for the huge province of the Keivy alkaline granite and granosyenite (Central Kola Block), which formed in the interval from 2674±6 to 2654±5 Ma [55] and covers the area of ca. 2500 km^2 (at the average thickness of layers in 500-700 m), that corresponds about the volume, which is similar to the bulk of the coeval SALK rocks in the other regions. That alone will do, if we speak about the megacyclic representativeness of the SALK peak (Fig. 9). On the Canadian Shield, the subalkaline and alkaline massifs and volcanites (of whose over 27 were dated), which are confined mainly to the vast boundary zone Ontario-Quebec, and are attached to the collision (2690-2660 Ma), which completed the evolution of the greenstone belts, which have mainly the ages within 2740-2710 Ma in the south-western part of the Abitibi Province [50]. Thus, the alkaline rocks there fix a

significant time shift towards the rejuvenation, that allows ascribing the SALK rocks to the activation of the underlying astenosphere in the Abitibi collision zone [57]. In the SE Greenland there is a vast alkaline province called Skioldungen, where syenite, carbonatite, monzonite, and foidolite have been dated to have the age within a narrow interval of 2698-2664 Ma. This fact allows regarding them as derivatives from the single plume magmatism. It should also be noted that, according to the prediction model of the Keivy deep structure [58] and geophysical and geological data for this area, a dome-like upper crust structure of the Keivy terrain dips in the north-east under the Murmansk Block, and in the south and south-west under the Imandra-Varzuga Block. In the lower crust there is a thick transition layer at the boundary with the mantle, i.e. at depths of 38-40 km. The thickness of the transition layer is about 10-12 km, i.e. over a quarter of the total crust under the Keivy region. On the whole, such a specific structure of the Earth's crust in the region made it possible to suppose the evolution of the mantle plume under the centre of the modern Keivy terrain at the Late Archean boundary.

This, the data on the SALK series of the all region seem to be quite reliable to ground an appearance of the first alkaline «megacyclic» peak, which is characterized by a shift of the SALK magmatism maximum towards the interval of 2660-2680 Ma, which is clearly younger in comparison with its average value of 2700-2720 Ma obtained by the total data body on the upper mantle (Fig. 6). The second «megacyclic» peak of ca. 1860-1840 Ma (Fig. 8, 9) reflects a shift by ca. 20-40 m.y. relative to the «megacyclic» mantle peak of 1880 Ma (Fig. 6). The third peak (Neoproterozoic SALK series) corresponds to the alkaline activation in the Grenville orogens in the interval of 1260-1060 Ma. The maximum of the alkaline activation (1160-1120 Ma, Fig. 8, 9) is also displaced towards the rejuvenation. The vast Palaeozoic alkaline activation on the Baltic Shield took place from 410 to 360 Ma ago [20] with a maximum of ca. 365-375 Ma, which is shifted relative to the older general mantle peak (ca. 415 Ma (Fig. 6) by 35-45 m.y. Thus, appearance of the superplume SALK magmatism products in the crust are clearly rejuvenated geochronologically within the mantle cycles, which reflect the total mantle endogenous activation. Therefore, the SALK magmatism represents just a part of the total upper mantle cycles, and the rest components of the mantle activation are still to be studied. The youngest Meso-Cainozoic plume peaks are not discussed here, but let us notice that they increase abruptly within relatively small interval parallel to other types of the plume magmatism.

Finishing the geochronological overview of the SALK series, let us emphasize availability of this information as applied to the surface plate tectonics controlling the processes of crowding and breakdown of the supercontinents, that has already been mentioned in the Introduction. So, the Rodinia supercontinent, according to the geotectonic, geochronological and paleomagnetic reconstructions, existed within the interval of 0.9-1.35 Ga [59], which coincides fully with a cycle of the Middle Proterozoic SALK magmatism activation (Fig. 8).

ON THE GENESIS OF THE SUPERGIANT ALKALINE DEPOSITS

The question, what provoked a rise of giant alkaline massifs enriched extremely in incoherent and volatile elements (Nb, Ta, Ti, Zr, REE, Sr, P, F, Cl etc.) still remains open, although the mechanisms of how the mantle zones with the increased concentration of the listed elements, being possible sources of alkaline rock generation, formed as a result of mantle metasomatism under the conditions of high oxygen fugacity, have already been developed due to experiments and real observations [16, 17, etc.]. However, among the hundreds of dated alkaline rocks, just a few massifs possess unique mineralization as regards incoherent elements. It is obvious that we still need more data on the petrology of the alkaline rocks to solve this problem. In particular, low distribution coefficients of incoherent elements in the rock-forming minerals and low melting degrees at the single generation of alkaline magmas can hardly provide enrichment in these elements up to the ore grade. We should search for additional criteria. One of them can be represented by a regional pattern of numerous SALK series manifestations in either region.

If we correlate the available data on the Late Archean manifestation of the SALK series in Canada, South Greenland and Baltic (2680-2660 Ma), for the Laurentia-Baltic craton of that epoch a discontinuous band of south-western and north-eastern rhumb of the simultaneous vast mantle alkaline activation, which is rather interpreted as a reflection of plume or superplume magmatism, is traced.

The second peak of the alkaline magmatism is registered there for the interval of 1880-1820 Ma. On the Canadian Shield the SALK series of this age are spread predominantly in the North-Western Territories, but scattered from the Baffin Land in the north to the Manitoba and Sascachevan in the south, on the Baltic Shield these are in Finland, Sweden, Karelia and on the Kola Peninsula (Soustov and Gremyakha-Vyrmes massifs [60]). In the West Greenland the SALK series of this age have not been found, but there are numerous basaltic dikes in the interval of 1980-1750 Ma.

The third peak (Neoproterozoic SALK series) corresponds to the alkaline activation in the Grenville orogens within the Rodinia supercontinent (1260-1080 Ma). On the Canadian Shield subalkaline series are confined to the Grenville Front (Ontario, Quebec, eastern Labrador) and spatially shifted towards the Late Archean magmatism peak. In the south and south-western Greenland alkaline and subalkaline complexes (Ilimaussak, Igaliko, Nunarssuit, Tugtutok etc.), including potassium alkaline massifs (Narssak etc.) and lamprophyre dikes are found in the zone of Late Archean magmatism. On the Baltic Shield the SALK series are described in Norway and Sweden, but they do not exist on the Kola Peninsula. However, a thick series of alkaline complexes occur also for the third time, but much later in the Palaeozoic, that corresponds to a 360 Ma megacyclic peak in the foidolite series and in the interval of 360-420 Ma for the other series (Fig. 9).

Thus, in these three regions following a different succession there is a repeated renewing of the SALK activation, the cycles of the alkaline magmatism

being connected to the same area in the South Greenland and Baltic Shield, and being scattered over a vast territory in the Canadian Shield.

It thus could be supposed that the territorial coincidence of the alkaline magmatism different in age in the two first regions reflects not only the relationship of the plume alkaline activity with the structural and tectonic features of the crust and mantle, but forces the youngest zones of the alkaline activation to inherit those geochemical variations in the composition of the mantle sources, which they accumulated at the earlier stages of the Archean and Early Proterozoic reworking during the mantle metasomatism. These ideas imply a suggestion that the metasomatic zones in the upper mantle could exist long and be a source for the alkaline magmatism. It should be also added that these upper mantle zones could be favourable «traps» for absorbing new portions of the overheated (firstly fluid) deep substance, which came from the middle and lower mantle. In the utmost, at the recurrent manifestation of the plume activation these zones should expect a supplementary inflow of volatiles and incoherent elements, resulting at the surface in the formation of strongly enriched in these elements alkaline massifs at the final stages of the alkaline activation in every region.

The attainability of this suggestion can be demonstrated by the examples of Greenland and Kola Peninsula, where the SALK activation has been reported to take place two or three times. Thus, among the Neoproterozoic alkaline and subalkaline complexes of the South-Western Greenland, the Ilimaussak layered agpaitic alkaline massif (1180±9 Ma [61]) shows a high concentration of volatiles (F, Cl, S) and rare (Li, Be, Rb, REE, Zr, Nb etc.) elements [62], which is comparable only with the Palaeozoic (371-361 Ma) layered alkaline Khibina and Lovozero massifs [62-66 etc.] of the central Kola Peninsula. These massifs are confined to the regions, where the various SALK series were earlier wide spread, but they had lower concentrations of rare and diffused elements comparable with the «common» SALK series of Canada and other regions.

The proposed analysis of the «inheritance» of the geochemical specialization of old mantle sources by the late SALK magmatism is to be considered as a attempt to attract attention to the importance of the suggested compositional heterogeneity of the upper mantle for the genesis interpretation not only of the alkaline rocks, but of the other plume magmatism, and to the need for special investigations in this field.

NATURE OF SOURCES FOR THE ALKALINE MAGMETISM

Since the formation of the subalkaline and alkaline magmatism is restricted by a wide range of the crustal and mantle depths, it is reasonable to expect that the parental mantle hearths should reflect quite a wide range of isotope and geochemical variations even for the one-type magmas, and bear signs of interaction with the country crustal substrate. To a first approximation we can judge a nature of the mantle sources from the correlation of isotope-geochemical

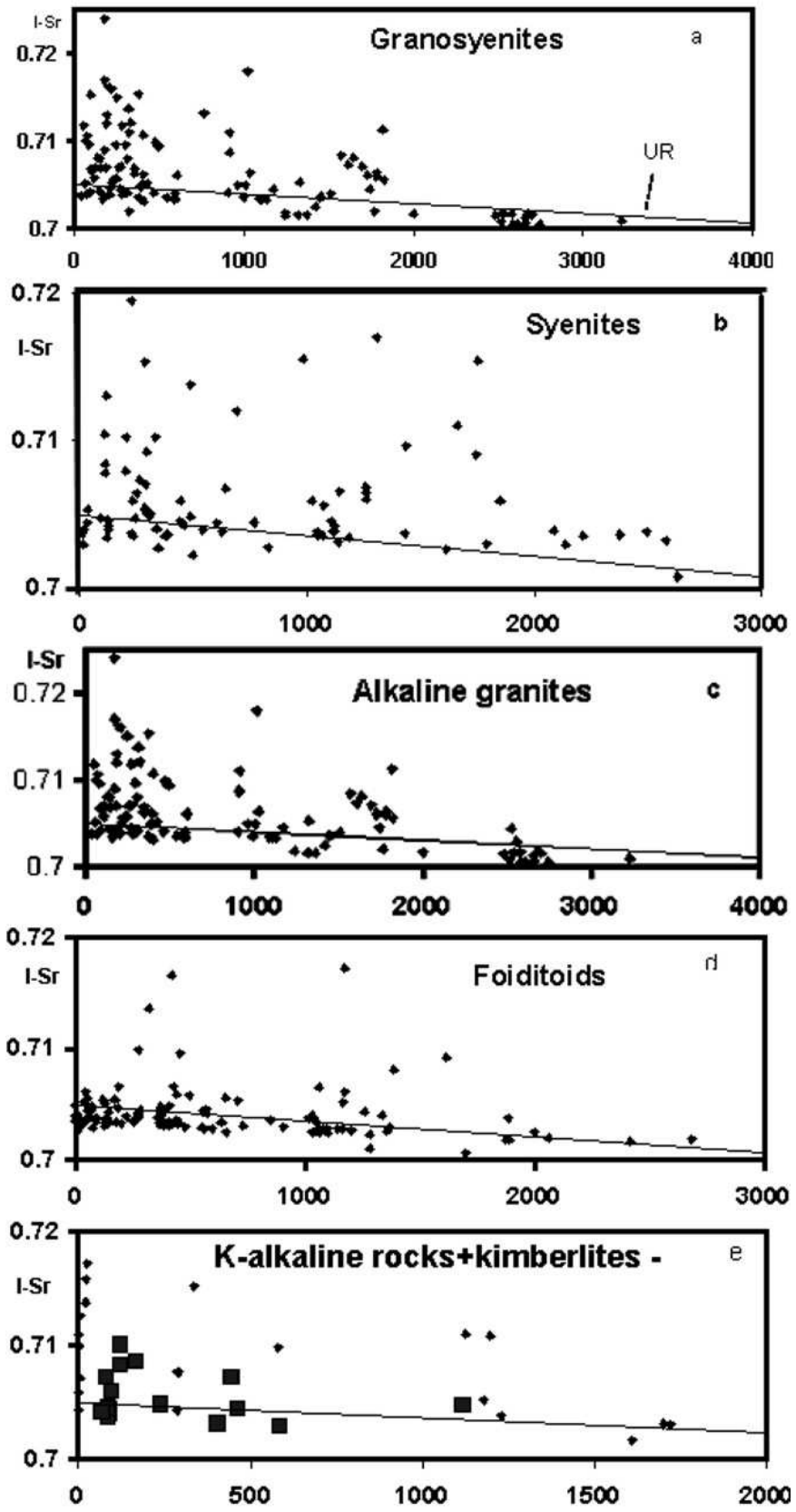

Fig. 10. **Variation in the initial Sr isotope ratio in the subalkaline and alkaline rock series relative to average mantle level (UR line).**

Vertical dotted lines indicate age, younger are the datings with typical crustal Sr isotope characteristics.

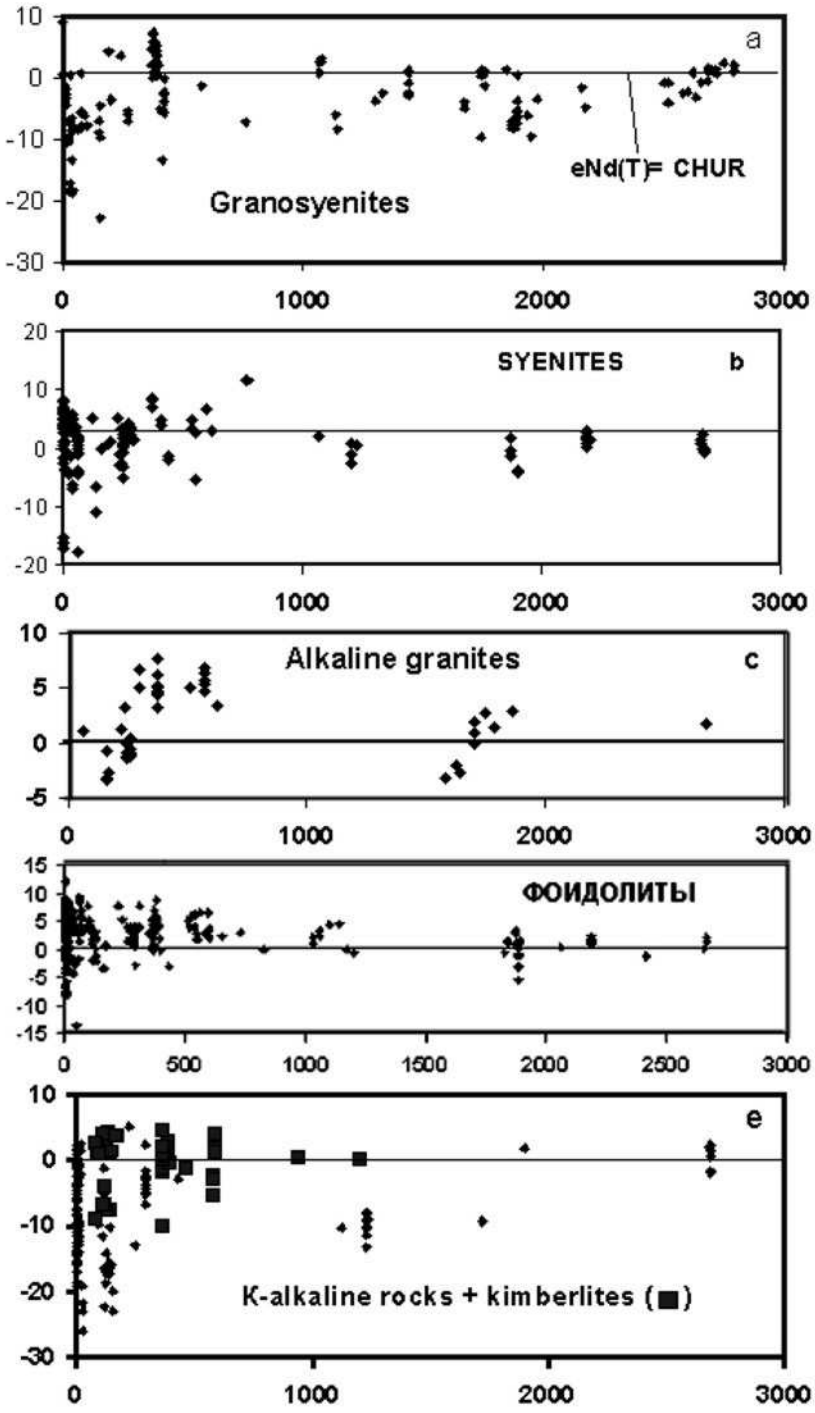

Fig. 11. **εNd(T) variations for the subalkaline and alkaline series relative to average mantle level (chondrite REE composition).**

Large squares show data for kimberlites.

parameters of the studied SALK series with the average mantle (UR) values of I-Sr = $(^{87}Sr/^{86}Sr)_t$ at the average mantle Rb/Sr = 0.30 (0.031-0.0294) [67, 68] and I-Sr(0) = 0.70475 (0.7045-0.7050) [69, 70], and average mantle (CHUR) εNd(t) at Sm/Nd=0.3245 [69, 71] and εNd(0) for the depleted mantle of 12 (10-14) [72, 73].

The data on the initial Sr ratio (I-Sr) of the studied SALK series (Fig. 10) are divided by a line o the average mantle ratio (UR) into three fields: 1) with isotope parameters, which are equal or close to the UR within the error for I-Sr determinations, 2) with those lower than in the UR (depleted sources field) and 3) with those higher than in the UR (enriched mantle and crust sources). It is visible that the first two groups of I-Sr values register clearly mantle nature of the most part of the SALK series, which is traced from the Phanerozoic to different intervals of the Archean (except for K-alkaline varieties, which are restricted by the interval of 1700-0 Ma). The same can be ascribed to the systematization of εNd(t) values, where $\varepsilon Nd(t) \geq 0$ corresponds to the mantle average (CHUR) and depleted mantle sources (Fig. 13).

The fact itself that the «syenite» and «foidolite» groups belong to the depleted mantle zones became known long ago [74 etc.]. But the analogous mantle sources to the primitive subalkaline group and alkaline granite in the Middle Archean has lately been found. The I-Sr data yield an interval of ca. 1800-1900 Ma, which initiates an abrupt abundance of rocks with crustal isotope parameters in the SALK series, and reflects most probably a lack of information, since the εNd(T) data in the SALK series show crustal Nd parameters in the Early Proterozoic (Fig. 11). The growing crustal effect towards the Phanerozoic, according to the total information for the two isotope systems, is beyond question. This is corroborated by the fragmentary data for the deepest in genesis rocks - kimberlites, which demonstrate the Proterozoic mantle isotope «marks» and some crust effect towards the end of the Phanerozoic epoch.

The common for the all SALK series tendency of expanding distribution of rocks with «crustal» Sr and Nd isotope parameters at the transition to the Neoproterozoic-Phanerozoic is most likely obliged to the effect of different factors: 1) it reflects increase in heterogeneity in the upper mantle due to the influx of crustal components by the subduction processes [75 etc.], 2) it resulted from the increase in heterogeneity of the lower crust composition due to the participation in melting of older metamorphosed fragments (fusion of some subalkaline magma), and 3) regional contamination of mantle magmas by the country crustal substrate (fenitization and other processes). In all cases not only variations in the source composition, but active fluid reworking during the mantle and crustal metasomatism are implied. This is confirmed by model estimations of Sr isotopes [66, etc.] and by data on the variations in stable isotope ratios. The expanding effect on the generating subalkaline and alkaline complexes combines with the activation of contrast tectonic processes, i.e. with more frequent manifestations of plate tectonics and subduction towards the Phanerozoic, and as a result with global expansion of mantle metasomatism activation and frequency of generation of intrusive and volcanogenic facies of subalkaline and alkaline rocks [16].

DISCUSSION AND CONCLUSIONS

The overview of the geochronological information on the crust evolution has shown that the selective application of a geochronological method even for the formal description of the crust thickening succession during the geological time is hardly plausible due to the contrast informational possibilities of the U-Pb, Sm-Nd, Rb-Sr, and K-Ar isotope systems and due to the data body obtained using these methods for the different rock types in the separate geological interval. Hence, in order to disclose the event of the crustal growth irregularity, it is essential to sum up the whole body of the geochronological information. However, such a summary should be accompanied by a separate informational analysis for both upper shell of the Earth, since the crust and the upper mantle are independent, but interrelated systems with the different rocks and endogenous processes.

As it has been shown, the difference is reflected in more intense evolution of the mantle processes during the simultaneous endogenous activation within the two shells and in more drastic reduction o the mantle activity during the fall in the endogenous activity in these shells. The difference in the activation dynamics does not contradict the event of the crust-forming «megacyclicity», which is roughly circumscribed by total information on the two shells, but allows outlining and disclosing the sense of the endogenous cyclicity, which reflects an inhibited crust reaction for the vicissitude of the processes proceeded in the mantle. As a result, it has been possible to establish a rather complicated nature of the mantle dynamics with a variable cycle duration, which may reflect the existence of three important intervals in the crustal evolution, including 1) the Early and Middle Archean with a cycle of ca. 200-250 m.y., 2) the Late Archean-Proterozoic with the clearly longest cycle (ca. 400 m.y.), and 3) the Phanerozoic with a sharply varying cyclicity from 5-10 to 100-130 m.y. However, this is only a statement of the fact, and the reasons of such an irregularity are still to be ascertained. Here it should be noted that when analyzing the regularity of the cinematic inversions in the mobile belts during the tectonic evolution, Morozov Yu.A. [76] arrived at a conclusion of the need to distinguish an increasing from the Phanerozoic to the Proterozoic and Archean duration of the cinematic stages from 25-30 to 100 m.y., that agrees with the geochronological systematization of the endogenous events in the Phanerozoic mantle. The detailed analysis of the 100-m.y. or minor cyclicity or periodicity, which is obvious within the large cycles of the mantle magmatism and endogenous events in the Precambrian crust, is to be separately studied and is not discussed here. Let us notice that the geodynamic sense of the heterospeed events in the two shells and reasons of the origin of various mantle cycles is to be interpreted, although in the preliminary draft changing in the duration of the maximal cycles can be treated as a consequence of the transition from the early (≈ 4.4-4.2 Ga) plume tectonics to the combination of the two geodynamic processes (plumes and subduction) with the subsequently expanding role of the deepest mantle magma generation.

By the example of subalkaline and alkaline magmatism analysis, we have made an effort to demonstrate that the cycles of the alkaline mantle activation agree completely with the global mantle cycles revealed by the total information for the mantle rocks through the comparison of these data with the endogenous events in the crust (Fig. 5-6 and 8-9). This is evident of the permanent contribution of the SALK series in the evolution of the mantle cycles, and, if we consider these as a specific example of the plume magmatism effect on the crust formation, we should speak also of a global nature of such an effect. The geochronology of the SALK series indicates a subsequent expansion of the petrological rock associations (from subalkaline to alkaline) at the transition from the Early-Middle Archean to the Late Archean and Proterozoic, as well as a generation depth range for the all SALK series towards the Phanerozoic. The whole body of this information can be regarded as a convincing example of the global effect of the gradual Earth's cooling on the character of the mantle products in the geological time. Besides, as the Sr and Nd isotope systematization has shown, in the same direction increases the intensity of the interaction between the mantle SALK series and crust on account of the crustal material inflow into the zones of the primary magmas generation and at the consolidation of mantle magmas within the crust. According to the early investigations [15, 16, 66, etc.], the most significant factors of this interaction are mantle and crustal metasomatism in the broad sense of this idea, which implies primarily intense influence or exchange of volatiles. It is not improbable that the mantle zones are enriched in volatiles and incoherent elements during the recurrent plume effect, and participate repeatedly in the alkaline magma generation, giving rise to alkaline massifs, which are optimally enriched in incoherent elements (up to the mining concentrations).

The investigation is supported by Program of the Basic Directions of Fundamental Researches RAS (topic 6,14) and Russian Fund of Fundamental Researches (grant 03-05-64740).

REFERENCES

1. **Gastil, G.** (1960).The distribution of mineral dates in time and space // Amer. J. Sci. V. 258. No 1. P. 1-35.
2. **Pushkarev, Yu.D.** (1990). Megacycles in the evolution of the crust-mantle system. L.: Nauka. Leningrad dep. 217 p. (in Russian)
3. **Armstrong, R.L.** (1981). Radiogenic isotopes: the case for crustal recycling on a near-steady-state no-continental-growth Earth // Phil.Trans.Roy.Soc.London. A301. P. 443-472.
4. **McCulloch, M.T., Bennett, V.C.** (1994). Progressive growth of the Earth's continental crust and depleted mantle: Geochemical constraints // Geochim. Cosmochim. Acta. V. 58. No 21. P. 4717-4738.
5. **Condie, K.C.** (1998). Episodic continental growth and supercontinents: a mantle avalanche connection // Earth and Planet. Sci. Lett. V. 163. P. 97-108.
6. **Balashov, Yu.A.** (1985). Isotope geochemical evolution of the Earth's mantle and crust. M.: Nauka, 221 p. (in Russian)
7. **Stein, M., Hofmann, A.W.** (1994). Mantle plumes and episodic crustal grouth // Nature. V. 372. 63-68.

8. **Kamazawa, M., Maruyama, S.** (1994). Whole Earth tectonics // J.Geol.Soc.Japan. V.100. P. 81-102.
9. **Van der Hillst, R. D., Widiyantoro, S., Engdahl. E.R.** (1997). Evidence for deep mantle circulation from global tomography // Nature. V. 386. P. 578-584.
10. **Van der Hillst, R. D., Karason, H.** (1999). Compositional heterogeneity in the bottom 1000 kilometers of Earth's mantle: Toward a hybrid convection model // Science. V. 283. P. 1885-1888.
11. **Avsyuk, Yu.N.** (1996). Tidal forces and natural processes // M. UIPE RAS. 188 p. (in Russian)
12. **Thompson, P.F., Tackley, P.J.** (1998). Generation of mega-plumes from the core-mantle boundary in a compressible mantle with temperature-dependent viscosity // Geophys. Res. Lett., V. 25. № 11. P. 1000-2002.
13. **Dobretsov, N.L., Kirdyashkin, A.G.** (2000). On the sources of the mantle plumes // DOKL. RAS. V. 373. № 1. P. 84-86. (in Russian)
14. **Letnikov, F.A.** (2002). Ultradeep fluid systems of the Earth and issues of the ore genesis // Proceedings of the II International Seminar «Deep magmatism, magmatic sources and plumes». Irkutsk-Bladivostok. P. 5- 24. (in Russian)
15. **Ionov, D.A., Hofmann, A.W.** (1995). Nb-Ta-rich mantle amphiboles and micas: Implications for subduction-related metasomatic trace element fractionations // Earth and Planet.Sci.Lett. V.131. P. 341-356.
16. **Kogarko, L.N.** (1998). Alkaline magmatism in the early history of the Earth // Petrology. V. 6. № 3, 251-258 p. (in Russian)
17. **Kogarko, L.N., Kurat, G., Ntaflos, T.** (2001). Carbonate metasomatism of the oceanic mantle beneath Fernando de Noronha Island, Brazil // Contrib.Miner.Petrol. V. 140. P. 577-587.
18. **Hart, S.R., Hauri, E.H., Oschmann, L.A., Whitehead, J.A.** (1992). Mantle plumes and entrainment: isotopic evidence // Science. V.256. P. 517-520.
19. **Hawkesworth, C.J., Lightfoot, P.C., Fedorenko, V.A., Black, S., Naldrett, A.J., Doherty, W., Gorbachev, N.S.** (1995). Magma differentiation and mineralisation in the Siberian continental flood bsalts // Lithos, V.34.P.61-88.
20. **Arzamastsev, A.A., Bea, F., Arzamastseva, L.V., Montero, P.** (2002). The Palaeozoic plume-lithosphere interaction in the NE Baltic Shield: TR-elements in the rocks and minerals of the Kola Peninsula as indicators of the alkaline melts' evolution // Proceedings of the II International Seminar «Deep magmatism, magmatic sources and plumes». Irkutsk-Bladivostok. P. 54- 86.
21. **White, R.S., McKenzie, D.M.** (1995). Mantle plumes and flood basalts // J. Geophys. Res. V. 100. № B9. P. 17543-17585.
22. **Garland, F., Turner, S., Hawkesworth, C.** (1996). Shifts in source of the Parana basalts through time // Lithos. V.37. P. 223-243.
23. **Ernst, R.E., Buchan, K.L., West, T.D., Palmer, H.C.** (1996). Diabase (dolerite) dyke swarms of the world: first edition. Geol. Surv. Can. Open File. No 3241. 104 pp.
24. **Tolstikhin, I.N., Kamensky, I.L., Marty, B., Nivin, V.R., Vetrin, V.R., Balaganskaya, E.G., Ikorsky, S.V., Gannibal, M.A., Weiss, D., Verhulst, A., Demaiffe, D.** (2002). Rare gas isotopes and parent elements in ultrabasic-alkaline-carbonatite complexes, Kola Peninsula: Identification of lower mantle plume component // Geochim. Cosmochim. Acta. V. 66. No 5. P. 881-901.
25. **Brandon, A.D., Norman, M.D., Walker, R.J., Morgan, J.W.** (1999). ^{186}Os-^{187}Os systematics of Hawaiian picrites // Earth and Planet. Sci. Lett. V.174. P. 25-42.

26. **Schärer, U., Corfu, F., Demaiffe, D.** (1997). U-Pb and Lu-Hf isotopes in baddeleyite and zircon megacrysts from the Mbuji-Mayi kimberlite: constraints on the subcontinental mantle // Chem. Geology. V. 143. No 1-2. P. 1-16.
27. **Kerschhofer, L., Scharer, U., Deutsch, A.** (2000). Evidence for crystals from the lower mantle:baddeleyite megacrysts of the Mbuji mayi kimberlite // Earth and Planet. Sci. Lett. V.179. N2. P. 219-225.
28. **Grachev, A.F.** (2000). Mantle plumes and issues of geodynamics // The Earth's physics. №4. P. 23-37. (in Russian)
29. **Prokoph, A, Veizer, J.** (1999). Trends, cycles and nonstationarities in isotope signals of phanerozoic seawater // Chem. Geol. V. 161. P. 225-240.
30. **Pechersky, D.M.** (1998). Palaeomagnetism of the Neogene – reflection of the processes at the core and on the Earth's surface // Russ. Mag. of the Earth's Sci. V. 1. № 2. P. 105-139. (in Russian)
31. **Solow, A.R.** (2002). Estimating event rates in the presence of dating error with an application to lunar impacts // Earth and Planet. Sci. Lett. V. 199. P. 1-6.
32. **Rytov, S.M. (**1979). Introduction into the statistic radiophysics. M. Nauka. 1976. 494 p.)in Russian)
33. **Nikitin, A.A.** Statistic methods for establishing geophysical anomalies. M., Nedra. 280 p. (in Russian)
34. **Dremin, I.M., Ivanov, O.M., Nechitailo, V.A.** (2001). Wavelets and their usage // Progress in physical sciences. V. 171, № 5, p. 465-501. (in Russian)
35. **Balashov, Yu.A.** (2001). Evolutional dynamics of the Moon-Earth system and meteorites // DOKL. RAS. V. 377. № 2. P. 227-230. (in Russian)
36. **Balashov, Yu.A.** (2002). Time conception in the geological history of the Earth // Geology and minerals of the Kola Peninsula (Volume to the 50th anniversary of the Geological Institute KSC RAS). New ideas and approaches to the geological investigations. V. 3. MUP «Poligraf», Apatity. P. 51-75. (in Russian)
37. **Kogarko, L.N., Khain, V.E.** (2001). Alkaline magmatism in the Earth's history: experience in the geodynamic interpretation // DOKL. RAS. V. 37. № 5. P. 677-679. (in Russian)
38. **Streckeisen, A.** (1979). Classification and nomenclature of volcanic rocks, lamprophyres, carbonatites, and melilitic rocks: Recommendations and suggestions of the IUGS Subcommission on the Systematics of Igneous Rocks // Geol. V.7. P. 331-335.
39. **Classification and glossary of igneous rocks** (ed. S.V. Yefremova). (1997). M.: Nedra. 248 p. (in Russian)
40. **Courtillot, V., Davaille, A., Besse, J., Stock, J.** (2003). Three distinct types of hotspots in the Earth's mantle // Earth and Planet Sci. Lett. V. 205. P. 295-308.
41. **Simakov, S.K.** (2001). Clinopyroxene barometry of the mantle peridotites and estimation of potential diamond content // DOKL. RAS. V. 376. № 6. P. 801-803. (in Russian)
42. **Allsopp, H.L., Bristow, J.W., Smith, C.B. et al.** (1986). A summary of radiometric dating methods applicable to kimberlites and related rocks // Kimberlites and related rocks (Ed. J.Ross, A..L.Jaques et al). V.1. Their composition, occurrence, origin and emplacement. Geol. Soc. Austral. Special Publ. N 14. Proc. of the 4th Intern. Kimberlite Conf. Perth. P. 343-368.
43. **Kinny, P.D., Griffin, B.J., Heaman, L.M. et al.** (1997). SHRIMP U-Pb ages of perovskite from Yakutian kimberlites // Russian Geology and Geophysics. V. 38. № 1. P. 97-105.
44. **Nelson, D.R., Trendall, A.F., Altermann, W.** (1999). Chronological correlations between the Pilbara and Kaapvaal cratons // Precambrian Res. V. 97. P. 165-189.
45. **Kamo, S.L., Davis, D.W.** (1994). Reassesssment of Archean crust development in the Barberton Moufain Land, South Africa, based on U-Pb dating // Tectonics. V. 13. No1. P. 167-192.

46. **Tabuns, E.V., Salnikova, E.B., Kovach, V.P. et al.** (2003). The Late Archean age of the ultrapotassic rocks (Ukduska massif, Aldan Shield): results of U-Pb investigation of single zircon grains // Proc. Of the II Russ. Conf. On the Isotope Geochronology. S.-Petersburg. P. 492-494. (in Russian)
47. **Kiviets, G.B., Phillips, D.** (1998). 40Ar/39Ar laser probe analyses of K-bearing titanates from kimberlites // ICOG-9, Beijing, China. Abstracts. P.65.
48. **Pidgeon, R.T., Smith, C.B., Fanning, C.M.** (1986). Kimberlite and lamproite emplasement ages in Western Australia // Proc. the 4th Intern. Kimberlite Conf. V.1. GSA Special Publ No 14. Perth. P. 369-381.
49. **Blichert-Toft, J., Arndt, N.T., Luden, J.N.** (1996). Precambrian alkaline magmatism // Lithos. V. 37. No1. P. 97-111.
50. **Corfu, F., Jackson, S.L., Sutcliffe, R.H.** (1991). U-Pb ages and tectonic significance late Archean alkalic magmatism and nonmarine sedimentation: Timiskaming Group, southern Abitibi belt, Ontario // Can. J. Earth Sci. V. 28. P. 489-503.
51. **Tilton, G.R., Bell, K.** (1994). Sr-Nd-Pb isotope relationships in Late Archean carbonatites and alkaline complexes: Applications to the geochemical evolution of Archean mantle // Geochim. et Cosmochim. Acta. V. 58. No15. P. 3145-3154.
52. **Nutman, A.P., Rosing, M.T.** (1994). SHRIMP U-Pb zircon geochronology of the late Archean Ruinneesset syenite, Skieldungen alkaline province, South-East Greenland // Geochim. et Cosmochim. Acta. V. 58. P. 3515-3518.
53. **Balashov, Yu.A., Mitrofanov, F.P., Balagansky, V.V.** (1992). New geochronological data on Archean rocks of the Kola Peninsula // Correlation of Precambrian formations of the Kola-Karelian region and Finland. Apatity. P. 13-34.
54. **Bayanova, T.B., Mitrofanov, F.P., Galimzyanova, R.M., Levkovich, N.V.** (1999). The Archean age of the Bely Tundra's alkaline granites (Kola Peninsula) // DOKL. RAS. V. 369. № 6. P. 806-808. (in Russian)
55. **Mitrofanov, F.P., Zozulya, Bayanova, T.B., Levkovich, N.V.** (2000). The world's oldest alkaline-granite magmatism in the Keivy structure of the Baltic Shield // DOKL. RAS. V. 374. № 2. P. 238-241. (in Russian)
56. **Kudryashov, N.M., Petrovsky, M.N.** (2000). Isotope age of the lamprophyre from the Kolmozero-Voronya greenstone belt // Proc. of the II Youth's Conf. (K.O. Kratts) «Geology and geoecology of the Fennoscandian Shield, north-west and centre of Russia. Petrozavodsk. P. 36-38. (in Russian)
57. **Wyman, D.A., Kerrich, R., Polat, A.** (2002). Assembly of Archean craton mantle lithosphere and crust: plume-arc interaction in the Abitibi-Wawa subduction-acretion comlex // Precambrian Res. V. 115. P. 37-62.
58. **Prediction model for the deep structure of the geophysical profile «2» location in the east of the Kola Peninsula.** (2000). Ed. F.P. Mitrofanov. Preprint of GI KSC RAS, Apatity, 49 p. (in Russian)
59. **Condie, K.C.** (2002). The supercontinent cycle: are there two patterns of cyclicity ? // J. Afr. Earth Sci. V. 53. p.179-183.
60. **Bea, F., Arzamastsev, A., Montero, P., Arzamastaeva, L.** (2001). Anomalous alkaline rocks of Soustov, Kola: evidence of mantle-derived metasomatic fluids affecting crustal materials // Contrib. Mineral. Petrol. V.140. P. 554-566.
61. **Larsen, L.M., Rex, D.C.** (1992). A review of the 2500 Ma span of alkakine-ultramafic, potassic and carbonatitic magmatism in West Greenland // Lithos. V. 28. N3-6, P.367-402.
62. **Blaxland, A.B., Van Breemen, O., Steenfelt, A.** (1976). Age and origin of agpaitic magmatism at Ilimaussaq, South Greenland: Rb-Sr study // Lithos. V. 9. 31-38.
63. **Gerasimovsky, V.I.** (1969). Geochemistry o fthe Ilimaussak alkaline massif. M.: Nauka. 174 p. (in Russian)

64. **Kogarko, L.N., Kramm, U., Granert, B.** (1983). New data on the age and genesis of the Lovozero alkaline rocks // DOKL. AN USSR. V. 268. № 4. P. 970-973. (in Russian)
65. **Gerasimovsky, V.I., Volkov, V.P., Kogarko, L.N., Polyakov, A.I., Balashov, Yu.A.** Geochemistry of the Lovozero alkaline massif. M.: Nauka. 395 p. (in Russian)
66. **Arzamastsev, A.A., Bea, F., Glaznev, V.N., Arzamastseva, L.V., Montero, P.** (2001). Kola alkaline province in the Palaeozoic: estimation of the primary mantle melts' composition and magma generation conditions // Russian magazine of the Earth's sciences. V. 3, №1. P. 3-24. (in Russian)
67. **Balashov, Yu.A.** (1985). Isotope geochemical evolution of the Earth's mantle and crust. M.: Nauka, 221 p. (in Russian)
68. **Hofmann, A.W.** (1988). Chemical differentiation of the Earth: the relationship between mantle, continental crust, and oceanic crust // Earth and Planet. Sci. Lett. V.90. P. 297-314.
69. **De Paolo, D.J., Wasserburg, G.J.** (1976). Inferences about magma sources and mantle structure from variations of $^{143}Nd/^{144}Nd$ // Geophys. Res. Lett. V. 3.P. 743-746.
70. **Carter, S.R., Evensen, N.M., Hamilton, P.J., O'Nions, R.K.** (1978). Continental volcanics derived from enriched and depleted source regions: Nd- and Sr-isotope evidence // Earth and Planet. Sci. Lett. V.37. P. 401-408.
71. **McDonough, W.F., Sun, S.** (1995). The composition of the Earth // Chem. Geol. V.120. P. 223-253.
72. **Goldstein, S.L., O'Nions, R.K., Hamilton, P.J.** (1984). A Sm-Nd study of atmospheeric dust and particulates from major river systems // Earth and Planet. Sci. Lett. V.70. P. 221-236.
73. **Balashov, Yu.A.** (1997). Pulsation model of mantle differentiation: Evolution, geochronological, geochemical, petrologic and geodynamic implications // Proc. 30th Intern. Geol. Congr. V.1. P. 79-95.
74. **Bell, K., Blenkinsop, J.** (1989). Neodymium and strontium isotope geochemistry of carbonatites // in Carbonatites: genesis and evolution (ed. By K.Bell).London-Boston-Sydney-Wellington.Unwin Hyman. P. 278-300.
75. **Nelson, D.R.** (1992). Isotopic characteristics of potassic rocks: evidence for the involvement of subducted sediments in magma genesis // Lithos. V. 28. P. 403-420.
76. **Morozov, Yu.A.** (2004). Cyclicity of cinematic inversions in mobile belts in light of Moon-Earth relations // Geotectonics. №1. P. 21-50.

UDK 552.33+550.42

Geochemistry of carbon and oxygen isotopes in carbonatites of Siberia and Mongolia and some geodynamic consequences

Vladykin N.V. [1], Morikiyo T. [2], Miyazaki T. [3]

[1] *lnstitute of Geochemistry of Siberian Branch, Irkutsk, Russia, e-mail: vlad@igc.irk.ru*
[2] *Department of Geology, Shinshu University, Asahi, Matsumoto, Japan*
[3] *Japan institute for Geothermal Sciences, Kyoto University, Beppu, Japan*

INTRODUCTION

Carbonatites are one of the most complex natural formations, associated with deep-seated silicate ultrabasic and alkaline rocks. Their magmatic genesis and the mantle pattern of initial magmas, which gave rise to these rocks as their differentiates does not call any doubts. As the surface does not always contain all members of carbonatite complexes and due to a poor outcropping of areas it is problematic to classify carbonate rocks as carbonatites. The mineralogical (availability of rare-metal Nb, Zr, TR-minerals) and geochemical criteria (heightened Ba, Sr, Nb, TR concentrations) are used for this purpose. The geochemistry of stable isotopes is of particular interest as it can be used for defining the type of mantle, which gave rise to carbonatites. However, there are a lot of problems of isotope geochemistry, which still remain unsolved, and the data accumulated results in expansion of existing boundaries of isotope "dogmas". For example, 20 years ago only rocks having the ratio of Sr isotope to be 0.703-0.704 were considered as mantle rocks. Progress in isotope Nd geochemistry and Nd isotope, Nd/Sr isotope ratio data show, that the ratio of Sr isotopes as 0.703 are characteristic of depleted mantle, while for enriched mantle EM-1 and particularly EM-2 mantle these values increase up to 0.720 (for example, in mantle lamproites of Australia and Spain). The scope of rocks which are associated with carbonatites has enlarged (for example, alkaline rocks of K- series) and occurrences of carbonatitic complexes [25]. It was earlier considered, that the carbonatitic complexes originate only on margins of platforms and shields. However, they are also abundant in areas of completed folding (e.g. Mongolia, Buryatia) [6-10]. As the carbonatitic complexes have the mantle genesis, associations of geodynamic settings and the type of primary mantle substratum is of particular interest [10, 19]. The given article discusses isotope data, obtained for carbonatitic occurrences of the Siberian Platform framing, Aldan shield, South Mongolia, Primor'e. It also gives the date concerning the massifs of the Kola Peninsula and Central Asia for comparison. Geochemical samples of carbonatites were collected for last 30 years by N.V. Vladykin, the isotope data were obtained by T.Morikiyo and T.Miyazaki in Shinshi, Kyoto and Niigata Universities (Japan). Besides, the article uses the

samples of E.A. Chernysheva, L.I. Panina and N.M. Podgornykh, the results of investigations were published in the joint article [12], which discusses the procedure of isotope analysis. Therefore here we give only a brief specification of this method.

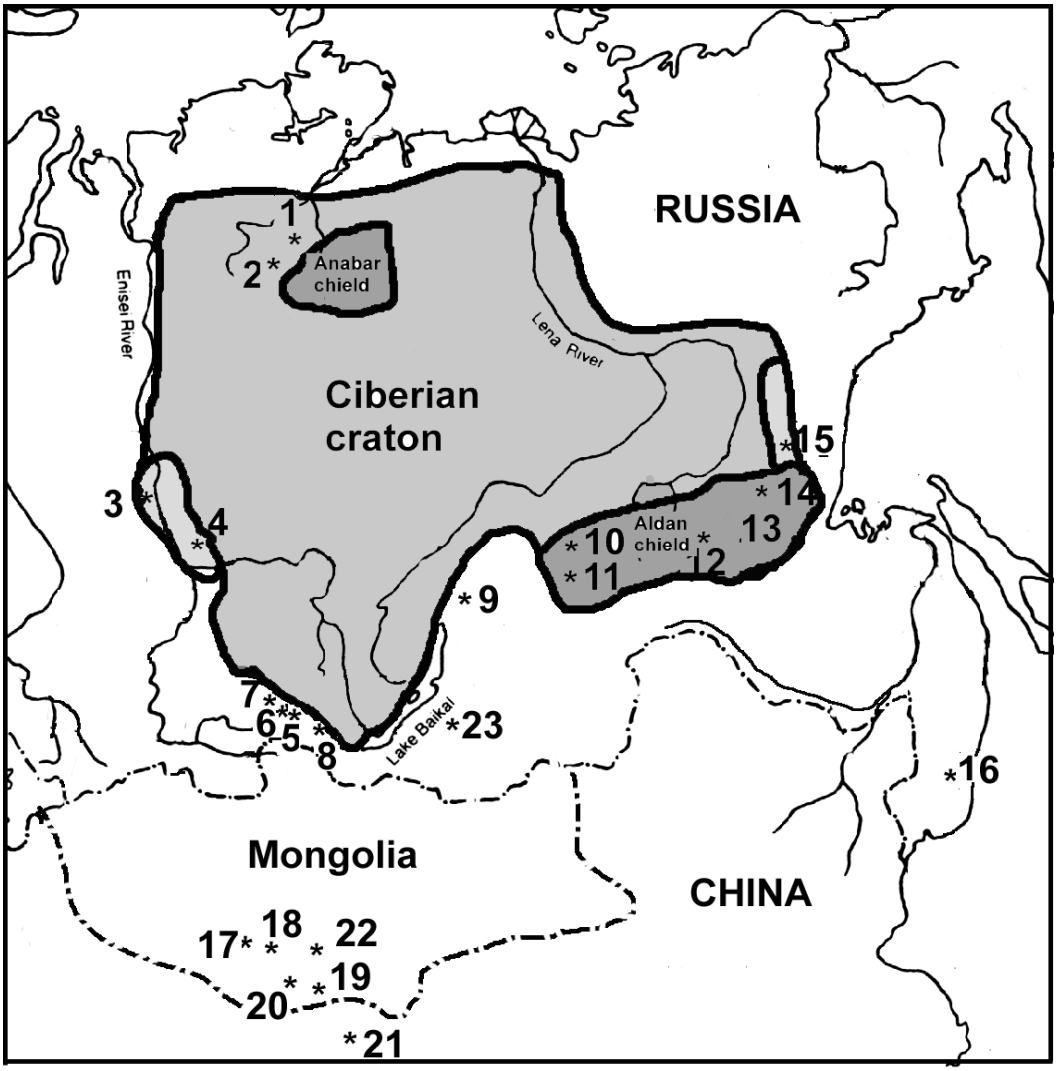

Fig. 1. **Geographic position of carbonatite massifs**.

Massifs: 1 - Guli, 2 - Essei, 3 - Kiya, 4 - Tatar, 5 - Belaya Zima, 6 - Srednaya Zima, 7- Tagna, 8 - Zhidoi, 9 - Burpala, 10 - Murun, 11- Khani, 12 - Bilibin, 13 - Arbarastakh, 14 - Ingili, 15 - Gornoe Ozero, 16 - Koksharov, 17- Mushugai, 18 - Bayan- Khushu, 19 - Lugingol, 20 - Khan-Bogdo, 21 - Bayan-Obo, 22 - Ulugei, 23 - Khaluta.

ANALYTICAL PROCEDURE

The experimental procedure for carbon and oxygen isotope ratio determination follows that outlined by [11]. The oxygen isotope fractionation factor determined by Sharma and Clayton [15], $\alpha_{CO2\text{-}CC}$=1.01025, was used to calculate the $^{18}O/^{16}O$ ratio of calcite. The isotopic data are presented in terms of the δ notation relative to PDB for carbon and SMOW for oxygen. Analytical

uncertainty is about ±0.1‰ for both $\delta^{13}C$ and $\delta^{18}O$.Concentrations of rare-earth elements of the carbonatites were determined by the instrumental neutron activation analysis at the Research Reactor Institute of Kyoto University following the procedure described by Koyama and Matsushita [4].

CARBONATITES OF THE SIBERIAN PLATFORM FRAMING

The given article considers the data on carbon and oxygen isotopes for the East-Sayan Province (Bolsheziminski, Srednezieminski, Tagninski and Zhidoi massifs), Maimecha-Kotui province (Guli and Essei massifs), Yenisei Ridge (Kiya and Tatar massifs). The location of massifs is shown in Fig. 1. The values of carbon and oxygen isotopes are given in Table 1.

Guli massif. This is the largest massif of carbonatitic complexes. The area of the massif is 600 km^2 (from geophysical data it is 2000 km^2). It is located in the north of the Siberian Platform and is included into the Maimecha–Kotui province. The massif has concentrically-zonal structure and contains [2]: dunites-peridotites, pyroxenites, melilitic rocks, olivine melanephelinites, ijolites, nephelinic and alkaline syenites. The magmatic series is terminated by calcite and dolomitic carbonatites. The variations of carbon isotopes in carbonatites are minor, within the range from -2.9 up to -5.3 (Table 1), while oxygen isotope values vary from 6.4 up to 11.6. The heaviest carbon and the lightest oxygen occur in the calcite carbonatite with pyroxene and pyrochlore, while the lightest carbon and heaviest oxygen are found in the dolomitic carbonatite (Fig. 2). In carbonatites, where calcite and dolomite coexist, the distribution between them is the following. In early forsterite - calcite carbonatites (which contain scarce dolomite) the oxygen isotope values are identical, and the carbon is heavier in dolomite. In dolomitic carbonatites (which contain scarce calcite) carbon isotope values in coexisting carbonates are identical, and oxygen is heavier in calcite. As a whole from early carbonatites to late there is an increase of values of both oxygen and carbon.

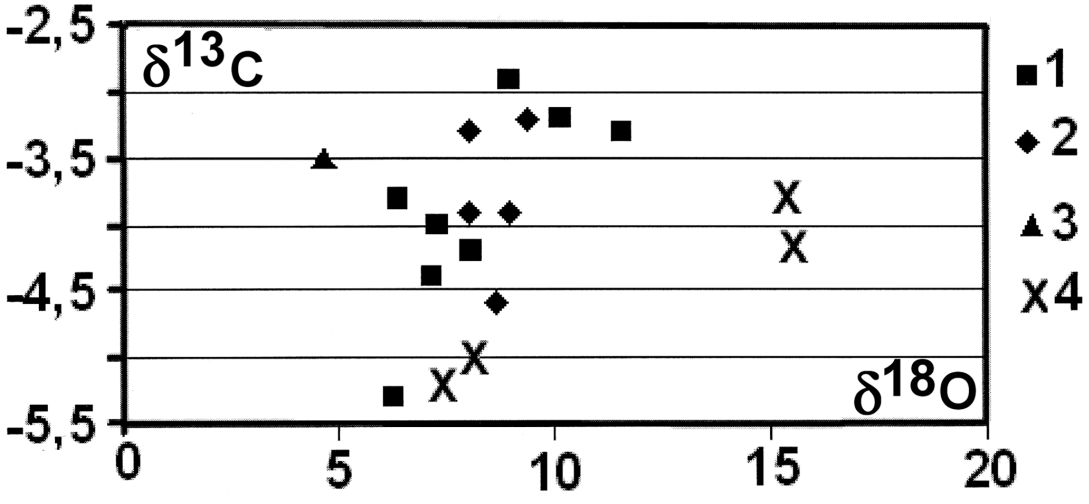

Fig. 2. **Carbon and oxygen isotope ratios in massifs: 1-Guli 2-Essei, 3-Kiya, 4-Tatarskiy.**

Table 1.

The values of carbon and oxygen isotopes in carbonatites of Siberia and Mongolia

#	Massif	№ sample	Rock name	Calsite		Dolomite	
				^{18}O	^{13}C	^{18}O	^{13}C
1	Essei	e2014	**Dol -Кс carbonatite with Ap и Mgt**	8,0	-3,9	8,0	-3,3
2		e200	**Fors.-Ap-Mgt rocks with Dol.-Кс.**	9,0	-3,9	9,4	-3,2
3		e2028	**Mgt –Ap rocks**	8,7	-4,6		
4	Guli	Gu-1	**Phl-Кс carbonatite with Py и pirokh.**	6,3	-5,3		
5		Gu-2	**Fors.-Кс carbonatite +Mgt+pirokh+bad**	7,2	-4,4	7,3	-4,0
6		Gu-3/4d	**Dol- carbonatite with pirokh**			6,4	-3,8
7		Gu802d	**Dol- carbonatite**			9,0	-2,9
8		Gu803/2	**Кс- carbonatite**	8,1	-4,2		
9		Gu823	**Dol.-Кс carbonatite**	11,6	-3,3	10,2	-3,2
10	Kia	Ki y-240	**Кс- carbonatite**	4,7	-3,5		
11	Tatarski	T2371/10	**Кс- Fors carbonatite**	15,5	-4,1	15,3	-3,8
12		T1704/27d	**Dol carbonatite**			7,4	-5,2
13		T162/35d	**Ank-dol carbonatite**			8,2	-5,0
14	Belay a Zima	B1a	**Gr-Py-Ne-Кс carbonatite**	7,4	-5,9		
15		B1b	**Gr-Py-Ne-Кс carbonatite**	6,6	-5,8		
16		B1c	**Gr-Py-Ne-Кс carbonatite**	6,7	-5,5		
17		B2a	**Py–Кс carbonatite with Mgt, Phl, Ap, pirokh**	6,6	-6,0		
18		B2b	**Py–Кс carbonatite with Mgt, Phl, Ap, pirokh**	6,9	-5,9		
19		B6w	**Ank carbonatite**	6,6	-5,7	6,1	-5,0
20		B6g	**Ank carbonatite**	7,3	-4,9	6,3	-4,8
21		B7	**Ank carbonatite**	10,7	-4,1	9,8	-4,0
22		B5/11	**Bt-Кс-Py carbonatite**	7,3	-6,0	6,5	-5,8
23		B66/2	**Кс-Phl-Py, carbonatite**	8,0	-5,9		
24		B521/6	**Кс-Phl carbonatite**	5,2	-4,5	4,8	-4,5
25		B549/4	**Кс-Py carbonatite**	8,1	-6,1		
26		B598/3	**Кс-Phl-Fors. Carbonatite with pirokh**	8,0	-5,3	8,10	-4,8
27	Srednjaja Zima	SB1/1	**БиBt-Кс carbonatite**	6,80	-5,5		
28		SB 86/7	**Bt-Py-Кс carbonatite**	7,60	-5,7		
29		SB 113/3	**Кс carbonatite**	6,90	-5,5		
30	Tagna	BT1	**Кс carbonatite**	12,0	-2,6		
31		BT2	**Кс carbonatite with Mgt-20%**	12,4	-3,1		
32		BT3-4	**Кс-Mi rocks**	13,9	-3,0		
33		BT5	**Bt-Fsp-Py rocks**	13,2	-3,7		
34		BT8/11	**Кс carbonatite**	12,5	-2,9		
35	Zidoi	Zd316/3	**Кс carbonatite with Ap**	7,5	-5,2		
36		Zd327	**Кс carbonatite**	7,1	-5,5		
37	Burpala	Bur311/21	**Qu-Кс carbonatite**	12,8	-1,8		
38	Коксharovski	Kw 22	**Кс carbonatite**	11,2	-4,2		
39	Darai-Pioz	Dp322	**Кс-Ap carbonatite with TR**	15,9	-3,2		
40		Dp91/1	**Кс-Py carbonatite**	16,3	-2,9		

Table 1 (End).

#	Massif	№ sample	Rock name	Calsite		Dolomite	
41	Mushugai Khuduk	Myw540a	**Ксенолиты Кс в меланефелинитовой лаве**	13,0	1,2		
42		Myw1986	**Кс carbonatite**	15,2	-1,6	16,6	1,3
43		Myw1910	**Кс carbonatite**	15,6	-0,7		
44		Muw1977	**Flu-Кс- carbonatite**	16,9	-1,5		
45	Lugingol	Ly1778	**Кс-sinkhisite carbonatite**	23,3	-1,5		
46		Ly1779	**Кс-bastnesite carbonatite**	24,6	-2,4	25,2	-2,1
47		Ly-1d	**Кс-bastnesite carbonatite**			19,1	-0,3
48	Bain-Khushu	Bax2031	**Кс-Flu-celistine carbonatite**	17,9	-0,9		
49		Bax2032d	**Dol Tuffs**			22,3	-0,6
50	Gornoe Ozero	ro1	**Кс - carbonatite**	8,5	-4,7	8,3	-4,4
51		ro2d	**Кс- carbonatite with TR (berbankite)**	17,8	-2,5		
52	Ingili	ung309	**Кс-Bt-Amf carbonatite**	8,0	-6,5		
53		ung314	**Bt-Кс carbonatite**	8,1	-6,6		
54		ung42/50	**Flu-Кс carbonatite**	13,0	-5,9	13,9	-5,4
55	Arbarastakh	Abc275	**Кс-Amf -Bt carbonatite**	9,3	-5,3		
56		Abc273	**Кс-Mgt-Ap carbonatite with pirokh**	7,6	-5,3	7,9	-4,6
57	Murun	Za136/52	**Кс--benstonite carbonatite**	9,4	-7,5		
58		Za137/5	**Qu-Кс carbonatite (grafic)**	9,7	-7,9		
59		Za143	**Кс carbonatite (Кс+Fsp+Py)**	7,9	-8,1		
60		Za157	**Benstonite carbonatite with Fsp**	8,3	-6,5		
61		Za173	**Charoite-Кс carbonatite**	9,4	-7,7		
62		Za186	**Кс- carbonatite with Tff, К-rikhterite**	10,4	-6,6	9,7	-6,2
63		Z1052/20	**Bt-Py-Кс carbonatite**	9,8	-5,2		
64	Khani	Xn205	**Кс- carbonatite with Fsp, Py, Ap**	8,6	-8,0		
65		Xn206	**Кс- carbonatite с Ap Fsp, Gr**	8,5	-8,4		
66	Bilibinski	Lam67/9	**Кс- carbonatite с Ap**	8,3	-4,6	7,5	-4,4
67	Turii Mys	Tu 316/4	**Phl-Кс carbonatite**	7,6	-2,4		
68		Tu 330 /4	**Bt carbonatite with Ap**	8,5	-2,8		
69		Tu 324/4	**Кс- carbonatite with Tff +dol**	8,1	-2,2	7,3	-2,0
70	Vuorijarvi	VJ1	**Fors-Кс- carbonatite**	7,5	-4,6		
71		VJ2	**Phl- Кс- carbonatite**	7,3	-3,4		
72	Kovdor	Kv-1d	**Dol carbonatite**			9,7	-1,7
73		Kv-2	**Dol-Кс carbonatite**	15,7	-1,2		
74		Kv-3d	**Dol carbonatite**			9,4	-1,8

Note. Dol.-dolomite, Кс-calcite, Ap-apatite, Mgt-magnetite, Fors.-forsterite, Py-pirocsene, Gr-garnete, Phl-phlogopite, Bt-biotite, Fsp-feldspate, Amf-amfibole, Tff-tetraferriphlogopite, Qu-quarz,Pirokh –pirochlore, Flu- fluorite, bad- baddeliite, Mi- mikrokline. Samples № 46,47,54, contain basnesite rathen than dolomite, sample № 51- contains berbankite.

Essei massif. It is located in the same province. The area of the massif is 6 km^2. It is composed of olivinites and peridotites, ijolites, forsterite–apatite-magnetite rocks (phoskorites) and calcite carbonatites [2]. Variations of carbon isotopes in carbonatites and phoskorites range from -3.2 to -4.6, while those of oxygen vary from 8.0 up to 9.4. The lightest carbon is found in apatite-magnetite

rock. In coexisting calcite and dolomite from carbonatites and phoskorites the oxygen isotope values are similar, and carbon is heavier in dolomite (content of dolomite in both rocks is minor).

Kiya massif. The massif is located in the North-West part of the Yenisei Ridge, the area is 15 km2. The massif contains ijiolites, nephelinic and alkaline syenites and carbonatites. In calcite carbonatites carbon isotope value is -3.5 and oxygen isotope value is 4.7. It is the lightest oxygen among all Siberian carbonatites, investigated by us.

Tatarskiy massif. It is located in the southeast part of the Yenisei Ridge [3]. The massif is composed of dolomitic, calcite-forsterite and ankeritic carbonatites. Silicate rocks have not been found in the massif. Xenoliths of strongly chloritized and serpentized rocks, which could be possibly the early rocks of the massif, are available. Variations of carbon isotope values in carbonatites range from -3.8 to -5.2, and those of oxygen vary from 7.4 to 15.52. In coexisting calcite and dolomite (calcite is much more abundant, than dolomite) oxygen isotope values are similar, and carbon is heavier in dolomite.

East-Sayan province. The province includes 4 massifs: Belya Zima, Srednyaya Zima, Tagna and Zhidoi [3].

Belaya Zima massif (Nizhesayanski). The area of the massif is 17 km^2. It contains [3] pyroxenites, ijolites, melilitic rocks, syenites and carbonatites. The massif also involves calcitic, dolomitic and ankeritic carbonatites, which are divided into 5 stages of carbonate formation. Variations of carbon isotope values in carbonatites are insignificant, from -4.0 up to -6.1 while those of oxygen are significant, ranging from 4.8 up to 10.7. In calcite carbonatites containing different minerals (pyroxene, garnet, phlogopite, forsterite, pyrochlore, sulfides) carbon isotope values vary from -4.8 to -6.0, and the oxygen isotope values remain similar (Fig. 3). In calcite - dolomitic and ankerite-calcitic carbonatites, where 2 carbonates coexist, carbon isotope data in pairs are similar, and the oxygen is heavier in calcite, though the content of calcite is much less, than that of ankerite.

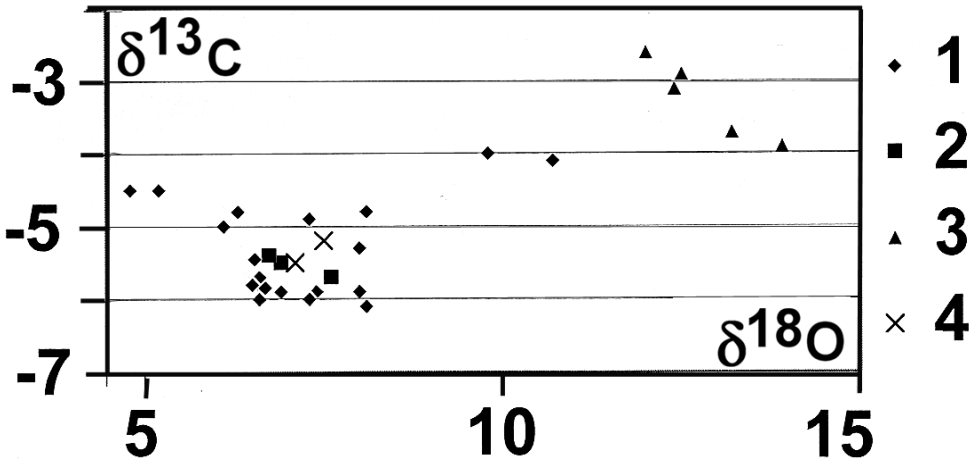

Fig. 3. **Carbon and oxygen isotope ratio in massifs.**

1- Belaya Zima, 2-Srednaya Zima, 3- Tagna, 4- Zhidoi.

Srednyaya Zima Massif (Verkhnesayanski). The area of the massif is 7 km^2. It is composed of ijolites, nephelinic syenites and carbonatites. Carbonatites are calcitic with biotite and pyroxene. Variations of isotope values are minor: carbon from -5.5 up to -5.7, and oxygen from 6.8 up to 7.6.

Tagna massif. The area of the massif is 9 km^2. It involves ijolites, alkaline syenites, microclinites, carbonatites and dikes of picrites, tinguaites and nephelinites. The carbonatites are divided into calcitic, calcite-fluoritic and ankeritic. Variations of carbon isotope values in carbonatites and microclinites vary from -2.6 to -3.9, while those of oxygen are from 12.0 up to 13.9. The Tagna massif contains the heaviest carbon among those three massifs.

Zhidoi massif. The massif is located southwards as opposed to the above three massifs.The massif is composed of pyroxenites, ijolites and dikes of syenites and carbonatites [22]. Carbonatites are of calcite composition with scarce apatite. A separate article is dedicated to a problem of isotope geochemistry of the Zhidoi massif [13]. The values of carbon and oxygen isotopes in carbonatites of the Zhidoi massif are similar to those of carbonatites from Belaya Zima massif.

For comparison with carbonatites of the Siberian Platform we have analyzed some of carbonatite samples from the Kola Peninsula (Kovdor, Vuoriyarvi massifs and the massif of Tur'ev peninsula) [3, 21].

Kovdor massif belongs to classic massifs of ultrabasic-alkaline rocks and carbonatite. The area of the massif is 40 km^2. The massif contains [3] olivinites, pyroxenites, melilitic and monticellite rocks, ijiolites and dikes of alkaline nepheline syenites. The younger rocks involve a large stock of phoskorites of the ore complex (magnetite-forsterite-apatite-phlogopite-calcite rocks), transferring on depth into calcitic and dolomitic carbonatites. In the center of the massif there is a large body of olivine, diopside- phlogopite rocks. The values of carbon isotopes in carbonatites vary within minor limits from -1.2 to -1.8, while oxygen isotopes range from 9.4 to 15.7 (Table 1, Fig.4). In dolomitic carbonatites isotope variations are insignificant, and dolomite-calcite carbonatite contains heavier carbon and oxygen, as opposed to pure dolomitic rocks (-1.2 and 15.7, accordingly).

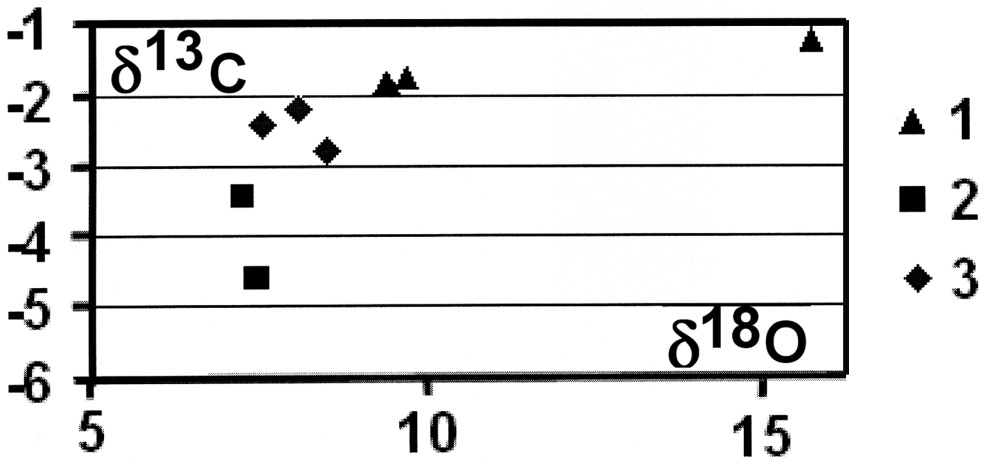

Fig. 4. **Carbon and oxygen isotope ratio in massifs.**

1-Kovdor, 2-Tur'ev mys, 3- Vuorijarvi.

Vuorijarvi massif. The area of the massif is 20 km^2. The massif comprises pyroxenites, ijiolites, phoskorites (apatite-magnetite-phorsterite rocks) and calcite carbonatites. The forsterite - calcite and phlogopite-calcite carbonatites do not differ in oxygen isotopes (7.3-7.5). Variations of carbon isotopes are more considerable, from -3,4 to -4,6, and phlogopite carbonatites contain heavier carbon.

Carbonatite occurrences of the Tur'ev peninsula. In region of carbonatite occur-rences the outcrops of pyroxenites, melilitic rocks, ijiolites, and apatite-magnetite rocks are available. Carbonatites are calcitic with phlogopite, apatite and tetraferri-phlogopite. Variations of carbon isotopes are minor from –2.2 to –2.8 and those of oxygen range from 7.6 to 8.5. The heaviest oxygen is found in apatite carbonatite. In terms of geochemistry isotopes carbonatites of the Kola Peninsula are similar to carbonatites of massifs of the Siberian platform framing.

CARBONATITES OF FOLDED BELTS

The given section considers the carbonatites of Mongolia, Primor'e and North Pribaikalie. Occurrences of carbonatites of K-series are found in Mongolia, South Gobi. They include volcanics of Mushugai-Khuduk and Bayan-Khushu [6,8] and Lugingol [5] massif of pseudoleucite syenites. The latter is located in 100 km from the occurrence of carbonatites with TR ores in China (Bayan-Obo).

Mushugai-Khuduk volcanic area. It is located in 100 km to the south of Dalandzagad city. The flows of lava and tufflava of melanephelenites, trachytes, phonolites, stocks of nepheline and alkaline syenites occur on the area of over 100 km^2. They are cut by dikes and diatremes of apatite-magnetite and carbonatitic composition. Carbonatites are mainly calcitic and calcitic-fluoritic. Cerussite-containing tuffs are found as well [20, 25]. The heavier carbon and oxygen isotopes are characteristic of all carbonatitic occurrences as opposed to carbonatites of other areas. Variations of carbon isotopes in Mushugai-Khuduk carbonatites range from - 1,6 up to + 1,2, and those of oxygen vary from 13 up to 16.9. The liquation separations of carbonatites in lavas of melanephelinites and melaleucite (Table № 540a) contain the heaviest carbon isotopes and the lightest oxygen ones (Fig. 5). The microgranulated dike of calcite and calcite–fluorite carbonatites are marked by the lightest isotopes of carbon and similar values of oxygen isotopes. The coexisting calcite–dolomite in carbonates have similar values of oxygen isotopes while the carbon isotopes n in dolomite are much heavier, as opposed to calcite.

Bayan-Khushu massif. It is located in 50 km eastward of Mushugai-Khuduk. The massif is composed of shonkinites, nephelinic and alkaline syenites, which are cut by dikes of calcite-fluorite –celestine (and barite) carbonatites. The hosting rocks contain the veined body of dolomitic tuff. Carbon isotope values vary from -0,6 up to -0,9, and oxygen isotopes range from 17,9 up to 23,8. The tuff is marked by heavier oxygen isotope as compared with carbonatite.

Lugingol massif is situated in 250 km south-westwards of Mushugai-Khuduk and in 100 km eastward of the largest Khan-Bogdo agpaitic massif of alkaline

granites [5, 16]. It is composed of nephelinic and pseudoleucite syenites of the major phase of the massif, which also contains the xenoliths of feld-spar pyroxenites and shonkinites. The syenites are cut by dikes of pseudoleucite syenites, pseudoleucite tinguaites and calcite carbonatites with bastnesite, sinkhisite. The carbon isotope values varying from -1,5 up to - 2,4 and very heavy oxygen from 23,3 up to 25,2 is typical of carbonatites. In coexisting calcite-bastnasite the calcite is marked by lighter isotopes. Shonkinite dikes occur in 50 km westward of Lugingol. In chemical and mineral composition they are similar to shonkinites of TR deposit Mautin-Pass (USA). The dyke of dolomitic carbonatites with bastnaesite (30 %) (Table 1 № Ly-1d) is found as well. Carbon isotope value for this carbonatite is -0,3 and that of oxygen is 19,1.

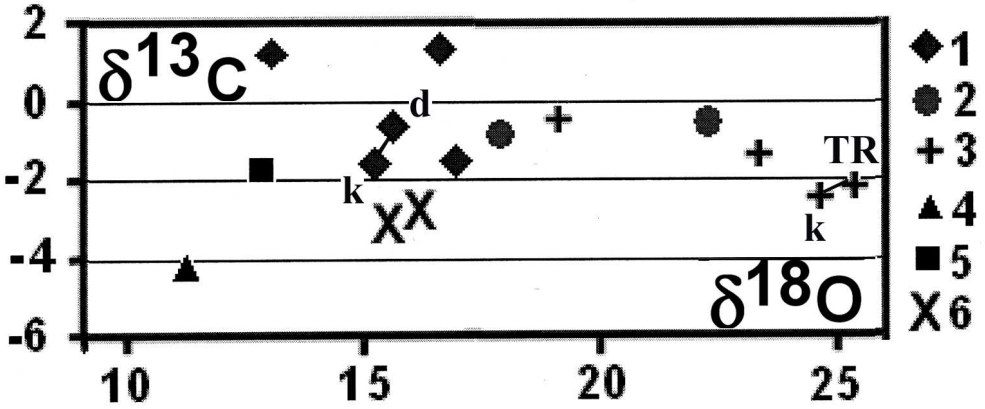

Fig. 5. **Carbon and oxygen isotope ratio in massifs.**

1 - Mushugai, 2 – Bayan-Khushu, 3 - Lugingol, 4 - Kokshar, 5 - Burpala, 6 - Darai-Pioz. The line connects co-existing calcite (k) -dolomite (d), and и calcite (k) - bastnaesite (TR).

Koskharovskiy massif in Primor'e is composed of pyroxenites, which are cut by dikes of agpaitic nephelinic syenites and calcite carbonatites [19]. The carbon isotope values as - 4,2 and those of oxygen as 11,2 are characteristic of carbonatites.

Burpala massif is located in the North Pribaikalie, in 100 km north-eastward of the northern margin of Lake Baikal [19]. The massif contains nephelinic, alkaline and quartz syenites, which are cut by numerous dikes of rare-metal agpaitic syenites-pegmatites.The central massif's zone comprises a large body of apatite-fluorite rocks, containing magnetite and mica (fluorite analog of phoskorites). The carbonatitic dikes of calcite composition with brewsterite are found in the center of the massif while calcite dikes with a quartz and pyrite occur in the host rocks. The latter has determinations of carbon and oxygen isotopes as -1,8 and 12,8 correspondingly.

Darai-Pioz massif is found in South Tyanshan at the altitude of 5000 m. The massif is composed of nephelinic, alkaline syenites and alkaline granites, which are cut by dikes of carbonatites and rare-metal alkaline-granite pegmatites. Calcite-pyroxene carbonatites contain rare metal mineralization [18]. Isotope variations in

carbonates are the following: carbon from -2,9 to - 3,2, oxygen from 15,9 up to 16.3. Lighter carbon and oxygen isotopes are characteristic of rare-metal carbonatite.

CARBONATITES OF RIFT ZONES OF SIBERIAN PLATFORM AND ALDAN SHIELD JOINING

The carbonatitic complexes of this structural region can be divided into 2 groups [26]. The first group includes complexes of the western and central parts while the second one comprises complexes of the eastern part [26]. The first group contain Mz –Murun massif and Bilibin massif and Pre-Cm –Khani massif while the second one includes Low Paleozoic Arbarastakh, Ingili and Mountain Lake massifs. The massifs of the second group can be probably assigned to the Siberian Platform framing.

Murun massif. The area of the massif is 150 km2, age is 145 Ma. It belongs to volcano-plutonic ultrapotassium stratified alkaline complex [23]. The massif contains complex of Bt-pyroxenites, K -ijolites, leucite shonkinites and fergusite (early comp-lex) with xenoliths of olivine-spinel monticellite-melilitic rocks. The rocks of the major phase involve the stratified complex of melanoctratic and leucocratic pseudoleucites, alkaline syenites and alkaline granites. At later stage tuff lavas and leucite phonolites and leucite lamproites flows were erupted and the dykes of leucite tinguites were intruded. The later phase contains a stratified silicate-carbonate comp-lex of microclinites, microcline-pyroxene rocks, charoite rocks, as well as calcite and benstonite carbonatites [27, 28]. Then all rocks were subjected to hydrothermal silici-fication and sulfidization, containing numerous ore mineralization. We have revealed 5 types of carbonatites and over-intrusive zone of calcite- K-rickterite-tetraferriphlo-gopite rocks [19]. Variations of carbon isotope range from –5.2 to - 8,1, and those of oxygen are from 7.9 to 10.4. The lightest isotopes of oxygen are typical of early calcite and benstonite carbonatites (Fig. 6). Moreover, calcite carbonatites contain lighter carbon. Similar values of oxygen isotopes from 9,4 to 10,4 but different values for carbon isotopes are characteristic of other types of carbonatites. Lighter carbon is found in silicate-carbonate calcite-charoite and quartz-calcite carbonatites, while the heaviest carbon occurs in mica-containing varieties. In the calcite - dolomitic pairs a lighter carbon and heavier oxygen are typical of calcite which is abundant.

Bilibin massif. The area of the massif is 150 km2. It belongs to K-leucite comp-lex of rocks [17]. The massif is composed of the stratified complex of micaceous peridotites, Bt- pyroxenites, olivine-leucite lamproites and leucite fergusites. Shonki-nites, leucite and alkaline systenites and alkaline granites were crystallized later. The second group of rocks has gradual transitions. A unique differentiation from ultraba-sic rocks to granites is common to the massif. A small clump of apatite - calcite carbonatites has been found among occurrences of ultrabasic rocks. The clump could be brought from the Arbarastakh massif, located in 100 km eastwards.

The dolomite phase has been also found in the calcite carbonatite. Heavier carbon and lighter oxygen are common to dolomite.

Khani massif (Ukduska site). The massif is composed of apatite-biotite pyroxenites, shonkinites, syenites and granites. Pyroxenites are cut by the dike of the layered syenite-carbonatites (calcite) and dike of olivine lamproites [19]. Carbon isotopes as -8,0 -8,4 and oxygen isotopes as 8,5 - 8,6 are characteristic of carbonatites.

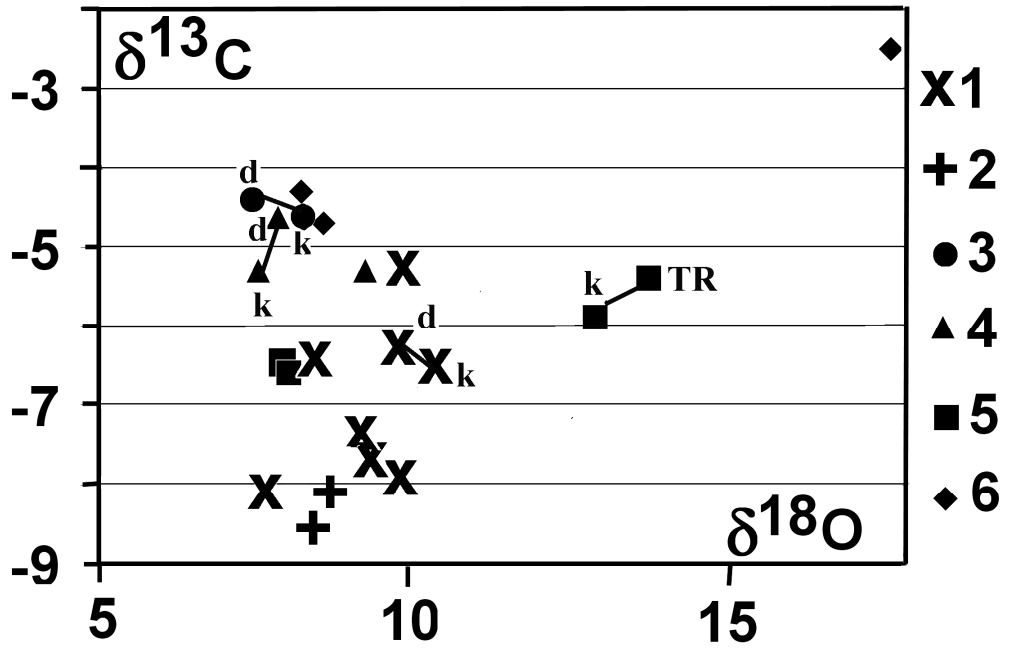

Fig. 6. **Carbon and oxygen isotope ratio in massifs.**

1 - Murun, 2 - Khani, 3 - Bilibinski, 4 - Arbarastax, 5 - Ingili, 6 - Gornoe Ozero. The line connects co-existing calcite (k) - dolomite (d), and и calcite (k) - bastnesite (TR)

Arbarastakh massif. The area of the massif is 42 km^2. The major phase of the massif contains pyroxenites with sites of biotite pyroxenites. The whole massif is cut by ring-type dikes of carbonatites and in some cases by cancretite and alkaline syeni-tes. The center of the massif is composed of phoskorites (apatite-magnetite-forsterite-calcite rocks). Similar values of carbon isotopes and variations of oxygen ranging from 7,6-9,3 are characteristic of calcite carbonatites. The calcite – dolomite pair in dolomite contains a heavier carbon.

Ingili massif. The area of the massif is 20 km^2. The massif contains amphibole-pyroxenites rocks and biotite pyroxenites, which are cut by dikes of ijolites, syenites and calcite carbonatites with amphibole and mica [19]. The authors use samples from the borecore to refine the magmatic scheme of the massif. Diatremes composed of basaltoid rocks (ingilites) with numerous xenoliths of the earth's lower crust have been found beyond the massif's contact. Similar values of isotopes are characteristic of calcite carbonatites with amphibole and mica. A younger (considering the time of intrusion) the calcite-fluorite carbonatite

with TR-carbonate veinlet contains heavier oxygen, moreover TR-carbonate contains heavier carbon and oxygen as compared with calcite.

Gornoe Ozero massif. The area of the massif is 9,3 km^2. It contains pyroxenites, ijolites, syenites, magnetite forsterite and carbonatite (calcite and rare-earth) rocks [3]. Oxygen and carbon isotopes in calcite-dolomite pair are almost identical (carbon -4,4 and - 4,7, and oxygen 8,3 and 8,5). Large separation of rare-earth carbonate underwent the structural disintegration into berbankite and other minerals. Thus, a heavier oxygen and carbon are common to it as opposed to calcite and dolomite of carbonatites.

As a whole it should be noted, that the oxygen and carbon isotope values in carbonatites originated in different geodynamic settings are considerably different, that will be discussed below.

THE ASSOCIATION ^{13}C AND ^{18}O ISOTOPES WITH THE TYPE OF MANTLE AND GEODYNAMIC SETTINGS

As known, the type of primary magma for massifs is determined from the data of Sr and Nd isotopes. Fig. 7 shows part of oxygen and carbon isotope data for [1] intrusive, volcanogenic etc. carbonatites of the world.

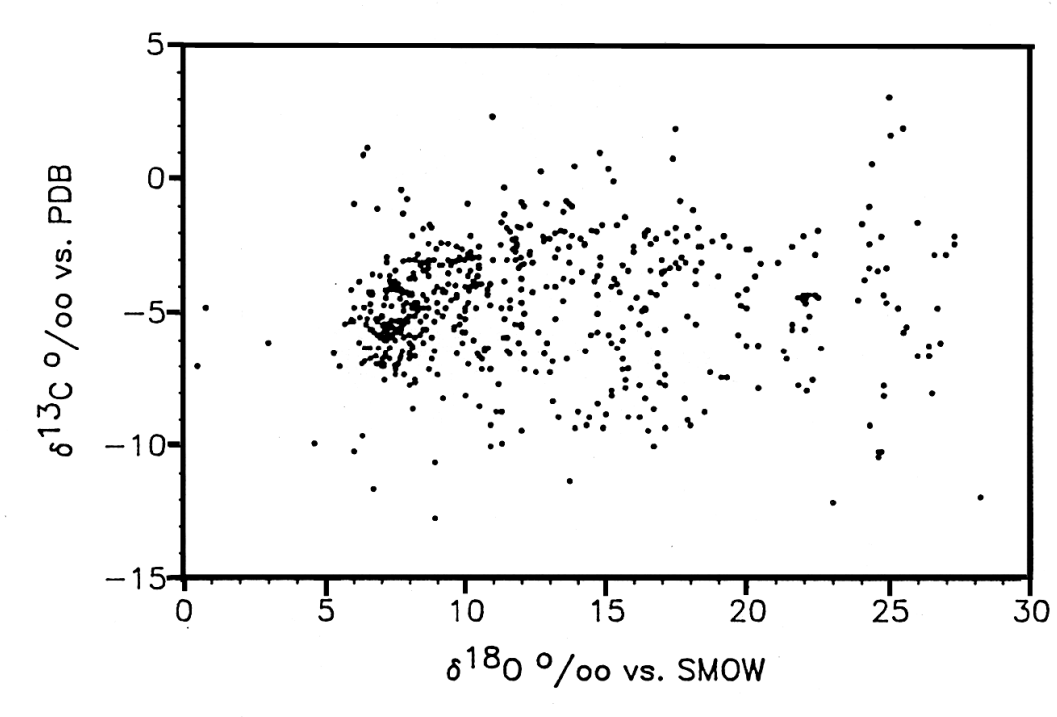

Fig. 7**. Carbon and oxygen isotope ratio in carbonatites of the world [1].**

There are great variations of the data, resulting from a number of factors, which are hardly to be interpreted. We made an attempt to systematize our data for carbonatites of Siberia and Mongolia. For the majority of samples we have Sr and Nd isotope data (Fig. 8). They are used for identifying type of the mantle, which gave rise to alkaline complexes [19, 24]. The geologic position and geodynamic

setting of the massifs under study provided an interesting deduction [24]. Different types of mantle (Fig. 8) are characterized by different geodynamic settings of alkaline rocks generation.

So, the massifs locating in the Siberian Platform framing and exhibiting subduction, were formed from depleted mantle. Massifs of folded belts (completed folding) have isotope determination of enriched EM-2mantle. Massifs locating in rift zone between the Siberian Platform and Aldan shield (as well as between North American Platform and Canadian shield) have isotope determinations of the deepest enriched EM-1 mantle [19]. We made an attempt to use the data concerning the mantle type obtained from the diagram of Sr and Nd ratio for the same samples on the plotof carbon and oxygen isotope ratios (Fig. 9). A rather compact pattern of separating massifs by mantle type has been obtained.

Massifs of the completed folding (Mongolia, Buryatiya, North Pribaikalie, Tyanshan etc.) fall into field 3. Their initial magmas generated from enriched mantle EM-2.

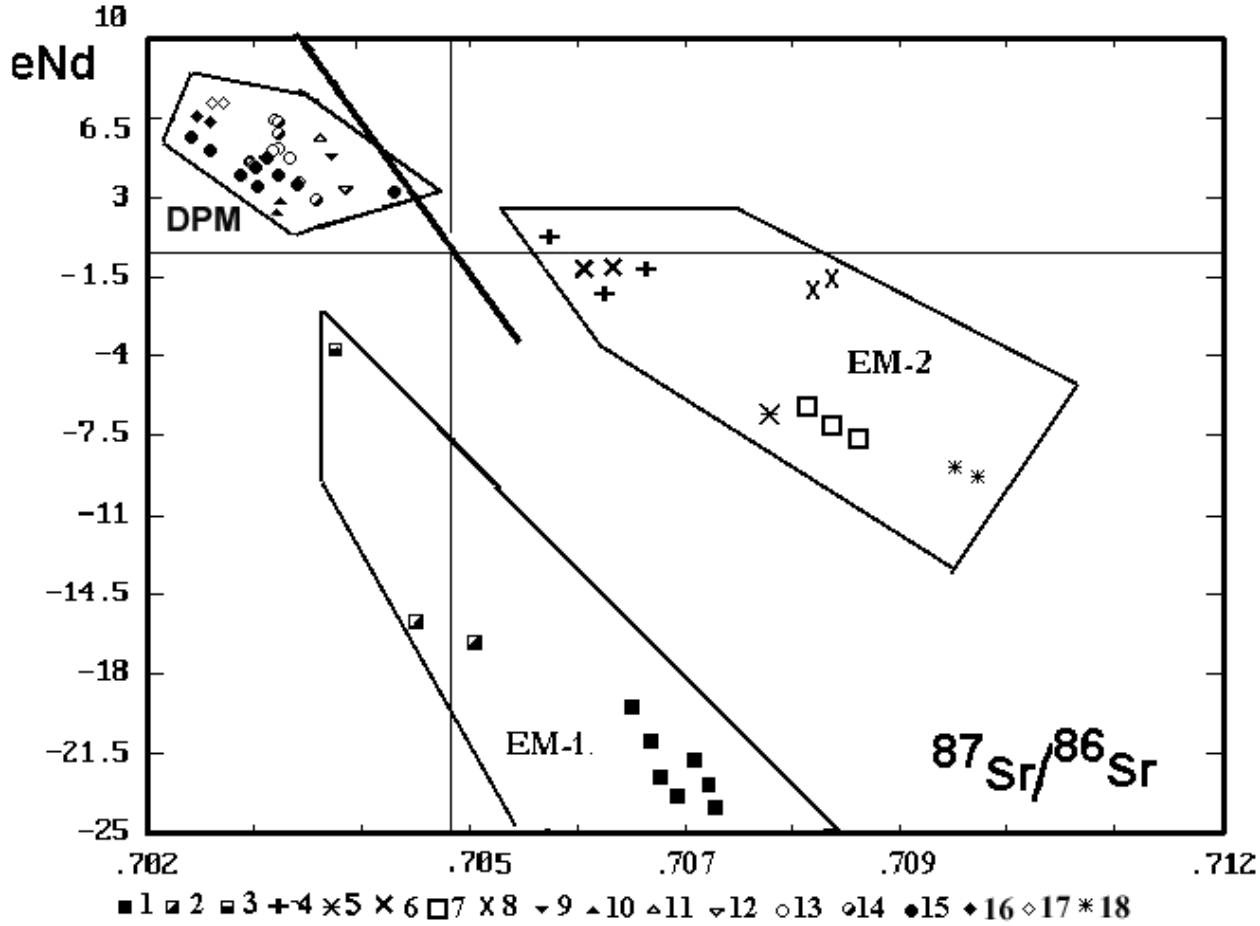

Fig. 8. **Sr/Nd isotope ratio**.

Massifs: 1 - Murun, 2 - Khani, 3 - Bilibinski, 4 - Mushugai, 5 - Burpala, 6 - Baian-Khushu, 7 - Darai-Pioz, 8 - Lugingol, 9 - Gornoe Ozero, 10 - Zidoi, 11- Kokshar, 12 - Kiya, 13 - Guli, 14 - Kola, 15 - Saiani, 16 - Ingili, 17 - Arbarastakh, 18 - Beltsin-Gol. DPM - depleted mantle.

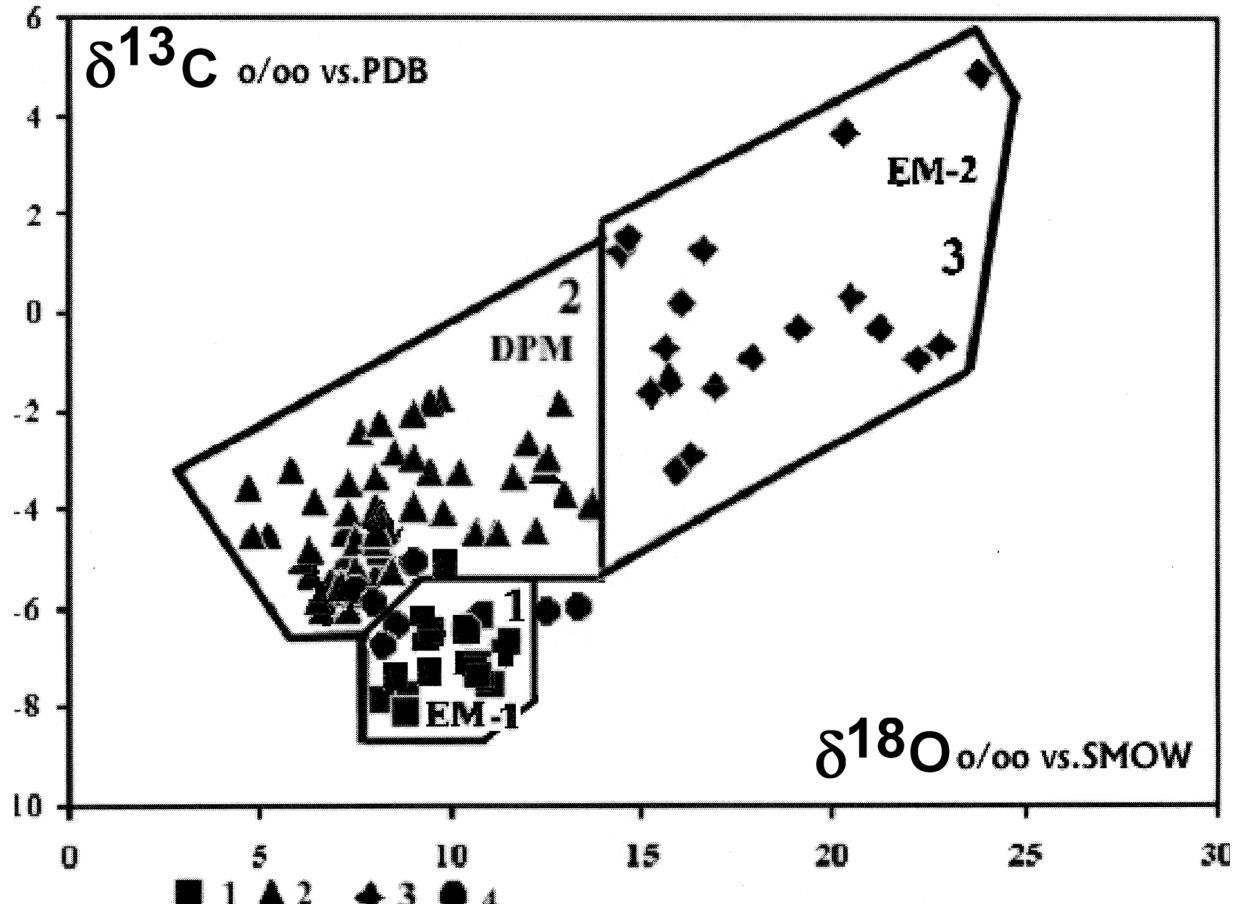

Fig. 9. **Carbon/oxygen isotope ratio and types of the mantle**.

Field 1 - EM-1 mantle. Field 2 - depleted mantle. Field 3 – EM-2 mantle. Conventional units. Massif: 1 - Murun, Khani, 2 - Bilibin, Inagli, Arbarastakh, 3 - massifs of the Siberian Platform framing, 4 - massifs of folded areas.

Earlier isotope determinations in the field 3 for carbonatites is conditioned by capturing of atmospheric oxygen and surface water during formation [14]. For the studied carbonatites this mechanism can act, but as secondary one. When rocks of the zone of the completed folding are generated the surface water was captured and these rocks have heightened values of heavy oxygen. When they subsided along Benioff zones to a considerable depth of the mantle they were mixed with the mantle changing isotope determinations. When the alkaline rocks were melted from this mantle they already had these new determinations. Thus, heavier oxygen is not an evidence of their contamination by crustal material as was considered by [14], but the effect of melting from contaminated mantle.

The massifs of the Siberian Platform framing, exhibiting subduction fall into field 2. The depleted mantle is typical of them. The carbonatites of massifs originated in rift zones between Aldan shield and Siberian Platform or on the shield itself fall into the field 1. This characteristic is common both to ultrapotassium Mz complexes of the Aldan shield (Murun and other massifs), and to Precambrian K-massifs (Khani massif). The influencing of plume processes,occurring in Asian continent at that time, on magma melting is more

probable [10]. Isotope values for ancient massifs of the Western Aldan (Arbarastakh, Ingili and Mountain Lake) are located on the boundary of fields 1 and 2. Such a position can be explained by lack of data concerning the geodynamic settings of areas in the Pre-Cambrian or by proximal position to the platform's margin with the depleted mantle type.

The above indicates that the proposed diagram can be applied for determining mantle type for carbonatites of the Asian continent. As the analysis of oxygen and carbon isotopes is much cheaper and easier than analysis of Sr and Nd isotopes, such application has sense. However, for new areas of carbonatite magmatism it is neces-sary to confirm the definition of mantle type using also data on Sr and Nd isotopes.

CONCLUSIONS

1. Carbon and oxygen isotope values and their ratio in carbonatites, derived in different geodynamic settings are discussed.

2. The ratios of oxygen and carbon isotopes in coexisting pairs (calcite - dolomite, calcite TR-F-carbonate and dolomite TR-F-carbonate) are considered.

The diagram of mantle type definition from carbon and oxygen isotope ratio in carbonatites has been proposed using the empirical data on the mantle type.

The investigations were supported by the Russian Foundation for Basic research (grant № 03-05-64146) and integration projects of SB RAS № 67 and RAS № 6-2-1.

REFERENCES

1. **Deines, P.** (1989). Stable isotope variations in carbonatites // Carbonatites. Genesis and Evolution (Edited by Keith Bell). London, pp. 301-359.
2. **Egorov, L.S.** (1991). Ijiolite-carbonatite plutonism, Nedra. 260 pp.
3. **Kogarko, L.N., Kononova, V.A., Orlova, M.P., Wooley, A.R.** "Alkaline Rocks and Carbonatites of the World. London, Glasgow, New York, Melbourne, Madras.
4. **Koyama, M., and Matsushita, R.** (1980). Use of neutron spectrum sensitive motions for Instrumental neutron activation analysis. Bull. Inst. Chem. Res., Kyoto Univ., vol.58, pp. 235-243.
5. **Kovalenko, V.I., Vladykin, N.V., et al.** (1974). The Lugingol massiff of pseudoleucitic syenites in the MNR // Izvestia Akademii Nayk SSSR, seria geologicheskaia, N 8, p. 38-49.
6. **Kovalenko, V.I., Vladykin, N.V., Goregljad, A.V.** (1977). East Mongolia-the new province of the rare metal mineralisazion. In: Main problems of geology in Mongolia. V.22, Nauka, p. 189-205.
7. **Kovalenko, V.I.,.Vladykin, N.V., et al.** (1977). Geochemical characteristics of rocks from near surface carbonatite kindred from Goby desert, Mongolia //Geochimia,N9, p.1313-1326.
8. **Kovalenko, V.I., Samoilov, B.S., Vladykin, N.V. et al.** (1979). Rare-metal carbonatites and apatite-magnetite rocks of Mongolia // Geology and magmatismes of Mongolia, v.30, Nauka, p. 158-167.
9. **Kovalenko, V.I., Yarmolyuk, V.V., Vladykin, N.V. et al.** (2002). Stages of formation, geodynamic setting and sources of rare-metal magmatism of central Asia // Petrology, v. 10, .№ 3, p. 227-253.

10. **Kovalenko, V.I, Yarmolyuk, V.V., Vladykin, N.V., Kozlovsky, A.M.** (2002). Problem of plumes and their bearing on sources of rare-metal magmatism in central asia // Deep-seated magmatic sources and the problem of plumes Vladivostok, pp. 23-42.
11. **McCrea, J.M.** (1950). On the isotopic chemistry of carbonates and a paleotemperature scale. // Jour. Chem. Phys., vol. 18, p. 849-857.
12. **Morikiyo, T., Miyazaki, T., Kagami, H., Vladykin, N.V.** (1998) Sr, Nd, C and O isotope characteristics of Siberian carbonatites // Chinese Science Bulletin, China, p. 90-92.
13. **Morikiyo, T., Tokana, K., Miyazaki, T., Kagami, H., Vladykin, N.V.** (2000). Sr, Nd, C and O isotopic compositions of carbonatite and peralkaline silicate rocks from the Zhidoy complex, Russia: evidence for binary mixing, liquid immiscibility and a heterogeneous depleted mantle source region // Journal of Mineralogical and Petrological, 2000, v. 95, pp. 162-172.
14. **Pokrovsky, B.G.** Crustal comtamination of mantle on evidance of isotope geochemistry // M, Nauka, 2000, 228 p.
15. **Sharma, T. and Clayton, R.N.** (1965). Measurement of O^{18}/O^{16} ratios of total oxygen of carbonates. Geochim. Cosmochim. Acta, vol.29, p. 1347-1353.
16. **Vladykin, N.V., Kovalenko, V.I., Dorfman, M.D.** (1981) Mineralogical and geochemical features Khan-Bogdo massiff alkaline granites.Nauka. Moskva, p.1-136.
17. **Vladykin, N.V.** (1996). Bilibin-massiff K-alkali rocks. DAN, v.349, N6, p. 972-975.
18. **Vladykin, N.V., Dusmatov, V.D.** (1996). Chemistry composition mikas Darai-Pioz massiff. ZVMO, N.3, p.84-94.
19. **Vladykin, N.V.** (1997). "Petrology and productivity of K-alkali rocks of Mongol-Okhotsk area of magmatism//The thesis in the of an scientific report, Irkutsk, p.1-80.
20. **Vladykin, N.V.** (1999), Ore-bearing tuffs and volcanics of the Mushugai Khuduk carbonatite complex, Gobi, Mongolia // Proceedings of Universities of Siberia, issue 4-5, p. 84-86.
21. **Vladykin, N.V., Morikiyo, T.** (1999) Geochemistry of isotopes of carbonatites Siberia and Kola peninsulu // Carbonatite of Kola peninsulu. C-Peterburg, p. 47-48.
22. **Vladykin, N.V., Morikiyo, T., Tokana, K.** (1999). New data about Zidui massif ultrabasik-alkali rocks and karbonatite // Geology and metalogenie preCm of Siberia. Irkytsk, p. 25-28.
23. **Vladykin, N. V.** (2000). Malyi Murun Volcano-Plutonic Complex: An Example of ifferentiated Mantle Magmas of Lamproitic Type // Geochemistry International, 2000, v. 38, suppl. 1, pp. 573-583.
24. **Vladykin, N.V., Morikiyo, T.** (2000). Sr-Nd systematies of carbonatites Siberia and Mongolia // XIX seminar «Geochemistry of magmatic rocks». Moskow, pp. 23-27.
25. **Vladykin, N.V.** (2001). Ore potential of carbonatite tuffs of K-alkaline complexes of Siberia and Mongolia // 100-anniversary of studies of carbonatites of the Kola Peninsula. S-Peterburg, p. 49-51.
26. **Vladykin, N.V.** (2001). The Aldan Province of K-alkaline rocks and carbonatites: problems of magmatism, genesis and deep sources // Alkaline magmatism and the problems of mantle sources. Irkutsk, pp. 16-40.
27. **Vladykin, N.V., Tsaruk, I.I.** (2003). Geology, chemistry and genesis of Ba-Sr-bearing ("benstonite") carbonatites of the Murun massif // Geology and Geophysics, v. 44, № 4, pp. 315-330.
28. **Vladykin, N.V., Viladkar, S.G., Miyazaki, T., Mohan, R.V.** (2003). Chemical composition of carbonatites of Tamil Nadu massif (South India) and problem of "benstoonite" carbonatites // Plumes and problems of deep sources of alkaline magmatism. Khabarovsk, pp.130-154.

UDK 552.33+550.42

Difference in Sr and Nd isotopic character of carbonatites and kimberlites from Siberia

MorikiyoT. [1], Weerakoon M.W.K. [2], Miyazaki T. [3], Vladykin N.V. [4], Kostrovitsky S.I. [4], Kagami H. [2], Shuto K. [2]

[1] *Department of Geology, Shinshu University, Asahi, Matsumoto, Japan*
[2] *Japan Niigata University, Igarashi, Niigata, Japan*
[3] *Department of Geology, institute for Geothermal Sciences, Kyoto University, Beppu, Japan*
[4] *lnstitute of Geochemistry of Siberian Branch, Irkutsk,Russia*

Whole-rock Sr and Nd isotopic compositions of 31 kimberlite and 38 carbonatite samples from Siberia are measured and the initial isotopic compositions are inferred based on the reported emplacement ages of the bodies. The Siberian kimberlites have initial ε Nd values of -1.6 to +4.6, with the exception of the Ingashin kimberlite located on the southern margin of the Siberian platform. The initial ε Sr values for the kimberlites vary widely, from -14.8 to +33.1. The very high ε Sr exhibited by some of the kimberlites is considered to be due to isotopic exchange with groundwater. The least-altered kimberlites typically have initial isotopic compositions of -1.6 to +4.6 ε Nd and -14.8 to +5.4 ε Sr, which is essentially similar to that of the Group Ikimberlites of South Africa. The Ingashin kimberlite has an initial isotopic composition of -10.3 ε Nd and +44.4 ε Sr, setting it close to the field of the Group Π kimberlites. The age, tectonic environment and chemistry of the Ingashin kimberlite is very different from the other kimberlites in the Yakutian province, and may be justifiably assigned to the Group Π kimberlites (orangeites).The Siberian carbonatites are classified into two groups on the basis of initial Si and Nd isotopic compositions. The Group 1 carbonatites are isotopically depleted, whereas the Group 2 mineralization is typically enriched. The Guli, Essei, Kiiskii, Srednetatarskii, Bolshetagninskii, Nizhnesayanskii, Verhnesayanskii, Zhidoy, Arbarastakh, Ingili, Ozernyi and Koksharovskii carbonatite bodies are classified as Group 1 carbonatites, and the Malomurunskii and Khani bodies are assigned to Group 2. The Group I carbonatites have initial isotopic compositions of -20.2 to -4.5 ε Sr and +2.7 to +7.0 ε Nd. Approximately half the Group 1 samples have ε Nd values higher than +4.6, in contrast to the kimberlites, which never exceed +4.6 ε Nd.This distinct difference in isotopic compositions between the kimberlites and carbonatites of this region represents compelling evidence that the two formations were generated from magmas from different sources, and are therefore not genetically related.

INTRODUCTION

The hypothesis that kimberlites and carbonatites are genetically related has been the subject of intense controversy. The overlap in trace element geochemistry and isotopic characteristics of Group I kimberlites and carbonatites, as well as the typically close spatial and temporal association of these two rocks [24] to suggest that a genetic relationship may exist between the source magmas. Recently,

melting experiments for the system CaO-MgO-Al_2O_3-SiO_2 -CO_2 by [10] revealed that liquids in equilibrium with lherzolite at 6 GPa systematically vary from carbonatitic to kimberlitic composition within a very narrow melting range. On the basis of these results, those authors went on to suggest that a certain systems of kimberlite and carbonatite occurring in close association, such as the rocks in the Sarfartoq region in west Greenland, were derived from the same source material with differing degrees of melting. Bell [3] suggested that carbonatitic and kimberlitic magmatism are related to plume activity and that the association of carbonatites and kimberlites could be explained by different degrees of melting of a carbonated lherzolite within a plume.

The contrasting viewpoint is that there is no such genetic connection. Mitchell [18] refuted the close relationship between kimberlite and carbonatite mainly on the basis of mineralogical evidence. Dawson [18] pointed out that kimberlites and carbonatites occur in different tectonic environments, and stated that on balance, there is little evidence for a genetic connection between kimberlites and carbonatites.

This paper reports the Sr and Nd isotopic compositions of kimberlites from Siberia. Although analytical Sr-Nd isotope data has already been reported for the Yakutian kimberlites [2, 16] the pool of data is as yet insufficient to understand the general features of the Siberian kimberlites, which consist of several groups of different ages. The present study aims to elucidate the common Sr and Nd isotopic character of Siberian kimberlites, and then compare these compositions with the Siberian carbonatites in order to investigate whether the two are indeed genetically related.

SPATIAL AND TEMPORAL DISTRIBUTION OF KIMBERLITES AND CARBONATITES

The distribution of kimberlites and carbonatites in Siberia is shown in Fig. 1. Several hundred kimberlite pipes and dykes are distributed in the Yakutia kimberlite province, east of the Anabar shield. Russian researchers engaged in kimberlite study have recognized three different zones in the Yakutia province, as follows:

Zone 1: Olenek-Anabar zone (Mesozoic in age)

Zone **2**: Daldin-Olenek zone(Paleozoic and Mesozoic in age)

Zone 3: ViluyMarhinsk zone (Paleozoic in age)

A number of kimberlites that occur outside of these zones are also examined in this study: the Serbiana pipe from the South Anabar kimberlite field, and the Achtah-2, Ulah-7, and Bazova-3 pipes from the Haramay field. The locations of the kimberlite fields and the extent of the 3 kimberlite zones are shown in Fig. 1.

The distribution of kimberlite within the Siberian platform is not limited to the Yakutia province. The Ingashin kimberlite dyke located in the East Sayan

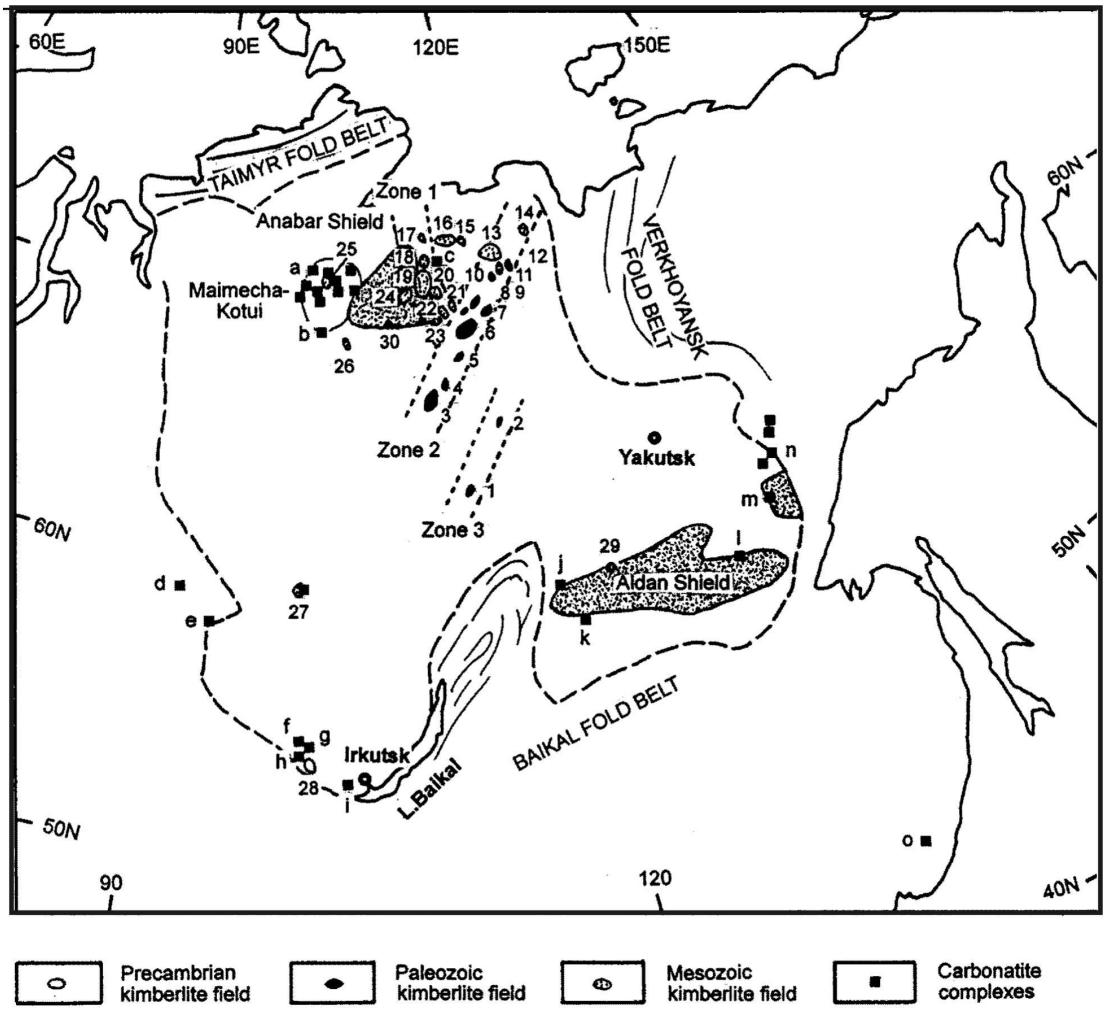

Fig. 1. **Distribution of kimberlites and carbonatites in Siberia.**

Data for kimberlites fields is taken from [1], and data for carbonatites is from [33]. Kimberlite fields: (1) Mirny, (2) Sredne-Markha, (3) Alakit, (4) Daldin, (б) Verhna-Muna, (6) Chomurdah, (7) OgonerYuryakh, (8) West Ukukit, (9) East Ukukit, (10) Merchimden, (11) Molodo, (12) Tbluop, (13) Kuoika, (14) Khorbusuon, (15) Tomtor, (16) Ebelyakh, (17) Orto-Yargin, (18) Starorechinsk, (19) Ari-Mastah, (20) D'uken, (21) Luchakan, (22) Birigindin, (23) Kurannakh, (24) Anabar, (25) Kotui, (26) Haramay, (27) Chadobets, (28) Ingashin, (29) Tobuk-Chompolion, (30) South Anabar. Carbonatite complexes: (a) Guli, (b) Essei, (c) Anabar, (d) Kiiskii, (e) Srednetatarskii, (f) Bolshetagninskii, (g) Nizhnesayanskii, (h) Verhnesayanskii, G) Zhidoy, (j) Malomurunskii, (k) Khani, (1) Arbarastakh, (m) Ingili, (n) Ozernyi, (o) Koksharovskii. Names of carbonatite complexes are according to [15].

province is distinct from the Yakutian kimberlites in that it occurs on the margin of the Siberian platform, and also in terms of its age 1268Ma, Rb-Sr [28].

A frequency distribution diagram for kimberlite and carbonatite dates for Sibeia is shown in Fig. 2. Kimberlites are generally contemporaneous with the carbonati-tes. However, carbonatites of around 600 Ma in age have been reported for several bodies, whereas no kimberlites of the same age have been identified in Siberia to date. This difference in age distribution may be significant.

Carbonatites occur in tectonically different regions to kimberlites. Some carbonatite bodies occur within the platform, while others occur in the folded regions. An example of the latter is the Koksharovskii body in the Shihote Alin

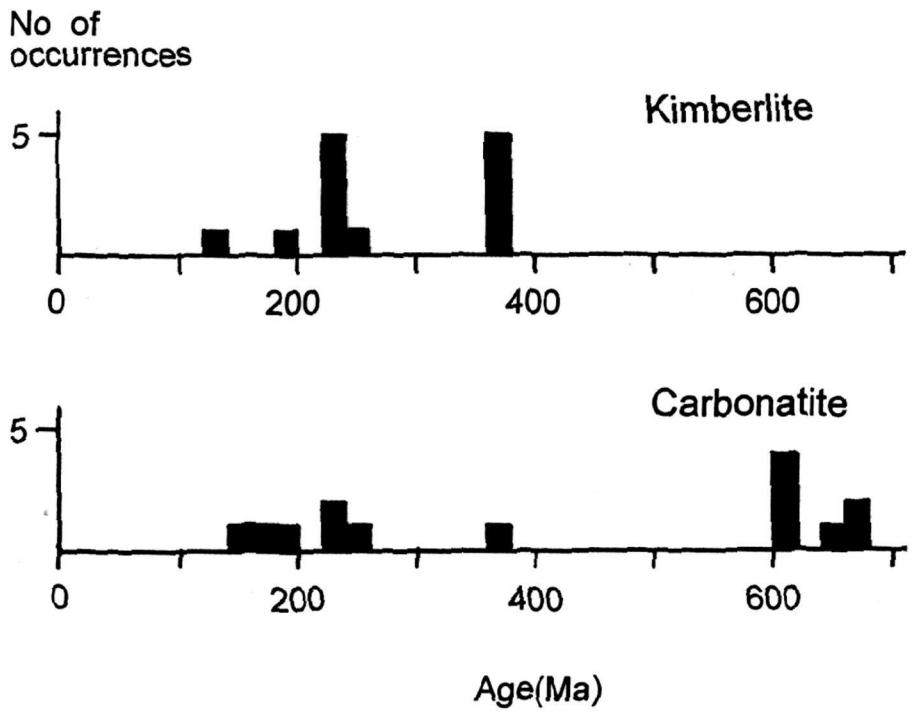

Fig. 2. **Frequency distribution of kimberlites and carbonatites in Siberia.**

fold belt. The tectonic settings of the carbonatite-alkaline rock occurrences in Siberia have been summarized by [8]. The carbonatites analyzed in this study were sampled from the following complexes: The Guli and Essei bodies from the Maimecha-Kotui province (Northwestern Siberian platform).' the Orto-Yrigakhsk and Nomotookhskoe dykes in the Anabar province; the Kiiskii and Tatarskii bodies in the Enisei province (within the Rephean fold belt),' the Bolshetagninskii, Nizhnesayanskii, Verhnesayanskii, and Zhidoy bodies in the East Sayan province (southern margin of the Siberian platform);the Murunskii, Khani, Arbarastakh, and Ingili bodies in the Aldan alkali province (southeastern Siberian platform); the Ozernyi body in the Sette-Daban range (eastern margin of the Siberian platform); and the Koksharovskii body in the Primorye region (part of the Sikhote-Alin fold belt).

The assignment of individual carbonatite bodies to the provinces above are based on the descriptions of [15]. The reader is referred to that work for the details of individual carbonatite bodies.

Among these provinces, the Anabar province is the only region in which carbonatite and kimberlite are known occur together [15]. Thisprovince corresponds to the Olenyok province of [6], and contains 7 carbonatite-alkaline rock complexes, the OrkrYrigakhskoe, Nomotookhskoe, Tomtor, and Bogdo bodies. The former two bodies, carbonatite dykes, are located within the Starorechinsk kimberlite field, and are the only carbonatites for which isotopic data is obtained in this study. Regrettably, the samples obtained from the Tomtor bodies were not suitable for isotopic study. The Anabar province contains Starorechinsk, Ari-Mastah, D'uken, Malo-Kuonamk, and Luchakan kimberlite fields of zone 1.

SAMPLES AND ANALYTICAL PROCEDURES

Most of the kimberlite samples were collected by S.I. Kostrovitsky. The kimberlite pipes from which the samples were taken are listed in Table 1. The kimberlite samples exhibiting the least alteration were broken into small pieces, and pieces free of crustal or mantle xenoliths were carefully selected for further grinding. Isotopic analysis of kimberlites was conducted using whole-rock powders. The carbonatite samples studied were collected by N.V. Vladykin, EA. Cherysheva, L.I. Panina and N.M. Podgornich from the bodies listed in Table 2.

The details of Sr and Nd isotopic analysis can be found in [22]. Initial $^{87}Sr/^{86}Sr$ and $^{143}Nd/^{144}$ Nd ratios and ε Sr and ε Nd values were calculated from the measured $^{87}Sr/^{86}Sr$, $^{87}Rb/^{86}Sr$, $^{143}Nd/^{144}Nd$, $^{147}Sm/^{144}Nd$ ratios and the reported ages for each rock body. Calculation of ε values was performed using the following parameters for Bulk Earth: $(^{87}Sr/^{86}Sr)pr = 0.7045$, $^{87}Rb/^{86}Sr = 0.0827$, $(^{143}Nd/^{144}Nd)pr = 0.512638$, $^{147}Sm/^{144}Nd = 0.1966$ [12, 14]. Isotopic analyses were conducted at Niigata University using a Finnigan MAT 262 mass spectrometer.

RESULTS

Isotopic compositions of carbonatites

The Sr, Nd, C and O isotopic compositions of the Siberian carbonatites have been reported by [23]. The data for Sr and Nd reiterated here for convenience, along with the data for carbonatite dykes in the Anabar province described by [16]. This data is presented in Table 2, and the corresponding initial ε Nd and ε Sr values are plotted in Fig. 5.

Carbonatites from Siberia can be classified into two groups in terms of their initial Sr and Nd isotopic compositions: carbonatites that exhibit depleted isotopic character (Group 1), and those that exhibit enriched character (Group 2) [23]. Among the Siberian carbonatites studied, only the Malomurunskii and Khani bodies are classified as Group 2, and the rest of the carbonatite bodies are classified as Group 1.

The isotopic composition of the Group 1 carbonatites lies between the MORB field and the composition of bulk earth. The initial ε Nd values range from +2.7 to +7.0 and ε Sr ranges from -20.2 to -4.5, with the exception of two samples from theBolshetagninskii body. The variance in isotopic composition of the Group 1 carbonatites is very small compared to that of the kimberlites, and the data plot along the depleted mantle array. The Group 1 carbonatites have similar carbon and oxygen isotopic compositions to mantle CO_2, inferred from MORB study.

However, the oxygen isotopic compositions of carbonatites are rather variable, ranging from +5 to $+18^0/_{00}$ with respect to SMOW [23].

The carbonatites from the Bolshetagninnskii body, which is classified as Group 1 have a wide range of initial Sr isotopic ratios (ε Sr = -10.6, +7.8, and +39.7). A tendency for the whole-rock Sr content to decrease with increasing ε Sr can be seen (Table l). The oxygen isotopic compositions of the calcite in the

Table 1.

Sr and Nd isotopic results for the kimberlites from Siberia

Pipe	Sm (ppm)	Nd (ppm)	$^{147}Sm/^{144}Nd$	$^{143}Nd/^{144}Nd$	$^{143}Nd/^{144}Nd$	Rb (ppm)	Sr (ppm)	$^{87}Rb/^{86}Sr$	$^{87}Sr/^{86}Sr$	$^{87}Sr/^{86}Sr^*$	εNd	εSr
Ari-Mastah kimberlite field(220Ma, Zone 1)												
Arktika	11.4	77.2	0.0891	0.51259	0.51246	67.5	595	0.3281	0.70503	0.70400	2.1	-3.4
Malo-Kuonamk (220Ma,Zone 1)												
Los	19.4	146	0.0807	0.51267	0.51255	55.3	1440	0.1109	0.70416	0.70381	3.8	-6.1
Universitetska	18.1	135	0.0809	0.51264	0.51252	72.3	806	0.2595	0.70401	0.70320	3.2	-14.8
Trudova	9.01	65.7	0.0830	0.51259	0.51247	31.1	1170	0.0769	0.70626	0.70602	2.2	25.2
Luchakan (220Ma, Zone 1)												
Otricyatelna	14.1	101	0.0849	0.51261	0.51249	141	635	0.6442	0.70587	0.70385	2.6	-5.5
Anomaly84	25.2	111	0.1366	0.51259	0.51239	74.2	776	0.2765	0.70445	0.70359	0.7	-9.3
Lihchan-1	20.7	148	0.0849	0.51240	0.51227	55.2	785	0.2033	0.70445	0.70381	-1.6	-6.1
Anomal98/65	25.4	172	0.0892	0.51262	0.51249	39.7	1360	0.0847	0.70401	0.70375	2.6	-7.0
Starorechinsk (180?Ma, Zone 1)												
Tokio	105	913	0.0695	0.51266	t.51258	25.6	2730	0.0271	0.70364	0.70358	3.4	-10.1
Dzho-severna	10.2	82.7	0.0747	0.51269	0.51260	36.5	722	0.1462	0.70387	0.70349	3.8	-11.3
Anomaly41n	13.5	109	0.0746	0.51269	0.51260	33.8	741	0.1319	0.70459	0.70426	3.8	-0.5
Haramay (250Ma)												
Achtah-2	9.33	68.2	0.0827	0.51253	0.51240	31.7	601	0.1525	0.70513	0.70459	1.6	5.4
Ulalb7	16.4	120	0.0831	0.51255	0.51241	84.5	304	0.8042	0.70680	0.70394	1.8	-3.8
Bazova-3	19.3	142	0.0822	0.51252	0.51239	74.7	1550	0.1392	0.70460	0.70411	1.4	-1.4
Ingashin (1268Ma)												
Ingashin	29.8	286	0.0631	0.51100	0.51048	84.3	2580	0.0944	0.70783	0.70613	-10.3	44.4
Daldin (360Ma, Zone 2)												
Udachna	10.8	81.5	0.0802	0.51257	0.51238	18.9	1110	0.0494	0.70460	0.70435	4.0	3.9
Alakit (360Ma, Zone 2)												
A'yhal	11.8	114	0.0624	0.51254	0.51239	27.2	749	0.1052	0.70465	0.70411	4.3	0.5
Malo-Botuobin (360Ma, Zone 3)												
International	12.1	87.4	0.0835	0.51261	0.51241	21.8	668	0.0945	0.70391	0.70342	4.6	-9.3
Verhna-Muna (360Ma, Zone 2)												
Novinka	10.6	68.1	0.0943	0.51262	0.51240	117	1000	0.3362	0.70611	0.70439	4.3	4.4
Zapolyarna	12.8	92.8	0.0831	0.51247	0.51227	93.5	1810	0.1497	0.70717	0.70641	1.9	33.1
Kuoika (1 10-140M a, Zone 2)												
Velikan	20.9	125	0.1012	0.51272	0.51263	89.3	1120	0.2302	0.70441	0.70395	3.4	-5.4
Zenit	32.4	248	0.0790	0451271	0.51264	15.2	849	0.0518	0.70430	0.70420	3.5	-1.9
Jila-87/2	9.52	65.6	0.0877	O.§1278	0.51270	115	749	0.4436	0.70446	0.70358	4.6	-10.8
Vtorogodnica	9.47	67.8	0.0844	0.51274	0.51267	433	1220	0.1027	0.70464	0.70444	4.1	1.5
Obnajenna	15.7	117	0.0809	0.51271	0.51263	72.6	2190	0.0958	0.70527	0.70508	3.4	10.6
Obnajenna	4.06	30.0	0.0817	0.51272	0.51264	155	511	0.8761	0.70806	0.70632	3.6	28.1
South Anabar (220Ma)												
Serbiana	15.0	93.8	0.0964	0.51247	0.51233	135	2060	0.1898	0.70500	0.70441	-0.4	2.4
Chomurdah(360M a, Zone 2)												
Chomur	15.9	97.9	0.0985	0.51256	0.51233	66.8	1010	0.1920	0.70601	0.70502	3.1	13.4
D'uken ($220Ma_9$ Zone 1)												
Anomaly 4a/90	20.8	136	0.0923	0.51266	0.51253	44.2	825	0.1548	0.70430	0.70382	3.4	-6.1
Anomaly 90/63	37.2	261	0.0862	0.51267	0.51255	88.2	649	0.3932	0.70506	0.70383	3.7	-5.9
Anomaly 37/89	18.6	115	0.0981	0,51267	0.51253	81.8	1110	0.2133	0.70449	0.70382	3.4	-5.9

Note. *- initial

Table 2.

Sr and Nd isotopic results for the carbonatites from Siberia

Sample	Sm (ppm)	Nd (ppm))	$^{147}Sm/^{144}Nd$	$^{143}Nd/^{144}Nd$	$^{143}Nd/^{144}Nd$	Rb (ppm))	Sr (ppm)	$^{87}Rb/^{86}Sr$	$^{87}Sr/^{86}Sr$	$^{87}Sr/^{86}Sr^*$	εNd	εSr
Guli (230Ma)												
Gl	5.57	32.3	0.1042	0.51274	0.51258	14.3	7370	0.0056	0.70309	0.70307	4.7	-16.4
G2	34.3	234	0.0889	0.51274	0.51261	0.62	4370	0.0004	0.70321	0.70321	5.2	-14.5
G3-4	12.0	80.8	0.0895	0.51273	0.51260	1.24	3720	0.0010	0.70316	0.70315	5.1	-15.2
Essei (230Ma)												
2000/8f	8.69	45.5	0.1155	0.51269	0.51252	2.80	2890	0.0028	0.70344	0.70343	3.5	-11.3
2014/14	7.68	48.9	0.0950	0.51272	0.51258	1.18	4190	0.0008	0.70334	0.70333	4.7	-12.7
Anabar (190Ma)												
90-74	32.4	275	0.0714	0.51268	0.51259	40.8	3880	0.0304	0.70371	0.70363	3.8	-9.2
78-1555	125	1450	0.0522	0.51270	0.51264	12.4	7070	0.0051	0.70348	0.70346	4.7	-11.6
Kiiskii (250Ma)												
K240	11.6	66.1	0.1062	0.51265	0.51248	10.6	928	0.0331	0.70400	0.70388	3.2	-4.5
Tatarskii												
162/35	93.5	552	0.1024	0.51250	0.51208	45.2	7220	0.0181	0.70268	0.70252	5.1	-17.4
1704/27	5.00	32.4	0.0943	0.51250	0.51211	1.38	6690	0.0006	0.70233	0.70233	5.7	-20.2
Bolshetagninskii (600Ma)												
BT1	2.21	19.9	0.0672	0.51230	0.51203	0.90	645	0.0040	0.70438	0.70434	3.3	7.8
BT34	2.31	25.6	0.0545	0.51227	0.51205	83.9	1550	0.1566	0.70439	0.70305	3.7	-10.6
BT5	6.36	41.2	0.0932	0.51237	0.51200	0.59	429	0.0040	0.70662	0.70658	2.7	39.7
Nizhnesayanskii (600Ma)												
HC1b	39.5	240	0.0995	0.51246	0.51207	22.0	4040	0.0157	0.70318	0.70305	4.0	-10.6
HC1c	16.4	130	0.0764	0.51235	0.51205	62.0	5800	0.0309	0.70321	0.70294	3.6	-12.1
HC6g	43.4	510	0.0515	0.51226	0.51205	0.45	11300	0.0001	0.70303	0.70303	3.7	-10.9
Verhnesayanskii (600Ma)												
Cl/1	26.0	158	0.0994	0.51249	0.51209	8.28	6940	0.0035	0.70295	0.70292	4.5	-12.4
CC86/7	19.4	118	0.1001	0.51250	0.51211	152	1580	0.2783	0.70547	0.70309	4.7	-10.0
CC113/3	22.7	139	0.0985	0.51247	0.51209	13.9	5400	0.0074	0.70303	0.70297	4.3	-11.7
Zhidoy (бООМа)												
Zhd316/3	57.4	393	0.0883	0.51241	0.51206	0.48	13600	0.0001	0.70300	0.70300	3.8	-11.2
Zhd327	46.6	348	0.0810	0.51233	0.51201	2.65	7770	0.0010	0.70318	0.70317	2.8	-8.8
• Malomurunskii (145Ma)												
Murl43	15.0	117	0.0777	0.51133	0.51125	15.7	41400	0.0011	0.70694	0.70694	-23.4	37.0
Murl36/52	25.2	199	0.0764	0.51141	0.51134	152	27200	0.0162	0.70711	0.70708	-21.8	39.0
Murl73	9.39	69.5	0.0817	0.51136	0.51128	55.5	23400	0.0069	0.70724	0.70722	-22.9	41.1
Murl37/5	2.84	18.3	0.0937	0.51139	0.51130	15.7	4730	0.00%	0.70680	0.70678	-22.5	34.8
Murl052/2	4.62	46.2	0.0606	0.51165	0.51159	25.5	29600	0.0025	0.70681	0.70681	-16.8	35.2
Murl86	2.33	22.2	0.0635	0.51129	0.51123	50.1	8060	0.018	0.70731	0.70727	-23.9	41.7
• Khani (1835Ma)												
Khn205	74.0	539	0.0831	0.51047	0.50946	126	4370	0.0837	0.70671	0.70450	-15.7	31.1
Khn206	146	1060	0.0834	0.51042	0.50942	16.1	4790	0.0097	0.70531	0.70506	-16.6	39.0
Arbarastakh(675Ma)												
Arb273	66.7	453	0.0890	0.51252	0.51213	1.65	7980	0.0006	0.70250	0.70249	7.0	-17.2
Arb275	39.8	279	0.086	0.51251	0.51212	28.5	3480	0.0237	0.70282	0.70260	7.0	-15.7
•Ingili (665Ma)												
Ing314	74.2	522	0.086	0.51250	0.51213	48.2	12200	0.0114	0.70257	0.70246	6.8	-17.8
Ing309	58.0	393	0.089	0.51251	0.51212	44.1	6600	0.0193	0.70257	0.70239	6.7	-18.9
• Ozernyi (360M a)												
Gol	19.4	150	0.077	0.51264	0.51246	34.2	3690	0.0268	0.70312	0.70298	5.5	-15.6
Go2	1250	16800	0.045	0.51253	0.51242	0.56	1530	0.0011	0.70376	0.70376	4.8	-4.5
• Koksharovskii (165Ma)												
Ksh22	34.4	228	0.09122	0.51281	0.51271	1.83	10300	0.0005	0.70363	0.70363	5.6	-9.6

samples a remarkably high ($\delta^{18}O$=12.0-13.9$^0/_{00}$), and the samples plot intermediate between the mantle CO_2 and the marine limestone fields in the $\delta\ ^{13}C$ / $\delta\ ^{18}O$ diagram [23].

The Group 2 carbonatites such as the Malomurunskii and Khani carbonatites a characterized by having negative ε Nd values and high positive ε Sr values. The enriched Sr and Nd isotopic feature of the Malomurunskii carbonatites has alrea < been reported by Mitchell et al. (1994). The carbon and oxygen isotopic compositions calcite in Group 2 carbonatites are similar to those of mantle CO_2 [23].

Isotopic compositions of kimberlites

Initial Sr and Nd isotopic compositions of the Siberian kimberlites are shown in Table 1 and plotted on an ε Nd /ε Sr diagram in Fig. 3. With the exception of the Ingashin kimberlite, the range of initial ε Nd values for these kimberlites is from –1.6 to +4.6, and initial ε Sr ranges from -14.8 to +38.1. These results are essentially similar to those obtained for the Yakutian kimberlites by [2, 16]. The data points fall in the upper quadrant of the ε Nd/ ε Sr diagram, and form an array parallel to the abscissa. The variation in the initial isotopic compositions of kimberlites is much greater than that of the Group 1 carbonatites from Siberia defined by [23].

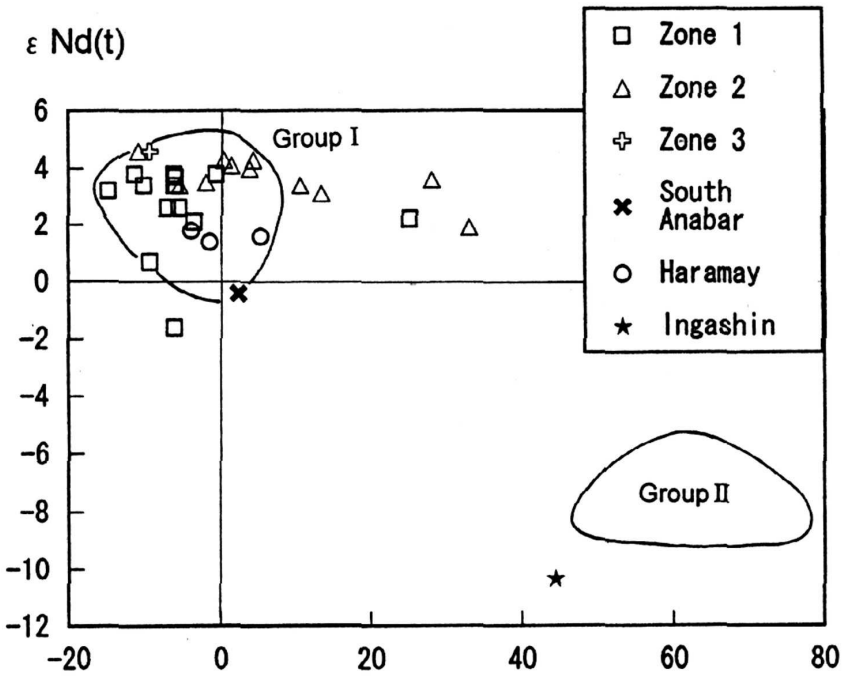

Fig. 3. **Initial ε Nd vs. ε Sr for kimberlites from the Siberian platform.**

The fields oi Group I and П South African kimberlites are from Smith [29].

Widely variable initial e Sr values were recognized even for samples collected from within a single kimberlite field. Figure 4 shows the Sr and Nd isotopic compositions of the kimberlites from the Kuoika kimberlite field (Zone 2). The initial ε Sr values of the kimberlites ranged from -10.8 to +28.1, whereas the ε Nd values were very consistent (ε Nd ~ +3.5) for all the Kuoika samples. Samples 7

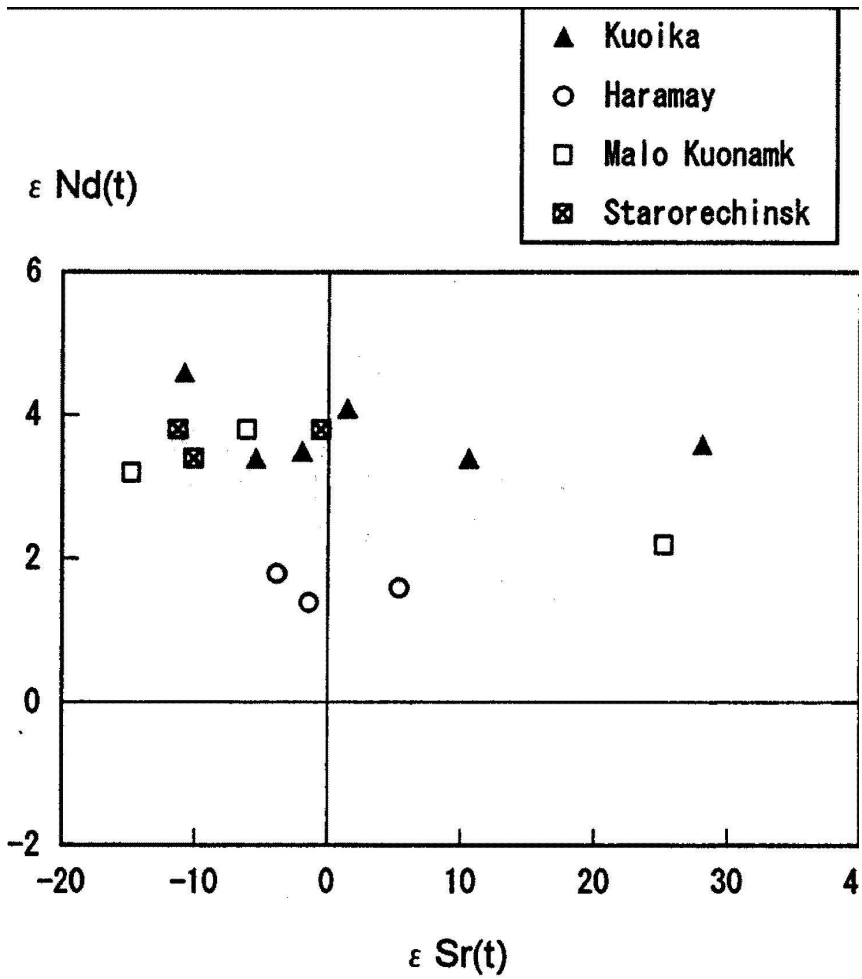

Fig. 4**. Initial ε Nd vs. ε Sr for kimberlites from the Kuoika, Haramay, Malo Kuonaml and Starorechinsk kimberlite fields.**

Data for each kimberlite field plot parallel to theAbscissa with almost constant ε Nd.

-384 and 7-388, taken from the same kimberlite pipe (Obnajenna pipe) of the Kuoika field, have very different ε Sr values of+10.6 and+28.1. Similar features were also observable for kimberlites from the Haramay (ε Sr = -3.8 to +5.4), Malo Kuonamk (ε Sr = -14/8 to +25.2), and Starorechinsk (ε Sr= -11.3 to -0.5) kimberlite fields (Fig. 4).

The Sr and Nd isotopic compositions of the Ingashin kimberlite 1268 Ma, [28] in the East Sayan province, -10.3 ε Nd and +44.4 ε Sr, differ greatly from those of the kimberlites occurring in Yakutia. The data fall close to the field of Group II kimberlites [19, 20] of South Africa in the ε Nd/ ε Sr diagram. The East Sayan province encompasses the Bolshetagninskii Niznesayannskii, Verhnesayanskii and Zhidoy carbonatite complexes, which have initial Sr and Nd isotopic compositions that fell in the depleted quadrant of the diagram, a feature that differs greatly from those of the Ingashin kimberlite. The mineralogical and geochemical character of the Ingashin kimberlite has been reported by [27], although they classified the rock as olivine lamproite.

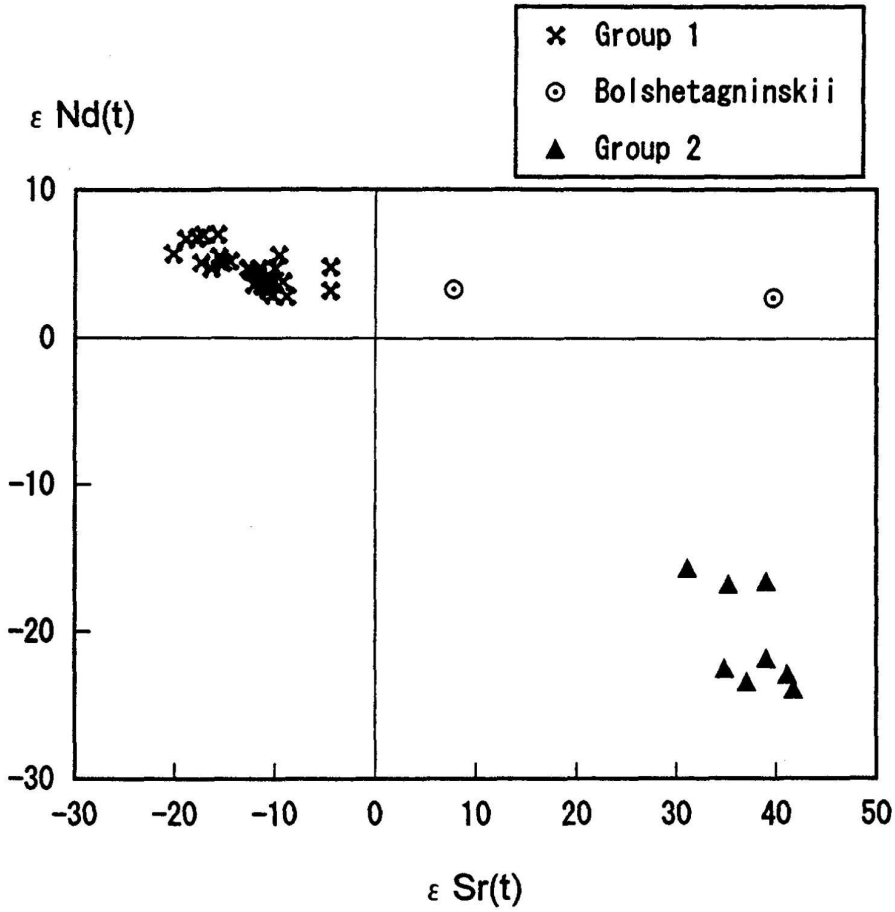

Fig. 5. **Initial ε Nd vs. ε Sr for carbonatites from Siberia.**

Although the Bolshetagninskii carbonatite is a member of the Group 1 carbonatites, it is distinguished because of the wide range of initial ε Sr and constant a Nd .

DISCUSSION

Groundwater alteration and inference of primary isotopic character of kimberlites

As described before, the kimberlite samples from the Kuoika field exhibit a widerange of initial ε Sr values, from-10.8 to +28.1,despite having almost constant ε Nd values of approximately +3.5 (Fig. 4). A similar feature is also recognized for the kimberlites from the Haramay, Malo kuonamk, and Starorechinsk kimberlite fields and for carbonatites from the Bolshetagninskii body. In the case of the carbonatites from the Bolshetagninskii body, a decrease in whole-rock Sr content with increasing ε Sr as well as overall ^{18}O enrichment in calcite are also recognized. These isotopic and chemical features strongly suggest that the $^{87}Sr/^{86}Sr$ ratios of kimberlites were elevated by interaction with groundwater [17, 29].

The samples with ε Sr values are higher than +10 are excluded from consideration here as samples that are expected to have undergone intense isotopic alteration. The least-altered kimberlites are considered to be those with isotopic compositions ranging from -1.6 to +4.6 ε Nd and -14.8 to +5.4 ε Sr (Fig. 6). These

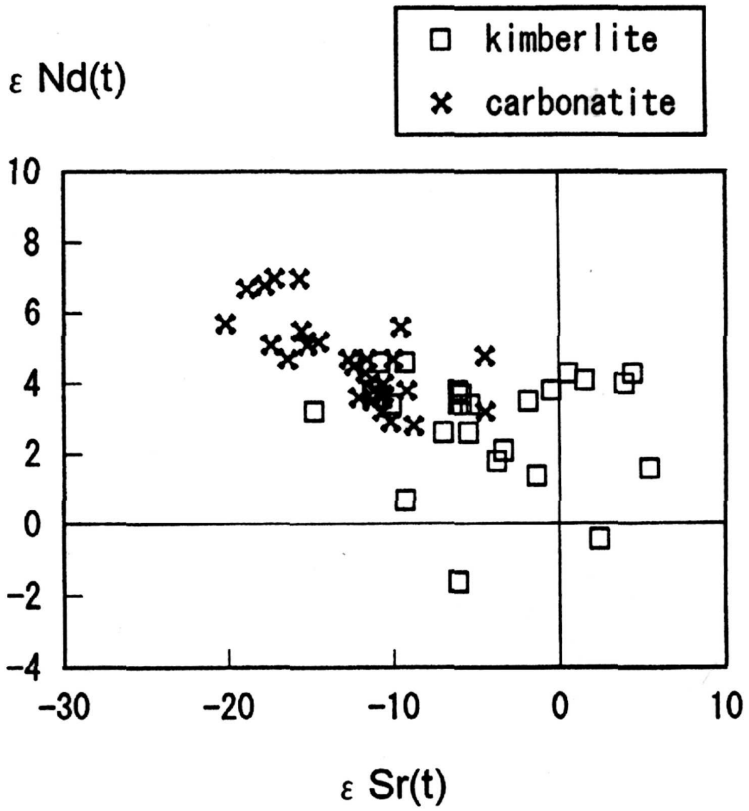

Fig. 6. **Initial ε Nd vs. ε Sr for the Siberian kimberlites compared to those of the Group 1 carbonatites.**

Kimberlite samples having £ Sr values higher than +10 and the Group 2 carbonatites are not chown.

ranges are essentially similar to those of the Group I kimberlites of South Africa *(*ε Nd = • 1 to +5, ε Sr = -18 to +8). Thus, it reasonable to conclude that the source for the Yakutian kimberlites is chemically similar to that of the Group I kimberlites of South Africa.

The Ingashin kimberlite on the southern margin of the Siberian platform, however, is different from the kimberlites of Yakutia, having Sr and Nd isotopic compositions consistent with Group Π kimberlites (orangeite) of South Africa. The isotopic composition of the rock, along with some peculiarities in whole-rock major and trace element concentrations reported by [27, 28], provide strong evidence for the assignment of the kimberlite to Group Π. It should be mentioned thhat Group Π kimberlite have not yet been recognized within the limits of the Siberian platform. As the Ingashin kimberlite pipe is Proterozoic in age, the occurrence of such an enriched kimberlite in the Siberian Craton has important implications for the chemical evolution of the subcontinental mantle beneath the Siberian Craton.

Comparison of isotopic compositions of kimberlites and carbonatites

Although the Sr and Nd isotopic compositions of both the kimberlites and carbonatites of Group 1 plot in a depleted quadrant in the ε Nd/ ε Sr diagram, the

kimberlites have lower e Nd relative to the carbonatites (Fig. 6). The kimberlites all have ε Nd values lower than +4.6, whereas half of the Group 1 carbonatites have ε Nd values higher than this value. Furthermore, the lowest ε Nd of the kimberlites is -1.6, whereas the lowest for the Group 1 carbonatites is +2.7. Although the initial Sr and Nd isotopic compositions of the two rock types overlap to some extent, it is evident that the kimberlites as a whole have lower initial Nd and higher initial Sr isotopic compositions than the carbonatites (Fig. 6). This does not support the hypothesis that kimberlites and carbonatites are generated from the same source mantle by differing degrees of partial melting, nor does it lend weight to the hypothesis that the two are derived from a single parental magma through magmatic differentiation such as liquid immiscibility or crystal fractionation. In fact, the isotopic evidence suggests that the source materials for kimberlites and carbonatites were chemically different.

Source region of the kimberlite magma

Boyd [7] reported that three different kinds of peridotite xenoliths can be found in the Udachnaya kimberlite pipe of the Daldin kimberlite field: spinel peridotite, lowtemperature garnet peridotite, and high-temperature garnet peridotite High-temperature garnet peridotite is deepest in origin, and analysis of the rock reveals equilibration temperatures of 1200 - 1300°C and pressures corresponding to 200 km depth. The pressure-temperature conditions for the garnet peridotite are within: the range of diamond stability. Thus, it is evident that the kimberlite magma of the Udachnaya pipe originated in the mantle region deeper than 200 km. The other kimberlites in the Yakutia province, at least those carrying diamond, are thought to be generated at similar depths.

The seismic lithosphere beneath the Siberian platform has been estimated to be as thick as 200 km on the basis of an analysis of surface waves [26]. Thus, the source region in which the kimberlite magma has been generated must correspond to convective asthenosphere deeper than 200 km. As high-pressure: mineral inclusions in diamond such as pyrope containing significant pyroxene solid solution have been reported for the kimberlites of the Arkhangelsk province in northwest Russia [30], there is a possibility that the kimberlite magma in fact originated much deeper than 200 km. Although the exact depth of kimberlitic magma generation remains unknown, the isotopic data suggests that the asthenospheric source region for kimberlitic magma is composed of less-depleted mantle materials.

Site of generation of the carbonatite parental magma

There are currently two different views concerning the source region of the parental magma for the carbonatite [5]. One hypothesis is that carbonatite magma originated in the h'thosphere beneath the continent [4], and the other is an asthenospheric source [24], in the form of magmatism associated with plume activity [3, 32].

The isotopic data, viewed in consideration of the spatial-temporal distribution of the Group 2 carbonatites, favors derivation from subcontinental lithosphere. The occurrences of the Group 2 carbonatites (Malomurunnskii and Khani carbonatitel bodies) are spatially restricted to the western part of the Aldan province. Although the isotopic features of the carbonatites are similar, the ages of emplacement are quite different: 130-138 Ma for the Malomurunskii body, as opposed to 1835 Ma for the Khani body. The fact that similar alkaline magmatism took place twice in different periods in the same province leads to the view that carbonatite magmatism is related not to plume activity but to localized melting of subcontinental lithosphere attached to the Siberian Craton [23]. As the source of the Group 2 carbonatites has isotopically enriched character, the source must have been isolated from the convective upper mantle for most of its evolution.

There is much less evidence from which to infer the site of generation of the Group 1 carbonatites. However, the evidence is consistent with derivation from the lithosphere assuming the following argument. The Group 1 carbonatites have more depleted isotopic character than Group I kimberlites, which are thought to originate from the asthenosphere. If the Group 1 carbonatites are also assumed to have originated in the convective asthenosphere, it is difficult to explain the isotopic difference between the kimberlites and carbonatites. Tainton and McKenzie [31] have shown that the depletion of the lithosphere decreases with depth. Thus, the Sr and Nd isotopic difference observed could be explained by a lithospheric source region for the carbonatite magma, shallower than the source for the kimberlites.

Boyd [7] deduced that subcontinental lithosphere beneath the Siberian craton consists mainly of Mg-rich Iherzolite and Mg-rich harzburgite, on the basis of a study on peridotite xenoliths entrained in the Udachnaya kimberlite. The Mg number (Mg/(Mg+Fe)) for the rocks is 92.5 to 93, which indicates depletion of the basaltic component in the peridotite. Thus, subcontinetal lithosphere beneath the Siberian Craton is also thought to have depleted features with respect to the Sr and Nd isotopic compositions. However, confirmation of the depleted signatures of the peridotites from Sr and Nd isotope measurements were unsuccessful, because the peridotite xenoliths exhibit highly heterogeneous isotopic compositions [25]. Even so, it may be reasonable to regard the peridotites as having depleted isotopic features on average. The widespread distribution of such depleted Group 1 carbonatites throughout Siberia and the existence of depleted subcontinental lithosphere beneath the Siberian Craton must therefore be related.

It has been shown that carbonatite melt of dolomitic composition can be generated by the partial melting of carbonated peridotite at pressures of 3 - 7 GPa (75 - 175 km), on the basis of experiments on the CaO MgO Al_2O_3-SiO_2-CO_2 system [9, 10]. This depth of 75 - 175 km corresponds to the depth of the lithosphere beneath the Siberian Craton. Therefore, the parental magmas for the carbonatite of both Group 1 and 2 are considered to have derived from the subcontinental lithosphere. The fact that the occurrence of carbonatites is largely restricted to the continental region is in accord with this hypothesis. The Group 1

carbonatites would then have been generated from depleted lithosphere that had undergone metasomatism, and the Group 2 carbonatites would have been derived from the metasomatized enriched lithosphere. According to this hypothesis, the site of generation for the kimberlitic magma will then be different from that for the carbonatite parental magma. Thus, the cause of mantle peridotite melting must differ between these magmas. This is further supported by the difference in spatial and temporal distribution of the kimberlites compared to the carbonatites in Siberia. Overall, there is strong evidence to suggest that the kimberlites and carbonatites in Siberia are not genetically related.

CONCLUSION

The Yakutia kimberlites have initial Sr and Nd isotopic compositions similar to those of the Group I kimberlites of South Africa. The kimberlite magma was inferred to have been generated at the convective asthenosphere, which has a less - depleted Sr and Nd isotopic signature.

The carbonatites in Siberia have been classified into two groups, Group 1 and Group 2, and the parental magmas of both were concluded to have derived from subcontinental lithosphere. The Group 1 carbonatites are derived from isotopically depleted lithosphere, whereas Group 2 carbonatites would have originated from isotopically enriched lithosphere.

The Yakutian kimberlites have initial Sr and Nd isotopic compositions that are less depleted than those of Group 1 carbonatites, and it is concluded based on this and other circumstantial evidence that the source regions for kimberlites and carbonatites differ, and that there is no direct genetic connection between the kimberlite and carbonatite of Siberia.

ACKNOWLEDGEMENTS

Appreciation is extended to Dr. A.P. Berzina of the United Institute of Geology, Geophysics and Mineralogy, Siberian Branch of the Russian Academy of Sciences, for considerable assistance at the beginning of this study.

The investigations were supported by the Russian Foundation for Basic research (grant 03-05-64146) and integration projects of SB RAS № 67 and RAS № 6-2-1.

REFERENS

1. **Afanasiev, V.P., Kryuchkov, A.I., Cherny, S.D.,** (1995). Geographic position and geological characteristics of the field trip area. In: Sobolev, N.V., Zuev, V.M., Afanasiev: V.P., Pokhilenko, N.P., Zinchuk, N.N. (Eds.), Kimberlites of Yakutia. Field Guide Book. United Institute of Geology, Geophysics and mineralogy, SB RAS, and Almazy Rossii-Sakha Co. Ltd, Novosibirsk, pp.9-11.
2. **Agashev, A.M., Orihashi, Y., Watanabe, T., Pokhilenko, N.P., Serenko, V.P.,** (2000). Isotope-geochemical features of the Siberian platform kimberlites in connection with the problem of their origin. Russian Geol. Geophys. 41, 87-97.

3. **Bell, K.,** (2002). Carbonatites and related alkaline rocks, lamprophyres, and kimberlites-indicators of mantle-plume activity. Abstr. vol. Int. Workshop, Role of superplumes in the Earth Systems, Tokyo, pp. 365-368.
4. **Bell, K., Blenkinsop, J.,** (1987). Archean depleted mantle: Evidence from Nd and Sr initial isotopic ratios of carbonatites. Geochim. Cosmochim. Acta 51, 291-298.
5. **Bell, K., Kjarsgaard, B.A., Simonetti, A.,** (1999). Carbonatites - Into the twenty-first century. J. Petrol. 39, 1839-1845.
6. **Borodin, L.S.,** (1974). The principal provinces and formations of alkaline rocks. Izdatel'stvo Nauka, Moscow, (in Russian)
7. **Boyd ,F.R., Pokhilenko, N.P., Pearson, D.G. Mertzman, S.A., Sobolev, N.V., Finger, L.W.** (1997). Composition of the Siberian cratonic mantle: evidence from Udachnaya peridotite xenoliths. Contrib. Mineral. Petrol. 128, 228-246.
8. **Butakova, E.L.,** (1979). Regional distribution and tectonic relations of the alkaline rocks of Siberia. In: Sorensen,H. (Ed.), The Alkaline rocks. John Wiley and Sons, London, pp. 172-189.
9. **Dalton, JA., Presall, D.C.,** (1998a). Carbonatitic melts along the solidus of model lherzolite in the system CaO-MgO Al_2O_3-SiO_2-CO_2 from 3 to 7 GPa. Contrib. Mineral. Petrol. 131, 123-135.
10. **Dalton, J.A., Presall, B.C.,** (1998b). The continuum of primary carbonatitic-kimberlitic melt compositions in equilibrium with lherzolitie: Data from the system CaO-MgO-$Al2O_3$-SiO2-CO_2 at 6GPa. J. Petrol. 39, 1953-1964.
11. **Dawson, J.B.,** (1980). Kimberlites and their xenoliths. Springer-Verlag, Berlin, Heidelberg, New York.
12. **DePaolo, B.J.,** (1988). Neodymium isotope geochemistry' An Introduction. Springer-Verlag, New York.
13. **Eggler, D.H.,** (1989). Carbonatites, primary melts, and mantle dynamics. In: Bell, K. (Ed.), Carbonatites. Unwin Hyman, London, pp.561-579.
14. **Goldstein, S., O'Nions, R., Hamilton, P.J.,** (1984). A Sm-Nd study of atmospheric dusts and particulates from major river system. Earth Planet. Sci. Lett.70, 221-236.
15. **Kogarko, L.N., Kononova, V.A., Orlova, M.P., Wooley, A.R.,** (1995). Alkaline rocks and Carbonatites of the world, Part 2: Former USSR. Chapman and Hall,London.
16. **Kostrovitsky, S.I., Morikiyo, T.,** (1998). Sr, Nd isotopic data of kimberlites and related rocks from North of Yakutian kimberlite province (Russia). Extended abstr.7th Int. Kimberlite Conf., Cape Town, South Africa, pp.466-468.
17. **Kramers, J.D, Smith, C.B., Lock, N.P., Harmon, R.S., Boyd, F.R.,** (1981). Can Kimberlites be generated from an ordinary mantle? Nature 291, 53-56.
18. **Mitchell, R.H.,** (1979). The alleged kimberlite-carbonatite relationship :Additional contrary mineralogical evidence. Am. J. Sci. 279, 570-589.
19. **Mitchell, R.H.,** (1995). Kimberlites, orangeites, and related rocks. Plenum press, New York.
20. **Mitchell, R.H.,** (1996). The Orangeite Clan. In: Mitchell., R.H. (Ed.), Undersaturated and alkaline rocks: Mineralogy, petrogenesis, and economic potential. MAC Short Course Series, Vol.24., Mineral. Assoc. Canada, Winnipeg, pp.245-257.
21. **Mitchell, R.H., Smith, C.B., Vladykin, N.V.,** (1994). Isotopic composition of strontium and neodymium in potassic rocks of the Little Murun complex, Aldan Shield, Siberia. Lithos 32, 243-248.
22. **Miyazaki, T., Shuto, K,** (1998). Sr and Nd isotope ratios of twelve GSJ rock reference samples. Geochem. J. 32, 345-350.
23. **Morikiyo.T., Miyazaki, T., Kagami, H., Vladykin, N.V., Chernysheva, E.A., Panina, L.I. Podgornych, N.M.,** (2001). Sr, Nd, C and O isotope characteristics of Siberian

carbonatites. In: Vladykin, N.V. (Ed.), Alkaline magmatism and problems of mantle sources. Irkutsk, pp.69-84.

24. **Nelson, D.R., Chivas, A.R., Chappell, B.W., McCulloch, M.T.,** (1988). Geochemical and isotopic systematics in carbonatites and implications for the evolution of ocean-island sources. Geochim. Cosmochim. Acta 52, 1-17.
25. **Pearson, D.G., Shirey, S.B., Carlson, R.W., Boyd, F.R., Pokhilenko, N.P., Shimizu, N.,** (1995). Re-Os, Sm-Nd, and Rb-Sr isotope evidence for thick Archean lithospheric mantle beneath the Siberian craton modified by multistage metasomatism. Geochim. Cosmochim. Acta 59, 959-977.
26. **Priestley, K., Debayle, E.,** (2003). Seismic evidence for a moderately thick lithosphere: beneath the Siberian Platform. Geophys. Res. Lett. 30, 1118.
27. **Sekerin, A.P., Menshagin, Y.V., Laschenov, V.A.,** (1991). New data about PreCm kimberlite of Prisayanye. Geol. Geophys., No.12, 75-81.(in Russian)
28. **Sekerin, A.P., Menshagin, Y.V., Egorov, K.N.,** (2001). Stages of magmatism and diamonds of central part of Uriksko-Iyskogo graben of Prisayanie. Otechestvennaya Geologiya, No.6, 38-43 (in Russian).
29. **Smith, C.B.,** (1983). Pb, Sr and Nd isotopic evidence for sources of southern Africs Cretaceous kimberlites. Nature 304, 51-54.
30. **Sobolev, N.V., Yefimova, E.S., Reimers, L.F., Zakharchenko, O., Makhin, A.I., Usov L.V.,** (1997). Mineral inclusions in diamonds of Arkhangelsk kimberlites province. Russian Geol. Geophys. 38, 379-393.
31. **Tainton, K.M., McKenzie, D.,** (1994). The generation of kimberlites, lamproites and their source rocks. J. Petrol. 35, 787-817.
32. **Toyoda, K, Horiuchi, H., Tokonami, M.,** (1994). Dupal anomaly of Brazilian carbonatites: Geochemical correlations with hotspots in the South Atlantic and implications for the mantle source. Earth. Planet. Sci. Lett. 126, 315-331.
33. **Woolley, A.R.,** (1989). The spatial and temporal distribution of carbonatites. In: Bell, K.(Ed.), Carbonatites. Unwin Hyman, London, pp.15-37.

UDK 552.48; 552.321.6

Metasomatism and partial melting in xenoliths from the kimberlites of Yakutia: implication to the origin of diamonds

Spetsius Z.V.

Institute of Diamond Industry, ALROSA Co. Ltd., Mirny, Yakutia,
e-mail: Spetsius@yna.alrosa-mir.ru

About 1000 samples of xenoliths from the kimberlite pipes Mir, Udachnaya and others of Yakutian province were examined by petrographically, chemically and isotopically on the evidences of metasomatism. These samples include different varieties of eclogite, pyroxenite and peridotite xenoliths. Relative distribution of metasomatized rocks in different parts of Siberian craton and intensity of metasomatic processes has been estimated.

Petrography, major chemistry and trace elements distribution suggest that mafic and ultramafic xenoliths from the Yakutian kimberlites undergone the metasomatic enrichment and late partial melting. The most impressive this is evidenced by widespread phlogopitization of the mantle xenoliths and kelephytization of garnet. Partial melting processes are observed in eclogite, alcremite and Gt-vebsterite xenoliths.

The cryptic metasomatism is recorded by the distribution of trace element in garnets and clinopyroxenes of peridotites and pyroxenites. Some peridotites have uniquely extreme Nd and Os isotopic characteristic indicative of ancient incompatible element enrichment. The predominant Archaean ages of mantle xenoliths from kimberlites indicate the longevity of the lithospheric mantle beneath the Siberian craton and long term coupling between crust and mantle.

According to the Re-Os determination of sulfide inclusions in olivines from the Udachnaya pipe the disturbing of Os systematic by metasomatic events took place after forming lithospheric mantle of the Siberian craton (3.5-2.9 Ga) from 2.8 till 2.0 Ga. These processes took have place repeatedly in lithospheric mantle of the Siberian craton and were manifested more intensive in the central part of the kimberlite province.

It is proposed that growth of diamonds in eclogite xenoliths could be repeated and connected with partial melting and metasomatose. These processes may take place in different time of mantle evolution and in some cases was connected with fluids interaction that has preceded the intruding of kimberlites.

INTRODUCTION

Due to intensive field works industrial pipes have been discovered on the Siberian platform and started to be exploited in the Yakutian kimberlite province. Since their discovery in 1955 [2], the mantle xenoliths embedded in kimberlites of different pipes of province have provided invaluable insights into the petrology

and composition of the subcontinental lithospheric mantle (SCLM) beneath the Siberian platform. Many xenoliths from different, especially from the exploited pipes have been intensively studied. The results of these investigations were the finding and description of many samples of diamondiferous eclogites and peridotites, discovering of eclogites with coesite and such unusual mantle rocks as alkremites [e.g. 2, 39, 51, and references therein]. The xenoliths studies have provided abundant data on composition, vertical and lateral heterogeneity of upper mantle and conditions of diamond formation.

The purpose of this paper is to describe the process of metasomatose and partial melting that fixed in mantle xenoliths from kimberlite pipes of Yakutia. Many of the mantle peridotites from Yakutian kimberlites have been subjected to a different stage of metasomatism in which new visible phases are developed; this tape has been referred to as “patent” or “modal” [9, 16 and reference therein]. Separate ultramafic xenoliths with obvious presence of phlogopite or other metasomatic minerals are found and described in many pipes of Yakutia [e.g. 41, 51] but in comparison with the date for the kimberlites of South Africa [e.g. 16, 26 and references therein] the systematic data on their distribution in different types of rocks don’t exist.

“Cryptic” metasomatism is less investigated between the ultramafic xenoliths from Yakutian kimberlites. It is possible to find in papers only some evidence about zoning of minerals or more rare data on trace elements distributions that suggest about enrichment rock or minerals [41, 51]. Here we have systematized the results on studying of xenoliths from the main investigated and worldwide known pipes. On this basis we have tried to do a first attempt to estimate the relative distribution of metasomatized rocks in different pipes, subsequently in different parts of Siberian craton and intensity of manifestation of metasomatic processes and coupled deformation of rocks. The presented data help to understand the formation and differentiation of lithosphere mantle and coupled crust as well as subsequent evolution of the SCLM.

The Siberian craton occupies about $4x10^9$ km^2, mostly buried beneath the Riphean-Phanerozoic sedimentary cover 1-8 km thick, averaging about 4 km. The main structure blocks and tectonic zones are given in [39]. According the concept of terranes, which appeared and developed independently as isolated sialic masses (microcontinents), the craton’s structure resulted from the collision and amalgamation (accretion) of heterochronous microcontinents [39]. The accretion of terranes seemed to occur in several stages, and generally lager units, superterranes or tectonic provinces had appeared before they consolidated to the craton structure. Kimberlitic pipes occur from the Viluy River in the south to the lower reaches of Olenek and Kotui Rivers in the north, over an area of more than 1100 km in longitude and to 800 km in latitude. Situated in the northearsten part of Siberian craton, the Yakutian kimberlite province occupies mostly the territory of the Anabar superterraine, including the Magan and Daldyn granulite-gneiss terranes as

well as the Markha granite-greenstone terrane. More detailed description is given in [39].

In past years, the source of diamonds was considered to be from the same melt that resulted in the kimberlite itself. As time went on and more studies were performed into the petrologic nature of kimberlites, it was discovered that many diamonds actually occurred in xenoliths carried from depths by the kimberlite. In fact, this evidence became so great that 15-20 years ago [27], it was generally considered that the kimberlite was simply the carrier of the diamonds that had originated in eclogitic and peridotitic rocks within the mantle. The single diamonds found in the kimberlite were considered to be simply broken-up portions of xenoliths, similar to the common xenocrysts of garnet and ilmenite. More recently [28 and reference therein], it has been argued that some portions of many diamonds (e.g., the outer, frosted, fibrous layers) are actually grown in the kimberlitic magma and that some micro-diamonds are possibly of the same origin. In paper [52] have been examine the evidence both for and against the genesis of diamonds within kimberlite versus in mantle xenoliths.

Ancient origin for SCLM of Siberian and Kaapvaal cratons supported by Re-Os and Sm-Nd model ages for eclogite and peridotite xenoliths. The age of some diamondiferous eclogites from South Africa, Canada and Yakutia varies between 2.8-3.5 Ga. Estimations of the ages of diamonds, based on their inclusions [e.g., 32, 33, 35] suggest that diamonds may have formed over a long period of Earth's history, especially diamonds of eclogite paragenesis. The only reasonable explanation for this is that after the eclogite formation, the diamonds grew by secondary metasomatic fluids.

SAMPLES

More than 1000 samples of mafic and ultramafic mantle xenoliths from the kimberlite pipes situated in different parts of Yakutian kimberlite province were studied. The modal analyses have been performed for the major part of xenoliths. For most samples rock chemistry was determined. Major-element analyses were performed for the rock-forming and minor minerals. Trace element composition was obtained for some minerals. All samples were classified into different varieties of eclogites and ultramafites according their petrographic and chemical features. A phase composition and element content of ore and sulfide minerals were investigated in many samples. All xenoliths were examined by petrographic, chemical and partly isotope methods to identify modal metasomatic minerals or other evidences of mantle metasomatism. These samples include different varieties of eclogites and ultramafic xenoliths from depleted dunites and harzburgites through coarse grained and sheared Gt-peridotites to ortho- and clino-pyroxenites.

ANALYTICAL TECHNIQUES

Major element compositions of silicate and oxide minerals in the xenoliths were determined with a Superprobe JXA-8800R electron microprobe at the ALROSA Co Ltd. (Mirny) and partly using a CAMECA SX-50 electron microprobe at Institute of Geology (Yakutsk). Part of rockforming garnets and clinopyroxenes and also different secondary phases of partial melting products were investigated by ESM with EDS at the University of Western Australia (Perth). Compositions of sulfide inclusions were analyzed on a CAMEBAX SX50 electron microprobe at the GEMOC ARC National Key Centre, Macquarie University. In all cases natural minerals and synthetic were used as standards. Analytical conditions included an accelerating voltage of 15 keV, a beam current of 20 nA, beam size of 5 μm, and 20 seconds counting time for all elements. All analyses underwent a full ZAF correction.

The trace elements (TRE) have been measured in rockforming and some secondary minerals of eclogites by laser Ablation ICP-MS (LAM) at the RSES of Australian National University, Canberra. The trace elements in minerals from ultramafite xenoliths have been measured by laser Ablation ICP-MS (LAM) at the Macquarie University in Sydney, with NIST 610 glass as external standard and Ca as internal standard; pit diameters were 40 –50mm.

Re-Os isotopes were analyzed using a Merchantek LUV266 laser microprobe with a modified ablation cell, attached to the Nu Plasma multi-collector ICPMS at GEMOC, Macquarie University. All ablations were carried out using He as the carrier gas. Most analyses were done at 4 Hz repetition rate and energies of ca 2 mJ/pulse; typical pit diameters were 50-80 microns. The analytical procedures for in situ Re-Os isotopic analysis have been described in detail previously [15].

COMPOSITION OF THE SCLM OF THE SIBERIAN CRATON

Investigation of deep-seated xenoliths from different kimberlite pipes of Yakutia show that the subcontinental lithospheric mantle (SCLM) of Siberian craton is differentiated both vertically and laterally [e.g., 44, 51]. The vertical heterogeneity is exhibited in a widespread spectrum of different types of mafic and ultramafic xenoliths in all kimberlite pipes of the province. First of all, the vertical heterogeneity of the SCLM is the result of differentiation and formation of the primary mantle substance during the Archaean time [e.g., 15, 31]. As shown by these dates, the SCLM of Siberian platform was formed and stabilized between 3.4-2.9 Ga. Not excluded that new addition to the mantle was made after main differentiation through the process of subduction. A probable subduction of the oceanic crust in the central Daldynsky terrane of kimberlite province is confirmed by the presence of Ky- and Cs-eclogites in the Udachnaya, Sytykanskaya and other pipes of this field. It is also verified by Sm-Nd and Rb-Sr isotope data for the eclogite xenoliths from the Udachnaya and Mir pipes [43, 58] as well by the

presence of isotopically light diamonds in eclogite xenoliths from the Udachnaya pipe.

The horizontal heterogeneity of the mantle results from the presence of highly aluminous rocks suite in the Udachnaya, Sytykanskaya, Zagadochnaya and other pipes of the central Daldyn-Alakitsky area of the kimberlite province. These rocks and particularly the Ky- and Cs-eclogites, alkremites and couplet with them lower crustal rocks such as eclogite-like rocks with kyanite are widespread in the Udachnaya and other kimberlite pipes from this area. However, they are not available on the south and north of the province in such pipes as Mir, International and Obnazhonnaya.

Rock chemistry and trace element data indicate that mafic and ultramafic xenoliths from the pipes located in the central part of the Yakutian province are divided into three well distinguished groups: peridotites, pyroxenites and eclogites [44]. This pattern changes for the southern and northern areas and such xenoliths are rather less distinguished between each other and the divided groups are overlapped. These data suggest the stronger diffirentiation of the mantle in the central part of the Siberian craton and probably their different follow-up evolution of the SCLM in the central and peripheral parts of the craton.

PARTIAL MELTING OF MAFIC XENOLITHS

Worldwide, most eclogite xenoliths from kimberlites display evidences of partial melting processes [e.g., 8, 9, 12, 31, 34, 47, 51]. This is particularly well observed in eclogites from the Udachnaya, Mir, and other Yakutian kimberlites. The crystallization products of these incomplete reactions, typically represented as a “spongy” texture around primary omphacite, include secondary clinopyroxene (with lesser Na2O), spinel, feldspar, and glass. In intergranular partial-melt veins, orthopyroxene, plagioclase, amphibole, and phlogopite are also present (Fig.1). With such melting of kyanite eclogites, corundum and mullite are encountered. Primary garnet may be partially melted with the formation of orthopyroxene, spinel, olivine, and glass, forming portions of the typical kelyphitic rims on garnet [51].

The chemistry of the systems involved indicate that the melting was not isochemical, but brought about by the introduction of metasomatic fluids rich in alkalis, mainly K, and probably volatiles. There are indications from the secondary assemblages that similar but different reactions occurred, as a function of the chemistry of the primary minerals and that of the metasomatic fluids.

Detailed petrographic investigations of xenoliths from pipes in the Daldyn-Alakit and Malo-Botuobia regions of Yakutia have demonstrated that the process of partial melting has occurred in the majority of xenoliths, especially in eclogites, as well as garnet websterites and pyroxenites. Such evidence is pronounced in both eclogites and kyanite eclogites, including diamondiferous varieties. Partially devitrified glass and other products of melting are clearly observed between garnet and clinopyroxene grains, sometimes in the form of veinlets that transect these

minerals. The degree of partial melting varies between xenoliths, as well as the modal abundances of the melt products, as shown in [52].

The modal abundances of the partial-melt products are highly variable [51, 52]. The intergranular melt typically consists of newly formed clinopyroxene, plagioclase, and spinel, and more rarely, orthopyroxene and amphibole, and with

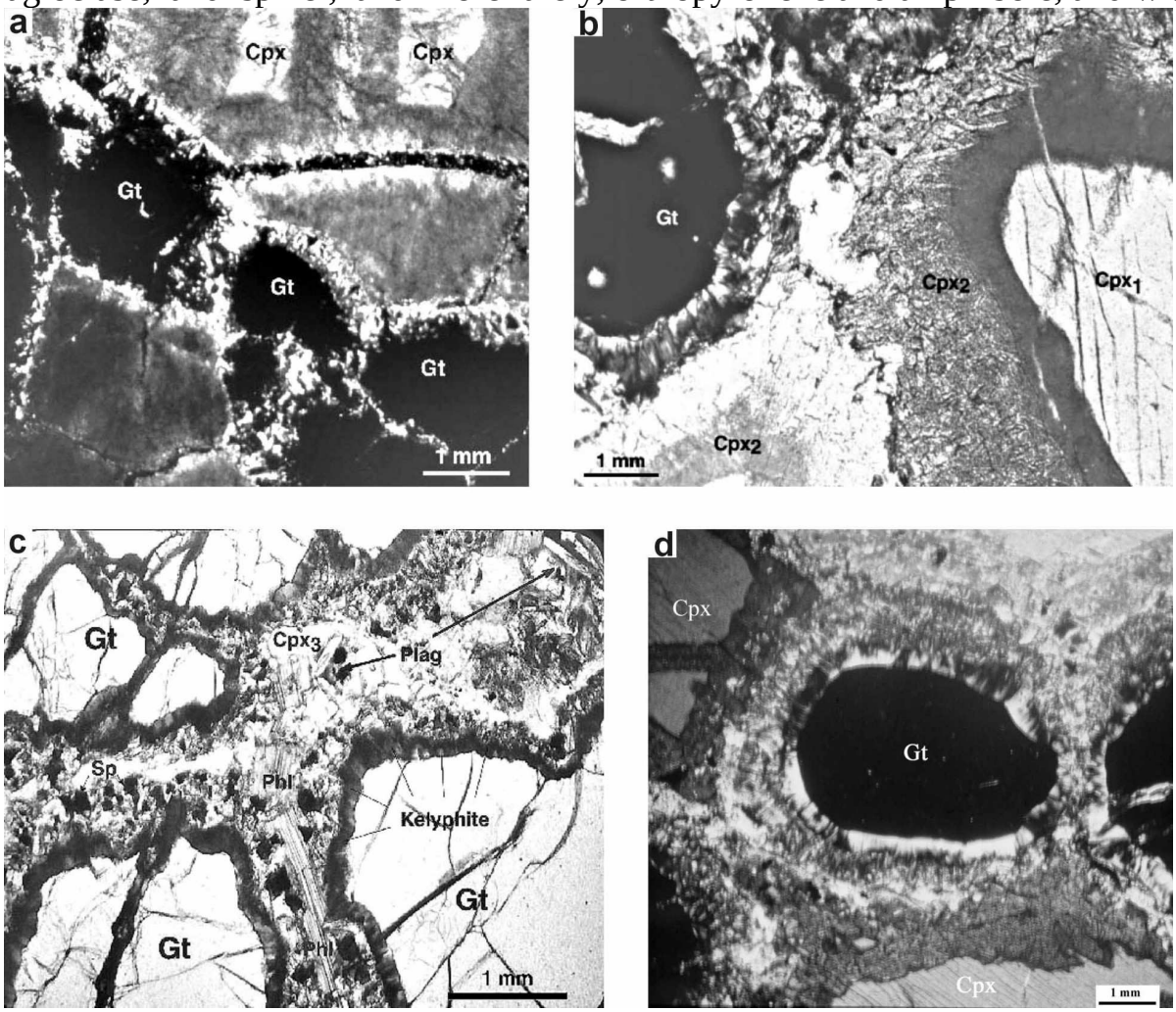

Fig. 1. **Partial melt-products in eclogite xenoliths from the Udachnaya kimberlite pipe.**

Crossed polarizers – a, b, d and c - plane-polarized light.
Legend for these photomicrographs is as follows: Gt = garnet, Cpx = primary omphacite, Cpx_2 = secondary clinopyroxene in spongy texture, Cpx_3 = secondary clinopyroxene in partial-melt veinlets, Sp = spinel, Plag = plagioclase, Phl = phlogopite.
(a) General view of fine-grained intergranular partial-melt products with pronounced ophitic textures between grains of garnet and clinopyroxene. Relicts of primary omphacite and garnet are present. Notice the intersecting partial-melting veinlets in the clinopyroxene. (b) Spongy texture of secondary pyroxene (Cpx_2) with plagioclase and glass. Garnet contains a kelyphitic rim. (c) Elongated needle of phlogopite encountered with secondary pyroxene, spinel, and plagioclase in intergranular partial-melt products. (d) A kelyphitic rim around garnet in intergranular partial-melt products.

possible phlogopite and or amphibole. The accessory minerals include calcite and sulfides. K-feldspar, with minor quartz, is present among the products in kyanite eclogites. Glass is typically availably, and secondary corundum and mullite occur around kyanite. Primary omphacite is replaced by a mixture of glass, plagioclase,

clinopyroxene, and often by veinlets of glass. The primary garnets and clinopyroxenes of these eclogites are well known; therefore, we will characterize mainly the minerals formed by crystallization of the melts. Selected representative, major-element analyses of the minerals of the partial-melt assemblage are given in [52].

MINERAL PHASES OF PARTIAL MELT

Clinopyroxenes are the most abundant in melt products, usually forming xenomorphic grains about 0.01-0.4 mm in size, sometimes appearing "sieve-like" due to spinel inclusions. Secondary clinopyroxenes [52] are always lower in Na_2O (to < 3 wt%) and Al_2O_3 (to < 1 wt%) and contain scarce jadeite component. Relative to the primary clinopyroxenes, they contain usually more MgO (12 to 16 wt% versus 8-11 wt%) and have variable Mg# from 70 to 87. CaO-contents are similar to those in the primary omphacites. Pyroxene is sometimes enriched in TiO_2-content (up to 1.2 wt%).

In some eclogites, secondary pyroxenes are included by prismatically elongated crystals up to 0.2 mm long and with a green-yellow pleochroism. This phase typically shows a high-Na_2O content (≈10 wt%), but with low Al_2O_3 (<1 wt%) concentration. This phase exhibits significantly higher FeO contents (>20 wt%) and corresponds to a large amount of an aegirine component [$NaFe^{3+}Si_2O_6$]. This drastic increase in Fe^{3+} indicates a large increase in oxygen activity in the late-stage metasomatizing fluids. Such aegirine-bearing clinopyroxene is also present in diamondiferous xenoliths [49].

Spinel as a phase from crystallization of the partial melt, is represented by grains 0.01-0.02 mm in size (see Fig. 1c). The spinel color is usually green, though grayish-brown and black spinel is seen in transmitted light. Dark opaque spinel is characteristic of ferruginous eclogites. Chemical zonation is abundant and is most pronounced in samples of Ky-tclogites with enhance of Al_2O_3 and MgO-content in outer rim zones of the grains, as a possible result of fractional crystallization. Electron microprobe analyses show that the general compositions of this spinel vary in composition between two end-members: spinel, $MgAl_2O_4$ and hercynite, $FeAl_2O_4$ [52]. Contents of TiO_2 and Cr_2O_3 are usually less than 0.5 wt%, but in some samples, spinel contains up to 3.5 wt% Cr_2O_3.

Plagioclase is present as elongated needles with a dominant size of 0.04-0.5 mm, rarely as lamellar crystals 0.02-1.0 mm in size. It is commonly polysynthetically twinned (albite law) with chemical zonations typically within the range of An 30-50. Plagioclase of An30 is developed about the primary omphacite, occasionally forming graphic intergrowths. However, the plagioclase is usually present as irregular segregations about 0.01-0.03 mm in size. Among the products of partial melting in some kyanite eclogites, bundles of albite are also present. It is the presence of this plagioclase that indicates the crystallization of the partial melt at pressures <10-15 kbars.

Phlogopite is typically developed in more-altered specimens, predominantly in kyanite eclogites, where the grain sizes vary from 0.1 to 1.0 mm. As revealed in

thin section, this phlogopite is formed late (Fig. 1c). Microprobe data yield variations in K_2O (8 to 13 wt%) and TiO_2 (0.70-3.20 wt%), but sometimes TiO_2 can range up to 9.50 wt% (Table 3). The Ba-content is usually below detectable limits (e.g., <0.04%), but in one xenolith, the phlogopite contained 0.65 wt% BaO.

Potash feldspar is encountered in certain kyanite eclogites, present in spongy-textures rims on clinopyroxene. This mineral was found in metasomatized lherzolite xenoliths from China (Snyder et al., 1997b) and noted in eclogites of Roberts Victor (Switzer and Melson, 1969). Sobolev et al. (1999) report alkali feldspar containing about 2 wt% CaO, but rich in K_2O (8 to 13 wt%) and poor in Na_2O (1 to 5 wt%).

Glass is noted in many eclogite xenolith samples, as the quench product of the melt remaining from the partial melting. It is intergranular in nature, usually in the interstices of plagioclase and spinel, and also as thin veinlets intersecting clinopyroxene. It is commonly found in the kelyphitic rims of garnet also. Partially devitrified glass, with microlites of plagioclase and clinopyroxene are encountered, often in kyanite eclogites (see Fig. 1b). In regular, bimineralic eclogites, the glass is largely devitrified and contains small euhedral plagioclase laths replaced by sericite and other alteration products. The color of the glass varies from dark-gray and brown to light brown. It is an alkali-rich glass containing 50-55% SiO_2 [52], and approaches plagioclase in composition. The high-silica compositions of some glasses are also manifested by the presence of quartz and silica spherulites in some of the crystallization products [50]. Glasses are rich in sodium contents, usually with about 6 wt% Na_2O and can be divided in two groups with high- and low-K_2O contents – e.g., 2.3-3.5 and <0.2 wt%. The high-K_2O glass contains the signature of the kimberlitic fluids; however, the low-K_2O glass commonly occurs in the partial-melt assemblage where plagioclase also has formed. Also, the glasses can vary broadly in Mg and Ti-contents [52]. The SiO_2-component can range as high as 61 wt%, higher than that of the primary clinopyroxene. This suggests possible addition of silica by the metasomatizing fluids.

CAUSES OF PARTIAL MELTING

There are two possible sources for the fluids that induced the partial melting of the eclogites. The difference between these two lies in the timing of the metasomatism. These two hypotheses are: 1) kimberlite metasomatism, with the alteration of captured xenoliths by fluids from the kimberlitic magma; and 2) pre-kimberlite metasomatism, with melting brought about by metasomatism in the mantle before entrapment of the xenoliths by the kimberlite.

Virtually all mantle xenoliths have undergone some form of metasomatism while resident in the mantle, mostly long before their entrainment in the kimberlite. Several observations are applicable here: a) although partial melting has occurred in samples of deep-seated xenoliths, little such evidence seems to have been noted from crustal rocks; b) eclogites which show evidences of extensive melting often

bear traces of deformation (cataclasis, mylonitization, etc.), supposedly only formed in the mantle before the kimberlite; c) a spatial connection between the intensity of melting versus the surface of the xenoliths does not seem to appear; d) an inhomogeneous distribution of the degree of partial melting within a given sample is available; e) intersecting veinlets of partial-melt products exist, as well as evidences for two or more types of melting events, perhaps closely related in time are the case; f) there is a rim on the exterior of some eclogites; it is the direct result of interaction with the kimberlite, as opposed to the partial melting which takes place throughout the xenolith; g) differences exist in the intensity of partial melting of similar xenoliths in the same pipe; and h) the degree of partial melting in eclogites varies from pipe to pipe within a given kimberlite field. Based upon the above factors and others [51], a possible scenario would have the first stage of the overall partial-melting process begins as mantle metasomatism under the influence of fluids that originated in deep mantle, possibly associated with a slight reduction in pressure. This process could have taken place close just preceding kimberlite eruption. The overall effects of metasomatism on mantle xenoliths and their trace-element fingerprints on the chemistry and mineralogy of eclogites were described in [18].

METASOMATISM OF ULTRAMAFITE XENOLITHS

Petrographic examination and set of data on major chemistry and trace elements distribution suggest that ultramafic xenoliths from the Yakutian kimberlites undergone the metasomatic enrichment and late partial melting in rare cases [51]. It is evidenced of widespread flogopitization of the mantle ultramafic xenoliths and kelyphitization of garnet. The presence of djerfisherite and sometimes titanomagnetite as well replacing some primary clinopyroxenes and garnets by the blebs consisting from phlogopite and other hidrous minerals also could evidenced about inducing of metasomatic agents and development of a new phases in result of metasomatism.

Phlogopite

Phlogopite in small proportion is encountered in almost all varieties of deep-seated xenoliths from all main kimberlite pipes. Its content varies from decimal parts up to 10-20% and in rare cases up to 80% of the rock volume. Peridotites and pyroxenites subjected to modal metasomatism contain a variety of phlogopites. Phlogopites from ultramaphic rocks are magnesian kinds of mica (20-30 wt% of MgO) with high variability of composition by the content of TiO_2, Al_2O_3, Cr_2O_3 and FeO (Table 1). The contents of Ti and Cr oxides in them vary for more than one order. The comparison of phlogopites from different rocks of peridotite-pyroxenite series enables to judge that, first, phlogopites from xenoliths of different pipes have some distinctive feature concerning their chemical composition; second, part of large megacrysts of phlogopites in kimberlites was formed at the expense of phlogopite-containing xenoliths [51].

Djerfisherite

Djerfisherite is one of the undoubtedly metasomatic minerals that present in about 1/3 part of ultramafic xenoliths from the Udachnaya, Obnazhonnaya and

Table 1.

Representative analyses of phlogopites in ultramafites from kimberlites of Yakutia

Sample	M-260	S-9/272	U-19/82	S-9/399	S-9/495	U-19/82	U-78/93	U-43	O-19/74	M-84	M-923
Analyses	1	2	3	4	5	6	7	8	9	10	11
SiO_2	44.95	45.63	42.1	46.57	44.23	40.63	39.88	42	42.76	43.76	39.99
TiO_2	0.2	0.24	0.54	0.3	0.25	2.8	3.02	2.53	2.05	3.8	1.68
Al_2O_3	11.41	13.92	13.02	11.76	11.58	12.88	10.68	13.5	13.62	10.38	14.44
Cr_2O_3	0.14	0.68	0.85	0.23	0.46	1.02	0.08	1.3	0.59	<0.03	2.53
FeO	4.13	4.96	3.87	2.81	4.77	4.41	9.07	4.61	6.17	7.1	3.25
MnO	0.06	0.01	0.03	0.01	0.01	<0.03	0.14	0.04	0.01	0.04	0.04
MgO	28.58	23.69	25.95	26.66	28.16	23.62	20.79	22.3	24.49	18.7	24.17
CaO	0.37	0.01	<0.03	0.01	0.01	<0.03	0.01	0.32	<0.03	0.04	n.d
Na_2O	0.42	0.19	0.22	0.02	0.07	<0.03	0.65	0.7	0.29	0.12	0.44
K_2O	7.75	6.89	10.35	10.71	10.21	11.03	9.92	8.97	7.61	9.3	9.73
Total	98.01	96.22	96.93	99.08	99.75	96.39	94.24	96.27	97.59	93.24	96.27

Note. Sample: 1, 2 –verlites, 3- ortopyroxenite, 4, 5- Sp-lherzolites, 6- Ilm-pyroxenite, 7-glimmerite, 8- Gt-peridotite, 9- Ilm-Gt-peridotite, 10- diamondiferous Gt-pyroxenite (Sobolev, 1977), 11- diamondiferous Gt-peridotite.

Table 2.

Representative analyses of djerfisherites in ultramafite xenoliths from kimberlites

	Sample	Fe	Ni	Co	Cu	S	K	Cl	Total
1	**U-1-80**	36.95	14.37	0.22	2.67	33.04	9.98	1.72	98.95
2	**U-3-80**	38.03	14.08	0.02	1.91	33.09	9.68	1.71	98.52
3	**U-10-81**	37	13.86	0.16	4.22	32.96	9.61	1.58	99.39
4	**U-25-81**	37.09	9.51	0.16	8.92	32.93	10	<0.03	98.64
5	**U-25-83**	41.42	10.4	0.28	2.41	32.95	10.01	1.69	99.16
6	**U-19-84**	38.71	16.19	0.15	1.92	31.93	9.5	1.7	100.1
7	**U-20-84**	36.86	19.35	0.08	1.08	32.4	9.17	0.18	99.12
8	**U-2249**	41.04	12.61	0.42	1.45	32.13	9.79	1.98	99.42
9	**U-2281-a**	39.43	12.72	0.35	3.55	32.13	9.22	1.34	98.74
10	**U-2281-b**	40.34	12.85	0.34	3.61	33.17	7.69	0.85	98.85
11	**U-2283**	36.39	14.41	0.8	4.12	32.32	9.94	1.78	99.76
12	**U-2298**	35.98	14.81	0.08	4.47	33.11	9.81	1.61	99.87
13	**O-3214**	34.35	10.79	0.1	10.47	32.57	7.14	1.66	97.08
14	**O-3251**	34.25	7.73	0.08	14	32.51	8.72	1.49	98.78
15	**O-3441**	37.72	11.07	0.1	7.08	33.09	8.94	1.68	99.68
16	**O-3445**	37.6	11.97	0.05	5.15	33.31	8.5	1.46	98.04
17	**O-1590**	34.16	11.78	0.11	8.44	33.72	9.88	1.54	99.63
18	**O-1608**	34.51	16.43	0.1	2.96	33.68	9.24	1.6	98.52

Note. 1, 3, 5, 7, 8, 12, 14, 16- Gt-peridotites; 4, 11- Gt-Ilm-peridotites; 2, 7, 14, 15, 17- Gt-verlites and olivinites; 6, 13- Gt-harzburgites; 9, 10, 18- Gt-vebsterites. U- Udacnaya pipe, O- Obnazhonnaya pipe.

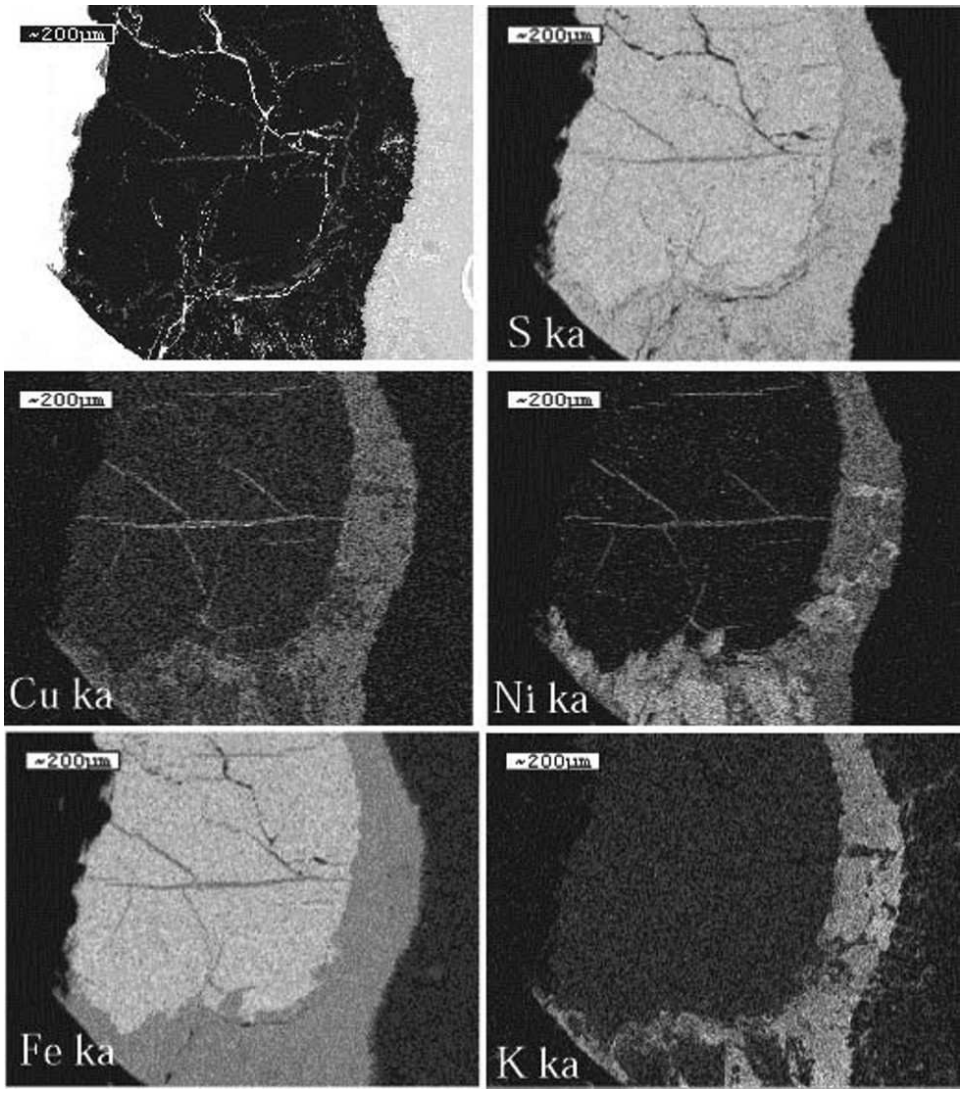

Fig. 2. **Images of typical sulfides grain (x-ray maps) in ultramafite xenolith from the Udachnaya pipe.**

Djerfisherite replace the pyrrhotite. Sample U-2281 (Gt-verlite).

others pipes and prevails between others sulfides in ultramafites [6]. It is the potassium-bearing sulfide with constant impurity of chlorine. This mineral replaces the primary Ni-Fe-sulfides - pyrrhotites and pentlandites that developed between grains of rockforming minerals. Usually djerfisherite forms outer rims on sulfide grains (Fig. 2). It should be stressed the composition inhomogeneity of this mineral not only in different grains of sulfides from one xenoliths but even in one given sulfide grain (sample U-2281, Table 2). That displayed in wide variations of Ni-, K- and Cl-contents. Such evidence as a high and non-constant K-content and presence of Cl in this mineral (Table 2) suggest about its more likely formation on the one of the last stages of metasomatism and probable relationship with the kimberlitic agents. Not excluded the origin of this mineral by inducing of the protokimberlitic fluids.

Partial melting processes are observed in rare clinopyroxenite xenoliths. Decrystallized and partly the glassy state products of melting are developed between rockforming minerals. Besides they form cutting veins, pockets and blebs up to 10-20 mm in size occupying sometimes about 20% the initial rock volume. By their compositions these partial melt product phases are adequate to partial melting minerals that are present in eclogite xenoliths. To a lesser extent, a partial melting has its sings in xenoliths of the peridotites and it is expressed in general kelyphitization of the garnet. The ultramafic rocks are subjected to cataclasis and deformation shears also. It is confirmed by the presence of porphyritic and porphyroclastic textures, fluidality and partial decrystallization of olivine matrix in xenoliths from all kimberlite pipes.

GARNET KELYPHITES IN ULTRAMAFITES

Kelyphitic rims are widespread on grains of garnet in kimberlites and mantle xenoliths from kimberlite pipes in Yakutia. Usually they consist of a mixture of secondary minerals such as phlogopite, spinel, clino- and orthopyroxene. Some rims are complicated especially on grains of garnets in kimberlites and consist of two or more zones with different composition. In xenoliths of garnet peridotite from Udachnaya pipe, garnets are mantled by coronas of phlogopite, spinel and secondary pyroxenes. While major and trace element zoning in garnet are explained as a result of metasomatic processes at depth [49], the formation of kelyphites around garnets usually is linked to interaction between garnet and ascending kimberlitic magma. To test this idea, trace element analysis has been undertaken on chemically homogeneous garnet grains with sharp kelyphitic rims more than 300-500 mm thick, in two peridotite xenoliths from Udachnaya kimberlite pipe: U-140/78 (sheared Gt-lherzolite) and U-2292 (mozaic-porphyroclastic Gt-harzburgite). Example of such kelyphitic rim is shown on Fig. 3. It is obvious that broad rim occupies about a half grain of primary garnet. Major element compositions of garnets and other minerals of these samples are given in Table 3. Major-element chemistry of rockforming minerals of both samples is very similar. Relicts of primary garnets have shown no zonation. Major-element chemistry of rockforming clinopyroxenes and olivines both samples are similar but garnets are differing by content of Cr_2O_3 and TiO_2 (Table 3). It should be noticed that kelyphite rims by compositions answer or close to phlogopite and consist from tiny intergrowths of spinel and phlogopite with predomination of the last. Trace elements were measured by laser-ablation ICP-MS; pit diameters were 40 –50mm.

TRACE ELEMENTS AS EVIDENCE FOR KELYPHITIC RIMS ORIGIN

Observations in thin-section show no notable interaction between peridotite xenoliths and kimberlite melt. There are no obvious relationships of the thickness of kelyphitic rims with the size of xenoliths or any increase in thickness in the

Table 3.

Analyses of rockforming minerals and garnets kelyphite rims in two garnet peridotite xenoliths from the Udachnaya

Sample	**U-2292**					**U-140/78**			
Analyses	Gt-1	Gt-kel-2	Gt-kel-3	Ol-4	Cpx	Gt core	Gt rim	Gt kel	Cpx
SiO_2	41.61	34.65	32.77	40.54	56.29	41.67	42.50	38.59	53.20
TiO_2	1.26	1.25	1.29	0.05	0.31	0.32	0.46	0.38	0.22
Al_2O_3	15.77	15.21	15.18	0.06	1.40	18.40	18.35	16.81	1.16
Cr_2O_3	7.23	6.98	7.24	0.04	1.47	5.64	5.46	5.62	1.31
FeO	7.32	8.24	7.67	8.64	3.65	7.83	7.48	8.05	2.24
MnO	0.33	0.37	0.31	0.12	n.d.	0.32	0.25	0.33	n.d.
MgO	20.03	21.27	19.41	47.76	19.10	20.17	20.06	23.80	19.25
CaO	5.81	6.04	7.38	0.04	17.40	5.44	5.32	4.24	19.91
Na_2O	0.16	0.36	0.47	0.03	1.36	n.d.	n.d.	n.d.	1.75
K_2O	n.d.	0.40	0.43	n.d.	n.d.	n.a.	n.a.	n.a.	n.a.
Total	99.52	94.77	92.15	9726	100.98	99.79	99.88	97.82	99.04

Note. Number: 1 to 4 answers to the points of analyses on Fig. 3.

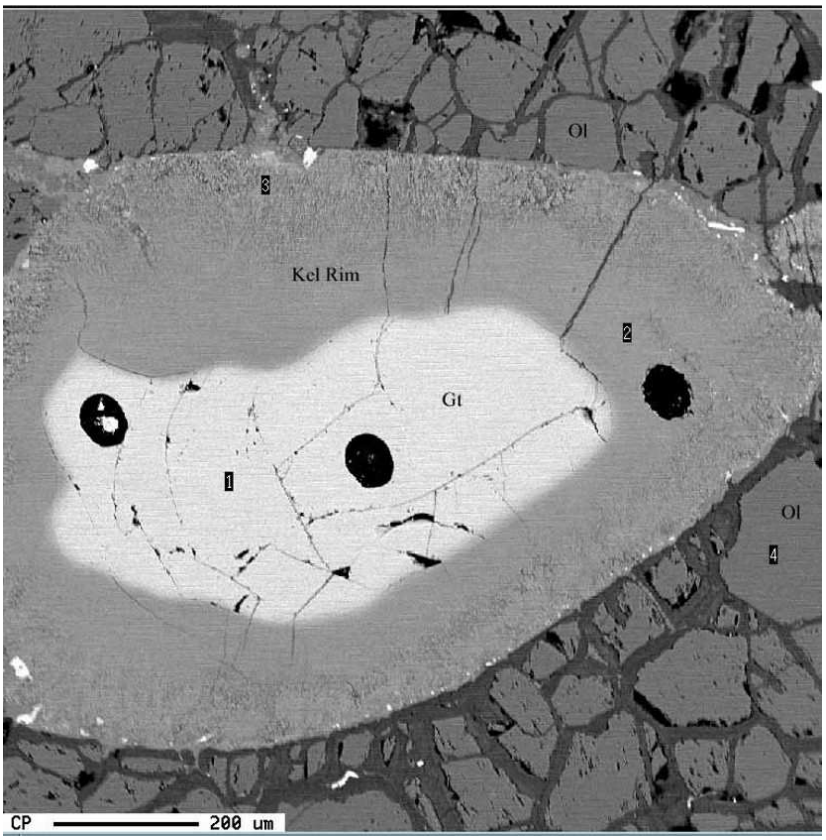

Fig. 3. **Scanning electron microscope back-scattered image of secondary kelyphitic rim replacing garnet in sheared garnet peridotite xenolith from the Udachnaya kimberlite pipe. (Sample U-2292).**

Points of microprobe analyses of minerals are shown (see data in Table 3) and three hols of ICP-MS laser beam drilling are obvious.

outer parts of samples. In areas where kimberlite is in contact with the minerals of the outer zone, there is a sharp border between garnet grains and kimberlite minerals. As was shown by Vishnevsky [59] kelyphitic rims on garnet in xenoliths usually represent a mixture of minerals: Phl + Sp ± Ol ± Cpx ± Opx. In our samples phlogopite predominates, as it is obvious from analyses of kelyphitic rims that in both cases represent nearly pore phlogopite (see table 3). Significant variations between core and rim in major and trace element composition were not observed in tested garnets from both samples. This suggests complete re-equilibration during or after ductile shearing in the mantle.

The REE compositions of the investigated garnets are similar, but garnet from sample U-2292 shows enrichment in MREE, while garnet from U-140 does not (Fig. 4). The kelyphites in the two samples have trace-element patterns different from one another, but essentially identical to their host garnet, except for enrichment in Sr. The REE patterns are significantly flatter than would be expected from equilibration with kimberlite magma [17]. The very high Sr contents probably reside in secondary clinopyroxene and locally high Ba (not shown) in secondary phlogopite. Otherwise, the similarity between garnet and kelyphite trace elements distribution suggests that kelyphitization has not involved extensive exchange with a metasomatic medium and not connected with the influence of kimberlitic agents.

Two models can be proposed to explain the petrographic features and trace element patterns of the kelyphites.

1. PT-estimates for the kelyphite overprint, using secondary minerals within coronas [14, 51]indicate temperatures of 1100-1250 ^{o}C and pressures of about 20 kbar. These data suggest that kelyphitization has occurred under upper mantle conditions. According to data of [14], in xenoliths from the Gibeon kimberlite these metasomatic processes have occurred within a magma chamber located close to the boundary between upper mantle and lower crust.

2. It was proposed an alternative explanation based in particular on trace element data and some petrographic evidence [49]. Analytical date suggest that the trace element patterns of the garnet kelyphites are not related to the kimberlitic magma, but resemble those of the garnet being replaced (Fig. 4), with addition of Sr, K and probably Ba; HFSE such as Zr, Hf, Ti and Nb, and the REE, were not affected. Experimental trace element partitioning data [3] indicate that at high pressure many of these trace elements do not partition into hydrous fluids to the same degree as into carbonatitic and silicate melts. This suggests that kelyphitization of garnet was not a result of interaction with silicate melt or carbonate-rich fluid, and that hydrous fluids play a more important role in formation of kelyphites on garnets (at this stage of mantle metasomatism). The fine grain size of kelyphite implies that the metasomatic processes, which caused replacement of garnet, were short-lived and probably were active not long before eruption of kimberlites, but the eruption process is very rapid. We therefore

suggest that kelyphite formed in response to the infiltration of hydrous fluids, prior to eruption. The source and precise nature of the metasomatic fluids remains

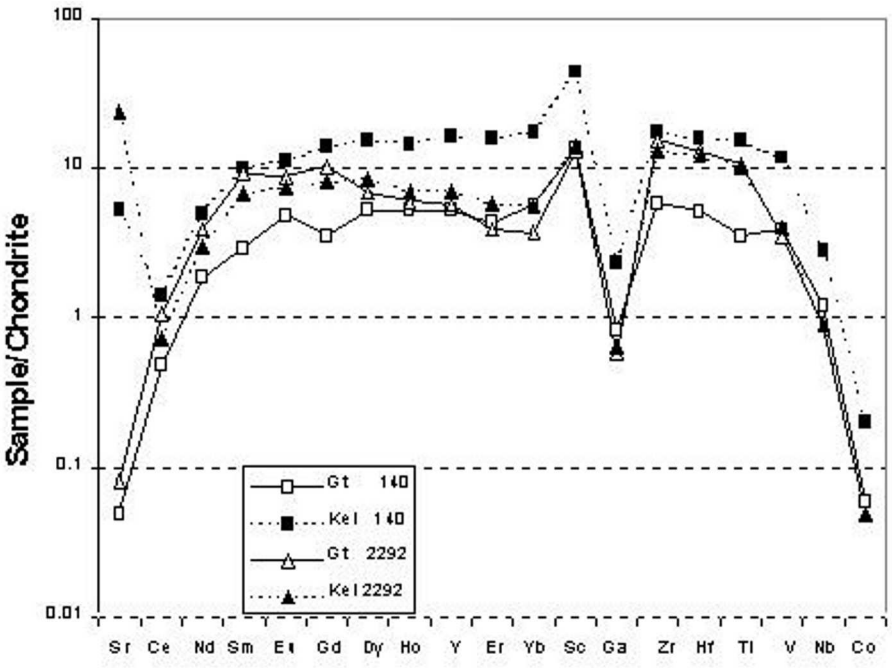

Fig. 4. **Chondrite-normalized trace element patterns for garnets and kelyphitic rims in sheared garnet peridotite xenoliths U-140/78 and U-2292 from the Udachnaya kimberlite pipe [49].**

problematic, but it is possible to speculate that they were related to a protokimberlitic magma.

In conclusion it should be stressed that garnet peridotite xenoliths from kimberlite pipe Udachnaya provide spectacular evidence of the metasomatic kelyphitization of garnets. Petrographic features, mineral associations and trace element patterns in kelyphites and garnet relicts suggest that these processes took place under upper mantle conditions in the presence of water-rich fluids. Most probably, this stage of metasomatism was caused by protokimberlitic fluids shortly before eruption of kimberlites.

TIMING OF METASOMATIC EVENTS

The majority of all known before estimations of ages of mantle xenoliths from kimberlite pipes of Yakutia are done by Sm/Nd or Re/Os methods [31, 30].The Nd and Sr isotopic date from diamond-bearing eclogites from the Udachnaya pipe and complex Sm-Nd isotope systematic in Siberian eclogites, are interpreted in [43] as indicating an early (> 4 Ga) differentiation event followed by subsequent (Early Proterozoic) eclogite crystallization from at least two different sources. The lowest peridotite osmium isotopic compositions require Re depletion in the mid-Archaean (3.2Ga) according to [33] and this age is interpreted as the time of differentiation of the Siberian lithospheric mantle. Ancient origin for Siberian lithosphere

supported by Re-Os and Sm-Nd model ages for eclogite and peridotite xenoliths from the Udachnaya and Mir pipes is obtained by different authors [19, 31, 43]. The age of formation of xenoliths and their differentiation in mantle according to isotopic data and other petrologic evidence is not less than 3.0 Ga, but as was shown [15, 31], the lithospheric mantle under the Siberian platform has complicated evolution which is displayed in multistage metasomatism. The trace element data for garnet and clinopyroxene inclusions and rockforming minerals of eclogite xenoliths from Udachnaya presented in [14, 48] also provide evidence that Siberian eclogites have experienced complex metasomatism and partial melting after their formation. In order to understand the evolution of the lithospheric mantle it is necessary to determine both the age of origin of mantle rocks and the age of subsequent mantle processes.

There are no precise and undoubted determinations of time of metasomatic events in lithospheric mantle of Siberian craton. Such attempt were made by Pearson et al. [31] that have estimated Archaean age for the lithospheric mantle beneath the Siberia craton and show that it was modified by multi-stage metasomatism. According to their data based on Rb-Sr isotope evidence metasomatism took place in a long period of evolution of the craton.

We have a possibility to estimate at least one stage of mantle metasomatism in the SCLM of the Siberia craton due to finding of the unique sample of garnet orthopyroxenite xenolith with the zircon in the Udachnaya pipe. The uniqueness of this sample is determined by the presence of secondary association of metasomatic minerals: phlogopite+rutile+zircon, that developed between grains of garnet and orthopyroxene and often crossing garnet (Fig. 5).

The modal composition of the sample is as follows: Opx - 30,4%, Gt - 29.4%, Fl - 36.6, Ru - 3.0, Zr - 0.6%. The orange grains of garnet are 1-10 mm, usually irregular or oval shape. The grains of garnet have been replaced relatively strong by kelyphitic rims. Orthopyroxene forms irregular and oval grains 3-6 mm. This rock is phlogopite-rich with regular crystals of phlogopite up to 5 mm long. Leists of phlogopite are situated usually between the grains of garnet and orthopyroxene. Rutile is present usually as inclusions in garnet 0.2-0.3 mm. Small grains of zircon, about 0.1-0.2 mm are associated with phlogopite. It should be stressed that both phlogopite and zircon are distributed not homogeneous in sample. Major elements composition of minerals from the analyzed sample shows that garnet is rich in pyrope-component and contains low Cr_2O_3 (Table 4). Phlogopite is titanium-rich what is usual for this mineral from ultramafic xenoliths of the Udachnaya and according to the low content of Cr_2O_3 may be define as primary mica. Rutile has a high content of FeO and rather high content of chromium. Major-element composition of primary minerals corresponds to typical garnets pyroxenites from this pipe (Table 4). Secondary minerals obviously replace primary garnet and orthopyroxene. It should be noticed also that secondary spinel and amphibole are presented in this sample, which most probably belong to the same secondary metasomatic association or represent next stage of metasomatose. The age of

zircons was determined at the Curtine University of Technology (Perth) using SHRIMP. U-Pb isotopic ratio and concentrations were determined in zircon grains *in situ* and were referenced to the Australian National University standart zircon

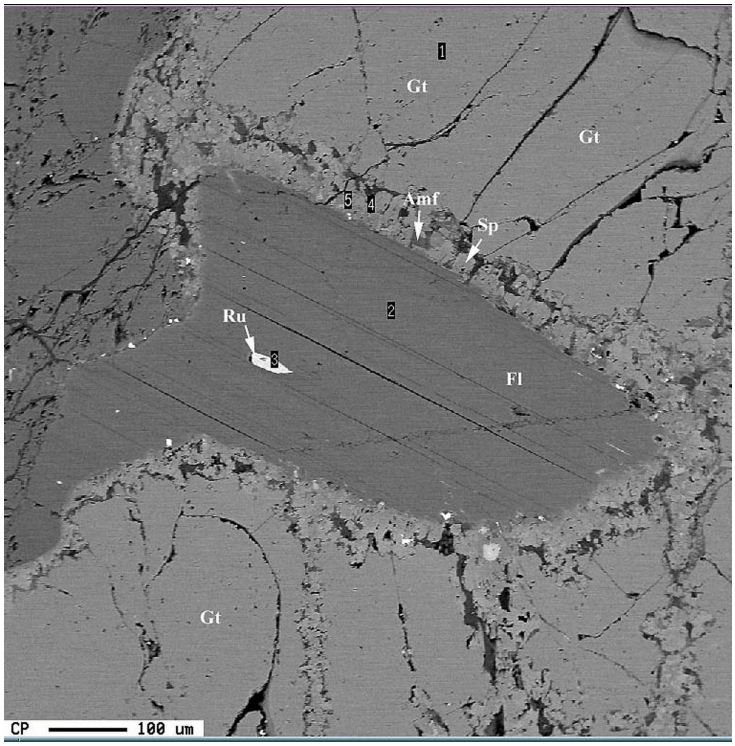

Fig. 5. **Scanning electron microscope back-scattered image of secondary phlogopite crossing garnet in the zirconbearing Gt-pyroxenite xenolith from the Udachnaya kimberlite pipe. (Sample U-2268).**

The phlogopite grain contains inclusion of rutile; additionally this phlogopite is corroding primary garnet. A rim consisting of secondary amphibole and spinel is obvious between garnet and phlogopite. Points of microprobe analyses of minerals are shown (data in Table 4).

Table 4.

Analyses of minerals of zirconbearing Gt-pyroxenite xenolith from the Udachnaya (sample U-2268)

Mineral	Opx	Gt (1)	Fl (2)	Ru (3)	Sp (4)	Amf (5)
SiO_2	52.96	41.08	39.61	0.03	0.1	48.85
TiO_2	0.08	0.03	2.49	95.67	0.15	0.18
Al_2O_3	4.7	22.75	13.46	0.02	59.63	9.37
Cr_2O_3	0.19	0.29	0.13	0.27	0.97	0.24
FeO	13.09	19.62	4.64	1.81	25.81	19
MnO	<0.03	0.55	0.01	0.11	0.36	0.61
MgO	28.58	13.67	22.35	0.17	11.77	20.6
CaO	0.27	3.76	0.05	0.01	<0.03	1.08
Na_2O	0.05	0.06	0.87	n.d.	n.d.	0.03
K_2O	n.d.	0.01	12.24	0.15	0.04	0.02
Total	99.96	101.81	95.86	98.24	98.83	99.97

Note. Numbers in parenthesis answer to the points of analyses on Fig. 5.

SL13 (572 Ma; 206Pb/238U=0/0928). Further details of the analytical procedure and data assessment are given in [20 and reference therein]. This estimation gives the Pb-U age of zircon 1.8 Ga (unpublished data). It should be noticed that this age is only one that defines the real timing of the metasomatic events in the SCLM of the Siberian craton.

Such petrographic evidence as inhomogeneous distribution in sample and secondary growth of phlogopite and associated with them zircon and rutile grains between rockforming garnet and orthopyroxene shows that these minerals were formed as secondary phases. Evidently they were formed in the process of global metasomatism of mantle rock under the Siberian platform. As was shown [51], the indications of mantle metasomatism manifested in deep-seated xenoliths are noted in many pipes of Yakutia among the rock of mafic and ultramafic composition. The only and relatively revealing criteria of infiltration metasomatism are micas and amphiboles that undoubtedly have metasomatic origin in mantle xenoliths but there are no sufficient data in order to judge the manifestation intensity of these processes in various areas of the Siberian platform. Reasoning from peculiarities of the phlogopite occurrence in the mantle rocks that is encountered as large grains commensurable with other minerals and also in the composition of kelyphite rims very likely that the metasomatic processes at the SCLM were repeated. In our case that shows a growth of phlogopite as a large grains like rockforming garnet and orthopyroxene more probably that origin of phlogopite and zircon had place on one of the stage of more intensive metasomatism, which more likely have occurred in time of global metasomatism of mantle. So, dated age of zircon from xenolith of garnet orthopyroxenite gives us the first correct estimation of time of global metasomatism of the mantle beneath the Siberian craton. It should be noticed that the age 1.8 Ga answer the timing of main crust formation [39] and thereby this suggests coincidence of these events.

GEOCHEMISTRY AND EVOLUTION OF REPRESENTATIVES OF THE SCLM OF SIBERIAN CRATON

Geochemical features of substance of the SCLM of upper mantle are discussed using the data on content and distribution of trace elements in mafic and ultramafic xenoliths as well as the data for megacrysts assemblage. As it was demonstrated by the results of proton probe and partly ICPMS data the content and distribution of the trace elements in eclogite xenoliths from the Udachnaya pipe and such pipes of South Africa as Monastery and others are very similar [49]. The main difference is high enrichment of eclogites from the Udachnaya pipe by Sr and Ga and depletion of garnets and clinopyroxenes by Y and Zr. Eclogitic clinopyroxenes of the Udacnaya are more LREE-depleted and less radiogenic than those from South Africa and garnet is enriched in LREE [18, 40, and 55]. Such a difference could be explained as a result of the more intensive metasomatic processes. ICPMS data for the eclogites from the Udachnaya pipe permitted the division into three groups in terms of trace element distribution [55]. Similar data

were obtained for the eclogites of Roberts Victor and Mbuji-Mayi [13, 38]. It should be emphasized that eclogites of the Udachnaya and Roberts Victor are very similar both in terms of their petrography, rock chemistry and geochemistry.

TRACE ELEMENT DISTRIBUTION IN MINERAL PHASES OF ECLOGITES FROM THE UDACHNAYA PIPE

The trace element data for mantle xenoliths have an important implications in many aspects: (a) the estimation of distribution in minerals and correct definition of partitioning of trace elements between minerals of mantle rocks in relationship with PT-conditions of their formation, (b) the deciphering of complicate history and evolution of mantle eclogites, that is an actual topic of discussion [18, 42, 43], (c) the elucidation of possible distinctions in behavior of trace elements in different mantle processes.

A suite of about 20 xenoliths from the Udachnaya kimberlite pipe has been studied on trace element composition of their minerals. Only 5 of the samples were simple bimineral or kyanite eclogites without diamonds. Diamondiferous xenoliths include not only bimineral eclogites, but one sample of garnet clinopyroxenite and two xenoliths of garnetites (with content of clinopyroxene less than 1%). Abundance of trace elements has been studied in coexisting garnets and clinopyroxenes in nearly all samples, and in secondary clinopyroxenes in some xenoliths. The special checking of core and rim parts of garnet grains shows that they are homogeneous in major and trace element composition. A little zonation of garnet is found only in two samples where rims are slightly enriched in Nd, Sm, Eu, Dy and Ho. It is necessary to stress that during the analysis of primary garnet and clinopyroxene in intensively metasomatized and partially melted xenoliths only the fresh relicts of these minerals were chosen.

The trace elements (TRE) have been measured in rockforming and some secondary minerals by laser Ablation ICP-MS (LAM) at the RSES of Australian National University, Canberra. The special checking of core and rim parts of garnet grains shows that they are homogeneous as by major and trace element composition. A little zonation of garnet is fixed only in two samples where rims are slightly enriched in Nd, Sm, Eu, Dy and Ho. Abundance of trace elements have been studied in coexisting garnets (Gt) and clinopyroxenes (Cpx) near in all samples and in some xenoliths were investigated also their distribution in phlogopite, rutile and secondary clinopyroxenes. It is necessary to stress that by analyzing of primary Gt and Cpx in intensively metasomatized and partially melted xenoliths the fresh relicts of these minerals were chosen.

Salient features of the results of LAM analyses can be summarized as follows: -chondrite-normalized REE pattern of garnets usually show a convex shapes and vary from slightly to strongly enriched in LREE (Fig. 6) whereas clinopyroxenes have characteristic high LREE abundance and show broad variations in MREE (Fig. 7):

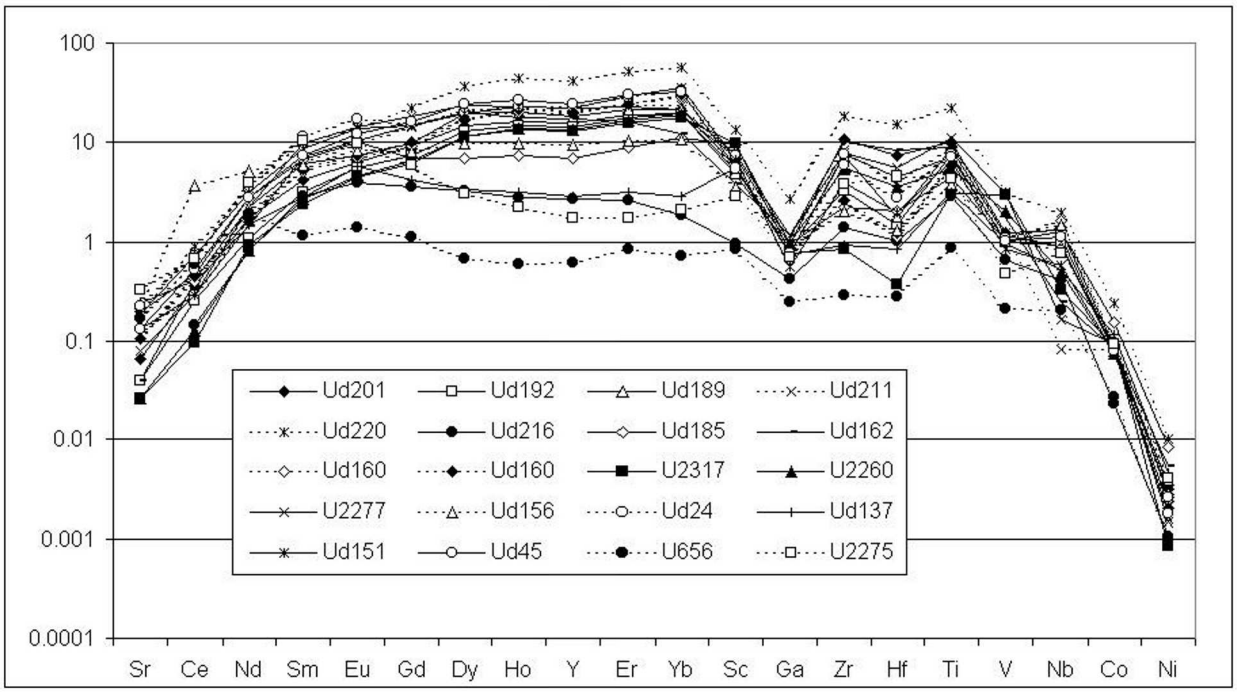

Fig. 6. **Chondrite-normalized REE diagram for garnets of eclogites from the Udachnaya kimberlite pipe. (Spetsius et al., unpublished data, 1998, ICP-MS, National University of Australia).**

Normalized against chondrite values of McDonough and Sun (1995).

- on the basis of the REE distribution three different types of garnets are distinguished in the studied eclogite xenoliths: (1) a “normal” group having upwardly convex pattern with initial steep progressive increase in LREE followed by a slower rate of increase in HREE, (2) a "HREE depleted" group in which the HREE show no marked increase from Dy to Yb and (3) an "Eu-anomalous group" in which there is a small positive Eu anomaly and a generally flat HREE pattern [55];

- the trace element content of most of the Group (1) garnets are similar, excluding garnetite sample (Ud-220) where this mineral is very rich in Sc, Ga, Yt, Nb, Zr, Ce, Gd, Dy, Ho, Er, Yb, Lu and Hf (Fig. 6);

- wide variations in REE and also in Sr are observed for clinopyroxenes (Fig. 7); the most suitable explanation for this enrichment is partial melting connected with metasomatism. Clinopyroxene Ud-2260 has especially high Y, Sm, Dy, Ho, Er and Yb;

- the highly aluminous xenoliths have slightly positive Eu-anomalies and low HFSE abundances that give some evidences for crustal protoliths, in accordance with the findings of [19];

- primary clinopyroxenes of most samples are enriched in LREE suggesting widespread cryptic metasomatism in many eclogite xenoliths from the Udachnaya; this confirming the results of petrographic observation [44].

It should be pointed that the substitution of Sr, Ba and such incompatible elements as V, Zr, Ni, and others into garnet and clinopyroxene is not controlled

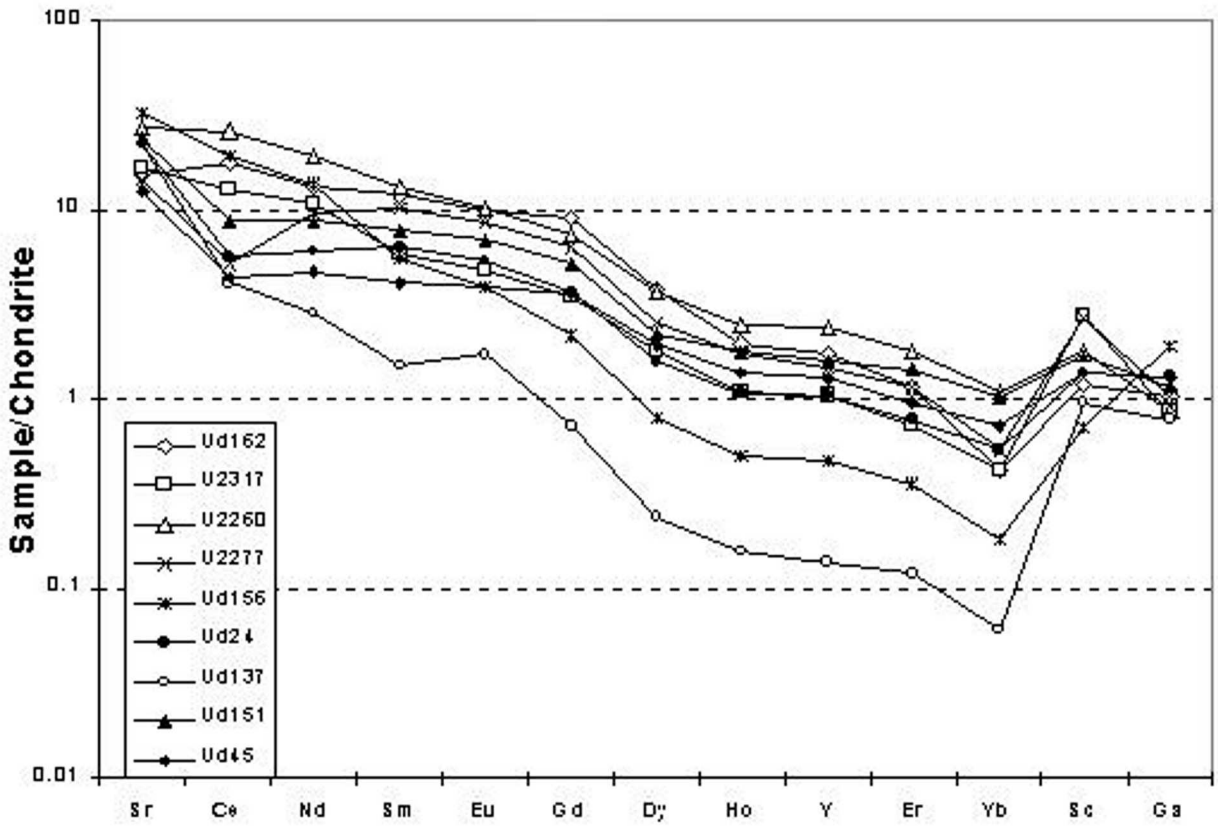

Fig. 7. **Chondrite-normalized REE diagram for clinopyroxenes of eclogites from the Udachnaya kimberlite pipe. (Spetsius et al., unpublished data, 1998, ICP-MS, National University of Australia).**

Normalized against chondrite values of [25].

essentially by T and P or bulk composition of minerals [55]. These observations indicate that the part of trace elements has independent behavior and support the suggestion [18] that enrichment or depletion of eclogite xenoliths rockforming minerals from Udachnaya pipe in some trace elements is due to complicated metasomatic and partial melting events. The REE abundance in coexisting garnets and clinopyroxenes and Cpx/Gt partition coefficients for some trace elements in eclogite xenoliths from Udachnaya [55] are similar to those found by O'Reilly and Griffin [29] for eclogites from South Africa, but these occurrences differ in Sr, Zr and Ni suggesting some differences in the evolution of the mantle eclogites of the Siberian and South Africa cratons.

TRACE ELEMENT EVIDENCE OF METASOMATISM IN ULTRAMAFITE XENOLITHS

Trace-element signatures in bulk rock can be used to some extent to fingeprint mantle processes [11]. REE patterns of SCLM clinopyroxenes are usually very similar to those of host peridotites, unless the peridotites contain another phases with a high distributions coefficient for REE [11]. That allowed using the trace

element distribution in clinopyroxenes of ultramafites for estimation their behavior in the whole rocks. Many mantle peridotites contain clinopyroxenes that show strong enrichment in LREE as a result of the metasomatic influence of LREE-enriched fluids. Evidence for the cryptic metasomatism is incompatible trace element concentrations in garnets and clinopyroxenes of fertile harzburgites and garnet peridotites from the Udachnaya pipe. This was established by ICPMS-data for minerals more than 15 samples. Fig. 8 shows typical REE patterns for clinopyroxenes in ultramafite xenoliths from the Udachnaya. It is obvious that many of peridotites contain clinopyroxenes with strong enrichment in LREE as a result of the metasomatic influence of LREE-enriched fluids. As was shown by Downes [11] REE patterns of SCLM clinopyroxenes are usually very similar to those of the whole rocks. This allowed us to use the distribution of trace elements in clinopyroxenes for estimation of intensity of metasomatic events in mantle xenoliths. Some evidence suggest that in many cases it could be a more correct method in comparison with the whole rock trace element data because many samples of mantle xenoliths from kimberlites contain evidence for the inducing of kimberlitic material or kimberlitic agents as a tiny veins or intergranular veinlets in xenoliths.

Representative data of trace element distribution in garnets of 18 samples ultramafite xenoliths from the Udachnaya confirm the wide development and presence of cryptic metasomatose between mantle ultramafites. According to [37], the results of the trace elements distribution study and above all REE-elements (Fig. 9) that show the convex shapes behavior of trace elements in garnets of ultramafites give a strong suggestion to this point of view. It not possible to discuss the time and stage of metasomatic events that are directly responsible for this effect but there are no doubts that in this case the metasomatose has nothing in connection with the influence of kimberlitic magma or fluids.

RE-OS SYSTEMATIC OF SULFIDES IN OLIVINES AND EVOLUTION OF THE SIBERIAN CRATON SCLM

As was shown above the data on the distribution of trace element in different types of ultramafites mainly from the Yakutian kimberlites are scarce. However, we could discuss the features of ultramafite geochemistry on the base of data obtained from Re-Os systematic of sulfides from the olivine macrocrysts of the Udachnaya pipe. Detailed Re/Os isotope compositions of sulfides were obtained for about 100 inclusions. The analytical procedures for in situ Re-Os isotope analysis and full data are presented in paper [15].

Sulfides in olivine macrocrysts from the Udachnaya pipe are presented predominantly by finely interfingered Ni-poor and Ni-rich monosulfide solid solution (MSS) with addition of pentlandite and chalcopyrite phases in some cases. Only 2/3 of all investigated sulfide inclusions give a reliable modal age. The modal age of about 60 sulfide inclusions varies from 2.4 to 3.5 Ga [15]. The main peaks

are found between 2.9 and 3.2. Ga. Multiple sulfide inclusions have been found and analyzed in 10 olivines. In most cases combinations of different sulfides

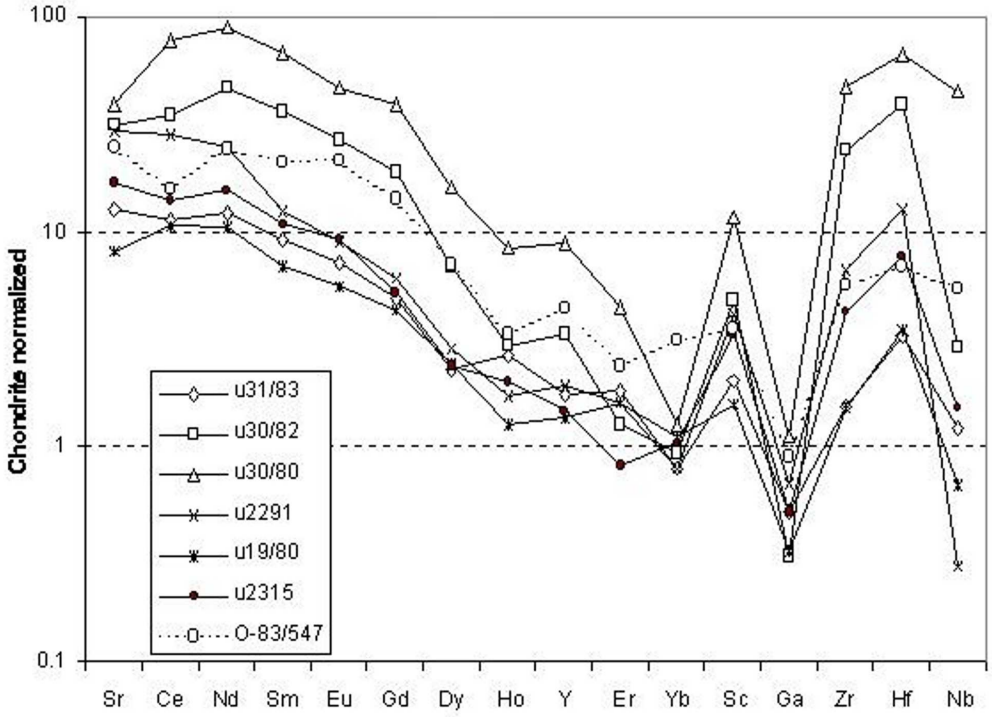

Fig. 8. **Chondrite-normalized REE diagram for clinopyroxenes of ultramafite xenoliths from the Yakutian kimberlites. (Spetsius and Griffin, unpublished data, 1998, ICP-MS, GEMOC).**

Normalized against chondrite values of [25].

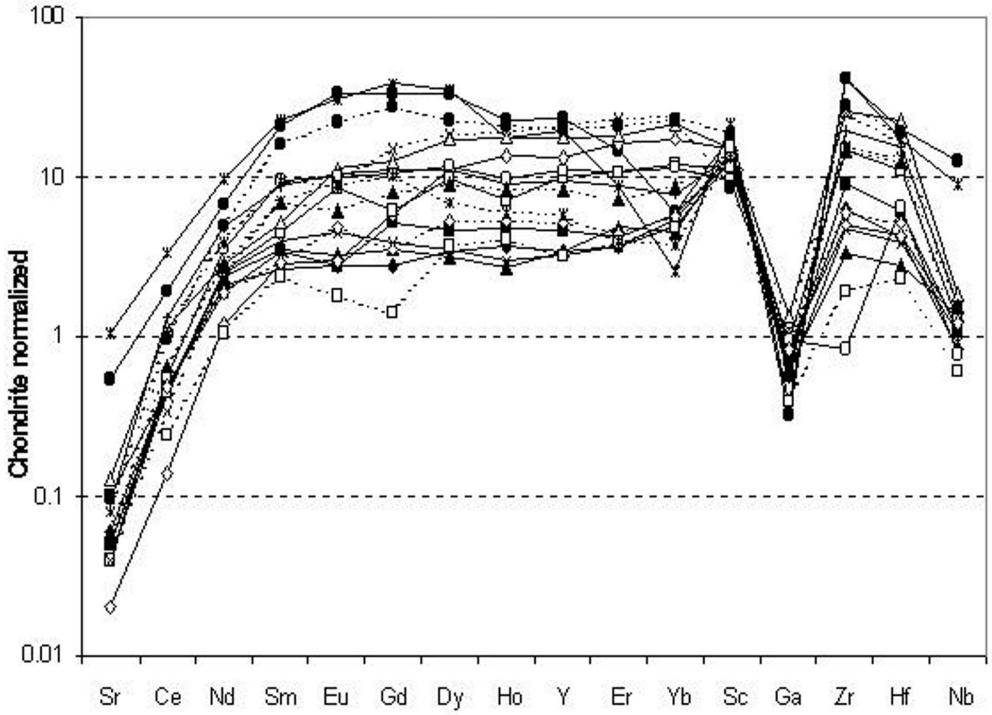

Fig. 9. **Chondrite-normalized REE diagram for garnets of ultramafite xenoliths from the Yakutian kimberlites. (Spetsius and Griffin, unpublished data, 1998, ICP-MS, GEMOC).**

Normalized against chondrite values of [25].

within a single olivine cannot yield Re-Os isochrones with meaningful ages and initial ratios. It suggests that these inclusions represent trapping of different sulfides generations in one olivine grain [15].

The majority of Re-Os determinations belong to the dating of sulfides in mantle xenoliths and diamonds from kimberlites. The characteristics of Re and Os isotopes distribution in mantle xenoliths are obtained for the whole rocks samples and provide ages from 2.8 to 3.2 Ga for mafic and ultramafic xenoliths from Yakutian kimberlites [31-33, 38]. Re-Os isotope ratio of sulfide inclusions in diamonds gives the model ages for Siberian mantle varying from 2.8 to 3.5 Ga [33]. As shown by results of in-situ Re-Os analysis of sulfide inclusions in olivines from the Udachnaya kimberlite pipe their model age varies from 2.4-3.5 Ga with the two peaks at 2.9 and 3.2 Ga [15]. Probably they reflect the main events in the SCLM of the Siberian platform.

Using the above data we can suggest that much of the SCLM beneath the Udachnaya pipe as well beneath the Siberian craton was formed between 3.4 and 2.9 Ga ago by one or more major melting events [15]. The results of Re-Os isotopes study of sulfide inclusions in the mantle megacrysts from the Yakutian kimberlites show that the SCLM beneath the Siberian craton was stabilized predominantly between 3.0 and 2.8 Ga ago. The major peak of T_{MA} values of sulfides in olivines around 2.9 Ga coincides with the time of the cratonization and the end of major SCLM formation as well as with the eclogite formation and remelting [15, 31, 36, 38]. Several sulfide inclusions in olivines with low Re/Os and T_{MA} 1.5-2.6 Ga may represent new additions to the lithosphere and connected with the late tectonic events and disturbing of Re-Os systematics through metasomatic events. These results clearly demonstrate the complicated history of the Siberian SCLM. Younger Proterozoic Re depletion ages are interpreted to be predominantly the result of open system behavior during the late igneous activity and probably metasomatism [15]. Such a possible scenario of a complicated history of Re-Os systematics confirms the longlivity of the lithospheric mantle beneath the Siberian craton. This scenario is consistent with the limited data on crustal formation in the Daldyn and other terranes [39].

Summarizing the results of investigations of metasomatic processes in ultramafic xenoliths from the Yakutian kimberlites it is possible to combine next evidence: i) modal metasomatic minerals or trace-element enrichment occur in the almost all varieties of xenoliths; ii) the most prominent features of the modal metasomatism are replacement of early phases by phlogopite with addition of spinel and other minerals and development of the kelyphitic rims. Trace elements distribution in garnet and their kelyphitic rims have suggested a deep origin for the kelyphitization; iii) another evidence for modal metasomatism in peridotite xenoliths are replacement of orto- and clinopyroxene by hydrous and ore phases

and development of partial melting blebs consisting of a new hydrous phases in garnets of coarse grained pyroxenites; iv) the metasomatic processes usually are synchronized or very close to the stage of mantle rock deformation; v) according to

Re-Os determination of sulfide inclusions in olivines from the Udachnaya, the Os system disturbing by igneous and metasomatic events took place after forming SCLM of the Siberian craton from 2.8 till 2.0 Ga; vi) one of the stage of the mantle metasomatism of the Siberian SCLM around 1.8 Ga is confirmed by U-Pb SHRIMP-dating of zircon in metasomatized Gt-pyroxenite from the Udachnaya; vii) the metasomatic and deformation processes are more intensive manifested in xenoliths from the central part (Daldyn-Alakitsky region) of the kimberlite province.

METASOMATIC ORIGIN OF DIAMONDS

Multi-Stage Diamond Formation Birefringence, laser- and cathodoluminescence investigation shows that less than 50% of diamonds from kimberlites grew in single-stage process [44]. Complicated growth is shown many diamonds that displayed in zonal growths, deformation and regrowths. Octahedral external forms of crystals may have central zones of different shapes. This provides evidence that diamonds have multistage and interrupted growths, which response to P-T and environment variations.

As it is accepted, diamonds are xenocrysts, along with ilmenite, garnet and zircon in kimberlites [e.g., 39, 51]. But there are a number of contradictions, hard to explain, on the assumption that all the diamonds in mantle were crystallizing as the first phases or simultaneously with the other rock-forming minerals of eclogites.

The complex and multi-staged history of growth is fixed for the part of diamonds both of peridotitic and eclogitic paragenesis. It is reflected in zonal growth of diamonds, resorption and deformation of crystals and their later recrystallization. The investigation of large diamond crystals of octahedron shape has shown that their central zones could be of different type: of cubic, round, cube-octahedron or octahedron form [4]. This testifies that growth of diamonds was multi-staged and interrupted in time, it was corresponding to the changes of chemical and P-T environment and, perhaps, to variations of volatile components.

Evidence for multi-stage formation of diamonds includes: (1) sharp boundaries between zones having different nitrogen content and aggregations stages; (2) large differences in $\delta^{13}C$ and $\delta^{15}N$ in inner and outer parts of diamonds; (3) abundance of sulfide inclusions and heterogeneity of sulphur isotope compositions; (4) combined inclusions associations of eclogitic and peridotitic paragenesis in one crystal; (5) heterogeneity of $\delta^{34}S$, as well as Pb isotopes, in sulfides within a single diamond. Strong evidence has been obtained recently through Re-Os isotope dating of individual sulfide inclusions in diamonds from the

Koffiefontein [32] that indicate two episodes of sulfide inclusions crystallization and respectively two ages of diamond formation.

METASOMATIC GROWTH OF DIAMONDS IN ECLOGITES

Diamondiferous eclogites contain petrographic and photographic evidence that the diamonds post-date the eclogites formation: a) a lack of diamonds within the primary garnets; b) the general observation that diamonds are correlated with zones of deformation and alteration in eclogites; c) the obvious resorption and possible growth features of diamonds in these alteration zones; and d) metasomatic, partially-melted Cpx (spongy texture) in both the alteration zones and as inclusions in the diamonds [4]. Some examples are given on Fig. 10.

There are also other direct proofs of secondary diamond growth and their relation to the metasomatic process. To such ones may be referred: a) occurrences of melted inclusions in diamonds from pipe Mir and in cubic crystals from Zaire and Botswana [4, 28], b) discovery of phlogopite and plagioclase in diamonds from pipe Monastery [28], c) finding syngenetic inclusions of metasomatic minerals [5, 22].

As a result of investigation of diamonds in eclogite xenoliths from pipe Udachnaya, it was ascertained that in rare samples there are two types of crystals different in morphology, color, physical and other features, which can be identified with two historically independent growth generations, different by P-T conditions and medium of diamond-formation [46].

Large monocrystals mostly of octahedral shape were formed most probably in stable conditions and crystallized from the melt according to the tangential law [4] simultaneously with basic rockforming minerals of eclogites. Their growth in process of metasomatism is also not excluded [58]. Such first generation diamonds in individual xenoliths exhibit signs of a complicated subsequent history - they may be deformed plastically, sometimes broken and resorbed [54].

There is an obvious distribution of second-generation diamonds, in some eclogites [46], where microdiamonds are located along zones of partial-melting or kelyphite rims around garnet, as well as along general zones of major metasomatic alteration. Such relations of diamonds in space have been found in eclogite xenoliths from Udachnaya, Sytykanskaya, and other Yakutian pipes. The diamonds of the second generation are represented by cubes, coated crystals (probably only surface zones of these crystals), and microdiamonds. Coats on diamonds and cubes were formed by an abnormal mechanism of growth under conditions with a high degree of carbon supersaturation. Such condition may be realized in last stages of partial melting when melt was enriched in carbon. Most probably they had been growing at lower P-T conditions and that they crystallized from sulfide-silicate melt saturated with fluids.

These facts and also the occurrence of diamonds in a number of eclogites, when the secondary character of diamonds in them is clear (the growth of

diamonds between and around the grains of rock-forming minerals and confinement of crystals to the veins of partial melting products) enable to put forward ***hypothesis of the late metasomatic diamond formation*** in some eclogites. The real proof of the similar opportunity is the distribution of diamond crystals in

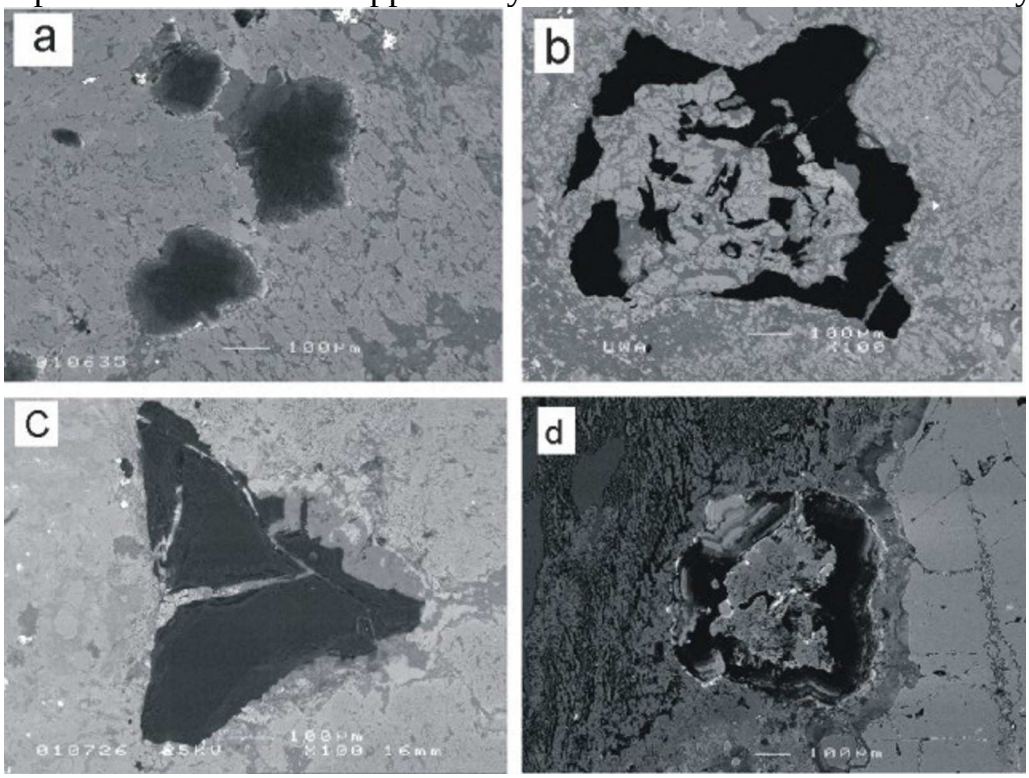

Fig. 10. **Diamonds associated with partial-melt products.**

(a) Microdiamonds in partial-melt products (Sample Ud-24 in BSE + CL). (b) Diamond with the inclusion of secondary clinopyroxenes and other phases of partial-melt (Sample Ud-161 in BSE). (c) Slightly zoned diamond with cutting veins of patial-melt products in secondary clinopyroxenes (Sample U-388 in BSE + CL). (d) Zoned crystal of hopper diamond with evidences for resorption by the partial melt which situated between partially melted clinopyroxene with 'spongy' texture and garnet (Sample Ud-45 in BSE + CL).

the products of partial melting, fringing garnet segregation. It is clearly seen that diamonds were growing around already formed garnets, therewith in one case diamonds of the second generation associate with kelyphite rim around garnet and are situated in the vein of partial melting products in clinopyroxene [46, 52].

A relationship between the partial melting process and growth of diamond is conceivable. There have been several studies that have demonstrated that diamonds undergo multistage and interrupted growth, caused by changes of the chemical and P-T environment (e.g., [45, 46, 52, 54, 58]). In particular, fibrous diamonds contain fluids that are highly enriched in K, Na. and other incompatible elements [28 and reference therein]. Zedgenizov et al. [60] published data on a potassic-bearing clinopyroxene included in diamond from the Sytykanskaya kimberlitic pipe. The core of this inclusion that composes of omphacite is surrounded by glassy matrix. These components would seem to be the same ones involved with the metasomatic fluids responsible for the partial melting of the eclogitic minerals.

It is entirely possible that the rims of some of the diamonds in the partial-melt regions may have grown as a result of this melting process. Others diamonds, like cubes and microdiamonds, may have grown as a result of the metasomatic fluid penetrations.

There are no unambiguous evidences of what stage of mantle metasomatism or partial melting these diamonds have been grown. However, interactions between diamonds and the partial melt are entirely possible, both with the stable and metastable growth of coatings, as well as resorption of the diamonds, as shown in Fig. 10 c, d. It is supposed that metasomatic growth of diamonds in eclogite xenoliths could be repeated and connected with partial melting. This process may take place in different time of mantle evolution and in some cases has been connected with fluids interaction that had preceded the intruding of kimberlites.

CONCLUSION

According to Re-Os and Sm-Nd dating the SCLM of the Siberian platform was formed in the Archaean. The vertical and lateral heterogeneities of the SCLM are the results of primary differentiations of the mantle substance and late addition of the oceanic crust during subduction in central part of the platform and subsequent development of mantle by the processes of mantle metasomatism and couplet tectonic deformation.

In Yakutian kimberlites the mafic xenoliths display evidences of partial melting. Modal and cryptic metasomatism is abundant in ultramafic mantle xenoliths from kimberlites. Often these processes are couplet with tectonic deformation of mantle rock and in rare cases with the partial melting. These processes took place repeatedly in SCLM of the Siberian craton and were more intensive in central part of the kimberlite province and are connected with the major tectonic-magmatic events observable in the upper crust.

The SCLM of the Siberian craton was formed in Archaean and has a resemblance in the distribution of petrographic types of mantle xenoliths and coupled crustal rocks in most areas of kimberlite province. The evolution of the SCLM of different regions inside kimberlite province could be different in timing of tectonic-magmatic events as well as in intensity of mantle metasomatism, partial melting and tectonic deformation.

It is supposed that metasomatic growth of diamonds in eclogite xenoliths could be closely associated with the metasomatism that caused some of the partial melting. This can occur both long before eruption deep in the mantle, as well as with kimberlite formation and eruption (e.g., fibrous-diamond growth on coated crystals).

ACNOWLEDGEMENTS

I thank Bill Griffin, Sue O’Reily and Wayne Taylor for the collaborative work on doing trace elements on ISPMS and their generous hospitality and

assistance during several visits to Australia. I am indebted to Brendon Griffin for his support with the diamond investigation and electron microprobe analyses of secondary phases in eclogites. I am grateful to Alexander Ivanov for help with the electron microprobe analyses and SEM images. I am pleased to Larry Taylor for discussing of partial melt process in eclogites that helped to understand their nature.

REFERENCES

1. **Beard, B. L., Fraracci, K. N., Taylor, L. A., Snyder, G. A., Clayton, R. N., Mayeda, T. and Sobolev, N. V.** (1996). Petrography and geochemistry of eclogites from the Mir kimberlite, Yakutia, Russia. Contrib. Mineral. Petrol. 125, 293-310.
2. **Bobrievich, A.P., Bondarenko, M.N., Gnevushev, M.A, Krasov, A.M., Smirnov, G.I. and Yurkevich, R.K.** (1959). The diamond deposits of Yakutia. Moscow: Gosgeoltekhizdat, 527 p. (in Russian).
3. **Brenan, J.M., Shaw, H.F., Ryerson, F.J. and Phinney, D.L.** (1995). Mineral-aqueous fluid partitioning of trace elements at 900^{o}C and 2.0 GPa: Constraints on the trace element chemistry of mantle and deep crustal fluids. Geochimica et Cosmochimica Acta 55, 2203-2214.
4. **Bulanova, G.P.** (1995). The formation of diamond. J. Geochem. Explor. 53, 1-23.
5. **Bulanova, G.P., Muchemwa, E., Pearson, D.G., Griffin, B.J., Kelly, S.P., Klemme, S. and Smith, C.B.** (2003). Syngenetic inclusions of yimengite in diamond from Sese kimberlite (Zimbabwe) – evidence for metasomatic conditions of growth. Ext. Abstracts of 8th Intern. Kimberlite Conf., Victoria, Canada.
6. **Bulanova, G.P., Spetsius, Z.V. & Leskova, N.V.** (1990). Sulfides in diamonds and xenoliths from kimberlite pipes of Yakutia. Novosibirsk: Nauka, 117 p. (in Russian).
7. **Chinner, J. A. and Cornell, D. H.** (1974). Evidence of kimberlite-grospydite reaction. Contribution Mineralogy and Petroogy, 45, 153-160.
8. **Dawson, J. B.** (1980). Kimberlites and their xenoliths. Berlin: Springer-Verlag, 252p.
9. **Dawson, J.B.** (1987). Metasomatized harzburgites in kimberlite and alkaline magmas: enriched restites and "flushed" lherzolites. In: Menzies, M.A. and Hawkesworth, C.J. (eds) Mantle metasomatism. London: Academic Press, pp. 125-144.
10. **Dawson, J. B.** (2002). Metasomatism and partial melting in upper-mantle peridotite xenoliths from the Lashaine volcano, Northern Tanzania. Journal of Petrology 43, 1749-1777.
11. **Downes, H.** (2001). Formation and modification of the shallow sub-continental lithospheric mantle: a review of geochemical evidence from ultramafic xenolith suites and tectonically emplaced ultramafic massifs of western and central Europe. Journal of Petrology 42, 233-250.
12. **Erlank, A.J., Water, F. G., Hawkesworth, C. J., Haggerty, S. E., Allsopp, H. L., Rickard, R. S., and Menzies, M.** (1987). Evidence for mantle metasomatism in peridotite nodules from kimberlite pipes, South Africa. In: Menzies, M.A. and Hawkesworth, C.J. (eds) Mantle metasomatism. London: Academic Press, pp. 221-311.
13. **Fadili, S. El. and Demaiffe, D.** (1999). Petrology of eclogite and granulite nodules from the Mbuji Mayi Kimberlites (Kasai, Congo): Significance of kyanite-omphacite intergrowths. In: Gurney, J.J., Gurney, J.L., Pascoe, M.D. and Richardson, S.H. (eds) Proceedings of 7th Intern. Kimberlite Conf. 1, Cape Town: Red Roof Design, 205-213.
14. **Franz, L., Brey, G.P. and Okrusch, M.** (1995). Metasomatic requuilibration of mantle xenjliths from the Gibeon kimberlite province (Namibia), Ext. Abstracts of 6th Intern. Kimberlite Conf., Novosibirsk, Russia, 169-171.

15. **Griffin, W.L, Spetsius, Z.V., Pearson, N.J., and O'Reilly, S.Y.** (2002). In-situ Re-Os analysis of sulfide inclusions in kimberlitic olivine: new constraints on depletion events in the Siberian lithospheric mantle. Geochemistry, Geophysics, Geosystems 1, N 11. GC000287.
16. **Harte, B., Winternburn, P.A., and Gurney, J.J.** (1987). Metasomatic and enrichment phenomena in garnet peridotite facies mantle xenoliths from the Matsoku kimberlite pipe, Lesotho. In: Menzies, M.A. and Hawkesworth, C.J. (eds) Mantle metasomatism. London: Academic Press, pp. 145-220.
17. **Hoal, K.E.O., Hoal, B.G., Erlank, A.J., and Shimizu, N.** (1994). Metasomatism of the mantle lithosphere recorded by rare earth elements in garnets. Earth and Planetary Science Letters 126, 303-313.
18. **Ireland, T. R., Rudnick, R. L and Spetsius, Z. V.** (1994). Trace elements in diamond inclusions from eclogites reveal link to Archean granites. Earth and Planetary Science Letters 128, 199-213.
19. **Jacob, D., and Foley, S.F.** (1999). Evidence for Archean oceanic crust with low high field strength element signature from diamondiferous eclogite xenoliths, Lithos 48, 317-336.
20. **Kinny, P.D., Black, L.P. and Sheraton J.W.** (1993). Zircon ages and the distribution of Archaean and Proterozoic rocks in the Rauer Islands. Antarctic Science 5, 193-206.
21. **Kinny, P.D., Trautman R.L., Griffin B.J., Fitzsimons, I.C.W. and Harte B.** (1999). Carbon isotopic composition of microdiamonds. Proceeding of 7th International Kimberlite Conference 1, 429-436.
22. **Kopylova, M.G., Rickard, R.S., Kleyenstueber, A., Taylor, W.R., Gurney, J.J. and Daniels, L.R.** (1997). First occurrence of strontian K-Cr loparite and Cr chevkinite in diamonds. The 6th IKC proceeding, Russian Geology and Geophysics 38, 405-420.
23. **Lappin, M.A.** (1978). The evolution of a grospydite from Roberts Victor Mine, South Africa. Contribution to Mineralogy and Petroogy 66, 229-241.
24. **McCormick, T. C., Smyth, J. R. and Caporuscio F. A.** (1994). Chemical systematics of secondary phases in mantle eclogites. In: Meyer, H.O.A. and Leonardos O.H. (ed) Kimberlites, related rocks and mantle xenoliths. Rio de Janeiro: Spec. Publ., Companhia de Pesquisa de Recursos Minerais, 405-419.
25. **McDonough, W. F. and Sun, S. S.** (1995). The composition of the Earth. Chemical Geology 120, 223-253.
26. **Menzies, M. A.** (1990). Petrology and geochemistry of the continental mantle: an historical perspective. In: Menzies M.A. (ed) Continental mantle. Oxford: Science Publication, 50-54.
27. **Meyer, H.O.A.** (1985). Genesis of diamond: a mantle saga. American Mineralogist 70, 344-355.
28. **Navon, O.** (1999). Diamond formation in the Earth's mantle. The 7th IKC proceeding 2, 584-605.
29. **O'Reilly, S.Y. and Griffin, W.L.** (1995). Trace-element partitioning between garnet and clinopyroxene in mantle-derived pyroxenites and eclogites: P-T-X controls, Chemical Geology 121, 105-130.
30. **Pearson, D.G.** (1999). The age of continental roots. Lithos 48, 171-194.
31. **Pearson, D. G., Shirey, S. B., Carlson, R. W., Boyd, F. R., Pokhilenko, N. P. and Shimizu, N.** (1995). Re-Os, Sm-Nd and Rb-Sr isotope evidence for think Archaean lithospheric mantle beneath the Siberia craton modified by multistage metasomatism. Geochimica et Cosmochimica Acta 59, 959-977.
32. **Pearson, D.G., Shirey, S.B., Harris, J.W. and Carlson, R.W.** (1998). Sulphide inclusions in diamonds from the Koffiefontein kimberlite, S. Africa: constraints on diamond ages and mantle Re-Os systematics. Earth and Planetary Science Letters 160, 311-326.

33. **Pearson, D.G., Shirey, S.B., Bulanova, G. P., Carlson, R.W. and Milledge, H.J.** (1999). Re-Os isotopic measurements of single sulfide inclusions in a Siberian diamond and its nitrogen aggregation systematics. Geochimica et Cosmochimica Acta 63, 703-711.
34. **Ponomarenko, A.I.** (1977). Partial melting of eclogites (natural processes), Doklady Akademy Nauk SSSR 235, 1416-1418 (in Russian).
35. **Richardson, S. H., Harris, J. W. and Garney, J. J.** (1993). Three generations of diamonds from old continental mantle. Nature 366, 256-258.
36. **Rosen, O.M., Serenko, V.P., Spetsius, Z.V., Manakov, A.V. and Zinchuk, N.N.** (2002). Yakutian kimberlite province: position in the structure of the Siberian craton and composition of the upper and lower crust. Russian Geology and Geophysics 43, 3-26 (in Russian).
37. **Shimizu, N. and Richardson, S. H.** (1987). Trace element abundance patterns of garnet inclusions in peridotite-suite diamonds. Geochimica et Cosmochimica Acta 51, 755-758.
38. **Shirey, S.B., Carlson, R.W., Richardson, S.H., Menzies, A., Gurney, J., Pearson, D.G., Harris, J.W. and Wiechert, U.** (2001). Archean emplacement of eclogitic components into the lithospheric mantle during formation of the Kaapvaal Craton. Geophysics Research Letters 28, p. 2509-2512.
39. **Sobolev, N.V.** (1977). Deep-seated Inclusions in Kimberlites and the Problem of Upper Mantle Composition, Novosibirsk: Nauka, Engl. Translation by Brown, D.A., and Boyd, F.R., (ed.), American Geophysics Union, Washington, D.C., 279 p.
40. **Sobolev, V.N., Taylor, L.A., Snyder, G.A Jerde, E.A., Neal, C.R. and Sobolev, N.V.** (1999). Quantifying the Effects of metasomatism in mantle xenoliths: Constraints from secondary chemistry and mineralogy in Udachnaya eclogites, Yakutia, In'l. Geology Review 41, 391-416.
41. **Sobolev, V.N., Taylor, L.A., Snyder, G.A., Sobolev, N.V., Pokhilenko, N.P. and Kharkiv, A. D.** (1997). A unique metasomatized peridotite from the Siberian Platform. Proceedings of 6th Intern. Kimberlite Conf. 1: Kimberlites, Related Rocks, and Mantle Xenoliths. Russian Geology and Geophysics 38, 218-228.
42. **Snyder, G.A., Taylor, L.A., Crozaz, G., Halliday, A.N., Beard, B.L, Sobolev, V.N. and Sobolev, N.V.** (1997). The origin of Yakutian eclogite xenoliths. Journal of Petrology 38, 85-113.
43. **Snyder, G.A., Taylor, L.A., Crozaz, G., Halliday, A.N., Beard, B.L., Sobolev, V.N. and Sobolev, N.V.** (1998). The diamond-bearing Mir eclogites, Yakutia: Nd and Sr isotopic evidence for the continental crustal imput in an Archean oceanic environment. Ext. Abstracts of 7th Intern. Kimberlite Conf., Cape Town, South Africa, pp. 826-828.
44. **Spetsius, Z.V.** (1995). Occurrence of diamond in the mantle: a case study from the Siberian Platform. Journal of Geochemical Exploration 53, 25-39.
45. **Spetsius, Z. V.** (1995). Diamondiferous eclogites from Yakutia: Evidence for a late and multistage formation of diamonds. Ext. Abstracts of 6th Intern. Kimberlite Conf., Novosibirsk, 572-574.
46. **Spetsius, Z.V.** (1999). Two generation of diamonds in the eclogite xenoliths. In: Gurney, J.J., Gurney, J.L., Pascoe, M.D. and Richardson, S.H. (eds) Proceedings of 7th Intern. Kimberlite Conf. 2. Cape Town: Red Roof Design, 823-828.
47. **Spetsius, Z.V. and Griffin, B.J.** (1998). Secondary phases associated with diamonds in eclogites from the Udachnaya kimberlite pipe: Implications for diamond genesis, Ext. Abstracts of 7th Intern. Kimberlite Conf., Cape Town, South Africa, 850-852.
48. **Spetsius, Z.V. and Griffin, W. L.** (1997). Trace elements in minerals from eclogites from the Udachnaya kimberlite pipe, Yakutia. Proceedings of 6th Intern. Kimberlite Conf., Russian Geology and Geophysics 38, 240-246.

49. **Spetsius, Z.V. and Griffin, W.L.** (1998). Trace element composition of garnet kelyphites in xenoliths from Udachnaya as evidence of their origin. Ext. Abstracts of 7th Intern. Kimberlite Conf., Cape Town, South Africa, 853-855.
50. **Spetsius, Z.V. and Ponomarenko, A.I.** (1979). The amorphozed eclogites - representatives of asthenosphere of the Earth, Doklady Akademy Nauk SSS, 235, 1415-1419, (in Russian)
51. **Spetsius, Z.V. and Serenko, V.P.** (1990). Composition of continental upper mantle and lower crust beneath the Siberian platform. Moscow: Nauka, 272 p. (in Russian).
52. **Spetsius, Z.V. and Taylor, L.A.** (2002). Partial Melting in Mantle Eclogite Xenoliths: Connection with Diamond Paragenesis. In'l. Geology Review 44, 973-987.
53. **Spetsius, Z.V. and Taylor, L.A**. (2003). Kimberlite xenoliths as evidence for subducted oceanic crust in the formation of the Siberian craton. Proceedings of 3d Intern. Workshop: Plumes and problem of deep sources of alkaline magmatism. Irkutsk, 5-19.
54. **Spetsius, Z.V. and Taylor, L.A.** (2003). Metasomatic diamonds in eclogite xenoliths: petrologic and photographic evidence. Ext. Abstracts of 8th Intern. Kimberlite Conf., Victoria, Canada.
55. **Spetsius, Z.V., Taylor, W.R. and Griffin, B.J.** (1998). Major and trace-element partitioning between mineral phases in diamondiferous and non-diamondiferous eclogites from the Udachnaya kimberlite pipe, Yakutia. Ext. Abstracts of 7th Intern. Kimberlite Conf., Cape Town, South Africa, 856-858.
56. **Switzer, G., and Melson, W. G.** (1969). Partially melted kyanite eclogite from the Roberts Victor mine. South Africa, Smithsonning Contribution Earth Science 1, 1-9.
57. **Taylor, L.A., Milledge, H.J., Bulanova, G.P., Snyder, G.A. and Keller, R.A.** (1998). Metasomatic eclogitic diamond growth: evidence from multiple diamond inclusions. Int. Geol. Rev. 40, 663-676.
58. **Taylor, L. A., Keller, R. A., Snyder, G. A., Wang, W. Y., Carlson, W. D., Hauri, E. H., McCandless, T., Kim, K.R., Sobolev, N. V.** (2000). Diamonds and their mineral inclusions, and what they tell us: A detailed "pull-apart"of a diamondiferous eclogite. Int. Geol. Rev. 42, 959-983.
59. **Vischnevsky, A.A.** (1991). Kelyphites on garnets in mantle xenoliths and kimberlites: compositions, genesis, petrological applications. Extended Abstracts of 5th International Kimberlite Conference, Araxa, Brasilia, pp. 571-572.
60. **Zedgenizov, D.A., Logvinova, A.M., Shatsky, V.S., Sobolev, N.V.** (1998). Inclusions in microdiamonds from some Yakutian pipes. Dokl. Ross. Akad. Nauk, Earth Sci. 359, 74– 76 (in Russian).

UDK 551.22 +552.11

Reconstructions of the mantle layering beneath the Alakite kimberlite field: comparative characteristics of the mineral geochemistry and TP sequences

Ashchepkov I.V.[1], Vladykin N.V.[2], Rotman A.Y.[3], Logvinova A.M.[1], Nikolaeva I.A.[1], Palessky V.S.[1], Saprykin A.I.[1], Anoshin G.N.[1], Kuchkin A.[1], Khmel'nikova O.S.[1]

[1]*United Institute of Geology Geophysics and Mineralogy SD RAS*
[2]*Novosibirsk Institute of Geochemistry SD RAS, Irkutsk*
[3] *Central Science And Research Geology And Prospecting Institute Of The Stock Company "ALROSA"*

Comparison of the mantle columns determined with the monomineral garnet and clinopyroxenes thermobarometry for the Aykhal and Yubileinaya, Komsomolskaya and Sytykanskaya kimberlites which are generally similar show a mantle layering consisting of 9 horizons. By using the P (kbar)- FeO, CaO, Al_2O_3 diagrams it became possible to show a detailed structural mutual correlation of the sequences. Chemical compositions of minerals of the mantle column are close despite of volume variations but TRE geochemistry is rather specific for mineral concentrates suggesting percolations through the whole mantle column and melt interaction processes. For the Aykhal where the mantle column is more depleted then in other pipes total Zr depletions in minerals are typical. K and LILE metasomatism is characteristic of the Yubileinaya pipe in lower horizons and Na-metasomatism and moderate depletion in HFSE were found for minerals from the Komsomolskaya and Sytykanskaya pipes. The sturtcures of mantle sections and feeding systems represented by ilmenites are close. Ti- rich associations (chromites, garnets etc) record the reactions around the feeding systems.

INTRODUCTION

The Alakite kimberlite region encounters several large pipes under exploration, four of them - Aykhal, Yubileinaya, Komsomolskaya, Sytykanskaya - compile the main diamond potential of the central part of the Yakutian diamond region (Fig. 1). This paper presents a comparison of the concentrates from these kimberlite diatreams to determine co-variations of mineral compositions between the pipes and based on PT reconstructions, mutual relationships and petro- and lithological features of the mineral chemistry and TRE (trace-element) geochemistry to determine the original mantle structure and possible evolution of the Alakite region. This together with the knowledge of diamond inclusion

geochemistry may help to explain the differences in diamond morphologies, their origin and to correlate the distribution of specific types of diamonds in the pipes.

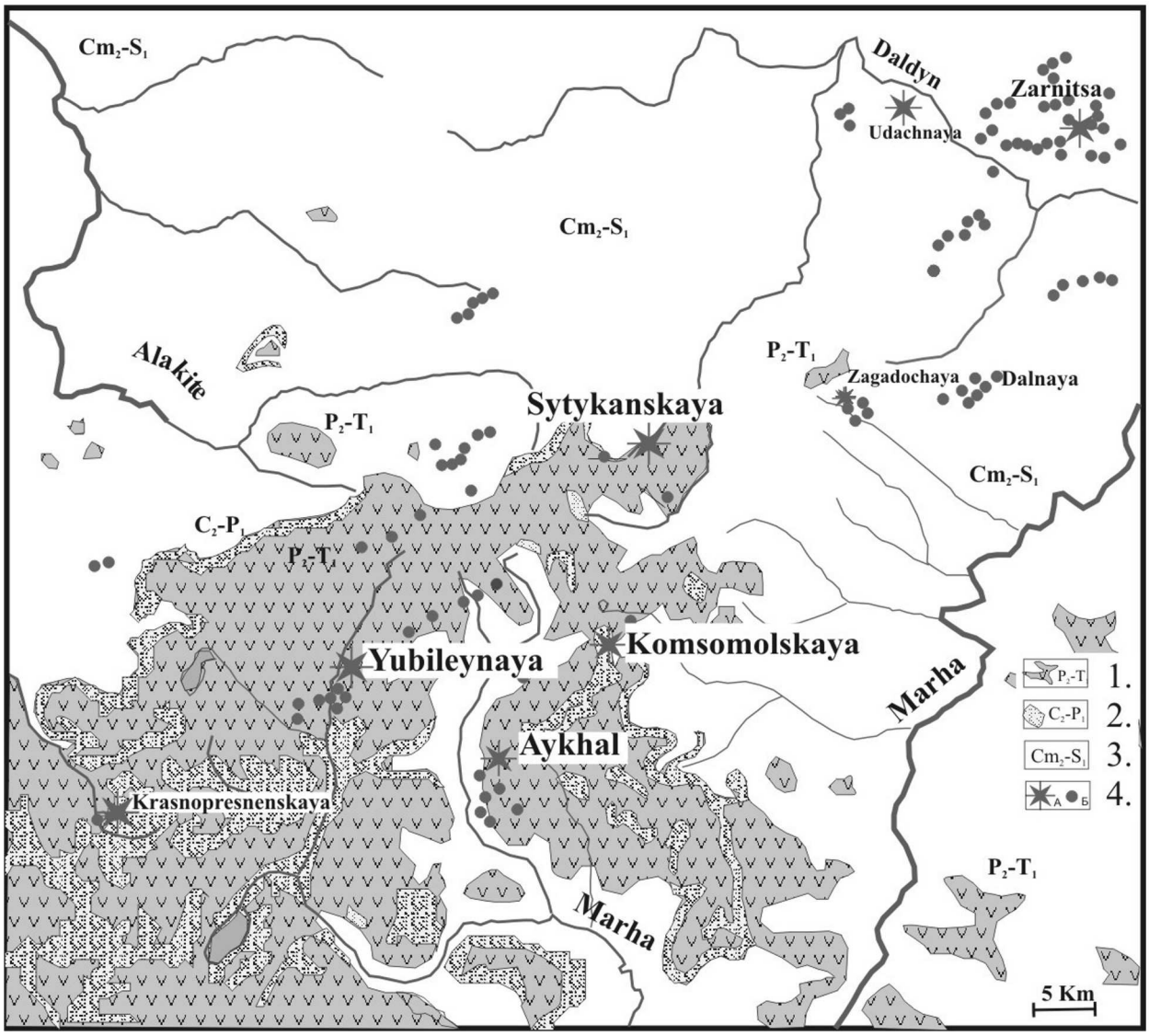

Fig.1. **Scheme of the pipe location in the Siberian platform and Alakite region.**

1 - P_2-T_1- basalts (trapps), 2 - C_1-P_1 sandstones and conglomerates, 3 - Cm_2-S_1 limestones, 4 - Middle and Upper Paleozoic kimberlites.

In this study we used only the microprobe data obtained in the UIGGM SB RAS on a CamebaxMicro mass-spectrometer and LAM ICP analyses made on a Finnigan Element mass-spectrometer, operators Nikolaeva I.A., Palessky V.S., and Kuchkin A.

Despite of the long study of kimberlites [1, 7, 9, 10, 13, 17-19, 24, 27-28, 34] and diamonds [27-28, 34-37] in the region under consideration the petrology of mantle xenoiths and columns remained unclear mainly due to the high degree of serpentinization and scarcity of material that may be analyzed by precise analytic methods.

The concentrates of minerals and comparison of mineral compositions with those of mantle xenoliths from other regions and pipes allowed us to judge about

the petrographic composition of the mantle. Single grain TP thermobarometry methods [3-5, 23] for different minerals allowed us to show positions of different rock varieties in the mantle sequences.

MINERALOGY

A concentrate of minerals was obtained by simple washing out of a large kimberlite portion and then by magnetic separation into 8 fractions. This allowed us to obtain a diverse grain sub-fraction with high concentrations of ilmenite, chromite, garnet, pyroxene, amphibole, mica and zircon.

Garnets in these pipes have highly variable composition and color. Theconfigurations of the diagrams for the separate pipes are close in general but reveal specific features (Fig. 2). The most abundant in the G9-10group is the

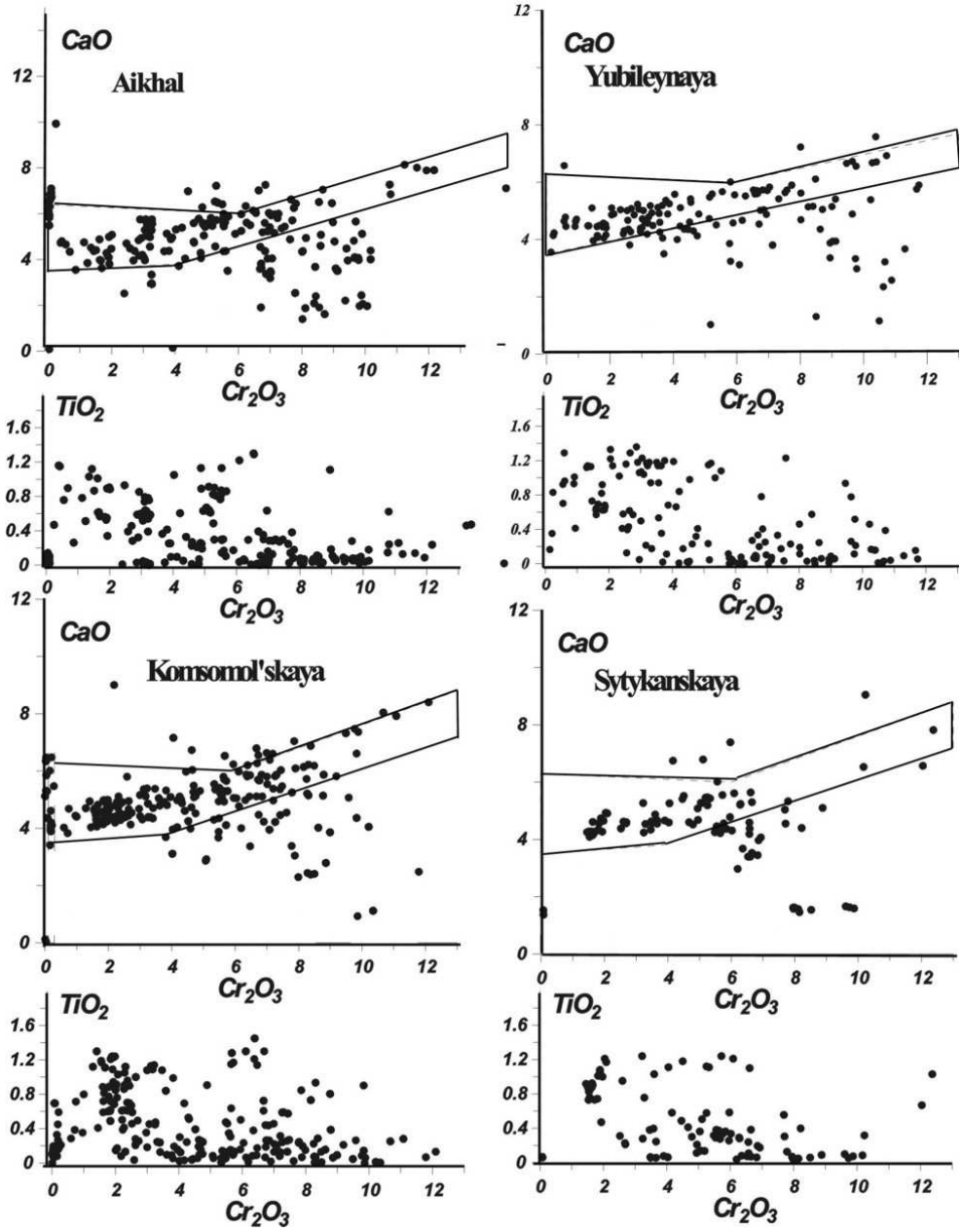

Fig. 2. **Variation diagrams for the garnets from four pipes for the Alkite kimberlite region.**

concentrate from Aykhal, especially the small rounded grains from the tuff- like breccias in the upper part of the section. A part of garnets traces the lherzolite in the Cr-rich part of the upper part of this field. Aykhal and Yubileinaya garnet [6] populations are close whereas Sytykanskaya garnets are similar to those from the Komsomolskaya pipe. The latter two pipes contain a great number of eclogitic orange garnets. The Sytykanskaya lherzolite trend is shorter. The deviations towards the fields of subcalcic garnets [12, 14] beginning from 3-4% Cr_2O_3 rise with the increasing Cr-content thus reflecting the increasing degree of depletion of the layers. Green Ca-Cr-rich pyropes (up to 14% Cr_2O_3) are found in the Aykhal and Yubileinaya concentrates.

The increased TiO_2 contents which are typical of pyroxenites are also characteristic of Komsomolskaya and Sytykanskaya garnet populations appeared at the 2%-boundary of the garnet facies, then at 4% (common pyroxenite lens) and then from 12-10% Cr_2O_3 reflecting the interaction with plume melts at the basement of the column. In the Komsomolskaya and Sytykanskaya pipes high TiO_2 contents are typical of the 1-5% Cr_2O_3 interval in the whole upper part of the mantle section. And only separate grains with high contents are found for deeper garnets reflecting separate interaction intervals near the feeding channels.

Clinopyroxenes in the concentrate belong to the Cr–diopside series and have variable compositions, which are mostly typical of the Yubileinaya pipe. The high contents of Cr_2O_3 (up to 6 %) and Na_2O (up to 5%) are typical of metasomatic associations. Aykhal clinopyroxenes in general are less Na_2O rich. In general the clinopyroxenes show the division onto 5 main clusters (Fig. 3). There are three groups with similar FeO contents (2-3%) and different Al-Cr-Na ratios, which usually co-variate and depend on the depths of their origin. The Fe–rich compositions (3-4% FeO) are close to the sheared peridotites [24] or the products of the melt–peridotite (4-5% FeO) interaction which are usually more TiO_2 enriched (up to 0.9%).

Ilmenite trends for these pipes are typical of kimberlites with decreasing TiO_2, MgO, NiO and increasing FeO (Fig. 4) are suggested to have resulted from magmatic differentiation [15, 22]. They could have been formed while ascending in the feeding vein systems precipitating on the walls of the channels and in intermediate chambers like megacrysts of alkaline basalts [6]. The trends are close for Komsomolskaya and Yubileinaya with a sharp division in Cr_2O_3 content and decrease of this component at the Ti-rich branch and the increase at the less Ti - trend more evident for the former pipe. Nearly continuous Cr–content with the rise only in the last part was found for the Aykhal pipe ilmenite trend. For the Yubileinaya pipe the dashed Ti-Cr trend with general rise of Cr_2O_3 is characteristic [2]. Al-trends decrease with FeO and TiO_2 for Komsomolskaya and Sytykanskaya and are nearly continuous for Aykhal and Yubileinaya and sharply decrease in the center part of the trend for Yubileinaya. The branching of the ilmenite trend in the finishing part is typical for two last pipes.

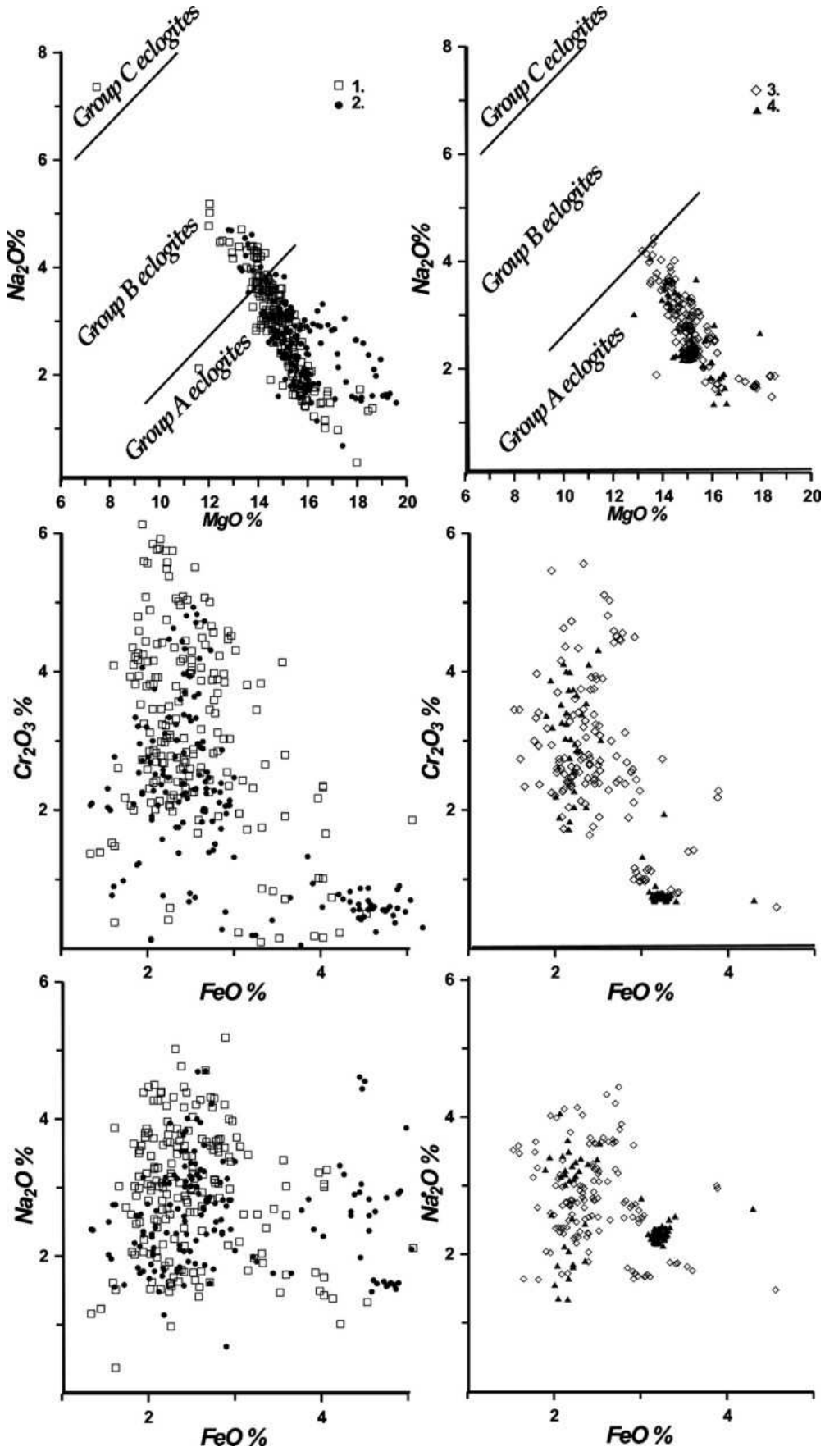
Group C eclogites
Group B eclogites
Group A eclogites
1.
2.
3.
4.
Na2O%
MgO %
Cr2O3 %
FeO %
Na2O %

Fig. 3. **Variation diagrams for the Cr- diopsides from four pipes for the Alakite kimberlite region.**

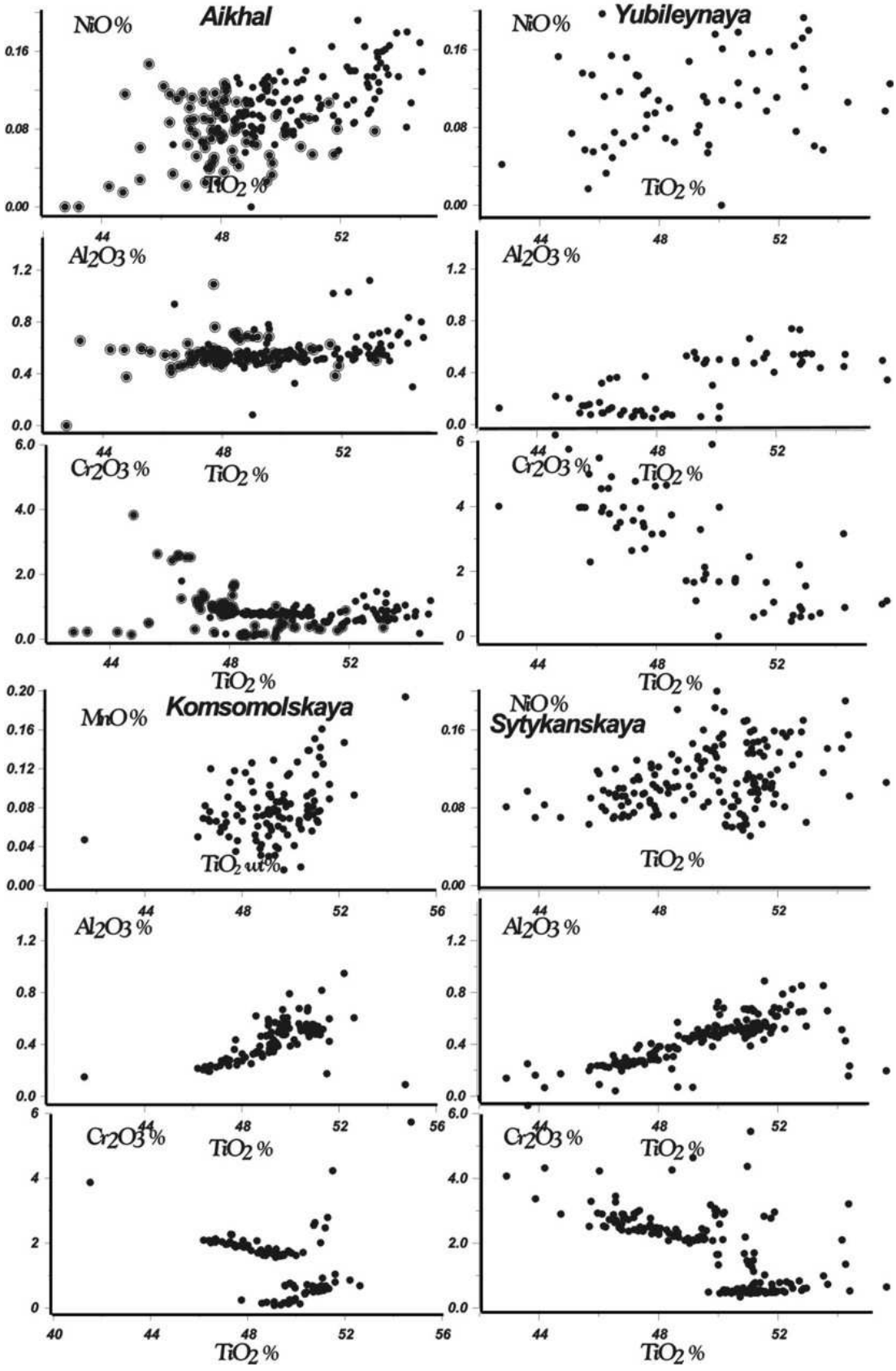

Fig. 4. **Variation diagrams for the ilmenites from four pipes for the Alakite kimberlite region.**

For Aykhal pipe the large grains represent the small rounded grains from the tuff- like horizons at the upper part of the sequence.

Amphiboles of mantle origin found in these pipes are of Ca series referring to the pargasite group except Yubileinaya pipe and are created at the upper part of the mantle sequence. The usual regularity is the joint rise of CaO –FeO, Al_2O_3 and TiO_2 and decrease of alkalis and MgO what except the crystallographic reasons reflect the rise of the Fe – basaltic components in the upper part of the mantle sequences.

Chromites are abundant in the Yubileinaya pipe [5] where they sharply separate into different groups according to the layering. For Aykhal the variations in the lower part of the section are not very high and simply split into the common FeCr-MgAl and FeCr–TiFe substitution. The latter trend is typical of the Sytykanskaya pipe and seems to be close to the Komsomolskaya pipe. For all the pipes the amounts of Cr rich compositions starting from 64%Cr Cr_2O_3 are higher revealing a log-normal distribution that corresponds to the diamond productivity of the pipes.

Micas in the mantle of each pipe are rather specific. In the concentrate from the Komsomolskaya pipe glimmeritic [38] and coarse Ti-rich micas prevail. For the Aykhal pipe Cr- phlogopites are more typical while in the Yubileinaya pipe the variations from rutile-bearing coarse-grained Ti-Fe enriched micas to fine-grained Cr-phlogopites were determined.

TP SEQUENCES

The TP reconstructions for the mantle of these pipes were made using monomineral clinopyroxene [4, 5, 23] and garnet [3] thermobarometry because xenoliths and orthopyroxene grains in the pipe material are rather rare. For each pipe 100 -200 grains of garnets and not less then 100 grains of clinopyroxene were analyzed. The correspondence of the PT estimates using this methods are rather good [3]. Practically all the obtained geotherms refer to 35 mv/m2 at the middle part (Fig. 5) like for the Udachnaya pipe [9]. The Aykhal geotherm is the most regular and cold one with good coincidence with the garnet and clinopyroxene based estimates thus implying essentially peridotitic compositions of most layers. But compared with the Yubileinaya mantle it is more depleted and the lens of coarse-grain dunites that were found beneath the Udachnaya pipe [25] and possible are common in the lithospheric keel basement is thicker. The hot branch was determined using garnet thermobarometry for Yubileinaya [2] is longer and possibly reflects hot interactions around the feeding system. For the Komsomolskaya pipe the hot garnet geotherm branch is more pronounced in the basement within the coarse Gar-dunite layer. It is similar to the Komsomolskaya pipe and has the most pyroxene- enriched mantle column even in the basement where they correspond to Fe rich Cr-low varieties. Fe-higher compositions are typical of the Aykhal mantle resembling many African Mesozoic pipes [20, 21] where the layering is also typical as well as of other cratons [22, 24].

The comparison of the data obtained with these methods gives us an idea about lithology of the mantle column (Fig. 6). The spinel facies zone of the

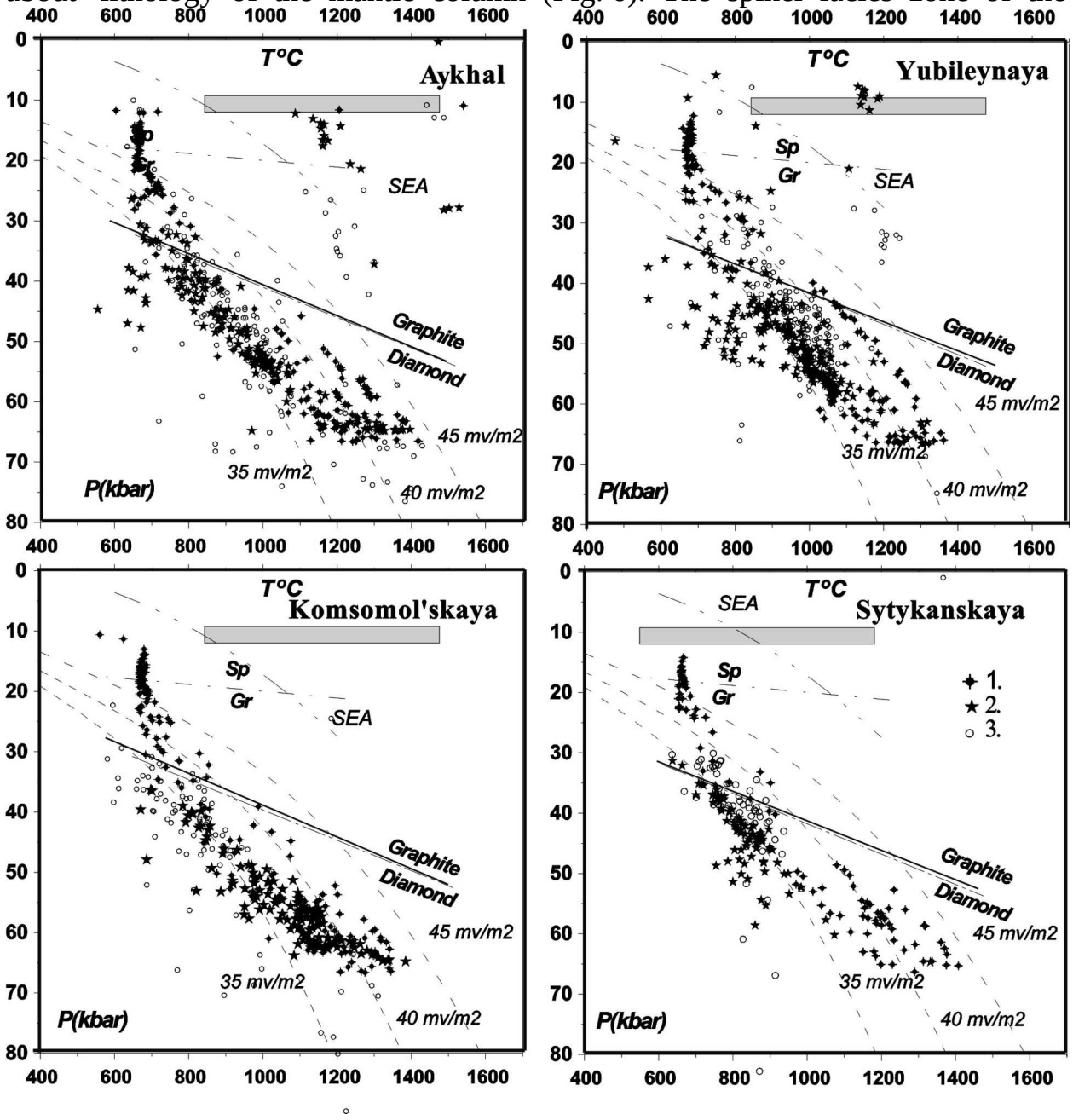

Fig. 5. **TP diagrams for the Aykhal, Yubileinaya , Komsomolskaya and Sytykanskaya pipes.**

1 - recostructions using [3] method for garnets, 2 - using [6, 23] methods and 3 - [23] method for clinopyroxenes.

Ubileyanaya and Aykhal pipes comprises Fe-lherzolites. The upper part of the mantle section at depths of 20-30 kbar must consist of garnet harzburgites. They are Fe–rich for all the pipes under description except the Aykhal. Pyroxene-rich layers appear near the 120 km boundary. For the Aykhal and Yubileyanaya pipes the pyroxene compositions are variable. The Komsomolskaya pipe is characterized by pyroxene enrichment toward the bottom and their rather constant compositions.

Enriched pyroxenes are found in the middle of the Sytytkanskaya mantle section with addition of more depleted compositions starting from 45-50 kbar. Despite of

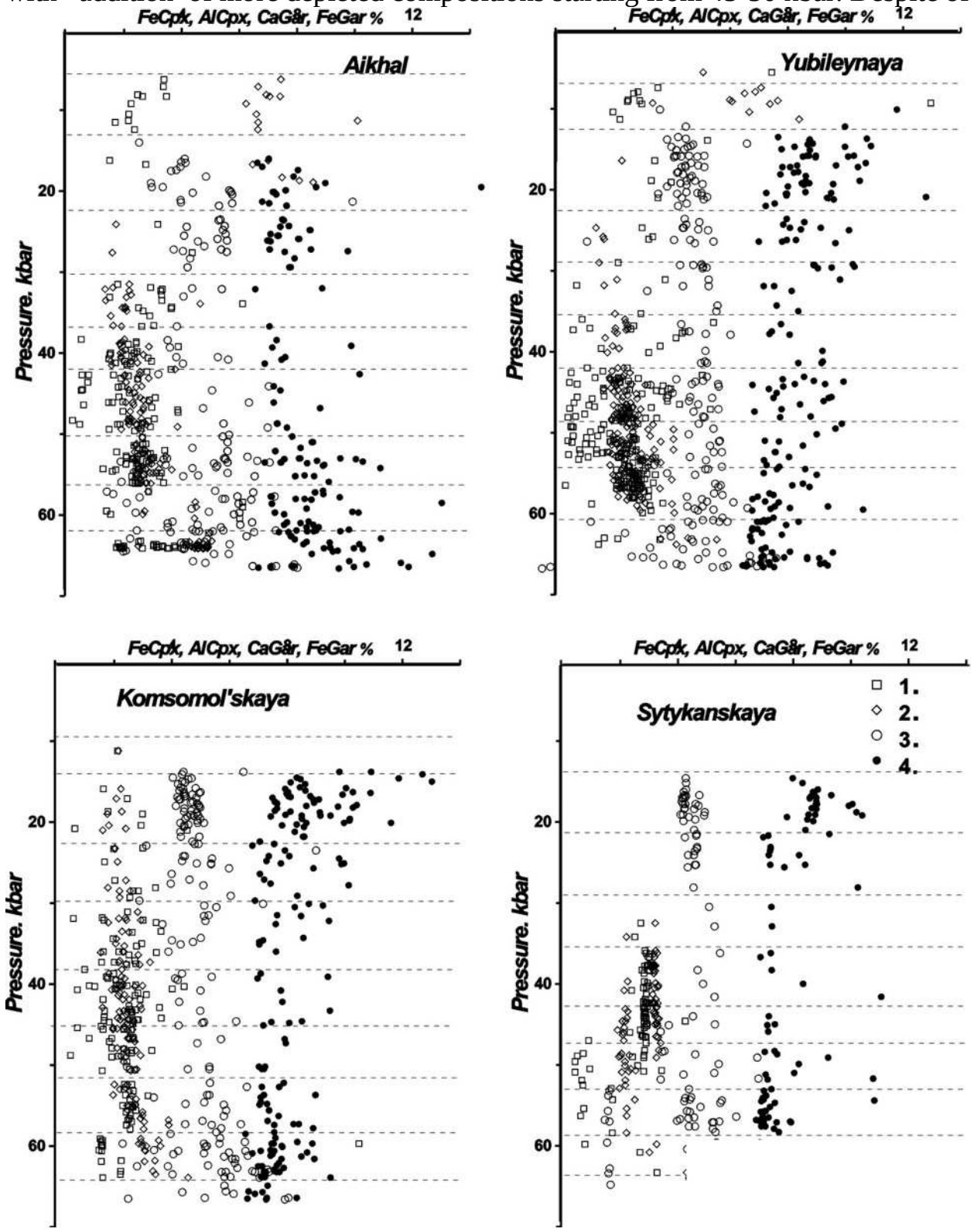

Fig. 6. **Reconstructions of the mantle layering for the four pipes using the variations of the**

1 - CaO in garnet from the pressure determined using [3], equation [3], 2 - FeO in garnet from the pressure determined using [3], equation [3], 3 - FeO in clinopyroxenes from the pressure determined using [4]. Al_2O_3 in clinopyroxenes from the pressure determined using [4].

some uncertainties in the layering we suggest 7-9 horizons in the mantle beneath the Alakite region. A general correlation is obvious for the Aykhal and Yubileinaya pipes. The Sytykanskaya and Komsomolskaya pipes have similar structures. From the NE to SW their structure changes from essentially eclogitic with mixed continental and oceanic mantle and crust signatures to peridotitic dominated by continental varieties enriched in modal, LILE and incompatible elements.

GEOCHEMISTRY

Minerals from the concentrate studied with the LAM ICP method show individuaд TRE element spectra for garnets and clinopyroxenes. All the pipes from the Alakite field display heterogenic mineral compositions.

Clinopyroxenes from the International'naya, Komsomolskaya and Sytykanskaya pipes have generally similar trace element compositions. The Yubileinaya (Fig. 8) clinopyroxenes display strong LREE enrichment with La/Ce_n >1. (Fig. 7). The La/Yb_n ratios are higher for clinopyroxenes from the Komsomolskaya pipe suggesting a higher Gar portion in peridotites. The Aykhal clinopyroxenes display HREE enrichment that is indicative of a depleted composition of the mantle column. In Komsomolskaya (Fig. 9) and Sytykanskaya (Fig. 10) clinopyroxenes show a low Ta-Nb minimum on the spider diagram while the Yubileinaya and Aykhal clinopyroxenes show TRE and Th enrichment. Zr minimum is typical of Aykhal clinopyroxenes however is less obvious in other pipes. U enrichment in Cpx's TRE patterns is more typical of two former pipes and less for two other pipes.

Garnets show S–type REE diagrams (G9-10) typical of the Komsomolskaya and Sytykanskaya and Aykhal pipes. Strong Zr depletion is typical of Aylhal due to abundant zircons in the concentrate. Hf-Zr minimums are typical of Komsomoskaya Cpx's while for Yubileinaya samples show Hf enrichment. Sytykaskaya garnets show no HFSE anomalies. Pb and Sr depletions are typical of most garnets however eclogitic garnets locally display weak Pb and Sr enrichments, Eu minimums and Ce anomalies. In that case peridotitic garnets are characterized by Ce minimums suggesting percolating processes in the mantle columns.

Ilmenites from all the pipes reveal different behavior despite a general similarity of their TRE patterns with high Ta-Nb-Zr-Hf-Ti maximums. Yubileaynaya samples show W-type REE patterns close to those of Komsomolskaya ilmenites but the latter are LREE enriched. Aykhal ilmenites possess U–shaped REE patterns whereas Sytykanskaya ilmenites have lower LREE. The REE behavior seems to be determined by the minerals reacting with

ascending protokimberlite magmas at a pre-eruption stage. Minerals dissolved during AFC processes result in similar REE distributions in Yubileinaya ilmenite and chromite and Aykhal ilmenite and garnet. The HFSE peaks are positively correlated with REE enriched in Komsomolskaya and Sytykanskaya ilmenites and

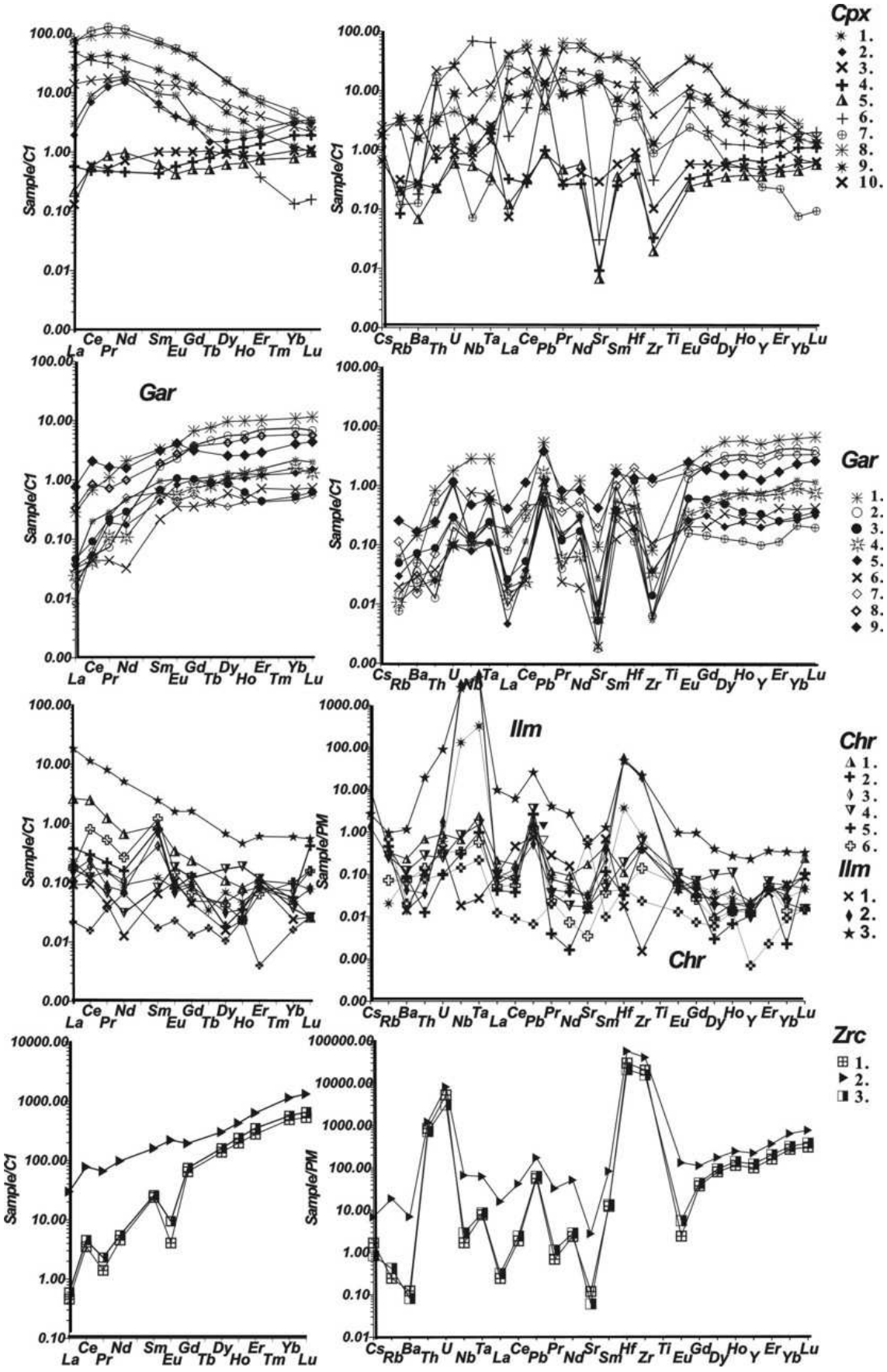

Fig. 7. **REE and TRE diagrams for the minerals from the concentrate for Aykhal pipe.**

The numbers are given for separate grains of each mineral.

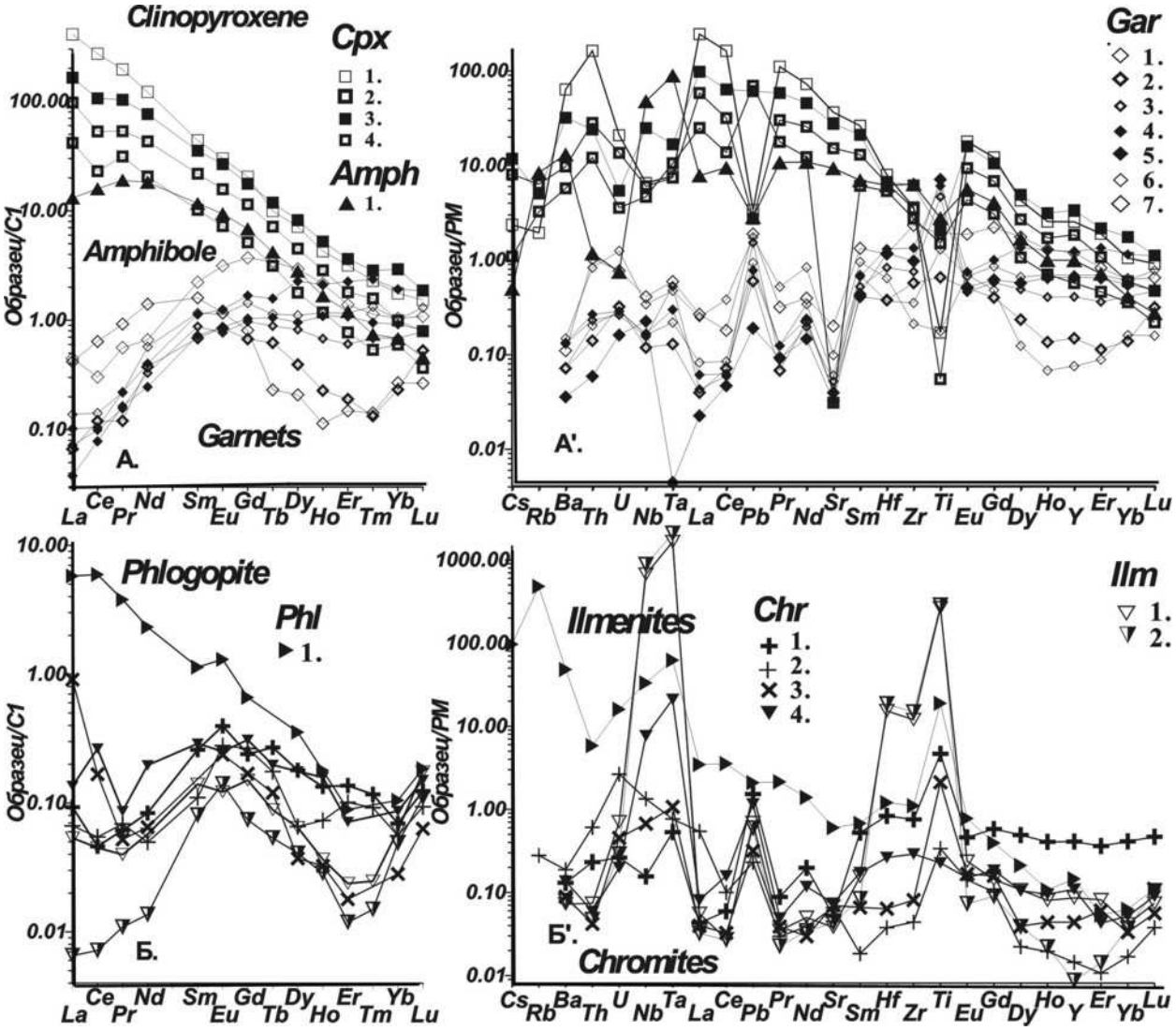

Fig. 8. **REE and TRE diagrams for the minerals from the concentrate for Yubileinaya pipe.**

The numbers are given for separate grains of each mineral.

negatively with Yubileinaya ilmenites. The processes of differentiation could have strongly affected such enrichment mainly pronounced at late stages for the samples plotted in the left part of the ilmenite trends. This is typical of the Sytykanskaya pipe where the most differentiated composition reveals REE 100 times exceeding the chondrite level in left part with $La/Yb_n > 100$. Kimberlite mica shows a different TRE composition with strong LREE enrichment (Yubileinaya) and moderate to flat REE patterns with weaker LREE enrichment (Komsomolskaya phlogopite).

DISCUSSION: PETROLOGICAL AND GEODYNAMIC ASPECTS OF THE MANTLE COMPOSITION AND STRUCTURE OF THE ALAKITE REGION

The mantle sections beneath the studied pipes a complex layered structure comprising at least 9 horizons which could have resulted from the coupling of

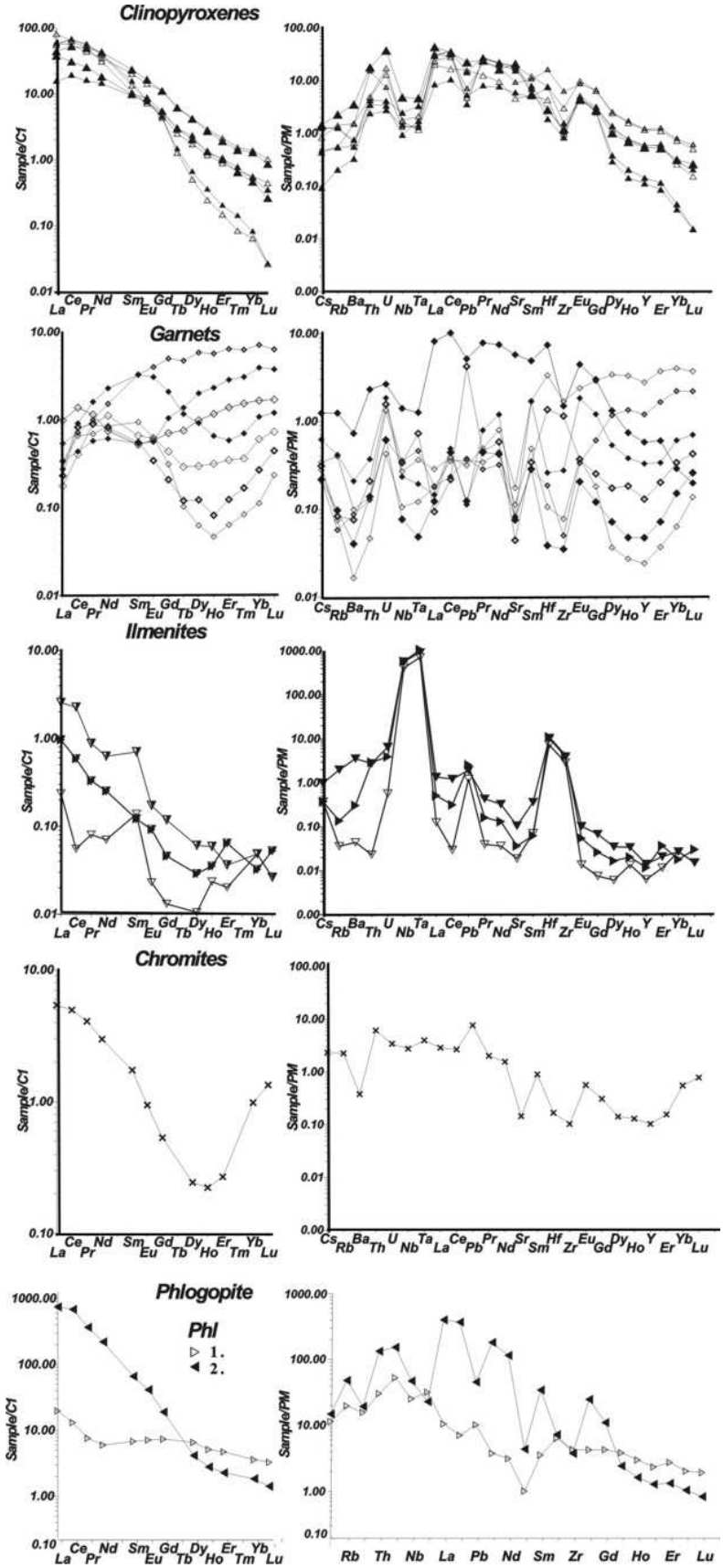

Fig. 9. **REE and TRE diagrams for the minerals from the concentrate for Komsomolskaya pipe.**

The numbers are given for separate grains of each mineral.

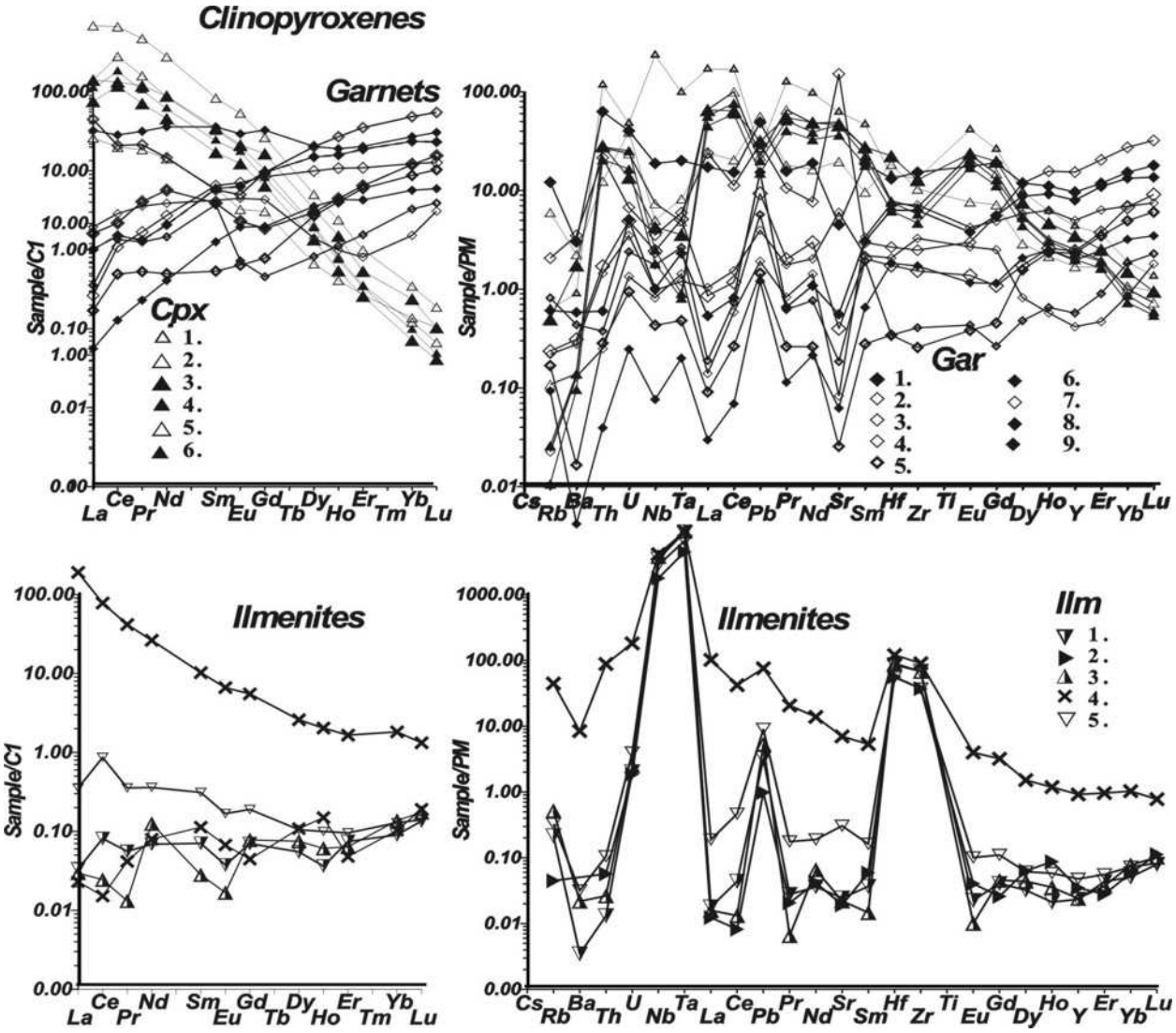

Fig. 10. **REE and TRE diagrams for the minerals from the concentrate for Sytykanskaya pipes.**

The numbers are given for separate grains of each mineral.

slabs consisting of lithospheric mantle and crust rocks formed in different geodynamic environments. Formation of new horizons could be related to new pulses of subduction which possibly periodicity refers to 60 Ma cycles, i.e. close to geological periods or plume cycles. The latter in turn can be related to global cosmogony events such as rotation of the Galaxy and changes of the gravitational field. The evidence for the mantle cake-like structure comes from abundant geophysical and petrologic data [13, 21, 25, 26] however there is a lack of direct information about extension of separate layers and their petrology and geochemistry. The Alakite pipes provide additional information which can help to solve this problem. The Aykhal and Yubileinaya and the Komsomol'kaya and Sytykanskaya kimberlite pipes are similar but the not completely suggesting a weak lateral zoning and possibly inclined layering.

All the pipes possess similar amount of layers and similar mineral chemistry. Major element compositions of diopside frequently coincide suggesting similar processes in the mantle columns but the amount of chemical groups is quite different. The differences in geochemistries may be explained by LAM ICP analyses of different varieties dominating in each certain pipe. Nevertheless Zr-depletions in Aykhal garnets and other specific compositional features show that those pipes have different major and trace element chemistry. The mantle column of each pipe experienced long vertical percolation which melt penetrated through mantle peridotites and interacted with them. During such process the minerals in the mantle column could be in partial equilibrium. It allows us to suggest that major geochemical signatures of the whole mantle column are determined by horizons of hydrated peridotites occurring at the basement of the lithospheric mantle. The phlogopite bearing horizons should have determined the K-LILE metasomatism of the Yubileinaya pipe and the Na-.H_2O enriched horizons of deeply subducted eclogites containing omphacites and hydrous minerals for the Sytykanskaya and Komsomolskaya pipes [29]. A “furnace” as a power engine for percolation processes may act as 1) a deep subduction responsible for general metasomatic features [38] and 2) interaction within the flow of ascending kimberlite masses during formation of feeding systems. The latter process is responsible for the formation of Ti-bearing associations including Ti–rich garnets (hot branches at TP plots), ilmenite–bearing associations with Ti-rich chromites (high ulvospinel), Ti–rich pyroxenites and micas of glimmerites and so on. The vertical Ti–metasomatism in mantle columns is evidenced by chromite variations even in simple Cr_2O_3 – TiO_2 diagrams. The development and vertical growth of the feeding system is illustrated by the prolongation of TiO_2–dependent trends of ilmenites in variation diagrams. The primary layering of the pipes and the structure of the feeding systems in the mantle columns are obviously mutually dependent as shown by Alakite pipes. The thick layering of the Komsomolskaya and Sytykanskaya mantle columns is illustrated by bi-modal ilmenite trends while the thin layering in the mantle under the Yubileinaya pipe is indicated by a dashed ilmenite trend built up for 7 separate groups of this pipe. The monotonous middle part of the Aykhal mantle column with a thicker layering in the upper part coincides with the linear ilmenite trend of the central part pf this pipe.

Similar behavior and mutual relationships of the TP sequences and megacryst associations represented in our case by ilmenite as well as compositions of reaction minerals and metasomatism are the rings of the same chain as well the formation of diamonds which seem to grow/enlarge also during the percolation processes affecting the mantle columns.

CONCLUSIONS

1. The TP sections and mineralogical features of the mantle columns of the Yubileinaya and Aykhal pipes on one hand and Komsomolskaya and Sytykanskaya pipes on the other hand are similar.

2. The mineral chemistry of each pipe in the Alakite region is individual despite similar general features and major element chemistry of minerals suggesting the through percolating processes in the mantel columns.

3. The layering of the mantle is closely related to the structure of mantle sections.

4. Each type of minerals reflects specific features of the processes taking place in different types of magmatic fluids and systems. Ilmenite and Cr-low pyropes are typical of the feeding systems of protokimberlite melts. Ti-bearing chromites and garnets are formed within reaction zones in peridotites. Mica-bearing associations and alkali pyroxenes result from metasomatic processes developed due to the heat impact of plume melts and/or directly from subduction processes. The mantle primary zoning and layering is preserved in the mantle column despite cutting processes.

5. Metasomatism and percolation types are related to geodynamics of the formation of mantle layers which change in the mantle column despite their through character.

Supported by RFBR grants 99-05-65688, 00-05-65288, 03-05-64146.

REFERENCES

1. **Amshinsky, A.N., Pokhilenko, N.P.** (1983). Characteristic features of the picroilmenite compositions from the kimberlite pipe Zarnitsa // Russian Geol Geophys. N11. pp .116-119.
2. **Ashchepkov I. V. Vladykin N. V., Nikolaeva I. V., Palessky S. V., Logvinova A. M., Saprykin, A. I., Khmel'nikova, O. S., and Anoshin, G. N.** (2004). Mineralogy and Geochemistry of Mantle Inclusions and Mantle Column Structure of the Yubileinaya Kimberlite Pipe, Alakit Field, Yakutia // Doklady Earth Sciences, Vol. 395A, No. 3, pp. 378–384.
3. **Ashchepkov, I.V.** Empirical garnet thermobarometer for mantle peridotites. Seattle Annual Meeting (November 2-5, 2003). Abstract ID: 65507.
4. **Ashchepkov, I.V.** Jd-Di barometer for mantle peridotites and eclogites // Experiment in Geosciences v.10, N1, 137-138.
5. **Ashchepkov, I.V.** More precise equation of the Jd-Di Barometr // Herald of the Earth department RAS. 2003, N1. pp. 45-46.
6. **Ashchepkov, I.V., André, L.** Pyroxenite xenoliths in picrite basalts (Vitim plateau):origin and differentiation of mantle melts // Russian Geol. Geophys. 2002. v. 43 (4). pp. 343-363.
7. **Ashchepkov, I.V., Vladykin, N.V., Saprykin, A.I., Khmelnikova, O.S.** (2001). Composition a thermal structure of the mantle in peripheral parts of the ancient shields within Siberian craton // Revista Brasileira de Geociencias. 31(4), pp. 527-636.
8. **Aulbach, S., Stachel, T., Viljoen, K.S., Brey, G.P., Harris, J.W.** (2002). Eclogitic and websteritic diamond sources beneath the Limpopo Belt —is slab-melting the link? // Contrib. Mineral. Petrol. v.143. pp. 56 –70.
9. **Boyd, F.R., Pokhilenko, N.P., Pearson, D.G., Mertzman, S.A., Sobolev, N.V., Finger, L.W.** (1996). Composition of the Siberian cratonic mantle: evidence from Udachnaya peridotite xenoliths // Contrib. Mineral. Petrol. 1997, V. 128. N 2-3. p. 228-246.
10. **Boyd, F.R., Pearson, D.G., Nixon, P.H., Mertzman, S.A.** (1993). Low-calcium garnet harzburgites from South Africa: their relations to craton structure and diamond crystallization // Contrib. Mineral. Petrol. 1993, v.113. p. 352 –366.

11. **Dawson, J.B.** (1980). Kimberlites and their xenoliths. Springer,Berlin Heidelberg New York, 295 p.
12. **Gregoire, M., Bell, D.R., Le Roex, A.P.** (2002). Trace element geochemistry of phlogopite-rich mafic mantle xenoliths: their classification and their relationship to phlogopite-bearing peridotites and kimberlites revisited // Contrib Mineral Petrol. 2002. v 142(5), pp. 603-625.
13. **Griffin, W.L., Ryan, C.G., Kaminsky, F.V., O'Reilly, S.Y., Natapov, L.M., Win, T.T., Kinny, P.D., Ilupin, I.P.** (1999). The Siberian lithosphere traverse: mantle terranes and the assembly of the Siberian Craton. // Tectonophysics. V.310. P. 1–35.
14. **Griffin, W. L., Fisher N. I., Friedman, J. H., O'Reilly, S. Y., and Ryan, C. G.** (2002). Cr-pyrope garnets in the lithospheric mantle. 2. Compositional populations and their distribution in time and space // Geochem. Geophys. Geosyst., v. 3 (12), 35 p.
15. **Griffin, W.L., Moore, R.O., Ryan, C.G., Gurney, J.J., Win, T.T.** (1997). Geochemistry of magnesian ilmenite megacrysts from Southern African kimberlites // Russian Geol. Geophys. 1997. v. 38(2). pp. 398-419.
16. **Jacob, D.E., Foley, S.F.** (1999). Evidence for Archean ocean crust with low high field strength element signature from diamondiferous eclogite xenoliths // Lithos. 1999. v. 48. p.317 –336.
17. **Khar'kiv, A.D., Zinchuk, N.N., Kr'ychkov, A.I.** Primary deposits of the diamonds in the World. Moscow, Nedra. 1998. 545 p.
18. **Koptil, V.I., Laz'co, E.E., Serenco, V.P.** (1975). Diamondiferous kyanite eclogite from kimberlite, pipe Sytykanskaya - new faunding in USSR // Dokl. Akad. Nauk SSSR, 225: 924-927. (in Russian)
19. **Kostrovitsky, S.I., De Bruin, D.** (2001). Garnets from the ultramafic associations in the groups Zagadochnaya and Bukovinskaya kimberlite pipes // Alkaline magmatism and the problem of mantle sources. Irkutsk, IGTU, pp. 170- 187.
20. **Leost, I., Stachel, T., Brey, G.P., Harris, J.W., Ryabchikov, I.D.** (2003). Diamond formation and source carbonation: mineral associations in diamonds from Namibia. Contrib Mineral Petrol., v.145, pp. 12-24.
21. **Lehtonen, M.L., O'Brien, H.E., Peltonen, P., Johanson, B.S., Pakkanen. L.K.** Layered Mantle at the Edge of the Karelian Craton: P-T of Mantle Xenocrysts and Xenoliths from Eastern Finland Kimberlites FLA_0260.
22. **Moor, R.O., Griffin, W.L., Gurney et al.** (1992). Trace element geochemistry of ilmenites megacrysts from the Monastery kimberlite, South Africa // Lithos. 1992. v. 29, pp.1-18.
23. **Nimis, P., Taylor, W.** (2000). Single clinopyroxene thermobarometry for garnet peridotites. Part I. Calibration and testing of a Cr-in-Cpx barometer and an enstatite-in-Cpx thermometer // Contrib. Mineral. Petrol. V. 139. N5. P. 541-554
24. **Nixon, P.H.** (1987). Kimberlitic xenoliths, their cratonic setting // In: P.H. Nixon (Editor). Mantle Xenoliths. Wiley, Chichester, pp. 215-239.
25. **Nixon, P.H., Boyd, F.R.** (1973). Petrogenesis of the granular and sheared ultrabasic nodule suite in kimberlites // In Lesotho Kimberlites (P.H. Nixon, ed.). Lesotho National Development Corporation, Maseru, Lesotho. (48-56).
26. **O'Reilly, S.Y., Griffin, W.L.** (2001). Poudium Diomany, Morgan P. Are lithospehers forever? // GSA Today. N11, pp.4-9
27. **Pokhilenko, N. P., Sobolev, N.V., Kuligin, S. S., Shimizu, N.** (2000). Peculiarities of distribution of pyroxenite paragenesis garnets in Yakutian kimberlites and some aspects of the evolution of the Siberian craton lithospheric mantle // Proceedings of the VII International Kimberlite Conference. The P.H. Nixon volume. pp. 690-707.
28. **Pokhilenko, N.P., Pearson, D.G., Boyd, F.R,. Sobolev, N.V.** (1991). Megacrystalline dunites, peridotites: Hosts for Siberian diamonds. Annu. Rep. Dir. Geophys. Lab. Carnegie Inst. Washington, 1990-1991: 11-18.

29. **Prouteau, G., Scaillet, B., Pichavant, M., Maury, R.** (2001). Evidence for mantle metasomatism by hydrous silicic melts derived from subducted oceanic crust // Nature v. 410. p. 197 –200.
30. **Rapp, R.P.,Watson, E.B.** (1995). Dehydration melting of metabasalt at 8 –32 kbar: implications for continental growth and crust – mantle recycling // J. Petrol. V.36. p. 891 – 931.
31. **Ryan, C. G., Griffin, W. L., Pearson, N. J.** (1996). Garnet geotherms: Pressure-temperature data from Cr-pyrope garnet xenocrysts in volcanic rocks. // J. Geophys. Res. B. 1996. V. 101. N 3. P. 5611-5625.
32. **Sobolev, N.V.** (1977). Deep-Seated Inclusions in Kimberlites and the Problem of the Composition of the Upper Mantle // Am. Geophys. Union, Washington, D.C. 1977. 279 p.
33. **Sobolev, N.V., Kaminsky, F.V., Griffin, W.L., Yefimova, E.S., Win, T.T., Ryan, C.G. & Botkunov, A.I.** (1997). Mineral inclusions in diamonds from the Sputnik kimberlite pipe, Yakutia // Lithos, v. 39, p. 135-157.
34. **Sobolev, N.V., Taylor, L.A., Logvinova, A.M., Koptil, V.A., Zinchuk, N.N., Zedgenizov, D.A., and Yefimova, E.S.** (2003). Mineral Inclusions In Diamonds From Komsomolskaya And Krasnopresnenskaya Pipes, Yakutia: Evidence For Deep Lithospheric Heterogeneities In Siberian Craton // 8th International Kimberlite Conference, Victoria, Canada.
35. **Spetsius, Z.V.** (1990). The diamond-bearing xenolith of garnet peridotite from the Mir kimberlite pipe // Dokl. Akad. Nauk SSSR, v. 313. p. 939-943 .
36. **Spetsius, Z.V.** (1995). Occurrence of diamond in the mantle: A case study from the Siberian Platform. In: W.L. Griffin (Editor), Diamond Exploration: Into the 21st Century. J. Geochem. Explor., v. 53. p. 25-39.
37. **Spetsius, Z.V., Serenco, V.P.** (1990). Composition of Continental Upper Mantle, Lower Crust Beneath the Siberian Platform // Nauka, Moscow, 1990. 272 pp. (in Russian).
38. **Van Achterberg, E., Griffin, W.L.** (2001). Steinfenhofer J. Metasomatism in mantle xenoliths from Letlhakane kimberlites estimation of element fluxes // Contrib. Mineral. Petrol. 2001. v. 141, pp. 397-414.

UDK 552.323.6

Kimberlites of Angola: structural-tectonic position and geology

Rotman A.Y.[1], Ganga J.[2], Nosyko S.F.[2], Shimupi J.[3], Zintchouk N.N.[1], Somov S.V.[2]

[1] *YaGEER&D CNIGRI ALROSA Co. Ltd., Russia, e-mail: rotman@cnigri.alrosa-mir.ru*
[2] *Mining-Ore Association "Catoca", Angola*
[3] *Endiama Co., Angola*

INTRODUCTION

Kimberlites are unique formations both in economic (basic magmatic source of diamonds) and in research (as the most abyssal volcanic rocks representing, according to Sobolev V.S., a window to the upper mantle) relations. At present they have been revealed practically on all ancient platforms, with the largest volumes on the African continent where unique resources of natural diamonds (68% of the world's resources) are fixed and more than the fifth part of them is concentrated in Angola. And this is the reason of interest to kimberlites of this country which is located on a large territory of south-western part of near-equatorial Africa with the least degree of geological investigation.

The discovery of the first in Angola kimberlite pipe Camafuka-Camazambo dates back to 1952. It is noteworthy that this pipe, located in the valley of river Shikapa in south-west of Lukapa city, is the leader in size – its surface area constitutes 1.6 km^2 [1]. Other numerous kimberlite pipes were discovered after this one reaching the total number of 638 [9], 105 of which are diamondiferous. But only one pipe – Catoca (north-eastern part of Angola, not far from Saurimo city) is being mined, though other bodies – pipes Camafuka-Camazambo, Chere, Camachia and others, were exploited to this or that degree. All kimberlite occurrences of this part of the country are located on the territory embracing two administrative provinces – Lunda Norte and Lunda Sul (Fig. 1) and characterized, together with primary, by broad distribution of placer deposits and diamond occurrences and distinguished as a geological-economic taxon – diamondiferous province Lunda Norte.

GENERAL GEOLOGICAL CHARACTERISTICS

The rule of Clifford T. N. [7] is fully realized on the example of Angola in distribution of diamondiferous kimberlites and their position within cratons with Archean consolidation: diamondiferous province Lunda Norte [11] is located on craton Angola-Cassai (see Fig. 1). All known kimberlites are attributed to linear zones of tectonic activization, part of which inherits ancient tectonic directions, and another part is related with new ones overlayed on the ancient basement and

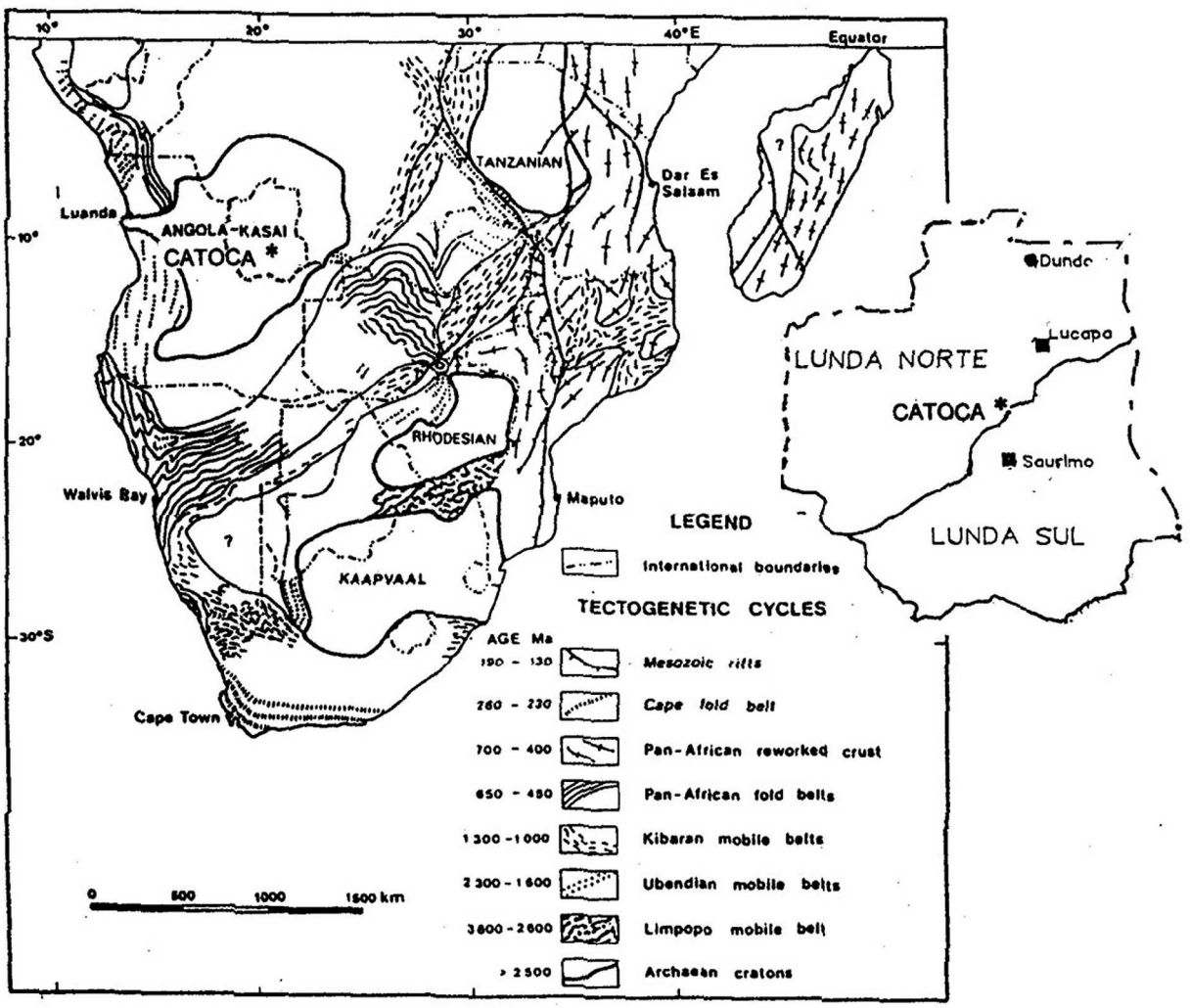

Fig. 1. **Basic cratons and mobile belts of near-equatorial Africa, according to Sohnge, 1986.**

cutting the system of cratons and mobile belts. By the time of occurrence kimberlite magmatism is usually attributed to the periods of epeirogenetic rising of areas (for instance, to rising of Cretaceous continent of South Africa). In the zones of tectonic activization kimberlite magmatism is distributed comparatively regularly but diamondiferous kimberlites occur only in the area of where they intersect Archean cratons (exposed or overlayed by platform cover) and on the sites of intersection with mobile belts – all kimberlite bodies are nondiamondiferous.

Almost all known kimberlite bodies of Angola are located along the Lacapa zone of faults (Fig. 2) which is traced along the whole continental part of the country from its south-western border (with Namibia) and crossing north-eastern one with prolongation to Zaire having more than 1600 km total length. There are preliminary data about the tendency of decreasing Angolan kimberlites' diamondiferousness from north-east to south-west [12]. According to the data of

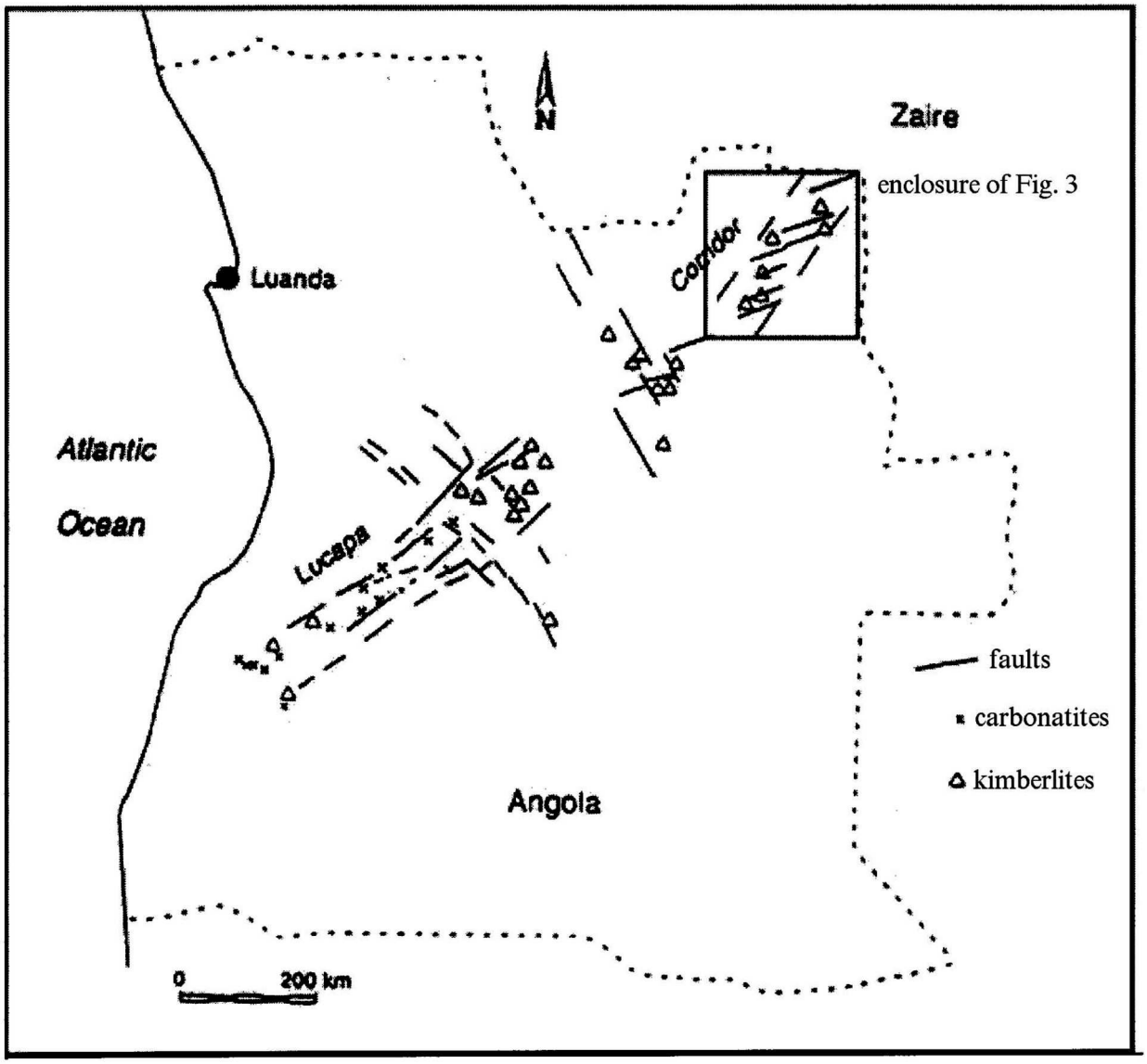

Fig. 2. **Positions' correlation of kimberlite occurrences and faults of the Lukapa zone.**

this researcher some part of kimberlite bodies belongs to Early Cretaceous age but on the whole this issue is poorly investigated.

Consequently, in the analyzed province there is confirmation of natural relation of kimberlite magmatism with linear zones of tectonic activization which is rather typical for dislocation of kimberlite bodies in South-African diamondiferous province and especially clearly is expressed on the example of "Lesotho trend" – sublatitudinal band with 600 km length and about 280 km width, where more than 200 kimberlite occurrences are located. Despite the marked tendencies, revealed in many regions of the world, there is still no universal conception which could explain structural-tectonic control of kimberlitic and other diamond-bearing rocks, as well as different in age kimberlites in a definite field or province.

A small value of erosional cut is a remarkable feature of the discussed diamondiferous province. Metamorphic rocks of the ancient African platform's

basement serve as kimberlite-hosting medium. Fragments of Triassic formation deposits, referred to “karroo” system and “intercontinental system” are marked north of the investigations area within shield Cassai, and Cretaceous continental formations preserved in province Lunda Norte and on adjoining territories (mainly within the “Congo” fall). They require more serious attention since they are related with placer deposits of diamonds. These deposits are subdivided into formations Calonda and Cuango. Within the described territory there is a developed formation Calonda which was revealed by geologists of “Diamang” company and referred to Apsian-Albsky interval of Cretaceous age. It consists of alluvial, lacustrine-alluvial and lacustrine sediments (mainly arkose sandstones from fine- to coarse-grained). Below polymict conglomerates, siltstones and argillites are observed. The rocks are weakly cemented, porous and colored mainly in red-brown to violet color. Sometimes fine streaks or lenses of interformational diamondiferous conglomerates occur. Thickness of the formation increases from south to north and reaches 40 – 50 m. Among the younger Paleogene-Eocene formations laterites are noted which were formed on post-Cretaceous peneplain surfaces, and sandy formations referred to Kalakhari group are typical of Eocene-Pliocene. Quaternary sediments are widely distributed on slopes or along river valleys. By genesis they are alluvial-proluvial and dealluvial-eluvial formations.

Among intrusive formations of the region one can distinguish a complex of Early and Late Archean, Early and Late Proterozoic, a complex of Cretaceous rocks, an undivided complex of Cretaceous – Paleogene rocks and a complex of rocks of indefinite age. Gabbro-norites of Early Archean are the most ancient intrusive rocks which are exposed in association with Archean and Early Proterozoic formations and are mapped as small massifs and bodies of altered basic rocks referred to gabbro-anorthosite complex. Within the Cassai shield they compose comparatively small bodies (up to 2-3 km in diameter) of gabbro-norite complex among metamorphic and ultra-metamorphic rocks of lower, rarely upper, groups of Early Archean. They are represented by orthoamphibolites which were formed in the result of pyroxene gabbro metamorphism. Intrusions of Late Archean are represented by a complex of granitoid rocks composing small bodies in the zone of contact between intrusions of Late Archean and metamorphic formations of the upper group of Lower Archean. Diorites and granodiorites occur together, sometimes one can observe gradual transition from one variety to another but granodiorite bodies are developed more. Rarely one can fix gradual transition from granodiorites to tonalites due to decrease of field spar content and correspondingly increase of plagioclase (andesine) quantity. One can also come across bodies of granites in the form of small intrusions associated with metamorphic and ultra-metamorphic rocks of Archean. Besides Archean and Proterozoic intrusions complexes of ultrabasic magmatic rocks of Mesozoic age (80 – 120 Ma) are widely developed on the territory of Angola, formation of which corresponds to Cretaceous period.

STRUCTURAL-TECTONIC POSITION AND GEOLOGY OF KIMBERLITE OCCURRENCES

Kimberlite magmatism is the main target of investigations. Numerous bodies of kimberlites are concentrated, as it was mentioned above, within the area of Archean consolidation of the basement (south-western slope of craton Cassai) and are controlled by the regional Lukapa zone of faults ("corridor Lucapa", graben Lucapa) of north-eastern stretch (see Fig. 2), the width of which varies from 55 to 85 km and the length (on the territory of Angola) reaches 1200 km. Its north-eastern prolongation determines positions of kimberlite occurrences of south-western part of Zaire and consequently traces sufficiently farther to north-east (more than 400 km). In south-western part of this structure pipe bodies of carbonatites and massifs of alkaline composition rocks are widely distributed together with kimberlites. Carbonatites expose to the day surface, where they are easily diagnosed, or they are hidden under silicified breccias or fenitizated rocks. Kimberlite pipes are attributed as a rule to the zones of fault intersection of north-eastern and north-western directions. The faults represent linearly stretched disturbances of the basement with a system of feathering fissures. The most investigated territory, from the point of view of kimberlite bodies' revelation and assessment of their perspectives, is the territory stretching along rivers Luembe, Chiumbe, Luachimo and Chicapa. As it was noted, kimberlite occurrences are attributed to grabens from where the trains of kimberlite indicator minerals start in Cretaceous (conglomerate Calonda) and modern alluvial sediments, from which the main mass of Angolan diamonds was mined before the discovery of primary deposits. One can note an interesting tendency of attribution of the most productive kimberlites to the areas of the most ancient Pre-Cambrian platform basement.

This region, where the main diamond resources of the country are concentrated [2, 3], includes four kimberlite fields – Camazambo, Catoca, Camutue and Camachia (Fig. 3) within which 70 kimberlite bodies are known by present. The form of occurrence in plan varies from regular rounded (pipes Catoca, Camachia and others) to irregular or greatly prolonged (Camafuca-Camazambo), and the size – from the first tens of meters to the first hundreds of meters in diameter, reaching 900 m (pipe Catoca) and more than 3 km (pipe Camafuca-Camazambo). The latter two pipes are among ten largest kimberlite occurrences of the world, and pipe Camafuca-Camazambo (basin of middle course of river Chicapa) is the fourth in this ten after M1, Mwadui and Orapa. The area of pipe Camafuca-Camazambo in the modern erosional cut constitutes 156 hectares, according to [4, 8], which corresponds to the second place in the world after M1. Constant presence of diamonds in the formations of a crater part and overlaying sediments, characteristics of diamond raw material (13,3% of octahedra and 24% of mixed type stones – octahedra-dodecahedra) place pipe Camafuca-Camazambo into a group of economically attractive deposits.

The largest pipe Camutue I in field Camutue is of 500x200 m size and is stretched in north-western direction. Hidden under 20-30 m thickness of Kalakhari

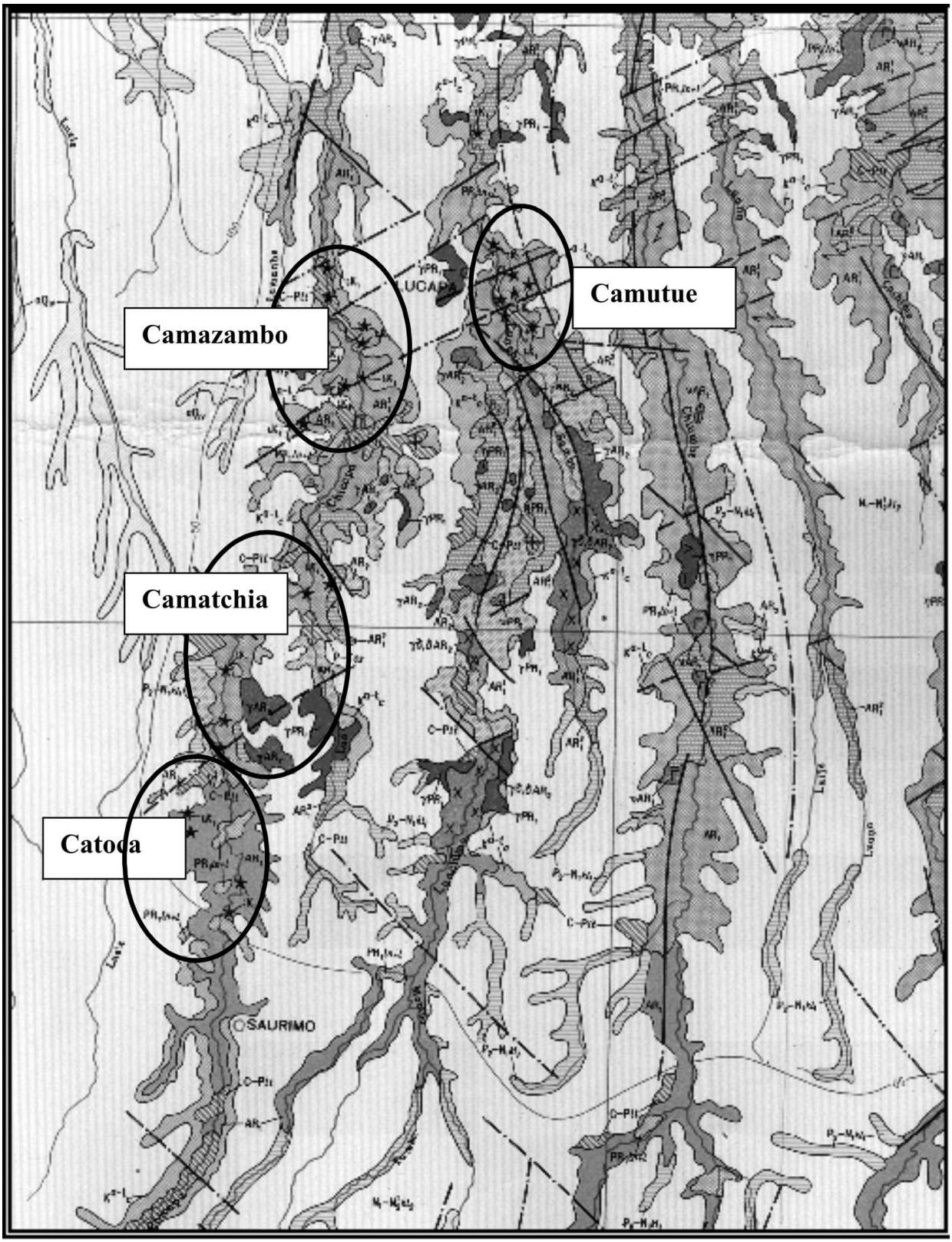

Fig. 3. **Disposition of basic kimberlite fields in diamondiferous province Lunda Norte** (fragment of a geological map of the region of 1:1000000 scale, according to Araujo et al. [2] with supplements of the authors).

Kimberlite fields are shown by separate contours.

sands it is slightly exposed in valley Rio Camutue and without sediments of Calonda includes 100 m thickness of crater part kimberlite formations, with the exception of an eastern part, where the rocks of diatreme facies come out to the surface of the pipe. Diamond grade in the upper part of the pipe is characterized by low values since kimberlites are diluted by disintegrated fragments of the frame, however quality of the crystals is rather high at sufficiently large size (the finds of stones weighing 80 car are not rare). One more large diatreme Cariue of 400x200 m size is 10 km to north. Its large axis is oriented in direction north-north-west and is located on the fissure of tearing off stretching under 145° angle. This pipe is distinguished by high concentration of heavy minerals reaching 100-250 kg/m^3. Besides these bodies one should note pipes-twins: Cambuazh I (550x250 m) and II (500x200 m). The data about sizes of other pipes are different.

Kimberlite field Camazambo is remarkable by the fact that it includes the above mentioned unusual pipe Camafuca-Camazambo – pipe-leader and one of the largest pipes in the world. Formations of its upper part are very diluted by sandstones Karroo which often complicates their diagnostics. Investigated kimberlite rocks of diatreme facies are composed by saturated with xenogeneic material breccia and basaltoid kimberlite with inclusions of pyroxene-garnet growths. Alluvium in sand-bars on river Shikapa usually contains diamonds and their indicator minerals. 8 km to north and down the river there is pipe Cagoa at the same tectonic disturbance, the upper part of which is composed by "xenotuffbreccia".

More than ten kimberlite diatremes with volcanogenic-sedimentary formations and tuffs in the upper part are located south of the pipe-leader. Other pipes of the field are characterized by similar structure, pipe Camuazanza, for instance – a rather large in area (11.5 ha) diatreme in the course of river Shikapa (diamondiferous micaceous kimberlite tuffs and tuff breccias), Cendzhamba (tuffs of kimberlites and kimberlite breccias), Camutongo, Cacola and Canzololo (volcanogenic-sedimentary formations), as well as pipe Camonbo (kimberlite tuffs). Kimberlite rocks of field Camazambo are distinguished by increased content of heavy minerals (up to 50 kg/m^3, sometimes more) while having rich view spectrum and diopside-ilmenite-garnet association of kimberlite indicator minerals, and more than half of the pipes are diamondiferous.

Field Camachia is the smallest in the province by the quantity of known kimberlite bodies (8). The field got its name from the largest pipe – Camatshia (Camachia), which is located in the place of the Chicapa and Luo rivers' confluence at the tearing off disturbance of latitudinal stretch broadly developed in the region. The size of the pipe is 600x500 m. The pipe is composed by volcanogenic-sedimentary rocks, kimberlite tuffs and tuff breccias, partially by basaltoid kimberlite. The rocks are very hard, dense, of brownish-green or dark-blue color. Nodules of picroilmenite occur. Relatively near is one more large pipe Camazhico of prolonged in north-eastern direction shape and attributed to the fault of the marked stretch, with 1000x420 m size. The pipe is composed (from up to

down) by volcanogenic-sedimentary rocks, kimberlite tuffs and tuff breccias, kimberlite breccias and porphyric kimberlites and is overlayed by diamondiferous fragment of formation Calonda (diamonds are most probably from another, unknown source). According to available data this pipe us the most productive in the described field.

Field Catoca is the most southern one in province Lunda (see Fig. 3) within which 25 kimberlite bodies are known grouping into a meridian zone of 18 km length and 12-14 km width, they are – Catoca, Lova, Tshikoa, Caissar, Caiputa and others (from south to north). Axes of most pipes are oriented in north-eastern and north-western directions, the shape of bodies is oval, isometric, or lens-like. Lova was one of the first discovered pipes, which is industrially diamondiferous, though its diamonds are characterized by lower quality than diamonds of pipe Catoca.

Pipe Catoca, one of the ten largest diatremes of the world, can serve as a model target both of the marked communities of kimberlite occurrences and the whole province. This pipe is distinguished by practically ideal rounded shape in plan at 900x900 m section and area of 65.7 ha. Beginning from 1997 this deposit, the first in Angola, is involved in modern industrial de4velopment. This pipe is the only one so far being mined large primary diamond deposit of Angola. More than 80% of its area is overlayed by Kalakhari formation sediments and interformational sands, including a clod layer of gritstones and conglomerates, observed only within the crater depression. Summarized capacity of this thickness is 40 m. The central part of the diatreme down to depth 100 – 140 m is composed by epiclastic sedimentary rocks – poorly lithificated sandstones and argillites of Mesozoic age formed in the crater lake. Before the development of the pipe kimberlite rocks of the diatreme's western part exposed to the day surface in the valley of creak Catoca. Hosting the pipe rocks – field spar-pyroxene gneisses and crystalline schists of Archean age. Complicated internal structure of pipe Catoca, stipulated by insignificant depth of erosional cut and preservation of a paleovolcano crater construction, has been established according to the data of production and geologic-prospecting works. Wide spectrum of forming the pipe rocks, represented by hypabyssal, diatreme, and crater facies has been established. Broad distribution of volcanogenic-sedimentary rocks, occupying a rather large volume in the section of the diatreme together with interformation sands, is noteworthy.

SPECIFIC FEATURES OF KIMBERLITE ROCKS' COMPOSITION

As it was noted above the rocks of hypabyssal, diatreme and crater facies take part in the sections of the prevailing part of the region's diatremes. According to textural-genetic classification [6, 10] all types of kimberlite rocks are present in the body.

Hypabyssal facies comprise the rocks of effusive appearance – porphyric and clustoporphyric kimberlites, usually composing autolithic fragments in eruptive breccias, as well as lapilli of various sizes and small in volume intrusive bodies in

crater formations, individual dykes have been noted. They contain minimal quantity (not more than 5%) of xenogenic material in the form of completely carbonatizated fine (3-5 mm) debris of country rocks. The texture is massive, the structure is fine-crystalline, fine-porphyric. The content of porphyric occurrences of olivine (pseudomorphs) of ovoid shape – 10-15%. Kimberlite also contains rare tabular crystals of phlogopite and partially substituted grains of ilmenite. The basic mass (matrix) is represented by fine (0.3-0.5 mm in average) idiomophic or hypidiomorphic pseudomorphs of serpentine on olivine (40-50%). They are distributed evenly but sometimes form growths from several grains. Large (0.8-1.2 mm) pseudomorphs are infilled by fine-scaly aggregate of subisotropic serpentine in association with magnetite. Fine (0.1-0.5 mm) pseudomorphs are completely substituted for calcite. Small crystals of oxide-ore minerals (spinel, ilmenite, magnesioferrites) cubic small crystals of perovskite, isometric or pillar grains of apatite are observed in the basic mass. The quantity of crystalline phase in matrix is much higher than mesosthasis.

The rocks of diatreme facies are represented by two genetic groups: effusive-fragmental (kimberlite breccias and autolithic kimberlite breccias, tuffisites) and explosive-fragmental (tuffs and tuff breccias). Petrographic varieties of the first of them are colored mainly in various tints of greenish-gray coloring. The texture is brecciated, autolithic in places, of the basic mass – massive. The structure is small-fragmental porphyric and clustoporphyric. Autoliths are rounded, isometric or ellipsoidal with clear concentric zoning. One can often come across autoliths of pellicle type with large pseudomorphs on olivine, monoclinic pyroxene or xenoliths of country rocks in core. The quantity of xenogenic material – fragments of metamorphic rocks – usually does not prevail 10-15%, constituting 5-7% in average. These fragments are practically completely substituted for poorly anisotropic mixed-layered mineral and carbonate (dolomite) with impurity of magnetite or hydroxides of iron. Relicts of hornblende, clinopyroxene, altered biotite, apatite have preserved in them. The basic mass (matrix) of autolithic kimberlite breccia is represented by serpentine-carbonate (sufficiently dolomitic) mesosthasis. Pseudomorphs on phenocrystals of the second generation olivine occupy a small volume (10-15%). They exhibit irregular distribution. Vermiculitizated of phlogopite (2-3%), rare leucoxenizated small crystals of perovskite and microisolations of oxide-ore minerals are observed in the basic mass of breccias. Interstices are infilled with subisotropic fine-scaly serpentine with rhomb-like crystals of dolomite.

The rocks of crater facies are most diverse in composition and include explosive-fragmental (tuffs and tuff breccias), sedimentary-volcanoclastic (tuffites), volcanogenic-sedimentary (tuff conglomerates, tuff gritstones, tuff sandstones, tuff siltstones, tuff argillites) and sedimentary deposits (heterolytic breccias consisting of the rocks' fragments composing geological section of the region; gritstones, sandstones, siltstones, argillites) with admixture of kimberlite material. They infill a cup-like body to 230-270 m depth and with washout are

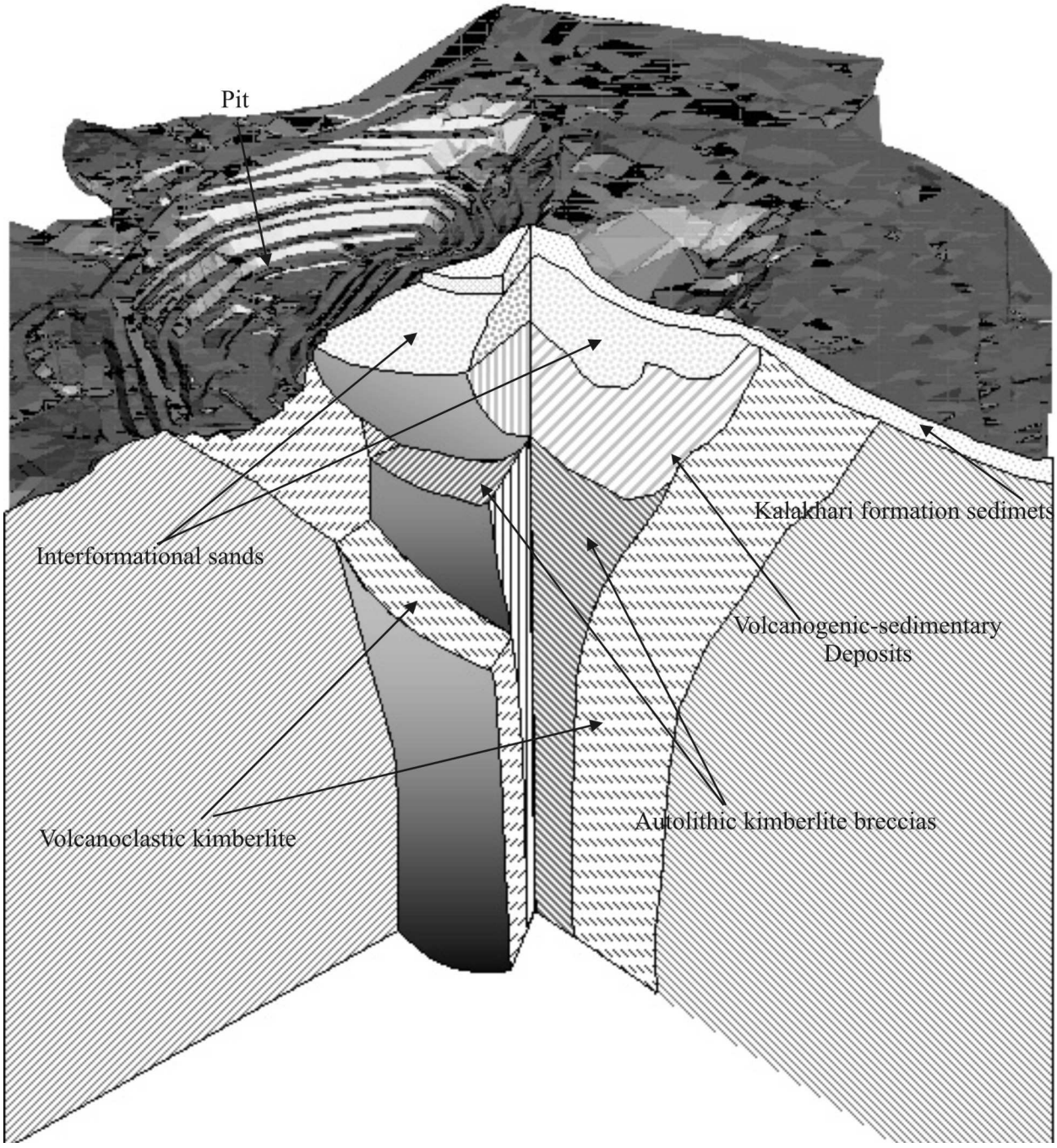

Fig. 4. **Schematic section of kimberlite pipe Catoca.**

deposited on the rocks of the crater facies (Fig. 4). Kimberlite tuff breccias, poorly sorted argillaceous tuff gritstones, tuff sandstones, tuff siltstones and epiclastic formations with various quantity of kimberlite material domain among them. The latter are lacustrine-continental deposits of paleocrater formed from the products of weathering of metamorphic and kimberlite rocks.

Initial kimberlite rocks respond to those from other regions of the world by mineral composition, structure and texture. Primary rock-forming silicates in them are substituted for minerals of serpentine group and olivine proper is practically

absent. Mixing of kimberlite material with debris of hosting granite-gneisses, joint weathering of which brought to the formation of specific composition of secondary products, typical of such ones, formed in sour medium, is the specific feature of diatreme Catoca initial rocks. And first of all – it is the development of saponite, on the one hand, and preservation of such metastable mineral as chrome-diopside in exogenous conditions, on the other hand. Secondary and hypergene minerals prevail in composition of investigated kimberlite rocks. Serpentine is one of the main among them, more seldom it is antigorite – its compact variety. Smectite, saponite and nontronite (group of montmorillonite), montmorillonite-hydromicaceous aggregates and veinlets of carbonates are widely represented in the formations of the crater part. Small admixture of chlorite is present. Down along the section of the pipe the content of smectite decreases and concentration of serpentine increases. Disperse admixture of quartz, oxides (pelitomorphous hematite) and hydroxides of iron are present.

Chemical composition of rocks of the exposed by boreholes part of pipe Catoca indicates sufficient content variations of all petrogenic components. Chemism of hypabyssal and diatreme facies rocks – porphyric kimberlites and eruptive kimberlite breccias (Table 1), is most close to "kimberlite frames", therewith. Up along the section one can fix noticeable variations in distribution of petrogenetic components. The largest quantity of SiO_2 is fixed in volcanogenic-sedimentary rocks (average content of SiO_2 prevails 65 mas.%) and individual samples of sedimentary formations (without visible kimberlite material) from the tops of the section – from 54.67 to 79.04 mas.% (Fig. 5) at reverse correlation of SiO_2 и MgO. On the whole formations of the crater facies, enriched by clustogene material, are characterized by high concentrations of silica, increased – alkali (Na_2O и K_2O), sometimes Al_2O_3, decreased – MgO and FeO. With transition down along the section to sufficiently kimberlitic formations the quantity of the latter components noticeably increases, and of the first ones falls at the most contrast decrease of SiO_2 contents. The share of TiO_2 is much higher in the rocks of diatreme facies. Concentrations of Cr, Ni, Co, Mn, Zn, and Sr are noticeably higher in the latter ones, in comparison with crater formations. Values of Ni/Co – ratio in average higher than 10 (see Table 1). Large limits of concentration fluctuations testify about extremely inconsistent distribution of elements-impurities in analyzed rocks which is stipulated by significant changeableness of mineral composition.

Diamonds in the province represent both peridotite and eclogitic sources [5]. Significant part among them possesses octahedral habit, there are many crystals of transitive and rhombic dodecahedral habits, as well as crystals with polycentric facets with insignificant quantity of bort, cubes and rounded shapes (first percents). Diamonds with inclusions of sulphides and garnets are recorded. On the whole qualitative and color characteristics of crystals put the diamonds of the province into a group of the best ones among primary deposits of Africa and the World.

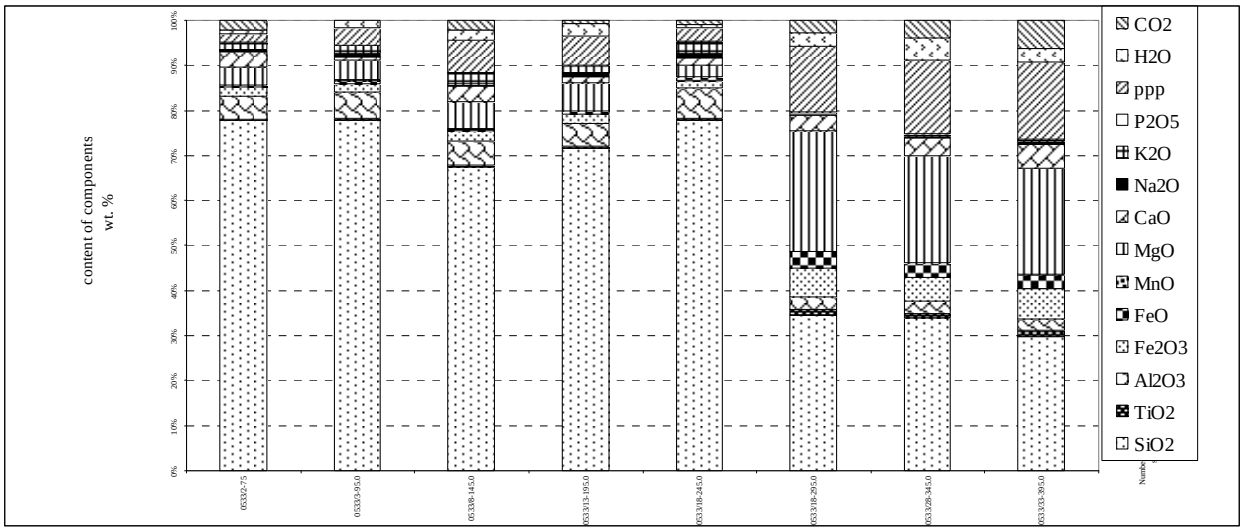

Fig. 5. **Petroghemical section of kimberlite rocks in borehole.**

Besides diamond garnets, zircons, ilmenite (picroilmenite), clinopyroxenes are practically not altered among primary minerals and mica is chloritizated. The highest concentrations of kimberlite indicator minerals, like of heavy fraction on the whole, with equal quantities of pyrope and picroilmenite have been recorded in the rocks of crater facies. Clinopyroxene is constantly noted, the largest quantities of which occur in epiclastic as well as in volcanogenic-sedimentary formations. Varying share of micas is also recorded, and increased quantity of amphiboles – in epiclastic and volcanogenic-sedimentary rocks of a crater part. High concentrations of kimberlite indicator minerals are specific for gritstones and sandstones of the upper part of the crater facies section. Garnet-pyroxene growths constantly occur in granulometric classes of more than 0.5 mm.

Monoclinic pyroxenes in kimberlites are represented by diopside (chrome-diopside) of prismatic form. Chrome-diopside with more than 2 mas.% contents of chrome, which characterizes the presence of juriite component ($NaCrSi_2O_6$). Non-chromic clinopyroxene with increased concentrations of Al_2O_3 и Na_2O, impoverished CaO and MgO (availability of jade component), analogous to omphacite from magnesial-ferriferous eclogites are also present. Growths of clinopyroxene with biotite and hornblende are recorded in autolithic breccia. Pyrope is represented by three color varieties: 1) violet and crimson-violet (prevails), 2) red and orange-red, 3) orange and yellow-orange, which is explained by content variations of Cr_2O_3 in them. Increased (more than 10%) quantity of high-chromic knorringite-bearing pyropes (Fig. 6) directly correlating with diamondiferousness of kimberlites is typical. Their compositions respond to garnets – growths with diamond and their inclusions in diamond.

Picroilmenite is widely represented, the content of which sometimes exceeds 5 vol.%. Two groups are distinguished by its chemism: the first one – with low contents of MgO (less than 6 mas.%), TiO_2 (less than 45 mas.%) and Cr_2O_3 (less than 1.6 mas.%) at increased quantities of Fe_2O_3 (more than 20 mas.%); the second

Table 1.

Average chemical composition of the Catoca pipe kimberlite rocks

Rocks	N	SiO_2	TiO_2	Al_2O_3	Fe_2O_3	FeO	MnO	MgO	CaO	Na_2O	K_2O	P_2O_5	H_2O
PK	4	35,18-36,33 35,76	0,78-1,13 0,96	2,18-2,59 2,39	3,91-4,43 4,17	4,67-6,18 5,43	0,14-0,16 0,15	29,53-30,68 30,11	4,8-5,8 5,3	0-0 0	0,16-0,31 0,24	0,33-0,34 0,34	0,69-0,78 0,74
AKB	7	32,63-38,98 36,52	0,75-1,49 1,15	2,12-3,47 2,84	4,06-7,4 5,68	2,44-5,35 3,97	0,14-0,16 0,15	25,2-27,78 26,53	4,27-7,73 5,43	0,0-0,62 0,33	0,08-0,24 0,2	0,15-0,55 0,35	0,84-5,19 3,81
KB	50	17,33-49,63 38,97	0,16-1,54 0,93	0,6-6,28 2,65	3,22-9,75 7,32	0,28-6,18 1,75	0,08-0,22 0,14	16,71-31,75 25,23	1,45-22,31 5,13	0,0-0,58 0,05	0,03-0,91 0,2	0,07-1,23 0,23	0,8-11,78 5,7
KB alt.	3	41,03-67,52 50,81	0,53-1,03 0,82	1,18-1,86 1,6	2,75-8,28 5,96	0,89-1,72 1,34	0,12-0,16 0,14	5,18-28,07 18,31	2,45-9,54 5,5	0,0-0,14 0,05	0,08-0,15 0,11	0,08-0,12 0,1	1,46-5,54 3,81
TB	12	40,14-71,0 49,95	0,31-1,27 0,76	2,88-5,39 4,03	2,76-8,66 5,65	0,25-1,72 0,74	0,09-0,14 0,12	6,98-25,37 17,2	2,03-10,11 4,6	0,00-0,65 0,13	0,2-1,63 0,77	0,11-0,59 0,22	3,6-10,64 7,28
VSR	30	35,52-79,14 65,82	0,18-1,12 0,52	1,44-6,88 4,93	0,26-9,34 3,11	0,18-2,04 0,59	0,04-0,15 0,11	2,46-29,8 9,87	0,79-15,31 3,39	0,0-1,03 0,36	0,07-2,7 1,45	0,05-0,82 0,16	0,86-9,81 4,16
SR	5	54,67-79,04 70,46	0,19-0,45 0,35	3,41-5,99 4,79	0,83-2,1 1,61	0,43-0,72 0,55	0,04-0,11 0,08	3,92-7,28 5,23	0,7-14,89 6,36	0,0-0,65 0,35	1,06-1,97 1,53	0,05-0,18 0,1	0,73-3,55 1,97

Rocks	N	CO_2	LOI	Cr	Ni	Co	Mn	Zn	Sr	Ba	Ni/Co	Sr/Ba
PK	4	3,74-4,4 4,07	14,92-15,29 15,11	646,0-818,0 732,0	1027,0-1257,0 1142,0	92,0-92,0 92,0	1030,0-1320,0 1175,0	68,0-71,0 69,5	434,0-450,0 442,0	125,0-409,0 267,0	11,16-13,66 12,41	1,06-3,6 2,33
AKB	7	2,86-6,82 4,46	14,49-18,87 16,77	651,0-1028,0 787,29	736,0-964,0 858,43	56,0-113,0 87	998,0-1378,0 1184,14	61,0-85,0 70,29	341,0-620,0 463,29	258,0-932,0 503,43	7,29-17,21 10,63	0,38-1,48 1,08
KB	50	0,0-21,34 3,43	6,68-28,41 17,45	169,0-1500,0 726,6	116,0-1387,0 955,3	25,0-129,0 72,2	315,0-3059,0 986,2	36,0-92,0 63,2	97,0-1748,0 417,5	133,0-1560,0 373,5	1,53-28,4 13,83	0,3-3,56 1,28
KB alt.	3	1,54-8,36 5,28	12,41-18,81 15,66	473,0-1192,0 808,67	266,0-1086,0 686	46,0-74,0 61,67	615,0-1205,0 943	23,0-65,0 50,33	213,0-581,0 335,67	72,0-445,0 198,33	5,78-14,68 10,44	1,31-2,96 2,33
TB	12	0,44-6,82 2,74	8,05-20,71 15,37	65,0-725,0 448,58	157,0-931,0 555,75	20,0-71,0 45,33	492,0-986,0 757,33	32,0-70, 51,83	316,0-750,0 482,92	250,0-850,0 492,67	2,21-26,64 13,19	0,51-2,67 1,08
VSR	30	0,0-11,0 2,03	2,97-20,86 9,52	79,0-1400,0 325,7	20,0-1469,0 305,0	20,0-72,0 30,5	129,0-1109,0 436,6	15,0-68,0 33,9	99,0-935,0 299,5	233,0-1113,0 525,5	0,8-20,4 9,6	0,16-2,49 0,6
SR	5	0,0-10,34 4,18	1,87-17,27 7,69	61,0-180,0 114,67	157,0-204,0 184	18,0-23,0 20,33	135,0-373,0 287	13,0-29,0 21,67	85,0-124,0 104,67	334,0-436,0 396,33	7,9-11,3 9,16	0,2-0,3 0,26

Note. PK - porphyric kimberlite, KB - kimberlite breccia, AKB - autolithic kimberlite breccia, KB alt. - altered kimberlite breccia, TB - tuff breccia, VSR – volcanogenic, SR - sedimentary rocks. In numerator - fluctuation limits, in denominator - average values sedimentary rocks,

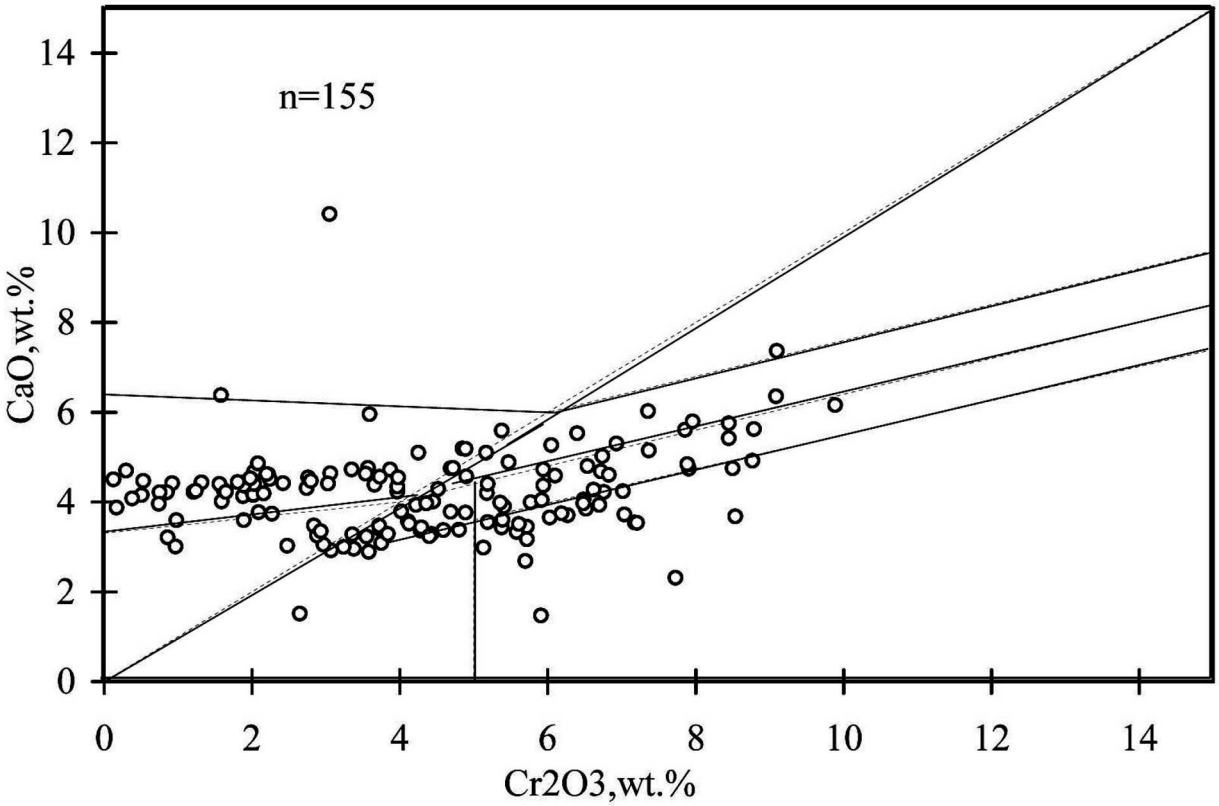

Fig. 6. **Composition of garnets from kimberlite rocks of the Catoca field pipes in diagram CaO-Cr_2O_3.**

one – with increased contents of MgO – more than 8 mas.%, TiO_2 – more than 45 mas.% (Fig. 7) and Cr_2O_3 – more than 1.6 mas.% at decreasing the quantity of Fe_2O_3 to 18.7 mas.%. Both paramagnetic and ferrimagnetic picroilmenite occur. The largest share of the latter is present in kimberlite rocks of pipe Chere where its quantity constitutes half of the concentration of usually dominating paramagnetic variety. In the rocks of pipe Catoca the ratio of paramagnetic and ferrimagnetic varieties corresponds approximately to 6:1. Composition of picroilmenite is distinguished by high chromic property and is analogous to the one from xenoliths of mantle rocks and nodules from kimberlites. By magnesial property it corresponds to paramagnetic ilmenite with increased share of geikielit minal. The greatest contents of large (more than 5 mm) picroilmenite grains are recorded in the layers of crater facies gritstones. Rare chrome-spinellids, often in growths with garnets and clinopyroxenes are close in chemism to high-chromic spinellids of lherzolite paragenesis with increased titanium property.

On the whole, specific features of composition of diamond indicator minerals and geochemistry of kimberlites testify about abyssal origin of initial melts in presence of garnet and restite mantle association. Judging from frequent presence of chromic garnets of abyssal diamond-pyrope facies formation of primary

kimberlite smeltings is supposed to take place on the border of lithosphere and asthenosphere, and wide variations of clinopyroxene and garnet chemism reflect heterogeneous composition of upper mantle.

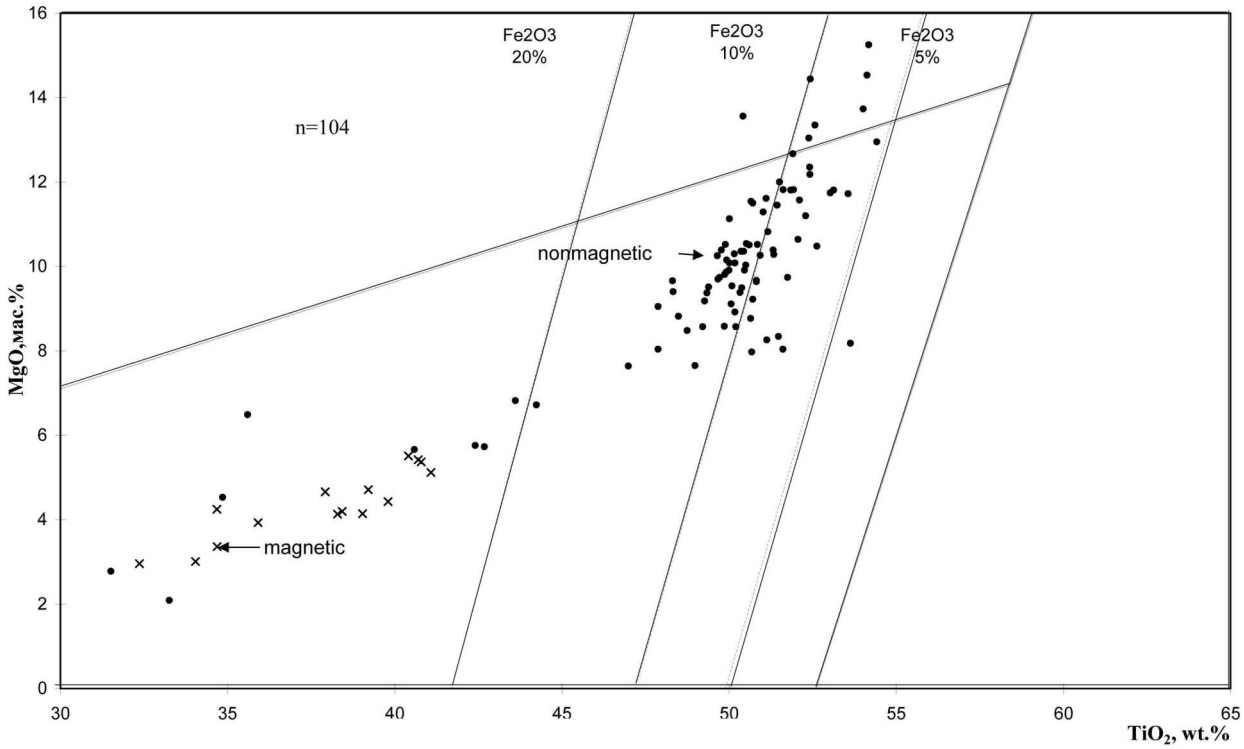

Fig. 7. **Composition of picroilmenite from kimberlites of pipe Catoca.**

CONCLUSION

Kimberlite occurrences of Angolan north-east are located within the ancient platform with Archean craton basement – craton Angola-Cassai, and are attributed to linear zones of tectonic activization, one part of which inherits ancient tectonic directions, and the other one is related with new directions overlayed on ancient basement and cutting the system of cratons and mobile belts. By the time of occurrence kimberlite magmatism is usually attributed to the periods of epeirogenetic rising of areas (probably to the rising of Cretaceous continent of South Africa). Almost all known kimberlite bodies of Angola are located along the zone of Lukapa faults which traces along the whole continental part of the country from its south-western border and crossing north-eastern one with prolongation into Zaire.

Almost all kimberlite pipes of Lunda Norte province are characterized by insignificant erosional cut and differ by the fact that all three facies of kimberlite diatreme theoretical model (hypabyssal, diatreme, and crater) are preserved within the frames of a separate geological body. Mixing of kimberlite material with that of hosting granite-gneissic rocks, with formation of heterogeneous in composition derivatives representing the mixture of rock and minerals, is specific feature of crater formations, which reflects on petrographic, mineralogical, and geochemical properties.

Specific features of composition of diamond indicator minerals and geochemistry of kimberlites testify about abyssal origin of initial melts in presence of garnet and restite mantle association. Judging from broad distribution of chromic garnets of abyssal diamond-pyrope facies formation of primary kimberlite smeltings is supposed to take place on the border of lithosphere and asthenosphere. Considerable part of diamonds possesses octahedral habit, there are many crystals of transitive and rhombic dodecahedral habits, as well as of crystals with polycentric facets at insignificant quantity of bort, cubes, and rounded shapes. Qualitative and color characteristics of the province crystals respond to diamonds of the best primary deposits of Africa and the World.

REFERENCES

1. **African Mining** (1998). Light of day for Angolan diamonds: African Mining, 2 (1), p.11-21.
2. **Araujo, A.G, Perevalov, O., Jukov, R. e out.** (1988). República Popular de Angola. Carta geologica de Angola, 1:1000000.: Luanda, Instituto Nacional de Geologia,
3. **Araujo, A.G., Perevalov, O., Guimarães, F.R. e out.** (1988). República de Angola. Carta de recursos minerais, 1: 1000000.: Luanda, Instituto Geologico de Angola.
4. **Bardet, M.G.** (1973). Geologie du diamant: Volume 2: Gisements de diamante d'Afrigue: Mémoir, BRGM 83, Paris, 229 pp.
5. **Boyd, F.R. and Danchin, R.V.** (1980). Lherzolites, eclogites and megacrysts from some kimberlites of Angola: American Journal of Science, 280A, p. 528-549.
6. **Clement, C.R., Skinner, E.M.W.** (1985). Textural-genetic classifications of kimberlites /trans/ Geol. Soc. S. Afr., Vol. 88, p. 403-409.
7. **Clifford, T.N.** (1966). Tectono-metallogenic units and metallogenic provinces of Africa: Earth and Planetary Science Letters, 1, p. 421-434.
8. **Janse, A.J.A.** (1995). A history of diamond sources in Africa: Part I: Gems and Gemology, Winter 1995, p. 228-255.
9. **Janse, A.J.A., and Sheahan, P.A.** (1995). Catalogue of world wide diamond and kimberlite occurrences: a selective and annotative approach: Journal of Geochemical Exploration, 53, p. 73-111.
10. **Mitchell, R.H.** (1986). Kimberlites: Mineralogy, Geochemistry and Petrology. New York: Plenum Press, 442 p.
11. **Nosyko, S.F., Rotman, A.Ya.** (2003). Specific character of kimberlite manifestation and perspectives of Angola north-east diamondiferousness: Peculiarities and principal results of the science-and-research and experimental-methodical works of the Yakutian Science-and Research Geology and Prospecting Institute of the stock company «ALROSA», p. 102-108.
12. **Reis, B.** (1972). Preliminary note on the distribution and tectonic control of kimberlites in Angola: 24th International Geological Congress, Section 4, p. 276-281.

UDK 551.22+552.11

Mir and International'naya kimberlite pipes – trace element geochemistry and thermobarometry of mantle minerals

Ashchepkov I.V.[1], Vladykin N.V.[2], Rotman A.Y.[3], Logvinova A.M.[1], Afanasiev V.P.[2, 3], Palessky V.S.[1], Saprykin A.I.[1], Anoshin G.N.[1], Kuchkin A.[1], Khmel'nikova O.S.[1]

[1] *United Institute of Geology Geophysics and Mineralogy SB RAS, Novosibirsk*
[2] *Institute of Geochemistry SB RAS, Irkutsk*
[3] *Central Scientific Investigation Geological Exploration Institute, ALROSA , Mirny*

Compositions of the mineral determined with EPMA and TRE for 40 elements analyses obtained with LAM ICP method from the concentrate of Mir and International'naya pipes were used to reconstruct the mantle sections. Garnet and clinopyroxenes single grain thermobarometry [4-6,24] give very close mantle column structures with 7 layers. The TP gradients for both pipes are close to 35 mv/m^2 in the central part and to 45 or more at the asthenospheric level. More heated condition and scattering of the PT estimates was determined for International'naya pipe at the basement of lithosphere. The mantle column beneath the later pipe is represented by the harzburgite – hybrid pyroxenite and eclogites mixture while for Mir by the enriched Phl lherzolites and pyroxenites of continental type A-type eclogites. The TRE from the International'naya show the Eu- Ce anomalies for the Cr– diopsides, chromites and ilmenites. The later means the participation of the eclogites in the protokimberlite melt generation. The TRE behavior for the clinopyroxenes from peridotites in Mir suggests continuous enrichment of the mantle minerals in LILE, LREE, HFSE contents to the upper part of the mantle section. The deeper part is constructed by the more depleted material partly revealing oceanic mantle signatures.

INTRODUCTION

Malo-Botuobinsky region [16] was long time the most productive for diamond region in the Siberian province. Despite on the long time study Mir [8,9,15,16,18-20, 23-30, 32-36] and close located kimberlite pipes [17] and their xenoliths the TP reconstructions of the mantle section and the description of the mantle was not made in detail. In this paper we are trying to compare composition of the minerals and reconstructed with thermobarometry mantle sequences beneath two pipes Mir and International'naya. Using heavy concentrate we'll try to determine compositions of peridotites in mantle layers and on the bases of the geochemical features of mineral briefly describe the processes took place beneath the kimberlite pipes bringing to the formation of the lithospheric keel.

For this purposes more then 900 EMPA analyses of garnets, clinopyroxenes, ilmenites, chromites from each pipe were made and LAM ICP analyses (~ 60) of minerals with the most characteristic compositions were accomplished.

MINERALOGY

Garnet compositions for Mir and International'naya pipes are different. The garnets from Mir pipe analyzed in this work belong mainly to the lherzolites field rising toward the boundary of the pyroxenite field (Fig. 1). Starting from 5% Cr_2O_3 some dunite garnets of G9-10 groups [11-13] occur. The compositions of the garnets from International'naya pipe (Fig. 1b) correspond also mainly to lherzolite field [32] but starting from the 6 % Cr_2O_3 garnet trend tends to shift to harzburgitic compositions. Rather high amount of the population refer to the pyroxenitic compositions revealing CaO content form 10 to 16% for the green garnets with 12-14% Cr_2O_3. TiO2 concentrations for garnets from Mir rapidly rise in the Cr- rich deep garnets while for International'naya population it is weakly continuously rising.

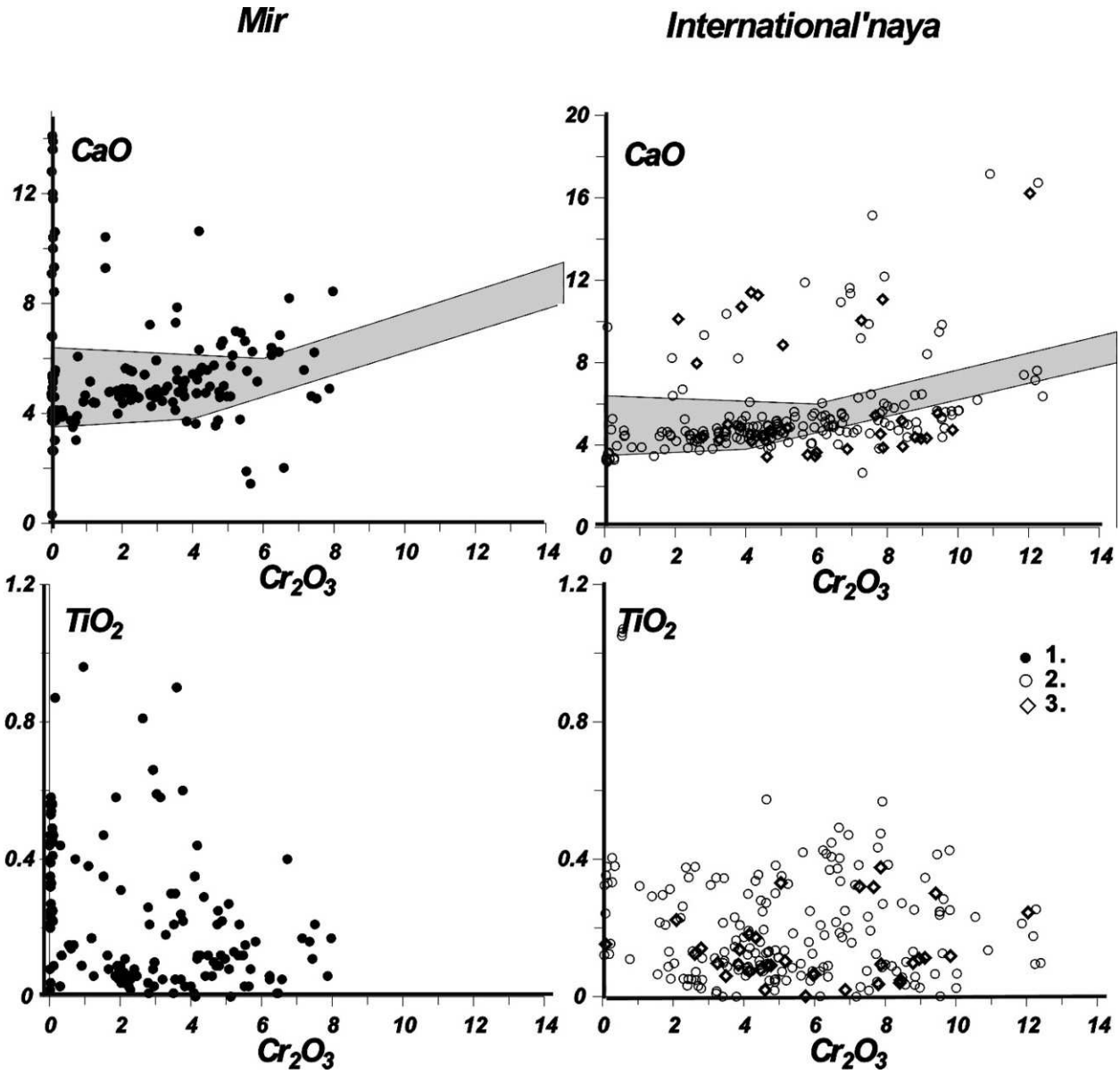

Fig. 1. **Variations of the garnet compositions of Mir and International'naya pipes.**

1 - Garnets from Mir pipe; 2 - Garnets from International'naya single grains; 3 - the same intergrowths.

Compositions of the ***Cr- diopsides*** (Fig. 2) also reveal different tendencies. For the International'naya the compositions with high Na, Cr, and Al rising together with the FeO and decreasing FeO content are characteristic – these are the typical features of the mantle sections with the high amount of eclogites [3, 33, 37, 38]. Some pyroxenes with 7% of Cr_2O_3 are quite unusual for distant from the center of craton regions of kimberlitic magmatism in Daldyn and Alakite – Markha region. Cr- diopsides form Mir pipe are lower in sodium content and related tetrahedral cations being more magnesial in general. Some typical A-type eclogites [15] without Cr were described for this pipe. TiO_2 content for clinopyroxenes from Mir pipe in general is higher. Amount of eclogitic pyroxenes for the Molo – Botuobinsky region is much higher them for the peripheral parts of the Siberian craton [15, 25, 32].

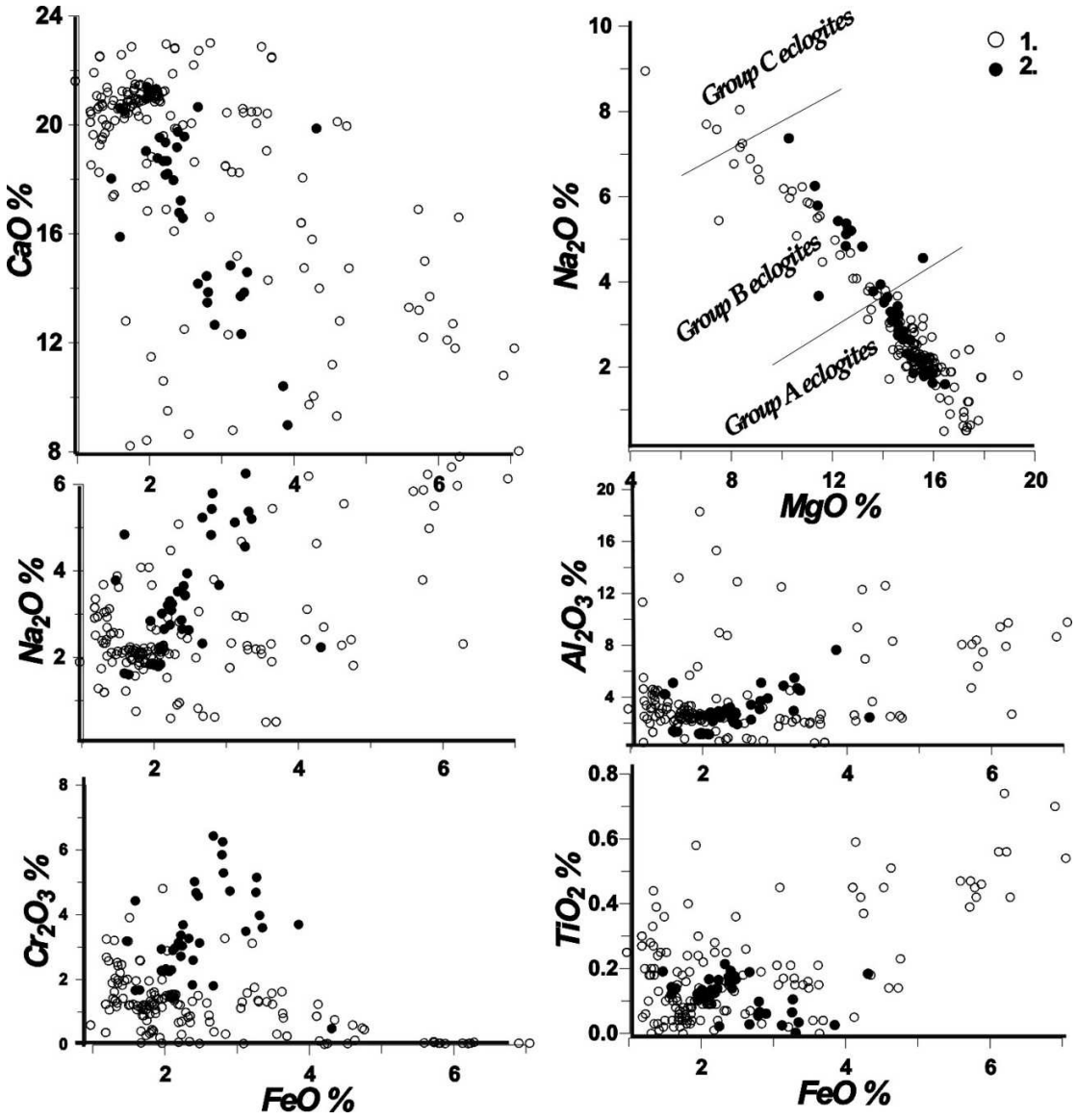

Fig. 2. **Variations of the clinopyroxene compositions from Mir (1) and International'naya (2) pipes.**

1 - Clinopyroxenes from Mir pipe; 2 - Cr- diopsides from International'naya pipe.

Ilmenites form the pipes of Malo- Botuobinsky region (Fig. 3) reveal rather low Cr_2O_3 content in the middle part of the trend (50-44% TiO_2) what suggest the lack of the interaction with the peridotite material or/ and essentially eclogitic composition of the mantle column in this part. The ilmenite trend for Mir pipe is very long 30-55% TiO2. As well as the trend from the Yubieynaya kimberlite [2] may be subdivided in to the 7 groups though the difference between groups is not sharp except the very beginning with Cr-Mg associations close to those from metasomatites [38] and the end where the Ni and Cr again rises. The hyperbolic curves for MgO, FeO, V_2O_5, Al_2O_3 in the middle part with the 5 groups suggest rather simple fractionation process [14, 22].

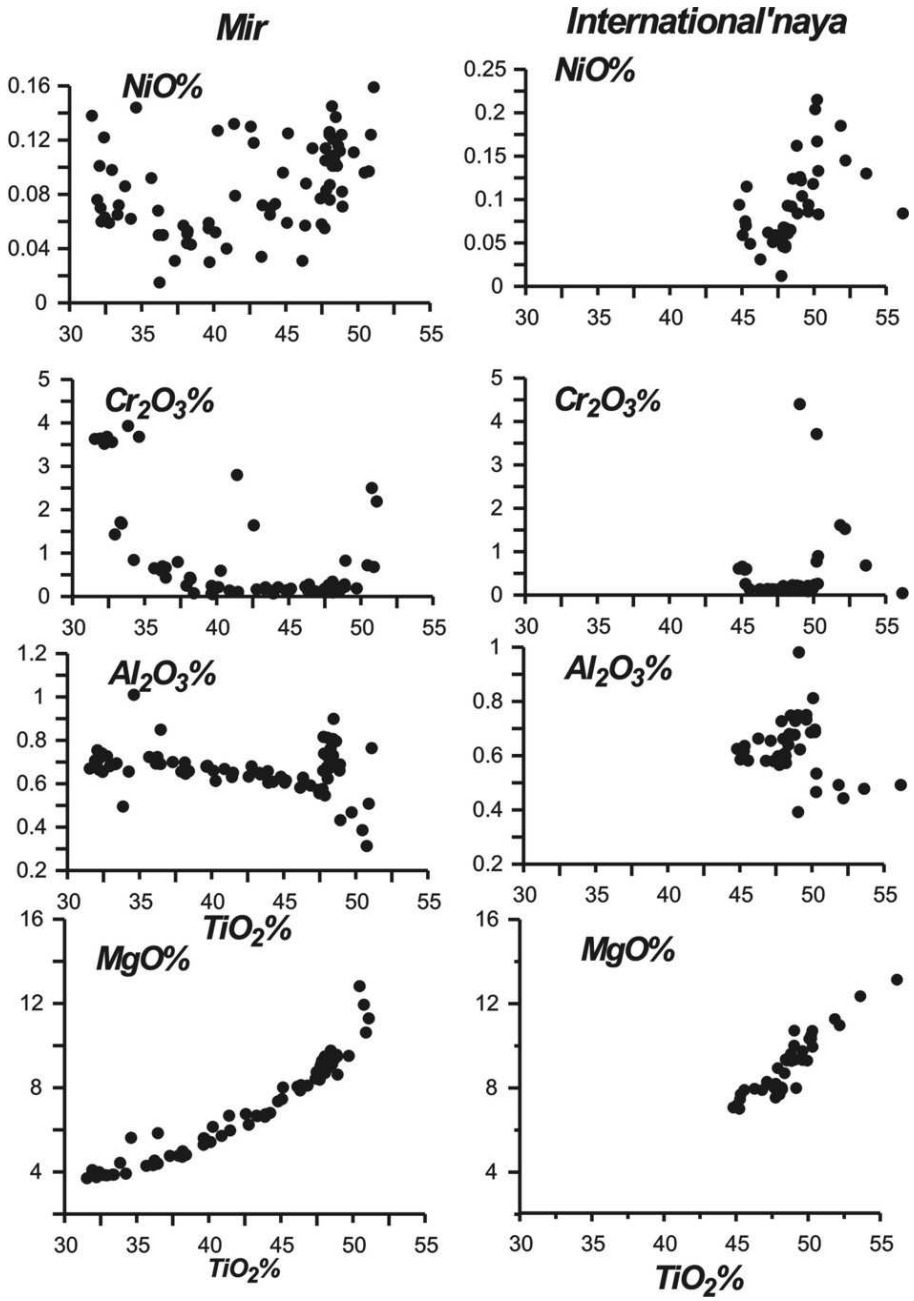

Fig. 3. **Variations of the ilmenite compositions from Mir and International'naya pipes.**

Ilmenite trend for International'naya pipe is restricted 55-40 what is closer o the pipes of the Daldyn and Alakite regions. Comparison with those from Mir pipe reveal very close configuration. More Cr- rich compositions in the beginning and more rapid fractionation of MgO and lack of the Fe- rich part of the trend may suggest the finishing of the fractionation which is likely developing in the rising feeding system at the middle part of the mantle column or the rising of the kimberlite masses in the upper part in another part of the mantle where the pre-eruption system did not reach. It may be suggested also that the rise of feeding system was faster and the finishing part of the trend was stopped at 40% TiO_2.

The other minerals were not studied in detail yet and will be described in another paper.

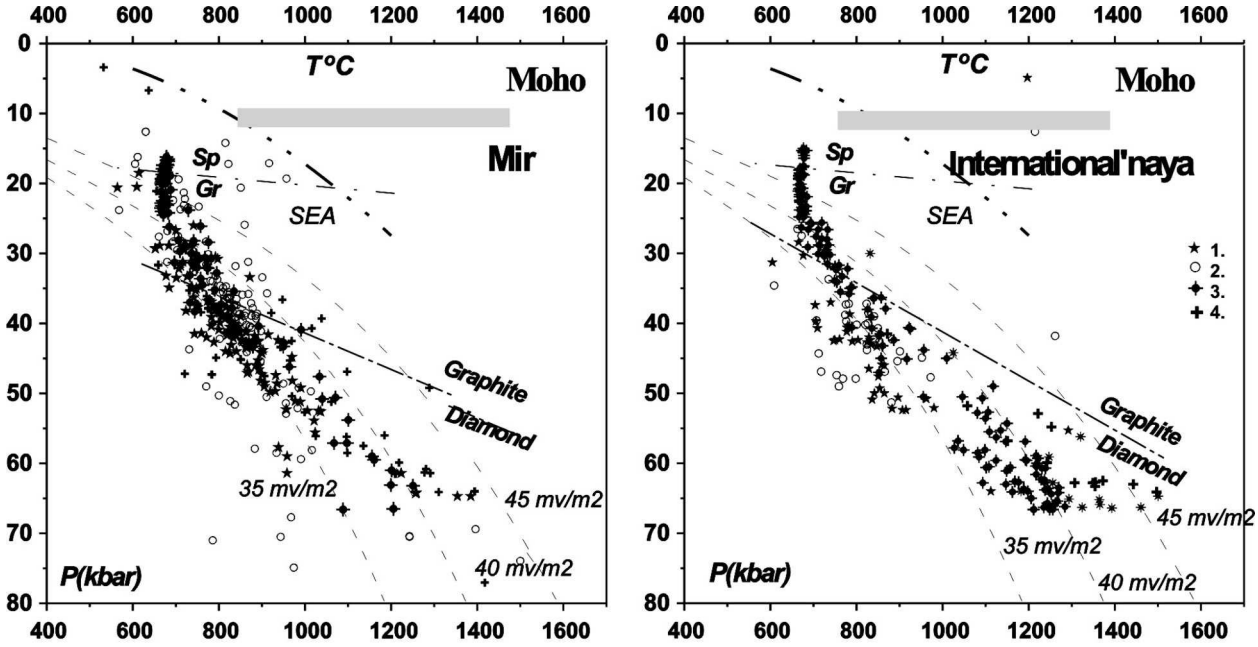

Fig. 4. **P-T diagrams for the Mir and International'naya pipes.**

Using: 1 - [4] method for garnets, 2 - [6], [17] methods, and 3 - [17] method for clinopyroxenes. T variations of the clinopyroxene compositions from Mir and International'naya pipes.

THERMOBAROMETRY

For the thermobarometry only two variant of the clinopyroxenes thermobarometry [5, 6, 23] and garnet thermobarometry [4, 28] were used. For the garnet – clinopyroxenes associations the combinations of Krogh thermometer [18] with the single pyroxene or garnet barometry were also taken. The comparison for the available from literature data for the complete lherzolite associations [20-25] reveal very good coincidence of the diagrams for the Mir pipe (Fig. 4) in general [1, 9, 20, 25] the constructed TP diagrams are rather similar for this pipes except of the lack of the abundant clinopyroxene's estimates for International'naya pipe. The geotherm in the 30-50 kbar intervals for Mir pipe is close to the 35 mv/m^2 gently rising to 65 kbar to 45 mv /m^2 . The 55—65 kbar interval is composed from the clinopyroxenes- free associations while in the middle part especially form 35 to

45 kbar the lherzolitic and Cr- diopside websterite associations very often with the phlogopite are abundant. They again became are in 30-20 kbar. Garnet geotherm for Mir pipe practically coincides with the clinopyroxenes- based giving in the branch in the deeper part very close to the geotherms typical for the South Africa [10-12, 38], Brasilia and some other cratons that derived from Gondwana. The estimates calculated from some garnet-Cpx intergrowths give the values correspondent to the asthenospheric peridotites [24, 31, 32]. For the International'naya pipe the geotherm reveal a bit less heated conditions in middle part giving the high scattering in deep part. The amount of the deep seated garnets Cr- rich garnets are much higher then for Mir pipe [9, 20, 25]. Partly this may be explained by the highly alkaline compositions of the clinopyroxenes that often bring to the lower temperatures that the estimates based on the Cpx- garnet thermobarometry [5, 18] and [4, 18] that produced the estimates > 1500^{o}C at the lower part of the section. Calculations of combinations with garnet barometry [4] and clinopyroxenes barometry [4, 5] produce practically the same results. The more heated then for Mir associations are developed in the 50-65 kbar interval of pressure. Pyroxene rich associations partly compile only 30-55 kbar interval.

The mantle layering. Using the dependence of the FeCpx, AlCpx and FeGar, CaGar from the pressure in the diagrams the mantle layering and the modal mineral compositions of the peridotites and other rock may be suggested (Fig. 5). For both pipes the 7 horizons – sequence is determined in the 65-12 kbar interval though the compositions of the layer are a different. For Internernational'naya the two horizons at the 65-55 kbar are composed from rare lherzolites and harzburgites with the some addition of the Ca- rich pyroxenites. Only few clinopyroxenes refer to the sheared peridotites. In the basement of the Mir mantle sequence the similar garnets referring to the harzburgites are determined but here lherzolitic pyroxenes as well as those close to Fe- enriched sheared varieties are developed. The thick horizon 45-56 kbar of both pipes are very similar in the compositions. It is compiled essentially from the pyroxenites and likely eclogites with addition of the garnet rich pyroxenites and harzburgites for International'naya pipe. Garnet lherzolites and Cr-diopside pyroxenites are most frequent in the 45-38 kbar interval that are close in modal compositions also for this pipes though for the Mir pipe the scattering for garnet composition is higher corresponding to the lherzolites and pyroxenites. For the International'naya the garnets are mainly of harzburgitic affinity. The next 38-28 kbar interval for Mir refer to the rapid rise of Al content in the clinopyroxenes for the International'naya it corresponds to the CaO decrease showing quite opposite tendencies of the enrichment to the top of he horizon in Mir pipe and general depletion for the International'naya. Nevertheless in mantle column the upper associations are essentially clinopyroxenitic. The garnet spinel facie 28-22 kbar for the Mir pipe refer to the motley compositions and mixed pyroxenite – lherzolite associations. For the International'naya it is represented by slightly depleted lherzolites. Different types of pyroxenites trace the spinel facie in Mir mantle sequence while in Internetional'naya the two main populations of the

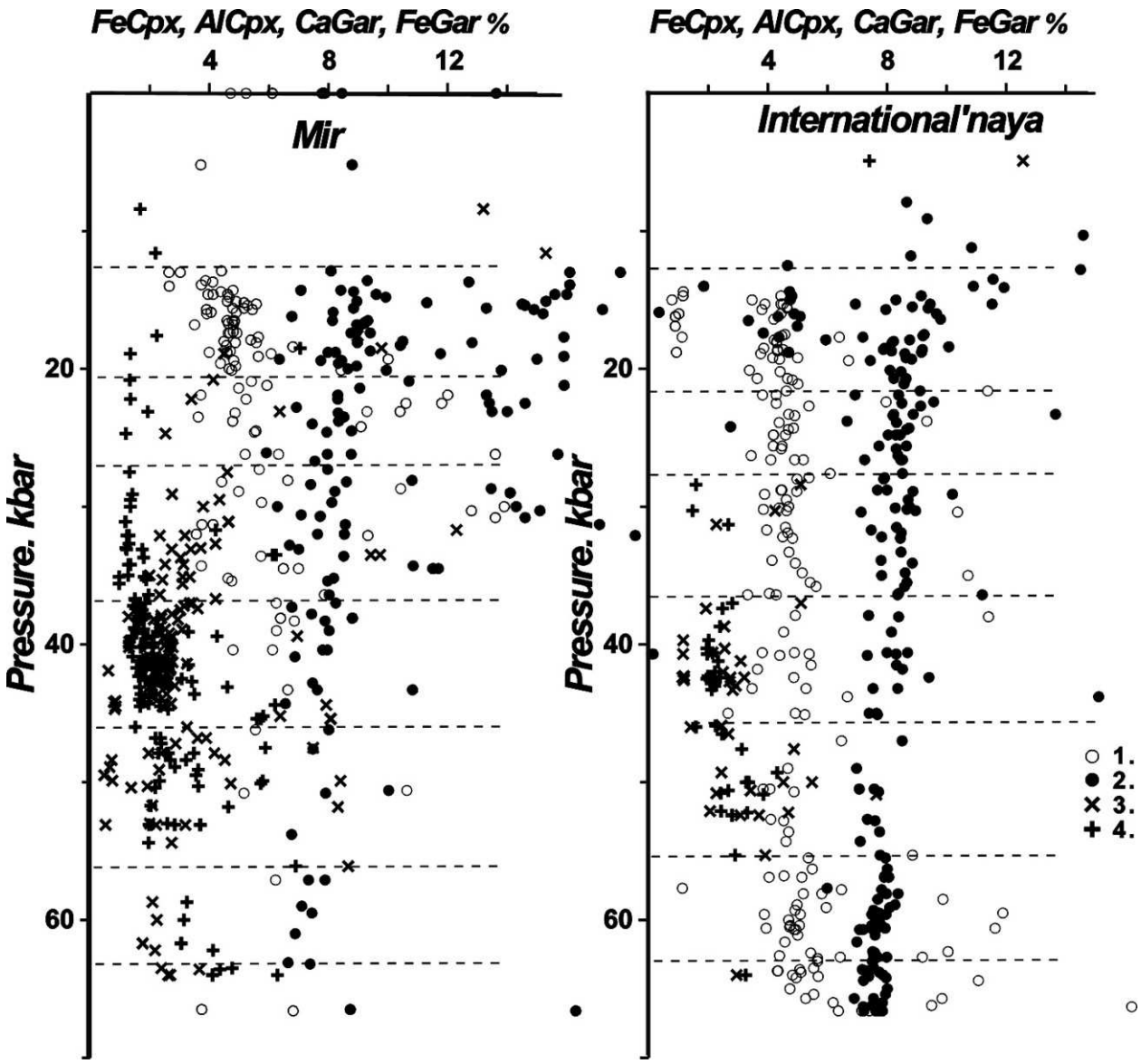

Fig. 5. **Reconstructions of the mantle layering for the four pipes.**

Using the variations of the 1 - CaO in garnet from the pressure determined using [4], equation (3); 2 - FeO in garnet from the pressure determined using [4], equation (3); 3 - FeO in clinopyroxenes from the pressure determined using [5]; and 4 - Al_2O_3 in clinopyroxenes from the pressure determined using [5].

pyroxenites with the Hi- Mg and temperate Fe- enriched compositions rising upward are determined.

TRACE ELEMENTS FOR THE MINERALS

The LAM ICP MS analyses for 40 components characterize mainly the peridotitic minerals from two pipes. Clinopyroxenes from Mir (Fig. 6) reveal trace element patterns differing in HREE content and configuration of the spectrums. For the lherzolitic assemblages the melting degree that negatively correlates with the La/Yb_n ratio and positively with general of the TRE are rising upward in the mantle section. It reflects also the decreasing of the Cpx/Gar with the depth. The

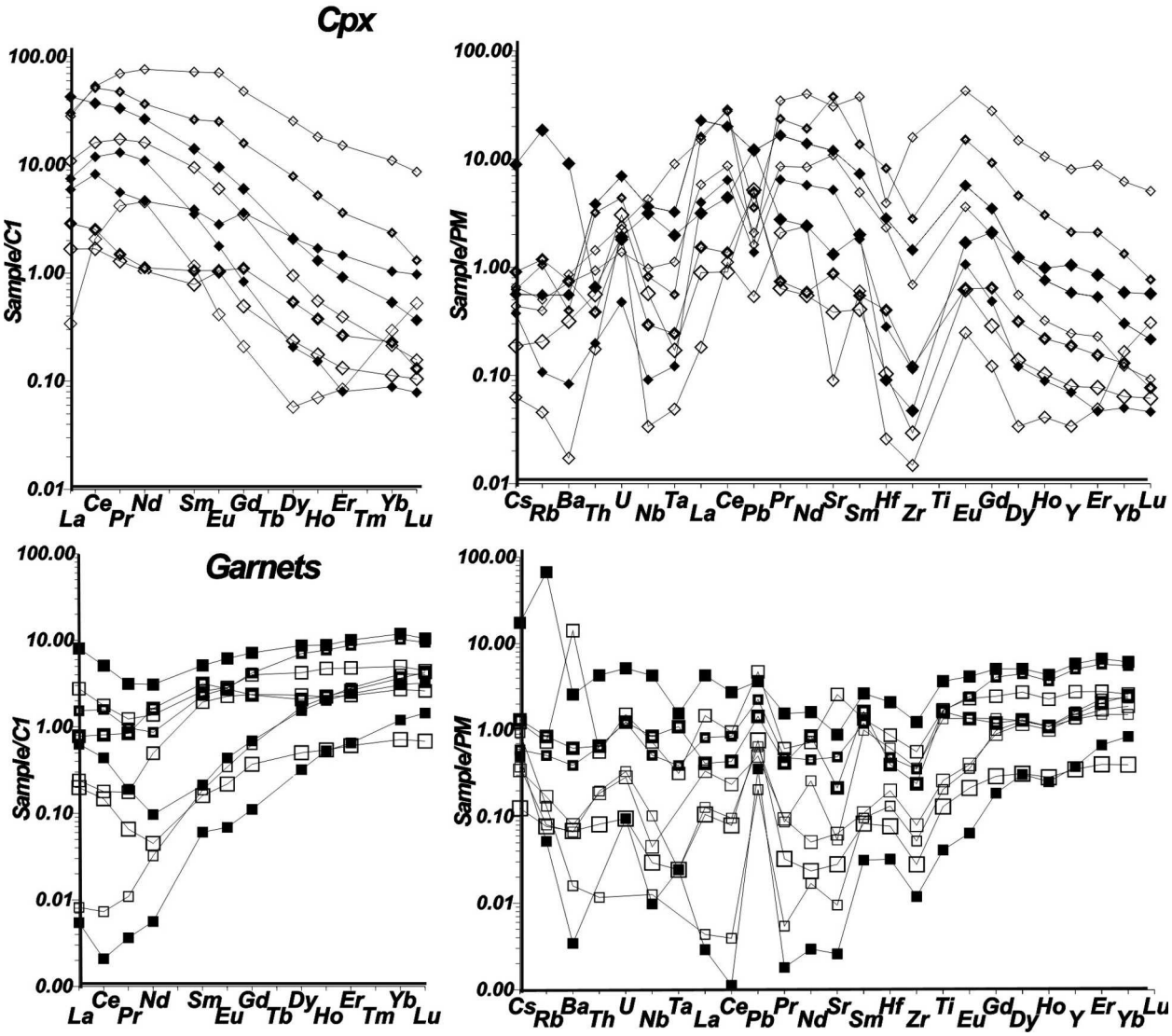

Fig. 6. **REE and TRE diagrams for the minerals from the peridotite xenoliths of Mir pipe.**

shape of the lherzolitic REE patterns for clinopyroxenes is simple and smoothed for the upper and middle part o the mantle column while for the pyroxenitic assemblages the level is varying and the shape is more inflected. The deeper clinopyroxenes demonstrate partly S shaped patterns as well as the garnets. The two folded patterns are also found at the middle part in the pyroxenite lens. The U maximum is typical for the pyroxenes with the low TRE content. The Zr/Hf ratio negatively correlates with the depth of the depression for these elements which became more pronounced for the deeper depleted Cpx's as well as the Pb peak. For the enriched composition Pb dip possibly suggest the additional differentiation of the intergranular melts. One Cr-diopside composition demonstrates small Eu depression enrichment in the LILE and Ce peak with the nearly strait REE line. For the garnets the LREE rise starting from Nd is typical. The garnets with the high REE content reveal nearly flat patterns while for the depleted varieties the La/Yb_n ratio rapidly fall down.

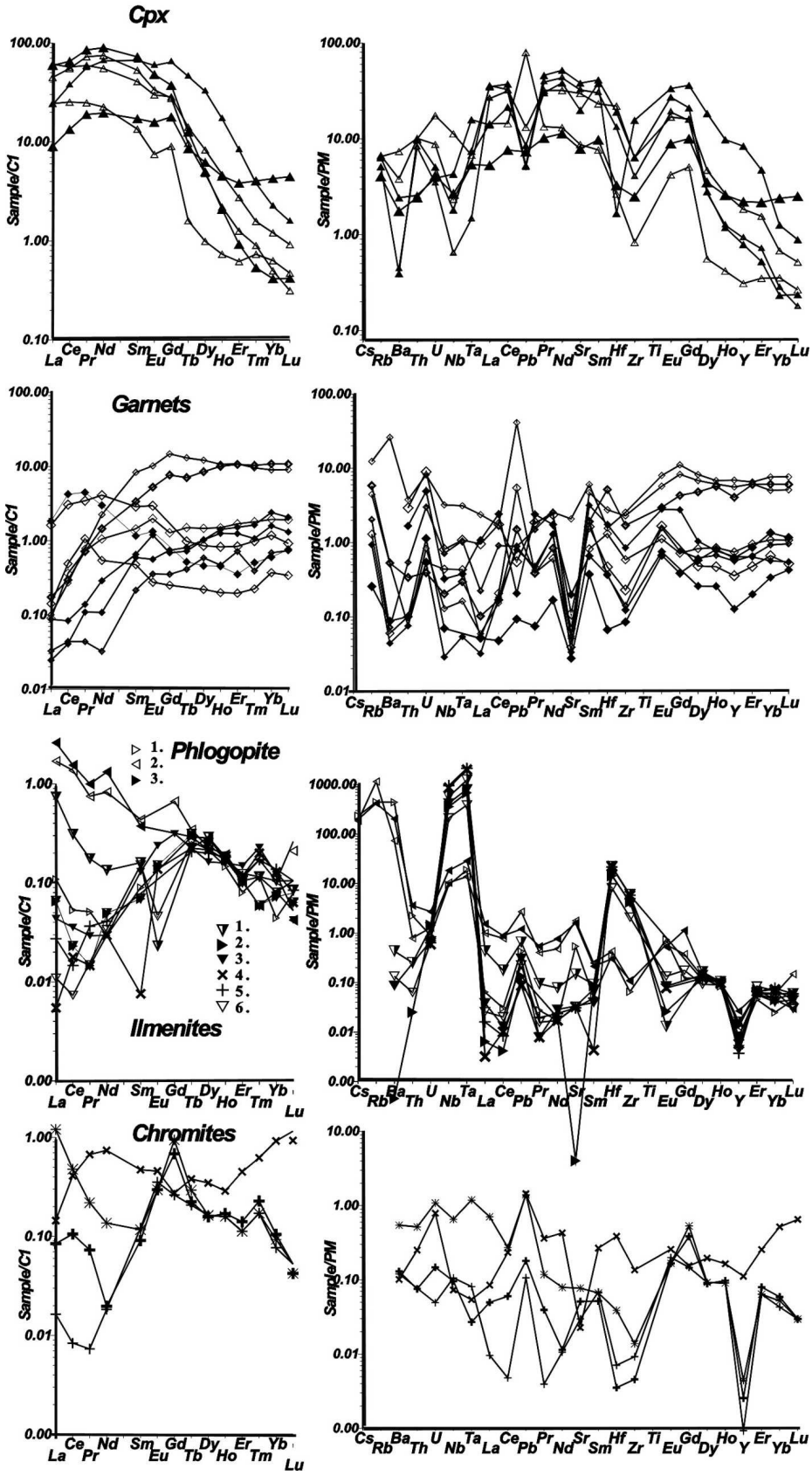

Fig. 7. **REE and TRE diagrams for the minerals from the concentrate for International'naya pipe.**

The numbers are given for separate grains of each mineral.

LREE enrichment is more pronounced for the compositions with inflected folded REE distribution curves and is lower for the deep depleted garnets. Pb* rises for the depleted compositions as well as the depth of Zr dips. The Ba peak was determined for one enriched composition found for one garnets while the others show Ba minima and U weak peaks typical fro the depleted varieties.

Clinopyroxenes from the International'naya (Fig. 7) show close conformed asymmetric hampered patterns. All of them demonstrate small Eu minima suggesting hybrid origin with the eclogite remelting. The HFSE (Nd, Zr) depression and Ta/Nb and Hf/Zr ration became higher for the less enriched clinopyroxenes. All except one demonstrate Pb depressions and small U peaks. Garnets from the International'naya show typical rounded patterns for the Hi-in-REE compositions. Three garnet patterns with S- type reveal the LREE enrichment; all garnets have strong U peaks and Sr minima. Pb peaks are found for more enriched varieties. The REE for the ilmenites are bell – like in shape. Two of six patterns show strong Eu minimums, all of the reveal Y depressing which became deeper with the rising REE and Pb peaks Zr-Hf Ta- Nb peaks are rising together with the REE Dark micas xenocrysts reveal the patterns very close to the ilmenites with the same peaks suggesting close origin differing only in the high LILE content. The chromites are quite different in the REE patterns. Three of them demonstrate the Eu peaks and one depression. The LREE enrichment is also typical. In general the shape is close to those of the ilmenites what also evidences about the origin according to the AFC process as for Yubileynaya pipe [2]. In spiderdiagram they also reveal the Y dips and Zr, Hf depressions. No serious evidence for the carbonatitic melt reactions were found for minerals from these pipes [26].

DIAMOND TRE GEOCHEMISTRY

Direct measurements with the LAM ICP MS method allowed determining the compositions for the several garnets from International'naya and Mir pipes. For the former rather low REE content ~0.1 relative to C1 (Fig. 8). Small Eu positive and negative anomalies suggest the eclogitic type of origin. In TRE pattern the elevated Zr-Hf and Ba, Sr, Pb peaks suggest the continental mantle origin with the subduction related component. The Y depression deepings with the rise of the REE content suggests the mechanism of the diamond TRE signatures. Such and Y anomaly was determined only for the ilmenites and chromites from the International'nya pipe and may be explained only by the fractionating AFC processes. Thus the most likely the diamond's TRE are produced during the interaction of the protokimberlitic melts in the contact zones around the feeding system but dominantly in the primary eclogitic layers.

For the diamonds from Mir pipe the similar signatures were found for few crystals in general the LILE enrichment is a bit lower Zr-Hf content is higher the Y anomaly is visible but it correlates with Nb dips. U peaks exist. The formation in peridotite and pyroxenites due to lack of Eu anomalies is more realistic. The

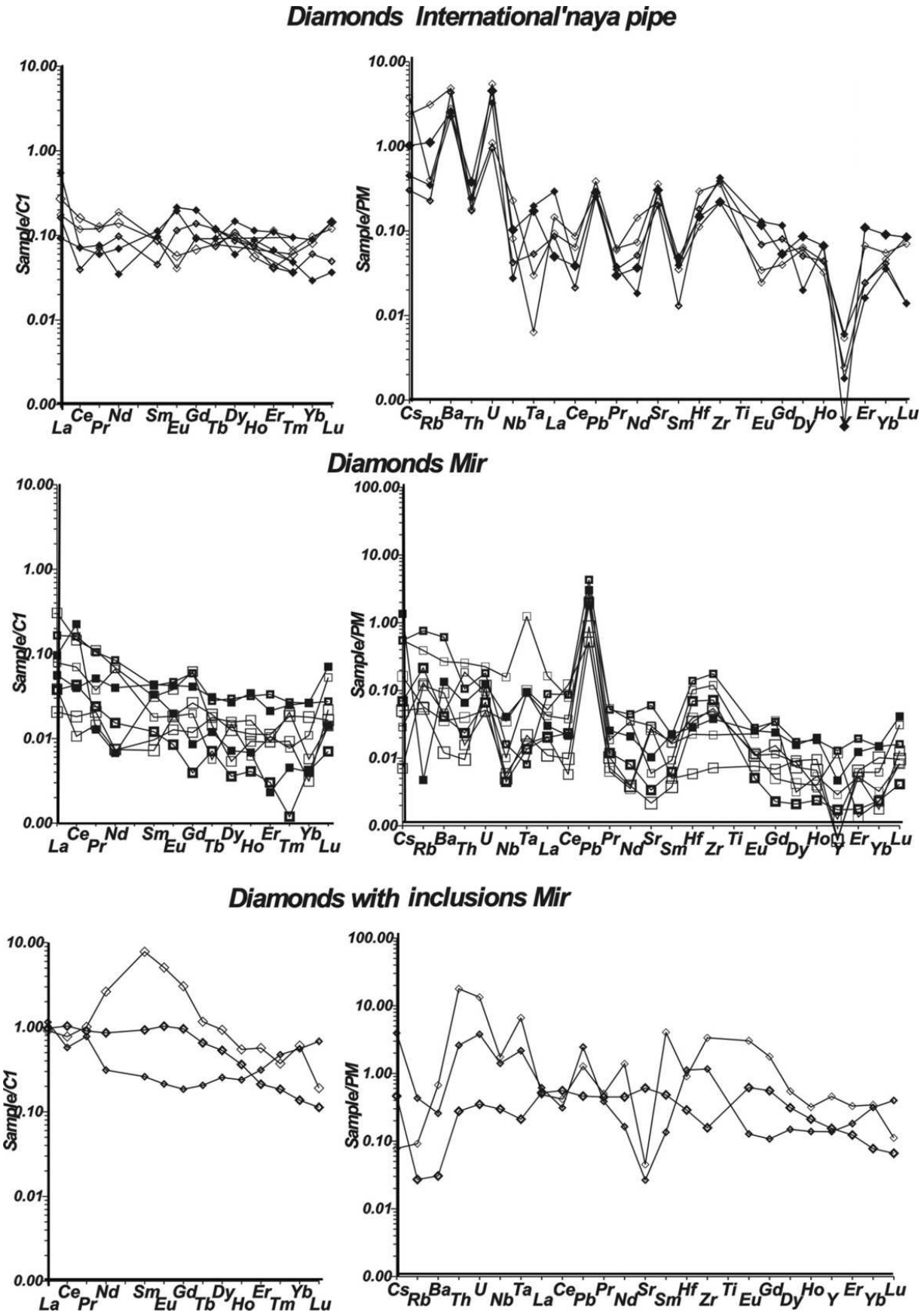

Fig. 8. **REE and TRE diagrams for the diamonds from Mir and International'naya pipes.**

The numbers are given for separate grains of each mineral.

reactions of the carbonatitic [25] or kimberlitic melts with peridotites or pyroxenites are also suggested.

All the feature of the trace elements well agrees to the data from mineral inclusions [31-36].

DISCUSSION

Despite on the difference in the mineralogical and some TRE features the general structure of mantle column for the International'naya and Mir pipe are very close. These may be explained by the lateral variations of the layers coupling with the mantle keel which are represented by the more depleted composition for the International'naya with the high amount o the eclogites

The trace element compositions and general mineral chemistry as well as the enriched character of the peridotites for the Mir reveal the features close to the continental mantle in the marginal facie The high LILE content and the enriched U, Th means the involving the continental crust material in the mantle melting what may be explained by the A- subduction. The International'naya mantle is closer t the continental arc environment also with the participation of the continental crust. The subduction type anomalies of Eu, Ce, LREE and LILE in the typical mantle peridotite minerals such as chromites Cr – diopsides and megacrysts of the ilmenites suggest that the passage of the subduction related melts cut through the entire mantle column. The Eu anomalies in the ilmenite show that crust material took place in the protokimberlite melt generation. Some crust signatures of the diamond may be also due to the passage of the hybrid melts in mantle column though the direct reaction around the feeding system is more realistic. High eclogitic content in the mantle column for the Malo-Botuobinsky region corresponds to the higher La/Yb_n ratios for the kimberlite melts in this region comparing to the other parts of Siberian craton. The difference in geochemistry for deeper and upper parts of the Mir and International'naya pipes suggest that the continental mantle material was joining mainly to the middle part of the mantle columns but deeper the more depleted material possibly of back arc or intra continental basing was coupled.

CONCLUSIONS

1. The mantle columns of the Mir and International'naya pipes are close but with the different major and trace compositions of the minerals as well as modal mantle rock composition.
2. Mir mantle column is essentially lherzolitic mantle with eclogites for the continental crust signatures while for the International'naya the continental arc or intracontinental basing mantle compositions with the is more realistic model.
3. Subducted material was participated in the generation of the mantle peridotite trace element and kimberlite signatures.

4. Diamonds from International'naya and Mir pipes are often reveal the eclogitic affinity in TRE. They were created in the contact system of the rising protokimberlite melts.

To the stuffs for the EPMA and ICPMS Laboratories of UIGGM SB RAS. Supported by RFBR grants 99-05-65688, 03-05-64146, and integration projects of SB RAS № 67 and RAS № 6-2-1.

REFERENCES

1. **Ashchepkov, I, Vladykin, N., Pokhilenko, N., Sobolev, N., et al.** (2003). Clinopyroxene geotherms for the mantle columns beneath kimberlite pipes from Siberian craton. //Extended Abstracts of the 8 International Kimberlite Conference..
2. **Ashchepkov, I. V., Vladykin, N. V., Nikolaeva, I. V., et al.** (2004). Mineralogy and Geochemistry of Mantle Inclusions and Mantle Column Structure of the Yubileinaya Kimberlite Pipe, Alakit Field, Yakutia. Doklady Earth Sciences, Vol. 395A, No. 3, pp. 378–384.
3. **Ashchepkov, I. V., Pokhilenko, N.P., Vladykin, N. V., et al.** (2003). Pyroxene geotherms and stratification of the mantle beneath the kimberlite pipes of the Siberian platform: reconstructions and the relation to diamond potention // Problems of prediction, prospection and investigation of the deposits of of the ore and mineral resources at the boundary of XXI century. Voronezh.. Voronezh State University.. pp. 352 – 355. (in Russian)
4. **Ashchepkov, I.V.** (2003). Empirical garnet thermobarometer for mantle peridotites. Seattle Annual Meeting Abstract ID: 65507.
5. **Ashchepkov, I.V.** Jd-Di barometer for mantle peridotites and eclogites // Experiment in Geosciences. v.10, N1, pp. 137-138.
6. **Ashchepkov, I.V.** (2003). More precise equation of the Jd-Di Barometr. Herald f of the Earth department RAS. N1. pp.45-46.
7. **Ashchepkov, I.V., Vladykin, N.V., Saprykin, A.I., Khmelnikova, O.S.** (2001). Composition a thermal structure of the mantle in peripheral parts of the ancient shields within Siberian craton. // Revista Brasileira de Geociencias. 31 (4), pp.527-636.
8. **Baroshinsky, Z.V., Kharkiv, A.D., Botkunov, A.L., Sobolev, N.V.** (1973). New data on diamonds from the eclogites of the Mir pipe // Geol. Geofiz. 14 (5), pp. 108–112. (in Russian)
9. **Beard, B.L., Fraracci, K.N., Taylor, L.A., et al.** (1988). Chemical differentiation of the earth: the relationship between mantle, continental crust, and oceanic crust // Earth Planet Sci Lett 90. pp. 297 –314
10. **Boyd, F.R., Finnerty, A.A.** (19800. Conditions of origin of natural diamonds of peridotite affinity. //J. Geophys. Res. v. 85, pp. 6911-6918.
11. **Boyd, F.R., Pearson, D.G., Nixon, P.H., Mertzman, S.A.** (1993). Low-calcium garnet harzburgites from southern Africa: their relations to craton structure and diamond crystallization // Contrib. Mineral. Petrol., V.113, pp. 352-366
12. Burgess, S.R., Harte, B. (1999). Tracing lithosphere evolution through the analysis of heterogeneous G9/G10 garnets in peridotite xenoliths, I: Major element chemistry // The J.B.Dawson volume,The VIIth Int.Kimb.Conf. Proc., pp. 66 -80.
13. **Griffin, W. L., Fisher, N. I., Friedman, J. H., O'Reilly, S. Y., Ryan, C. G.** (2002). Cr-pyrope garnets in the lithospheric mantle, 2. Compositional populations and their distribution in time and space // Geochem. Geophys. Geosyst., 3(12), 35 p.
14. **Griffin, W.L., Moore, R.O., Ryan, C.G., Gurney, J.J., Win, T.T.** (1997). Geochemistry of magnesian ilmenite megacrysts from Southern African kimberlites // Russian Geol. Geophys. v.38 (2). pp. 398-419

15. **Jacob, D., Jagoutz, E., Lowry, D., Mattey, D., Kudrjavtseva, G.** (1994). Diamondiferous eclogites from Siberia:remnants of Archean oceanic crust //Geochim Cosmochim Acta. V. 58. pp. 5191 –5207
16. **Khar'kiv, A.D., Zinchuk, N.N., Kr'ychkov, A.I.** (1998). // Primary deposits of the diamonds in the World. Moscow. Nedra. 545p.
17. **Krogh, E.J.** (1988). The garnet-clinopyroxene Fe-Mg geothermometer – a reinter-pretation of existing experimental data // Contrib. Mineral. Petrol., v. 99, pp. 44–48
18. **Kudryvtzeva, G.I., Bovkun, A.V., Garanin, V.K., Cherny, S.D.** (2003). Typomorphic features of the ilmenites from the kimberlites of the Malo - Botuobinsky field (Yuakutian diamond province // Problems of prediction, prospection and investigation of the deposits of of the ore and mineral resources at the boundary of XXI century. Voronezh, Voronezh State University. pp. 322 – 328. (in Russian)
19. **Kuligin, S.S., Pokhilenko, N.P.** (1998). Mineralogy of xenoliths of garnet pyroxenites from kimberlite pipes of Siberian platform // Extended Abstracts 7IKC. Cape Town. pp. 480-482.
20. **Laz'ko, E.E., Roden, M. F.** (2003). Garnet peridotites and pyroxenites in the subcontinental lithosphere of the central part of Sierian craton (xenoliths from the Mir pipe) Problems of prediction, prospection and investigation of the deposits of of the ore and mineral resources at the boundary of XXI century. Voronezh, Voronezh State University. pp. 307 – 317 (in Russian)
21. **Mitchell, R.H.** (1995). Kimberlites, orangeites and related rocks. New York: Plenum, 500 p.
22. Moor, R.O., Griffin, W.L. Gurney, et al. (1992). Trace element geochemistry of ilme-nites megacrysts from the Monastery kimberlite, S. Africa // Lithos. v. 29, pp. 1-18.
23. **Nimis, P., Taylor, W.** (2000). Single clinopyroxene thermobarometry for garnet peridotites. Part I. Calibration and testing of a Cr-in-Cpx barometer and an enstatite-in-Cpx thermometer // Contrib. Mineral. Petrol. V. 139. N 5. pp. 541-554.
24. **Nixon, P.H., Boyd, F.R.** (1973). Petrogenesis of the granular and sheared ultrabasic nodule suite in kimberlites // In: Lesotho Kimberlites (P.H. Nixon, ed.). Lesotho National Development Corporation, Maseru, Lesotho, pp. 48-56.
25. **Rege, S., Davies, R.M., Griffin, W.L., Jackson, S., O'Reilly, S.Y.** (2003). Trace element analysis of diamond by LAM ICP MS: preliminary results Extended Abstracts of the 8 International Kimberlite Conference.
26. **Roden, M.F., Laz'ko, E.E., Ponomarenko, A.I., Serenko, V.P.** (1995). Mineralogy of peridotite xenoliths from the Mir kimberlite, Yakutia, Russia. 5IKC Extended Abstracts. Novosibirsk, pp. 462-464.
27. **Rudnick, G., McDonough, W.F., Chappell, B.W.** (1993). Carbonatite metasomatism in the northern Tanzanian mantle // Earth Planet. Sci. Lett. V. 114. pp. 463-475.
28. **Ryan, C. G., Griffin, W. L., Pearson, N. J.** (1996). Garnet geotherms: Pressure-temperature data from Cr-pyrope garnet xenocrysts in volcanic rocks // J. Geophys. Res. B. V. 101. N 3. pp. 5611-5625.
29. **Smith, D., Boyd, F.R.** (1987). Compositional heterogeneities in a high-temperature lherzolite nodule and implications for mantle processes. In: Nixon, P.H. (Ed.), Mantle Xenoliths. Wiley, New York, pp. 551–561.
30. **Smith, D., Griffin, W.L., Ryan, C.G.** (1993). Compositional evolution of high-temperature sheared lherzolite PHN 1611. Geochim. Cosmochim. Acta 57, pp. 605–613.
31. **Sobolev, N.V., Snyder, G.A., Taylor, L.A., et al.** (1998) . Extreme chemical diver-sity in the mantle during eclogitic diamond formation: evidence from 35 garnet and 5 pyroxene inclusions in a single diamond. Int Geol Rev 40. pp. 567 –578.
32. **Sobolev, N.V.** (1977). Deep-Seated Inclusions in Kimberlites and the Problem of the Composition of the Upper Mantle // Am. Geophys. Union, Washington, D.C. 279 p.

33. **Spetsius, Z.V., Bulanova, G.P., Griffin, W.L.** (1992). Eclogite containing diamond with a garnet inclusion from the Mir pipe // Dokl. Ross.Akad. Nauk, v.332, pp. 134–137.
34. **Spetsius, Z.V.** (1990). The diamond-bearing xenolith of garnet peridotite from the Mir kimberlite pipe // Dokl. Akad. Nauk SSSR, v. 313. pp. 939-943
35. **Spetsius, Z.V.** (1995). Occurrence of diamond in the mantle: A case study from the Siberian Platform. In: W.L. Griffin (Editor), Diamond Exploration: Into the 21st Century. J. Geochem. Explor., v. 53. pp. 25-39.
36. **Spetsius, Z.V., Serenco, V.P.** (1990). Composition of Continental Upper Mantle, Lower Crust Beneath the Siberian Platform // Nauka, Moscow, 1990. 272 p. (in Russian).
37. **Taylor, L.A., Gregory, A., Snyder, A. et al.** (2001). Petrogenesis of group A eclogites and websterites: evidence from the Obnazhennaya kimberlite, Yakutia // Contrib Mineral Petrol., v.145, pp. 424-443.
38. **Van Achterberg, E., Griffin, W.L., Steinfenhofer, J.** (2001). Metasomatism in mantle xenoliths from Letlhakane kimberlites estimation of element fluxes // Contrib. Mineral. Petrol.. v. 141, pp. 397-414

UDK 552.11.548.4

Liquid carbonate-carbonate-salt immiscibility and origin of calciocarbonatites

Panina L.I., Usol'tseva L.M.

Institute of Mineralogy and Petrography, Novosibirsk, Russia,
e-mail: Panina@uiggm.nsc.ru

Primary silicate-salt, carbonate-salt and salt inclusions have been studied in the minerals of the melilite and monticellite rocks of the Krestovskaya intrusion. They helped us to document the moment of separation of carbonate melts from parental silicate magma and for the first time to characterize all the stages of their evolution up to the final stages of occurrence and crystallization of Ca-rich (calcite) rocks. Silicate-salt inclusions present in perovskite-I of the plutonic melilite rocks are characterized by silicate-carbonate liquid immiscibility at 1230-1250^{o}C. This was manifested as separation of carbonate-salt globules in silicate (alkali-basic) melt. The chemical composition of these globules was hyperalkali-carbonate (wt.%): 14-24 CaO, 17-22 alkalies, from 2 to 3-5 SiO_2, FeO, MgO, P_2O_5, SO_3, and 0.2-0.3 SrO, BaO, Cl. This composition, undoubtedly, reflects the composition of initial carbonatite melts equilibrated with silicate parental magma. In silicate-salt inclusions contained in perovskite II, along with silicate-carbonate immiscibility at 1200-1190^{o}C, additionally, carbonate-salt liquid immiscibility occurred which caused separation of carbonate-salt melt into immiscible portions of various compositions. Primary silicate, carbonate, carbonate-salt and salt inclusions in melilite and monticellite of studied rocks are the result of spatial separation of immiscible silicate-carbonate-salt portions. The inclusions in chemical composition are identical (or close) to the fractions in immiscible silicate-salt inclusions or to those having simpler composition compared with them. Among carbonate-salt and salt inclusions in these minerals we found inclusions of initial hyperalkaline carbonate melts, alkali-Ca-rich carbonate melts, alkali-sulfate, alkali-phosphate, alkali-chloride, and calciocarbonate melts. The later melts appeared at the final stages of evolution and were the latest residual fraction of initial carbonate melt. The conclusions is made that the occurrence of such processes in macroconditions at appropriate saturation of initial carbonatite magma in Na, K, F, Cl, S, and P could result to occurrence of various types of carbonatites – alkali-sulfate, alkali-phosphate, alkali-chloride, and the most abundant, calcite.

INTRODUCTION

Most researchers believe that carbonatites are igneous rocks but many problems of their genesis have not been solved yet: for example, the initial composition of carbonatite melts; mechanism and PT-parameters of their generation and crystallization; reasons for the enrichment of effusive carbonatites in alkalies and lack of the latter in plutonic rocks; reasons for the enrichment of some carbonatites in S, F, P, Cl, etc. Studies of melt inclusions in minerals of various rocks from the alkali-ultrabasic Krestovskaya intrusion (Polar Siberia) helped us to solve some of these questions. For the first time we were able to trace

the evolution of carbonate melts from the moment of their isolation from parental silicate magma and their further separation up to the final crystallization stage of calcitic fractions.

BRIEF GEOLOGICAL DESCRIPTION OF THE KRESTOVSKAYA INTRUSION

The Krestovskaya intrusion is located in the Maimecha-Kotui province of alkali-ultrabasic carbonatite rocks [7] in the zone of the immediate contact of the Yenisei-Khatanga accumulative plain and Middle-Siberian Plateau. The intrusion occupies the central part of a volcano-plutonic structure and is a layered body of ultramafic rocks consisting of alternating thick (a few tens of meters) layers of olivinites, wehrlites, and clinopyroxenites. The root part of this body is located at the depth of more than 4.5-5 km from the day surface [33]. In the west and east of the massif in the marginal zones of the layered series of ultrabasic rocks one can observe the layer injections of melilite and associated monticellite rocks. According to isotope-geochemical studies [33], the age of the ultrabasic rocks is 250 Ma.

Host rocks are represented by subalkali basalts and melanonephelinites of the Nizhne-Tyvakanskaya Suite. They are hornfelzed in the contact aureole and phlogopitized in some parts. The intrusion and enclosing effusive series contain dikes of dolerites, nephelinite and melilite lamprophires, alkaline picrites, and calciocarbonatites. They are most widespread in the endo- and exocontact zones of the intrusion and in the places where rocks of different mineral compositions make contacts. The dikes group into swarms and belts to 70 m in thickness, extending through the massif at a distance 100-120 m from each other. In the center of the intrusions the dikes form an arching bend parallel to the southern contact of the massif. The only dike of calciocarbonatites was exposed by a borehole at a depth of 15 m in the northwest of the massif among olivine-monticellite-melilite rocks. It is rather thin (30 cm). Its mineral composition, in addition to prevailing calcite, involves to 3-5 vol.% magnetite and less than 1 vol.% perovskite and phlogopite. Mafic minerals are segregated into separate subparallel alternating bands responsible for the taxitic structure of the rock.

The composition of volcano-plutonic rocks from the Krestovskaya intrusion and chemistry of their minerals are discussed in detail by Sazonov et al. [33], Pridannikov et al. [29], Legezina [16], and Panina et al. [25].

METHODS OF STUDIES OF MELT AND FLUID INCLUSIONS IN MINERALS

To heat inclusions in minerals and to determine their homogenization temperatures, we used a high-temperature heating stage with a contact heater. The heating stage was equipped with a microscope [20]. This allowed us to observe all the processes occurring in inclusions from the moment of heating to homogenization

of their content. The heating stage was calibrated by the melting points of chemically pure salts and noble metals. The accurracy of temperature measurements was ±10-15°C.

The chemical composition of inclusions and minerals was determined on a "Camebax"-electron microprobe of the United Institute of Geology, Geophysics and Mineralogy, Siberian Branch of the RAS, Novosibirsk. International standards of minerals and glasses were used. The analysis was conducted with accelerating voltage of 20 kV, beam current of 40 nA, counting time of 10 sec, and a 2-3 μm spot beam. The accuracy of analysis was 1-1.5 wt.%. Salt fine-crystallized inclusions were analyzed by scanning the surface with a focused beam. To determine the composition of silicate and carbonate-salt components in inclusions indicating liquid immiscibility, we heated inclusions only to temperatures of complete melting of contained silicate and salt crystal phases and further immiscibility of melt, and after that they were quenched. The most serious difficulties occurred during preparation of heated salt and, especially, silicate-salt inclusions for analysis, as their salt microcrystalline quenched aggregate often decomposed during opening. Some difficulties arose in analyzing salt globules in immiscible inclusions because of their small size and entrapment of silicate component by probe beam. Therefore, among tens of analyzed globules we could use only single, best analyses.

To determine the approximate amount of CO_2 and H_2O present in daughter minerals of salt and carbonate-salt inclusions, the chemical analyses were calculated in terms of normative composition. The calculation was based on molar ratios of components in the analysis. The following assumptions were made in the calculation: 1) All silicon is a common component of silicate minerals and, mainly, a component of host minerals of inclusions; 2) SO^{3-}, Cl^-, and PO^{4-}anions predominantly form ion pairs with alkalies and, when alkalies are lacking, with CaO; 3) excess cations bind with CO_2 (in case of the deficiency of anionic components), 4) to the balance the total to 100%, we used water which was, most likely, present in crystallization or constitution state (with sulfates, carbonates, phosphates, and silicates), less often, in a free state as thin films enveloping salts in inclusions.

To exclude possible overestimation of the amount of water in melt inclusions, the normative composition was calculated only for those inclusions for which the total of oxides was not evidently underestimated for technical reasons (owing to small sizes of inclusions, burning of salts under the electron beam, inhomogeneitie of inclusion content, etc.).

RESULTS OF STUDIES OF MELT INCLUSIONS IN MINERALS

According to previous fluid inclusion studies [25], silicate rocks of the Krestovskaya intrusion formed, the same as in most alkali-ultrabasic carbonatite plutons [24], during crystallization differentiation and fractionation of parental alkali-ultrabasic magma. Crystallization of magma started from separation of

olivine and proceeded by the following scheme: olivine → clinopyroxene → perovskite→ melilite → monticellite.

We obtained information about physicochemical conditions of generation of initial carbonatite melts and features of their evolution when studying ***carbonate, carbonate-salt,*** **and** ***silicate-salt inclusions*** in minerals of silicate rocks. Silicate-salt inclusions were found mainly in perovskite, much less often, in melilite of olivine-melilite, and monticellite-melilite rocks. These inclusions had a complex mineral composition and underwent complex phase transformations during heating. Their chemical analysis was technically difficult and had errors. Carbonate and carbonate-salt inclusions were simpler in all aspects and were more abundant than silicate-salt inclusions. Therefore, we believe that discussion of obtained results should begin with them.

CARBONATE AND CARBONATE-SALT INCLUSIONS

This inclusions are present mainly in melilite and monticellite of melilite-monticellite rocks in which they are primary. Rarely they occur as pseudo-secondary inclusions in melilite and garnet of melilitolites and apatite of olivine-monticellite rocks. In earlier minerals, olivine and clinopyroxene of clinopyroxenites and olivine-clinopyroxene rocks they occur as secondary inclusions. In chemical composition and homogenization temperatures, uniform of primary and secondary inclusions are quite comparable with each other. They are also similar in morphology. Their sizes vary from few to 20-30 μm and even to 50-60 μm. Their shape is rounded, tetrahedral and hexagonal, prismatic, partly faceted, and, occasionally, irregular. The content of inclusion is fine- or coarse-crystallized. The inclusions differ from each other mainly in chemical composition and, to a lesser degree, in melting points of salt phases and homogenization temperatures. The main components of inclusions are alkalies, Ca, P, Cl, SO_3, and CO_2. Depending of the ratios of these components and predominance of one of them, the inclusions can be divided into 6 groups (types): 1) hyperalkaline carbonate melts; 2) alkali-Ca-rich carbonate melts; 3) alkali-sulfate carbonate melts; 4) alkali-phosphate carbonate melts; 5) alkali-chloride carbonate melts; 6) calciocarbonate melts. Interestingly, a primary of carbonate and carbonate-salt inclusions with different compositions often occur in one and the same growth zones of host monticellite and melilite and coexist with microliths of phlogopite, apatite, nepheline. The inclusions consist of colorless, brownish and greenish aggregates among which one can observe smallest ore segregations and deformed gas bubbles (Fig. 1). The ratios of variously colored salt phases in different types of inclusions are differ. The rations of diverse-colored salt phases in different types of inclusions are variable: in inclusions of hyperalkali-carbonate and alkali Ca-rich melts they are equal, in calciocarbonate inclusions the colorless phases are generally dominant, in alkali-chloride inclusions the colorless and brownish salts are dominant, in alkali-phosphate inclusions the greenish salts coexist with colorless and brownish phases; alkali-sulphate inclusions contain the mixture of colorless and greenish salt phases. On heating, the first to melt (~300^{o}C) are brownish, thereafter colorless

phases, while at 510-580°C, melting of greenish salt crystals takes place. At these temperatures the gas bubble becomes spherical and easily moves in inclusions vacuole. The features and homogenization temperatures for different types of inclusions are very similar, but some differences exist.

Inclusions of hyperalkaline carbonate melts (Fig. 1-1). At about 800°C, liquid in this inclusions often separates into brownish and greenish portions. On further heating, most inclusions were in leakage. Few inclusions at 850-985°C homogenize into a salt melt.

In the chemical composition of inclusions (Table 1) alkalies either clearly predominate over Ca, or occur in approximately equal ratios with it. The total amount of alkalies varies from 20 to 32 wt.% with predominance of Na over K. The inclusions contain (in wt.%) from 7-9 to 18-30 CaO, about 1 FeO and to 2 MgO, 1-2 SrO, less than 1 BaO, to 1-3 P_2O_3, 6-8 SO_3, and 0.5 Cl.

The normative composition of inclusions is represented mainly by carbonates of alkalies (gregoryite, nyerereite, trona and natrite) and calcite (10 to 40 wt.%). It also contains alkaline sulfates (from 8 to 15 wt.% arcanite) and, occasionally, alkaline and Ca phosphates (to 10-18 wt.% nahpoite and 5 wt.% apatite). Minor amounts (to 1 wt.%) of magnetite, halite, and Mg and Ba carbonates are commonly present as well. According to calculations, the amount of bound water is 4-6 wt.% and that of bound CO_2, 26-40 wt.%.

Inclusions of alkali Ca-rich carbonate (Fig. 1-2). On 750-780°C two phases appear in some inclusions: greenish in the center and colorless around it. But on further heating, inclusions most often decrepitate. Single registered homogenization temperatures correspond to 890-975°C.

The chemical compositions of inclusions heated to 900°C (Table 2, ans. 1-13) is dominated by CaO (30-38 wt.%). They also contain from 10 to 15-18 wt.% alkalies (mainly, Na), 1-3 wt.% SrO, and 0.2-0.3 wt.% BaO. The anionic part includes aprreciable amounts of SO_3 and P_2O_5 (from 2-3 to 5 wt.% and from 1 to 2 wt.%, respectively) and to 0.1-2 wt.% Cl. The content of bound CO_2, from the calculation of normative composition of inclusions, is 33-37 wt.%, but water is absent.

According to calculations, the normative minerals are dominated by calcite (more than 50 wt.%) and alkali carbonates – nyerereite and gregoryite (to 20 wt.%). Other minerals are strontianite, magnesite, apatite, and arcanite (from 1.2-2 to 5-6 wt.%) and magnetite, halite, and sulfides (less than 2 wt.%).

We made an attempt to compare the obtained results with calculated data on unheated inclusions, which in addition to predominant (70-80 vol.%) of fine-crystallized carbonate component (Table 2, ans. 14,18) also contained large daughter phases – apatite (Table 2, ans. 15,19) and alkali chlorides (Table 2, ans. 16,20) as well as ore minerals – magnetite and djerfisherite (Fig. 1-2a). The calculated data show that the preserved inclusions contained (wt.%): 36-39 CaO, 15-16 alkalies, 1-3 SrO, 2.4-4 P_2O_5, 1-5 Cl, 0.5-1.0 SO_3 (Table 2, ans. 17,21), i. e.,

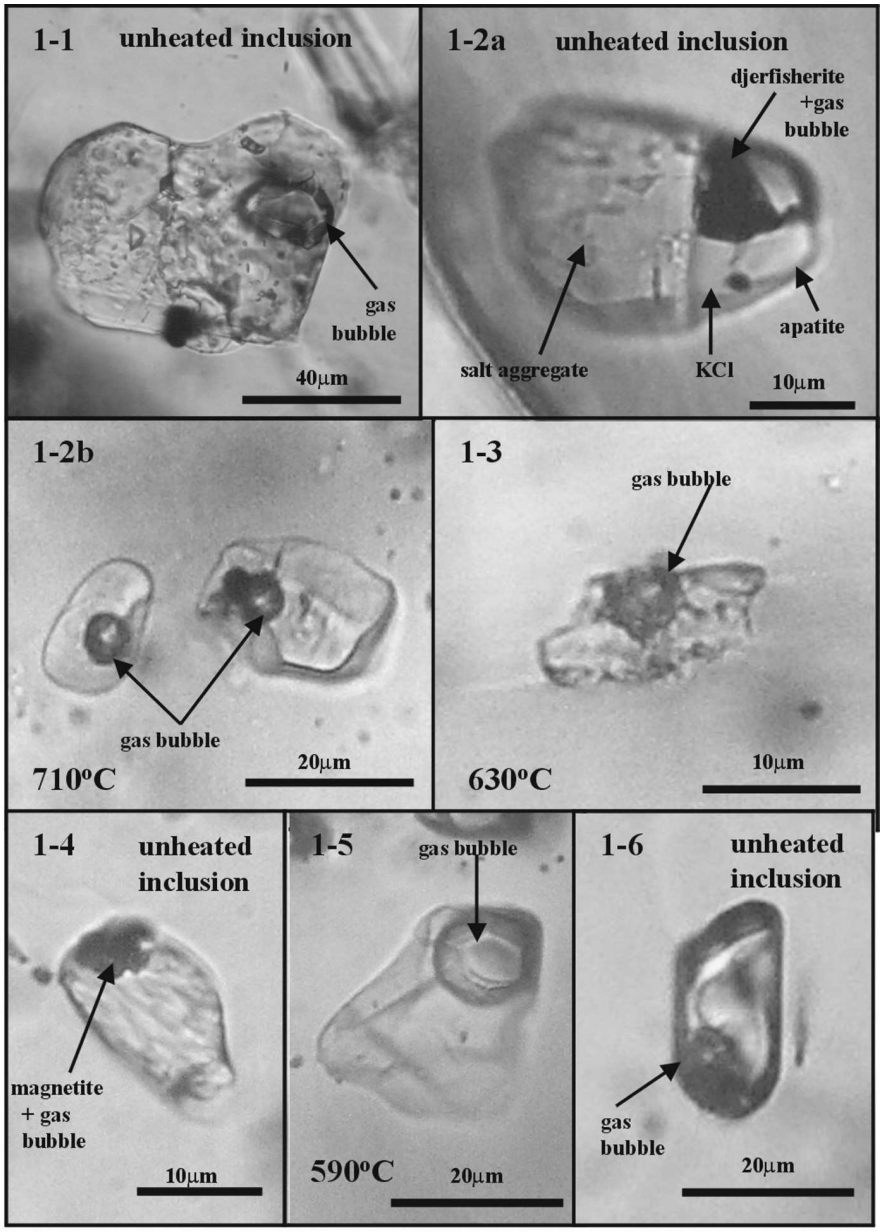

Fig. 1. **Carbonate and carbonate-salt iinclusions in minerals of rocks from the Krestovskaya intrusion.**

1-1. Unheated inclusion of hyperalkaline-carbonate melts in monticellite of olivine-monticellite rocks. Chemical analysis 15 in Table 1

1-2. Inclusions of alkali-Ca-rich-carbonate melts: a – coarse-crystallized unheated inclusions in melilite of olivine-monticellite-melilite rocks. Chemical analyses of salt aggregate, daughter apatite and daughter chloride K see in Table 2 (no 14-16). b – heated inclusions in monticellite of olivine-monticellite rocks. Chemical analysis 1 in Table 2.

1-3. Heated alkali-sulfate carbonate inclusion in monticellite of olivine-monticellite rocks. Chemical analysis 1 in Table 3

1-4. Unheated alkali-phosphate carbonate inclusion in monticellite of olivine-monticellite rocks. Chemical analysis 8 in Table 4

1-5. Heated alkali-chloride inclusion in melilite of melilitolites. Chemical analysis 7 in Table 5

1-6. Inclusion of calciocarbonate melts in clinopyroxene of clinopyroxenites. Chemical analysis 3 InTable6

Table 1.

Chemical composition of hyperalkali-carbonatite melt inclusions in minerals of rocks from the Krestovskaya intrusion (wt.%)

#	1	2	3	4	5	6	7	8	9	10	11	12	13	14	15
n	1	1	1	1	1	1	1	1	3	1	1	1	2	1	5
SiO_2	0.30	0.35	4.22	0.87	0.84	2.47	1.82	1.69	3.95	4.08	1.42	3.74	0.10	0.07	0.01
TiO_2	0.00	0.00	0.04	0.06	0.00	0.00	0.17	0.02	0.03	0.00	0.19	0.05	0.03	0.00	0.00
Al_2O_3	0.00	0.00	0.00	0.00	0.00	0.00	0.11	0.00	0.27	0.00	0.00	0.00	0.00	0.00	0.00
FeO	0.49	0.24	2.45	1.08	0.73	1.11	0.35	0.85	0.92	0.89	2.88	2.42	0.29	0.04	0.13
MgO	0.30	0.31	3.66	1.24	1.21	1.88	0.84	2.67	1.42	1.24	0.00	2.12	0.77	0.03	0.01
CaO	6.67	9.50	9.91	13.61	18.28	20.20	22.07	23.92	23.52	24.91	26.34	27.48	26.42	29.13	30.97
Na_2O	**20.20**	**16.76**	**25.09**	**18.59**	**22.67**	**14.25**	**25.65**	**18.06**	**8.69**	**13.71**	**9.24**	**18.49**	**11.50**	**13.81**	**21.87**
K_2O	**12.58**	**8.83**	**6.22**	**8.66**	**8.75**	**8.14**	**1.55**	**4.32**	**11.59**	**5.25**	**5.82**	**4.64**	**5.54**	**9.18**	**2.03**
BaO	0.46	2.16	0.57	0.39	0.57	0.42	0.00	0.06	1.30	0.22	0.31	-	0.04	0.00	0.00
SrO	0.37	0.36	1.73	1.03	2.80	1.88	1.26	2.48	0.71	0.94	1.56	1.26	1.57	0.46	0.71
P_2O_5	1.56	2.49	7.16	2.10	3.07	0.72	1.41	9.11	0.24	0.99	1.52	0.27	0.10	0.48	0.26
Cl	0.22	0.61	0.72	0.29	1.12	0.15	6.03	0.64	2.20	1.22	0.82	2.39	0.00	0.00	0.18
SO_3	3.79	7.81	8.72	6.88	7.79	8.06	4.51	5.88	6.40	4.86	6.73	3.02	1.43	0.00	0.92
Total	46.94	49.42	70.49	54.80	67.83	59.28	65.77	69.70	61.24	58.31	56.83	65.90	47.69	53.23	57.09
Less O=Cl	0.05	0.14	0.16	0.07	0.25	0.03	1.35	0.14	0.48	0.28	0.19	0.52	0.00	0.00	0.04
Total	46.89	49.28	70.33	54.73	67.58	59.25	64.42	69.56	60.76	58.03	56.64	65.38	47.69	53.23	57.05

Note. Inclusions: 9 - in melilite and 12 - in monticellite of melilitolites, 7 - in apatite , and others - in monticellite of olivine-monticellitic rocks. 13-15 - unheated, others - heated inclusions content. Registered homogenization temperatures of inclusions: 1,9 ~ 980°C, 3 – >> 770°C, 11 - 870-890°C, n – number of analyses.

#	1	2	3	4	5	6	7	8	9	10	11	12	13	14	15	16	17	18	19	20	21
n	1	1	1	1	1	1	1	1	1	2	1	1	2	1	1	1	1	1	1	1	1
SiO_2	2.70	1.22	8.22	0.63	1.41	0.20	4.91	1.29	6.50	1.24	2.43	0.81	0.63	0.23	0.65	11.10	1.88	0.08	1.32	0.16	0.13
TiO_2	0.03	0.15	0.15	0.08	0.00	0.09	0.14	0.00	0.28	0.02	0.09	0.00	0.00	0.00	0.00	0.00	0.00	0.00	0.00	0.00	0.00
Al_2O_3	0.00	0.00	0.35	0.00	0.00	0.00	0.95	0.00	1.48	0.00	0.00	0.00	0.00	0.00	0.00	0.85	0.13	0.00	0.00	0.00	0.00
FeO	0.00	0.46	1.92	1.06	0.56	0.12	0.44	0.36	1.60	0.46	0.62	0.88	0.38	0.05	0.17	0.47	8.10	0.12	0.70	0.34	2.82
MgO	4.05	1.06	1.98	3.31	1.68	0.05	3.38	1.27	3.16	1.02	2.03	1.07	1.45	0.11	0.00	2.43	0.45	0.09	0.05	0.10	0.08
CaO	25.93	29.13	30.76	31.63	32.84	2.86	32.92	33.30	33.72	35.35	35.72	36.85	37.70	44.51	52.30	11.06	35.66	40.12	51.30	0.71	39.38
Na_2O	4.02	7.95	2.38	11.63	13.09	9.23	5.84	14.33	5.92	13.61	5.64	17.11	11.51	7.11	0.47	0.60	5.42	13.20	0.37	53.58	12.33
K_2O	5.63	7.14	3.55	6.86	7.80	7.65	10.48	4.30	4.47	2.12	4.74	2.41	3.90	5.47	0.00	40.49	10.20	4.86	0.23	0.51	4.29
BaO	0.21	0.16	0.24	0.28	0.35	0.27	1.46	0.00	0.20	0.00	0.00	0.00	0.08	0.00	0.00	0.00	0.00	0.00	0.00	0.00	0.00
SrO	3.43	2.76	0.36	2.95	3.50	0.62	1.20	0.98	0.93	1.34	2.47	1.60	4.22	1.13	0.91	0.38	0.90	3.90	1.91	0.06	3.43
P_2O_5	0.61	0.56	0.09	1.51	5.35	2.19	2.82	0.75	1.49	0.76	1.82	0.85	2.66	0.81	39.95	0.00	2.73	0.21	39.72	0.34	4.05
Cl	0.55	0.56	1.98	0.59	0.06	0.14	1.49	2.40	0.07	0.18	0.34	0.22	0.44	0.12	0.15	29.58	4.59	0.04	0.15	57.36	0.96
SO_3	4.87	3.79	2.11	4.25	5.32	0.02	2.09	3.51	1.49	1.38	2.46	1.54	2.39	0.00	0.07	0.00	0.63	1.26	0 07	0.28	1.09
Total	52.03	54.94	54.10	64.78	71.96	53.44	68.12	62.49	61.31	57.48	58.36	63.34	65.36	59.59	94.77	97.08	70.69	63.89	95.82	113.43	68.56
Less O=Cl	0.12	0.12	0.45	0.13	0.01	0.03	0.43	0.54	0.01	0.05	0.08	0.5	0.10	0.02	0.03	6.47	1.00	0.00	0.03	12.94	0.21
Total	51.91	54.82	53.65	64.65	71.95	53.41	67.78	61.95	61.30	57.43	58.38	63.29	65.26	59.57	94.74	90.61	69.69	63.89	95.79	100.49	68.35

calculated compositions appeared to be close to averaged compositions of alkaline Ca-rich melts in heated inclusions (Fig. 1-2b).

Alkali-sulfate carbonate inclusions (Fig. 1-3). At 800°C the content of this inclusions becomes absolutely colorless, and then at 820-840°C, homogeneous.

The chemical composition of inclusions (Table 3) is characterized by high concentrations (from 7-10 to 17 wt.%) of SO_3 and significant amount (from 26 to 45 wt.%) of alkalies at considerable predominance of Na over K, and rather low (mainly 7-8, rarely 15-18 wt.%) contents of CaO at appreciable amounts P_2O_5 (2-7 wt.%), SrO (~ 1%), and Cl (from 0 to 2-3 wt.%). The calculations show that the normative compositions of inclusions are as follows (wt/%): from 11 to 45-50 gregoryite, 15-30 arcanite, 10-20 calcite, to 10 thenardite, 0-25 mirabilite, from 0 to 24 trona, 1-10 nahpoite, 1-1.5 strontianite, 0-5 halite, about 1 ankerite, magnesite, and witherite, and minor amounts of silicate and ore minerals. According to calculations, the content of bound CO_2 and H_2O in these inclusions might reach 17-25 and from 0.3 to 10 wt.%, respectively.

Alkali-phosphate carbonate salt inclusions (Fig. 1-4). Inclusions homogenize in a rather wide temperature range – from 850 to 985°C and, most likely, to a certain degree depend on the chemical composition of conserved melt (Table 4).

In general, this melt is enriched in P_2O_5 (from 12 to 35-39 wt.%), CaO (from 20 to 30 wt.%), and alkalies (in total reaching 25-35 wt.% at significant predominance of Na over K), which are in particular ratios with each other. It was established that an increase in P_2O_5 content in a salt melt is accompanied by a

Table 3.

Chemical composition heated of alkali-sulfatic carbonate melt inclusions from monticellite of olivine-monticellitic rocks (wt.%)

#	1	2	3	4	5	6	7	8	9	10	11
SiO_2	0.42	1.49	1.52	0.59	0.78	4.32	7.08	1.55	0.70	1.75	0.50
TiO_2	0.05	0.00	0.00	0.00	0.00	0.05	0.00	0.05	0.09	0.00	0.00
Al_2O_3	0.04	0.00	0.00	0.00	0.00	0.00	0.00	0.00	0.00	0.00	0.00
FeO	0.00	0.38	0.32	0.86	0.69	4.59	1.83	1.14	0.85	0.28	0.97
MgO	3.15	0.91	0.72	0.64	0.73	4.73	1.39	1.04	0.50	0.98	0.91
CaO	17.44	8.34	15.34	8.14	7.70	6.81	18.08	8.53	6.69	7.32	5.07
Na_2O	**15.98**	**39.10**	**27.84**	**14.74**	**28.11**	**17.40**	**18.28**	**23.18**	**34.49**	**25.35**	**42.59**
K_2O	**5.70**	**7.79**	**10.27**	**11.14**	**7.32**	**11.15**	**7.85**	**6.20**	**9.15**	**20.14**	**12.16**
BaO	0.14	0.70	0.51	0.67	0.57	0.56	0.40	0.43	0.62	0.33	1.07
SrO	1.59	1.36	1.54	0.42	1.07	0.17	1.12	1.16	0.93	0.09	0.90
P_2O_5	2.94	3.85	4.56	4.73	7.28	1.22	0.38	8.94	2.67	4.31	2.46
Cl	0.11	1.49	1.45	0.31	2.26	1.94	0.00	3.08	0.60	0.25	5.07
SO_3	**6.59**	**10.05**	**11.57**	**11.66**	**12.56**	**13.10**	**13.38**	**14.14**	**16.27**	**17.07**	**17.68**
Total	54.14	75.45	75.64	53.90	69.07	66.04	69.79	69.44	73.56	77.87	89.38
Less O=Cl	0.02	0.33	0.33	0.07	0.51	0.44	0.00	0.70	0.14	0.06	1.14
Total	54.12	75.12	75.31	53.83	68.56	65.60	69.79	68.74	73.42	77.81	88.24

Table 4.

Chemical composition of alkali-phosphatic carbonate melt inclusions in minerals of rocks from the Krestovskaya intrusion (wt.%)

#	1	2	3	4	5	6	7	8	9	10	11	12	13	14	15	16	17
n	1	1	2	2	1	1	2	3	2	1	2	1	1	1	2	1	2
SiO_2	1.15	2.02	3.15	2.69	2.73	1.27	1.39	0.37	0.82	2.74	3.72	1.80	3.12	0.49	4.15	0.28	0.87
TiO_2	0.00	0.07	0.03	0.02	0.00	0.81	0.00	0.00	0.00	0.00	0.00	0.00	0.00	0.00	0.00	0.00	0.13
Al_2O_3	0.00	0.02	0.00	0.00	0.00	0.00	0.00	0.00	0.00	0.00	0.00	0.00	0.00	0.80	0.00	0.00	0.00
FeO	0.72	0.60	0.59	0.75	0.51	0.64	1.37	0.21	0.27	0.46	0.81	0.60	0.76	0.62	0.55	0.34	0.43
MgO	2.82	1.67	2.31	2.35	1.81	2.13	2.42	1.47	1.10	1.67	4.14	1.23	2.23	1.25	1.75	0.91	1.07
CaO	22.05	22.04	38.23	20.85	23.95	19.37	24.24	20.53	23.91	25.51	24.05	24.60	26.29	22.29	30.68	25.08	25.94
Na_2O	**25.76**	**17.26**	**6.21**	**32.75**	**15.90**	**25.73**	**17.61**	**23.14**	**24.42**	**20.81**	**22.10**	**26.67**	**23.27**	**13.00**	**19.87**	**24.66**	**22.99**
K_2O	**4.46**	**7.59**	**2.81**	**1.27**	**3.43**	**3.65**	**3.48**	**4.81**	**3.00**	**4.21**	**2.45**	**4.18**	**2.40**	**3.38**	**1.76**	**3.48**	**3.23**
BaO	0.00	0.70	0.00	0.08	0.39	0.22	0.42	0.62	0.37	0.11	0.33	0.30	0.15	0.58	0.28	0.35	0.30
SrO	2.46	1.85	2.35	1.38	1.56	1.26	1.45	1.93	1.63	1.94	1.56	1.97	1.78	1.39	1.58	0.35	1.72
P_2O_5	**11.91**	**13.06**	**13.73**	**17.92**	**20.18**	**21.60**	**27.99**	**28.20**	**30.69**	**30.82**	**32.10**	**32.08**	**33.00**	**33.11**	**33.74**	**34.29**	**34.41**
Cl	0.29	0.11	0.76	0.07	0.00	0.05	0.02	0.01	0.04	0.00	0.00	0.00	0.00	-	0.00	0.03	0.00
SO_3	4.89	7.20	2.42	4.97	6.43	0.31	3.78	4.46	3.25	1.73	1.99	1.95	1.35	0.80	1.25	2.23	1.72
Sum	76.58	74.16	72.59	85.10	76.91	79.46	84.17	85.75	89.50	90.93	93.25	95.38	94.35	79.50	95.61	93.45	92.81
Less O=Cl	0.07	0.02	0.16	0.02	0.00	0.01	0.00	0.00	0.01	0.00	0.00	0.00	0.00	0.00	0.00	0.00	0.00
Total	76.51	74.14	72.43	85.08	76.91	79.45	84.17	85.75	89.49	90.93	93.25	95.38	94.35	79.50	95.61	93.45	92.81

Table 4(End).

#	18	19	20	21	22	23	24	25
n	3	2	1	1	2	1	1	1
SiO_2	2.07	4.99	3.87	2.75	0.76	0.43	1.88	1.61
TiO_2	0.01	0.00	0.00	0.00	0.00	0,00	0.00	0.00
Al_2O_3	0.00	0.00	0.00	0.00	0.00	0,00	0.00	0.00
FeO	0.35	0.57	0.49	0.53	0.29	0.18	0.39	0.24
MgO	1.29	1.79	1.12	2.20	1.06	0.23	1.19	1.10
CaO	27.70	32.01	34.00	28.25	27.12	26.47	29.19	31.61
Na_2O	**23.18**	**17.73**	**14.84**	**19.68**	**22.68**	**21.95**	**20.59**	**19.74**
K_2O	**2.89**	**1.47**	**1.94**	**3.00**	**3.38**	**2.78**	**2.03**	**2.33**
BaO	0.19	0.35	0.21	0.29	0.43	0.85	0.24	0.13
SrO	1.81	1.45	1.14	1.77	1.27	2.27	1.68	0.82
P_2O_5	**34.43**	**34.47**	**34.75**	**34.80**	**35.04**	**35.38**	**35.56**	**39.60**
Cl	0.00	0.00	0.00	0.00	0.03	0.05	0.00	0.00
SO_3	1.05	0.67	1.41	1.23	2.13	1.65	1.85	0.95
Total	94.97	95.50	93.77	94.50	94.19	92.24	94.60	98.13
Less O=Cl	0.00	0.00	0.00	0.00	0.00	0.01	0.00	0.00
Total	94.97	95.50	93.77	94.50	94.19	92.23	94.60	98.13

Note. Inclusions: 14 - secondary in olivine, others - primary in monticellite of olivine-monticellitic rocks; 4, 8, 10, 12, 14, 23 - unheated, others - heated to homogenization. Registered homogenization temperatures of inclusions: 6 ~ 910°C, 11 – 980-985°C, 15 – > 780°C, 18, 21 – > 850°C, 19 – >> 805°C. n – number of analyses for different sites of one inclusion.

minor increase in the contents of CaO and decrease in alkalies with predominant drop in the amount of K_2O. But SrO and BaO present in the melt in noticeable amounts (1.5-2 and 0.2-0.5 wt.%. respectively) remain at the same level, but the contents of SO_3 reduce (from 5 to 1-2 wt.%). i. e., phosphorus becomes a predominant anion in the melt.

Based on normative composition, the amount of bound CO_2 in maximum phosphorus-rich fractions is only 1-2 wt.%, whereas in phosphorus-poor fractions its concentration might reach 15-20 wt.%. The content of bound water in the melts, from calculations, increases with growing phosphorus content and may reach 1.5-7 wt.%.

The normative composition of inclusions shows that by alkali phosphates (bushveldite, nahpoit, brianite) and apatite (from 20 to 65 and from 3 to 15 wt.%, respectively) as well as by alkali carbonates (gregoryite, nyerereite) and alkali sulfates (arcanite, thenardite) are dominant phases. The inclusions also contain appreciable amounts of calcite (15-30 wt.%) and, often, portlandite (from 0 to 20 wt.%). Carbonates of Sr and Ba as well as magnetite are present constantly but in minor amounts. The presence of halite and alkaline silicate, combeite, is also probable.

Table 5.

Chemical composition of inclusions of alkali-chloridic carbonate melts in minerals of rocks from the Krestovskaya intrusion (wt.%)

#	1	2	3	4	5	6	7	8	9	10	11	12
n	5	1	1	2	1	1	1	1	1	1	3	1
SiO_2	1.19	1.65	0.00	5.28	6.93	5.30	9.41	1.19	3.30	0.49	0.00	0.77
TiO_2	0.00	0.00	0.22	0.00	1.35	1.48	0.06	0.28	0.12	0.24	0.10	0.00
Al_2O_3	0.00	0.05	0.00	0.00	1.07	1.10	0.31	0.37	0.24	0.08	0.00	0.02
FeO	1.73	0.85	5.42	1.96	1.72	1.69	0.44	1.26	0.69	0.34	0.10	0.81
MgO	0.10	0.99	4.96	0.00	0.00	0.00	2.99	0.00	0.00	0.00	0.00	0.00
CaO	**32.90**	**27.23**	**19.91**	**41.05**	**3.90**	**3.03**	**10.07**	**2.29**	**1.95**	**1.14**	**3.12**	**1.44**
Na_2O	**2.84**	**6.15**	**8.52**	**6.15**	**22.16**	**22.01**	**8.22**	**29.90**	**31.25**	**38.30**	**0.07**	**44.57**
K_2O	10.51	11.13	18.16	12.46	20.32	19.25	31.91	2.29	4.72	16.98	55.69	1.21
BaO	0.19	-	1.20	0.18	0.00	0.00	0.20	0.00	0.00	0.00	0.00	-
SrO	0.08	0.62	0.25	0.00	0.00	0.03	0.29	0.00	0.00	0.03	0.13	0.04
P_2O_5	0.12	0.12	0.07	0.04	-	-	0.01	0.10	0.10	0.00	0.00	0.00
Cl	**5.63**	**9.20**	**10.71**	**12.84**	**22.37**	**24.57**	**33.47**	**35.67**	**41.44**	**41.78**	**41.39**	**45.76**
SO_3	6.10	3.71	5.39	1.36	0.02	0.04	0.00	0.20	0.13	-	0.00	0.43
Total	67.40	61.70	74.81	81.32	78.50	78.50	97.38	73.55	83.94	99.38	100.45	95.05
Less O=Cl	1.27	2.07	2.41	2.90	5.05	5.54	7.33	8.05	9.35	9.43	9.30	10.32
Total	66.13	59.63	72.40	78.42	74.79	72.96	90.05	65.50	74.59	89.95	91.15	84.73

Note. Inclusions: 2, 12 – in monticellite of melilitolites, 1, 3, 4, 7, 11 – in melilite of melilitolites, 5, 6, 8-10 – in clinopyroxene of clinopyroxenites. Homogenization temperatures of inclusions: 4 – 680°C, 7-9, 11 – 720-790°C, 1, 3 – at 840 °C liquid immiscibility occurs. 10 – K- and Cl-rich fraction from two-phase unheated inclusion. Second fraction has alkali-enriched Ca-rich-carbonate composition (Table 6, an. 10), n – number of analyses.

Inclusions of alkali-chloride carbonate melts (Fig. 1-5).Chemical composition drastically varies from Ca-rich with appreciable amounts of Cl, SO_3, and alkalies (Table 5, ans. 1-4) to highly alkaline with a very high content of Cl (Table 5, an. 9-12). Homogenization temperature of inclusions to a certain degree depends on the chemical composition of inclusions (Table 5): at high contents of alkalies and Cl, i. e., when inclusions are dominated by halite and sylvite, inclusions homogenize at 720-790^{o}C. At lower contents of these elements and high CaO, inclusions homogenize at lower temperatures, 670-680^{o}C. In some of such inclusions boiling of salt melt occurs. Ca-rich inclusions containing simultaneously high concentrations of Cl and SO_3 (Table 5, ans. 1, 3) at 840^{o}C exhibit immiscibility which develops as separation of melt into brownish and greenish liquids. We failed to homogenize these inclusions as they decrepitated. We also find an immiscible unheated inclusion consisting of the phase of alkaline Ca-rich carbonates (Table 6, an. 10) and the phase of alkali chlorides (Table 5, an. 10) in melilite of melilite rocks.

The normative composition of inclusions, in addition to predominant halite, also present varying amounts of sylvite, calcite, alkaline carbonates (trona, natrite, shortite, nyerereite), magnetite, and portlandite. The amount of bound water in salt melt might reach 5-10 wt.%, CO_2 ranges from few percent to 25 wt.% in inclusions with a high content of Ca.

The inclusions of calciocarbonate melts (Fig. 1-6). Inclusions homogenize at 810-790^{o}C.

The chemical composition of inclusions (Table 6) is uniform. Cationic part is represented mainly (43-54 wt.%) by CaO and minor (0.2-0.4 wt.%) amounts of FeO and MgO and to 2 wt.% SrO. Rarely, alkalies are present in rather considerable amounts (2-13 wt.%) (Table 6, ans. 8-11) and P_2O_5 is minor. Cl^- and SO^{3-}anions are normally absent and only occasionally occur in minor amounts. Traces of Si seem to be a result of entrapment of the host mineral of inclusions by the probe beam. It is interesting that in the immiscible inclusion from melilite of melilitolites, consisting of the phase of alkali chlorides (Table 5, an. 10) and Ca-rich phase, the composition of the latter is identical to the composition of secondary Ca-rich phase of carbonate inclusions from clinopyroxene of clinopyroxenites. This coincidence is additional evidence of the governing role of liquid immiscibility during separation of initial carbonatitic melt into separate fractions of a more simple composition.

According to calculations, the normative composition of Ca-rich inclusions might vary from essentially calcite with traces of strontianite (to 2 wt.%) and apatite (about 0.5 wt.%) (Table 6, ans. 1-6) or carbonates of alkalies (to 10-12 Na_2CO_3 and 5-8 K_2CO_3; Table 6, an. 8-10) to a mixture of calcite (~ 40 wt.%) with portlandite (60 wt.%: Table 6, an. 7). Portlandite-enriched inclusions may contain to 14.5 wt.% bound water.

Table 6.

Chemical composition of inclusions of calciocarbonate melts in minerals of rocks from the Krestovskaya intrusion (wt.%)

#	1	2	3	4	5	6	7	8	9	10	11	12
SiO_2	0.51	1.20	1.11	1.76	0.18	0.40	0.22	0.72	0.61	0.18	2.12	3.43
TiO_2	0.07	0.00	0.06	0.04	0.10	0.05	0.01	0.00	0.15	0.00	0.00	0.00
Al_2O_3	0.35	0.00	0.00	0.00	0.00	0.00	0.00	0.03	0.00	0.00	0.09	0.00
FeO	0.43	0.27	0.21	0.16	0.17	0.20	0.18	0.33	0.13	0.51	0.65	0.00
MgO	0.39	0.37	0.45	0.46	0.03	0.10	0.03	1.65	0.11	0.00	1.69	0.00
CaO	**54.73**	**55.31**	**50.24**	**54.32**	**58.90**	**58.01**	**67.95**	**47.30**	**45.06**	**43.45**	**45.75**	**51.89**
Na_2O	0.00	0.00	0.00	0.04	0.06	0.05	0.06	4.74	7.56	7.42	2.04	0.03
K_2O	0.00	0.00	0.05	0,00	0.00	0.00	0.02	3.56	5.87	5.70	0.08	0.01
BaO	0.04	0.00	0.00	0.04	0.00	0.00	0.00	0.00	0.00	0.00	-	-
SrO	0.34	0.21	1.03	1.70	0.68	0.60	0.02	2.15	1.98	0.85	-	0.10
P_2O_5	0.16	0.15	0.12	0.14	0.21	0.20	0.00	0.52	0.17	0.83	-	0.10
Cl	-	-	-	-	-	-	0.00	0.04	-	0.07	-	0.03
SO_3	0.00	0.00	0.00	0.00	0.00	0.06	0.33	0.00	0.00	0.00	-	0.60
Total	57.02	57.51	53.27	58.66	60.33	59.67	68.82	61.04	61.64	58.61	52.48	56.19
Less O=Cl	-	-	-	-	-	-	0.00	0.01	-	0.01	-	0.00
Total	57.02	57.51	53.27	58.66	60.33	59.67	68.82	61.03	61.64	58.60	52.48	56.19

Note. Host mineral of inclusions: 1-7, 9 – clinopyroxene from clinopyroxenites, 8 – olivine and 11 – monticellite from monticellitolite, 10 – melilite from melilitolite, 12 – garnet from melilitolite. 1-6, 9, 10, 12 – unheated inclusions, the others are heated ones. 10 – Alkali-enriched Ca-rich carbonate fraction of two-phase inclusion. Second fraction is K- and Cl-rich (Table 5, an.10). Homogenization temperature of the content of heated inclusions: 7 ~ 790°C, 8 – 810°C, 11 – >> 660°C.

SILICATE-SALT INCLUSIONS

Silicate-salt inclusions occur throughout in perovskite and rarely in melilite. **Perovskite** contains abundant inclusions but they are distributed nonuniformly. In large zonal phenocrysts (Fig. 2), inclusions occur mainly in the central parts composed of dark perovskite-I and in peripheral light zones consisting of perovskite-II. The intermediate zone between them is normally sterile from inclusions. Small grains of perovskite-I contain lesser inclusions. In general, perovskite-II contains more inclusions than perovskite-I. The shape of inclusions in perovskite-I is isometric and rounded. In perovskite-II, their shape is elongate-rounded, rarely, irregular; size is 20-30 μm. The content of inclusions is partly or completely crystallized. The phase composition of unheated inclusions in transmitted light of microscope is hard to identify, especially in perovskite-I, but in the reflected light, the inclusions clearly demonstrate individual daughter phases among which is a fine-crystallized carbonate-salt residual aggregate. Microprobe analysis of daughter phases in perovskite-I detected [25] the following minerals: clinopyroxene, kalsilite, apatite, phlogopite, combeite, rankinite, magnetite, djerfisherite, pyrrhotite, and sphene. In inclusions from perovskite-II the paragenesis of daughter minerals is

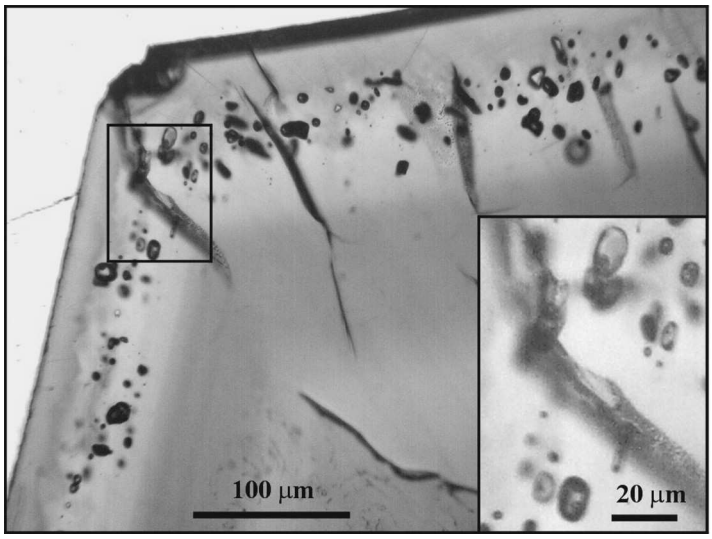

Fig.2. **Fragment of zoned phenocryst of perovskite in olivine-monticellite-melilite rock with silicate-salt inclusions in colorless rim (perovskite II).**

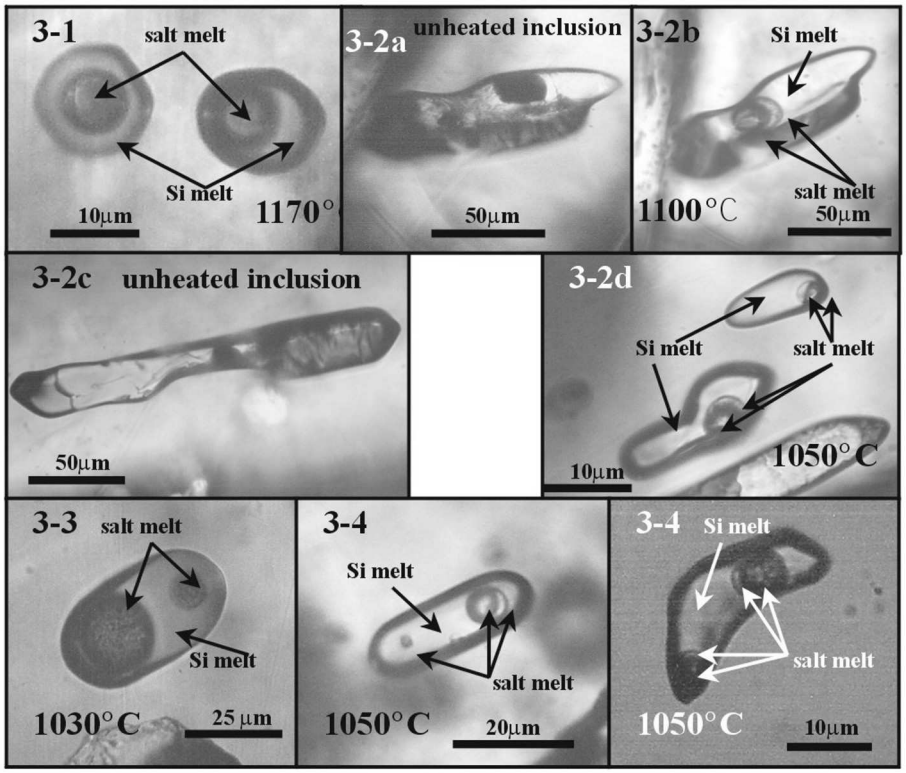

Fig. 3. **Silicate-salt inclusions in perovskite.**

3-1. Inclusion with silicate-carbonate immiscibility, heated to 1170°C, in perovskite-I from monticellitolite. Chemical composition of carbonate-salt phase (globule) in Table 7, an. 2

3-2. Inclusions of silicate-salt melts in perovskite II from olivine-monticellite-melilite rocks: a,c – unheated inclusions; b, d – inclusions heated to 1100 and 1050°C. It is well seen in heated inclusions that isolated carbonate-salt fraction (globule) is heterogeneous and is separated into immiscible phases;

3-3. Inclusion with three-phase silicate-carbonate-salt immiscibility in perovskite II, heated to 1130°C. Immiscible carbonate-salt phases of inclusion spatially separated in glass. Chemical composition of salt phases is given in Table 7 (no 3, 4);

3-4. Heated inclusions with multi-phase silicate-carbonate-salt immiscibility in perovskite II. It is seen in inclusions that carbonate-salt globules are heterogenenous and spatially separated into immiscible phases.

somewhat different and includes: phlogopite, kalsilite, haüyne, pectolite, magnetite, and rutile.

On heating, the content of inclusions in ***perovskite-I*** gradually lightens and at about 700-780°C one can observe melting of salt aggregates. At temperatures higher than 1000°C silicate phases start to melt. At 1130-1150°C many inclusions exhibit spherical isolation (globule) of salt liquid in silicate melt with distinct boundary between them (Fig. 3-1). On further heating, the salt globule begins to decrease and at 1230-1250°C, it disappears in most inclusions and the melt becomes homogeneous. The remaining heterogeneous inclusions on further heating decrepitate. After quenching, the inclusions reveal silicate-carbonate immiscibility. The ratio of immiscible phases is predominantly 1:10, but sometimes deviates to 1:5, i.e., some inclusions are evidently abnormal. Probably, at some stage of conservation of inclusions in perovskite-I the melt was already heterogeneous due to partial separation of salt portion from silicate melt. Nevertheless, we believe that the temperature 1250-1230°C at a minor assumption can be regarded as the temperature of silicate-carbonate liquid immiscibility.

The chemical composition of silicate component of inclusions corresponds to alkali-basic melts [25] and contains on the average (wt.%): 32.20 SiO_2, 6.12 TiO_2, 5.78 Al_2O_3, 11.73 FeO, 6.47 MgO, 18.87 CaO, 6.23 Na_2O, 6.54 K_2O, 0.28 BaO, 0.25 SrO, 1.57 P_2O_5, 0.35 SO_3, 0.19 Cl.

The chemical composition of salt globules (Table 7, ans. 1, 2) is characterized by predominance of alkalies (17-22 wt.%), significant concentrations of CaO (14-20 wt.%), small amounts (from 2 to 3-5 wt.%) of SiO_2, TiO_2, FeO, MgO, SO_3, and P_2O_5, and trace contents (0.2-0.3 wt.%) BaO, SrO, and Cl. The content of bound CO_2, according to the calculation on normative composition , might reach 20-24 wt.%, whereas the amount of bound water is only < 1 wt %. The normative composition of salt phase is dominated by carbonates of alkalies (gregoryite and nyerereite to 20 wt.%) and calcite (to 30 wt.%) with small amounts of carbonates of Sr, Ba, Mg. It may also contain considerable (to 10 wt.%) alkali sulfates and phosphates (arcanite, nahpoite) and to 1-3 wt.% silicate (combeite, K-feldspar) and ore (magnetite, perovskite, or rutile) minerals. These data in their characteristics most closely correspond to hyperalkaline carbonate melts conserved in melilite of melilitolites and monticellite of olivine-monticellite rocks (Table 1). They, most probably, characterize the composition of initial carbonatite melts separated from parental silicate magma as a result of liquid immiscibility.

In light perovskite-II, melting of salt phases in inclusions becomes evident already at 660°C, whereas at 1000°C silicate phases begin to melt. At 1030-1050°C, in inclusions one can observe separation of several salt globules in silicate melt. At further increase in temperature, salt globules in some inclusions decrease in size and come closer to each other, while at 1190-1200°C all globules join into one bubble. Total decrepitation of inclusions prevented their homogenization. After cooling to 1050-1100°C and quenching, in silicate glass of heated inclusions one could easily observe inhomogeneous salt globules consisting of two coexisting immiscible phases

Table 7.

Chemical composition of salt globules from heated inclusions of silicate-salt melts in perovskite and melilite (wt.%)

#	1	2	3	4	5	6	7	8
n	1	8	4	4	1	1	2	1
SiO_2	2.97	5.54	0.26	2.30	5.65	6.76	4.06	7.59
TiO_2	4.83	4.13	0.96	0.57	1.75	2.39	1.67	0.03
Al_2O_3	0.33	1.19	0.00	0.61	1.18	0.33	0.58	0.48
FeO	0.72	4.48	0.06	1.24	2.13	2.03	2.51	0.78
MgO	0.70	2.33	0.08	1.15	3.59	1.47	0.94	7.79
CaO	20.01	13.91	4.65	16.19	17.14	18.72	13.44	22.15
Na_2O	4.00	11.75	10.78	5.42	12.36	10.01	3.48	5.01
K_2O	17.50	5.20	19.99	12.90	6.68	7.93	14.75	13.69
BaO	0.00	0.49	0.11	0.98	0.82	1.10	0.77	0.75
SrO	0.22	0.35	0.19	0.74	0.93	0.98	0.54	0.38
P_2O_5	0.07	1.90	0.42	6.65	0.57	4.92	3.15	0.02
Cl	-	0.18	0.16	0.61	0.51	0.24	0.27	6.62
SO_3	4.56	1.03	17.05	7.02	14.93	10.02	8.42	1.02
Sum	55.91	58.02	54.71	54.78	68.24	66.93	54.58	66.36
Less O=Cl	-	0.04	0.03	0.13	0.11	0.05	0.05	1.45
Total	55.91	57.98	54.68	54.65	63.85	66.88	54.53	64.91

Note. Inclusions: 1,2 - in perovskite I, 3-7 - in perovskite II of melilitic and olivine-monticellitic rocks, 8 - in melilite of melilitolites. 3-4 - spatially separated salt globules in silicate glasses from one heated inclusion. n – number of analyses for different sites of one inclusion.

(Fig. 3-2). Some inclusions in silicate melt exhibited spatial separation of two salt globules (Fig. 3-3), one of them being represented by two immiscible phases (Fig. 3-4). Hence, this suggests that at 1190-1200°C the initial carbonate melt itself started to separate into immiscible fractions.

Because of small sizes of salt globules only in one case we managed to qualitatively analyze both salt globules in one silicate-salt inclusion. One of them appeared to correspond to the composition of inclusions of alkali-sulfate carbonate melts (Table 7, an. 3), whereas the other has an intermediate composition between the inclusions of alkali-sulfate and alkali-phosphate carbonate melts (Table 7, an. 4). The chemical composition of single heterogeneous salt globules from inclusions in perovskite-II was similar to the composition of alkali-sulfate carbonate melts enriched in P (Table 7, an. 5-7). Hence, the crystallization stage of perovskite-II was marked not only by silicate-salt immiscibility of parental silicate melt but also by heterogenization and spatial separation of salt melt into simpler immiscible components (fractions). The composition of silicate melt remained as before similar to alkali-basic one.

Melilite contains scarce silicate-salt inclusions; their shape is rounded and irregular. Their size reaches 10-20 μm, their content is partly or completely

crystallized. Among daughter phases in inclusions we found [25]: clinopyroxene, phlogopite, rankinite (?), larnite (?), magnetite, djerfisherite, pyrrhotite, as well as brownish and greenish salt aggregates. On heating, the first to melt at 640-680^{o}C are salt phases. At 900-945^{o}C some inclusions exhibit two liquid phases: a greenish salt phase in the center and a brownish silicate phase forming a rim around it. Their ratios vary from 1:1 to 1:10, which suggests conservation of initially heterogeneous melt by inclusions. Because of decripitation of inclusions at high temperatures, we failed to homogenize them.

The chemical composition of silicate part of heated and thereafter quenched inclusions is idential to the composition of the silicate components of similar inclusions in perovskite I, the only difference being in smaller amounts of TiO_2. Only once we succeeded in qualitative analysis of the composition of salt component of these inclusions (Table 7, an. 8). It was close to the composition of alkali-chloride carbonate inclusions in melilite and monticellite of melilite-monticellite rocks (Table 5, ans.1,2), i. e., as major components it contained (wt.%): 13.7 CaO, 5 Na_2O, 13.7 K_2O, 6.62 Cl and about 1 SO_3. The salt melt was also slightly enriched in Si and Mg.

DISCUSSION OF RESULTS

The studies of inclusions in minerals of various rocks from the Krestovskaya intrusion allowed us to establish occurrences of liquid immiscibility: at 1250-1230^{o}C, two-phase carbonate-silicate and, starting from about 1200-1190 to 800^{o}C, multiphase silicate-carbonate-salt. The occurrence of two-phase silicate-carbonate immiscibility in parental silicate magma seems to cause generation and separation of initial carbonatite melts in magma chamber. The immiscibility concurred with the beginning of crystallization of perovskite. The evidence for this comes from the fact that the cores of phenocrysts of perovskite-I contained primary silicate-salt inclusions which at 1230-1250^{o}C separated into two silicate and carbonate immiscible liquid phases. The ratio of quenched immiscible silicate and salt phases in normal inclusions was approximately 1:10. The composition of silicate glass in quenched inclusions was similar to the that of alkali-basic melts, whereas the composition of salt components corresponded to that of hyperalkaline carbonatites significantly enriched (few percent) in SiO_2, SO_3, P_2O_5, SrO, BaO, and Cl (Table 1). This composition was quite comparable to that of alkali-carbonatite lavas from the 1960 and 1988 eruptions of volcano Oldoinyo Lengai, Tanzania [5] and, most likely, was identical or close to the composition of initial carbonatite melts.

Spatial separation of silicate and carbonate components of parental silicate magma, obviously, started at once. This is evidenced by the fact that phenocrysts of perovskite-I, along with normal inclusions, contain inclusions with abnormal ratios of silicate and carbonate-salt phases which on heating did not homogenize but decrepitated. This conclusion is also supported by the presence (in the same growth zones of melilite) of syngenetic spatially separated silicate and salt inclusions whose chemical composition is close to that of fractions from heated silicate-salt inclusions in perovskite.

Extremely interesting were silicate-salt heated inclusions in perovskite-II (phenocryst rim), which on heating exhibited multiphase liquid immiscibility: silicate-carbonate at 1250-1230 and carbonate-salt at 1190-1200°C. After heating and quenching, silicate glasses of such inclusions contained either single heterogeneous salt globules composed of two immiscible phases (Fig. 3-2) or two salt globules of different compositions (Fig. 3-3). In the latter case, the composition of both globules was highly alkaline but in one of them it was SO_3-rich, while in the other, along with SO_3, it included aprreciable amounts of P_2O_5. In melilite, crystallized at close temperatures with perovskite [25], the composition of salt globule from silicate-salt inclusions was enriched in Cl (Table 7, an. 8). These facts, undoubtedly, suggest separation of initial carbonate-salt melt into simpler immiscible fractions. This assumption is supported by finding in melilite and monticellite of studied rocks of primary carbonate-salt and salt inclusions some of which were similar in composition to carbonate-salt globules from heated silicate-salt inclusions in perovskite and melilite. Others had a simpler composition in which of decisive importance was one or another anion present in the initial carbonate melt – SO_3, Cl, P_2O_5, or CO_2.

Thus, all the variety of carbonate-salt and salt inclusions is represented: initial hyperalkaline-carbonate melts and their derivatives: alkali-Ca-rich melts, alkali-sulfate, alkali-phosphate, alkali-chloride, and calciocarbonate melts. During separation and occurrence of liquid immiscibility, major components of initial carbonate melts were redistributed as follows (Fig. 4).

CaO concentrated in alkali-Ca-rich and calciocarbonate melts, amounting to 30-40 and 45-55 wt.%, respectively. In alkali-phosphate melts its amount remained at the same level, while in alkali-sulfate and alkali-Cl-rich melts decreased to 5-8 and 1.5-5 wt.%, respectively.

The highest contents of **alkalies** appeared to be associated with sulfate (from 26 to 40-43 wt.%) and extreme rich in Cl (to 45-55 wt.%) salt melts; in alkali-phosphate melts the content of alkalies did not change, while in alkali-Ca-rich melts it decreased to 16-18 wt.% and in calciocarbonate ones was minimum (0-12 wt.%).

SrO during separation of initial carbonate melt accumulated in alkali-Ca-rich and alkali-phosphate carbonate melts (on the average about 1.9 and 1.6 wt.%, respectively). Its content somewhat decreased (on the average to 0.8-0.9 wt.%) in alkali-sulfate and calciocarbonate melts, falling to 0.0-0.1 wt.% in alkali-chloride melts.

BaO concentrated mainly in alkali-sulfate melts in which its content varied from 0.5 to 1 wt.%. It slightly decreased in alkali-phosphate and alkali-Ca-rich melts (on the average to 0.31 and 0.23 wt.%, respectively). In alkali-chloride and calciocarbonate melts BaO was either absent or present in trace amounts.

Major amounts of **phosphorus** were redistributed into alkali-phosphate melts, in which they accounted for 12-39 wt.% P_2O_5. Essentially enriched were alkali-sulphate and, to a lesser degree, alkali-Ca-rich melts, containing on the average

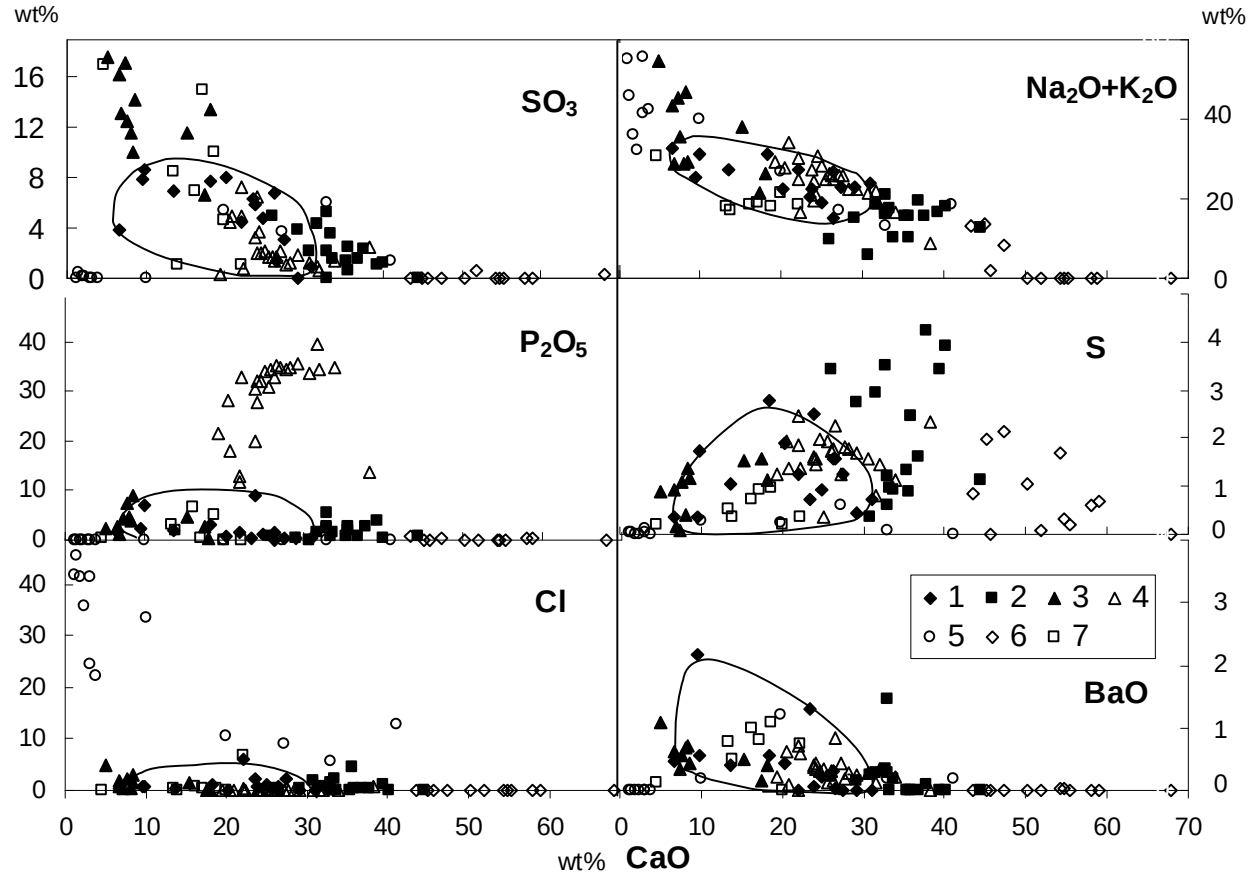

Fig. 4**. Plots of CaO versus SO_3, P_2O_5, Cl, ∑ Na_2O+K_2O, SrO, and Ba for carbonate and carbonate-salt inclusions in melilite and monticellite, also for carbonate-salt fractions from inclusions with silicate-salt immiscibility in perovskite.**

Inclusions of: 1 – initial hyperalkaline carbonate melts; 2 – alkali-Ca-rich carbonate melts; 3 – alkali-sulfate carbonate melts; 4 – alkali-phosphate carbonate melts; 5 – alkali-chloride carbonate melts; 6 – calciocarbonate melts; 7 – carbonate-salt fractions (globules) from heated silicate-salt melts in perovskite. The field defined by the initial hyperalkaline-carbonate melts

about 3.9 and 1.6 wt.% P_2O_5, respectively. In calciocarbonate and alkali-chloride melts the amount of P_2O_5 drastically decreased to 0.1-0.2 wt% or was absent at all.

During the occurrence of immiscibility, most **SO_3** from initial carbonatite melt migrated to alkali-sulfate liquid, where its amount on the average was about 13 wt.% (varying from 8 to 18 wt.%). In alkali-Ca-rich and alkali-phosphate melts its content decreased on the average to 2.5 wt.%. In alkali-chloride melts the content of SO_3 was in inverse dependence on that of Cl. In calciocarbonate SO_3 was absent.

Cl, besides high concentrations in alkali-chloride melts, was also present in appreciable amounts (on the average 1.34 wt.%) in alkali-sulfate melts. In alkali-Ca-rich liquids its content was on the average 0.65 wt.%, while in other immiscible carbonate-salt fractions, no more than tenths fractions of percent.

The amount of **CO_2**, according to calculations of the chemical composition of inclusions to normative composition, on the occurrence of carbonate-salt liquid

immiscibility considerably increased in calciocarbonate melts (to 42-44 wt.%) and alkali-Ca-rich melts (to 33-37 wt.%). In other immiscible fractions the content of CO_2 decreased considerably. The higher the content of the leading anion component (SO_3, P_2O_5, Cl), the lower the concentration of carbonate component. CO_2 could be present in the following amounts: from 17 to 25 wt.% in alkali-sulfate melts, from 1-3 to 15-25 wt.% in alkali-phosphate melts, and from 0-8 to 25 wt.% in alkali-chloride melts.

The concentration of bound **water**, from calculations, is not constant. Its highest values (to 14.5 wt.%) are specific of calciocarbonate melts. Alkali-sulfate and alkali-chloride carbonate melts could contain from few to 10 wt.% bound water and from 1.5 to 7 wt.% H_2O in alkali-phosphate melts. Its content, most likely, grew with increasing amount of P_2O_5.

An important fact is the establishment of coexistence of carbonate-salt and salt inclusions with different chemical compositions in the same growth zones of the host minerals. This evidences syngenetic separation of chemically different salt fractions and their simultaneous entrapment by growing minerals. Most likely, at the crystallization stage of perovskite II as a result of drastic changes in the physicochemical conditions of magmatic medium (which is indicated by the high saturation of peripheral zone of perovskite phenocrysts in inclusions) the salt melt became inhomogeneous because of separation of immiscible fractions with different compositions in it.

Separation into simpler components, obviously, continued in isolated salt fractions as well. This is supported by the occurrence of liquid immiscibility at 840-800^oC in the inclusions of alkali-Ca-rich melts (Table 2, an. 5) and alkali-chloride melts with high contents of SO_3 (Table 5, ans. 1,3). This seems to have been promoted by the instability of physicochemical conditions of crystallizing magmatic medium. The reflection of this is conservation in monticellite of abundant primary salt and carbonate-salt inclusions and boiling of melt found in alkali-chloride inclusions. The instability of conditions led to disturbance of phase equilibria of magmatic system and promoted spatial migration of salt fractions. At a microlevel, this was expressed in the appearance of secondary carbonate-salt inclusions in olivine and clinopyroxene of olivine-clinopyroxene and clinopyroxenite rocks as a result of penetration of some salt fractions into microcracks of these high-temperature minerals.

Separation of carbonate-salt melt can be substantiated theoretically as follows. Since carbonate-salt melts are ionic liquids, according to the polarity rule, the equilibria of exchange reactions in them are shifted toward combination of strong acid anions with the strongest alkali cations. Inhomogeneity and immiscibility in these melts occur when the interaction energy of some ion pairs is significantly higher than that of others [13]. In the considered initial carbonate melts cations are represented mainly by alkalies and Ca, while anions, by Cl, SO_3, PO_4, CO_3 (in decreasing order of their basic and acid properties, respectively). Since the melts contained stronger acid bases than CO_3, this allowed alkalies (as for stronger

bases) to establish mainly bonds with them, creating inhomogeneities and expanding the fields of immiscibility when replacing a weaker acid anion by a stronger one. As carbonates Ca are the lowest energy pair, they terminated separation of initial carbonate melt.

Thus, the data obtained on melt inclusions indicate immiscible separation of carbonate-salt melts from parental alkaline silicate magma at 1250-1230^{o}C. The carbonate-salt melts, in turn, starting from 1200-1190^{o}C in unstable physicochemical conditions separated into simpler immiscible fractions.

The reality of occurrence of two-phase carbonate-silicate immiscibility in nature causes no doubt nowadays. They were established in petrographic and geochemical researches [34, 15], supported experimentally, and documented in fluid inclusion studies.

Thus, it was found experimentally [9, 10, 11, 3] that carbonate-silicate liquid immiscibility in many cases is responsible for the separation of carbonatite liquid from silicate melt, is well manifested in the systems with an excess of alkalies, occurs in a wide range of PT-parameters, and an increase in the content of alkalies, especially potassium, considerable broadens its field.

With the help of studies of melt inclusions in minerals, silicate-carbonate immiscibility was also found to occur during formation of melilitolites of the Gardiner complex in Greenland [23] and during crystallization of melilite-monticellite-olivine rocks of the Malyi Murun alkaline massif in Aldan [26] and K-basaltoids of Eastern Pamir [35]. In general, silicate-carbonate immiscibility is typical of alkali-ultrabasic and alkali-basaltoid magmas.

The phenomena of three-phase silicate-carbonate-salt and carbonate-salt immiscibility is much less common. These were documented in natural silicate melts enriched with S, F, Cl, Na, K and carbonates. Thus [14], in the zones of alteration of harzburgite nodules from the volcano Montana-Clara (Canarian Archipelago) in association with minerals of II generation (olivine, clinopyroxene, spinel) syenite glass was found with globules of monosulfides of Ni, Fe, Cu, and globules of Ca-carbonates (Ca/Ca+Mg from 0.85 to 0.95). Carbonate globules in structure corresponded to rapidly cooling liquid. The character of relationships between carbonates, alkali-silicate glass, and sulfides suggests coexistence of three immiscible liquids in reduced conditions of the upper mantle.

According to the results of studies of melt inclusions in minerals [1, 2, 22], the formation of alkaline-carbonatite-bearing Mushugai-Khuduk complex (South Mongolia) also proceeded under multi-phase liquid immiscibility. It was established that at temperatures above 1220^{o}C, the initial alkali-basic magma enriched in F, P, S, and CO_2 separated into immiscible silicate and silicate-phosphate melts. Then at 1200^{o}C, a phosphate-carbonate liquid considerably enriched in Ca, P, F, S separated from silicate-phosphate melt. At the later magmatic stage, the formation of the rocks of these complex was influenced by sulfate, fluoride-sulfate, and chloride-sulfate salt melts. The character of their genetic relations with silicate and phosphate-carbonate melts was not established

but the researchers admit the probability of their separation from alkaline-basic magma during differentiation.

The formation of calcite carbonatites of the Malyi Murun alkaline massif (Aldan) was also related to three-phase silicate-carbonate-salt immiscibility [27]. It was found that at 1280-1260^{o}C, Ca-rich carbonate melt enriched in alkalies and SO_3 separated, as a result of liquid immiscibility, from the initial alkaline-basic magma. At lower temperatures (1200-1170^{o}C), this melt separated into alkali-sulfate and Ca-carbonate liquids. Spatial isolation at a macrolevel and crystallization of Ca-rich carbonates melts at 850-750^{o}C resulted in calcite carbonatites. The influence of alkali-sulfate melts on host rocks led to the formation of fenites and development of various sulfate mineralization widespread in the massif.

A rare example of sulfate-carbonate immiscibility, which occurred at a macrolevel is carbonatitic lavas of Oldoinyo Lengai (Tanzania) of 1966 eruption [6]. Here, in melanite from lapilli macroinclusions of irregular shape were found composed of Na-rich sulfate material (22.7-33.8 wt.% Na_2O, 23.85-49.42 wt.% SO_3) also containing varying amounts (wt.%) of CaO (3.8-16.8), SiO_2 (3.3-16), TiO_2 (1.5-5.2), Fe_2O_3(2-10.8). In addition, alkali-carbonatite cement of the same lapillae was found to contain two types of isolated globules consisting of intergrowing: a) alkali phosphates and carbonates, b) K-bearing Fe-sulfides and carbonates. The content of sulfur in the latter type of isolations was 21-32 wt.%. The formation of globules is related to quenching of S- and P-enriched salt liquids separated from the magmatic carbonate melt.

In the groundmass of porphyritic natrocarbonatite lavas erupted in 1995 from the above-mentioned volcano R.H Mitchell [21] found "textures indicative carbonate-carbonate immiscibility. The immiscible fractions are considered to involve: a Na-K-Ca-CO_2-Cl-rich, Fe-bearing fluid crystallizing gregoryite, sodian sylvite, potassium neighborite as well as a complex Ba-rich carbonate; and a Na-rich, Cl-poor carbonate liquid approximating to a nyerereite-gregoryite cotectic composition... Textural and paragenetic data are interpreted to suggest that these recent lavas are more evolved than previously investigated Oldoinyo Lengai lavas and that natrocarbonatite is a highly evolved rather than a primitive magma".

Carbonate-salt liquid immiscibility can be also responsible for schlieren-like isolations of apatite in carbonatite lavas of Kontozera on the Kola peninsula [30] and oriented ellipsoidal isolations of apatite in sövite dike of the Fen complex.

It is beyond question nowadays that the phenomena of three-phase and multiphase silicate-carbonate-salt immiscibility are related to the fact the alkali- and carbonate-enriched silicate melt contain abundant volatile components – F, Cl, S, P, and CO_2, which, because of the high activity of alkalies, cannot separate from melt in the form of gas phase. This seems to lead to a structural change in alkali-aluminosilicate melts and creates conditions for the occurrence of immiscibility. This opinion is supported by experimental data. Thus, S in silicate melts forms stable sulfate and sulfide associates, which are highly soluble if fluids enriched with alkalies

and pressure in the system is high [18]. The highest solubility levels of S are typical of sulfate forms [4]. P in alkali-rich magmas is present in the form of easily soluble complex compounds of the type $(K, Na)_{3-n}$ $(PO_{4-n})F$ and $(K, Na)_{3-n+2m}[PO_{4-n}(F,Cl)_nCO_3)]$ [19]. Their high content in particular physicochemical conditions might cause immiscible separation of melt into silicate and phosphate-silicate components [12]. Separation of carbonate-salt liquids into simpler fractions is supported by experimental works of Suk [36]. He experimentally studied a silicate-carbonate system modeling separation of carbonate liquids from silicate melts at T = 1100 and 1250^{o}C and P = 2 bar. It was established that addition of alkalies, P, Cl, and F causes inhomogeneities in the isolated salt melt and appearance of immiscible phases in it. That is: a) high concentrations of alkalies in a silicate-carbonate system result in separation of salt melt into alkaline (mainly, Na) and alkali-Ca (predominantly,Ca) fractions; b) in a phosphate-carbonate-silicate system a salt melt is separated into alkali-phosphate and carbonate liquids; c) in a chloride-carbonate-silicate system a salt liquid is separated into chloride and carbonate components. It was found that an increase in pressure and decrease in temperature favor broadening of the field of immiscibility of melts.

Thus, analysis of literature data shows that some elements of carbonate immiscibility were repeatedly documented by researches in natural objects and tested in experimental conditions. But, unfortunately, in most cases the features of immiscibility are hard to detect and they disappear because of the high mobility and agressiveness of separated fractions enriched in alkalies. At the same time, the separation of initial carbonatite melts into immiscible fractions, most likely, occurs widely in nature, if not throughout, especially in deep conditions on slow cooling and long-term evolution of magma. Indirect evidence for this is revealing and distinguishing of various types of carbonatites: ***alkali-sulfate***, for example, carbonatites of Western Transbaikalia [31], Mushugai-Khuduk in Mongolia [1, 2], Mountain Pass in California [17], ***alkali-phosphate*** – apatite-polycarbonate eruptive dikes and welded tuff of phosphate composition from the Tomtor Massif in Siberia [8] and ***essentially calcite*** – the most abundant type of intrusive carbonatites. Calcite carbonatites are undoubtedly an exhausted residual melt of initial alkali-carbonatite magma and appear at the final stages of its evolution. The composition of initial alkali carbonatite magma can be preserved only at rapid eruption of melt into the surface and in the absence of intermediate magma chambers.

CONCLUSIONS

1. Initial carbonate melts in alkali-ultrabasic carbonatite Krestovskaya intrusion are a result of two-phase silicate-carbonate liquid immiscibility of parental silicate magma at 1250-1230^{o}C.

2. The chemical composition of separated carbonate melts was hyperalkalic (to 20-32 wt.% of total of alkalies at predominance of Na over K), contained from 7-9 to 18-30 wt.% CaO and had elevated concentrations of SO_3, P_2O_5, Cl, SrO, BaO.

3. Disturbance of physicochemical stability of magmatic system at 1200-1190°C favored occurrence of multi-phase carbonate-salt liquid immiscibility in isolated carbonate melt and caused appearance of inhomogeneities. As a result of separation and redistribution of major petrogenic components the initial carbonate melt separated into 5 chemically different immiscible liquids: alkali-Ca-rich, alkali-sulfate, alkali-phosphate, alkali-chloride, and calciocarbonate melt.

4. The process of immiscibility of carbonate melt continued up to 800°C and led to simplification of component of composition of immiscible fractions and their spatial separation.

5. Calciocarbonate melts were the final exhausted product of evolution, which terminated disintegration of initial hyperalkali-carbonate melt. Their crystallization at 790-810°C is responsible for the formation of calcite carbonatites in the Krestovskaya intrusion. The presence of other immiscible carbonate-salt and salt melts at a macrolevel is not quite obvious. Probably, this is due to their minor separated volumes, removal outside magma chamber, or interaction with early minerals of parental silicate magma. Nevertheless, the homogenization temperatures of inclusions suggest that alkali-Ca-rich, alkali-sulfate, and alkali-phosphate melts could exist up to 850-820 and alkali-chloride, up to 790-720°C, after which they were to crystallize.

6. From the viewpoint of the results obtained, calcite and other types of carbonatites can appear only as a result of long-term evolution of initial hyperalkaline carbonatite magma. The primary composition of this magma might be preserved only in volcanic environment in rare cases of their rapid eruption and quenching on the day surface.

The work was financially supported by grant 02-05-64617a from the Russian Foundation for Basic Research and the Integratoin Project CSB № 67.

REFERENSES

1. **Andreeva IA, Naumov VB, Kovalenko VI, Kononkova NN** (1998) Fluoride-sulfate and chloride-sulfate salt melts of carbonate-bearing Mushugai-Khuduk complex, Southern Mongolia. Petrologiya 6: 307-315.
2. **Andreeva IA, Naumov VB, Kovalenko VI, Kononkova NN** (1999) Composition of magmas and genesis of theralites of carbonate bearing Mushugai-Khuduk complex (Southern Mongolia). Geokhimiya 8: 826-841.
3. **Brooker RA, Hamilton DL** (1990) Three-liquid immiscibility and the origin of carbonatites. Nature 346: 459-462.
4. **Carroll MR, Rutherford MJ** (1985) Sulfide and sulfate saturation in hydrous silicate melts. Geophys Res 90: 601-612.
5. **Dawson JB, Pinkerton H, Norton GE, Pyle DM** (1990) Physico-chemical properties of alkali carbonatite lavas: Data from the 1988 eruption of Oldoinyo Lengai, Tanzania. Geology 18: 260-263.
6. **Dawson JB, Smith JV, Stelle IM** (1992) 1966 ash eruption of the carbonatite volcano Oldoinyo Lengai: mineralogy of lapilli and mixing of silicate and carbonate magmas. Mineral Mag 56: 1-16.
7. **Egorov LS** (1985) Alkali-ultrabasic magmatism and its mineralogy. Geologiya Rudnykh Mestorozgdenii 4: 24-40.

8. **Entin AR, Zaitsev AI, Nenashev NI, Vasilenko VB, Orlov AM, Tjan OA, Olhovik YuA, Olchtinskii SP, Tolstov AV** (1990) On the sequence of geologic events related to the intrusion of the Tomtor Massif of ultrabasic-alkaline rocks and carbonatites. Russian Geology and Geophysics 31: 42-51.
9. **Freeston IC, Hamilton DL** (1980) The role of liquid immiscibility in the genesis of carbonatites: an experimental study. Contrib Mineral Petrol **7**3: 105-117.
10. **Kjarsgaard BA, Hamilton DL** (1988) Liquid immiscibility and the origin of alkali-poor carbonatites. Mineral Mag 52: 43-55.
11. **Kjarsgaard BA, Hamilton DL** (1989) The genesis of carbonatites by immiscibility. In: Bell K (ed) Carbonatites: genesis and evolution. London: Unwin Hyman, pp 388-409.
12. **Kogarko LN** (1977) Problems of genesis of agpaitic magmas (in Russian). Nauka, Moscow.
13. **Kogarko LN** (1978) Principle of polarity of chemical bond and its petrologic significance. In: Problems of petrology of the Earth's crust and upper mantle (in Russian). Nauka, Moscow, pp 222-228.
14. **Kogarko LN, Henderson CMB, Pacheco H** (1995) Primary Ca-rich carbonatite magma and carbonate-silicate-sulphide liquid immiscibility in the upper mantle. Contrib Mineral Petrol 121: 267-274.
15. **Le Bas MJ** (1977) Carbonatite-nephelinite volcanism. Wiley, New York.
16. **Legezina OG** (1999) Rocks of the Krestovskaya intrusion (north of the Siberian Platform). In: Geology and mineral resources of the Krasnoyarsk Territory (in Russian). Krasnoyarsk, pp 189-190.
17. **Lieber Werner** (1997) Bastnasit from Mountain Pass, California. Aufschluss 48: 137-142
18. **Luhr JF** (1990) Experimental phase relations of water- and sulfur-saturated arc magmas and the 1982 eruptions of E1 Chichon Volcano. J Petrology 31: 1071-1114.
19. **Marakushev AA** (1968) On the genesis of apatite deposits in Precambrian series of magnesian marbles. In: Apatites (in Russian). Nauka, Moscow, pp 339-347.
20. **Mikhailov MYu and Shatskii VS** (1975) A silicon carbide heating element for a high-temperature microscopic stade. In: Mineralogy of endogenic rocks (in Russian). Nauka, Novosibirsk, pp 109-110.
21. **Mitchell R** (1997) Carbonate-carbonate immiscibility, neighborite and potassium iron sulphide in Oldoinyo Lengai natrocarbonatite. Mineral Mag 61: 779-789
22. **Naumov VB, Kovalenko VI, Sobolev AV, Tihonenkov PI, Samoilov VS** (1986) Immiscibility of silicate melts from data on studies of inclusions in high-temperature fluorite. Dokl AN SSSR 288: 453-456.
23. **Nielsen TFD, Solovova IP, Veksler IV** (1997) Parental melts of melilitolite and origin of alkaline carbonatite: evidence from crystallized melt inclusions, Gardiner complex. Contrib Mineral Petrol 126: 331-344.
24. **Panina LI** (1985) Physicochemical conditions of formation of rocks in intrusions of alkali-ultrabasic formation. Russian Geology and Geophysics 26: 33-51.
25. **Panina LI, Sazonov AM, Usol'tseva LM** (2001) Melilitic and monticellite-bearing rocks of the Krestovskaya intrusion (north of Siberian Platform) and their genesis. Russian Geology and Geophysics 42: 1313-1332.
26. **Panina LI, Usol'tseva LM** (1999) Alkali-Ca-rich sulfate-carbonatitic inclusions in melilite-monticellite-olivine rocks of the Malyi Murun alkaline massif (Aldan). Petrologiya 7: 653-659.
27. **Panina LI, Usol'tseva LM** (2000) Role of liquid immiscibility in the formation of calcitic carbonatites of the Malyi Murun Massif (Aldan). Russian Geology and Geophysics 41: 655-670.

28. **Poulson SR, Ohmoto H** (1990) An evalution of the solubility of sulfide sulfar in silicate melts from experimental data and natural samples. Chem Geol 85: 57-75.
29. **Pridannikov AV, Il'in SS, Betkher MYa, Sazonov AV, Krasnova TG** (1999) Chemical composition of the Krestovskaya intrusion. In: Physicochemistry and technology of inorganic materials (in Russian). Krasnoyarsk, pp 25-28.
30. **Pyatenko IK, Saprykina LG** (1976) On finding of carbonatitic lavas and pyroclastics in the Paleozoic volcanosedimentary series of the Kantozera region on the Kola peninsula. Dokl AN SSSR 229: 919-921.
31. **Ripp GS, Kobylkina OV, Doroshkevich AG, Sharakshinov AO** (2000) Late-Mezozoic carbonatites of Western Transbaikalia (in Russian). Nauka, Ulan-Ude.
32. **Ryabchikov ID** (1987) Mantle magma formation. In: Evolution of magmatism in the Earth's history (in Russian). Nauka, Moscow, pp 349-371.
33. **Sazonov AM, Zvyagina EA, Leontiev SI, Gertner IF, Krasnova TS, Kolmakov YuV, Panina LI, Chernyshov AI, Makeev SM** (2001) Platinum-Bearing alkaline-ultrabasic intrusions of the Polar Siberia (in Russian). Tomsk.
34. **Shastry A, Kumar S** (1995) Petrogenesis of carbonatite veins and associated melanephelinite from Sarnu-Dandali Igneous Complex, Barmer, Rajasthan. Ind Nat Acad Sci Lett 18: 139-143.
35. **Solovova IP, Girnis AV, Ryabchikov ID** (1996) Inclusions of carbonate and silicate melts in minerals of alkaline basaltoids from Eastern Pamir. Petologiya 4: 339-363
36. **Suk NI** (2001) Experimental study of silicate-carbonate systems. Petrologiya 9: 547-558.

UDK 549.322+552.323.6

Genesis of djerfisherite from kimberlites and xenoliths of the Udachnaya diatreme, Yakutia, Russia

Sharygin V.V., Golovin A.V., Pokhilenko N.P.

Institute of Mineralogy and Petrography, UIGGM SD RAS, Novosibirsk, Russia, e-mail: sharygin@uiggm.nsc.ru

Djerfisherite has been found in different unaltered rocks of the Udachnaya-Eastern pipe: in kimberlite breccias, in veined monticellite kimberlites and in a phlogopite-spinel lherzolite. In kimberlite breccias it is observed both a groundmass mineral and a phase of secondary melt and sulphide inclusions which forms trails in olivine. Djerfisherite is the main sulphide mineral in the groundmass and it forms individual irregular or rounded grains (up to 50-100 μm) or association with magnetite. In secondary melt inclusions (5-80 μm) djerfisherite occurs together with other daughter/trapped phases (carbonates, Na-K-chlorides, silicates, magnetite, sulphates and Fe-Ni-sulphides). Homogenisation of secondary melt inclusions occurred at 700-800°C. Monticellite kimberlites form the 2 cm-thick veins in kimberlite breccias. Here K-sulphide forms rounded isolations (up to 20 μm) in the groundmass or sulphide blebs in poikilitic sodalite, rarely it occurs as a phase of secondary inclusions in olivine. In the xenolith djerfisherite is mainly intergranular phase, which forms rims (up to 100 μm) on primary mantle sulphides or individual xenomorphic grains. The broad compositional variations (especially, in Fe, Ni and Cu) are typical of djerfisherite from different occurrences of the Udachnaya pipe. The textural relations and microprobe data are evidenced that djerfisherite from the Udachnaya-Eastern pipe kimberlites is a common groundmass mineral which appeared at the late magmatic stage. During formation of kimberlite breccias the melt due to phenocryst crystallisation gradually evolved towards carbonatites. Crystallisation of carbonates from volatile-rich silicate-carbonate melt probably permits djerfisherite to be stable. It crystallised at shallow depths and T≤700-800°C. In contrast, K-sulphide found in phlogopite-spinel lherzolite is seems to be product of infiltration of evolved kimberlite magma into xenolith or of reaction of evolved kimberlite fluid/melt with xenolith at shallow depths. In general, it partially or completely replaces the primary sulphide assemblages. The same genesis may be considered for djerfisherite from sulphide associations in diamonds and xenoliths from world-wide kimberlites.

INTRODUCTION

Djerfisherite, generally $K_6Na(Fe,Ni,Cu)_{24}S_{26}Cl$, was firstly discovered in meteorites [18]. Later it was found in Cu-Ni-ores, kimberlites, alkaline ultramafic and carbonatitic rocks, alkaline agpaitic rocks as well as in skarns around alkaline and intermediate massifs. Clarke et al. [6] summarized the majority of data on occurrences and origins of djerfisherite. The information about new occurrences of this mineral in carbonatites and related silicate rocks was given in [2, 11, 12,

21, 27, 30, 37, 45]; in peralkaline rocks – [1, 9, 14, 22, 31, 33, 47, 48]; in skarns – [23, 26, 36, 39, 46]; and in some chondritic meteorites – [16, 25, 32].

This sulphide is very rare in kimberlites and their xenoliths. Djerfisherite was commonly established in diamonds and xenoliths from kimberlites of Yakutia and South Africa as phase rimmed primary Fe-Ni-Cu-sulphides [3, 5, 7, 13, 15, 20, 41, 42, 49]. Genesis of djerfisherite from these associations normally interprets as metasomatic transformation of xenoliths and diamonds due to invasion of K-Cl-S-rich fluid either in the mantle prior to trapping by kimberlitic magma or at a late stage of kimberlite formation [3, 5, 7, 15, 34, 41-43]. At present day, the findings of this sulphide in kimberlite itself are scarce. It was firstly mentioned (without chemical data) as groundmass mineral in kimberlites of the Muza pipe, Yakutia [15]. Later djerfisherite was found in the groundmass of kimberlites from Northwest Territories (Canada) as a late primary magmatic phase [4, 6].

In this work, we report new data about the occurrences of djerfisherite from unaltered kimberlitic rocks of the Udachnaya-Eastern pipe, Yakutia. Initially djerfisherite was found and analysed from secondary melt inclusions in olivine of kimberlite breccias [19]. Later this mineral was observed in the groundmass of kimberlite breccias and veined monticellite kimberlites [40]. Recently we found abundant djerfisherite in a phlogopite-spinel lherzolite from unaltered kimberlite breccias of this pipe. This work is a first detailed description of djerfisherite from the groundmass of the Yakutian kimberlites in comparison with K-sulphide from mantle xenoliths.

ANALYTICAL TECHNIQUES

Doubly-polished rock sections of about 50-100 μm in thickness have been used for optical microscopy in transmitted and reflected light. Quantitative analyses of djerfisherite and other sulphides were performed using a CAMEBAX electron microprobe equipped with an energy-dispersion system at the United Institute of Geology, Geophysics and Mineralogy (UIGGM), Novosibirsk, Russia. Operating conditions were accelerating voltage 20 kV, beam current 15-30 nA, beam diameter about 2 μm, counting time 30 seconds. The precision for major elements were better than 2 % relative. Mineral standards and synthetic alloys were used for controls: chalcopyrite and pyrrhotite for Fe, Cu and S, synthetic Fe-Ni-Co alloy for Ni and Co, albite for Na, sanidine for Si, Al and K, chlorapatite for Cl. Tl was not detected in analysed djerfisherites, Ag and Li were not determined. The K-sulphide grains with size more than 10 μm were selected for microprobe analysis. International mineral standards were use for analyses of silicates and oxides from mantle xenolith and groundmass of kimberlites. Back-scattered electron images (BSE) were carried out with a JEOL electron scanning microscope at UIGGM, Novosibirsk. X-ray powder diffraction data for kimberlites and some minerals were obtained by means of X-ray diffractometer DRON-3 (IMP UIGGM) using CuKα radiation.

BRIEF GEOLOGICAL BACKGROUND OF THE UDACHNAYA DIATREME

The Udachnaya pipe (Middle Paleozoic) is situated in the Daldyn-Alakit field of the Yakutian kimberlite province. It consists of two bodies (western and eastern), which were connected on the surface forming eight in plan. Upper-middle Cambrian and Lower Ordovician dolomites, dolomitic limestones, mudstones, sandstones, and calcareous conglomerates are the main country sedimentary rocks of the Udachnaya pipe. The eastern diatreme was comprised at least by four intrusive phases: the three phases are different types of kimberlite breccias, the fourth phase is veined and dyke kimberlites [24]. The studied kimberlite breccias and monticellite kimberlite are related to the main third and fourth stages, respectively. These rocks were exposed on the 350-650 m depth. It should be noted that, in general, kimberlites of the eastern body are essentially fresher than rocks of the western body.

MINERALOGY AND PETROGRAPHY

Kimberlite breccias of the main third stage of the Udachnaya-Eastern diatreme contain abundant mantle-derived xenocrysts and xenoliths as well as the crustal xenogeny material. Olivine and phlogopite are the main macrocrysts and phenocrysts in these rocks. Fine-grained groundmass consists of olivine, calcite, phlogopite, perovskite, zoned spinel (chromite-Ti-magnetite-magnetite), ilmenite, djerfisherite and other sulphides, and Ca-Na-carbonates. The well-faceted gypsum crystals and zeolites occur in cavities of kimberlites as post-magmatic phases.

Monticellite kimberlite is the later intrusive phase than kimberlite breccias. In some cases it forms large blocks and injections in the Udachnaya-Eastern pipe [29]. We studied the 2 cm-thick black veined injections of monticellitic rocks in the kimberlite breccia. The abundance of xenogeny material do not exceed 5 vol. %. These rocks contain olivine and rare phlogopite as macro- or phenocrysts in fine-grained groundmass consisting of olivine, perovskite, phlogopite, monticellite, Ti-magnetite, sodalite, djerfisherite and scarce calcite.

The secondary alterations are normally absent in all studied kimberlite species. It should be also noted that djerfisherite is the dominant sulphide phase in these kimberlitic rocks. According to previous data [38] and our X-ray powder diffraction data, all rocks of the Udachnaya-Eastern pipe contain also fine-dispersive Na-K-chlorides, but their nature is unclear yet. Possibly they have post/late magmatic origin due to infiltration of Na-K-solutions or melts in kimberlites [10, 38]. Our recent field observations showed that kimberlite breccias of the third stage also contain abundant large isolations (sometimes, up to 0.5x1 m) of halite-sylvite rocks, sometimes in association with shortite and northupite. We do not exclude that they may be xenoliths of the country Cambrian evaporates trapped by kimberlitic magma during uplifting.

The studied phlogopite-spinel lherzolite was found in kimberlite breccia of third stage. This xenolith is rounded in the shape (size – up to 20 cm) and rimmed by light kimberlitic rock (up to 1-2 cm) labelled as autolithic kimberlite [34]. In general, it is orthopyroxene-rich and its primary paragenesis contains orthopyroxene, olivine, clinopyroxene, Cr-spinel, phlogopite and Fe-Ni-sulphides (monosulphide solid solution + pentlandite or pentlandite + pyrrhotite). The intergranular space in the xenolith is filled with the association consisting of olivine, clinopyroxene, Cr-spinel, phlogopite and djerfisherite+pyrrhotite. Moreover, the small cavities in the xenolith contain halite+sylvite, Na-Ca-carbonates and sulphides. The chemical compositions of minerals from both primary and interstitial associations are given in Table 1. It should be noted that chemistry of the same minerals from primary and interstitial paragenesises is drastically different. The chemical composition of primary minerals allows roughly estimate the PT-conditions for this xenolith as 31-33 kb and 700-800^{o}C.

OCCURRENCES OF DJERFISHERITE IN THE UDACHNAYA-EASTERN PIPE

Djerfisherite is observed in the secondary inclusions, which form trails in the macrocrystal and phenocrystal olivine, rarely – in the groundmass olivine of kimberlite breccia and monticellite kimberlite (Fig. 1 A, C). In this mineral djerfisherite occurs as individual sulphide blebs (up to 30 μm) and as a daughter phase in the secondary melt and polycrystalline inclusions (5-80 μm, Fig. 1). In secondary melt inclusions in olivine of kimberlite breccia it is associated with carbonates (calcite, Na-Ca-carbonates, dolomite, magnesite-siderite, northupite), silicates (tetraferriphlogopite, olivine, humite-clinohumite, diopside, monticellite), magnetite, Na-K chlorides and sulphates, rarely – with Mg-phosphate and Ni-rich pyrrhotite (or monosulphide solid solution, 4.4 wt % Ni). Ti-poor magnetite and djerfisherite are closely associated in the melt inclusions, whereas tetraferriphlogopite is common among silicate phases. The size of inclusion djerfisherite grains ranges from 2 to 15 μm. Homogenisation of melt inclusions occurred at 700-800^{o}C, and they were trapped at shallow depth [19]. During heating djerfisherite and magnetite disappeared near homogenisation temperatures. Polycrystalline inclusions contain the association calcite + magnetite + djerfisherite (Fig. 1 E). The secondary inclusions in olivine of monticellite kimberlite have the phase composition like those from kimberlite breccia.

K-sulphide in the groundmass of kimberlite breccia is the latest mineral phase. It either forms individual subhedral grains (up to 50-100 μm) in association with magnetite and rarely with pyrrhotite or fills the interstitial space between other groundmass minerals. Olivine, calcite and other groundmass minerals occur as crystal inclusions in the grains of djerfisherite (Fig. 2 A-D). In monticellite kimberlite djerfisherite is also late mineral. It forms rounded isolations (up to 20 μm) in the groundmass or individual sulphide blebs in poikilitic sodalite together with monticellite, perovskite, and magnetite (Fig. 2 E-F).

Table 1.

Chemistry (wt. %)of minerals from phlogopite-spinel lherzolite, Udachnaya-Eastern pipe

	Primary association					**Interstitial association**					
Phase	Ol-1	Opx-1	Cpx-1	Sp-1	Phl-1	Ol-2	Cpx-2	Sp-2	Phl-2	Phl-2	Phl-2
n	6	6	7	4	27	9	7	3	1	1	2
SiO_2	41.52	56.75	54.27	0.00	37.68	41.55	54.68	0.00	42.08	39.33	38.93
TiO_2	0.00	0.05	0.09	0.04	4.09	0.00	0.24	0.06	0.09	1.70	4.28
Cr_2O_3	0.01	0.64	1.47	30.55	1.36	0.12	0.30	39.43	0.40	0.87	0.03
Al_2O_3	0.00	2.29	3.11	36.98	14.35	0.00	0.21	27.46	11.99	12.28	11.42
FeO	6.86	4.63	1.69	16.47	2.50	5.86	2.38	17.82	1.85	4.10	7.05
MnO	0.09	0.10	0.05	0.17		0.30		0.42	0.02	0.01	0.07
MgO	50.98	35.31	15.70	15.05	22.49	51.57	17.76	13.54	26.74	24.94	22.14
CaO	0.00	0.29	22.15	0.00	0.02	0.36	23.84	0.00	0.10	0.07	0.03
BaO	0.00		0.00	0.00	2.16	0.00	0.00	0.00		0.27	0.62
Na_2O	0.00	0.04	1.54	0.00	0.17	0.00	0.42	0.00	0.14	0.47	0.56
K_2O	0.00	0.00	0.00	0.00	9.34	0.00	0.00	0.00	10.50	9.90	9.13
NiO	0.47	0.10	0.04	0.12		0.31		0.10	0.28		
F										2.05	1.50
Cl										0.01	0.01
Total	99.92	100.20	100.12	99.37	94.15	100.08	99.84	98.84	94.20	96.00	95.76
Mg#	0.93	0.93	0.94	0.65	0.94	0.94	0.93	0.62	0.96	0.92	0.85

Note. Ol = olivine; Opx = orthopyroxene; Cpx = clinopyroxene; Sp = spinel; Phl = phlogopite. *n* - number of analyses. For silicates **Mg#** means $Mg/(Mg+Fe_{tot})$, for spinels – $Mg/(Mg+Fe^{2+})$.

Djerfisherite in phlogopite-spinel lherzolite is an interstitial phase (Fig. 3 A). It usually forms the rims (up to 100 μm) around early sulphide isolations (monosulphide solid solution + pentlandite or pentlandite+pyrrhotite, Fig. 3 B-E) and individual xenomorphic grains or rims around pyrrhotite in the intergranular space of xenoliths (Fig. 3 F). Early sulphide associations without djerfisherite rim occur scarcely (Fig. 3 G). In some cases, djerfisherite is observed in trails, which fill the microfractures in primary silicate minerals of xenolith (Fig. 3 H-I). The textural relations in the xenolith interstices show that djerfisherite crystallised after silicate phases and pyrrhotite.

K-sulphide also occurs in autolithic kimberlite, e.g. on the contact between xenolith and kimberlite breccia. Like mineral from xenolith interstices this djerfisherite also form rims around pyrrhotite and individual xenomorphic or rounded grains (Fig. 4). Sometimes Cu-rich sulphide (chalcopyrite ?) occurs in djerfisherite filling with microfractures in the host (Fig. 4 G). Mineral relations show that pyrrhotite and djerfisherite crystallised after olivine, calcite and other groundmass phases. In some cases, the connection between kimberlite and interstices in xenolith was observed (Fig. 4 A). The compositions of Fe-Ni-sulphides from xenolith and contact are given in Table 2. It should be noted that these phases are virtually free in Cu.

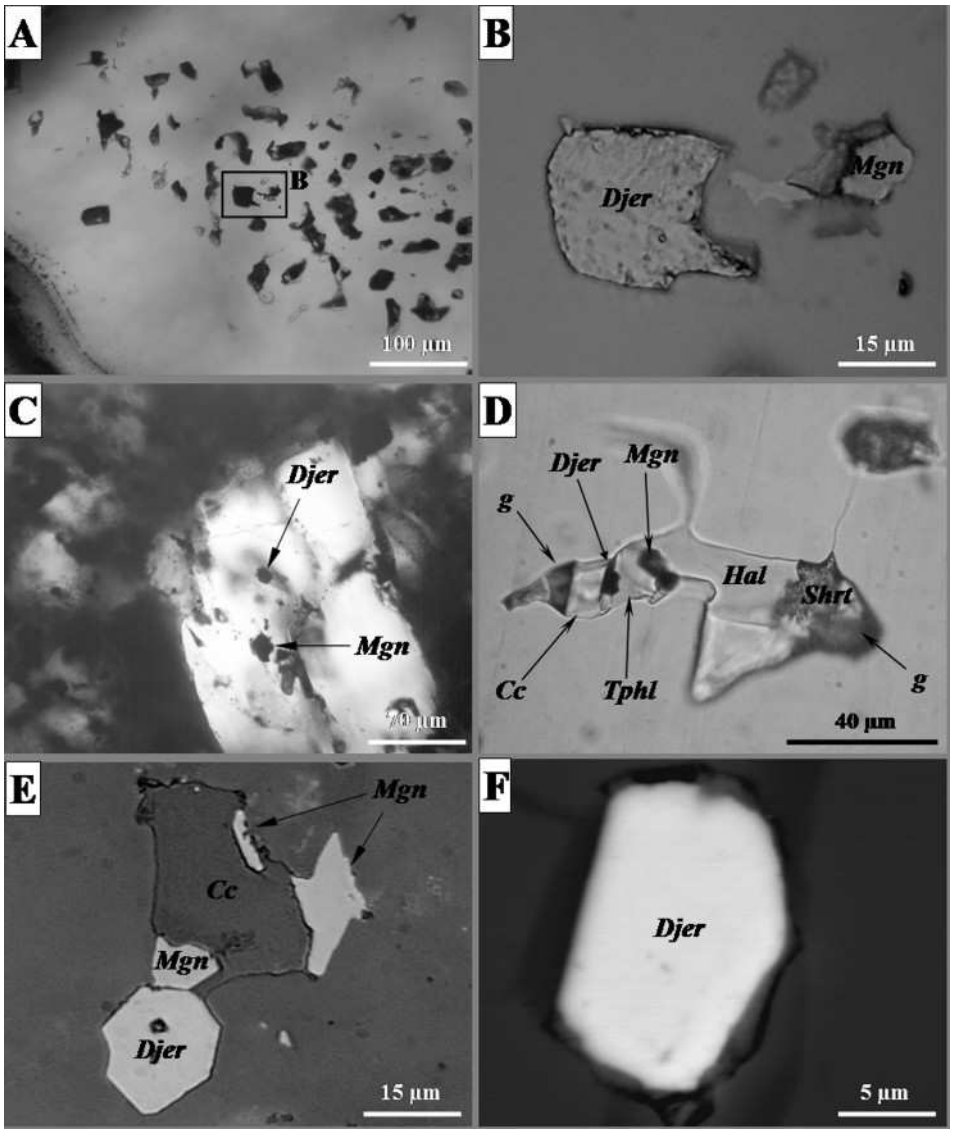

Fig. 1. **Djerfisherite from secondary inclusions in olivine of kimberlite breccias, Udachnaya-Eastern pipe.**

A – general view of trail of secondary inclusions in macrocrystal olivine, ordinary light; B – djerfisherite in association with magnetite, reflected light; C – djerfisherite and magnetite from trail of secondary inclusion in groundmass olivine, ordinary light; D – secondary melt inclusion containing djerfisherite, calcite, halite, tetraferriphlogopite, shortite and magnetite, ordinary light; E – polycrystalline inclusion consisting of calcite, djerfisherite and magnetite, reflected light; F – individual djerfisherite bleb in olivine, BSE image.
Symbols: *Djer* – djerfisherite; *Mgn* – magnetite; *Hal* – halite; *Tphl* – tetraferriphlogopite; *Cc* – calcite; *Shrt* – shortite; *g* – gas bubble.

CHEMICAL COMPOSITIONS OF DJERFISHERITE

The broad compositional ranges are most characteristic for djerfisherite from inclusions in olivine of kimberlite breccias (based on 26 analyses, in wt. %): Fe – 32.6-38.8; Ni – 4.2-23.1; Co – 0.2-0.5; Cu – 0.1-17.6; K – 8.9-9.3; Na – 0.04-0.7; S – 32.5-33.4; Cl – 1.2-1.4. In contrast, K-sulphide from olivine-hosted inclusions in monticellite kimberlite has Fe-rich composition (based on 4 analyses, in wt. %): Fe – 40.2-49; Ni – 6-8; Co – 0.1-0.3; Cu – 0.2-7; K – 9.1-9.5; Na – up to 0.5; S –

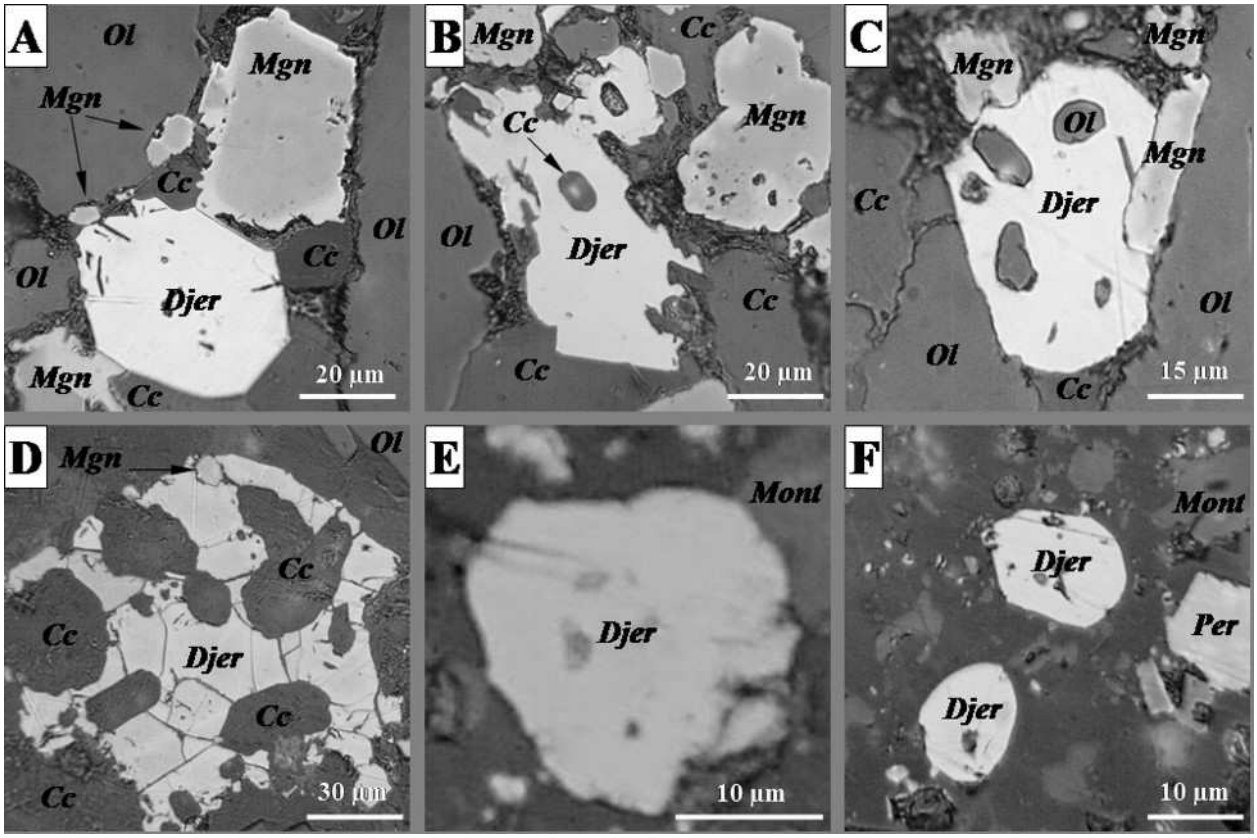

Fig. 2. **Djerfisherite from kimberlite groundmass of the Udachnaya-Eastern pipe (reflected light).**

A-D – in kimberlite breccia: A – polygonal grain in groundmass in association with zoned spinel, olivine and calcite; B – xenomorphic isolation with calcite inclusion; C – grain with olivine inclusions; D – xenomorphic isolation with calcite inclusions; E, F – rounded blebs of djerfisherite in association with monticellite and perovskite inclusions in poikilitic sodalite from monticellite kimberlite.
Symbols: *Mgn* – zoned spinel (core - Cr-spinel, middle – Ti-magnetite, rim – magnetite); *Ol* – olivine; *Mont* – monticellite; *Per* – perovskite. Other symbols see Figure 1.

33.2-33.5; Cl – 1.3-1.6. However, the variations in Fe, Ni and Cu are insignificant within single grains from the core to rim (Table 3).

In general, djerfisherites from the groundmass of kimberlite breccias and monticellite kimberlites are richer in Fe and poorer in (Ni+Co) than mineral of olivine-hosted inclusions. The core-to-rim deviations within single grains are also minimal. Thus, djerfisherite from groundmass of kimberlite breccias has the following compositional variations (based on 57 analyses, in wt. %): Fe – 37.0-42.7; Ni – 2.0-6.3; Co - 0.2-0.4; Cu – 9.9-14.9; K – 8.8-9.4; Na – 0-0.2; S – 32.6-33.3; Cl – 1.2-1.5. Potassium sulphide from groundmass of monticellite kimberlites is characterized by lower Cu and higher Ni (based on 36 analyses, in wt. %): Fe – 38.1-43.5; Ni – 5.8-9.2; Co – 0.1-0.2; Cu – 6.1-10; K -9.1-9.6; Na – 0.2-0.4; S – 33.1-33.5; Cl – 1.3-1.5. Table 4 presents some representative compositions of djerfisherite from groundmass of different rock species of the Udachnaya-Eastern pipe.

Intraxenolith djerfisherites are rich in Ni and poor in Cu (based on 40 analyses, in wt. %): Fe – 34.0-42.2; Ni – 12.5-19.6; Co – up to 0.2; Cu – 0.4-5.7; K

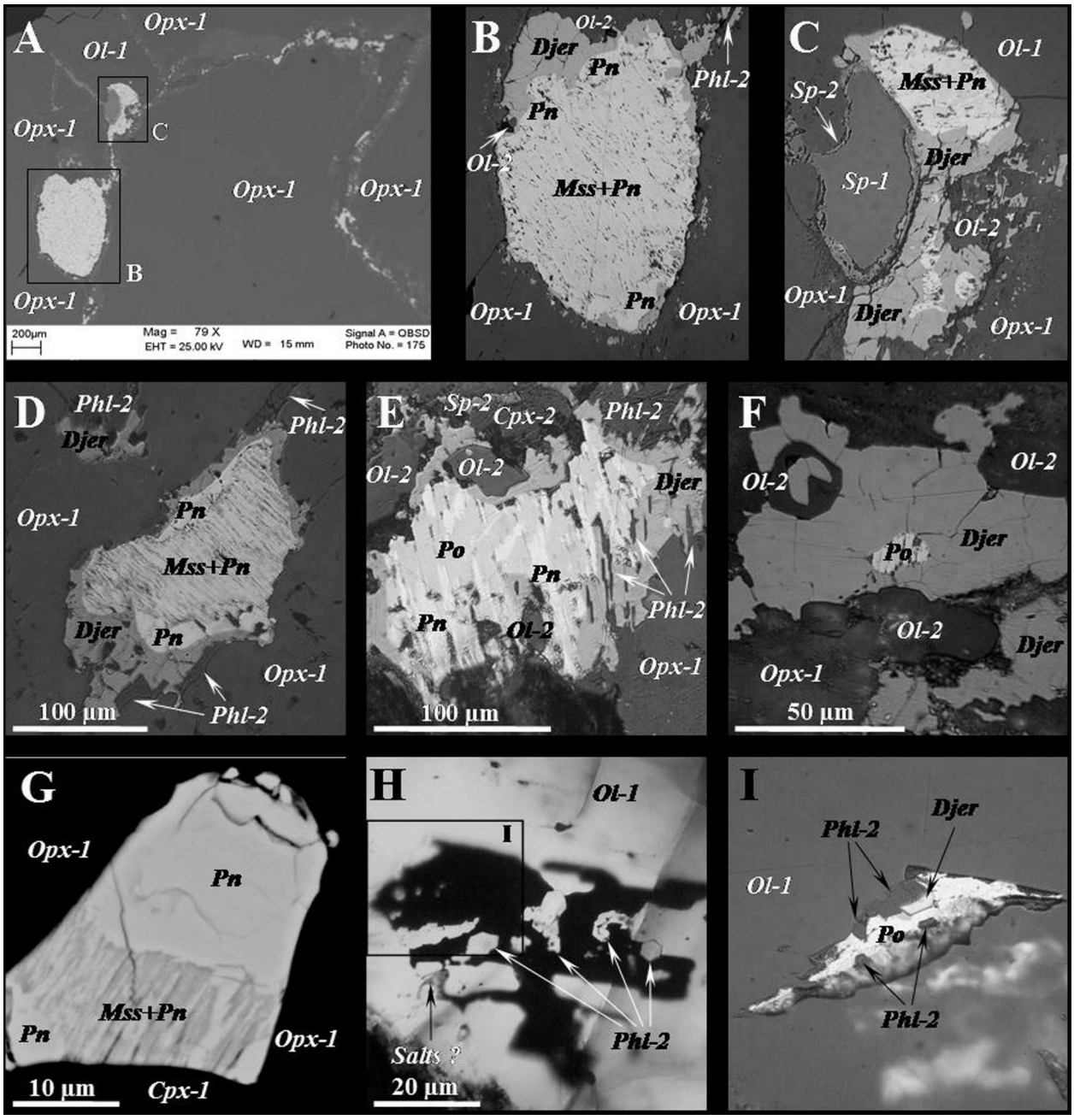

Fig. 3. **Djerfisherite and Fe-Ni-sulphides in phlogopite-spinel lherzolite from the Udachnaya-Eastern pipe.**

A – distribution of sulphides in the xenolith; B-G – interstitial sulphide associations in xenolith; H-I – trails of inclusions in xenolith olivine-1. A, G – BSE images; B-F, I – reflected light; H – ordinary light. Symbols: *Opx-1, Ol-1, Cpx-1, Sp-1* –primary orthopyroxene, olivine, clinopyroxenes and Cr-spinel of xenolith; *Ol-2, Phl-2, Cpx-2, Sp-2* – olivine, phlogopite, clinopyroxene and Cr-spinel from interstices of xenolith; *Mss* – monosulphide solid solution; *Pn* – pentlandite, *Salts?* – chlorides+sulphates+carbonates. Other symbols see Figures 1-2.

– 9.0-9.5; Na – 0-0.2; S – 33.0-33.5; Cl – 1.3-1.5. K-sulphides from small cavities in xenolith have similar compositional variations. In contrast, djerfisherites on the contact between xenolith and kimberlite are richer in Fe and poorer in Ni (based on 33 analyses, in wt. %): Fe – 41.1-49.8; Ni – 4.5-8.6; Co - 0.1-0.6; Cu – 0.5-8.3; K – 9.1-9.5; Na – 0.1-0.2; S – 33.2-33.5; Cl – 1.3-1.5 (Table 5).

Table 2.

Chemistry of Fe-Ni-sulphides from phlogopite-spinel lherzolite and from the contact of xenolith and kimberlite breccia, Udachnaya-Eastern pipe

#	Sulphide association	Phase	*n*	Fe wt.%	Ni	Co	Cu	S	Total
1	**Mss+Pn+Djer**	**Mss**	5	55.04	8.47	0.23	0.01	36.35	100.10
		Pn in Mss	3	40.96	24.80	0.66	0.03	33.63	100.09
		Pn	4	35.60	29.70	1.50	0.03	33.36	100.19
2	**Mss+Pn+Djer**	**Pn**	1	36.04	29.33	0.84	0.02	33.78	100.00
3	**Mss+Pn+Djer**	**Pn in Mss**	1	33.44	32.45	0.73	0.07	33.40	100.09
		Pn	1	32.91	32.56	0.98	0.06	33.47	99.98
4	**Pn+Po+Djer**	**Pn**	1	40.03	25.19	1.77	0.02	33.16	100.17
		Po	2	62.67	0.27	0.00	0.01	36.64	99.58
5	**Pn+Po+Djer**	**Pn**	2	38.51	25.95	2.07	0.03	33.53	100.08
		Po	2	63.06	0.14	0.00	0.00	36.82	100.02
6	**Pn+Po+Djer**	**Pn**	1	35.82	29.64	0.48	0.06	33.55	99.54
7	**Po+Djer**	**Po**	1	62.85	0.17	0.00	0.00	36.78	99.80
8	**Po+Djer**	**Po**	2	62.77	0.17	0.00	0.00	36.81	99.75
9	**Mss+Pn+Djer**	**Mss**	1	54.82	8.80	0.26	0.03	36.08	99.99
		Pn	2	40.20	25.57	0.33	0.13	33.83	100.05
10	**Mss+Pn+Djer**	**Pn**	2	37.82	28.35	0.77	0.03	32.75	99.72
11	**Mss+Pn+Djer**	**Mss**	1	55.26	8.66	0.42	0.02	35.82	100.18
		Pn	1	37.22	28.84	1.09	0.02	32.89	100.06
12	**Po+Djer**	**Po**	2	63.24	0.03	0.00	0.00	36.52	99.79
13	**Po+Djer**	**Po**	2	63.25	0.06	0.01	0.00	36.66	99.97
14	**Po+Djer**	**Po**	2	63.12	0.05	0.00	0.04	36.61	99.82
15	**Po+Djer**	**Po**	1	63.20	0.03	0.00	0.02	36.61	99.86
16	**Po+Djer**	**Po**	1	63.14	0.08	0.01	0.00	36.76	99.99

Note. 1-8 - intraxenolith suphides; 9-11 - sulphides from cavities in xenoliths, in association with Na-Ca-carbonates and halite; 12-16 - sulphides on the xenolith-kimberlite breccia contact; Mss = monosulphide solid solution; Pn = pentlandite; Po = pyrrhotite; Djer - djerfisherite, *n* = number of analyses.

All data (Tables 3-5) show that Cl is an essential component of djerfisherite at approximate level of one atom per formula unit and Na is not very significant element (excepting some djerfisherites from inclusions).

DISCUSSION

The variation diagrams (Fig. 5) show the pronounced differences between djerfisherites from olivine-hosted inclusions and from groundmass of kimberlite breccias and monticellite kimberlites. Djerfisherite from kimberlite breccia groundmass forms two compositional clusters in the Cu abundance. The first cluster overlaps with some djerfisherite compositions from olivine-hosted inclusions. Possibly it is evidenced that some djerfisherites from inclusions may be result of the invasion of residual kimberlite melt, which forms the groundmass of kimberlite breccias. Other djerfisherites probably originate due to complete

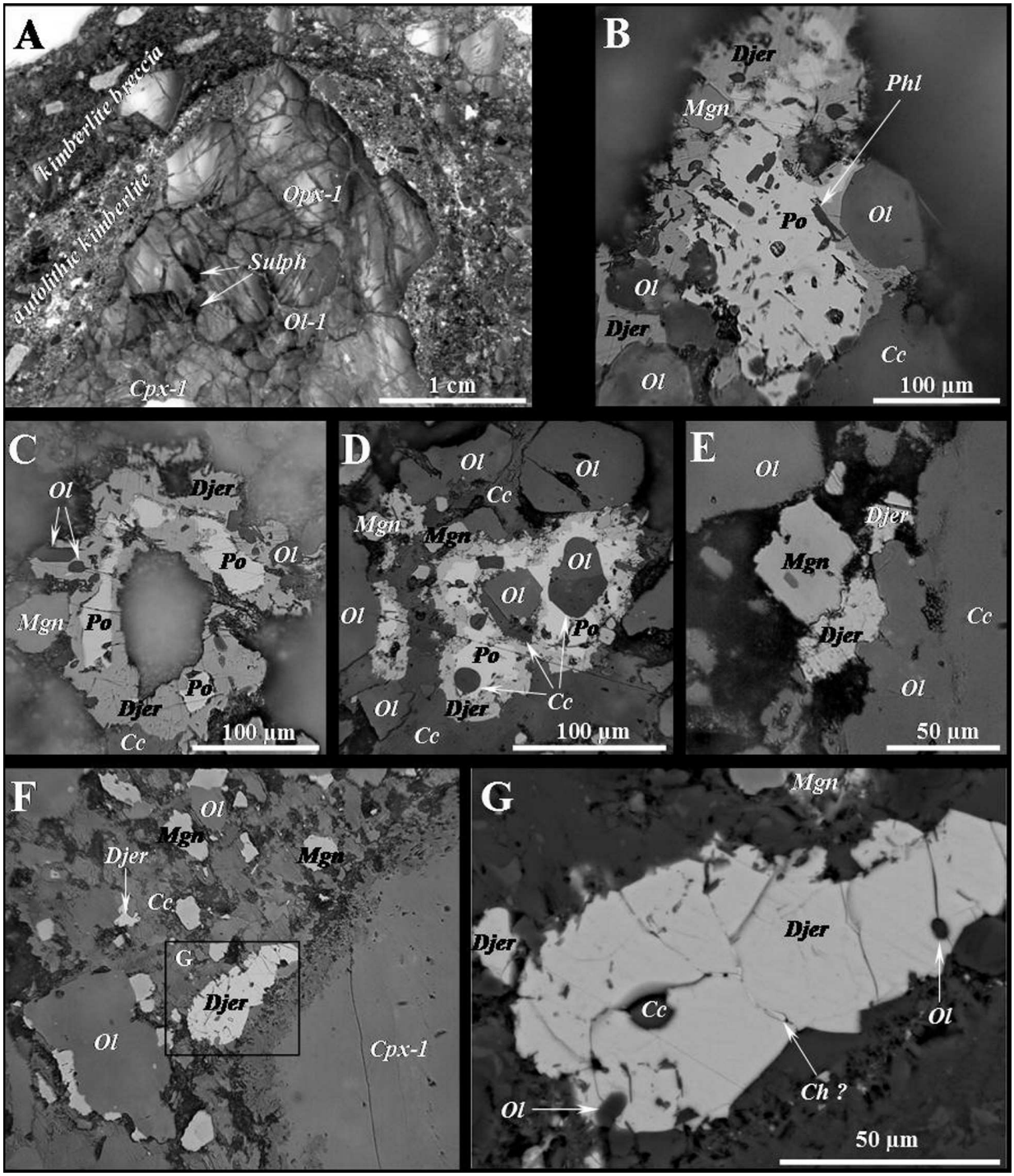

Fig. 4. **Djerfisherite and pyrrhotite on the contact between kimberlite breccia and phlogopite-spinel lherzolite, Udachnaya-Eastern pipe.**

A – light zone in kimberlite (autolithic kimberlite) on the contact with xenolith; B-G – djerfisherite and other sulphides in autolithic kimberlite on the contact. A – ordinary light; B-F – reflected light; G – BSE image. *Sulph* – polysulphide associations in xenoliths; *Ch ?* – Cu-rich sulphide (chalcopyrite?); other symbols see Figures 1-3.

replacement of primary sulphides in xenocrystal and macrocrystal olivine. In general, djerfisherites from groundmass of kimberlite breccias and monticellite kimberlite show negative correlations between Cu and Fe evidencing about

Table 3.

Representative analyses of djerfisherite from olivine-hosted inclusions in kimberlite breccia and monticellite kimberlite, Udachnaya-Eastern pipe

wt.%	1	2	3	4		5	6	7		8		9		10	11	12
				c	r			c	r	c	r	c	r			
K	8.97	9.10	8.89	8.97	8.92	9.08	9.08	9.08	9.08	9.15	9.27	8.95	8.85	9.12	9.18	9.40
Na	0.06	0.10	0.05	0.08	0.06	0.03	0.06	0.04	0.04	0.00	0.00	0.69	0.44	0.00	0.53	0.35
Fe	35.32	34.31	34.78	36.00	36.03	36.41	35.98	35.40	35.17	37.08	37.06	34.78	34.94	49.03	41.64	40.23
Ni	20.34	20.28	17.54	15.98	15.94	12.17	11.59	10.26	10.52	5.30	5.28	5.33	5.37	5.97	6.99	7.99
Co	0.43	0.39	0.45	0.36	0.38	0.27	0.24	0.31	0.27	0.18	0.20	0.16	0.14	0.28	0.08	0.10
Cu	0.21	1.47	3.57	4.47	4.30	7.54	8.53	10.98	10.79	14.43	14.18	15.95	16.04	0.23	6.52	7.01
S	33.36	33.01	33.35	32.93	32.97	32.89	32.94	32.86	32.74	32.53	32.91	32.80	32.81	33.40	33.16	33.52
Cl	1.33	1.39	1.38	1.33	1.29	1.39	1.24	1.22	1.36	1.38	1.38	1.28	1.43	1.55	1.32	1.37
Total	100.02	100.05	100.01	100.12	99.89	99.78	99.66	100.15	99.97	100.05	100.28	99.94	100.02	99.58	99.41	99.97
Formula based on 26 sulphurs																
K	5.733	5.877	5.683	5.807	5.768	5.886	5.877	5.891	5.913	5.997	6.005	5.817	5.751	5.821	5.902	5.979
Na	0.065	0.110	0.054	0.088	0.066	0.033	0.066	0.044	0.044	0.000	0.000	0.763	0.486	0.000	0.574	0.380
Fe	15.803	15.514	15.566	16.317	16.311	16.523	16.303	16.080	16.034	17.013	16.808	15.827	15.895	21.911	18.743	17.914
Ni	8.658	8.724	7.468	6.891	6.865	5.254	4.996	4.434	4.563	2.314	2.278	2.308	2.324	2.538	2.993	3.385
Co	0.182	0.166	0.191	0.155	0.161	0.116	0.104	0.132	0.117	0.079	0.088	0.067	0.062	0.120	0.032	0.041
Cu	0.084	0.584	1.404	1.781	1.711	3.007	3.397	4.383	4.323	5.819	5.652	6.379	6.413	0.090	2.579	2.743
S	26.000	26.000	26.000	26.000	26.000	26.000	26.000	26.000	26.000	26.000	26.000	26.000	26.000	26.000	26.000	26.000
Cl	0.937	0.990	0.973	0.950	0.920	0.994	0.885	0.873	0.977	0.997	0.986	0.918	1.025	1.091	0.936	0.961

Note. Microprobe beam diameter was 2 μm. 1-9 - kimberlite breccia; 10-12 - monticellite kimberlite; c = core, r = rim of djerfisherite grains.

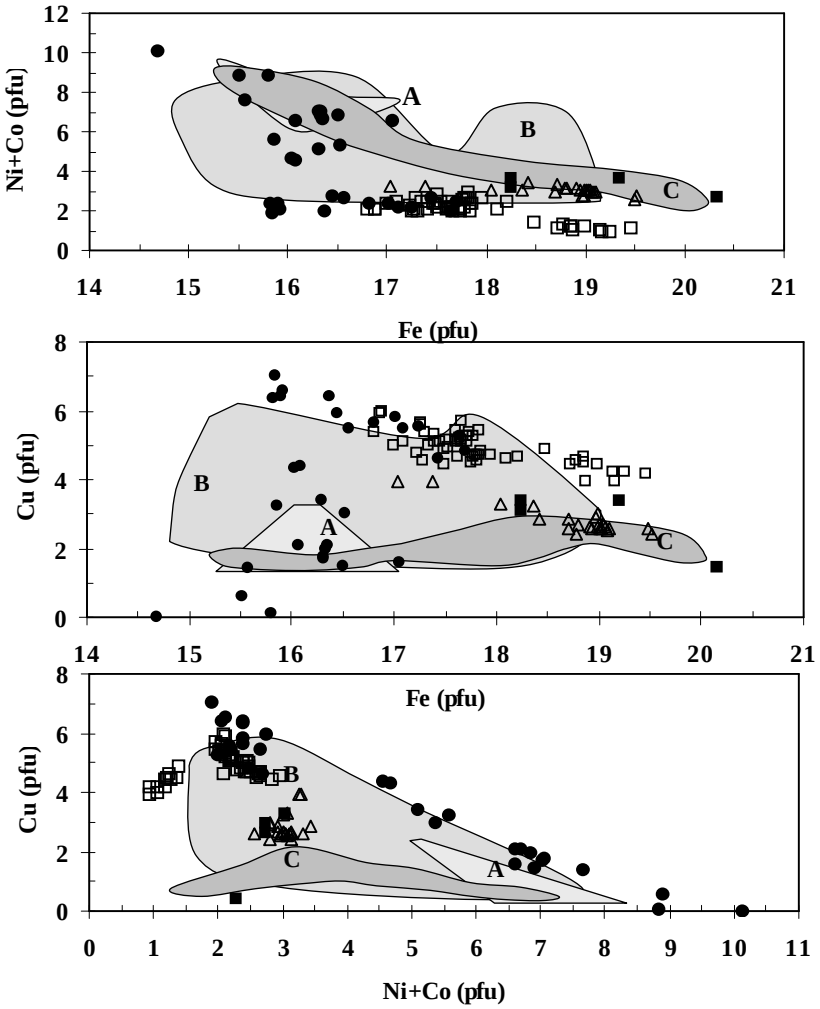

F ig. 5. **Compositional variations of djerfisherite (in apfu) from kimberlites of the Udachnaya-Eastern pipe.**

Solid circles – from inclusions in olivine of kimberlite breccia; solid squares - from inclusions in olivine of monticellite kimberlite; open squares – from groundmass of kimberlite breccia; open triangles – from groundmass of monticellite kimberlite. Compositional fields of djerfisherite: A – from primary sulphide inclusions in diamonds of Yakutia [3, 49]; B – from sulphide associations in deep-seated xenoliths from the Yakutian and South Africa kimberlites [3, 5, 7, 15, 41, 42]; C – from groundmass of the Elwin Bay kimberlites [6].

possible isomorphism of these elements in the djerfisherite structure. Moreover, there are no pronounced correlations between Cu and (Ni+Co). Unlike groundmass, djerfisherites from olivine-hosted inclusions have negative correlation between Cu and (Ni+Co).

The compositional data on djerfisherite from kimberlites of the Udachnaya-Eastern pipe have compared with literature compositions for K-sulphide from

sulphide associations in diamonds and xenoliths from the Yakutian and South

Table 4.

Representative analyses of djerfisherite from groundmass of kimberlite breccias and monticellite kimberlites, Udachnaya-Eastern pipe

wt.%	1	2	3		4		5		6		7	8	9		10	11
			c	r	c	r	c	r	c	r			c	r		
K	9.07	9.36	9.15	9.14	9.07	9.10	9.21	9.12	9.07	9.02	9.21	9.17	9.25	9.28	9.11	9.18
Na	0.00	0.12	0.00	0.00	0.00	0.00	0.00	0.00	0.00	0.00	0.00	0.00	0.00	0.00	0.00	0.00
Fe	41.72	42.35	38.86	38.80	38.86	39.08	37.91	37.79	37.14	37.03	42.01	42.43	42.13	42.13	40.90	38.63
Ni	2.26	2.24	4.79	4.75	4.79	4.59	4.34	4.33	4.72	4.60	7.17	6.90	6.32	6.33	6.91	7.48
Co	0.21	0.20	0.32	0.33	0.34	0.30	0.39	0.36	0.18	0.18	0.18	0.21	0.20	0.19	0.17	0.15
Cu	9.99	10.60	12.82	12.76	13.04	13.14	14.00	14.09	14.87	14.86	6.20	6.54	7.54	7.37	8.16	9.92
S	32.99	33.02	32.84	32.91	32.89	32.91	32.78	32.69	32.87	32.75	33.38	33.28	33.11	33.15	33.24	33.18
Cl	1.35	1.29	1.40	1.30	1.27	1.22	1.38	1.33	1.34	1.34	1.39	1.38	1.38	1.37	1.43	1.43
Total	97.59	99.18	100.18	99.99	100.26	100.34	100.01	99.71	100.19	99.78	99.54	99.91	99.93	99.82	99.92	99.97
Formula based on 26 sulphurs																
K	5.861	6.043	5.940	5.921	5.879	5.895	5.990	5.948	5.883	5.872	5.882	5.874	5.956	5.968	5.843	5.899
Na	0.000	0.133	0.000	0.000	0.000	0.000	0.000	0.000	0.000	0.000	0.000	0.000	0.000	0.000	0.000	0.000
Fe	18.876	19.143	17.662	17.597	17.635	17.724	17.262	17.254	16.865	16.876	18.785	19.029	18.992	18.969	18.365	17.377
Ni	0.973	0.963	2.071	2.050	2.068	1.981	1.880	1.881	2.039	1.995	3.050	2.944	2.711	2.712	2.952	3.201
Co	0.089	0.086	0.140	0.144	0.148	0.127	0.169	0.155	0.076	0.077	0.078	0.089	0.085	0.083	0.071	0.062
Cu	3.972	4.211	5.121	5.086	5.201	5.237	5.602	5.654	5.934	5.952	2.436	2.578	2.987	2.916	3.220	3.922
S	26.000	26.000	26.000	26.000	26.000	26.000	26.000	26.000	26.000	26.000	26.000	26.000	26.000	26.000	26.000	26.000
Cl	0.962	0.919	1.002	0.929	0.908	0.872	0.990	0.957	0.958	0.962	0.979	0.975	0.980	0.972	1.011	1.013

Note. 1-6 - kimberlite breccias; 7-11 - monticellite kimberlites.

Table 5.

Representative analyses (wt. %) of djerfisherite from phlogopite-spinel lherzolite and from the contact of xenolith and kimberlite breccia, Udachnaya-Eastern pipe.

#	1	2	3	4	5	6	7	8	9	10	11	12	13	14	15	16
Sulphide associat.	Mss+Pn+	Djer	Pn+Po+Djer		Po+Djer		Djer		Mss+Pn+Djer		Po+Djer		Djer			
n	10	2	2	1	1	2	1	2	1	1	2	3	2	4	3	2
K	9.38	9.32	9.29	9.25	9.30	9.33	9.23	9.23	9.04	9.05	9.36	9.33	9.39	9.32	9.34	9.23
Na	0.00	0.00	0.00	0.00	0.00	0.00	0.00	0.00	0.05	0.05	0.00	0.00	0.00	0.00	0.00	0.00
Fe	35.61	36.34	38.65	34.54	37.11	35.56	33.99	34.64	41.51	35.78	48.39	47.87	49.53	45.21	41.85	41.05
Ni	18.71	16.00	16.64	19.00	18.17	17.82	19.61	15.86	12.77	15.47	6.04	5.48	4.54	7.79	6.74	6.64
Co	0.08	0.01	0.20	0.13	0.18	0.18	0.16	0.00	0.07	0.08	0.46	0.32	0.10	0.14	0.12	0.11
Cu	1.62	3.59	0.49	2.18	0.52	2.25	2.40	5.67	1.95	5.14	0.71	1.89	1.14	2.49	7.10	8.16
S	33.17	33.36	33.45	33.39	33.38	33.35	33.48	33.09	33.28	33.17	33.53	33.35	33.33	33.36	33.38	33.23
Cl	1.38	1.27	1.33	1.31	1.33	1.33	1.32	1.25	1.31	1.33	1.44	1.45	1.39	1.39	1.39	1.38
Total	99.94	99.87	100.05	99.80	99.98	99.81	100.19	99.74	99.98	100.07	99.91	99.69	99.41	99.69	99.93	99.79
Formula based on 26 sulphurs																
K	6.028	5.954	5.921	5.906	5.940	5.965	5.878	5.947	5.791	5.817	5.949	5.964	6.006	5.955	5.963	5.922
Na	0.000	0.000	0.000	0.000	0.000	0.000	0.000	0.000	0.054	0.057	0.000	0.000	0.000	0.000	0.000	0.000
Fe	16.025	16.262	17.246	15.440	16.594	15.917	15.153	15.625	18.617	16.100	21.544	21.424	22.180	20.230	18.715	18.438
Ni	8.012	6.810	7.064	8.080	7.730	7.587	8.317	6.806	5.449	6.623	2.558	2.333	1.932	3.314	2.869	2.838
Co	0.032	0.003	0.085	0.055	0.074	0.078	0.068	0.001	0.031	0.032	0.192	0.135	0.043	0.057	0.051	0.045
Cu	0.640	1.410	0.192	0.856	0.204	0.885	0.940	2.246	0.769	2.033	0.278	0.742	0.448	0.978	2.791	3.221
S	26.000	26.000	26.000	26.000	26.000	26.000	26.000	26.000	26.000	26.000	26.000	26.000	26.000	26.000	26.000	26.000
Cl	0.981	0.895	0.935	0.922	0.937	0.934	0.927	0.888	0.925	0.943	1.006	1.022	0.977	0.980	0.981	0.973

Note. 1-8 - interstities in Phl-Sp lherzolite; 9-10 - from cavities in xenolith, in association with Na-Ca-carbonates and halite; 11-16 - on the xenolith-kimberlite breccia contact. Symbols as in Table 2.

Africa kimberlites as well as from groundmass of kimberlites at Elwin Bay [3, 5-7, 14, 15, 41, 42, 49]. Majority of djerfisherites from the Udachnaya-Eastern pipe generally fall in the compositional fields of this mineral from the Yakutian diamonds and xenoliths as well as from Frank Smith (Fig. 5). Djerfisherite from the Udachnaya kimberlite groundmass is richer in Cu than K-sulphide from kimberlite groundmass at Elwin Bay [6]. The mineral of the Canadian kimberlites has essential variations in Fe, Cu and Ni showing zoning from Cu-rich interior to Ni-rich rim. In contrast, as it is mentioned above, the core-to-rim deviations in djerfisherites from the Udachnaya kimberlites are insignificant.

The comparison of the Udachnaya djerfisherites from phlogopite-spinel lherzolite, kimberlite breccia and their contact indicate that they are also drastically different in composition (Fig. 6). In general, intraxenolith mineral forms compositional cluster similar to djerfisherite from sulphide assemblages in diamonds and peridotite xenoliths of Yakutia. They are rich in Ni and poor in Cu. In contrast, kimberlite groundmass K-sulphide is rich in Cu and poor in Ni. Djerfisherite from the kimberlite-xenolith contact has an intermediate position in Cu and Ni being Fe-rich variety like K-sulphide from groundmass of monticellite kimberlites (Fig. 5-6). Such compositional differences should relate to the origin of particular djerfisherites. Intraxenolith mineral has clear features of mineral, which partially or completely replaced early Ni-Fe-rich and Cu-poor associations (monosulphide solid solution + pentlandite, pentlandite + pyrrhotite). Djerfisherite from the contact replaced pyrrhotite, while groundmass mineral crystallised from kimberlite melt.

The data obtained show that djerfisherite in unaltered kimberlites of the Udachnaya-Eastern pipe is a late primary magmatic mineral belonging to the stage of groundmass crystallisation. During formation of breccias the kimberlitic melt due to phenocryst crystallisation gradually evolved towards carbonatitic compositions [19]. Crystallisation of carbonates from volatile-rich silicate-carbonate melt probably permitted djerfisherite to be stable. It should be noted that djerfisherite and other potassium sulphides are common late phases for volcanic and intrusive carbonatites and related alkaline silicate rocks [1, 8, 11-12, 21, 35, 37, 44-45, 47].

Monticellite kimberlite principally differs in chemical and mineral composition of the groundmass from kimberlite breccia in particular due to the paucity of carbonates and the appearance of monticellite and sodalite. Kornilova *et al.* [29] interpreted monticellite kimberlite as crystallisation product of evolved kimberlite melt, which possibly assimilated evaporates from the country sedimentary rocks around the Udachnaya pipe. Apparently, the assimilation may be possible to explain the appearance of such Cl-rich mineral as sodalite. The different trends for residual portions of kimberlitic melt were likely to determine the differences in composition of djerfisherite from the particular kimberlite species of the Udachnaya pipe.

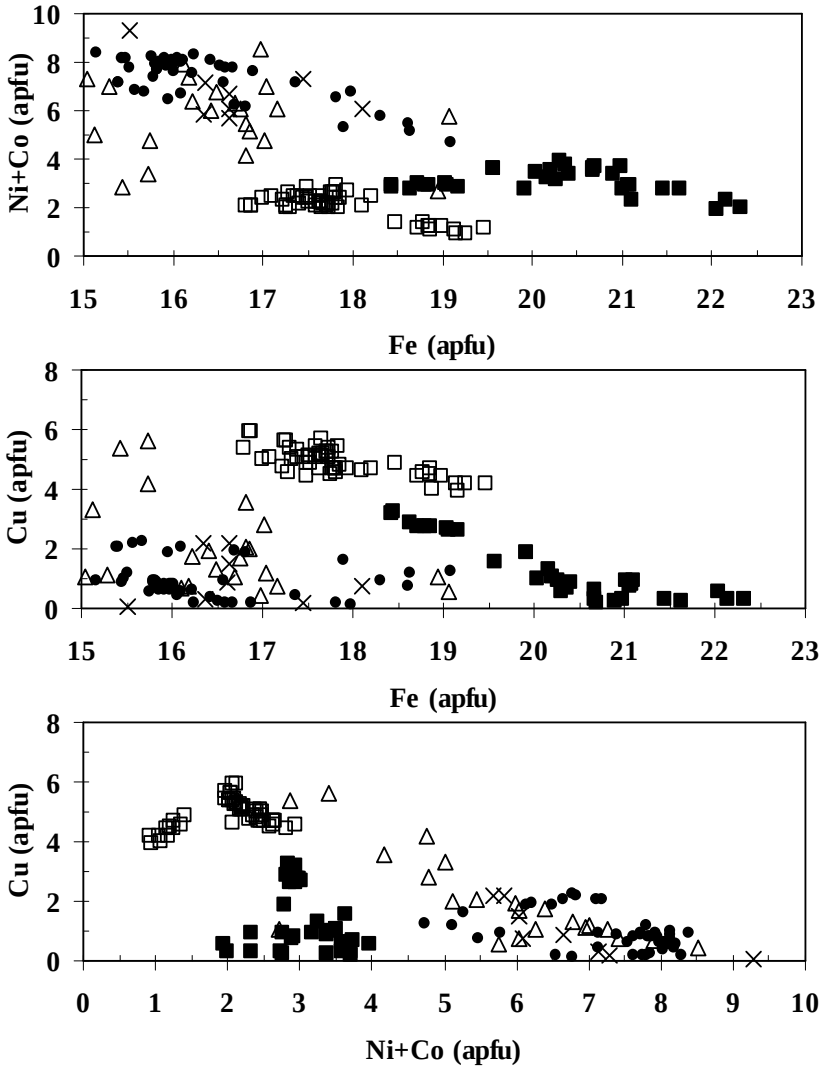

Fig. 6. **Compositional variations of djerfisherite (in apfu) from Phl-Sp lherzolite and contact between kimberlite breccia and xenolith, Udachnaya-Eastern pipe.**

Solid circles – from Phl-Sp lherzolite; solid squares – on the contact between kimberlite breccia and xenolith; open squares – from groundmass of kimberlite breccia; open triangles – from sulphide associations of peridotite xenoliths in kimberlites of Yakutia [3, 42]; crosses - from primary sulphide inclusions in diamonds of Yakutia [3, 49].

The occurrence of djerfisherite in the studied lherzolite and on the contact with kimberlite possibly assumes its reactionary nature, e.g. due to infiltration of evolved kimberlitic fluid/melt into xenolith as more realistic agent.

The comparison of chemical data on djerfisherite from mantle-derived xenoliths and host kimberlites allow us to make some suggestions about the origin of this sulphide in xenoliths and xenocrysts. Previous investigations [3, 5, 7, 15, 20, 41, 42] directly showed that djerfisherite is normally secondary after primary mantle sulphides due to interaction of metasomatising fluid/melt. However, in most cases it is unclear what source of metasomatising agent and what P-T-

conditions for its interaction on the primary sulphides. At present day two dominant points of view exist: (1) metasomatic event occurred in the mantle prior to entrapment by kimberlitic melt [7, 15, 41-42]; (2) metasomatism took place during the transportation of xenolith [34, 40]. Like in the case of phlogopite-spinel lherzolite of the Udachnaya pipe we can suggest that djerfisherite in diamonds and xenoliths from kimberlites may be product of the reaction between evolved kimberlitic melt or fluid and primary sulphides at shallow depth conditions. Namely, metasomatising agent acted on xenocryst/xenolith might be kimberlitic melt itself or its fluids. In the case of the primary sulphide blebs in diamonds and primary minerals of mantle-derived xenoliths, where djerfisherite forms outer rims, it may suggest the penetration of this fluid/melt through microfractures, which occur around the inclusions after crystallisation and transformation of sulphide melt [3]. For the mantle sulphide associations occurring in intergranular space of xenoliths it may assume not only reactionary nature of djerfisherite, but and its crystallisation from kimberlitic melt itself. In this case the primary sulphides, especially pentlandite owing to the similarities of their crystal structures [17], might be the seed for crystallisation of djerfisherite from residual kimberlitic melt penetrating into xenoliths through intergranular space.

The occurrences of djerfisherite as late magmatic and reactionary mineral in diverse magmatic and metasomatic rocks suggest different conditions of its origin. The synthesis of K-Fe-Ni-sulphides [5] indicated that djerfisherite may be formed at temperatures from 356^{o}C to at least 950^{o}C, i.e. at temperatures both above and below the solidus in the sulphide system K-Fe-Ni-S-Cl. The homogenisation temperatures of secondary melt inclusions in kimberlite olivine of the Udachnaya-Eastern pipe show that djerfisherite may crystallise at T≤700-800^{o}C [19]. The study of the Frank Smith xenolith assumes that this K-sulphide may be formed in the solid state after pentlandite and pyrrhotite at T≤600^{o}C [5, 7]. The crystallisation of djerfisherite in skarns was estimated as 700-820^{o}C [23, 26, 28, 36, 39, 46].

The review of literature data on K-sulphide-containing rocks shows that djerfisherite and other potassium sulphides crystallised in carbon-rich systems, i.e. where carbonates, graphite or CO_2/CH_4-rich fluid occur. Possibly, the presence of carbon-rich phases is responsible for reduced conditions and permits K-sulphides to be stable.

The appearance of such K-Cl-bearing sulphides as djerfisherite and bartonite in magmatic and metasomatic rocks also assume high concentrations of Cl in system. The presence of Cl-rich solutions is ordinary phenomena for skarns. The gradual increasing of Cl is very common for the evolution of carbonatitic and peralkaline magmas that is favourable to the appearance of Cl-rich silicates and chlorides as late products of crystallisation [12, 21, 31, 35, 37, 44]. In case of the Udachnaya kimberlites, the abundance of Cl is suggested due to both evolution of kimberlitic magma and assimilation evaporates from country rocks or presence of Cl-rich brines [19, 29, 38]. However, the mineralogy and petrography of the Elwin Bay kimberlite do not assume the presence of evaporates and brines near this

diatreme [6]. Thus, like in carbonatites and peralkaline rocks, the abundance of Cl in kimberlites may be a result of kimberlite evolution. Nevertheless, chlorine is not very necessary component for crystallisation of K-Cl-bearing sulphides. Chlorine-poor or even chlorine-free djerfisherite and bartonite may occur in some magmatites and skarns [1-2, 8, 15, 26, 31, 44], sometimes they coexist in rock together with Cl-rich varieties suggesting the Cl↔S substitution in the crystal structure of these minerals.

Unfortunately, our attempts to compare compositions of djerfisherite from all world-wide occurrences were failed because of broad variations. Possibly, it deals with that in most cases djerfisherite is secondary phase after primary sulphides. It is suggested that composition of this sulphide strongly depends on composition of primary sulphides. Fe-, Ni-, Cu- and even Co-rich varieties of djerfisherite occur in nature.

CONCLUSIONS

The data obtained for the Udachnaya-Eastern pipe allow postulate two main conclusions:

1. Djerfisherite in kimberlite breccia and monticellite kimberlite is a late primary magmatic mineral belonging to the stage of groundmass crystallisation. It was crystallised at shallow depths and $T \leq 700\text{-}800^{o}C$.
2. K-sulphide found in phlogopite-spinel lherzolite is seems to be product of infiltration of evolved kimberlite magma into xenolith or of reaction of evolved kimberlite fluid/melt with xenolith at shallow depths. It partially or completely replaces the primary mantle sulphides and rarely occurs as individual grains.

ACKNOWLEDGMENTS

Authors would like to thank L.N.Pospelova and A.T.Titov (UIGGM, Novosibirsk) for assistance during microprobe analysis and scanning microscopy, respectively. We are greatly indebted to V.S. Pavlyuchenko and S.N. Fedorova (IMP UIGGM, Novosibirsk) for X-ray diffraction data.

This work was supported by Russian Foundation of Basic Research (grant no. 02-05-64620) and Siberian Division of RAS (integration project no. 67).

REFERENCES

1. **Balabonin, N.L., Voloshin, A.V., Pakhomovskii, Y.A., Polyakov, K.I.** (1980): The composition of djerfisherite from alkaline complexes, Kola Peninsula. Mineral. Zh., 2, 90-99 (in Russian).
2. **Barkov, A.Y., Laajoki, K.V.O., Gehör, S.A., Yakovlev, Yu.N., Taikina-Aho, O.** (1997): Chlorine-poor analogues of djerfisherite – thalfenisite from Noril'sk, Siberia and Salmagorsky, Kola Peninsula, Russia. Can. Mineral., 35, 1421-1430.
3. **Bulanova, G.P., Spetsius, Z.V., Leskova, N.V.** (1990): Sulfides in diamonds and xenoliths from kimberlitic pipes of Yakutia. Publ. H. Nauka, Novosibirsk, 120 p. (in Russian).

4. **Chakhmouradian, A.R. & Mitchell, R.H.** (2001): Three compositional varieties of perovskite from kimberlite of the Lac de Gras field (Northwest Territories, Canada). Mineral. Mag., 65, 133-148.
5. **Clarke, D.B.** (1979): Synthesis of nickeloan djerfisherites and the origin of potassic sulphides at the Frank Smith mine. in "The Mantle Sample: Inclusions in Kimberlites and Other Volcanics". Proc. Second Int. Kimberlite Conf., 2, 300-307.
6. **Clarke, D.B., Mitchell, R.G., Chapman, C.A.T., MacKay, R.M.** (1994): Occurrence and origin of djerfisherite from the Elwin Bay kimberlite, Somerset Island, Northwest Territories. Can. Mineral., 32, 815-823.
7. **Clarke, D.B., Pe, G.G., MacKay, R.M., Gill, K.R., O'Hara, M.J., Gard, J.A.** (1977): A new potassium – iron – nickel sulfide from a nodule in kimberlite. Earth Planet. Sci. Lett., 35, 421-428.
8. **Czamanske, G.K., Erd, R.C., Leonard, B.F., Clark, J.R.** (1981): Bartonite, a new potassium iron sulfide mineral. Am. Mineral., 66, 369-375.
9. **Czamanske, G.K., Erd, R.C., Sokolova, M.N., Dobrovol'skaya, M.G., Dmitrieva, M.T.** (1979): New data on rasvumite and djerfisherite. Am. Mineral., 64, 776-778.
10. **Dawson, J.B.** (1980): Kimberlites and their xenoliths. Springer-Verlag.
11. **Dawson, J.B., Smith, J.V., Steele, I.M.** (1992): 1966 ash eruption of Oldoinyo Lengai: mineralogy of lapilli, and mixing of silicate and carbonate magmas. Mineral. Mag., 56, 1-16.
12. **Dawson, J.B., Smith, J.V., Steele, I.M.** (1995): Petrology and mineral chemistry of plutonic igneous xenoliths from the carbonatite volcano, Oldoinyo Lengai, Tanzania. J. Petrol., 36, 797-826.
13. **Distler, V.V., Ilupin, I.P., Laputina, I.P.** (1987): Sulfides of deep-seated origin in kimberlites and some aspects of copper-nickel mineralization. Int. Geol. Review, 29, 456-464.
14. **Dmitrieva, M.T.** (1976): The crystallochemical formula of djerfisherite according to structural positions. Izv. Akad. Nauk SSSR, Ser. Geol, 4, 97-101 (in Russian).
15. **Dobrovol'skaya, M.G., Tsepin, A.I., Ilupin, I.P., Ponomarenko, A.I.** (1975): Djerfisherite from Yakutia kimberlites. in "Mineraly i Paragenezisy Mineralov Endogennykh Mestorozhdenii", P.M. Tamarinov, ed. Publ. H. Nauka, Leningrad, 3-11 (in Russian).
16. **El Goresy, A., Grögler, N., Ottemann, J.** (1971): Djerfisherite composition in Bishopsville, Pena Blanca Springs, St. Marks and Toluca meteorites. Chem. Erde, 30, 77-82.
17. **Evans, H.T. & Clark, J.R.** (1981): The crystal structure of bartonite, a potassium iron sulfide, and its relationship to pentlandite and djerfisherite. Am. Mineral., 66, 376-384.
18. **Funchs, L.H.** (1966): Djerfisherite, alkali copper-iron sulfide: a new mineral from enstatite chondrites. Science, 153, 166-167.
19. **Golovin, A.V., Sharygin, V.V., Pokhilenko, N.P., Mal'kovets, V.G., Kolesov, B.A., Sobolev, N.V.** (2003): Secondary melt inclusions in olivine from unaltered kimberlites of the Udachnaya-Eastern pipe, Yakutia. Dokl. Russ. Acad. Sci., Earth Sci. Sect., 388, 93-96.
20. **Govorov, I.N., Blagodareva, N.S., Kiryukhina, N.I., Khar'kiv, A.D., Shcheglov, A.D.** (1984): Primary potassium minerals in deep-seated eclogites of Yakutia. Int. Geol. Review, 26, 1290-1294.
21. **Henderson, C.M.B., Kogarko, L.N., Plant, D.A.** (1999): Extreme closed system fractionation of volatile-rich, ultrabasic peralkaline melt inclusions and the occurrence of djerfisherite in the Kugda alkaline complex, Siberia. Mineral. Mag., 63, 488-495.
22. **Ifantopulo, T.N., Yushko-Zakharova, O.Y., Dubakina, L.S.** (1978): Djerfisherite from the Lovozero massif. Dokl. Acad. Sci. USSR, Earth Sci. Sect., 243, 199-200 (in Russian).
23. **Jamtveit, B., Dahlgren, S., Austrheim, H.** (1997): High-grade contact metamorphism of calcareous rocks from the Oslo Rift, Southern Norway. Am. Mineral., 82, 1241-1254.

24. **Khar'kiv, A.D., Zinchuk, N.N., Kryuchkov, A.I.** (1998): Diamond primary deposits of the world. PH Nedra, Moscow, 555 p.
25. **Kumira, M., El Goresy, A.** (1988): Djerfisherite compositions in EH chondrites: a potential parameter to the geochemistry of the alkali elements. Meteoritics, 23, 279-280.
26. **Kislov, Y.V., Orsoev, D.A., Pushkarev, Y.V.** (1994): Halogens in djerfisherite from a magnesian skarn in the Yoko-Dovyren platinum-bearing massif (northern Pribaikal'ye). Russ. Geol. Geophys., 35 (11), 54-57.
27. **Kogarko, L.N., Plant, D.A., Henderson, C.M.B., Kjarsgaard, B.A.** (1991): Na-rich carbonate inclusions in perovskite and calzirtite from the Guli intrusive Ca-carbonatite, Polar Siberia. Contrib. Mineral. Petrol., 109, 124-129.
28. **Konev, A.A. & Samoilov, V.S.** (1974): Contact metamorphism and metasomatism in aureole of the Tazheran alkaline intrusion. Publ. H. Nauka, Novosibirsk, 244 p. (in Russian).
29. **Kornivola, V.P., Egorov, K.N., Safronov, A.F., Filippov, N.D., Zaitsev, A.I.** (1998): Monticellite kimberlite from the Udachnaya-Eastern pipe and some aspects for evolution of kimberlite melts. Otech. Geol., no. 1, 48-51 (in Russian).
30. **Korobeinikov, A.N., Mitrofanov, F.P., Gehör, S., Laajoki, K., Pavlov, V.P., Mamontov, V.P.** (1998): Geology and copper sulphide mineralization of the Salmagorskii ring igneous complex, Kola Peninsula, NW Russia. J. Petrol., 39, 2033-2041.
31. **Kostyleva-Labuntsova, E.E., Borutskii, B.E., Sokolova, M.N., Shlyukova, Z.V., Dorfman, M.D., Dudkin, O.B., Kozyreva, L.B.** (1978): The mineralogy of the Khibini massif. V. 2 (minerals). Publ. H. Nauka, Moscow, 586 p. (in Russian).
32. **Lin, Y., El Goresy, A.** (2002): A comparative study of opaque phases in Qingzhen (EH3) and MacAlpine Hills 88136 (EL3): Representatives of EH and EL parent bodies. Meteorit. Planetary Sci., 37, 577-599.
33. **Lisitsin, D.V., Dobrovol'skaya, M.G., Tsepin, A.I., Shcherbachev, D.K., Trubkin, N.V., Kononkova, N.N.** (2002): Sulfide mineralization in high-alkaline pegmatites of the Koashva deposit (Khibiny Massif, Kola Peninsula). Geol. Ore Deposits, 44 (5), 385-395.
34. **Mitchell, R.H.** (1986): Kimberlites: Mineralogy, Geochemistry and Petrology. Plenum Press, New York, 442 p.
35. **Mitchell, R.H.** (1997): Carbonate-carbonate immiscibility, neighborite and potassium iron sulphide in Oldoinyo Lengai natrocarbonatite. Mineral. Mag., 61, 779-789.
36. **Orsoev, D.A., Kislov, Y.V., Zaguzin, G.N.** (1993): Djerfisherite from magnesian skarns of the Yoko-Dovyren layered intrusion. Russ. Geol. Geophys., 34 (5), 121-126.
37. **Panina, L.I., Sazonov, A.M., Usol'tseva L.M.** (2001): Melilite- and monticellite-bearing rocks of the Krestovskaya intrusion (northern Siberian Platform) and their genesis. Russ. Geol. Geophys., 42 (9), 1243-1263.
38. **Pavlov, D.I. & Ilupin, I.P.** (1973): Halite in the Yakutian kimberlites: its relationships with serpentine and question about source of solutions precipitated it. Dokl. Acad. Sci. USSR, Earth Sci. Sect., 213, 1406-1409 (in Russian).
39. **Pertsev, N.N., Konnikov, E.G., Kislov, Y.V., Orsoev, D.A., Nekrasov, A.N.** (2003): Merwinite-facies magnesian skarns in xenoliths from dunites of the Dovyren layered massif. Petrology (Petrologiya), 11 (5), 464-475.
40. **Sharygin, V.V., Golovin, A.V., Pokhilenko, N.P., Sobolev, N.V.** (2003): Djerfisherite in unaltered kimberlites of the Udachnaya-Eastern pipe, Yakutia. Dokl. Russ. Acad. Sci., Earth Sci. Sect., 390, 554-557.
41. **Solov'yeva, L.V., Barankevich, V.G., Zav'yalova, L.L., Lipskaya, V.I.** (1988): Metacomatic alterations in ferromagnesian eclogites from the Udachnaya pipe. Dokl. Acad. Sci. USSR, Earth Sci. Sect., 303, 107-110.
42. **Spetsius, Z.V., Bulanova, G.P., Leskova, N.V.** (1987): Djerfisherite and its genesis in kimberlitic rocks. Dokl. Acad. Sci. USSR, Earth Sci. Sect., 293, 133-136.

43. **Spetsius, Z.V., Griffin, W.L., O'Reilly, S.** (2003): Re-Os isotope analysis and dating of sulfide inclusions in olivine from the Udachnaya kimberlite pipe. in " Problemy prognozirovaniya, poiskov I izucheniya mestorozhdenii poleznych iskopaemych na poroge XXI veka". PH Voronezh State University, 624-628 (in Russian).
44. **Stoppa, F., Sharygin, V.V., Cundari, A.** (1997): New mineral data from the kamafugite-carbonatite association: the melilitolite of Pian di Celle, Italy. Mineral. Petrol., 61, 27-45.
45. **Sukharzhevskaya, E.S. & Artyukhova, A.A.** (2000): Sulfide mineralization in carbonatites of the Vuoriyarvi massif. in "Mineralogicheskie Muzei v 21 veke", Saint Peterburg, 113 (in Russian).
46. **Takechi, Y., Kusachi, I., Nakamuta, Y., Kase, K.** (2000): Nickel-bearing djerfisherite in gehlenite-spurrite skarn at Kushiro, Hiroshima Prefecture, Japan. Resource Geol., 50, 179-184.
47. **Yakovenchuk, V.N., Pakhomovsky, Y.A., Men'shikov, Y.P., Ivanyuk, G.Y., Krivovichev, S.V., Burns, P.C.** (2003): Chlorbartonite, $K_6Fe_{24}S_{26}(Cl,S)$, a new mineral species from a hydrothermal vein in the Khibina massif, Kola Peninsula, Russia: Description and crystal structure. Can. Mineral., 41, 503-511.
48. **Yeremeev, N.V., Dobrovol'skaya, M.G., Miravitskaya, G.N.** (1982): A new find of djerfisherite in rocks of the potassic alkaline series of the Inagli complex (Aldan Shield). Dokl. Acad. Sci. USSR, 263, 1210-1212 (in Russian).
49. **Zedgenizov, D.A., Logvinova, A.M., Shatskii, V.S., Sobolev, N.V.** (1998): Inclusions in microdiamonds from some kimberlite diatremes of Yakutia. Dokl. Russ. Acad. Sci., Earth Sci. Sect., 359, 204-208.

UDK 552.331 (571.54)

Mineral composition and geochemical caracteristic of the **Veseloe carbonatites (Northern Transbaikalia, Russia)**

Ripp G.S., Badmatsyrenov M.V., Doroshkevich A.G., Isbrodin I.A.

Geological Institute SB RAS, Ulan-Ude, e-mail: ripp@gin.bsc.buryatia.ru

The endogenous carbonate rocks were discovered in the North Transbaikalia and were classified as carbonatites. It is supposed that they are a part of new carbonatite area forming in Late Riphean. The carbonatites are represented by dykes of beforsites and situated in Early Precambrian protrusion edges. The Veseloe carbonatite occurrence is disposed to the west of North-Muya block. The first results of mineralogical and geochemical investigation of carbonatites are exhibited in this article. The chemical composition, trace element and REEs contents, composition of main and accessory minerals were determined in rocks.

The mineral composition and geochemical features of rocks resemble with carbonatites of different regions of world. The REEs composition, high content of Sr, $\delta^{13}C$ and $\delta^{18}O$ isotope values in carbonate, $^{87}Sr/^{86}Sr$ initial ration in rocks and non-rubidium minerals also testifies about this.

Peculiar composition fine resorbed aggregates with Cr-bearing minerals were detected in carbonatites. Structural and textural properties permit to attribute them to mantle xenoliths.

ANALYTICAL METHODS

The chemical composition of rocks is determined by atomic absorptive method, trace element by roentgen fluorescent method and REEs by spectral method with precut chemical enrichment. In the latter case as standard example with certified content of REEs the apatite ore and apatite were used. The minerals were analyzed using electron-probe micro-analysis (EPMA) (accelerating voltage of 20 kV, a beam current of 40 nA, a beam size of 3-4 ηm and 20 second-counting time) and scanning electron microscopy (LEO-1430) with energy-dispersion spectrometry (IncaEnergy-300) (SEM-EDS). Strontium isotope value in non-rubidium minerals is determined using mass-spectrometer MI-1201 T. All methods are realized in laboratories of the Geological Institute SD RAS.

The $\delta^{13}C$ and $\delta^{18}O$ isotope values were analyzed in isotope laboratory of Analytical Center FESC RAS. Analysis fallibility in carbonates and magnetite are not exceeded ± 0,02 and ± 0,5‰ accordingly.

GEOLOGICAL DESCRIPTION OF THE VESELOE AREA

The Veseloe carbonatites were found in the North Transbaikalia. The occurrence is situated to the west of North-Muya block. The muscovite-quartz-

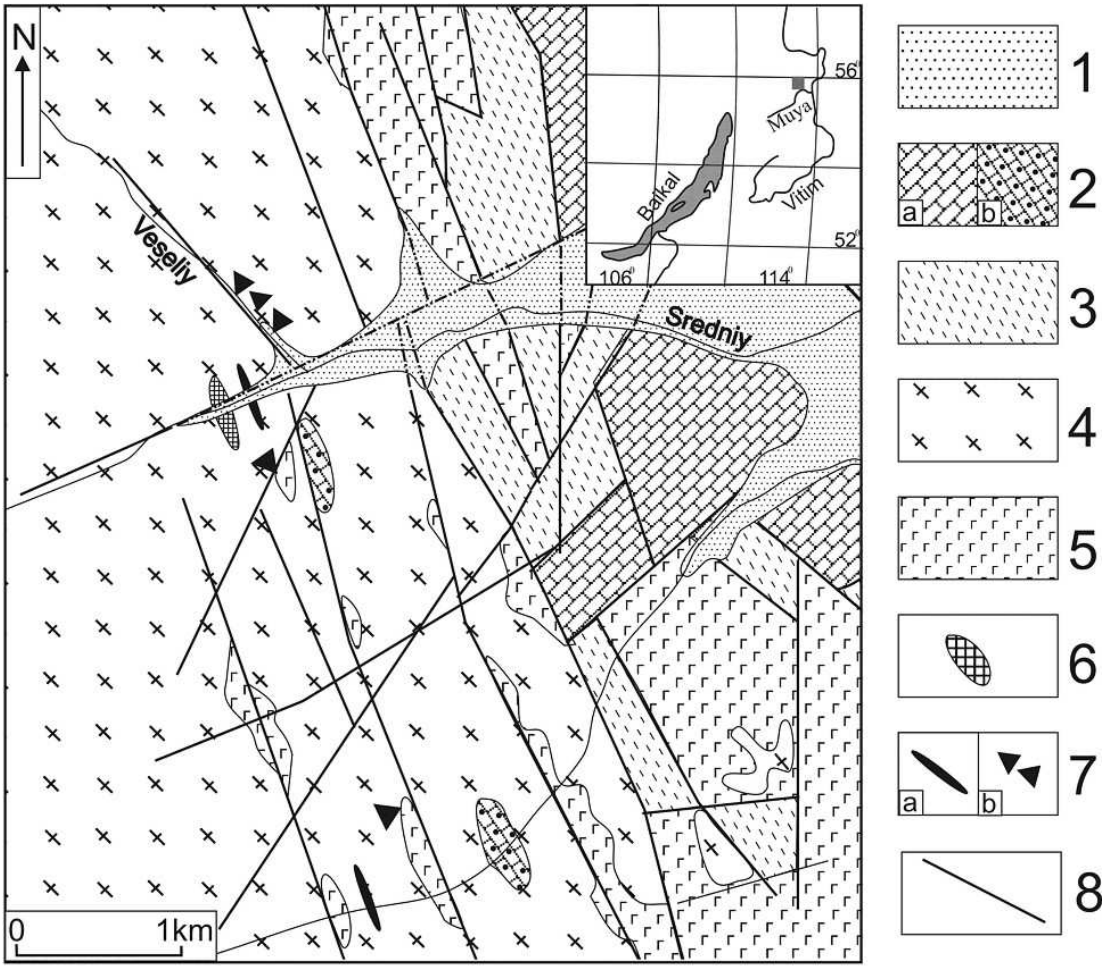

Fig. 1. **Schematic geological map of the Veseloe area.**

1 - loose recent deposits; 2a – Cambrian limestones; 2b – dolomite marble of Riphean; 3 – crystalline shales of Early Riphean; 4 – gneissis, gneissose granites and crystalline shales of Late Riphean; 5 – gabbro of Late Riphean; 6 – talk-carbonate rocks and listvenites; 7 – dykes (a) and deluvium (b) of carbonatites; 8 – faults.

feldspar crystalline schists, gneisses, amphibolites and dolomite marbles of Late Precembrian compose the area (Fig. 1). The Early Palaeozoic limestone blocks were mapped on east part of the occurrence area. Metamorphic rocks are intruded by gneissose granites, altered basic rocks, listvenites and ultrabasites modifying in talk-carbonate rocks. The comagmatic alkaline silicate rocks were not disclosed on the Veseloe occurrence. The dykes of chloritizated and epidotizated basic rocks are essentially earlier than carbonatites.

In core of area among gneisses and crystalline schists of Riphean the dolomite marbles are presented. They compose lenslike masses and contain high-magnesium phlogopite dissemination. The non-ferriferous dolomite (about 22 wt.% MgO) composes rocks and characterized low trace element content (Table 1, analysis 1-2).

In mineral the SrO amount not exceed hundredth percent, also strontium are not detected in analyzed samples of marble (Table 2, analysis 1-2). The $\delta^{13}C$ and $\delta^{18}O$ isotope values were analyzed in two dolomite samples from marble

Table 1.

Chemical composition of rocks from the Veseloe occurrence, wt.%, ppm

Component	1	2	3	4	5	6	7	8	9	10
SiO_2	4.60	7.80	32.10	37.70	42.62	1.60	6.80	1.60	2.30	3.30
TiO_2	<0.02	<0.02	0.02	0.12	1.63	0.22	0.39	0.35	0.38	0.85
Al_2O_3	0.50	0.90	0.90	15.30	15.30	0.30	0.60	0.90	0.30	0.90
Fe_2O_3	<0.05	<0.05	2.76	0.87	2.25	1.20	< 0.05	< 0.05	0.76	2.01
FeO	0.55	0.78	5.10	4.63	8.63	2.08	4.55	3.76	4.63	2.61
MnO	0.02	0.05	0.15	0.10	0.21	0.11	0.13	0.10	0.11	0.11
MgO	21.03	19.85	30.62	10.12	7.12	10.46	12.84	14.60	12.70	11.33
CaO	28.60	28.90	5.10	8.66	8.01	39.80	33.65	34.08	35.81	37.44
Na_2O	0.03	0.13	0.01	0.20	2.87	0.08	0.07	0.04	0.07	0.07
K_2O	0.02	0.07	0.01	3.61	2.16	0.01	0.08	<0.10	0.02	0.04
P_2O_5	0.06	<0.05	<0.05	<0.05	0.12	5.12	6.64	6.30	8.10	5.65
LOI	44.46	40.97	22.79	17.61	8.90	37.71	34.56	37.67	34.51	35.01
Total	99.87	99.45	99.56	99.03	99.80	98.69	100.31	99.50	99.69	99.32
CO_2	43.11	40.95	8.71	13.49	4.46	36.95	33.34	36.10	33.55	34.19
S	<0.10	<0.10	<0.10	0.13	<0.10	0.20	<0.10	<0.10	0.28	0.22
F	0.02	0.02	-	-	0.22	0.52	0.76	0.60	0.76	0.57
Cr	-	-	3100	560	44	96	78	96	96	200
V	-	-	50	61	210	50	50	50	0.0061	0.061
Ni	-	-	68	<50	<50	100	82	130	140	190
Rb	<3	<3	<3	64	n.a.	<3	4	6	4	<3
Sr	480	130	640	230	n.a.	10300	8500	5850	6800	8300
Y	35	9	2	3	n.a.	58	37	25	46	60
Zr	5	12	7	11	n.a.	100	80	55	90	250
Nb	<2	<2	<2	<2	n.a.	6	15	5	6	19
Ba	<50	500	650	240	n.a.	2000	4000	130	850	700
Cu	<10	<10	14	23	n.a.	<10	<10	<10	<10	56
Zn	-	-	30	56	n.a.	20	48	30	34	24
Pb	<3	3	<5	16	n.a.	40	57	26	12	23
REE	36.5	157.9	n.a.	n.a.	n.a.	961	835	545	1554	1143

Note. 1-2 - dolomite marble, 3- talk-carbonate rock, 4 –listvenites, 5 - dyke of modified basic rock, other samples – carbonatites, n.a. – element not analyzed. Macrocomponents were determined by atomic-absorptive method (analysts Tsirenova A.A., Ivanova V.A., Borzhonova I.V.), trace elements were analyzed by roentgen fluorescent method (analyst Zhalsaraev B.Zh.) and REEs by chemical spectral method (analysts Kazantseva T.A. and Levantueva L.A.). Geological Institute SB RAS, 2003-2004.

(+3,1‰ $\delta^{13}C$ and 15,7‰ $\delta^{18}O$) and are similar by values in metamorphic sedimentary carbonate rocks.

The body of talk-carbonate rock and listvenite is situated in 80 m to the west of carbonatites in right edge of Sredniy river and has thickness about 10 m. The chemical composition of the rocks (see Table 1, analysis 3-4) allow to ultrabasites. In the rocks the carbonate minerals mainly are presented by dolomite (see Table 2, analysis 3, 5). Ferriferous magnesite (see Table 2, analysis 4) is widespread in talk-carbonate rocks containing magnetite disseminations.

Table 2.

Chemical composition of carbonate minerals in rocks from the Veseloe area, wt.%

№	FeO	MnO	MgO	CaO	SrO	№	FeO	MnO	MgO	CaO	SrO
1	0.35	-	22.01	29.75	-	14	7.89	n.a.	16.64	28.72	0.35
2	0.24	-	22.36	30.30	-	15	5.30	n.a.	16.80	29.0	0.60
3	5.48	0.10	1.91	30.00	-	16	6.45	n.a.	17.04	29.24	-
4	8.05	0.13	42.05	0.09	-	17	5.19	n.a.	17.46	28.25	0.79
5	0.53	0.17	21.28	29.26	0.33	18	5.83	n.a.	17.30	28.65	0.70
6	1.98	0.07	21.65	30.59	-	19	3.76	n.a.	17.63	28.68	0.89
7	2.18	0.07	21.31	29.11	-	20	6.19	0.10	16.98	29.77	0.51
8	4.92	0.17	18.09	29.17	0.36	21	5.36	0.20	18.04	29.19	0.77
9	5.08	0.25	18.48	30.60	-	22	1.02	-	1.70	49.27	0.93
10	8.71	0.093	15.65	28.71	0.43	23	1.89	-	0.67	48.02	0.46
11	5.15	0.19	17.67	29.29	0.33	24	0.70	-	0.75	49.85	0.62
12	4.48	0.15	18.25	29.43	0.34	25	0.56	-	0.51	50.64	0.79
13	4.96	0.18	17.86	29.82	0.39	26	1.09	-	0.96	49.83	0.75

Note. 1-2 – from dolomite marbe. 3 – from listvenite, 4-5 – from talk-carbonate rock, 6-7 – from dolomite-quartz vein, 8-19 – dolomite from carbonatite, 20-21– dolomite from carbonate vein intersecting carbonatite and containing Sr-bearing barite, 22-26– interstitial calcite between dolomite, n.a. – element not analyzed. Data of EPMA and SEM-EDS (analysts Kanakin S.V. and Karmanov N.S., Geological Institute SB RAS, 2003-2004).

In dolomite from listvenite the $\delta^{13}C$ and $\delta^{18}O$ isotope values have 1,4‰ and 12,1‰ accordingly. Fengite is presented in listvenite and contains up to 0,5 wt.% Cr_2O_3. Dykes of basic rocks occur rarely. One of the dykes is characterized by low SiO_2 content and high alkalinity (see Table 1, analysis 5). The rock is altered and composed of albite aggregate, chlorite with biotite relic and epidote.

Quartz, calcite-quartz and dolomite-quartz veins, also zones of silicification, pyritization, chloritization occurs widely on the Veseloe occurrence. They were formed after carbonatites and have not genetic relationship with latter. According to the $\delta^{13}C$ and $\delta^{18}O$ isotope values (-0,1‰ $б^{13}C$ and 16,7‰ $б^{18}O$) the carbonate-quartz veins are related with processes of metamorphism of carbonate rocks.

STRUCTURAL AND TEXTURAL FEATURES OF CARBONATITES

Some bodies of carbonatites mostly presenting slide-rocks were founded in area 0,5-0,7 km wide and about 4 km long. One of them was observed on 120 m long and 20-30 m wide in left edge of Veseliy stream. Parameter of carbonatite body was not determined, because the body are overlaped by deluvium of country rocks. The scope of carbonatite distribution could be determined by geochemical anomaly of phosphorus (near 4 km^2).

The carbonatites are presented massive fine-grained rocks with banding. The banding is conformal to contacts of the rocks and is cause by common orientation of apatite crystals, dolomite grains and bands of magnetite and rutile. The carbonatites have tectonic contacts of with country rocks, therefore the material of

Table 3.

Chemical composition of micas and amphiboles in rocks from the Veseloe area, wt.%

№	SiO_2	TiO_2	Al_2O_3	Cr_2O_3	FeO	MgO	CaO	Na_2O	K_2O	F	Total
1	50.85	1.97	22.45	-	5.98	3.68	-	-	11.37	1.14	102.01
2	50.56	1.17	25.43	-	1.32	3.28	-	-	11.35	1.05	98.80
3	47.12	1.11	25.71	-	7.22	2.86	-	-	10.93	0.84	100.46
4	50.95	-	28.48	-	2.10	3.34	-	-	12.44	-	97.30
5	39.89	1.03	13.17	-	9.38	20.37	-	0.07	10.51	3.71	102.60
6	39.40	0.76	12.67	-	9.17	20.99	-	-	10.65	4.15	102.28
7	40.84	0.70	12.57	-	8.62	20.73	-	-	10.59	3.96	102.50
8	40.68	0.93	12.97	-	8.14	20.28	-	-	10.97	3.79	102.26
9	48.71	0.79	26.44	1.72	3.72	2.56	-	-	11.96	-	95.92
10	47.10	0.61	26.58	1.45	3.74	2.33	-	-	12.13	-	93.95
11	47.39	0.38	29.77	1.13	4.02	1.43	-	-	11.81	-	95.92
12	55.50	0.15	0.78	-	21.35	10.82	1.81	6.23	0.04	n.a.	98.66
13	56.24	-	1.08	-	21.58	10.21	0.96	6.60	-	n.a.	98.68
14	54.54	-	0.66	-	7.70	18.70	8.76	2.19	1.18	n.a.	94.35
15	57.20	-	0.63	-	8.10	20.03	9.30	2.50	1.90	n.a.	99.93
16	54.80	-	0.75		9.85	18.64	8.54	2.18	1.74	n.a.	95.61

Note. 1-4 – fengite from country crystalline schists, 5-8 – phlogopite from contact zones of carbonatite bodies, 9-11 – Cr-bearing fengite from xenoliths in carbonatites, 12-16 – amphiboles from carbonatites: 12-13 - magesioriebeckite, 14-15 – richterite, n.a. – element not analyzed. Data of EPMA and SEM-EDS (analysts Kanakin S.V. and Karmanov N.S., Geological Institute SB RAS, 2003-2004).

latter “rub” in carbonate matrix. In some case the thin phlogopite zones are saved on contacts. Pyritization, chloritization and quartz veinlets are noted here.

The carbonatites and country rocks have undergo a processes of regional metamorphism. The mineral paragenesis compositions of country crystalline slates conform to epidote-amphibolite and amphibolite phases of metamorphism. The carbonatites and slates contain neogenetic phengite. The mineral (Table 3, analysis 1-4) has more than 0,5 f.k. of Fe and Mg, and Si content varies from 3,30 up to 3,45 f.k., that by [2] these values correspond to 7,5-10 kbar at 500 ^{0}C.

The dolomite and calcite veinlets with Sr-bearing barite and barite-celestine disseminations were formed after carbonatites, also on dolomite have neocrystallization of talk. The later silicification, pyritization and chloritization are confined to tectonic dislocations.

MINERAL COMPOSITION OF CARBONATITES

Carbonatites are composed of dolomite (70-80%), apatite (10-20%) and calcite (5-15%). Magnetite, rutile, fluorophlogopite and alkaline amphiboles are minor minerals (1-3%). Zircon is commonness among accessory minerals. Monazite, titanite, ilmenite, molibdenite, allanite, celestine and barite are met rarely. These minerals are represented or single grains or small assemblages

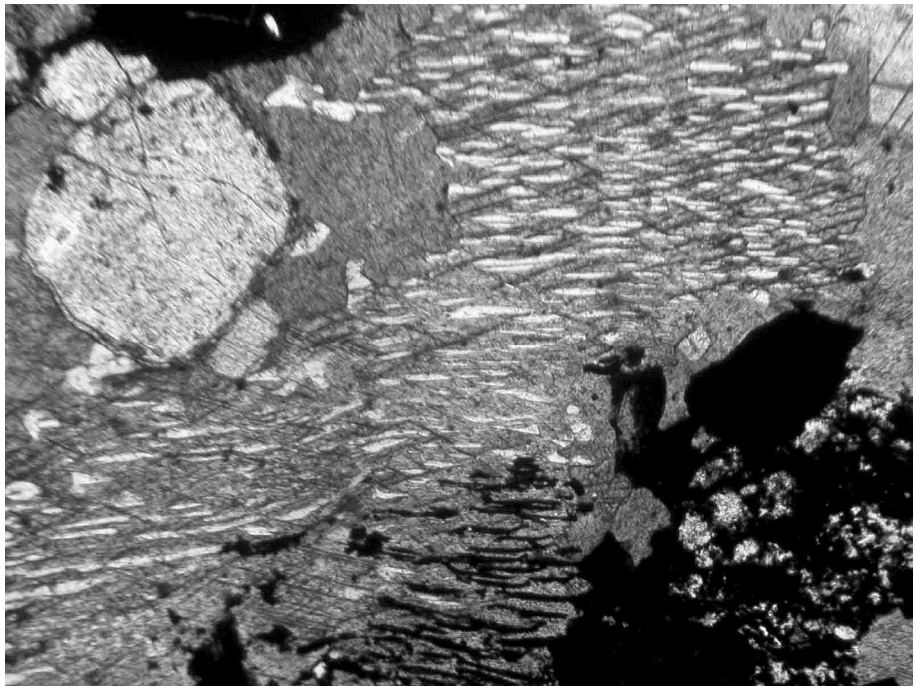

Fig. 2. **Dolomite exolutions (light) in calcite.**

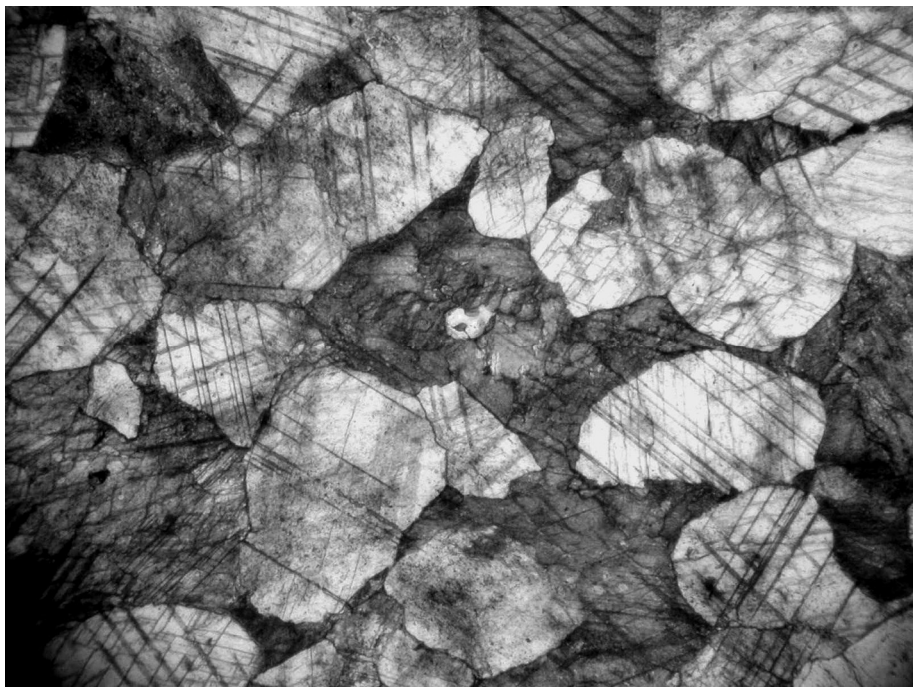

Fig. 3. **Interstitial calcite (grey) between dolomite grains.**

elongated according to banding of rocks. Some minerals are associated with post-carbonatite veinlets.

Dolomite is main mineral of carbonatites. Its composition (see Table 2, analysis 8-19) has steadily 5-7 wt.% FeO and 0,3-0,7 wt.% SrO. In dolomite the content of manganese not exceed first-tenth a part of a percent. Dolomite

composed vienlets with calcite and Sr-bearing barite the veinlets has analogous composition (see Table 2, analysis 20-21). Furthermore dolomite is noted as lenticular exsolutions in calcite presenting solid solution (Fig. 2). Amount of exsolutions (lamellas) varies from 5 to 30% of area of calcite grains.

Calcite irregularly is distributed among apatite-dolomite matrix. Basically mineral has interstitial fill between dolomite (Fig. 3). It is forming sections with content variation from single grains to 20-30% volume of rocks. The main part of calcite grains contains lamellas of dolomite presenting solid solution. Calcite has essential amounts of Mg, Fe and Sr (see Table 2, analysis 22-26). In addition not large (usually up to 1 cm) calcite and dolomite-calcite veinlets are occurring in carbonatites rarely.

Apatite forms idiomorphic prismatic crystals oriented according to banding of rocks. It is formed on early stage of carbonatite crystallization. The mineral is distributed irregularly and varies from first up to 20-30% in rock. The mineral is fluorapatite with limiting F content (up to 3.9 wt.%). The typical feature of apatite is high Sr content, in average of 1,5 wt.%. In single samples the LREEs are present up to 0,4-0,8 wt.%. In these samples simultaneously with REEs are noted tenth part of percent of Na_2O.

Single grains and small aggregates of amphiboles are presented in dolomite matrix. The compositions of amphiboles (see Table 3, analysis 12-16) are magnesioribekite (6,6 wt.% Na_2O) and K-bearing richterite (up to 1,9 wt.% K_2O).

Phlogopite is rare mineral. It forms both single grains and assemblage in contact zones of carbonatites. The mineral is characterized by low Ti and high F contents (see Table 3, analysis 5-8) and is diagnosed as fluorphlogopite.

The main feature of carbonatites is higher amounts of Cr (0,0106%) and Ni (0,0122%). The contents are more in three-four times than in average carbonatite [6]. There are conditioned of presence of fine (up to 3-5 mm) resorbed aggregates with Cr-bearing minerals. These aggregates according to structure and texture features may attribute to xenoliths. They contain high-titanous minerals with Cr and some cases Ni that are various degrees altered of late processes. There are assemblage of fine accrete disintegrated grains of magnetite, rutile, ilmenite, titanite. The primary silicate phases (excluding titanite) were not kept and replaced of fengite and chlorite. Cr is determined in magnetite, rutile, titanite, ilmenite, chlorite and fengite. The Cr_2O_3 content in chlorite is varies from 1,68 to 6,15 wt.%. The mineral also contains up to 1,33 wt.% NiO. In fengite the Cr_2O_3 concentration run up to 1,7 wt.% (see Table 3, analysis 9-11).

Magnetites and rutiles are presented several generations. Their amount not exceeds 1-2% volume of carbonatites. The minerals are differing compositions of trace element. The main part of magnetite is paragenous with dolomite and composes disseminations, grain chains elongated along banding of rocks. In this group of magnetite is distinguished two generations (see Fig. 4). One of them (magnetite-1) is presented as inclusions in magnetite-2. These magnetite inclusions

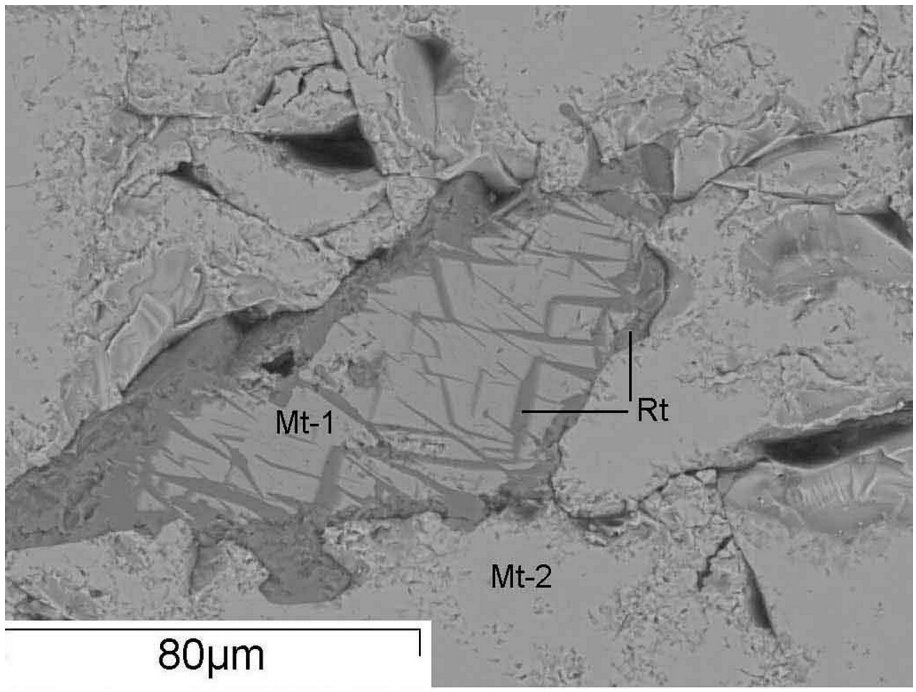

Fig. 4. **Two generations of magnetite are paragenous carbonatite.**

Magnetite-1 (inclusion) contain lamellar rutile (dark grey). A core of magnetite-1 has margin of rutile. Magnetite-2 compose main field. Backscattered electron image.

have ring and lamellas of rutile (Fig. 4). Magnetite has higher content of Ti and V (0,6-1,65 wt.% V_2O_3) and is not contain of Cr (Table 4, analysis 1-3).

In second generation (magnetite-2) the content of Ti and V are decreased and also Cr is absent (see Table 4, analysis 4-6). Later generation (magnetite-3) compose thin (2-3 mm) monomineral veinlets and intersected the carbonatite. Magnetite-3 is sharply depleted of Ti and V and not contains Cr (see Table 4, analysis 7).

Cr-bearing magnetites were met in xenoliths. Among them are determined two groups. One of them (magnetite-4) is presented single grains in association with ilmenite, titanite, rutile (Fig. 5). Magnetite-4 contain up to 4-18 wt.% Cr_2O_3 (see Table 4, analysis 8-13). Often the mineral is characterized high Ti content (up to 16-21 wt.% TiO_2). Usually the magnetite grains are broken and presented angular and splinter crystalloclasts. The morphology of mineral and correlation with different minerals including magnetite are seeing on figures 5-6. These minerals are derived of breakup of Fe-Ti mineral.

The latter magnetite (magnetite-5) forms symplectic intergrowth with rutile making the breakup of solid solution. These aggregates have sharp boundary with host-matrix and contain inclusions of titanite and ilmenite grains. The structure features are shows on figures 5-6. This magnetite is depleted of Cr and characterized more homogeneous dispensing of this element. Usually Cr_2O_3 contents are 0,5-2,5 wt.% (see Table 4, analysis 14-29). Ti content in mineral is reduced and has some amount of V.

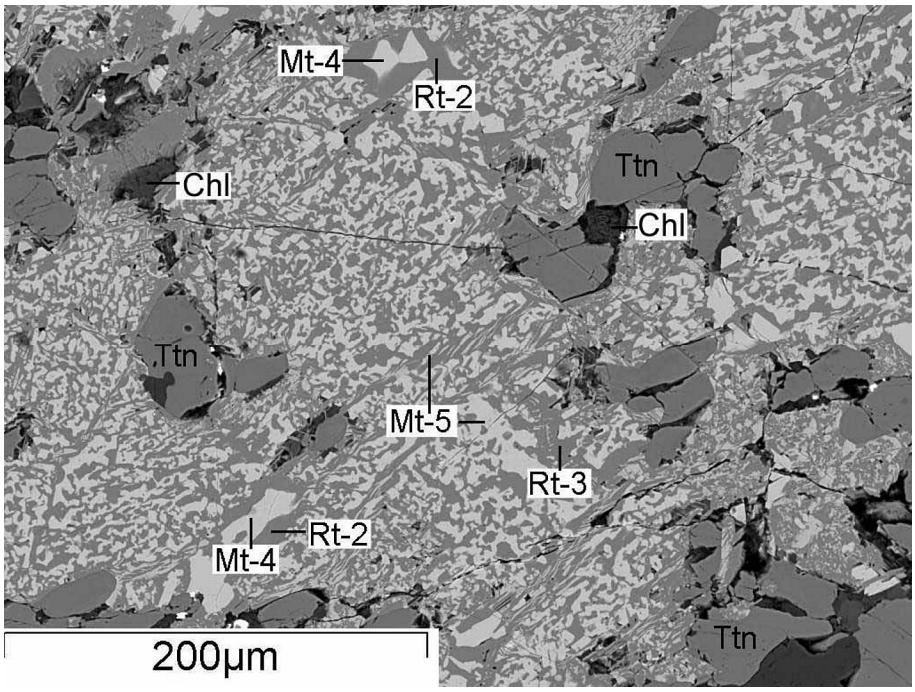

Fig. 5. **Association of titanite (grey grains), Cr-bearing rutile-3 intergrowth with Cr-bearing magnetite-5 assembly and magnetite-4 crystalloclasts with rutile-2 margin.**

Cr-bearing chlorite has black grains and dolomite dark grey. Backscattered electron image.

The case as with magnetite some generations of rutile are presented in carbonatites. The rutile is paragenous with dolomite (rutile-1) and compose the disseminations and the grain chains elongated along banding of rocks. It is not contain of Cr, Ni and the V is presented steadily (Table 5, analysis 1-6). In mineral in higher amount the iron also is detected.

The rest generations of rutile are marked in xenoliths. One of them (rutile-2) is associated with high-chromous magnetite and composes the ring around the last. The main feature of rutile is the presence 0,95-2,30 wt.% Nb_2O_5 (see Table 5, analysis 7-13). Second generation (rutile-3) is formed solid solution with magnetite (see Fig. 5-6). Rutile-3 also is enriched of Cr. The content of Cr_2O_3 in mineral is varies from 0,3 to 2,9 wt.%, constituting 0,5-0,7 wt.% in the majority of samples (see Table 5, analysis 14-25).

Cr in ilmenite is determined in lesser amount (not determined in some samples). The mineral composes the single grains scattered in titanite-rutile-magnetite aggregate. In ilmenite also is increased the contents MgO and CaO (Table 6, analysis 15-21).

Furthermore in 9 from 15 analyzed of titanite samples, which are typical mineral of xenoliths, are determined 0,3-0,5 wt.% Cr_2O_3. The single titanite grains are dispersed among rutile-magnetite aggregates and compose the small assemblages in xenoliths. The later titanite forms ring on contact of xenoliths with dolomite (Fig. 6). The mineral composition (see Table 6, analysis 1-14) is typical.

Table 4.

Chemical composition of magnetite from the Veseloe carbonatites, wt.%

№	TiO_2	Cr_2O_3	FeO	V_2O_3	Total
Magnetite-1 and magnetite-2 are paragenous of carbonatite					
1	8.57	-	83.54	1.62	93.73
2	9.16	-	82.87	1.65	93.68
3	4.20	-	87.00	1.38	92.57
4	0.34	-	82.66	0.74	93.73
5	-	-	93.88	0.86	94.75
6	-	-	93.30	0.73	94.03
Veinlet of magnetite-3 in carbonatite					
7	0.24	-	95.42	0.31	95.97
Magnetite-4 and magnetite-5 from xenoliths					
8	3.67	3.67	88.95	-	92.28
9	0.52	18.27	71.65	-	93.58
10	9.20	6.10	75.83	0.50	92.16
11	1.66	3.93	88.74	0.28	95.06
12	2.46	4.27	89.10	-	95.83
13	1.89	3.02	92.19	-	97.10
14	1.95	3.74	90.11	0.33	96.13
15	2.03	2.55	90.59	0.32	95.49
16	4.85	0.32	90.72	0.32	96.21
17	3.72	0.22	92.58	0.27	96.79
18	2.46	4.27	89.10	-	95.83
19	2.88	0.86	92.75	-	96.49
20	1.89	3.02	92.19	-	97.10
21	3.34	0.42	94.50	-	98.25
22	3.00	1.63	93.20	-	97.84
23	5.13	0.62	93.11	-	98.86
24	5.55	0.57	91.89	-	98.02
25	3.39	0.33	93.44	-	97.17
26	1.66	3.93	88.74	0.28	95.06
27	3.63	0.67	92.00	0.29	96.58
28	2.69	2.34	90.48	0.47	95.98
29	3.01	1.66	90.89	0.27	95.82

Note. 1-3 – magnetite-1 (early generation), 4-6 – magnetite-2 (late generation), 7 – magnetite-3 from veinlet intersecting carbonatite, 8-29 – magnetite-4 and magnetite-5 from the xenoliths: 8-13 – crystalloclasts of magnetite-4, 14-29 – magnetite-5 from exolution with rutile. Data of SEM-EDS (analyst Karmanov N.S., Geological Institute SB RAS, 2004).

The most interesting feature of titanite is presence of Cr and V up to tenth part of percent in some samples.

The sulphate minerals were formed on post-carbonatite stage. A part of them composes the disseminations and small assemblages in calcite-dolomite veinlets. Thin (up to 0.5 cm) monomineral sulphate veinlets are found. The composition of sulphates is changeable. In general they are presented of barite containing up 4 to 20 wt.% SrO. Barite-celestine with similar ration of celestine and barite minal is met rarely.

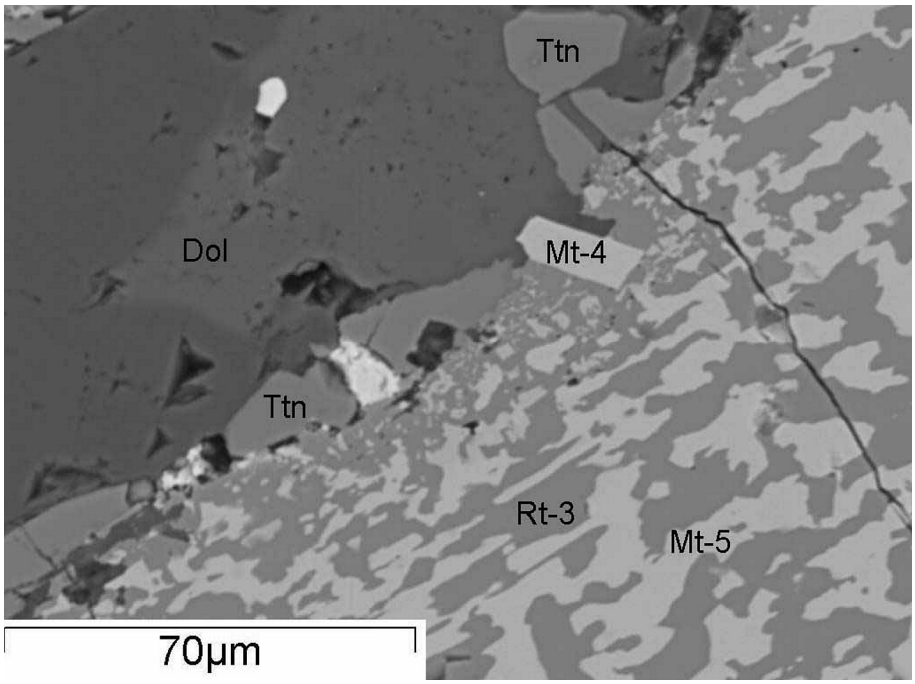

Fig. 6. **Titanite (grey) grains are confined to contact of xenolith with carbonatite.**

Xenolith is composed Cr-bearing magnetite-4, magnetite-5 and rutile-3. Barite-celestine has light single grains. Backscattered electron image.

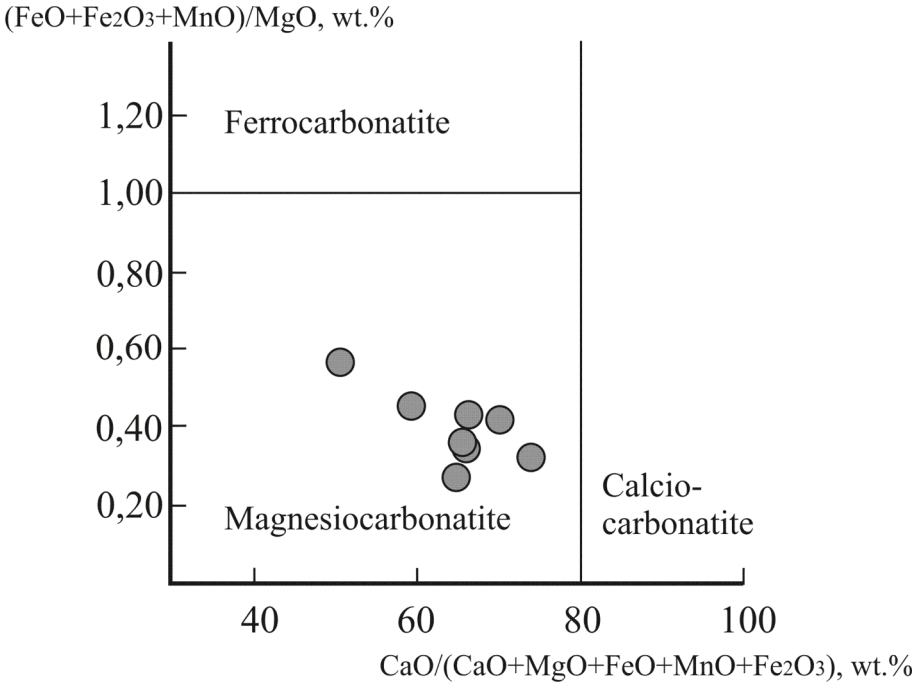

Fig. 7. **Composition of Veseloe carbonatite into the classification diagram, field outline according to [6].**

A big part of monazite, sinchisite and allanite are related with secondary processes. They are presented of disseminations in area of silicification, carbonatization of rocks and apatite recrystallization. Allanite and monazite are enriched of light rare earth elements selectively. Monazite has most stable cerium

Table 5.

Chemical composition of rutile from the Veseloe carbonatites, wt.%

№	TiO_2	Cr_2O_3	FeO	V_2O_3	Nb_2O_5	Total
Rutile-1 is paragenous of carbonatite						
1	89.74	-	9.31	1.34	-	99.05
2	95.88	-	4.43	1.08	-	101.39
3	84.81	-	14.34	1.12	-	100.27
4	97.28	-	1.79	0.99	-	100.06
5	96.47	-	1.87	1.76	-	100.12
6	98.57	-	1.58	1.03	-	101.18
Rutile-2 and rutile-3 from xenoliths						
7	97.84	1.58	0.37	-	1.46	101.25
8	95.93	2.11	-	-	0.95	98.99
9	93.84	2.90	0.38	0.93	2.30	100.35
10	96.02	2.74	-	-	1.75	100.51
11	98.61	1.33	-	-	-	99.94
12	98.13	1.01	-	0.88	-	100.02
13	98.36	1.40	0.36	-	-	100.12
14	98.97	0.51	1.03	-	-	100.51
15	98.79	0.52	1.38	-	-	100.68
16	98.59	0.27	1.02	0.92	-	100.80
17	89.36	0.65	8.69	1.22	-	99.95
18	97.76	0.70	1.57	-	-	100.04
19	95.40	0.79	3.45	-	-	99.64
20	96.13	0.61	3.95	-	-	100.70
21	96.23	0.87	3.08	-	-	100.17
22	97.59	0.34	1.20	0.85	-	99.97
23	97.00	0.30	1.27	0.71	-	99.37
24	97.91	0.82	1.53	-	-	100.27
25	97.00	1.14	0.97	-	-	99.12

Note. 1-6 – rutile-1 is paragenous of carbonatite, 7-25 - rutile-2 and rutile-3 from xenoliths: 7-13 – rutile-2 from xenoliths, 14-23 – rutile-3-magnetite exolution. Data of EPMA and SEM-EDS (analysts Kanakin S.V. and Karmanov N.S., Geological Institute SB RAS, 2003-2004).

content and most wide variations of lanthanum and neodymium contents. In monazite also is typical the presence of strontium (from 0,5 to 4,23 wt.% SrO) and small amount of thorium.

Zircon forms the single translucent prismatic crystals and idiomorphic grains and scattered in dolomite matrix. The assemblages in 2-3 crystals are marked rarely. As apatite, the long axles of grains are oriented according to banding of rocks. In zircon not detected Hf and other trace elements.

CHEMICAL COMPOSITION OF CARBONATITES

The chemical composition of the rocks of Veseloe occurrence is hit in magnesiocarbonatite field (Fig. 7). They have a high magnesium content and decreased ferruginosity. The main feature of rocks is increased the concentrations of P, Ti and F (see Table 1, analysis 6-10) and decreased of Nb, Zr, Mn, and Ba

Table 6.

Chemical composition of titanite and ilmenite from the Veseloe carbonatites, wt.%

№	SiO_2	TiO_2	Cr_2O_3	FeO	MgO	CaO	V_2O_3	Total
1	30.00	39.00	-	1.21	-	27.02	0.61	97.85
2	29.82	38.30	0.38	1.26	-	27.11	-	97.77
3	30.74	37.86	0.27	1.04	-	27.61	-	99.00
4	30.43	39.05	0.34	1.23	-	27.57	-	98.60
5	30.28	38.68	-	1.08	-	27.35	-	98.04
6	29.78	38.12	-	1.73	-	26.50	-	96.55
7	30.19	38.77	0.52	1.55	-	27.28	-	99.31
8	29.75	38.33	-	1.45	-	26.97	-	97.41
9	29.93	38.53	0.33	1.42	-	26.97	-	97.18
10	29.28	38.23	-	1.37	-	27.21	0.57	97.45
11	30.58	38.68	-	1.61	-	27.72	0.52	99.49
12	30.25	38.53	0.30	1.51	-	27.95	-	98.54
13	29.93	38.47	0.54	1.17	-	27.36	-	98.60
14	29.71	38.62	0.27	1.12	-	27.98	0.56	99.47
15	-	49.75	1.14	44.47	1.85	0.72	-	97.93
16	-	50.64	-	45.30	1.99	0.99	-	99.23
17	-	49.42	0.69	49.61	-	-	-	99.72
18	-	51.91	0.29	46.71	1.81	0.86	-	101.59
19	-	51.06	0.40	46.83	1.82	0.82	-	100.94
20	-	51.04	-	48.42	0.62	1.06	-	101.54
21	-	54.05	1.33	44.19	-	-	-	99.58

Note. 1-14 – titanite, 15-21 – ilmenite. Some samples of titanite contain up to 1 wt.% of Nd_2O_3, Ce_2O_3, Y_2O_3. Data of SEM-EDS (analyst Karmanov N.S., Geological Institute SB RAS, 2004).

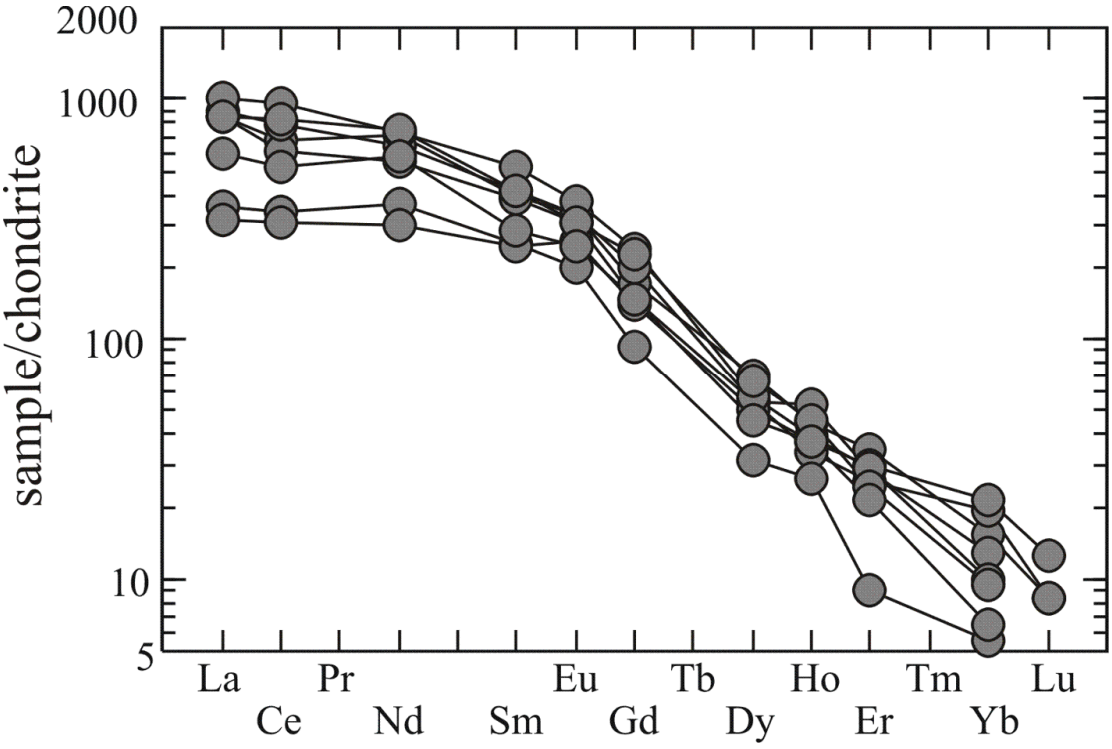

Fig. 8. **REEs spectra in the Veseloe carbonatites, normalized according to [5]**

contents. There are Cr and Ni. Their amount is higher in four times than in average carbonatite [6]. The strontium and REEs concentrations are similar by average carbonatite.

The REEs compositions and them plot normalized by chondrite (Fig. 8) are similar of carbonatite compositions from other regions of world. Light rare earth elements predominate among REEs.

Table 7.

Isotope composition of C, O and Sr in rocks of the Veseloe area

Analyzed rocks	Mineral	$\delta^{13}C$‰, PDB	$\delta^{18}O$‰, SMOW	$^{87}Sr/^{86}Sr$
Quartz-dolomite vein	**dolomite**	-0.1	16.7	
Listvenite	**dolomite**	-1.9	12.0	
	--//--	-0.9	12.2	
Dolomite marble	**dolomite**	2.8	16.1	
	--//--	3.4	15.3	
Carbonatite	**dolomite**	-1.9	10.2	0.70398
	--//--	-2.2	8.9	0.70396
	--//--	-1.9	10.1	
	magnetite		1.5	
Post-carbonatite calcite-dolomite veinlet	**calcite**	-2.3	9.8	

Note. Analysis of dolomite from listvenite is obtained by Damdinov B.B. (data not published). Isotope composition of O and C were determined Analitical Center FESC RAS, Sr - Geological Institute SB RAS (analyst – Posokhov V.F.), 2003-2004.

ISOTOPE CHARACTER OF CARBONATITES

The $\delta^{13}C$ and $\delta^{18}O$ isotope values and $^{87}Sr/^{86}Sr$ initial ration were studied in minerals from carbonatites. Two samples of dolomite from marbles, which are situated nearby of carbonatites, carbonates from listvenites and quartz-carbonate vein were analyzed for comparison. The results of analyses are shown in a table 7.

$^{87}Sr/^{86}Sr$ initial ration in dolomite from carbonatite has a value to similar by mantle source of Late Riphean.

The $\delta^{13}C$ isotope value in dolomite from main matrix of carbonatites has -1,9 and -2,2‰. It is heavier of average value for mantle rocks. The $\delta^{18}O$ isotope value is similar to mantle source.

The $\delta^{18}O$ isotope values in magnetite, which is paragenous of carbonatite (magnetite-2) has 1,5‰ $\delta^{18}O$ and is analogous of magmatic magnetite from basic rocks.

The $\delta^{13}C$ and $\delta^{18}O$ isotope values in calcite from post-carbonatite dolomite-calcite veinlet containing the disseminations of Sr-bearing barite are similar by dolomite from carbonatite.

Dolomite from marble that is situated near carbonatites has differed isotope value. The $\delta^{13}C$ and $\delta^{18}O$ isotope values are heavier and are analogous by value for metamorphized marine limestone. In marble the $^{87}Sr/^{86}Sr$ initial ration has low value (0,70409) that is cause of strontium pollution from carbonatites. Sr content in

carbonatites is more 1200 ppm and average content of this element in marble not exceed of one hundred ppm. Sr is not detected in monomineral dolomite samples (limit of detection about 270 ppm).

The $\delta^{13}C$ and $\delta^{18}O$ isotope values in dolomite from quartz-carbonate veinlets also are differed (see Table 7). The values are similar to values of metamorphized sedimentary carbonate rocks.

The $\delta^{13}C$ and $\delta^{18}O$ isotope values in carbonate minerals from listvenites situating near carbonatites have other values. And $\delta^{13}C$ and $\delta^{18}O$ from these minerals are enriched by heavy isotopes relatively mantle value (see Table 7).

CONCLUSIONS

In investigated carbonatites, the composition of mineral paragenesises is similar to carbonatites of other regions of world. Dolomite, apatite, calcite, rutile, magnetite, zircon and alkaline amphiboles are typomorphic minerals here. The $\delta^{18}O$ isotope values and the $^{87}Sr/^{86}Sr$ initial rations are analogous by average carbonatite. The only the $\delta^{13}C$ isotope value in carbonate is heavier. It is interesting to note that the carbonates from listvenites contain the heavy $\delta^{13}C$.

Dolomite composition and absence of calcite carbonatites are most important features of the Veseloe carbonatites. Absence of comagmatic silicate rocks also is nonordinary.

These carbonatites on many features are similar by linear type of carbonatites [1]. For this type of carbonatites are suppose their formation from mantle directly.

As distinct from the Pogranichnoe [3] carbonatites situating in this area the Veseloe carbonatites have larger concentrations of apatite and titanium content, but less of magnetite and strontium and REEs concenrations. The Pogranichnoe rocks on chemical composition are hit in ferrocarbonatites field and the Veseloe carbonatites are magnesiocarbonatites.

The carbonatites, though not big on scale, discovered in the North Transbaikalia are evidence of existence of new carbonatite area.

The presence of Cr-bearing mineral assamblages in the Veseloe carbonatites allows diagnosing them as mantle xenoliths. There is necessitating of consideration that carbonatites were smelt from mantle matrix. It and also special mineralogical composition and geochemical features of rocks make necessary to carry out more detailed historic analysis to study geologic development of zones where folded areas joint with Siberian craton and crystalline basement.

The studies have been carried out under support of the RFBR (grant №03-05-65270), Integration project of SB RAS (grant №67), Lavrent'ev Foundation of SB RAS (grant №92) and Russian Science Support Foundation.

REFERENCES

1. **Bagdasarov, U.A.** (1986). Chemistry of magnetites from carbonatites of different formation types and facies of depth this rocks // Mineral clarks and nature theirs stability. Mater. IV Vses. Miner. Seminara. Dushanbe. P. 223-224. (In Russian)

2. **Massone, S., Schreyer, W.** (1989). Stability field of the high-pressure assemblage talk-phengite and two new phengite barometers // Eur. J. Miner. № 1. P. 391-410.
3. **Ripp, G.S., Badmatsyrenov, M.V., Doroshkevich, A.G.** (2003). Mineral composition and geochemical characteristic of the Pogranichniy carbonatites (Northern Transbaikalia) // Plumes and problem of deep sources of alkaline magmatism. Irkutsk-Khabarovsk, P. 88-108. (In Russian)
4. **Ripp, G.S., Badmatsyrenov, M.V., Skulyberdin, A.A.** (2002). A New Carbonatite occurrence in Northern Transbaikalia // Petrology. V. 10. № 4. P. 442-446. (In Russian)
5. **Sun, S., McDonough, W.F.** (1989). Chemical and isotopic systematics of oceanic basalts: implications for mantle composition and processes // Eds. Saunders A.D. & Norry M.J. Magmatism in the ocean basins. Geol. Soc. Special Publ. № 42. P. 313-345.
6. **Woolley, A.R., Kempe, R.C.** (1989). Carbonatites: Nomenclature, average chemical composition and element distribution. Carbonatites: Genesis and Evolution. London: Unwin Hyman, P. 1-46.

UDK 550.42; 552.111

Geochemistry of oceanic basalts of the Katun accretionary wedge in northern Gorny Altai: evidence for mantle plume magmatism

Safonova I.Yu., Buslov M.M.

Institute of Geology SB RAS, Novosibirsk, Russia, e-mail: inna@uiggm.nsc.ru

Geological and geochemical studies of basaltic-sedimentary terranes have been performed in the Katun accretionary wedge (Vendian-Middle Cambrian units). We identified the fragments of Vendian-Early Carboniferous oceanic crust of the Paleo-Asian Ocean. The Katun accretionary wedge of Early Cambrian age recorded a stage of the Kuznetsk-Altai island arc evolution. The presented study of the fragments of oceanic crust allowed a conclusion that hot-spot volcanism was active at the early stages of the Paleo-Asian Ocean history. The fragments of weakly to strongly differentiated varieties of oceanic and island-arc basalts have been preserved in accretion-collision zones and gave us information about chemical composition and petrology of volcanic rocks composing the oceanic crust.

Two types of oceanic basalts are present in the 560 Ma Katun accretionary wedge of Gorny Altai. Ti-high (oceanic island basalts - OIBs) and Ti-medium (mid-oceanic ridge basalts – MORB or island-arc tholeiites) varieties co-exist within this geological structure. The least altered Ti-high basalts are characterized by enriched LREE and flat HREE patterns (La/Sm_N =1.03-1.7, Eu/Yb_N = 1.6-2.7). They have small negative Zr (Hf) anomalies relative MREE. Mg# varies from 48 to 60 over a relatively narrow range of SiO_2 (48-52 wt%).Ti-medium basalts have slightly depleted LREE and flat HREE (La/Sm_N =0.22-0.66, Eu/Yb_N = 0.47-1.4), negative Zr (Hf) anomalies and Nb-Ta negative anomalies (Nb/La_N =0.18-0.25, La/Ta_N= 1.1-2).

Two types of Katun oceanic metabasalts could have been melted at different degrees of partial melting and at different depths. Otherwise they could be produced from one mantle source, but then differently influenced and/or contaminated by the upper mantle matter. Our interpretation of geochemical data suggests that Katun metabasalts were formed within mid-oceanic ridges and oceanic islands or oceanic plateau of the Paleo-Asian Ocean.

INTRODUCTION

At present most investigators accept the idea about mantle plumes ascending from the lower-upper mantle boundary or lower mantle/outer core boundary. Such plumes while moving up result in the melting of mantle rocks and therefore produce special basaltic melts erupting at the surface not at plate boundaries but within oceanic and continental plates to form oceanic islands and oceanic and continental basaltic plateaux [23]. It is necessary and important to determine the tectonic setting of mafic volcanism because compositions of magma are strongly related to tectonic setting. The geochemistry of oceanic island basalts provides

information on the composition of the mantle, and the processes and dynamics of mantle melting. Because primitive basaltic magmas (e.g. oceanic island basalts) travel from their mantle sources to the surface without significant cooling and crystallization ***en route***, compositional variations within them provide direct information on the sources and processes of partial melting in the mantle [31].

The Paleo-Asian Ocean existed in Vendian time between Siberia and East Gondwana and could be up to 4000 km wide (e.g. [15, 27, 34, 41]). It was closed in Late-Carboniferous-Permian time as a result of the collision of the Kazakhstan and Siberian continents. The fragments of the oceanic crust of the Paleo-Asian Ocean, including ophiolites and plume-types basalts (oceanic island/plateau basalts – OIB/OPB) have been preserved in Altai-Sayan area (ASA) – a Caledonian collisional zone at the western and southern margins of the Siberian continent [8, 33]. In Vendian time, the Siberian continent's SW margin was bounded by an island arc system, which remnants together with the fragments of the oceanic crust have been found in South Siberia and Mongolia (Fig. 1). Their ages are believed to be Vendian-Cambrian by many investigators of the Altai Mts. typically referred to as Gorny Altai. Gorny Altai is a western mountainous part of the Altai-Sayan area (ASA), which is a Caledonian accretion-collisional complex of South Siberia containing large fragments of Vendian- Cambrian island arcs formed after the closing of the Paleo-Asian Ocean and fragments of the oceanic crust [3, 8, 17, 41].

Many investigators have studied oceanic terrains in ASA since the early 1990's. The Katun accretionary complex or wedge is a part of the above mentioned Caledonian folded structure in the southern frame of the Siberian craton, which incorporates multiple fragments of basaltic units. Katun units have been previously identified as island-arc, MORB and oceanic island basalts formed over the Vendian-Early Cambrian crust of the Paleo-Asian Ocean [4, 8, 10, 17, 18, 33, 41].

The paper presents the results of the geochemical study of the Katun basalts incorporated in the Katun accretion-collision zone (Fig. 1). The Katun accretionary wedge comprising fragments of an oceanic island was described in many publications (e.g. [4, 18]). This paper reviews the data on the previously recognized oceanic crust of Vendian-Early Carboniferous age formed in different structural setting and presents additional information on its chemical composition.

GEOLOGICAL SETTING

The tectonic structure of the Altai-Sayan foldbelt is a collage of terranes of different ages separated by numerous large-scale thrusts, strike-slip faults and nappes [3, 4, 11, 16, 17, 41]. The terranes are classified mainly based on Vendian-Cambrian geodynamic units of the Paleo-Asian Ocean. Fig. 1 shows the major structural units, which are a part of the Central Asian foldbelt, within the area in between the Kazakhstan and Siberian continents. The tectonic pattern of Altai-Sayan includes three groups of structural and tectonic units: 1) the Gondwana-derived Altai-Mongolian terrane; 2) terranes of different ages – Kalba-Narym,

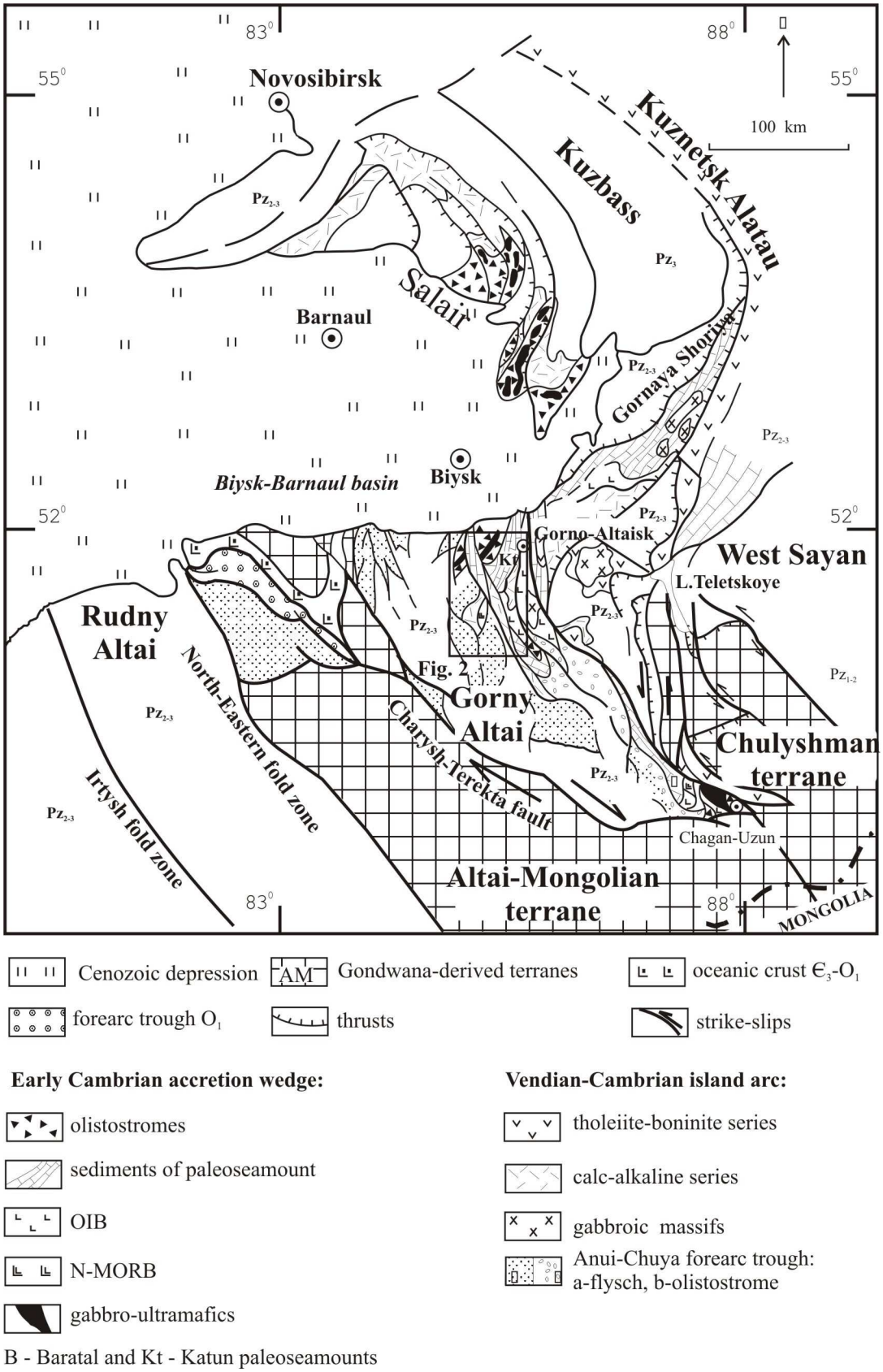

Fig. 1. **Location and regional geology of Gorny Altai and North-West Altai.**

Rudny Altai, Gorny Altai - composed of fragments of Caledonian and Hercynian accretion-collision zones. Accretionary prisms (wedges) consist of fragments of subducted terranes of oceanic lithosphere – ophiolites, seamounts and ocean islands - which had accreted to island arcs and/or active continental margins; 3) systems of strike-slip faults and thrusts of different ages – Chara, Irtysh, North-West, Charysh-Terekta, Kurai, Teletsk-Bashkauss - separating collisional terranes from the margins of collided continents [8].

The Gorny Altai terrane contains a complete set of Vendian-Cambrian rocks [10]. Previous petrochemical studies by Buslov et al. [4, 6, 8] deciphered the tectonic settings of volcanic rocks. A number of Early Cambrian accretionary units including OIB and N-MORB and Vendian-Cambrian island arc units are recognized and contact each other in the Kurai (west of Chagan-Uzun Village) and Katun (nearby Gorno-Altaisk city) zones of the Gorny Altai [6, 8, 9, 35].

Katun oceanic island units include pillow lavas and their associated siliceous, siliceous-terrigenous-carbonate and carbonate sediments. The Katun paleoseamount terrane is 70x20 km size and it is a part of the Katun accretionary wedge consisting of alternating basalts and olistostrome and ophiolite tectonic sheets.

The Katun accretionary wedge is situated north of the Kurai accretionary wedge and extends over a distance of more than 120 km along the Katun River, south of Gornoaltaisk (Fig. 1). It involves three types of paleo-oceanic island rock units: 1) limestones, black silicilites, dolomites, siliceous shales, and thin basaltic flows; 2) high-Ti tholeiites and alkali basalts; 3) reef limestone and dolomite. These units are suggested to be fragments of a single unit formed in the oceanic island setting [18]. Fragments of paleo-oceanic islands occur in association with olistostromes (Fig. 2).

There are two types of Vendian-Early Cambrian volcanic rocks in the Katun paleo-island: a) thin flows of tholeiitic basalts – the relicts of oceanic crust - formed in deep-water setting; and b) large volcanic buildups and submarine plateaux of alkali basalts with subordinate tholeiites. The first type volcanics are aphyric tholeiites with sporadic fine phenocrysts of olivine and clinopyroxene. The second type volcanics are aphyric olivine-bearing tholeiites, porphyric hawaiites, and aphyric or Pl-porphyric alkali basalts, consisting of olivine, pyroxene and plagioclase phenocrysts and glassy matrix [4, 21].

The Katun accretionary wedge is overlain by basal conglomerates containing carbonate rocks of the Shashkunar Formation, which takes the lowest position in the sequence of the Early-Middle Cambrian island arc. The tectonic sheets of the accretionary wedge and carbonate rocks of the Shashkunar Formation are cross-cut by island-arc dikes of pyroxene-plagioclase porphyrites, diabase, and gabbro.

Volcanogenic, siliceous-limestone and carbonate paleo-oceanic units extend to the northeast to Gornaya Shoriya, and form a 40X250 km structure. In the northwestern part of the Katun accretionary wedge the tectonic sheets and

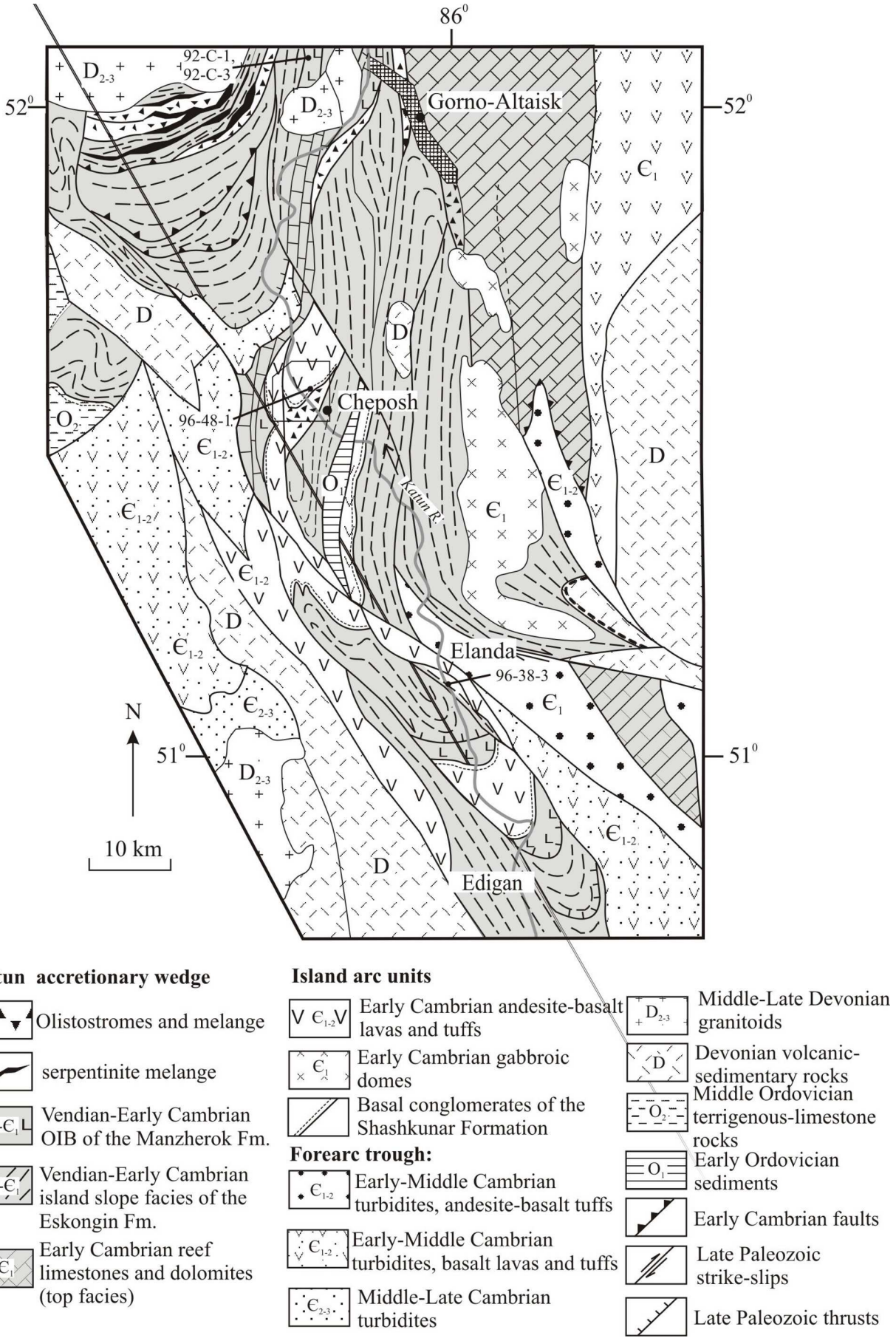

Fig. 2. **Geological map of the Katun accretionary wedge.**

olistostromes are surrounded by serpentinitic melange and basalts with N-MORB characteristics [4, 21] (Fig. 2).

ANALYTICAL METHODS AND GEOCHEMICAL APPROACHES

For geochemical investigation of metabasalts from all the localities considered in the paper samples with few or no veinlets and vesicles were collected from the least deformed and altered outcrops. In all samples analyzed, olivine, pyroxene and volcanic glass were replaced by chlorite and epidote and most plagioclase was albitized. All analyses were made at the United Institute of Geology, Geophysics and Mineralogy, SB RAS. Major elements and some trace elements (Rb, Sr, Y, Zr, Nb) were determined using a "Nauchpribor" X-ray fluorescence spectrometer (analytical procedure following Russian state analytical standard OST-41-08-212-82 Mingeo SSSR; analyst – A.D. Kireev). REE and other trace elements were analyzed with the neutron-activation method (INAA) by V.A. Bobrov using Ge detectors for Y-rays higher that 30 KeV and below 2000 KeV (REE and HFSE), atomic absorption spectrometry (LILE) using a 3030 AA spectrometer and XRF (Rb, Sr, Y, Zr, Nb).

The diagrams applied below use high field strength elements (HFSE) such as Ti, Zr, Y, Nb and several others which are thought to be relatively immobile in aqueous fluids unless there are high activities of F^- (not observed in our case). This means that these elements will be stable under conditions of hydrothermal, sea-floor weathering and up to medium metamorphic grades (mid-amphibolite facies) [32].

The Nb/Y ratio was used for the distinction of alkaline and subalkaline series [39]. MORB-normalized trace element patterns [26], MnO-TiO_2-P_2O_5 diagram [29] and 2Nb-Zr/4-Y systematics [28] were utilized to identify tectonic setting of formation. Nb/Y-Nb/Zr diagram was used to compare with superplume-related oceanic island basalts [37].

GEOCHEMISTRY OF BASALTS

Wholerock analyses of 49 selected samples of tholeiitic, subalkaline and alkaline metabasaltic rocks and amygdaloidal pillow-lavas from 4 sites of the Katun accretionary wedge – Surtaika, Ust-Syoma, Cherga and Cheposh - are given in Table 1. Table 2 shows trace element analyses of 9 Katun basalts. The basalts are in the low-temperature greenschist facies of regional metamorphism and probably also underwent sea-floor metamorphism. The pillows consist of a Cpx-porphyrite core and siliceous-carbonate outer part. Pyroxene is replaced by chlorite and epidote and the matrix comprises actinolite, epidote, chrolite and albite. The Katun metabasaltic rocks are dominantly subalkaline and alkaline basalts (Fig. 3a). The SiO_2 versus Nb/Y diagram shows two groups of basalts as well: subalkaline and alkaline basalts (Fig. 3b). The samples display a clear Fe-enrichment trend with advancing fractionation and TiO_2 increase with increasing FeO*/MgO is not

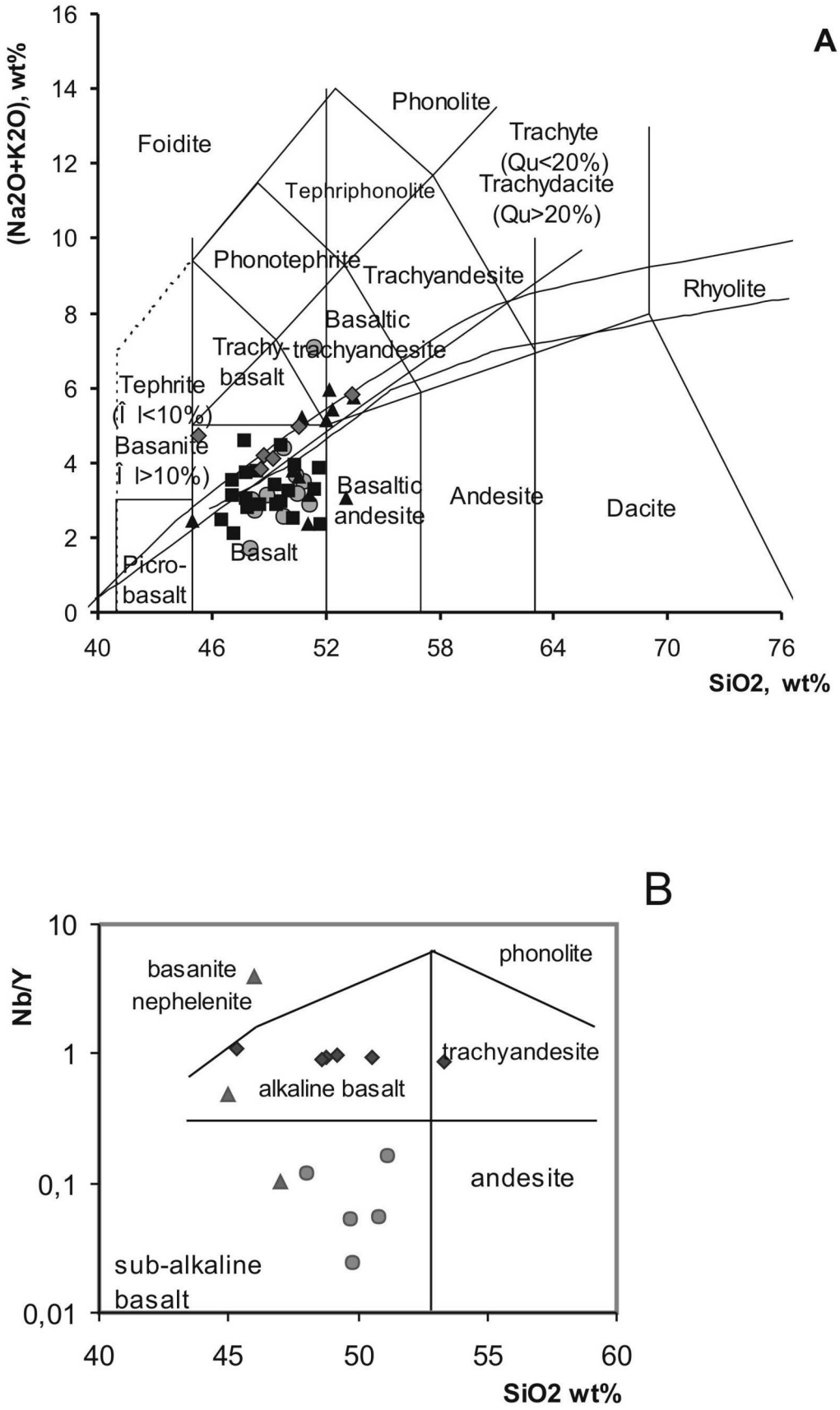

Fig. 3. **Classification diagrams: A - SiO_2 versus total alkali (TAS); B – Nb/Y vs SiO_2 [39].**

Symbols - filled rhombs: Surtaika metabasalts, circles: Ust-Syoma metabasalts, triangles: Cherga metabasalts, squares: Cheposh metabasalts.

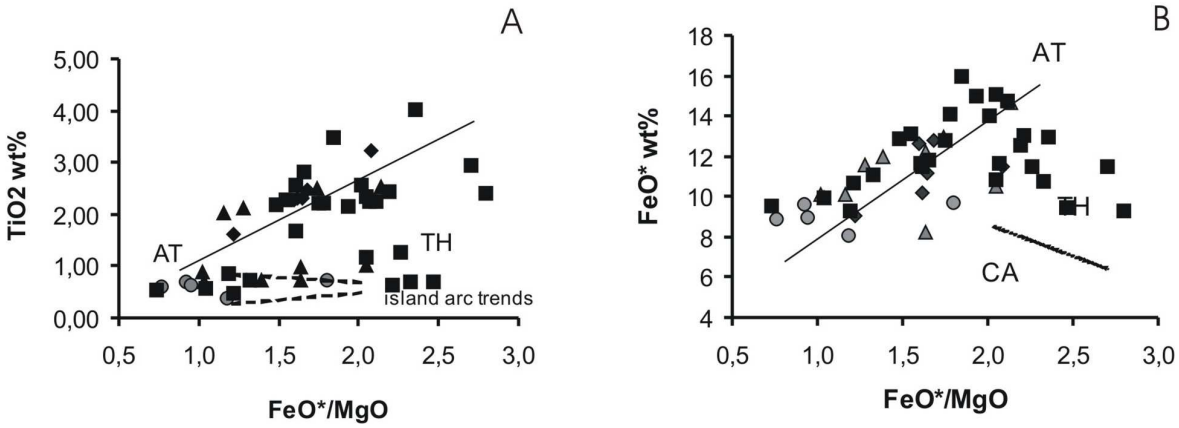

Fig. 4. **Major element plots: A – FeO* vs FeO*/MgO; B – TiO_2* vs FeO*/MgO.**

Discriminant fields and trends of abyssal tholeiite (AT), tholeiite (TH) and calc-alkaline volcanic rocks (CA) are after Miyashiro (1973). Symbols as in Fig. 3.

as obvious (Fig. 4a) showing weak tholeiitic and calc-alkaline (island-arc) trends. The Fe-enrichment trend is close to those characteristic of strongly differentiated tholeiitic suite (Miyashiro, 1973). Katun samples have FeO*/MgO ranging mostly from 1 to 2.5 and showing a medium degree of differentiation (Fig. 4b) and they are characterized by a relatively large range of Mg# (40-70) and Fe_2O_3 (8-16 wt.%) contents over a restricted range of SiO_2 (46-52 wt.%). Compared to island-arc tholeiites Katun metabasalts are depleted in LILE (K, Rb, Ba) and have higher HFSE (Zr, Nb, Th, Hf) contents [19].

All samples have variably high LOI (2.1-6.9%), indicating different degrees of alteration (Table 1). Na, Ka and low-field-strength elements are mostly mobile and susceptible to change during alteration (e.g. [24]), while HFSE and REE are essentially immobile during the most severe sea-floor hydrothermal metamorphism (e.g. [40]. Thus, only immobile HFSE and REE were used to identify the magmatic affinity and petrogenesis of these altered mafic volcanic rocks.

The TiO_2 and P_2O_5 contents range from 0.37-0.83 wt% (Ti-medium varieties) to 2.1 -3.89 wt % (Ti-high varieties) and from 0.04 to 0.43 wt%, respectively. Al_2O_3 ranges from 10.3 wt% to 19.5 wt%, that is in average a little lower than in IAT. The mafic volcanic rocks of Katun are slightly depleted in LILE and enriched in HFSE, Cr and Mg compared to IAT (Table 2). According to HFSE and LILE concentrations and K/Rb, K/Ba and Zr/Nb ratios we may distinguish two types of samples.

Ti-high Type 1 includes Surtaika samples and Ti-enriched Cherga and Cheposh samples, which are also enriched in HFSE, depleted in Sr, Rb and Ba and have high K/Rb, K/Ba and Zr/Nb ratios (Table 1). Type 1 alkaline and tholeiitic basalts have intermediate Nb/Zr (0.14-0.18) and Nb/Y (0.86-1.08) bulk ratios (Table 2, Fig. 9). In these basalts, La/Sm_N ranges from 1.03 to 1.7 and Eu/Yb_N ranges from 1.6 to 2.7 (Table 2). The Ti-high basalts have small positive Nb

anomalies with respect to La (Nb/La_n =1.4-2.0) and negative Th anomalies (Th/La_n

Table 1.

Major element analyses of metabasaltic rocks from the Katun accretionary wedge, wt.%

	Sample	SiO_2	TiO_2	Al_2O_3	Fe_2O_3	MnO	MgO	CaO	Na_2O	K_2O	P_2O_5	L.O.I.	Total
1	*92-C-1*	52,32	2,26	12,44	11,11	0,10	6,19	7,60	5,04	0,68	0,29	2,76	100,79
2	*92-C-2*	48,50	2,20	12,74	11,85	0,09	6,48	9,02	4,20	0,56	0,24	4,43	100,31
3	*92-C-3*	47,62	2,40	13,04	13,85	0,14	7,42	8,81	3,70	0,41	0,31	3,42	101,12
4	*92-C-4*	47,13	2,21	12,01	13,59	0,16	7,65	10,27	3,23	0,48	0,24	4,03	101,00
5	*96-38-3*	42,26	1,51	14,79	9,40	0,23	6,94	13,59	3,95	0,46	0,17	6,98	100,27
6	*96-48-1*	46,94	3,07	13,79	12,17	0,16	5,26	9,86	2,36	1,55	0,28	4,76	100,20
7	*96-39-1*	49,03	0,37	19,27	8,58	0,17	6,55	9,10	1,13	1,66	0,06	4,02	99,94
8	*96-39-2*	48,05	0,69	18,01	10,37	0,20	5,18	9,70	3,79	0,46	0,14	3,52	100,12
9	*96-39-3*	47,05	0,67	12,22	10,48	0,21	10,21	15,25	0,96	0,71	0,15	2,10	100,01
10	*96-40*	47,67	0,56	10,36	9,48	0,20	11,18	13,65	1,55	0,91	0,12	4,18	99,86
11	*96-50-2*	49,13	0,63	14,68	9,66	0,15	9,19	9,89	3,29	0,08	0,04	2,98	99,72
12	*260*	49,90	0,70	19,80	8,80		4,85	6,88	3,60	1,31	0,11	4,38	100,33
13	*259/2*	48,50	0,67	16,00	10,59		9,21	7,34	2,99	0,50	0,11	4,89	100,80
14	*259*	41,80	0,67	18,10	12,39		8,03	9,64	1,83	0,44	0,07	6,67	99,64
15	*257*	48,70	0,95	14,10	13,09		7,20	9,18	2,80	0,27	0,07	4,16	100,52
16	*242/2*	47,10	1,00	15,60	11,40		5,02	14,69	1,85	0,80	0,11	2,82	100,39
17	*242*	47,10	0,86	15,90	10,79		9,54	8,95	2,28	0,72	0,11	4,52	100,77
18	*241*	48,50	1,94	15,00	10,80		8,37	7,80	3,16	0,65	0,17	4,35	100,74
19	*239*	44,20	2,42	13,00	15,50		6,53	10,79	1,99	0,39	0,24	5,03	100,09
20	*238/2*	46,20	2,06	13,90	12,40		8,70	10,33	2,37	0,36	0,18	3,81	100,31
21	*238/1*	45,40	2,42	14,20	13,90		7,20	11,02	1,67	0,37	0,18	4,05	100,41
22	*1513-2*	44,60	3,29	16,53	16,80	0,17	8,19	1,35	2,84	0,51	0,43	5,30	100,01
23	*1514-1*	46,22	3,89	15,08	13,95	0,19	5,34	7,16	2,92	1,53	0,62	3,15	100,05
24	*1520*	49,62	2,72	13,42	12,63	0,18	6,86	6,66	3,03	0,69	0,36	3,94	100,11

Table 1 (End).

	Sample	SiO2	TiO2	Al2O3	Fe2O3	MnO	MgO	CaO	Na2O	K2O	P2O5	L.O.I.	Total
25	*1566*	46,16	2,34	16,38	13,50	0,17	5,55	8,65	2,79	0,82	0,26	3,57	100,19
26	*1567*	46,67	2,48	15,51	12,35	0,17	6,90	8,34	2,27	1,39	0,49	3,35	99,92
27	*1567-3*	47,63	2,30	19,52	9,89	0,17	3,18	8,55	3,66	0,63	0,49	3,94	99,96
28	*3563*	44,23	2,08	15,18	13,35	0,19	6,86	8,66	2,03	0,90	0,46	6,29	100,23
29	*3579-1*	48,44	2,11	13,30	12,09	0,19	5,27	9,73	1,82	0,40	0,27	6,40	100,02
30	*1507-1*	47,95	2,11	13,73	13,93	0,18	8,45	7,74	2,39	0,42	0,24	2,93	100,07
31	*1507-4*	45,97	2,24	12,74	16,07	0,19	7,06	8,68	2,66	0,27	0,28	4,01	100,17
32	*1507-8*	48,65	2,09	12,04	16,07	0,17	7,49	7,50	2,29	0,17	0,25	3,37	100,09
33	*1507-9*	46,44	2,13	12,72	15,03	0,18	7,59	8,65	2,53	0,25	0,29	4,37	100,18
34	*1507-10*	48,56	2,20	13,52	14,16	0,19	8,25	6,72	2,88	0,28	0,26	3,04	100,06
35	*1508*	47,63	2,46	14,59	15,00	0,16	6,71	6,40	2,94	0,35	0,32	3,56	100,12
36	*1508-2*	48,35	2,19	12,78	15,99	0,17	6,81	7,97	2,68	0,21	0,28	2,62	100,05
37	*1508-10*	49,19	2,82	12,73	12,21	0,17	4,06	11,02	2,03	1,14	0,41	4,50	100,28
38	*1523*	50,00	1,15	17,02	11,76	0,17	5,16	4,71	2,61	4,30	0,47	2,75	100,10
39	*1559*	46,74	1,62	16,41	12,55	0,17	7,03	9,60	2,12	0,81	0,20	2,80	100,05
40	*3557*	49,15	1,24	16,41	12,42	0,17	4,94	9,29	1,50	2,06	0,31	2,57	100,06
41	*1510-7*	50,02	0,70	12,97	11,62	0,19	7,90	7,67	1,07	1,79	0,27	6,02	100,22
42	*1516-3*	49,25	0,62	14,93	13,95	0,19	5,67	8,34	1,51	1,50	0,33	3,90	100,19
43	*3551-1*	48,41	0,52	13,33	10,24	0,16	12,55	7,17	1,59	2,05	0,28	3,84	100,14
44	*3551-3*	49,29	0,55	14,00	10,74	0,17	9,30	7,68	0,63	4,45	0,37	2,96	100,14
45	*3590-1*	48,66	0,46	13,33	11,30	0,18	8,38	10,42	1,14	1,10	0,27	5,05	100,29
46	*1507-7*	50,70	0,67	17,96	10,18	0,18	3,72	7,81	2,52	2,74	0,38	3,27	100,13
47	*1509*	49,48	0,67	19,06	11,33	0,18	4,38	3,97	3,71	1,92	0,17	5,30	100,17
48	*1509-6*	52,06	0,83	13,35	10,07	0,18	7,61	7,47	2,08	3,53	0,24	2,67	100,09

Note. Surtaika site: 1-6, Ust-Syoma site: 7-11, Cherga site: 12-21, Cheposh site: 22-48.

Table 2.

Trace element analyses of metabasaltic rocks from the Katun accretionary wedge, ppm

Sample	92-C-1	92-C-3	96-38-3	96-39-1	96-39-2	96-39-3	96-40	96-48-1	96-50-2
La	9,5	11	11	0,8	5,5	1,5	3	17	0,4
Ce	24,5	36	25	4	9,2	6	9,2	32	2,2
Nd	15	24,5	16	3	6	3	4,8	18	2,8
Sm	47	5	3,8	1,1	2	1,4	1,8	5	1,1
Eu	1,4	1,72	1,2	0,47	0,86	0,68	0,65	2	0,45
Gd		5,2		1,6		2,4		4	1,95
Tb	0,82	1,05	0,7	0,24	0,42	0,4	0,34	0,8	0,57
Yb	1,9	2,2	2,1	0,9	1,7	1,5	1,8	2,1	2,7
Lu	0,29	0,31	0,3	0,14	0,32	0,25	0,3	0,26	0,35
Sc	23,6	23	39	30	37	65	54	30	38
Th	0,6	0,6	0,9	0,3	0,4	0,5	0,3	1,5	
Hf			2,1	0,35	1	0,6	0,9	4	0,2
Ta	1,1	1,2	0,9	0,04	0,1	0,08	0,02	1,4	
Ba			95	680	200	530	500	350	370
Co			40	35	85	54	50	56	60
Cr			100	52	34	650	740	100	710
Rb	6,5	2,56	5	25	20	7	15	25	3
Sr	120,4	267,8	300	900	1150	405	275	800	240
Y	23,9	18,7	13	12	28	17	25	27	18
Zr	140,8	124,4	80	30	50	37	40	170	14
Nb	20,5	17,7	14	2	1,5	2	0,6	26	1
K/Rb	428,9	656,6	377,2	272,2	94,3	415,9	248,7	254,2	109,3
K/Ba			19,85	10,01	9,43	5,49	7,46	18,16	0,89
Zr/Nb	6,87	7,03	5,71	15,00	33,33	18,50	66,67	6,54	14,00
(Nb/La)N	1,19	1,41	0,70	1,38	0,15	0,74	0,11	0,85	1,38
(La/Ta)N	0,97	0,65	0,87	1,42	3,90	1,33	10,65	0,86	
(La/Yb)N	3,37	3,37	3,53	0,60	2,18	0,67	1,12	5,46	0,10
$(La/Sm)_N$	1,25	1,36	1,79	0,45	1,70	0,66	1,03	2,10	0,22
$(Eu/Yb)_N$	2,10	2,22	1,62	1,48	1,44	1,29	1,03	2,71	0,47
$(Nb/La)_N$	2,03	1,51	1,20	2,35	0,26	1,25	0,19	1,44	2,35
$(La/Ta)_N$	0,53	0,56	0,74	1,22	3,34	1,14	2,03	0,74	
$(Th/La)_N$	0,49	0,43	0,64	2,94	0,57	2,61	0,78	0,69	

=0.42-0.78). In the Nb-Zr/4-Y diagram Type 1 samples plot in the plume-type MORB (P-MORB) field (Fig. 5). Thus, Type 1 metabasalts resemble OIB basalt of Hawaii.

Ti-medium Type 2 comprises HFSE-depleted and LILE-rich Ust-Syoma samples and low-Ti Cherga and Cheposh samples with low K/Rb, K/Ba and Zr/Nb ratios (Table 1). Type 2 tholeiitic and subalkaline basalts have low Nb/Zr (0.02-0.07) and Nb/Y (0.02-0.06) bulk ratios resembling those of MORB (Table 2, Fig. 9). In these basalts, La/Sm_N ranges from 0.2 to 0.6 and Eu/Yb_N ranges from 0.5 to 1.4. The Type 2 basalts have clear negative Nb anomalies (Nb/La_n =0.18-0.25) (Table 2). In the 2Nb-Zr/4-Y diagram Type 1 samples plot in the fields of within-plate alkali basalts and tholeiites and Type 2 samples plot in the field of N-MORB

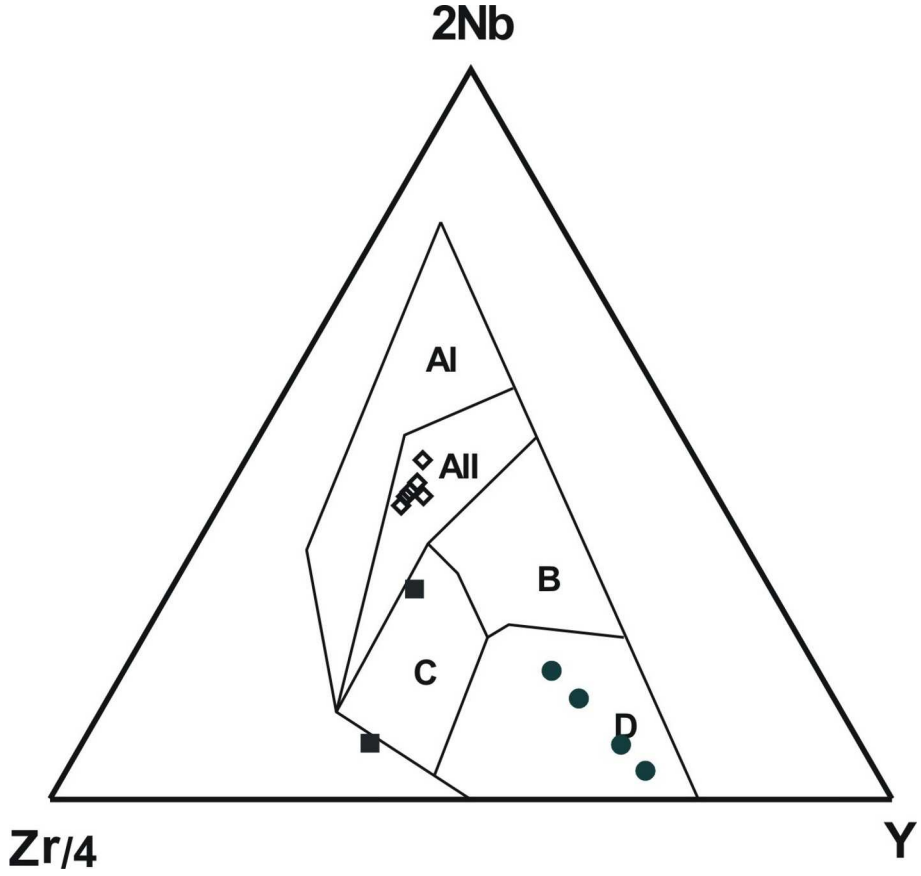

Fig. 5. **The Zr/4-2Nb-Y discrimination diagram after Meschede [28].**

The fields are defined as follows: AI - within-plate alkali basalts; AII - within-plate alkali basalts and within-plate tholeiites; B - E-type MORB; C - within-plate tholeiites and volcanic-arc-basalts; D - N-type MORB and volcanic-arc basalts. Symbols as in Fig. 3.

(Fig. 5). Thus, Type 2 possesses N-MORB affinities. In average, Type 1 basalts have lower MgO content than those of Type 2. Samples 96-38-3, 241, 1523, 1559 and 3557 we regard as chemically intermediate (Tables 1 and 2).

The support for consideration of such two groups also comes from the MnO-TiO_2-P_2O_5 discrimination diagram after Mullen [29], where all samples split into two groups: those chemically close to oceanic island tholeiitic or alkaline basalts and those with island-arc tholeiitic or calc-alkaline basalts affinities (Fig. 6).

REE patterns for the samples of Type 1 show an obvious LREE enrichment (Fig. 7) with La_N = 30-54, $(La/Yb)_N$ = 3.3-5.4. Most samples have no Eu anomalies. Type 2 samples are LREE-depleted with La_N = 2-4.8, $(La/Yb)_N$ = 0.1-0.6. Sample 96-39-2 has intermediate LREE and HREE with La_N = 9, $(La/Yb)_N$ = 1.1 and a short Eu maximum. The sample takes a transitional position between Type 1 and Type 2. Sample 96-40 has a flat REE pattern with La_N = 17.4, $(La/Yb)_N$ = 2.18 and a short Eu maximum (Fig. 7).

In the chondrite-normalized spidergrams the basalts of Type 1 (OIB) display mild Nb-Ta enrichments relative to La (i.e. $Nb/La_N > 1$) unlike Type 2 having clear depletions in Nb-Ta (i.e. $Nb/La_N < 1$) (Fig. 8). Thus, the OIB group resembles

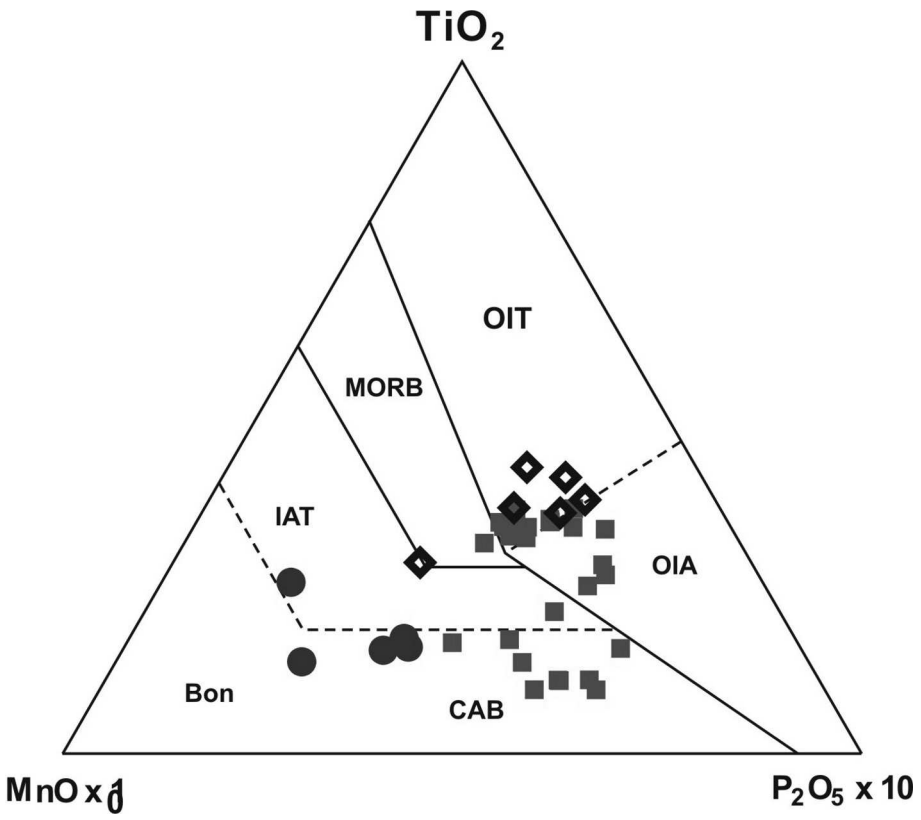

Fig. 6. **The MnO-TiO_2-P_2O_5 discrimination diagram after Mullen [29].**

The fields are MORB, OIT - oceanic-island tholeiite or seamount tholeiite; OIA – oceanic-island alkali basalt or seamount alkali basalt; CAB island-arc calc-alkaline basalt; IAT – island-arc tholeiite, Bon – boninite. Symbols as in Fig. 3.

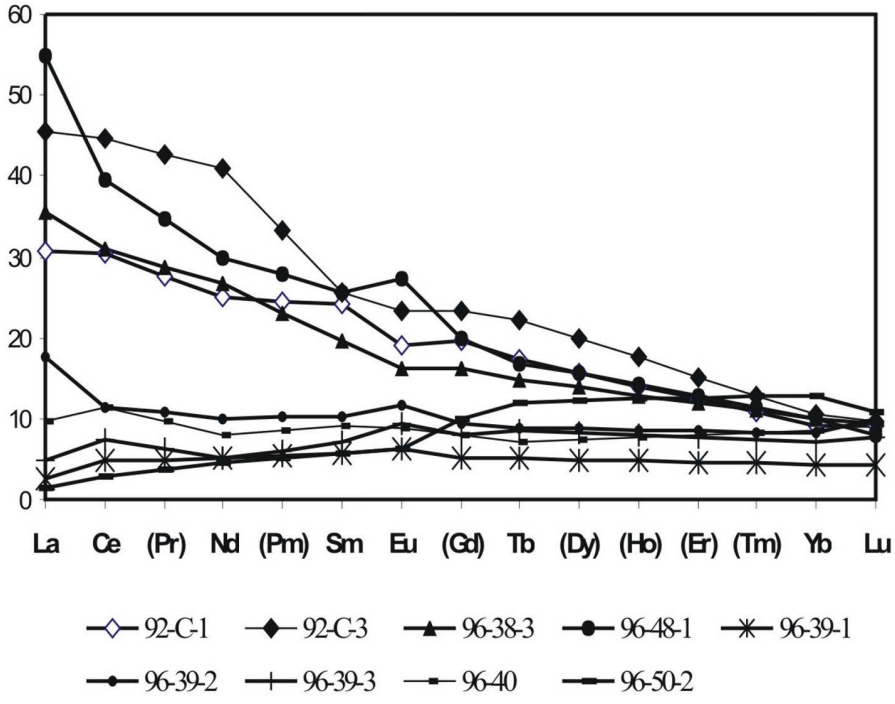

Fig. 7. Chondrite-normalized rare-earth –element (REE) plots.

The normalizing values are from McDonough and Sun [26].

many oceanic alkali basalts formed without crustal contamination. For the MORB samples, despite Nb-Ta depletions, we also cannot suggest crustal contamination because of their depletions in Th and Hf (Table 2, Fig. 8). Nb and Ta negative anomalies in Type 2 suggest that these magmas were generated by fractional crystallization of basaltic magma and/or involving crystallization of Nb, Ta-rich minerals, such as Ti-Te oxides. The samples of Type 2 display strong Sr enrichments indicating a possible spilitization of basalts during their eruption in sea-floor environment.

In the Nb/Zr versus Zr/Y diagram the compositional points of Katun metabasalts also split into two groups. The Ti-high samples plot in the field of Hawaii oceanic island basalts, whereas the Ti-medium samples plot in the field of MORB (Fig. 9).

The obtained data indicate that Katun metabasalts represent MORB to OIB transitional basaltic series, which possibly formed within an environment of oceanic islands related to hot spots at various degrees of melting.

DISCUSSION

Hot spot volcanism has been under investigation and regarded from the point of view of the Paleo-Asian Ocean evolution. The entities of the study were possibly hot spot induced oceanic basalts presently incorporated in a Caledonian accretion-collision zone of Vendian-Early Cambrian (Katun zone).

The Katun accretion-collision zone of Gorny Altai comprises the rock units, which formed over the oceanic crust of the Paleo-Asian Ocean and were incorporated in the accretionary wedge during its subduction under the Siberian continent and its collision with the Altai-Mongolian terrane. The accretionary wedge is characterized by a sheeted structure and consists of ophiolites from the basement of an island-arc and the rocks of a deformed oceanic crust (the Paleo-Asian oceanic plate). MORB and oceanic islands submerged into the subduction zone together with the plate and, later, they were incorporated into an accretionary wedge. During the subduction the oceanic islands collided with an island arc. The fragments of paleoseamounts in the accretionary wedge are as a rule cemented by olistostromes consisting of broken seamount and island arc units [18].

In general, the lithology and composition of Katun paleooceanic island sedimentary rocks records the evolution of their accumulation in an opened oceanic realm. The oceanic sedimentary rocks are shallow-water reef-type units with a basaltic basement, slope-facies carbonate and siliceous rocks/ deep-water siliceous sediments and foot breccia of oceanic islands [18].

Our performed geochemical studies of basaltic rocks – both with OIB and MORB affinities – show that upper and lower mantle derived basalts incorporated in accretionary terranes may illustrate the history of hot-spot volcanism and its relation to the evolution of the Paleo-Asian Ocean. Most of the studied samples are tholeiites, subalkaline basalts and alkaline basalts.

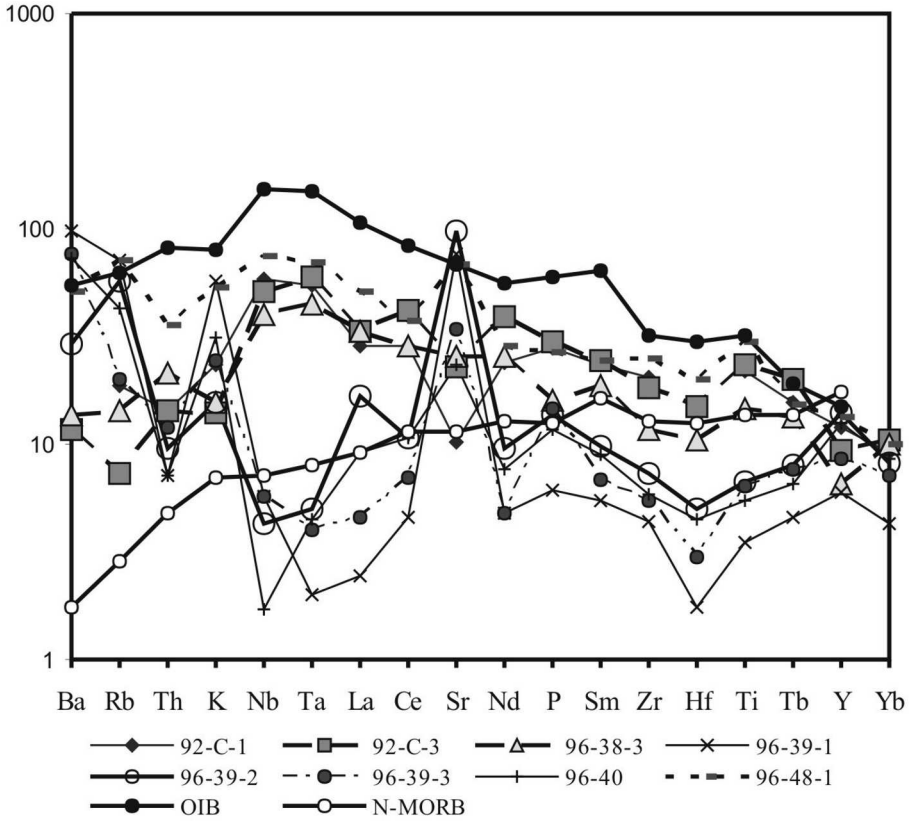

Fig. 8. **Chondrite-normalized multi-element diagrams.**

The normalizing values are from Sun and McDonough [36].

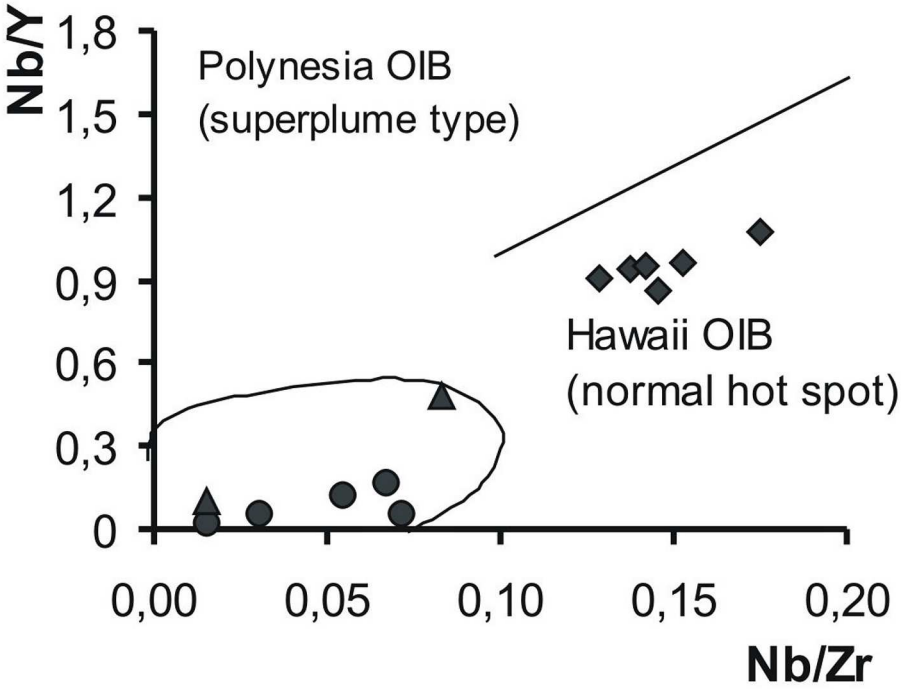

Fig. 9. Nb/Zr versus Nb/Y plot.

Discriminant fields after Tatsumi et al. [37]. Symbols as in Fig. 3.

The interpretations are mainly based on REE and trace elements. Variable element mobility is a possibility for Vendian-Early Cambrian volcanic rocks that have undergone sea-floor hydrothermal alteration and greenschist to mid-amphibolite facies, and multi-stage deformation, but there is a general agreement that REE, HFSE and some transitional metals are least sensitive to mobility ([32, 39] and the references cited therein). The samples with high values of LOI or large Eu anomalies were not used for petrogenetic interpretation. Primary clinopyroxene is present in the Katun basalts.

In the studied group of least altered basaltic rocks, evidence for low mobility of Th, HFSE and REE comes from the following: 1) there is no significant enrichment of depletion of groups of elements (e.g. LILE) in a given rocks type over a range of metamorphic grade from greenschist to epidote-amphibolite facies; 2) REE and chondrite-normalized multi-elements diagrams of given basaltic suites exhibit coherent patterns for HFSE and REE (Figs. 7 and 8) relationships between Th, Nb and La contents do not correlate with loss on ignition (LOI). The abundances of rare-earth elements (REE) have been used extensively to evaluate the petrogenesis of basalts. There are three types of REE patterns (Fig. 5): LREE-enriched, LREE-depleted and MORB-like. The distribution of REE depended either on the degree of differentiation and degree of partial malting in the mantle reservoir. Light-REE abundances vary and are considerably enriched (35-55) relative to chondrites, whereas heavy-REE abundances have much smaller ranges from 6 to 13 times that of chondrites (Fig. 5).

Chondrite-normalized REE abundances show three groups of greenstones: MORB-like, OIB and transitional (Fig. 8). Those with OIB affinities are qualitatively similar to those in other suites of alkaline and tholeiitic oceanic island basalts [13, 19, 20, 25, 38]. In the multi-element diagrams the samples display Sr enrichment relative K that can be explained by the action of sea-water during the basaltic eruption in sea-floor environments (Fig. 8). MORB-like samples display moderate Nb-Ta depletion suggesting a similar way of fractional differentiation and a clear enrichment in LILE (Fig. 8). The “humped” multi-element patterns are probably due to LILE added during secondary alteration.

Contamination by continental crust is quite probable, however many geological features are consistent with an intra-oceanic setting of the Katun basaltic sequences. The present of massive island-top-like limestones and thin cherts layers within tholeiitic pillowed basalts and flows suggest a marine environment for the eruption of the volcanic rocks [10, 18]. Another support for the absence of crustal contamination comes from the lack of zircon xenocrysts. The granitic intrusions in the region under study are younger then the accretionary belt [4].

Negative Nb anomalies in Ti-medium greenstones could possibly reflect some crustal contamination (Fig. 8), however there are negative Th anomalies (Th/La_{pm} =0.5-0.7) and no other data can support contamination. In general, low Th abundances (0.3 to 0.9 ppm) also support the idea about the lack of crustal

contamination. These special geochemical features are unlikely to have resulted from sialic crustal contamination, but rather from mafic lower crust or lithospheric mantle (Li et al., 2002).

As for the melting processes, the Katun Ti-medium basalts have depletions of Nb relative to LREE generating high La/Nb ratios. Bach et al. [1] regarded the Nb depletions a result of the second stage of the melting of a mantle source that had previously experience melt extractions under extremely low degrees of partial melting. Thorium depletion occurs in the Ti-medium varieties along with the Nb depletions that is consistent with low degree partial melting. Therefore, based on the negative range of Nb and Th anomalies displayed by the Ti-medium samples we suggest a partial melting episode in a mantle source. We can no suggest garnet facies depth melting because no suites have fractionated HREE, which is a possible garnet signature [22].

There is a significant variation of Mg# in Ti-medium basalts therefore we may conclude about a fractional crystallization control over Nb anomalies. Moreover, Nb is compatible in Fe-Ti-oxide minerals, which are likely fractionating phases in mafic liquids. Ti-high display no notable Mg# variations.

The Katun oceanic metabasalts from Gorny Altai may be clearly divided into two groups which could have been melted at different degrees of partial melting and at different depths. On the other hand they could have melted from one mantle source, but then differently influenced and/or contaminated by the upper mantle matter, for example, a weakly depleted oceanic mantle could interact with upwelling plume melts.

CONCLUSIONS

The Katun accretionary wedge in Gorny Altai demonstrates that fragments of oceanic crust comprise not only ophiolitic rock units, but also paleo-oceanic island units, which are important features in the structure of foldbelts.

The presented combined study of the fragments of oceanic crust involved in an accretionary terrane allowed a conclusion that hot-spot volcanism was active at the early stages of the Paleo-Asian oceanic evolution. The fragments of weakly to strongly differentiated varieties of oceanic and island-arc basalts have been preserved in accretion-collision zones providing information about chemical composition and petrology of volcanic rocks composing the greatest volume of the oceanic crust.

The geochemical data indicate that the Altai metabasalts could have been formed within mid-oceanic ridges, island arcs and oceanic islands of the Paleo-Asian Ocean in Vendian time.

The interpretation of structural, lithological, geochemical and biostratirgaphic data shows that the Vendian-Cambrian oceanic lithosphere of the Paleo-Asian Ocean was structurally and compositionally similar to the present Pacific. Further detail geochemical investigation would allow more complete reconstruction of the

ancient oceans and better understanding of petrologic processes, which resulted in the formation of the paleo-oceanic crust.

ACKNOWLEDGEMENTS

The auhtors thank Prof. N.L. Dobretsov, Drs. O.M. Turkina and A.E. Izokh, all from UIGGM SB RAS, Prof. Y. Fujiwara, S. Okada, S. Maruyama and Dr. T. Ota for fruitful discussions and joint field missions, and Dr. V.A. Bobrov for REE and trace element determinations.

The research was sponsored in parts by funds from RFBR grants no. 02-05-64627 and 03-05-64668. Prof. Shigenori Maruyama partly sponsored the 1996-2000 field expenses in Gorny Altai.

REFERENCES

1. **Bach W., Erzinger J., Dosso L., Bollinger C., Baugnault H., Etaubleau J., Sauerwein, J.** (1996) Unusually large Nb-Ta depletion in North Chile ridge basalts at 36°-50° to 38°-56° S: major element, trace element and isotopic data. Earth Planet. Sci. Lett, v. 142, pp. 223-240.
2. **Ben-Avrahem, Z., Nur, A., Jones, D. and Cox, A.** (1981) Continental accretion: from oceanic plateau to allochthonous terranes. Science, v. 213, pp. 47-54.
3. **Berzin, N.A. and Dobretsov, N.L.** (1994) Geodynamic evolution of Southern Siberia in Late Precambrian – Early Paleozoic time, In: Coleman, R.G. (Ed.) Reconstruction of the Paleo-Asian ocean. Utrecht, The Netherlands, pp. 53-70.
4. **Buslov, M.M., Berzin, N.A., Dobretsov, N.L. and Simonov, V.A.** (1993) Geology and Tectonics of Gorny Altai. Novosibirsk, UIGGM Publ., Novosibirsk, 122 p.
5. **Buslov, M.M., Fujiwara, Y., Saphonova, I.Yu, Okada, Sh. and Semakov, N.N.** (2000) The junction zone of the Gorny Altai and Rudny Altai terranes: structure and evolution. Russian Geol. Geophys., v. 41, pp. 377-390.
6. **Buslov, M.M., Saphonova, I.Yu. and Bobrov, V.A.** (1998) New geochemical data on boninites from Kurai ophiolites, Gorny Altai. Dokl. RAN, v. 361, pp. 244-247.
7. **Buslov, M.M., Saphonova, I.Yu and Bobrov, V.A.** (1999) An exotic terrane of the Late Cambrian-Early Ordovician oceanic crust in the northwestern Gorny Altai (Zasurin Formation): structural position and geochemistry. Dokl. RAN, v. 368, pp. 650-654.
8. **Buslov, M.M., Saphonova, I.Yu., Watanabe, T., Obut, O.T., Fujiwara, Y., Iwata, K., Semakov, N. N., Sugai, Y., Smirnova, L.V., Kazansky, A.Yu. and Itaya, T.** (2001) Evolution of the Paleo-Asian Ocean (Altai-Sayan Region, Central Asia) and collision of possible Gondwana-derived terranes with the southern marginal part of the Siberian continent. J. Geosci., v. 5, N 3, pp. 203-224.
9. **Buslov, M. M. and Watanabe, T.** (1996) Intrasubduction collision and its role in the evolution of an accretionary wedge: the Kurai zone of Gorny Altai, Central Asia. Russian Geol. Geophys., v. 36, pp. 83-94.
10. **Buslov M. M., Watanabe T., Saphonova I. Yu., Iwata K., Travin A., Akiyama M.** (2002) A Vendian-Cambrian island arc system of the Siberian continent in Gorny Altai (Russia, Central Asia), Gondwana Res., v. 5, no. 4, pp. 781-800.
11. **Buslov, M.M, Watanabe, T., Smirnova, L.V., Fujiwara, Y., Iwata, K., De Grave, J., Semakov, N.N., Travin, A.V., Kirjanova, A.P. and Kokh D.A.** (2003) Role of strike-slip faults in Late Paleozoic-Early Mesozoic tectonics and geodynamics of the Altai-Sayan and East Kazakhstan folded zones. Russian Geol. Geophys., v. 44, pp. 49-75.

12. **Chekhovich, V.D.** (1997) On the accretion of oceanic rises. Geotektonika, v. 4, pp. 69-79 (in Russian).
13. **Clague, D.A. and Frey, F.A.** (1982) Petrology and trace element geochemistry of the Honolulu volcanic, Oahu; implication for the oceanic mantle below Hawaii. J. Petrol., v. 23, pp. 447-504.
14. **Coleman, R.G.** (1977) Ophiolites. Springer- Verlag, Berlin.
15. **Didenko, A.N., Mossakovskii, A.A., Pecherskii, D.M., Ruzhentsev, S.V., Samygin, S.G. and Kheraskova , T.N.** (1994) Geodynamics of the Central-Asian Paleozoic oceans. Russian Geology and Geophysics, v. 35, no. 7-8, pp. 48-61.
16. **Dobretsov, N.L. and Zonenshain, L.P.** (Eds.) (1985) Riphean-Paleozoic ophiolites of North Eurasia. Nauka, Novosibirsk (in Russian).
17. **Dobretsov, N.L., Berzin, N.A. and Buslov, M.M.** (1995) Opening and tectonic evolution of the Paleo-Asian Ocean. Int. Geol. Rev., v. 35, pp. 335-360.
18. **Dobretsov, N.L., Buslov, M.M. and Uchio,Yu.** (2003) Fragments of oceanic islands in accretion-collision areas of Gorny Altai and Salair, southern Siberia, Russia: early stages of continental crust growth of the Siberian continent in Vendian-Early Cambrian time. J. Asian Earth Sci. (accepted for publication).
19. **Frolova, T.I. and Burikova, I.A.** (1997) Magmatic formations in modern geotectonic environments. Moscow Univ. Press, 319 p.
20. **Garcia, M.O., Frey, F.A. and Grooms, D.G.** (1986) Petrology of volcanic rocks from Kaula Island, Hawaii: implications for the origin of Hawaiian protoliths. Contrib. Miner. Petrol., v. 94, pp. 461-471.
21. **Gibsher, A.S., Esin, S.V., Izokh, A.E., Kireev, A.D. and Petrova, T.V.** (1996) Cambrian diopside-bearing basalts from the Cheposh zone in Gorny Altai. Russian Geol. Geophys., v. 38, pp. 1760-1773.
22. **Hirschman, M.M. and Stolper, E.M.** (1996) A possible role for garnet pyroxenite in the origin of the "garnet signatire" in MORB. Contrib. Miner. Petrol., v. 124, pp. 185-208.
23. **Hofmann, A.W.** (1997) Mantle geochemistry: the message from oceanic volcanism. Nature, v. 385, pp. 219-229.
24. **Humphris, S.E. and Thompson, G.** (1978) Hydrothermal alteration of oceanic basalts by seawater. Geochim. Cosmochim. Acta, v. 42, pp. 107-125.
25. **Li, X., Li, Zh.-X., Zhou, H., Liu, Y. and Kinny, P.D.** (2002) U-Pb zircon geochronology, geochemistry and Nd isotopic study of Neoproterozoic bimodal volcanic rocks in the Kandigan Rift of South China: implications for the initial rifting of Rodinia. Precambrian Research, v. 113, pp. 135-154.
26. **McDonough, W.F. and Sun, S.** (1995) The Composition of the Earth. Chem. Geol., v. 120, pp. 223-253.
27. **McKerrow, W.S., Scotese, C.R. and Brosier, M.D.** (1992) Early Cambrian reconstruction. J. Geol. Soc. Lond., v. 149, pt. 4, pp. 589-606.
28. **Meschede, M. (1986)** A method of discriminating between different types of Mid-Oceanic Ridge Basalts and continental tholeiites with the Nb-Zr-Y diagram. Chem. Geol., v. 56, pp. 207-218.
29. **Mullen, E. D.** (1983) $MnO/TiO_2/P_2O_5$: a minor element discriminant for basaltic rocks of oceanic environments and its implications for petrogenesis. Earth Planet. Sci. Let., v. 62, pp. 53-62.
30. **Miyashiro, A.** (1973) The Troodos ophiolitic complex was probably formed in an island arc. Earth Planet. Sci. Let., v. 19, pp. 218-224.
31. **Reiners P.W.** (1998) Reactive melt transport in the mantle and geochemical signatures of mantle-derived magmas. J. Petrol., v. 39, pp. 1039-1061.

32. **Rollinson, H.R.** (1993) Using Geochemical Data: Evaluation, Presentation, Interpretation. Longman Group UK Ltd., 352 p.
33. **Safonova I.Yu., Buslov M.M., Iwata K., Kokh D.A.** (2004) Fragments of Vendian-Early Carboniferous oceanic crust of the Paleo-Asian Ocean in foldbelts of the Altai-Sayan region of Central Asia: geochemistry, biostratigraphy and structural setting. Gondwana Research, v. 7, no. 3, pp. 771-790.
34. **Sengör, A.M.C., Natal'in, B.A. and Burtman, V.S.** (1993) Evolution of the Altaid tectonic collage and Paleozoic crustal growth in Eurasia. Nature. 364, 299-307.
35. **Simonov, V.A., Dobretsov, N.L. and Buslov, M.M.** (1994) Boninite series in structures of the Paleo-Asian Ocean. Russian Geology and Geophysics, v. 35, pp. 182-199.
36. **Sun, S. and McDonough, W.F.** (1989) Chemical and isotopic systematics of oceanic basalts: Implications for mantle composition and processes. In: Saunders, A.D. and Norry, M.J. (Eds.) Magmatism in the Ocean Basins. Geol. Soc. London. Spec. Publ., v. 42, pp. 313-345.
37. **Tatsumi, Y., Shinjoe, H., Ishizuka, H., Sager, W.W. and Klaus, A.** (1998) Geochemical evidence for a mid-Cretaceous superplume. Geology, v. 26, pp. 151-154.
38. **Ueda, H., Kawamura, M. and Niida, K.** (2000) Accretion and tectonic erosion processes revealed by the mode of occurrence and geochemistry of greenstones in the Cretaceous accretionary complexes of the Idonappu zone, southern central Hokkaido, Japan. The Island Arc, v. 9, pp. 237-257.
39. **Winchester, J.A. and Floyd, P.A.** (1977) Geochemical discrimination of different magma series and their differentiation products using immobile elements. Chem. Geol., v. 20, pp. 325-343.
40. **Wood, D.A., Joron, J.L. and Treuil, M.** (1979) A re-appraisal of the use of trace elements to classify and discriminate between magma series erupted in different tectonic settings. Earth Planet. Sci. Let., v. 45, pp. 326-336.
41. **Zonenshain, L.P., Kuzmin, M.I. and Natapov, L.M.** (1990) Geology of the USSR: A Plate tectonic synthesis. Geodynamic Monograph, American Geophysical Union, Washington, 242 p.

UDK 550.4

Peculiarities of compositional variations in xenoliths of mantle spinel peridotite: possible mechanisms of their formation in fold and stable areas

Prikhodko V.S.[1], Petukhova L.L.[1], and Chubarov V.M.[2]

[1] *Institute of Tectonics and Geophysics, FEB RAS, Khabarovsk, vladimir@itig.as.khb.ru*
[2] *Institute of Volcanology, FEB RAS, Petropavlovsk-Kamchatsky*

Compositional variations of rocks and minerals in spinel peridotite xenoliths from the Alchanskiy and Sviyaginsky alkali-basalt volcanoes have been considered. Xenoliths from the former one characterize the upper mantle material in the Sikhote-Alin nappe-fold system, while the xenoliths in the Sviyaginskiy location – the upper mantle of the Khanka craton terrain. Petrochemical diagrams show similar compositional variations in spinel peridotite xenoliths from those volcanoes thus testifying to similar mechanisms of their formation; peculiarities of the structure testify to the fact that partial melting of the upper mantle material was such a mechanism. In general, the peculiarities revealed in the chemical compositional variations in the minerals of spinel peridotite xenoliths from the Alchanskiy volcano dependent on MgO content in rock correspond to the theoretical calculations and results of experimental investigations of the upper mantle partial melting processes.

INTRODUCTION

The existing assessments of the Earth's upper mantle composition show that it is mainly composed of ultramafic rocks, the fragments of which are being carried to the surface by alkali-basaltoid or kimberlite melts. Studying fragments of these rocks is a direct method of studying the composition and structure of deep-seated material, also allowing to estimate the scale of magmatic and metamorphic processes in the mantle, which are responsible for their formation. Such questions have been weakly described in the literature mainly due to fragmentary data on the composition of xenoliths and component minerals. It does not allow to adequately characterize local and lateral peculiarities of rock composition and to discuss possible mechanisms of the upper mantle material transformation under various tectonic structures. This paper discusses the nature of rock and mineral compositional variations of spinel peridotite xenoliths within individual alkali-basaltoid volcanoes characterizing the mantle material under stable (Sviyaginskiy volcano) and fold (Alchanskiy volcano) areas in the south of the Far East.

GEOLOGIC SETTING

The territory under discussion covers the Khanka median massif, Sikhote-Alin nappe-fold system and East Sikhote-Alin volcanic belt. These are main tectonic structures in the continental part of the Russian Far East south. The

manifestations of the Cenozoic alkali-basaltoid volcanism, in the products of which there are xenoliths of spinel peridotite, occur throughout the region. Representative collections of deep rock samples from alkali-basaltoid volcanoes situated within the above-mentioned tectonic structures of the region were studied [5]. The Khanka median massif lithosphere is characterized by xenoliths from the Sviyaginskiy and Medvezhiy volcanoes, East Sikhote-Alin volcanic belt – the rock samples from the Sanku creek (the Koppi river left tributary). All other samples (from the Alchanskiy, Anyuiskiy, Barkhatniy, Bolonskiy and Innokentiyevskiy volcanoes) represent the upper mantle of various sectors of the Sikhote-Alin system. The descriptions of volcanoes, compositions of effusives, distribution and conditions of xenolith occurrences have been given in many papers [1, 2, 4, 5, 6].

A comparative analysis of spinel peridotite xenolith's material composition aimed at estimating the degree of heterogeneity of deep-seated material within the continental block of the Far East was carried out based on the database about the rock compositional variations within the above-mentioned individual volcanoes. The peridotite xenoliths under discussion are characterized by distinct negative correlations between MgO content in rock and the contents of SiO_2, Al_2O_3, CaO, and Na_2O. Based on the concept of distribution of main petrogenic oxides (Al_2O_3, CaO, MgO) local and lateral variations of the mantle material composition at the level of spinel peridotite facies were studied in the paper [5]. On the basis of the average concentration and Al_2O_3 distribution, two groups of deep rocks were recognized. The first one (the maximum in the collection is at the interval of 2-3 weight %, there are samples with Al_2O_3 content lower than 1 weight %) combines deep-seated xenoliths from the Sviyaginskiy, Medvezhiy and Bolonskiy volcanoes. The second group is characterized by the maximum values of Al_2O_3 at the interval of 3-4 % and absence of low contents of this oxide. It includes rocks from the Alchanskiy, Anyuiskiy, Barkhatniy, Innokentievskiy volcanoes and "Sanku" location. These groups are equally clearly observed on the diagram for CaO and MgO distribution in rocks. Thus, petrochemically depleted peridotite was found in the mantle blocks under the Khanka median massif (Medvezhiy and Sviyaginskiy volcanoes) and the Sikhote-Alin nappe-fold region (Bolonskiy volcano). These rocks refer to the "continent marginal-oceanic", ultimately depleted type of the Earth's mantle ultramafic substrate [3]. Another group of xenoliths, characterizing the upper mantle of the Sikhote-Alin system and East Sikhote-Alin volcanic belt, can correspond to weakly depleted "mid-oceanic" ultramafic substrate [3].

SAMPLES AND METHODS OF INVESTIGATION

Representative sample collections of spinel peridotite xenoliths from the Alchanskiy and Sviyaginskiy volcanoes were studied. The first one is situated in the Bikin river basin, near its right tributary of the Alchan river. The volcano pinnacle is a small hill made up by flows of massive basalt. The effusives are substantially saturated with small (to 10 cm) angular fragments of spinel lherzolite. The Sviyaginskiy volcano pinnacle (near Sviyagino railway station) is cut by the

Khabarovsk-Vladivostok highway. A lot of small rounded xenoliths of spinel peridotite occur in massive basalt.

From each volcano, at random, there was collected a representative collection of samples of spinel peridotite xenoliths, allowing to characterize petrochemical peculiarities of this group of deep rocks. The main requirements are as follows: no products of secondary alteration, and the size of xenoliths must not be less than 7 cm. These samples after the corresponding processing (taking away basalt coating and other foreign materials) were cut into two parts, one of which was crashed and powdered for the subsequent silicate analysis. The silicate analysis of the samples was done at the Institute of Tectonics and Geophysics FEB RAS by analysts V.Ye. Zazulina, L.S. Bokovenko, and N.I. Il'ina. From the second part of the sample, under a microscope there were selected relatively clean grains of olivine, chrome spinel, ortho- and clinopyroxene, the composition of which was further studied at "Camebax" microanalyzer at the Institute of Volcanology FEB RAS by analyst V.M. Chubarov. Five grains of each mineral from one sample of xenoliths were analyzed; each grain was characterized by three analyses (center, rim). The samples studied rather uniformly characterize the total sample deep rock collection as regards MgO content and other mineralogical parameters.

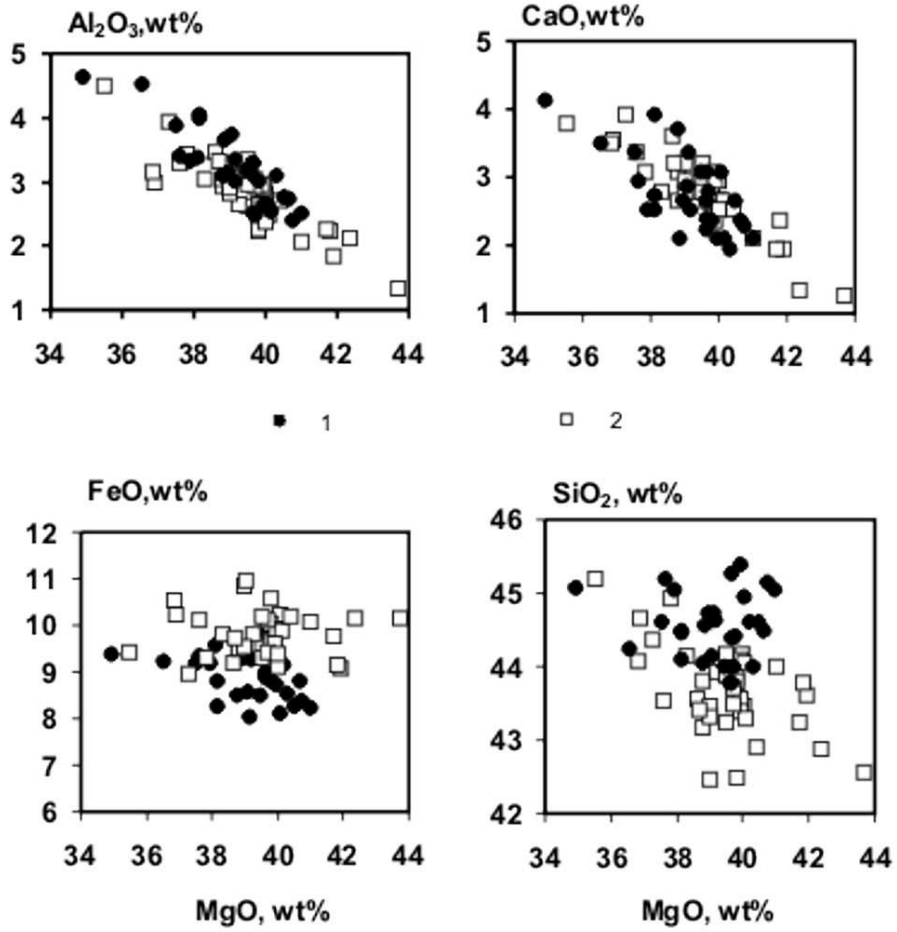

Fig. 1. **Variation diagram of rock-forming oxides in spinel peridotite xenoliths from Sviyagin and Alchan alkali-basaltoid volcanoes:** 1 – Alchan, 2 – Sviyagin.

RESULTS

Chemical compositions of spinel peridotite xenoliths from the Alchanskiy and Sviyaginskiy volcanoes (Fig. 1) show that these sample collections are rather uniform, the Alchanskiy one being more compact. Here are the average compositions of xenoliths from the Alchanskiy (29 samples) SiO_2-44.55; TiO_2-0.11; Al_2O_3-3.22; FeO_{total} -8.81; MgO-39.09; CaO-2.77; Na_2O-0.22; Cr_2O_3-0.42) and Sviyaginskiy volcanoes (32 samples): SiO_2-43.67; TiO_2-0.32; Al_2O_3-2.81; FeO-9.54; MgO-39.51; CaO-2.80; Na_2O-0.20; Cr_2O_3-0.45. Certain variations in petrochemical characteristics of xenoliths from two volcanic centers are illustrated by variational diagrams in Fig. 1. These sample collections of peridotite xenoliths are characterized by distinct negative correlations between MgO content in rock and Al_2O_3 and CaO contents. The correlation between SiO_2 and FeO contents with MgO content is less stable, still a general tendency is preserved, i.e. with MgO enrichment in rock, SiO_2 and FeO contents are decreased.

Let us consider the changes in the compositions of the minerals of xenoliths in the Alchanskiy and Sviyaginskiy volcanoes depending on MgO content. As the main chemical parameters of the minerals (most changeable) we used Cr contents in ortho- and clinopyroxene, spinel, aluminum in pyroxene, sodium and a wollastonite molecule in clinopyroxene.

Fig. 2 a, b, c, presents a series of diagrams illustrating the correlation between Cr_2O_3 content (mass%) in minerals of xenoliths and MgO content (mass%) in rock: (a – in orthopyroxene, b – in clinopyroxene, c – in chrome spinel). First of all, different nature of correlation between the named parameters in the Alchanskiy and Sviyaginskiy volcanoes' spinel peridotite xenoliths should be noted. The Alchanskiy volcano xenoliths are characterized by a stable tendency of Cr content increase in orthopyroxene (most intensive), in clinopyroxene and spinel when MgO content grows in rock. The figurative points of Cr_2O_3 concentrations in clinopyroxene and spinel of the Sviyaginskiy volcano xenoliths (Fig. 2 b,c) form a subhorizontal plateau. The dependence of Al_2O_3 contents in ortho- and clinopyroxene on MgO content in spinel peridotite is shown in Fig. 3 a,b. A similar nature of this oxide's alteration in orthopyroxene of the Alchanskiy and Sviyaginskiy volcanoes' xenoliths has attracted our attention. In clinopyroxene there is observed a considerably more complicated change in Al_2O_3 contents: in the Alchanskiy volcano minerals there is a slight decrease when MgO content grows, but in the second volcano's xenolith clinopyroxene there is a slight increase. Fig. 4 demonstrates the character of sodium content alteration in clinopyroxene of spinel lherzolite: a stable decrease of sodium in clinopyroxene of xenoliths from the Alchanskiy location, and an increase in case of clinopyroxene of the Sviyaginskiy volcano spinel peridotite. The dependence between the content of wollastonite minal in clinopyroxene on MgO content in rock is illustrated in Fig. 5. The figurative points for the compositions of minerals of xenoliths from the two volcanoes can be described with parabolic curves; in both cases their minima correspond to 39% of MgO in rocks.

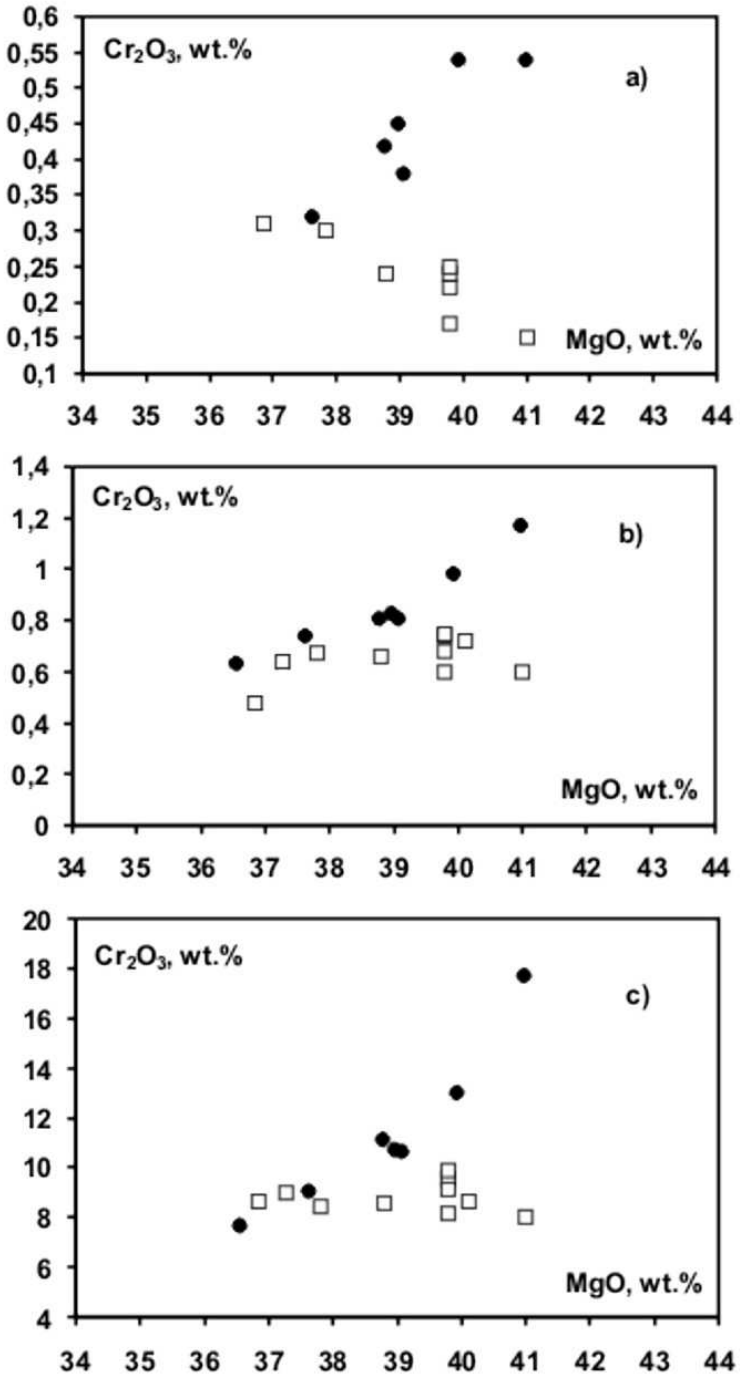

Fig. 2. **Correlation between Cr_2O_3 content (mass%) in minerals of xenoliths and MgO content (mass%) in rock:** (a – in orthopyroxene, b – in clinopyroxene, c – in chrome spinel).

DISCUSSION OF RESULTS

The petrochemical diagrams (Fig. 1) show similar compositional variations of spinel peridotite xenoliths from the Alchanskiy and Sviyaginskiy volcanoes testifying to similar mechanisms of their formation. The conception of the mantle ultramafic rock formation in the process of partial melting of deep material is most appreciated in modern geological literature. A linear dependence between the contents of petrogenic oxides in spinel peridotite (negative linear correlations

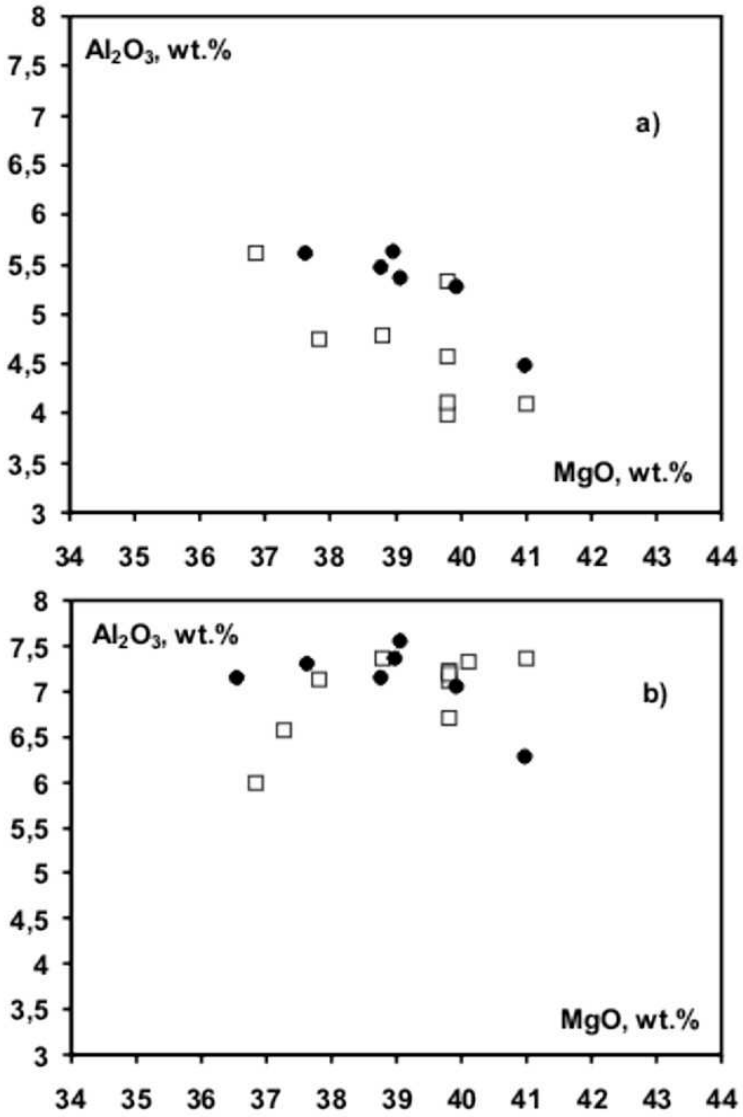

Fig. 3. **Correlation between Al_2O_3 content (mass%) in minerals of xenoliths and MgO content (mass%) in rock:** (a - in orthopyroxene, b – in clinopyroxene).

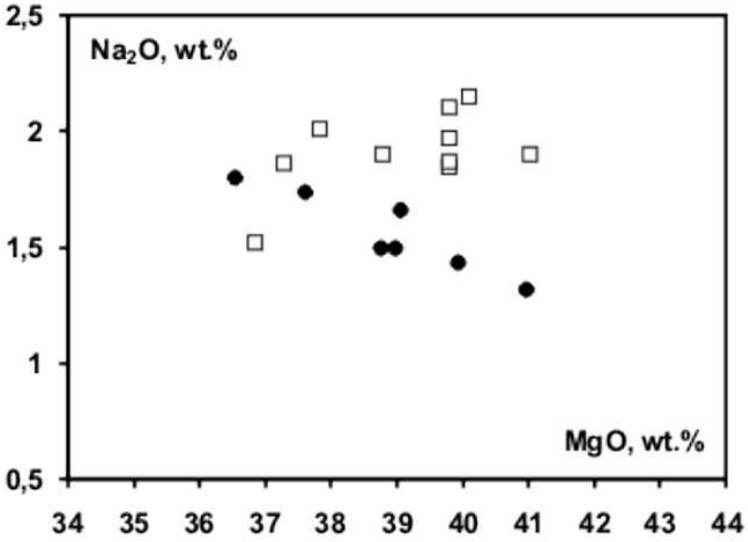

Fig. 4. **Correlation between Na_2O content (mass%) in clinopyroxene and MgO content (mass%) in xenoliths of spinel peridotite.**

between MgO content and the contents of FeO, Al_2O_3, CaO, SiO_2, etc.) is suggestive of their restite character within the model of partial melting. When the "initial" mantle material is separated from basaltic or picritoid liquids there appears variously depleted peridotite. The composition of complementary members (melts and restite) is controlled by the chemistry of mantle material, the degree of melting, and coefficient of the elements' distribution between a liquid and solid phases. It is suggested, that spinel peridotite with the minimum (36-38 weight%) MgO contents can be regarded as primitive, i.e. with the composition similar to the initial mantle material. More magnesian varieties of rocks, depleted in easily movable components (Al, Ca, Na) are infusible remains (restite) after taking away the melts. The higher the temperature and, therefore, the degree of the initial material melting, the more depleted is the composition of restite. The experiments with ultramafic systems have shown that rock-forming minerals transform into the melt as follows: Cpx – Opx – Ol, each one in a certain temperature interval [3].Clinopyroxene disappears when the degree of melting the initial rock reaches 25%. Peculiarities of the partial melting process of the natural ultramafic parageneses vividly illustrate a linear distribution of the figurative points for the compositions of spinel peridotite in coordinates CaO-A_2O_3 (ratio approaches 1). Judging by the value of this ratio, which is considerably lower than in clinopyroxene (2.8 and more), it can be suggested that the second aluminiferous phase, chrome spinel, participates in melting.The participation of this mineral in melting processes is confirmed by a positive correlation between Ca_2O_3 contents in spinel and MgO in rock. It is known, that when the melting degree increases, which is equal to the formation of more magnesian parageneses, in chrome spinel there grows the value of Cr/Al ratio [3]. For this isomorphic row of spinel it is analogous with the grows of Cr content in them.

Earlier we presented some petrochemical considerations as regards the processes of partial melting of ultramafic rocks at the conditions of the upper mantle and summarized the results of experimental investigations of melting processes of ultramafic rocks.

It should noted that the revealed peculiarities of compositional variations of spinel peridotite xenolith minerals in the Alchanskiy volcano (Fig. 2, 3, 4) depending on MgO content in rocks in general correspond to theoretical calculations and results of experimental investigations of partial melting processes. Most representative are the changes in Cr content in chrome spinel, ortho- and clinopyroxene – a stable increase of this component is connected with the growth of MgO content in rocks (Fig. 2). Likewise, the decrease of aluminum content in orthopyroxene and sodium content in clinopyroxene with the growth of MgO content in spinel peridotite has been distinctly demonstrated. More complicated are the variations in the aluminum content in clinopyroxene. Probably it is due to a dual position of aluminum in the structure of clinopyroxene: a jadeite and a chermakite molecules. Partial melting should result in the decrease of jadeite and increase (?) of chermakite minals. The position of the figurative points on the

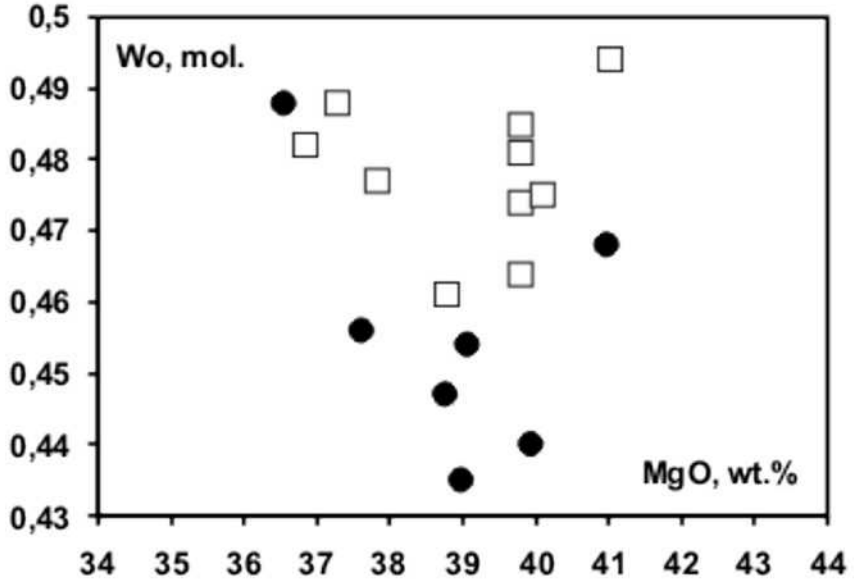

Fig. 5. **Correlation between content of wollastonite molecule in clinopyroxene and MgO content (mass%) in xenoliths of spinel peridotite.**

diagrams in the coordinates: MgO content in rock and wollastonite in clinopyroxene can be an indirect confirmation to the above information (Fig. 5).

The compositional variations of spinel peridotite minerals in the Sviyaginskiy volcano appears to be more complicated, though the petrochemical structure of this sample collection of xenoliths is rather simple and agrees with the regularities of the partial melting process of the upper mantle material. But the trends for the compositions of the minerals from this volcano's xenoliths mainly have the opposite tendencies relative to the trends for the compositions of the minerals in the Alchanskiy volcano (see Fig. 2, 3, 4), which requires some special consideration.

We explain this fact as follows. The spinel peridotite xenoliths in the Sviyaginskiy volcano characterize the modern upper mantle in the Khanka craton terrain. At the early stage of the Earth's evolution, the Khanka block was a component part of a larger craton, the upper mantle of which was relatively cold and was mainly composed of garnet peridotite. Further, as a result of structural reconstructions in the Pacific margin of Asia and activation of magmatic processes, there happened an increase of a geothermal gradient within the Khanka craton terrain. This resulted in the transformation of the mantle garnet peridotite into spinel peridotite. It is suggested that the petrochemical structure of spinel peridotite formed at the early stages as a result of partial melting of the initial mantle material represented by garnet peridotite. It is likely that in the instance with the Sviyaginskiy volcano xenoliths, the peculiarities of the compositions of the minerals and their trends are defined by the nature of the elements' distribution during solid phase reactions between minerals when garnet peridotite is transformed into spinel peridotite.

CONCLUSIONS

It has been established that the peculiarities revealed in the chemical compositional variations in the minerals of spinel peridotite xenoliths from the Achanskiy volcano depending on MgO content in rocks are stipulated by the partial melting processes. The petrochemical structure of rocks from this sample collection and the peculiarities in the compositions of spinel peridotite xenoliths' minerals formed during partial melting of the mantle material at the level of spinel peridotite facies.

It has been established that the petrochemical structure of the sample collection of xenoliths from the Sviyaginskiy volcano is relatively simple and agrees with the regularities of the partial melting of the upper mantle material. However, the trends for the compositions of the minerals in xenoliths from this volcano in general have the opposite tendencies relative to the trends for the compositions of the minerals in the Alchanskiy volcano xenoliths. It is suggested that the petrochemical structure of spinel peridotite formed as a result of garnet peridotite partial melting; the compositional peculiarities of the minerals and their trends are defined by the nature of the elements' distribution during solid phase reactions between the minerals during the transformation of garnet peridotite into spinel peridotite.

REFERENCES

1. **Govorov I.I., Ilunin I.P., and Harkin A.D.** (1980).Geochemistry of deep volcanic rocks and xenoliths. Moscow, Nauka.
2. **Esin S.V.** (1991).Ultramafic moduli from Cenozoic alkaline basaltoids of the Sovgavan plateau (East Sikhote Alin)// Hyperbasitic associations of fold areas. Irkutsk, Nauka,
3. **Magmatic rocks (ultramafic rocks)**. (1988). Edited by Ye.Ye. Laz'ko, Ye.V. Sharkov. Moscow, Nauka.
4. **Prikhodko V.S., Bekhtold A.F., Berdnikov N.V.** (1985). Deep petrology of active continental margins. Moscow, Nauka,
5. **Prikhodko V.S., Ponomarev G.P., and Karetnikov A.S.** (19930. Deep xenoliths and upper mantle in the Far East south. In: Structure and Geokinematics of Lithosphere of Russian East. Magadan.
6. **Scheka S.A.** (1983).Nasite-hyperbasitic intrusions and inclusions in effusives of the Far East. Moscow, Nauka.

UDK 550.4

Slab melt-mantle interaction, sub-arc metasomatism and possible implications for the origin of cratonic lithosphere

Kepezhinskas P.K.

National Resource Corporation, Moscow, Russia, e-mail: pavel_k7@yahoo.com

This paper discusses mineralogical and geochemical composition of island-arc ultramafic xenoliths from Kamchatka convergent margin with comparison to other arc peridotites (Kuriles, Japan, Cascades, Philippines, Papua New Guinea, Lesser Antilles) and cratonic peridotites. Trace element geochemistry of minerals, glasses and bulk peridotite xenoliths from volcanic arcs indicates their depleted nature resulted in refractory composition of olivine, clinopyroxene and spinel. Presence of hydrous phases (primarily amphibole) and silicic (dacitic) veins and glasses indicates pervasive metasomatism by hydrous fluids and, possibly, silicic melts above subduction zones. Chemical composition of silicic glasses – high Al and Na contents, high Sr concentrations, high Sr/Y, La/Yb and Zr/Sm ratios – suggests their similarity to Cenozoic slabd melts (adakites). However, elevated MgO contents suggest intense interactions with peridotitic mantle wedge above subduction zones which is also a feature of Precambrian TTG suites believed to be derived via slab melting and contamination by mantle peridotites. Similarities between mineralogical compositions of subduction-related and cratonic peridotites as well as presence of slab melt metasomatic signatures in both cases may suggest that processes somewhat similar to modern subduction regimes played an important role in generation of Archean cratonic lithosphere.

INTRODUCTION

Generation of siliceous Sr and LREE-enriched, water-saturated melts via partial melting of subducted slab under amphibolite to eclogite facies (adakites) is important in hot subduction zones (ridge subduction, subduction of young and hot oceanic crust, initiation of subduction, or oblique convergence) or in Archean convergent margins [2]. Slab-derived melts vigorously interact with the overlying sub-arc mantle wedge during their ascent and become progressively enriched in Mg, Cr and Ni resulting in generation of a high-Mg andesite or "transitional adakite" [2,3,4]. Melting of slab melt-metasomatized source yields Nb-enriched alkaline basaltic melts (NEABs) with otherwise arc-like geochemical characteristics. The adakite-mantle interaction was even more profound in Archean subduction zones due to the higher thermal gradient in the early Earth [13]. Large-scale derivation of tonalite-trondhjemite-granite (TTG) slab melts in Archean was synchronous with formation of diamondiferous cratonic roots via accretion of ultra-depleted (relative to MORB) island-arc mantle at the base of continental lithosphere [4]. The TTG melt-mantle interaction may also have been responsible

for generation of Archean high-Mg granodiorites and high-Nb lamprophyres and shoshonites.

SLAB MELTS IN SUB-ARC MANTLE WEDGE

Metasomatic veins of dacitic composition were documented in ultramafic mantle-derived xenoliths from Kamchatka [3,4]. These veins are depleted in Ti, Zr and Y and are enriched in Al, Sr and display Na/K ratios of 3-7 (Fig. 1).

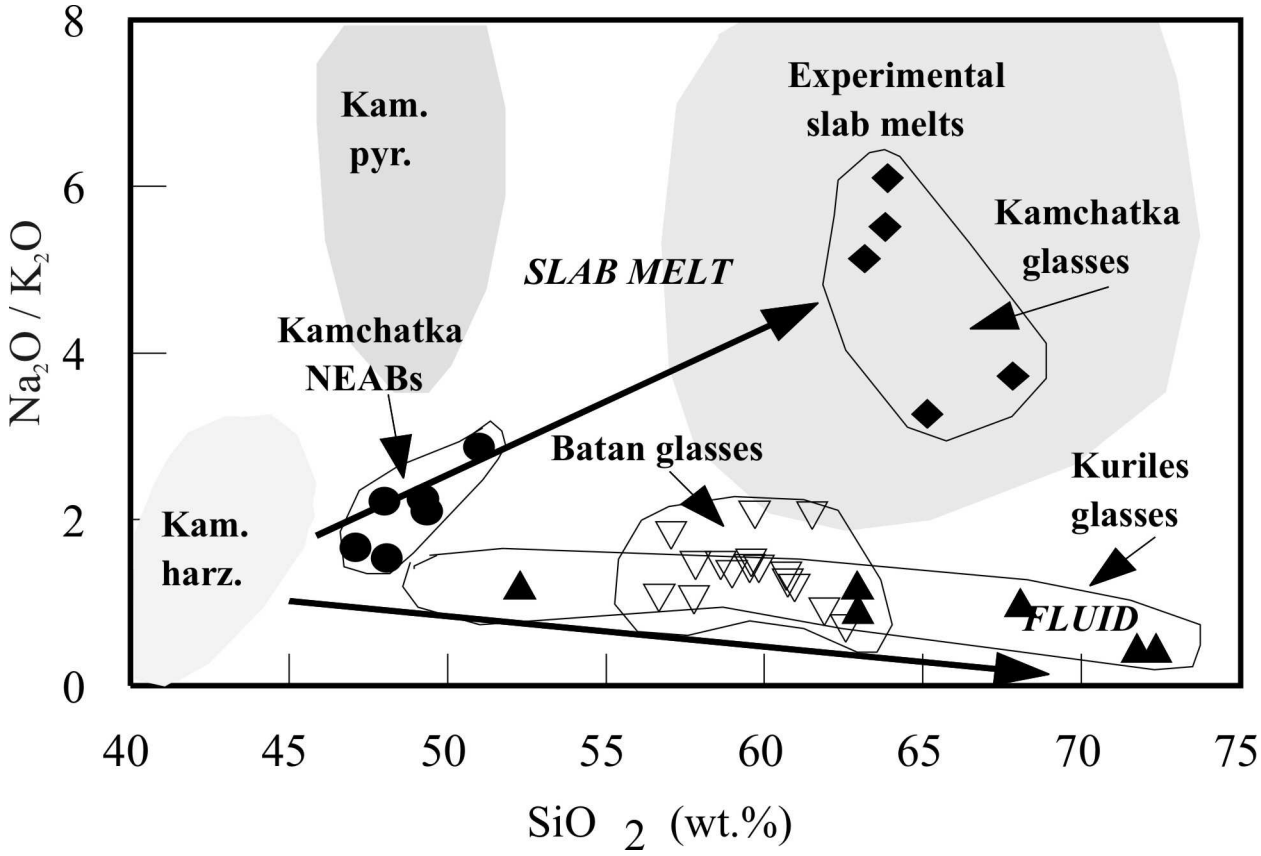

Fig. 1**. Chemical composition of glasses in sub-arc mantle xenoliths from Kamchatka [3], Batan [10] and Kuriles [12] compared with expermental slab melts [8], Kamchatka NEABs [3] and Kamchatka pyroxenite (Kam. pyr.) and harzburgite (Kam. harz.) xenoliths [4].**

Typical siliceous glasses from mantle xenoliths in alkaline intraplate basalts have Na/K ratios less than 2 and high Ti contents resembling TiO_2 concentrations in their host alkaline basalts. Glasses in Kamchatka mantle xenoliths are compositionally similar to the experimental melts derived via partial melting of metabasalt at 15-32 kbars (Figure 1). Ion-probe analyses of Kamchatka mantle glasses reveal high Sr (1040-1736 ppm), La (66-125 ppm) and low Y (6-17 ppm) contents coupled with high Sr/Y (60-285), La/Yb (20-30), Sr/Sm (46-209), Nb/La (0.198-0.280) and low Ti/Eu (71.4-128.3) and Y/Er (2.88-3.48) ratios. Typical arc andesites and dacites have Sr/Y ratios < 20-40 and La/Yb ratios < 20, while slab melts have Sr/Y ratios > 30 and La/Yb ratios > 20 [2]. Kamchatka siliceous glasses generally display high Cr contents (50-348 ppm) suggesting that some reaction

with peridotite took place prior to transport of the slab melt-metasomatized xenolith by an ascending basaltic magma. Siliceous glass inclusions from Batan Island (Philippines) mantle xenoliths have high Al_2O_3 contents (17.2-19.7 wt.%) along with high Sr (279-810 ppm), La (31.2-69.2 ppm) and low Y (2.2-12.1 ppm) concentrations and high Sr/Y (41-238) and La/Yb (24-100) ratios [10]. These glasses have variable Na/K ratios of 0.6-2.05 and plot slightly below the compositional field of experimental slab melts potentially reflecting various degrees of interaction with ultramafic material (Fig. 1). Siliceous glasses in ultramafic xenoliths from Kurile arc have high Al and low Ti contents and variable Na/K ratios of 0.45-1.2 [12]. Kurile glasses display a decreasing Na/K ratio at increasing SiO_2 content which is typical of calc-alkaline arc magmas (Fig. 1). We interpret these glasses as a result of partial melting of fluid-fluxed (abundant amphibole and phlogopite in glass-bearing xenoliths) sub-arc mantle.Slab melts are found in the mantle wedge overlying both hot (northern) and cold (southern) subduction zone environments within the Kamchatka convergent margin [4]. This suggests that slab melt may be a ubiquitous component of sub-arc mantle even if current subduction conditions do not favor slab melting. This may very well explain a frequent occurence of high-Mg andesites, transitional adakites and NEABs in the "not-so-hot" subduction zones (e.g., Aleutians, Andes, Philippines) which may be linked together via the process of interaction between adakite magmas and sub-arc mantle wedge [2, 14].

CHEMICAL SIGNATURES OF SLAB MELT-MANTLE WEDGE INTERACTION

Slab melts ascend into and react with the mantle wedge and become enriched in MgO, Cr and Ni while retaining their slab melt geochemical signature (e.g., high Sr/Y, La/Yb, Zr/Sm and low Y and Yb). During the course of this interaction, slab melt becomes progressively saturated in in mantle components and starts to precipitate Al-Na-rich augite, garnet, Na-plagioclase and Al-rich spinel as observed in the ultramafic xenoliths from Kamchatka [3]. High-Mg andesites (transitional adakites) in northern Kamchatka show high MgO and Cr contents and relatively low Sr/Y and La/Yb ratios which can be modelled by addition of peridotite to a pristine slab melt [3]. Kamchatkan transitional adakites contain olivine (Fo_{89-90}), clinopyroxene (Mg# =85-88) and Cr-spinel (Cr/(Cr+Al) > 70) xenocrysts indicating that they reacted with mantle peridotite on the way to the surface.

Slab melt-contaminated mantle xenoliths from the Kamchatka arc show enrichments in Sr, La and Ta which are correlated with modal contents of metasomatic disseminated phases (Al-Na-augite clinopyroxenes, amphiboles, and Al-rich spinels) which can be used as a rough estimate of the extent of slab melt-mantle wedge interaction (Fig. 2). This enrichment is coupled with Nb enrichments

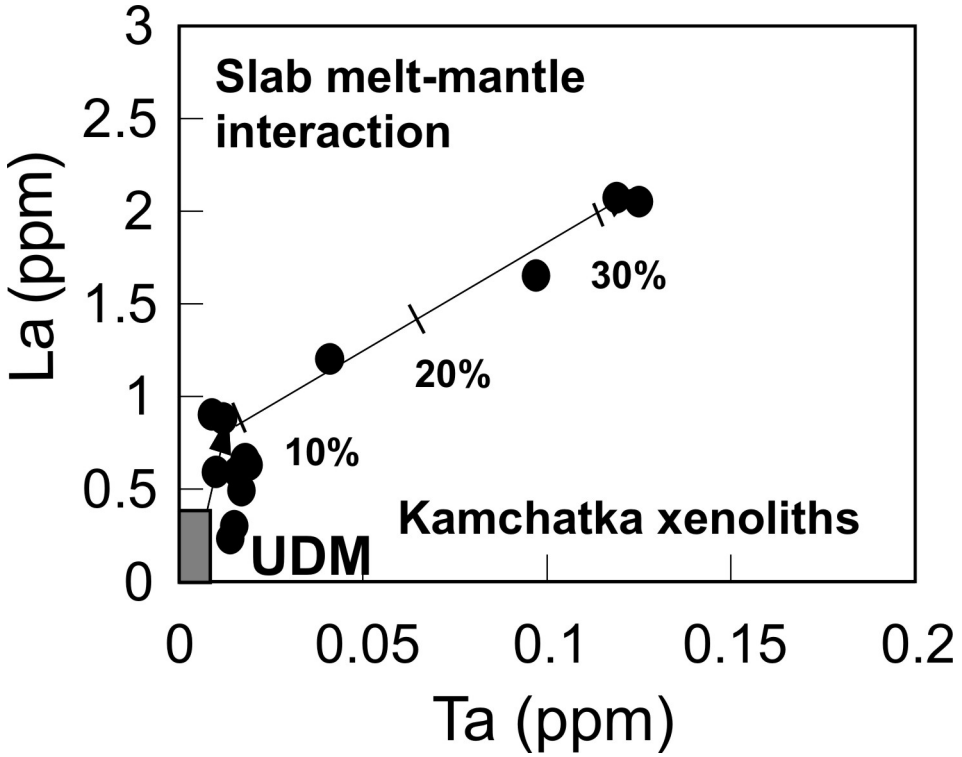

Fig. 2. **La vs. Ta variation in variably metasomatized ultramafic xenoliths from the Kamchatka arc.**

Percentages reflect extent of slab melt-induced metasomatism estimated from petrographic studies (modal content of metasomatic Al-Ti-Na-augites and Al-Fe-Mg-spinels) and ion-microprobe data on mantle clinopyroxenes [3]. UDM- ultra-depleted unmetasomatized mantle xenoliths from Kamchatka.

detected in siliceous glasses from Kamchatka ultramafic xenoliths. This suggests that extensive slab melt-mantle interaction can produce HFSE (Nb and Ta) enrichment in both metasomatizing slab melt and the sub-arc mantle wedge [11]. Slab melt-mantle interaction will also cause LILE (Sr) and LREE (La) and Na enrichment in the sub-arc mantle (Figures 1 and 2). Unmetasomatized to slightly metasomatized harzburgite xenoliths in Kamchatka have relatively low Na/K ratios while metasomatic wehrlites and pyroxenites exhibit elevated Na/K ratios of 3-11 due to the reaction with the Na-rich slab melt (Figure 1). Sub-arc wedge metasomatism by slab melt-mantle interaction produces a veined mantle source (matrix- harzburgites, veins- pyroxenites) enriched in HFSE (Nb and Ta), LILE (Sr) and LREE (La) capable of arc-related alkaline (high-Na) magma generation [3].

IMPLICATIONS FOR ARC MAGMATISM IN HOT SUBDUCTION ZONES

Slab melt-mantle interaction in convergent margins associated with ridge subduction, oblique convergence or initiation of subduction results in hybridization of both ascending slab melts and sub-arc mantle sources. Major element relationships between adakites, transitional adakites, high-Mg andesites and boninites suggest common petrogenetic link [2].

NEABs which are commonly spatially and temporally associated with adakites and transitional adakites have typical arc depletions in HFSE even though they have high absolute concentrations in these elements. The NEABs are enriched in Nb relative to island-arc basalts and are lower in HFSE compared with oceanic-island basalts [2]. Based on the correlated Sr, La and Ta enrichments in slab melt-metasomatized mantle wedge xenoliths in Kamchatka, we suggest that progressive slab melt-mantle interaction in hot subduction zones will produce a hybrid source with selective vein enrichment in Nb, Ta, Sr and LREEs (Figures 1 and 2). Melting of this slab melt-metasomatized source will generate arc magmas with "OIB-like" signatures (HFSE enrichment) coupled with typical arc signatures (Sr and LREE enrichment) without actual involvement of OIB-type mantle sources [11]. We suggest that a lithologic association of adakite- transitional adakite-high-Mg andesite-NEAB exists in arc tectonic settings associated with ridge subduction, subduction of young and hot oceanic crust, initiation of subduction, or oblique convergence or in Archean convergent margins [2, 3, 4].

SLAB MELT-METASOMATIZED MANTLE WEDGE: A POSSIBLE PROTOLITH FOR THE CRATONIC LITHOSPHERE

Kamchatka harzburgite xenoliths exhibit mantle olivine (Fo_{91-93}), spinel - Cr/(Cr+Al) of 0.65 to 0.81,and Al_2O_3 in opx - 0.4-1.6 wt.%. The modal opx content ranges from 10 to 25%. These harzburgites exhibit extremely low TiO_2 (0.01-0.03 wt.%) and Al_2O_3 (0.4-0.6 wt.%) and high Cr (2635-4360 ppm), Ni (2361-2600 ppm) and refractory PGEs (Os- 3-6 ppb, Ir- 3.4-6.8 ppb, Ru- 10-28 ppb). Some harzburgite xenoliths contain graphite-coated diamonds with $d^{13}C$ values of -33.4 and -35.1 $^{0}/_{00}$ indicating a potential slab sedimentary origin for carbon.Kamchatka harzburgite xenoliths are systematically more depleted than the MORB mantle in both mineral and bulk compositions (Fig. 3). The Kaapvaal-type cratonic peridotites have notable compositional similarities to the Kamchatka peridotites: low Al content of co-existing orthopyroxene and spinel, high olivine Fo content, high modal orthopyroxene abundance. Both Kaapvaal and Kamchatka peridotites contain orthopyroxene-rich veins interpreted as a result of slab melt-mantle interaction [4,9]. We propose a three-stage melt extraction model to achieve the depleted (relative to MORB mantle) chemistry of sub-arc mantle wedge (Kam. PMM in Figure 3), cratonic peridotites and peridotitic inclusions in diamonds: 1) extraction of MORB melt at mid-ocean ridges; 2) extraction of back-arc basaltic melt in back-arc spreading centers and 3) hydrous partial melting in a sub-arc mantle wedge to produce arc magmas. This backarc-island arc re-melting of the MORB-type mantle in Archean was probably accompanied by voluminous derivation of TTG suites via partial melting of young and hot oceanic crust and introduction of carbon necessary for diamond formation into the overlying depleted mantle wedge. This is consistent with an apparent synchronicity of TTG

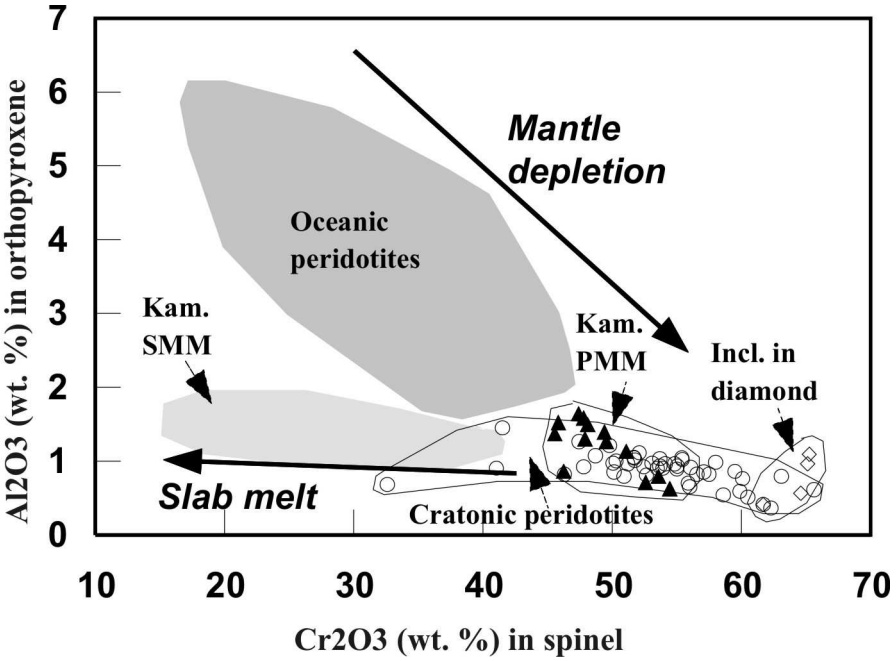

Fig. 3. **Al_2O_3 in orthopyroxene vs. Cr_2O_3 in co-existing spinel for Kamchatka pre-metasomatized mantle peridotites (Kam. PMM) and slab melt-metasomatized peridotites and pyroxenites (Kam. SMM) compared with oceanic peridotites [1], inclusions in diamond [5], and cratonic peridotites [9].**

crustal production (3.5-2.1 Ga), Sm-Nd ages for diamonds (3.4-1.9 Ga), Os model ages for cratonic lithospheric peridotites (3.5-2.7 Ga) and kimberlite-borne eclogites (3.4-2.6 Ga) [6]. This slab melt-metasomatized mantle was subsequently carried below cratons and underplated at the base of growing continental lithosphere.

REFERENCES

1. **Bonatti, E., & Michael, P.J.** (1989). Mantle peridotites from continental rifts to oceanic basins to subduction zones // Earth and Planetary Science Letters, 91, 297-311.
2. **Drummond, M.S., Defant, M.J., & Kepezhinskas, P.K.** (1996). Petrogenesis of slab-derived trondhjemite-tonalite-dacite/adakite magmas // Transactions of the Royal Society of Edinburgh, Earth Sciences, 87, 205-215.
3. **Kepezhinskas, P.K., Defant, M.J., & Drummond, M.S.** (1996). Progressive enrichment of island arc mantle by melt-peridotite interaction inferred from Kamchatka xenoliths // Geochimica et Cosmochimica Acta, 60, 1217-1229.
4. **Kepezhinskas, P.K., & Defant, M.J.** (1996). Contrasting styles of mantle metasomatism above subduction zones: constraints from ultramafic xenoliths in Kamchatka // In: Bebout, G.E., Scholl, D.W., Kirby, S., and Platt, P.J, eds., Dynamics of Subduction, AGU Monograph.
5. **Gurney, J.J., & Zweistra, P.** (1995). The interpretation of the major element compositions of mantle minerals in diamond exploration // Journal of Geochemical Exploration, 53, 293-309.

6. **Pearson, D.G., Carlson, R.W., Shirey, S.B., Boyd, F.R., & Nixon, P.H.** (1995). Stabilization of Archean lithospheric mantle: a Re-Os isotope study of peridotite xenoliths from the Kaapvaal craton // Earth and Planetary Science Letters, 134, 341-357.
7. **Polat, A., & Kerrich, R.** (2001). Magnesian andesites, Nb-enriched basalt-andesites, and adakites from late-Archean 2.7 Ga Wawa greenstone belts, Superior Province, Canada: Implications for late Archean subduction zone petrogenetic processes // Contrib. Mineral. Petrol., 141, 36-52
8. **Rapp, R.P., & Watson, E.B.** (1995). Dehydration melting of metabasalt at 8-32 kbar: Implications for continental growth and crust-mantle recycling // Journal of Petrology, 36, 891-931.
9. **Rudnick, R.L., McDonough, W.F., & Orpin, A.** (1994). Northern Tanzanian peridotite xenoliths: A comparison with Kaapvaal peridotites and inferences on metasomatic reactions // In: Meyer, H.O.A., and Leonardos, O., eds., Proceedings of the 5th International Kimberlite Conference, CPRM, Brasilia.
10. **Schiano, P., Clocchiatti, R., Shimizu, N., Maury, R.C., Jochum, K.P., & Hofmann, A.W.** (1995). Hydrous, silica-rich melts in the sub-arc mantle and their relationship with erupted arc lavas // Nature, 377, 595-600.
11. **Stolz, A.J., Jochum, K.P., Spettel B., & Hofmann A.W.** (1996). Fluid- and melt-related enrichment in the subarc mantle: Evidence from Nb/Ta variations in island-arc basalts // Geology, 24, 587-590.
12. **Volynets, O.N., Avdeiko, G.P., Tsvetkov, A.A., Ananyev, V.V., Antonov, A.Yu., Gladkov, N.G., & Markov, I.A.** (1990). Peridotite inclusions in Quaternary lavas from the Kuriles Island Arc // Transactions of the USSR Academy of Sciences, Geological Series, 3, 43-57 (in Russian).
13. **Wyman, D.A., Ayer, J.A., & Delaney, J.R.** (2000). Niobium-enriched basalts from the Wabigoon subprovince, Canada: evidence for adakitic metasomatism above an Archean subduction zone // Earth Planet. Sci. Lett., 179, 21-30.
14. **Yogodzinsky, G.M., Kay, R.W., Volynets, O.N., Koloskov, A.V., & Kay, S.M.** (1995). Magnesian andesite in the western Aleutian Komandorsky region: implications for slab melting and processes in the mantle wedge // Geol. Soc. Amer. Bull., 107, 505-519.

UDK 552.33

Fluid regime and ore-bearing of late Paleozoic granitoids in west Transbaikalian zones of deep faults

Khrustalev V.K.

Geological Institute SB RAS, Ulan-Ude,e-mail: smetanina@gin.bsc.buryatia.ru

The massives of Late Paleozoic granitoids in zones of deep faults and outside them have been studied. The granitoids that evolve in deep fault zones are characterized by higher contents of rare elements, gases and water. High content of fluids with the water domination in their composition decrease the temperature of melt solidus and decrease that of hydroxyl-containing mineral stability, hamper isomorphic dispersion of ore elements and contribute to origin of accessory mineralization in quiet tectonic setting. Activization of tectonic processes in the above-intrusive zones of the massives causes transition of ore-bearing solutions into the upper structural stages and provides the conditions for formation of the concentrated rare metal mineralization.

The Late Paleozoic hypabyssal massives of leucocratic granites are widespread in the West Transbaikalian region. The rare metal mineralization is spatially associated with some of them. It occurs not ubiquitously and with various intensity. The reasons of such anomalies in spatial distribution of the mineralization have not been analyzed by anybody. Moreover, no systematic studies on geochemistry of the Late Paleozoic granites and correlation of these data with their structural position have been carried out. The reliable estimate of their potential ore-bearing is in fact impossible without them.

The systematic petrological and geochemical studying some massives of the Late Paleozoic leucocratic granites localized in the Turka and Kydzhimit River basins that was carried out by us in the recent years allowed to establish some definite regularities between their geochemical specific features, and structural and geological positions [4]. In particular, we showed that spatial position of the leucocratic granite massives or their individual parts that have features of rare metal geochemical specialization is controlled by the zones of the foundation obscure deep faults (DF) (as viewed by I.N. Thomson), whereas the analogous granite massives localized outside the zone of DF influence have a standard geochemical habit [1]. All this permits to suggest that separate sections of DF zone and knots of their intersections were active fluid conduit structures in the process of the Late Paleozoic granite formation. Therefore some differences should be expected both of quantitative and qualitative characters in composition of volatile components in rocks and minerals of the granite massives that lie in DF zones and outside them that must eventually determine their different potential ore--bearing as well [4].

Some special fluid and geochemical analyses of minerals and rocks from the granites that occur in zones of DF influence (Ona-Kydzhimit massif) and outside them (Khil'minsky massif) have been performed so that to verify the present suggestion. The determination of the fluid phase (H_2O, CO_2, CO, H_2, CH_4, N_2) composition included into feldspars and granite quartz with sensitivity $1 \cdot 10^{-3}$ % has been made in the Institute of the Earth's Crust SB RAS (Irkutsk) with the use of the chromatographic technique by L.V. Baranova. The quantitative spectral measurements of rare metal contents in rocks and minerals have been made in the Institute of Geochemistry SB RAS (Irkutsk).

The Ona-Kydzhimit and Khil'minsky massives lie in the basin of the upper Kydzhimit River among the Low Paleozoic volcanogenic-sedimentary and magmatic rocks, that they have clear intrusive contacts with. The modern contact of the Ona-Kydzhimit massif coincides with the zone of latitudinal Turka-Vitim DF, and the zone of submeridional Vershino-Shovokikan DF crosscuts its west margin. The Khil'minsky massif is located outside the influence of the mentioned DF zones. Both massives have relatively simple structure. Their central parts are composed of middle-grained leucocratic granites gradually changed by fine-grained varieties in the periphery. The granite-porphyries of endocontact facies are fragmentally preserved in the western and eastern margins of the Ona-Kydzhimit massif. Aplites, fine-grained granites of the veined facies and fine- and irregular-grained miarol granites of the schlieren facies are widely developed in the Ona-Kydzhimit massif in contrast to the Khil'minsky one. It is specific that the maximum concentration of the schlieren miarol granite bodies (20-30% of massif volume) is confined to the western margin of the massif located in zone of the Vershino-Shovokikan DF and Turka-Vitim DFs contact. The schlieren bodies are spatially isolated from each other and have diffused contacts with the middle-grained granites hosting them. The endocontact zones of the schlieren bodies consist of fine-grained granites with micropegmatite structure that are changed by the middle-grained varieties with miarol cavities and block isolations of quartz and microcline in the schlieren central parts. These facts indicate that the formation of such bodies occurred from the enriched in volatiles residual melts that were partially degassed in the precrystallization period.

The rock-forming minerals in granites of the Ona-Kydzhimit and Khilminsky massif are represented by albite-oligoclase No5-15 (20-25%), microcline-perthite (46-49%), quartz (27-32%) and biotite (1-2%) with slight variations in some facies varieties.

It is characteristic that biotites from granites of the Khilminsky and Ona-Kydzhimit massives outside the DF zones are differed by the higher magnesium-bearing ($x\mathrm{Bi}_{\mathrm{Mg}}$= 0.40) compared to biotites of the Ona-Kydzhimit massif granites in DF zone ($x\mathrm{Bi}_{\mathrm{Mg}}$= 0.30). Magnetite, zircon, cyrtolite, apatite, ilmenite, rutile, brookite, anatase, orthite and rare sphen are typomorphic accessory minerals in rocks of both massives. Cassiterite, tourmaline and molybdenite have been found only in granites of the Ona-Kydzhimit massif that is located in DF zone.

The contents level of most litophile rare elements in granites of the Khilminsky and Ona-Kydzhimit massives localized outside DF zones are close to the clark values of the low-calcium granites (from Turekjyan and Vedepol). In addition, concentrations of such elements as tungsten, beryllium and molybdenum in them are 1.5-2 times higher than the clark values at the anomalously low contents of fluorine (Table 1). It is characteristic that the fine-grained granites as tungsten, beryllium and molybdenum are 1.5-2 times higher than the clark values at the anomalously low contents of fluorine (Table 1).

It is specific that fine-grained granites of the schlieren and veined facies and granites of the Ona-Kydzhimit massif main facies outside the DF zones are not really differed by the level of all rare element content, i.e. no noticeable tendency toward accumulation of rare and volatile components is marked in the residual melt.

The significant accumulation of all the rare and volatile elements has been established in granite of the Ona-Kydzhimit main facies that formed in the DF zone. They contain 5 times more lithium and boron, and 2 times higher tin, molybdenum, beryllium, tungsten and fluorine compared to the granites of the rest parts in the massif. In addition, decrease in contents of most rare elements up to the level that is specific of granites outside the DF zone is observed in the miarol granites of the schlieren facies. However, they are differed by the higher contents of lithium (4 times) and boron (2 times) compared to the latter ones.

The sharp depletion of the schlieren facies granites in all the rare and volatile elements compared to the source granites of the main facies in the DF zone is likely caused by partial loss of the fluid phase at the stage prior to crystallization of residual melts. The indicated mechanism of the schlieren facies granite formation is reflected in their textural and structural peculiarities, when marginal zones of schlieren have fine-grained and micropegmatite structures, and miarol cavities and block pegmatoid coarse-grained aggregates of quartz-feldspar composition are present in the central parts of the schlieren.

Various geochemical habits of granites that occur in and outside the DF zones suggest an addition of rare and volatile elements into the magmatic chamber of the Ona-Kydzhimit massif by the deep transmagmatic fluids. The peculiarities of the volatile component regime largely determine the subsequent geochemical fate of rare elements in the process of magma crystallization. The comparison of tin distribution in minerals of granites (biotite, quartz) that are variously enriched in the volatile components (B, F) is of obvious interest in this respect.

The comparison of the obtained data (Table 1) with the results of the earlier paper [3] indicates that the lowest tin concentrations are fixed in more ferriferous biotites from granites with the maximum bulk contents of this element and volatile components. In contrast to biotite, the tin content in quartz directly depends on the bulk concentrations of tin and volatiles in rock. It is specific that accessory cassiterite (Ona-Kydzhimit massif in the DF zone) is contained in granites with the minimum tin amount in biotite.

Table 1.

Average contents of rare elements in the Late Paleozoic granites

NN	Position	Number of analyses	%		ppm							
			K	Na	Li	Rb	Be	Sn	W	Mo	F	H
1	**Outside DF zones**	8	3.4	2.7	51	220	5.7	4.5	1.3	2.6	240	18
2		10	3.8	2.9	21	220	5.5	4.4	1.6	2.4	220	10
3		9	3.7	2.6	23	260	5.4	4.9	2.4	2.6	170	10
4	**In DF zone**	11	4.0	2.8	270	220	7.1	9.5	4.8	5.2	550	55
5		11	3.4	3.0	85	200	4.9	3.9	2.6	3.4	350	20

Note. 1,2,4 – leucocratic granites of main facies; 3 – alpites and fine-grained granites of veined facies; 5 – pegmatoid granites of schlieren facies (1 – the Khilminsky massif; 2-5 – the Ona-Kydzhimit massif). Analysis has been carried out at the Institute of the Earth' Crust SB RAS (Irkutsk) by chromatographic technique. Analysist is L.V.Baranova, 1996.

Therefore, the elevated contents of the volatile components in the melts prevent from isomorphic dispersion of tin in biotite, provide the conditions for its accumulation in the mineral of the crystallization late stage (quartz) and origin of accessory cassiterite.

The data on the contents of water and gases in feldspars and quartz of granites from the Khilminsky and Ona-Kydzhimit massives that are presented in Table 2 testify to the formation of both massives having occurred in mostly oxidized setting, the sum of the oxidized fluids (H_2O+CO_2) significantly dominates over that of the reduced gases (CH_4+CO+H_2). The fluid division into two groups with CH_4+H_2 (bonding force r=+0.6) in one group and H_2O+CO_2 (r=+0.3) in the other one is specific of the considered granites on the whole due to the cluster [3]. A very weak negative association is outlined between these groups. The similar structure of the cluster attributes to the fact that the two relatively independent fluid systems, i.e. the reduced (CH_4+H_2) and oxidized (H_2O+CO_2) ones participated in formation of the Late Paleozoic granites. The oxidized fluids can both have the crust nature and form at the parental magma generation due to oxidation of deep, significantly reduced fluids (CH_4+H_2). The outlined negative CO association with the group CH_4+H_2 from the one hand and with H_2O+CO_2 one from the other hand can indicate to CO origin due to oxidation of CH_4 with its subsequent oxidation up to CO_2.

The comparison of granites that develop in the DF zones and outside them attributes to the various quantitative and qualitative compositions of fluids in the process of their formation. Thus, for instance, the feldspars of the Ona-Kydzhimit massif granites in the DF zone contain more H_2O, CO_2 and N_2, but less H_2 in comparison with feldspars in the Khilminsky massif. The maximum extent of fluid oxidation both by the ratio H_2/H_2O and CO/CO_2 (Table 2) is typical for them. The comparison of fluid composition in the row of leucocratic granite – pegmatoid granite shows that the contents of CH_4, H_2, CO and H_2O decrease and those of CO_2

and N_2 increase in the residual melt in the process of the massif crystallization in the DF zone. It follows from the obtained data that the massif crystallization occurs

Table 2.

Average contents of fluid components in the Late Paleozoic granites, cm^3/g

	Khil'minsky massif			**Ona-Kydzhimit massif**	
	Leicocratic granites			**Pegmatoid granites**	
Component	1	2		4	5
	Feldspars (4)	Quartz (4)	Quartz (1)	Feldspars (5)	Feldspars (5)
	Outside DF zones			**In DF zone**	
H_2O	1.12	0.20	0.23	1.90	1.80
CO_2	0.08	0.04	0.05	0.23	0.33
CO	0.05	0.03	0.02	0.05	0.04
CH_4	0.02	-	-	0.02	0.006
H_2	0.24	-	-	0.09	0.014
N_2	0.029	0.046	0.024	0.034	0.062
H_2/H_2O	0.19	-	-	0.034	0.062
CO/CO_2	0.65	0.60	0.40	0.26	0.16
KB= $\frac{CH_4+CO+H_2}{CO_2+H_2O}$	0.28	0.18	0.25	0.08	0.02
H_2O/CO_2	16.1	5.0	4.6	9.5	6.5
$\Sigma gas/H_2O$	0.46	0.60	0.41	0.23	0.28

Note. 1,2,4,5 – the same as in Table 1. Numbers in brockets – number of analyses. Analyses have been carried out at the Institute of Geochemistry SB RAS (Irkutsk) by photometric, atom-absorption and spectrographic techniques. Analysists are D.Kh.Nikolaeva, T.N.Shrefer, L.N.Svadkovskaya, L.L.Petrov and A.D.Glazunova, 1990.

on the background of CH_4, H_2 and CO oxidation and its partial degassing mainly at the cost of H_2O loss. Due to the cluster [3], the granites in the DF zone are specific of rather close association of primarily reduced fluids CO, CH_4 (r=0.72) that are attached by H_2(r=+0.40), and as the product of its oxidation H_2O, CO_2 and N_2 are found to have a weak negative association with this group. The general structure of the cluster [3] and data presented in Table 2 indicate that granite evolution in the DF zone occurred at the stationary seepage of the reduced gases, H_2O and CO_2 generating in deep horizons at the cost of the latter ones oxidation. In the present case, CO, CH_4 and H_2 in granites are likely to characterize the relic part of the deep fluids. Since the fluid oxidation is followed by the significant heat release, the melt crystallization in the DF zone takes place in the exothermostated conditions that contributes to its long evolution. In the course of the massif crystallization, the access of fluids from deep horizons becomes difficult, and the residual melts (pegmatoid granites of the schlieren facies) that are isolated from the main part of the massif behave like autonomous bodies with their parameters of existence. Nearly complete CH_4 and H_2 "burning down" occurs during their crystallization.

Quite an other behavior of fluid components is observed during the process of granite crystallization in the Khilminsky massif that develops outside DF zones. The comparison of fluid compositions in feldspars and quartz of this massif

indicates to the sharp decrease in H_2O, CO_2 and CO and lack of CH_4 and H_2 contents in the latter one (Table 2), i.e. complete oxidation of H_2 and CH_4 and throwing off H_2O significant amounts take place by the moment of quartz crystallization. The N_2 accumulation is only fixed. The structure of the cluster in the Khilminsky massif granites [3] testifies to the mixed nature of fluids in the process of their formation, as both the oxidized and reduced fluids are united into the same group in it.

It can be said rather confidently that H_2O generation occurred at the cost of H_2 oxidation during the process of the Khilminsky massif crystallization. The presence of CO strong negative association with CH_4, CO_2 and H_2 is likely to be the consequence of complex evolution of fluids in the process of crystallization, when possible oxidation proceeds on line $CH_4 \rightarrow CO+H_2$ and further on $H_2 \rightarrow H_2O$ and $CO \rightarrow CO_2$. In addition, it is characteristic that the extent of CO oxidation in quartz remains really at the same level as in feldspars (CO/CO_2 =0.65 and 0.60 respectively), and H_2O/CO_2 ratio decreases 3 times. The constant level of CO oxidation in the late products of crystallization (quartz) and CO_2 relative accumulation in them are likely to be a universal regulation.

Therefore, it is demonstrative that compositions of fluids and their oxidized-reduced parameters in quartz of granites in the Ona-Kydzhimit massif that occur outside the zone of DF influence are close to quartz fluid compositions of the Khilminsky massif (Table 2). It follows from this comparison that the granites in the Khilminsky and Ona-Kydzhimit massives that occur outside the zones of DF influence from in similar oxidized-reduced regime. It is also confirmed by the same level of iron oxidation in them ($Fe_2 O_3/FeO$=1.2). At the same time, the feldspar fluids of granites that are found in the zone of DF influence are in maximum more oxidized than in quartz both by the summary extent of oxidation and CO/CO_2 value that is agreed well with the maximum extent of iron oxidation (Fe_2O_3/FeO=1.5 and 3.1) in rocks as well.

Thus, the granites in the DF zones are characterized by higher bulk amount of fluids and maximum extent of their oxidation in contrast to the granites that form outside the DF zones. The similar levels of the reduced gas contents in both massives are likely the result of their incomplete oxidation that is associated with the low buffer ability of leucocratic granite melts. Therefore, it is logical to assume that enrichment of granites in H_2O and CO_2 that develop in DF zones occurs at the cost of the deep reduced gas oxidation in the lower parts of magmatic chambers, decreasing T of melt solidus and eventually determining the ways of its crystallization. In this respect, the presence of direct correlation between the ratio value Σ_{gas}/H_2O and Mg-bearing of biotites and granites in DF zones and outside them is demonstrative [3]. It is logical to assume that the ratio value Σ_{gas}/H_2O is directly dependent on PH_2O in the melt-fluid system. Therefore it can be suggested that granite formation within the Ona-Kydzhimit massif in the DF zone occurred at higher value than that of the Khilminsky one. It is generally known that PH_2O increase decreases the temperature of granite melt solidus and shifts biotite field of

stability into the higher-T field at $P_{tot.} > PH_2O$ in the P-T plot. Therefore, the increase in water partial pressure in melt at $P_{tot.}$=const will result in increase of the ferriferous biotite stability in other similar conditions. The maximum biotite Fe-bearing in granites with the minimum value of ratio $_{\Sigma gas}/H_2O$ (Ona-Kydzhimit massif in DF zone) gets clear in this respect. Since PH_2O increase shifts the fields of stability not only of OH-containing minerals, but oxides as well [2] in the field of high TT, the highest content of accessory cassiterite in leucocratic granites of the Ona-Kydzhimit massif main facies within DF zones and its lack outside them can be simply elucidated.

It should be noted that most tin ore occurrences of the tin-bearing pegmatites and cassiterite-quartz formations are also localized just in those parts of the Ona-Kydzhimit massif that lie within the Vershino-Shovokikan and Turka-Vitim DFs and particularly at their intersection.

Thus, all the sum of the structural-geological and petrological-geochemical data testify to a decisive role of the foundation closed faults in formation of the Late Paleozoic granitoid geochemical habit and localization of rare metal mineralization spatially associated with them. It can be suggested that the most favorable sites for the origin of rare metal leucogranite massives should be the knots of intersection or joint of the greatest number of the foundation closed fault zones, various orientations and depths of location, as in this case, the heat and fluid flows controlled by them will be summed up. The quantitative and qualitative compositions of the fluids that migrate through the magmatic chambers in the DF zone eventually determine geochemical habit of granitoids and ways of their differentiation and crystallization. Of course, the granite massives with higher contents of rare and volatile components should have higher potential ore-bearing in other similar conditions, compared to the granites of the standard geochemical habit. However, its realization depends on the possibility and mechanism of ore-bearing fluid mobilization.

REFERENCES

1. **Khrustalev V.K.** (1990). Geochemistry and ore-bearing of the Paleozoic granitoids on the Vitim upland. Novosibirsk, Nauka, 135p. (in Russian)
2. **Khrustalev V.K.** (1997). Fluid regime and evolution of magmatogenic and hydrothermal systems in West Transbaikalia // In: Ore mineralization and granitoid magmatism in the North Pacific. Abstracts of reports of All-Russia meeting. Magadan, Nauka, 251-252. (in Russian)
3. **Komarov Yu.V., Kopylov E.N., Belogolovkin A.A., Khrustalev V.K. et al.** (1978). Tin mineralization of the Turka-Vitim deep fault in West Transbaikalia. Novosibirsk, Nauka, 95p. (in Russian)
4. **Kopylov E.N., Khrustalev V.K. and Baranova L.V.** (1996). Fluid regime and potential ore-bearing of the West Transbaikalian Late Paleozoic granitoids in zones of closed deep fault influence // Geology and Geophysics, v.37, N12, 42-54.